UNIVERSITÄT
LEIPZIG

REPORT
Institute für Physik
The Physics Institutes
2017

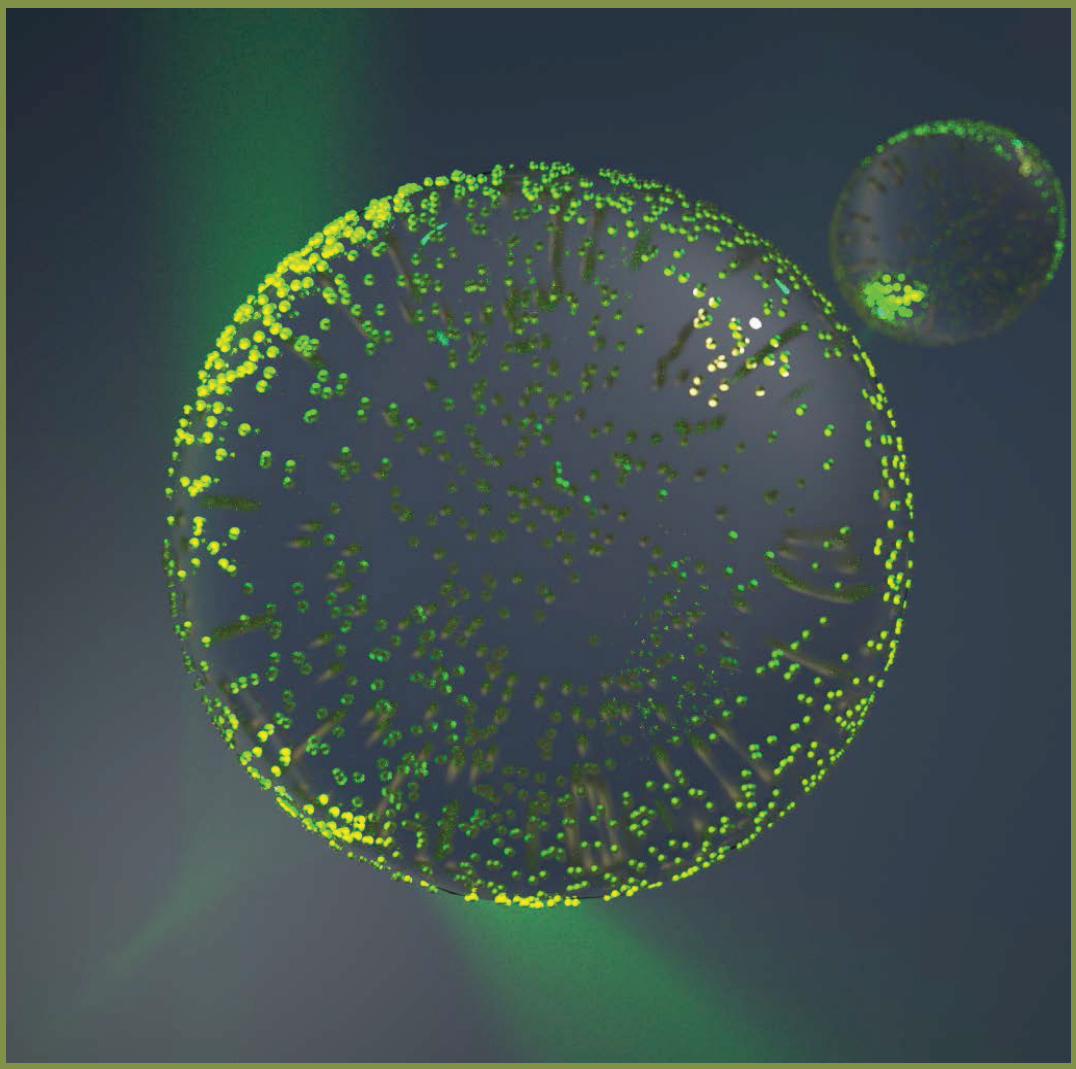

The Physics Institutes of Universität Leipzig, Report 2017
M. Grundmann (Ed.)

Technical Editor: Anja Heck

Printed in Germany by
MERKUR Druck und Kopierzentrum GmbH, Leipzig

online available at
http://nbn-resolving.de/urn:nbn:de:bsz:15-qucosa-151238

Front cover
The images shows a symmetric swimmer, that is a polymer particle decorated with gold nanoparticles which moves by optical heating of the gold nanoparticles.

Back cover
TCO2019

Peter-Debye-Institut für Physik der weichen Materie
Felix-Bloch-Institut für Festkörperphysik
Institut für Theoretische Physik

Fakultät für
Physik und Geowissenschaften

Universität Leipzig

Peter Debye Institute for Soft Matter Physics
Felix Bloch Institute for Solid State Physics
Institute for Theoretical Physics

Faculty of Physics and Earth Sciences

Universität Leipzig

Report 2017

Addresses

Peter Debye Institute for Soft Matter Physics

Linnéstraße 5
D-04103 Leipzig, Germany
Phone: +49 341 97-32654
Fax: +49 341 97-32598
WWW: https://www.physgeo.uni-leipzig.de/fakultaet/institutebereiche/peter-debye-institut/
Mailing address: Postfach 100 920, D-04009 Leipzig, Germany

Felix Bloch Institute for Solid State Physics

Linnéstraße 5
D-04103 Leipzig, Germany
Phone: +49 341 97-32650
Fax: +49 341 97-32668
WWW: https://www.physgeo.uni-leipzig.de/fakultaet/institutebereiche/felix-bloch-institut/
Mailing address: Postfach 100 920, D-04009 Leipzig, Germany

Institute for Theoretical Physics

Brüderstraße 16
D-04103 Leipzig, Germany
Phone: +49 341 97-32420
Fax: +49 341 97-32548
WWW: https://www.physgeo.uni-leipzig.de/fakultaet/institutebereiche/theoretische-physik/
Mailing address: Postfach 100 920, D-04009 Leipzig, Germany

Preface

The 2017 Report of the Physics Institutes of the Universität Leipzig provides an overview of the structure and research activities of the three institutes.

We are happy to announce that Prof. Dr. Caudia Schnohr from Universität Jena will join the Felix Bloch Institute for Solid State Physics beginning 2019 filling the vacant position in the department for Solid State Optics. Dr. Johannes Deiglmayr from ETH Zurich will establish an independent department for Quantum Optics at the same institute.

Various academic events have enriched our year, among them the "Topological matter and flat bands" conference in August, an official satellite meeting of the 28th International Conference on Low Temperature Physics (LT28, Gothenburg/Sweden) that was organized by Prof. Pablo Esquinazi. The TCO2017 conference organized by Prof. Marius Grundmann and Dr. Holger von Wenckstern brought together about eighty national and international experts, young scientists and students in the fields of transparent conductive oxides and oxide semiconductors. At the end of November the by now traditional 18th International Workshop on Recent Developments in Computational Physics "CompPhys17" organized by Prof. Wolfhard Janke took place in Leipzig. Around sixty scientists from over ten different countries exchanged ideas and discussed recent progress in several fields of computational physics.

As it is meanwhile a tradition, the Peter Debye Institute for Soft Matter Physics has organized its annual Soft Matter Day also in 2017. On June, 23th all departments of the institute presented their current research in talks and posters. About one hundred scientists and students have been enjoying very lively discussions together with members of other institutes and faculties and a BBQ.

Work has successfully continued in the DFG-funded Centers of Excellence (Sonderforschungsbereiche) SFB 762 "Functionality of Oxide Interfaces" and SFB TRR 102 "Polymers under Multiple Constraints: Restricted and Controlled Molecular Order and Mobility" as well as in several Research Units (DFG Forschungsgruppen), Priority Programs (DFG Schwerpunktprogramme) and EU-funded projects. The International Graduate College "Statistical Physics of Complex Systems" of the Deutsch-Französische Hochschule (DFH-UFA) run by the computational physics group in cooperation with the partners Université de Lorraine in Nancy, France, Coventry University, UK, and the Institute for Condensed Matter Physis of the National Academy of Sciences of Ukraine in Lviv, Ukraine, started in January 2017 the 4th funding period from 2017-2020.

We are grateful to our guests for enhancing our academic year with their contributions in the colloquium and within our work groups. We mention especially Prof. Dr. Ulrich H.E. Hansmann (University of Oklahoma, USA) who has spent from June to December 2017 his Sabbatical and Prof. Dr. Handan Arkin-Olgar (Ankara Univer-

sity, Turkey) who has spent her Alexander-von-Humboldt Fellowship for Experienced Researchers in the group of Prof. Janke.

Our activities and success are enabled through the generous support from various funding agencies for which we are very grateful and which is individually acknowledged in the brief reports.

Leipzig,
November 2018

F. Cichos
M. Grundmann
W. Janke
Directors

Contents

III Institute for Theoretical Physics 209

1

Structure and Staff of the Institutes

1.1 Peter Debye Institute for Soft Matter Physics

1.1.1 Molecular Nano-Photonics, Molekulare Nanophotonik [MON]

Prof. Dr. Frank Cichos

Technical staff

Dipl.-Phys. Andrea Kramer
Dipl.-Phys. Uwe Weber

PhD candidates

Alexander Fischer, M.Sc.
Martin Fränzl, M.Sc.
André Heber, M.Sc.
Santiago Muiños Landin, M.Sc.
Dipl.-Phys. Romy Schachoff
Tobias Thalheim, M.Sc.

Students

Alice Abend
Hans Falk
Andreas Hentrich
Sergio Ortega
Ricardo Rose
Nicola Söker

1.1.2 Molecular Physics, Molekülphysik [MOP]

Prof. Dr. F. Kremer

Secretary

Kerstin Lohse

Technical staff

Dipl.-Ing. (FH) Jörg Reinmuth
Dipl.-Phys. Wiktor Skokow

Academic staff

Dr. Wilhelm Kossack
Dr. Arthur Markus Anton

PhD candidates

M. Edu. Falk Frenzel

Students

cand. M. Edu. Patricia Prinz

1.1.3 Soft Matter Physics, Physik der weichen Materie [PWM]

Prof. Dr. Josef A. Käs

Secretary

Claudia Brück

Technical staff

Dr. Undine Dietrich
Dipl.-Phys. Bernd Kohlstrunk

Academic staff

Dr. Thomas Fuhs
Dr. Jörg Schnauß
Dr. Mareike Zink

PhD candidates

Katharina Anna Bela, M. Sc.
Martin Glaser, M. Sc.
Tom Golde, M. Sc.
Dipl.-Phys. Tina Händler

Paul Heine, M. Sc.
Kantida Juncheed, M. Sc.
Hans Kubitschke, M. Sc.
Jürgen Lippoldt, M. Sc.
Philine Hietschold M. Sc.
Erik Morawetz, M. Sc.
Dipl.-Phys. Steve Pawlizak
Dipl.-Phys. Carsten Schuldt
Frank Sauer, M. Sc.
Dipl.-Phys. Enrico Warmt
Astrid Weidt, M. Sc.

Students

Diana Rodriguez Bonet
Carlotta Ficorella
Pablo Gottheil
Yookyung Ha
Sebastian Henn
Yonah Karkheck
Thomas Lettau
Till Möhn
Paul Mollenkopf
Friederike Muth
Hannah-Marie Scholz-Marggraf
Markus Sommerfeld
Teresa Tschirner
Cary Tutmarc
Joey Wittenbecher
Isabella Marie Fornacon Wood

1.1.4 Biological Physics, Biologische Physik [BIP]

Prof. Dr. Claudia Mierke

Secretary

Kerstin Lohse

Technical staff

Dipl.-Ing. Kathrin Koch

PhD candidates

Stefanie Puder, M.Sc.
Dipl.-Phys. Tony Fischer
Tom Kunschmann, M.Sc.
Jeremy Perez, M.Sc.
Nils Wilharm, M.Sc.
Frank Sauer, M.Sc.

Students

Alexander Hayn
Anne-Dorette Ziems
Christian Aermes
Sebastian Ronneberger

1.1.5 Molecular Biophysics, Molekulare Biophysik [MBP]

Prof. Dr. Ralf Seidel

Secretary

Kerstin Lohse

1.2 Felix Bloch Institute for Solid State Physics

1.2.1 Office of the Director

Prof. Dr. Marius Grundmann (director)
Prof. Dr. Pabolo Esquinazi (vice director)

1.2.2 Magnetic Resonance of Complex Quantum Solids, Magnetische Resonanz Komplexer Quantenfestkörper [MQF]

Prof. Dr. Jürgen Haase

Secretary

Sophie Kirchner
Sandra Meurer

Technical staff

Gert Klotzsche
Stefan Schlayer
Horst Voigt

Academic staff

PD Dr. Marko Bertmer
Prof. Dr. Dieter Freude
Dr. Michael Jurkutat
Prof. Dr. Andreas Pöppl
Dr. Richard Reznicek
PD Dr. Rustem Valiullin

PhD candidates

Dipl.-Phys. Nina Dvoyashkina
Stefan Friedländer, M. Sc.
Nataliya Georgieva, M. Sc.
Robin Gühne, M. Sc.
Seungtaik Hwang, M. Sc.
Dipl.-Phys. Alexander Jäger
Arafat Hossain Khan, M. Sc.
Dipl.-Phys. Jonas Kohlrautz
Anastasiia Kultaeva, M. Sc.
Kathrin Lorenz, M. Sc.
Dipl.-Phys. Matthias Mendt
Steven Reichardt, M. Sc.
Daniel Schneider, M. Sc.

1.2.3 Nuclear Solid State Physics, Nukleare Festkörperphysik [NFP]

Prof. Dr. Jan Meijer

Secretary

Birgit Wendisch

Technical staff

Dipl.-Phys. Steffen Jankuhn
Carsten Pahnke
Dipl.-Ing. Joachim Starke

Academic staff

Dr.-Ing. Michael Kieschnick
Dr. Sébastien Pezzagna

PhD candidates

Sascha Becker, M.Sc.
Tobias Herzig, M.Sc.
Dipl.-Math. Roger John, B.Sc.
Tobias Lühmann, M.Sc.
Nicole Raatz, M.Sc.
Paul Räcke, M.Sc.
Clemens Scheuner, M.Sc.
Robert Staacke, M.Sc.
Ralf Wunderlich, M.Sc.

Students

Camila Bräutigam, B.Sc. (till January 2017)
Jakob Helbig, M.Sc. (till October 2017)
Alexander Kühne, B.Sc.
Johannes Küpper, M.Sc. (till November 2017)
Frederic Renner, B.Sc. (till June 2017)
Marcel Rietzschke, M.Sc. (till September 2017)
Erik Wiedemann, M.Sc. (till March 2017)

1.2.4 Semiconductor Physics, Halbleiterphysik [HLP]

Prof. Dr. Marius Grundmann

Secretary

Anja Heck
Birgit Wendisch

Technical staff

Dipl.-Phys. Gabriele Benndorf
Monika Hahn
Dipl.-Ing. Holger Hochmuth
Dipl.-Phys. Jörg Lenzner
Dipl.-Phys. Axel Märcker
Gabriele Ramm
Roswitha Riedel
Dipl.-Ing. Ulrike Teschner

Academic staff

Prof. Dr. Michael Lorenz
PD Dr. Rainer Pickenhain
Prof. Dr. Bernd Rheinländer (retired)

Dr. Rüdiger Schmidt-Grund
Dr. Daniel Splith
Dr. Chris Sturm
Dr. Holger von Wenckstern
Dr. Chang Yang
Dr. Zhipeng Zhang

PhD candidates

Sofie Bitter, M.Sc.
Oliver Herrfurth, M.Sc.
Stefan Hohenberger, M.Sc.
Robert Karsthof, M.Sc.
Max Kneiß, M.Sc.
Abdurashid Mavlonov, M.Sc.
Tom Michalsky, M.Sc.
Anna Reinhardt, M.Sc.
Steffen Richter, M.Sc.
Peter Schlupp, M.Sc.
Alexander Shkurmanov, M.Sc.
Lukas Trefflich, M.Sc.
Haoming Wei, M.Sc.
Anna Werner, M.Sc.
Marcel Wille, M.Sc.
Vitaly Zviagin, M.Sc.

Students

Philipp Bischoff
Ron Hildebrandt
Rebecca Hölldobler
Tanja Jawinski
Florian Jung
Evgeny Krüger
Oliver Lahr
Stefan Lange
Steffen Lanzinger
Manuel Raphael Lindel
Sophie Müller
Karim Nafis Imtiaz
Ahsan Rasheed
Fabian Schöppach
Philipp Storm
Laurenz Thyen
Benjamin Wehr

1.2.5 Solid State Optics and Acoustics, Festkörperoptik und -akustik [FKO]

vacant

1.2.6 Superconductivity and Magnetism, Supraleitung und Magnetismus [SUM]

Prof. Dr. Pablo Esquinazi

Secretary

Mrs. Sandy Ehlers

Technical staff

Dr. Winfried Böhlmann
Dipl.-Krist. Annette Setzer

Academic staff

Prof. Dr. Michael Ziese
Dr. José Barzola-Quiquia
Dr. Séverine Diziain
Dr. Israel Lorite Villalba
Dr. Yogesh Kumar

PhD candidates

M. Sc. Francis Bern
M. Sc. Johannes Küpper
M. Sc. Christian Eike Precker
M. Sc. Bogdan Semenenko
M. Sc. Markus Stiller

Students

B. Sc. Lukas Botsch
B. Sc. Tiago Rafael Silva Cordeiro
B. Sc. Stefan Dietel
cand. B. Sc. Anthony Ogbuehi
cand. B. Sc. Devesh Jawla

1.3 Institute for Theoretical Physics

1.3.1 Office of the Director

Prof. Dr. Wolfhard Janke (director)

Secretary

Gabriele Menge
Susan Moreno
Lea Voigt

1.3.2 Computational Quantum Field Theory, Computerorientierte Quantenfeldtheorie [CQT]

Prof. Dr. Wolfhard Janke

Academic staff

Dr. Stefan Schnabel
Dr. Jonathan Gross
Dr. Suman Majumder

PhD candidates

M.Sc. Johannes Bock
M.Sc. Henrik Christiansen
M.Sc. Momchil Ivanov
M.Sc. Stanislav Kazmin
M.Sc. Ravinder Kumar ("co-tutelle" with Coventry University, UK)
Dipl.-Phys. Martin Marenz
Dipl.-Phys. Marco Müller
Dipl.-Phys. Hannes Nagel
Dipl.-Phys. Andreas Nußbaumer
M.Sc. Philipp Schierz

Students

Kieran Austin
Thomas Els
Lisa Fiedler
Hans-Joachim Lange
Fabio Müller
David Oberthür
Simon Schneider
Franz Paul Spitzner
Ronja Stübel

Dimitrij Tschodu
Tobias Weiss
Chris Allen
Jakob Bürgermeister
Adrian Häußler
Michel Michalkow

1.3.3 Quantum Field Theory and Gravity, Quantenfeldtheorie und Gravitation [QFG]

Prof. Dr. Rainer Verch (Speaker)

Prof. Dr. Gerd Rudolph (retired)

Academic staff

Prof. Dr. Rainer Verch
Priv.-Doz. Dr. Michael Bordag
Dr. Thomas-Paul Hack
Dr. Matthias Schmidt

PhD candidates

Tobias Diez, M.Sc.
Erik Fuchs, M.Sc.
Michael Gransee, M.Sc.
Mathias Hänsel, M.Sc.
Felix Kurpicz, M.Sc.

Students

Mohammed Belhassen
Sandesh Bhat
Stanislaw Kazmin
Sebastian Knappe
Richard Neidhardt
Justus Neumann
Thies-Albrecht Ohst
Marie Rodal
Maik Wessling
Johannes Zähle

Retired

Prof. em. Bodo Geyer
Prof. em. Gerd Rudolph
Prof. em. Armin Uhlmann

1.3.4 Statistical Physics, Statistische Physik [STP]

Prof. Dr. Bernd Rosenow

Academic staff

Dr. Casper Drukier
Dr. Andreas Kreisel

PhD candidates

Giovanni Frigeri, M.Sc.
Lukas Kimme, M.Sc.
Martin Treffkorn, M.Sc.
Heinrich-Gregor Zirnstein, M.Sc.
Niels John, M.Sc.

Students

Florian Knoop
Enrico Lohmann
Pit Strub
Matthias Thamm
Tobias Leckel
Sina Teichert
Thomas Suchanek

1.3.5 Theory of Condensed Matter, Theorie der kondensierten Materie [TKM]

Prof. Dr. Klaus Kroy (Speaker)

Prof. Dr. Ulrich Behn (retired)
Prof. Dr. Dieter Ihle (retired)
Prof. Dr. Adolf Kühnel (retired)

Academic staff

Dr. Viktor Holubec

PhD candidates

Gianmaria Falasco, M.Sc.
Stefano Steffenoni, M.Sc.
Dipl.-Phys. Jakob Bullerjahn
Dipl.-Phys. Marc Lämmel
Richard Pfaller, M.Sc.

Sven Auschra, M.Sc.
Daniel Geiss, M.Sc.
Constantin Huster, M.Sc.

Students

Benjamin Streitz, B.Sc.
Katharina Tholen, B.Sc.
Paul Cervenak, B.Sc.
Roland Wiese, B.Sc.
Joscha Mecke
Erik Rohkamm
Omer Rochman
Wei Liu

1.3.6 Theory of Elementary Particles, Theorie der Elementarteilchen [TET]

Prof. Dr. Stefan Hollands

Prof. Dr. Klaus Sibold (retired)

Academic staff

PD Dr. Roland Kirchner (retired)
PD Dr. Holger Perlt
PD Dr. Arwed Schiller
Dr. Jochen Zahn

PhD candidates

Dipl.-Phys. Steffen Pottel
Mojtaba Taslimi Tehrani, M.Sc.

Students

En-Hung Chao, B.Sc.
Sebastian Drawert, B.Sc.
Onirban Islam, B.Sc.
Marek Kozon, B.Sc.
Narek Papoyan
Frederieke Richert
Carlos Serrano

I

Peter Debye Institute for Soft Matter Physics

2

Molecular Nano-Photonics

2.1 Introduction

Studying dynamic processes at the level of single molecules and particles in soft materials, the group has recently started to explore the release of heat from single molecules and nanoparticles. These absorbing chromophores are able to convert optical energy into heat if their fluorescence quantum yield is low. This released heat is generating a steady state spatial temperature profile as they are embedded in a large heat bath, which is their solvent environment. This local temperature profile allows a number of new studies, which range from fundamental physical aspects of Hot Brownian Motion (HBM) to the active motion of self-propelled particles. In particular this field of research of the group addresses

- Thermally propelled particles and micromachines
- Manipulation and trapping of single nano-objects in solution
- Transmission microscopy of Rayleigh- and Mie-particles
- Manipulation of living cells by local temperature fields
- Heat conduction at the nanoscale

During the year 2017 the Molecular Nanophotonics Group has celebrated a number of achievements. Among them are:

- The group is part of the priority program SPP 1726 "Microswimmers", which has been successfully extended in the year 2017.
- Prof. Dr. Alois Würger from the University of Bordeaux has been a guest in the group for one month working on thermoelectric effects at the nanoscale.

Collaborations with the groups of Prof. Dr. Klaus Kroy (Universität Leipzig), Prof. Dr. Michael Mertig (TU Dresden), Prof. Dr. Alois Würger (University of Bordeaux) and Prof. Haw Yang, PhD (Princeton University) have been very fruitful. A new collaboration with the group of Prof. Giovanni Volpe, PhD from the University of Gothenburg in Sweden has been started.

Frank Cichos

2.2 Manipulation of single molecules in a thermophoretic trap

T. Thalheim, M. Braun, F. Cichos, M. Mertig*, D. Huster†

*TU Dresden, Kurt Schwabe Institute of Instrumentation and Sensor Engineering Meinsberg
†Universität Leipzig, Institute for Medical Physics and Biophysics

Nano-objects in a viscous medium are governed by Brownian motion which is erratic and jerky in nature. Thus, for a long-term investigation of these objects sophisticated devices, as, e.g., optical tweezers or the so-called Anti-Brownian Electrokinetic trap (ABEL trap) were invented to confine this stochastic dynamics. The ABEL trap applies a feedback-controlled homogeneous electric field generated by four electrodes to even trap single molecules [1]. Multi-particle studies are therefore difficult to realize since due to the homogeneity of the electric field these objects are shifted by the same amount in this trap when the Brownian motion of one object has to be counteracted.
Recently, we devised an all-optically controlled technique which employs highly localized thermal fields instead of electric fields [2, 3]. These temperature fields are produced by converting optical energy of a focused laser into temperature using a laser-printed plasmonic nanostructure (Figure 2.1A and B). The physical phenomenon utilized in these experiments is termed thermophoresis or Ludwig–Soret effect. Our setup allows to control the number of particles or molecules in the trap using an optical feedback

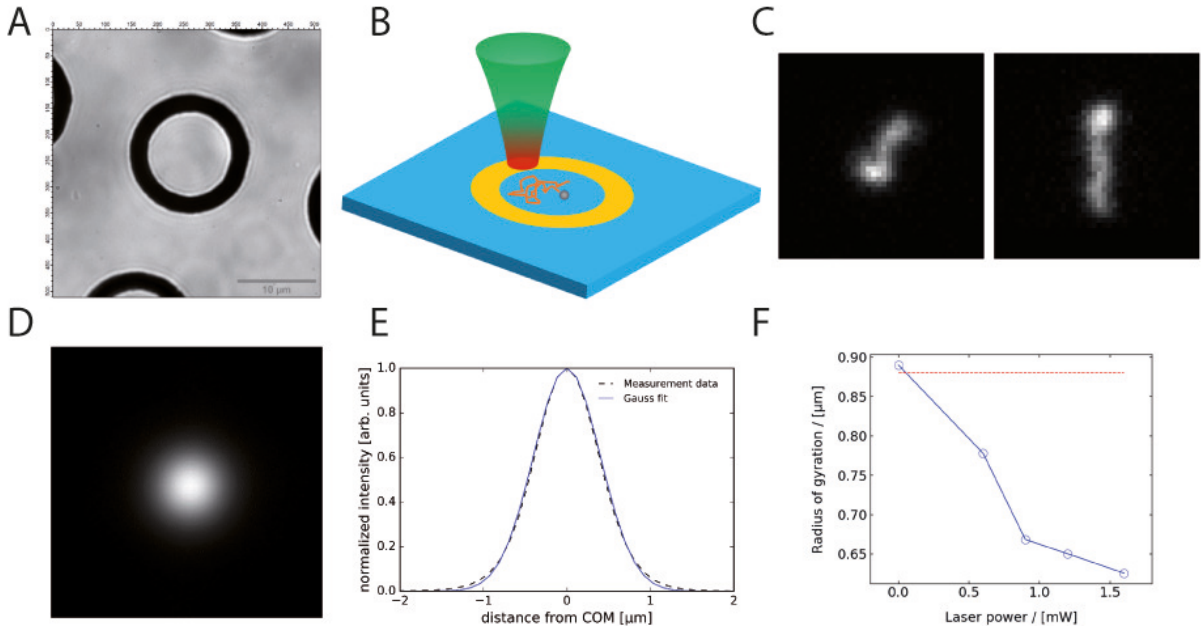

Figure 2.1: **A**) Laser-printed array of plasmonic gold nanostructures as thermophoretic traps. **B**) A laser beam is focused on the gold structure generating an inhomogeneous temperature profile. **C**) Snapshots of λ-DNA in COM coordinates during a trapping experiment. **D**) Accumulated intensity distribution of all recorded images in COM. **E**) The line profile through the accumulated intensity distribution resembles a Gaussian distribution very well. Hence, a width can be extracted. **F**) Decreasing radius of gyration of the T4-DNA with increasing heating power.

mechanism. Hence, completely new types of bio-molecular interaction dynamics assays on single molecules by avoiding surface attachment can be realized.
As a first insight into these studies, we have already shown that it is possible to trap multiple colloids as well as single DNA molecules [4]. Figure 2.1C shows two snapshots of a T4-DNA molecule whose center-of-mass (COM) motion was confined in a thermophoretic trap. Due to the inhomogeneous temperature gradient generated by the focused laser beam (Figure 2.1B), which is decaying approximately with the inverse distance from the heat source, parts of the DNA in close proximity to the heating laser experience a higher thermophoretic drift velocity than parts of the DNA which are further away. The T4-DNA is therefore a single polymer chain which is not in thermal equilibrium. Different positions along the chain experience different temperatures. We therefore expected the T4-DNA to be compressed in the thermophoretic trap in addition to the confinement of the COM motion. Therefore, the DNA molecule in every recorded image of a trapping experiment was shifted into the COM frame and the accumulated intensity distribution was calculated (Figure 2.1D). A line profile through this intensity distribution can be reasonably well approximated with a Gaussian distribution (Figure 2.1E). As the temperature gradients along the chain become stronger with increasing heating power at the trap structure, a decrease of the radius of gyration of the T4-DNA is observed (Figure 2.1F). With the help of such experiments a more detailed analysis using a principle component analysis is possible, which shall reveal the dynamics of the compression and expansion of a single DNA molecule. Other biopolymers under current research are actin strands and amyloid-β fibrils whose nucleation as well as fibrillation dynamics are under investigation.
The project is funded within the CRC TRR 102 "Polymers under Multiple Constraints".

[1] A. Cohen, W. Moerner: PNAS **86**, 093109 (2005), doi:10.1063/1.1872220
[2] M. Braun, F. Cichos: ACS Nano **7**, 11200 (2013), doi:10.1021/nn404980k
[3] M. Braun et al.: PCCP **16**, 15207 (2014), doi:10.1039/C4CP01560F
[4] M. Braun et al.: Nano Lett. **15**, 5499 (2015), doi:10.1021/acs.nanolett.5b01999

2.3 Optically driven thermoviscous flows

M. Fränzl, F. Cichos

We investigated optically generated circular fluid flows in thin films. A circular rapidly moving hot spot is generated by heating a 50 nm gold film with a 532 nm laser using an acousto-optic deflector (Figure 2.2A). 250 nm gold nanoparticles are used as tracer particles to probe the flow in the sample. A circular flow opposite to the laser movement is observed at high rotation frequencies (Figure 2.2B). The resulting flow velocities are in the range of micrometers per second, well below the speed of the heating laser. The opposite flow is, in fact, resulting from the temperature-dependent density as well as the temperature-dependent viscosity of the fluid.
To sketch the basic physical principles let us consider a moving warm spot in a fluid that moves to the left (Figure 2.2C). At its front the fluid is heated. At its back it cools down. The heating is causing a thermal expansion and thus a diverging flow in the front of the spot. In the back the fluid contracts upon cooling. Since the viscosity of the

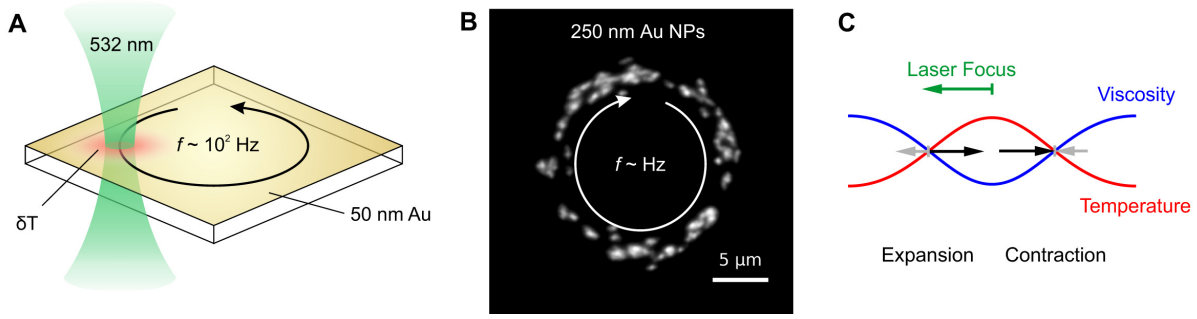

Figure 2.2: A) Sketch of the experimental design. The fluid is contained between two glass cover slides with a gap of about 2.5 μm (top cover slide not shown). The bottom glass cover silde is coated with about 50 nm gold film and heated using a focused 532 nm laser from below. 250 nm gold nanoparticles are used as tracer particles. **B**) Darkfield image from gold nanparticle tracers moving in the generated flow field. **C**) Basic physical principle of thermoviscous flows.

fluid drops with temperature, the expansion and contraction takes place in a gradient of viscosity, leading to a net fluid flow to the right.
A theoretical treatment [1] shows that the flow velocity depends linearly on the rotation frequency of the laser and quadratically on the excess temperature in agreement with our experiments. However, our observations suggest an additional attractive contribution due to thermo-osmotic flows [2] or thermoelectric effects [3] which we are currently investigating.
The project is funded within the DFG-ANR project "Thermoelectric Effects at the Nanoscale".

[1] F.M. Weinert, D. Braun: J. Appl. Phys. **104**, 104701 (2008), doi:10.1063/1.3026526
[2] A.P. Bregulla et al.: PRL **16**, 188303 (2016), doi:10.1103/PhysRevLett.116.188303
[3] A. Majee, A. Würger: PRL **108**, 118301 (2012), doi:10.1103/PhysRevLett.108.118301

2.4 Active systems learning at the microscale

S. Muiños-Landin, F. Cichos, K. Ghazi-Zahedi*

*Max Planck Institute for Mathematics in the Sciences, Leipzig

Living organisms are able to sense and process information about the environment they live in. They are also able to update this information in order to construct solutions for real life problems such as finding food or avoiding danger. This active adaption process, that in the long run drives the evolution of species, is the result of a short time scale evolution of the knowledge of an organism that we know as learning. At the microscale the learning is hampered by stochasticity given that the intrinsic Brownian noise makes it difficult to build a feedback between stimulus and action. In this project, we investigate a system based on a self-themophoretic microswimmer that allows the application of artificial intelligence algorithms at the microscale. Our swimmer consists of a 2 μm polymer sphere homogeneously covered with gold nanoparticles. The particle suspended in water can be controlled using self-thermophoresis by illuminating it

asymmetrically with a focused laser beam. This way we increase the level of control compared with other swimmers. Using reinforcement learning we show that even under noisy conditions a system is able to learn how to optimize a simple navigation task. We study the influence of noise and the situation where multiple agents can share information to carry out specific tasks. For that we explore different learning processes at different velocities which, by the definition of the Peclet number, implies the variation in the relationship between directed and diffusive motion. As a consequence the process becomes more or less deterministic. This way we show how adaptation and intelligent collective behavior can be studied in artificial microswimmers systems and what the role of Brownian noise in these processes is.

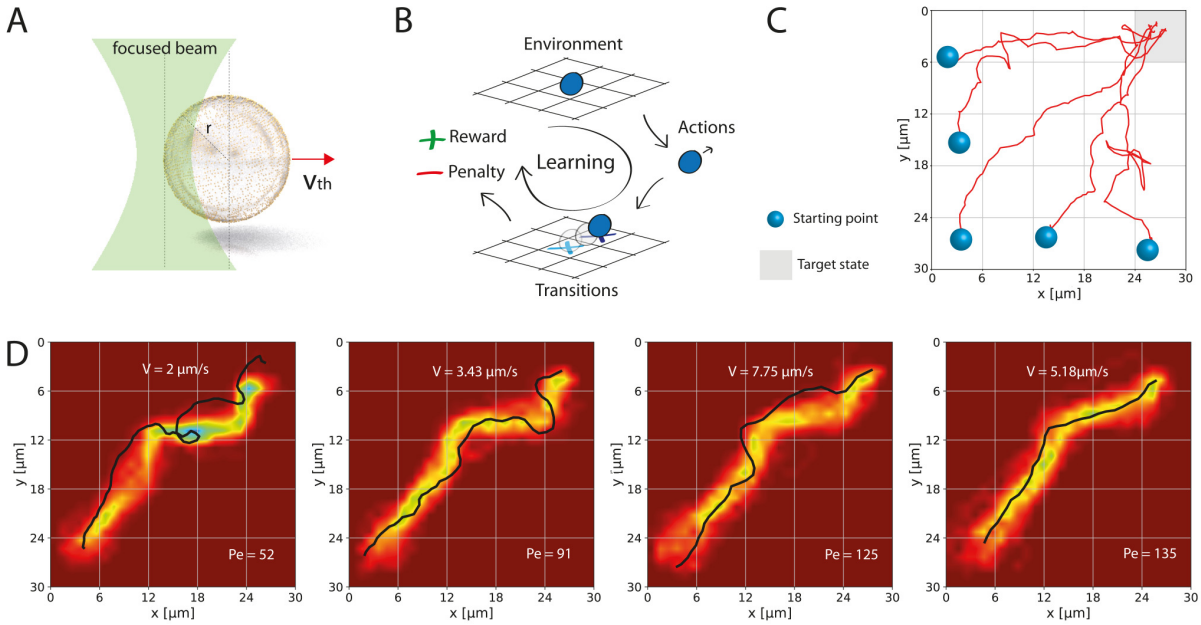

Figure 2.3: Active system learning. **A**) Illuminating a symmetric microswimmer asymmetrically, a temperature gradient can be created on its surface and changing the laser position, the propulsion direction can be changed. **B**) Reinforcement learning idea applied in our microswimmer context. The swimmer explores its environment by executing different actions that produce transitions between a set of states. The transitions are evaluated through the definition of a reward or a penalty and during the exploration the information is propagated and correlated by the system. **C**) Trajectories of the swimmer after learning. After the system has explored the environment enough in order to correlate its information on the question which is the best action to execute in each state, the system is able to navigate towards a target state independent of the starting point of the swimmer. **D**) The density map of the trajectories after learning and changing the Peclet number of the process shows how the determinism of the process is affected by the velocity of the swimmer. This also has an impact in the learning process.

2.5 Multiagent active systems behavior

S. Muiños-Landin, F. Cichos

Different species are able to find or optimize solutions to real life problems through interactions with the environment. However, when other individuals are present in this

environment, the interactions between them increase the capability of solving problems showing what we know as collective behavior. Examples of this can be found in nature at different scales, from bacteria to schools of fish or flocks of birds. In this project we investigate an artificial system based on self-thermophoretic microswimmers. The symmetric geometry of our swimmer makes a high level of control in real time of each individual in a group possible. We create artificial interactions by a feedback rule coupling the actions of one swimmer to the other swimmers positions and combine these interactions in a distributed algorithm based on swarm intelligence. In this context a collective of individuals tries to complete a task (usually an optimization problem). Each element of the collective is finding a potential solution for the given problem and all the information collected by each individual is available for any member of the group. This reduces a more complex multi-agent problem to a problem where a swarm of agents acts as a single entity. This might improve the performance of a collective in applications like surrounding, trapping and transport of microscopic objects. With this the application of machine learning techniques is also extensible to the self-adaptive behavior of a collective of self-propelled particles.

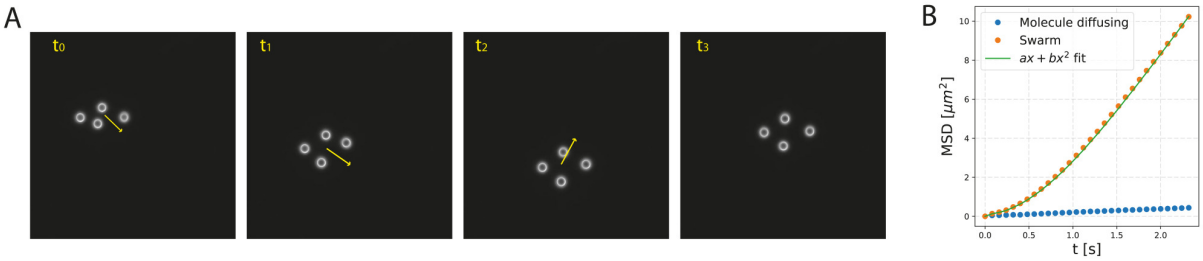

Figure 2.4: Multiparticle active system. **A**) Active structure of four microswimmers self-assembled via artificial interactions. The swimmer structure becomes active once the components of the swarm exchange information with each other via swarm intelligence behaving as a pure social active system and navigating as a flock. **B**) Mean square displacement of the passive multiparticle system (blue) and the system where the particles exchange information to navigate (orange).

2.6 Hot Brownian motion on short time scales

A. Fischer, F. Cichos, K. Kroy*

*Universität Leipzig, Institute for Theoretical Physics

We have recently in collaboration with the group of Prof. Kroy from the theory department shown that the Brownian motion of heated spherical nanoparticles can be described by new effective parameters for the temperature and the viscosity of the surrounding medium. One of the interesting effects is that the effective temperature is now coupled to the hydrodynamic flow field created by the motion of the nanoparticle thereby dissipating its kinetic energy. Thus, different degrees of freedom such as the rotational and translational motion possess in this thermal non-equilibrium different effective temperatures.

To measure this effective temperature we use an optical tweezers setup. Particles which can be heated by a solid-state laser at 532 nm are trapped by an infrared laser (1064 nm). The laser heating is supplied in counter-propagating beams to prevent a displacement of the particle due to radiation pressure. The fluctuations of the particle are imaged onto a knife-edge prism and recorded by a balanced photodiode and a fast analog-to-digital converter. With the help of this setup we were able to measure the mean squared displacement and velocity autocorrelation function on a time scale down to nanoseconds and with a spatial resolution in the angstrom regime. By determining the ratio of the mean squared displacement of an unheated and a heated particle we found the first evidence that the hot Brownian motion influences the characteristic time-constants τ_p and τ_f (depicted in Figure 2.5).

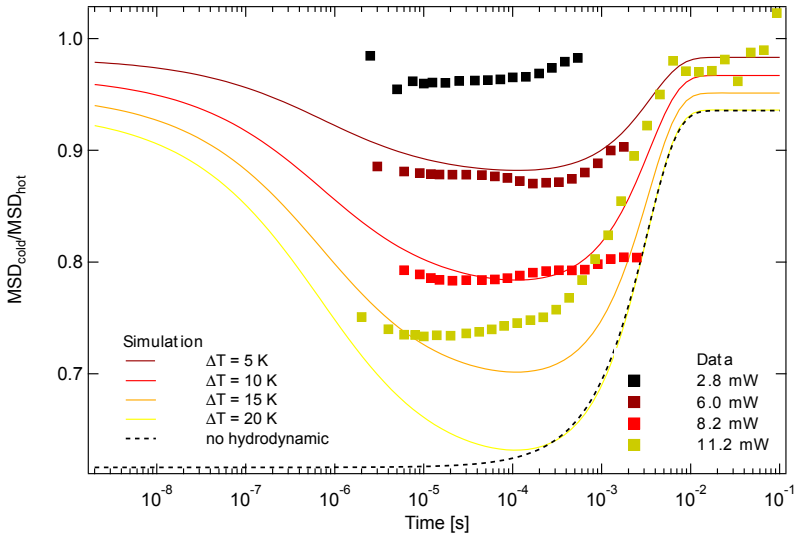

Figure 2.5: Ratio MSD_{cold}/MSD_{hot} for different heating powers. The lines correspond to the calculations done for a heated particle. A gold-coated polystyrene particle was heated with different heating powers. The calculated MSD ratio is represented by the squares. Note that the simulated ratio of the MSD is just a visual guide for the rough trend of the function for different temperature increases.

2.7 Feedback-controlled active particle assemblies

A. Fischer, F. Cichos, G. Volpe*

*University of Gothenburg, Sweden

Active particles are simple microscopic model systems for living objects such as birds, fish or people and mimic in particular the propulsion of bacteria or cells without the complexity of physical properties and chemical networks in living objects. With their bare function of self-propulsion they are, however, missing an important ingredient of life, which is sensing and feedback, that all living objects from cells up to whole organisms have in common. All of their living relatives have signaling inputs which they use to gain information on the environment. Using this external information, birds or fish can self-organize into flocks or schools and, on a microscopic level, cells

may regulate gene expression. The structure formation, though, depends on the active motion of the animal and its ability to steer based on its perception of the environment. While active particles do not have such sensory inputs and feedback mechanisms built in yet, suitable control mechanisms may introduce this complexity fostering the exploration of new emergent phenomena.
We recently developed such control mechanisms for a particular new type of active particles. These active particles comprise a melamine resine particle of about one micrometer in diameter. The surface of this particle is homogeneously covered by gold nanoparticles of about 10 nm diameter at a surface coverage of 30 percent. These gold nanoparticles can be heated optically by a focused laser. If this heating is asymmetric with respect to the particle center, thermo-osmotic surface flows develop and result in a self-propulsion of the particle. By controlling the heating laser position on the circumference of the particle a precise steering is achieved and by modulating the heating power different activities can be achieved.
The project considers the self-organization of such active particles by means of feedback control. In various steps we explore the importance of signaling between the environment and between the particles and its effect on a collective behavior. The experiments shall, for example, evaluate the importance of a feedback delay as a single control parameter for an aggregation or segregation of particles, i.e., the occurrence of positive and negative tactic behavior as observed for bacteria. The simulated behavior of an active swimmer in an external field including a delay is shown in Figure 2.6.

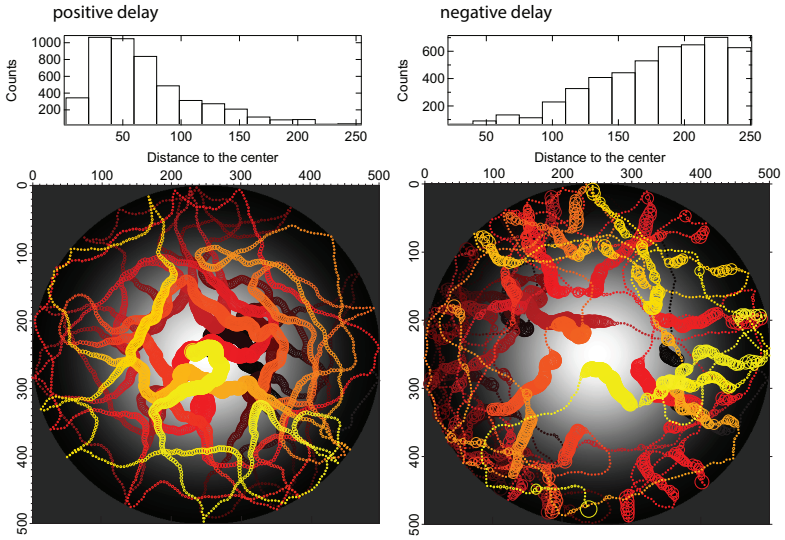

Figure 2.6: Simulated path of an active swimmer in an external field adjusting its speed to the measured intensity. On the left side a positive delay is used which leads to an aggregation. On the right side a negative delay is used which leads to a separation. The aggregation and separation is revealed in the histograms displaying the distance to the position with highest intensity.

2.8 Active Brownian particles in activity gradients

N. Söker, F. Cichos

Spatial variations in the swimming velocity of active Brownian particles lead in general to agglomeration in regions with lower velocity, i.e. activity. For swimmers without any interactions or translational diffusion the time-averaged spatial probability density is merely proportional to the inverse of their swimming speed. By adding walls or immobile objects to the scenario, active particles agglomerate around them as they slide along the objects' surface. If now particles at a surface are sampled, their orientation will point towards this surface. By adding another diffusive process this otherwise delta-like layer of directed orientation is smeared out. Now, a boundary connecting two regions with differing activities can be seen as an equivalent: the boundary of regions with differing activity is an oriented layer, smeared out into both regions by adding translational diffusion.
In this project, these population and orientation effects are studied threefold: in an experiment by artificial microswimmers, by single-particle overdamped Brownian dynamics simulations and by a Fokker–Planck formalism. It is shown that putative polarization of active Brownian particles can merely be caused by spatial variations in activity, or other intrinsic parameters of activity, e.g. correlation times, without introducing an external force. Further, the particle density was found to scale with the square root of the effective diffusion constant for the long-time behavior of the active particle. Another important observation is that introducing a delay in the active particles' response can have moderate influence on the emerging scenario. Figure 2.7 shows an example trajectory of a microswimmer in a stepwise activity field and the time-averaged orientation plotted for a passive region sandwiched between two active regions.

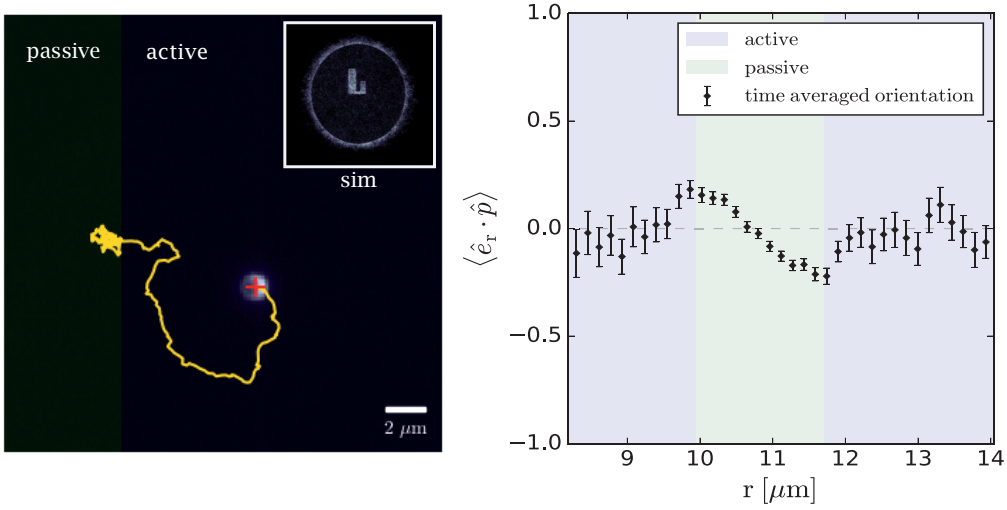

Figure 2.7: The left image shows an example trajectory of a microswimmer in a stepwise activity field. The inset shows the particle density for a simulated active particle exploring a confined region with an L-shaped passive region. The right plot shows experimental data for the mean orientation emerging for a passive stripe sandwiched between active regions.

2.9 Funding

DFG-ANR: Thermoelectric Effects at the Nanoscale
F. Cichos in collaboration with A. Würger (University of Bordeaux, France)
DFG, CI 33/14-1

DFG SPP 1726, TP Propulsion and Interaction of Hot Brownian Swimmers
F. Cichos in collaboration with K. Kroy
DFG, CI 33/16-1

CRC/TRR 102, TP B10: Interaction of Single Polymer Chains in a Thermophoretic Trap
F. Cichos
DFG CRC/TRR 102

Leipzig School of Natural Sciences – Building with Molecules and Nano-objects (BuildMoNa)
F. Cichos (Principal Investigator)
founded as DFG GSC 185

2.10 Organizational Duties

Frank Cichos

- Director of the Peter Debye Institute for Soft Matter Physics
- Vice Speaker of the Collaborative Research Center Transregio 102 "Polymers under Multiple Constraints"
- Member of the Scientific Advisory Board of the Kurt Schwabe Institute of Instrumentation and Sensor Engineering Meinsberg
- Member of the Steering Committee of the Graduate School BuildMoNa
- Vice Head of the Board of the Faculty for Quality Management
- Member of the Examination Board (Physics/Meteorology)
- Referee: Phys. Rev. B, Phys. Rev. Lett., Nature, Nature Photonics, Chem. Phys. Lett., Appl. Phys. Lett., ACS Petroleum Research Fund, Medical Research Council

2.11 External Cooperations

Academic

- MPI for Intelligent Systems, Stuttgart
  Prof. Peer Fischer, PhD
- Princeton University, USA
  Prof. Haw Yang, PhD
- TU Berlin
  Prof. Dr. Regine von Klitzing
- TU Chemnitz
  Prof. Dr. Christian von Borczyskowski

- TU Dresden
  Prof. Dr. Michael Mertig
- Universität Konstanz
  Prof. Dr. Clemens Bechinger
- Universität Mainz
  Prof. Dr. Thomas Basché
- University of Bordeaux, France
  Prof. Dr. Alois Würger
- University of Gothenburg, Sweden
  Prof. Giovanni Volpe, PhD

2.12 Publications

Journals

A. Herms, K. Günther, E. Sperling, A. Heerwig, A. Kick, F. Cichos, M. Mertig: *Concept, synthesis, and structural characterization of DNA origami based self-thermophoretic nanoswimmers*, Phys. Status Solidi A **214**, 1600957 (2017)

A. Heber, M. Selmke, F. Cichos: *Thermal diffusivities studied by single-particle photothermal deflection*, ACS Photonics **4**, 681–687 (2017)

F. Cichos, T. Thalheim, M. Mertig, K. Günther: *Manipulating single and multiple biomolecules with dynamic temperature fields*, Optical Trapping Applications, OtM3E.1 (2017)

F. Schmidt, A. Magazzu, A. Callegari, L. Biancofiore, F. Cichos, G. Volpe: *Microscopic engine powered by critical demixing*, Optical Trapping Applications, OtM3E.2 (2017)

Talks

S. Muiños-Landin, K. Ghazi-Zahedi, F. Cichos: *Reinforcement learning of artificial microswimmers*, DPG Spring Meeting, Dresden, 19–24 March 2017

F. Cichos: *Manipulating single and multiple biomolecules with dynamic temperature fields*, Optical Trapping Applications, San Diego, USA, 02–05 April 2017, invited

F. Cichos: *Single molecules in dynamic temperature fields*, Future Trends in DNA-based Nanotechnology, Dresden, 29 May – 2 June 2017, invited

F. Cichos: *Motion of particles and molecules in feedback controlled dynamic temperature fields*, Seminar Talk at ICFO – The Institute of Photonic Sciences, Barcelona, Spain, 12 June 2017, invited

M. Fränzl, F. Cichos: *Transport of charged colloids driven by thermoelectricity*, Soft Matter Day, Leipzig, 23 June 2017

R. Schachoff, K. Günther, M. Mertig, F. Cichos: *Hot nanoswimmers*, Soft Matter Day, Leipzig, 23 June 2017

M. Fränzl, F. Cichos: *Thermoelectric charging of a hot spot in electrolyte solution*, Gordon Research Conference Plasmonically-Powered Processes, Hong Kong, China, 25–30 June 2017

T. Thalheim, M. Braun, F. Cichos: *Thermophoretic trapping of single nano-objects*, Doctoral Students Seminar CRC/TRR 102, Leipzig, 30 June 2017

S. Muiños-Landin, K. Ghazi-Zahedi, F. Cichos: *Reinforcement learning of artificial microswimmers*, Workshop New Directions in Biocomputation, Dresden, 12–13 September 2017

F. Cichos: *Hot microswimmers*, Microswimmers – From Single Particle Motion to Collective Behavior, Cargèse, France, 18–22 September 2017, invited

Posters

A. Abend, R. Schachoff, F. Cichos: *Photothermal detection of single gold nanoparticles in living fibroblasts*, DPG Spring Meeting, Dresden, 19–24 March 2017

A. Fischer, F. Cichos: *Hot Brownian motion on short time scales*, DPG Spring Meeting, Dresden, 19–24 March 2017

M. Fränzl, F. Cichos: *Thermoelectric charging of a hot spot in electrolyte solution*, DPG Spring Meeting, Dresden, 19–24 March 2017

A. Heber, F. Cichos: *Thermal diffusivity measurements with single particle photothermal microscopy*, DPG Spring Meeting, Dresden, 19–24 March 2017

R. Rose, A. Heber, F. Cichos: *Detection of pressure and density waves by gold nano particle near phase transition temperature in liquid crystal*, DPG Spring Meeting, Dresden, 19–24 March 2017

R. Schachoff, K. Günther, M. Mertig, F. Cichos: *Hot nanoswimmers*, DPG Spring Meeting, Dresden, 19–24 March 2017

T. Thalheim, M. Braun, A. Bregulla, F. Cichos: *Thermophoretic trapping of single molecules*, DPG Spring Meeting, Dresden, 19–24 March

T. Thalheim, M. Braun, F. Cichos: *Feedback-assisted thermophoretic trapping of single molecules*, 4th Miniworkshop CRC/TRR 102, Leipzig, 12 May 2017

A. Abend, R. Schachoff, F. Cichos: *Photothermal detection of single gold nanoparticles in fibroblasts*, Soft Matter Day, Leipzig, 23 June 2017

A. Fischer, F. Cichos: *Hot Brownian motion on short time scales*, Soft Matter Day, Leipzig, 23 June 2017

A. Hentrich, M. Fränzl, F. Cichos: *Darkfield and phase contrast imaging with LED array illumination*, Soft Matter Day, Leipzig, 23 June 2017

S. Muiños-Landin, K. Ghazi-Zahedi, F. Cichos: *Reinforcement learning of artificial microswimmers*, Soft Matter Day, Leipzig, 23 June 2017

R. Rose, A. Heber, F. Cichos: *Detection of pressure and density waves by gold nano particle near phase transition temperature in liquid crystal*, Soft Matter Day, Leipzig, 23 June 2017

T. Thalheim, M. Braun, A. Bregulla, F. Cichos: *Thermophoretic trapping of single molecules*, Soft Matter Day, Leipzig, 23 June 2017

M. Fränzl, F. Cichos: *Thermoelectric charging of a hot spot in electrolyte solution*, Gordon Research Conference Plasmonically-Powered Processes, Hong Kong, China, 25–30 June 2017

U. Khadka, V. Holubec, H. Yang, F. Cichos: *Information controlled structure formation in artificial microswimmer systems*, Workshop New Directions in Biocomputation, Dresden, 12–13 September 2017

T. Thalheim, M. Braun, F. Cichos: *Applying principal-components analysis to single DNA molecules in a thermophoretic trap*, International Discussion Meeting on Polymer Crystallization, Wittenberg, 17–20 September 2017

2.13 Graduations

Doctorate

- André Heber
  Application of single optically heated gold nanoparticles to sensing and actuation
  November 2017

Master

- Alice Abend
  Photothermal detection of single gold nanoparticles in mammalian cells
  September 2017

Bachelor

- Hans Falk
  Thermophoretische und thermoelektrische Effekte in dielektrischen Flussigkeiten an Polystyrol Nanopartikeln
  December 2017
- Andreas Hentrich
  Quantitative Phasenkontrastmikroskopie mithilfe eines LED-Arrays
  December 2017

2.14 Guests

- Prof. Dr. Alois Würger
  University of Bordeaux, France
  06 June – 06 July 2017
- Prof. John Bechhoefer, PhD
  Simon Fraser University, Canada
  18–19 December 2017

3

Molecular Physics

3.1 Introduction

Our research in 2017 was focused essentially on two projects,(i) a “Knowledge-transfer-project (Erkenntnistransfer-Projekt)” together with Prof. Veronika Strehmel, FH Krefeld and Merck KGaA in Darmstadt about “Neue Polymermaterialien auf der Basis von funktionalisierten ionischen Flüssigkeiten für Anwendungen in Membranen” and (ii) a project on “Broadband Dielectric and IR Spectroscopy to study molecular dynamics and order in nanometer domains of end-fixed polymers” within the Collaborative Research Center (CRC) of the universities in Halle and Leipzig, “Polymers under multiple constraints: restricted and controlled molecular order and mobility”. In both an important progress could be achieved as demonstrated in the publications. Additionally a book project was realized about “The scaling of relaxation processes” (Eds.: F. Kremer and A. Loidl), which will appear in the series “Advances in Dielectrics” (Series Editor: F. Kremer). It will appear in summer 2018.

Friedrich Kremer

3.2 Molecular Dynamics and Charge Transport in Highly Conductive Polymeric Ionic Liquids

F. Frenzel, R. Guterman*, A.M. Anton, J. Yuan*, F. Kremer

*Max-Planck Institute for Colloids and Interfaces, Potsdam-Golm

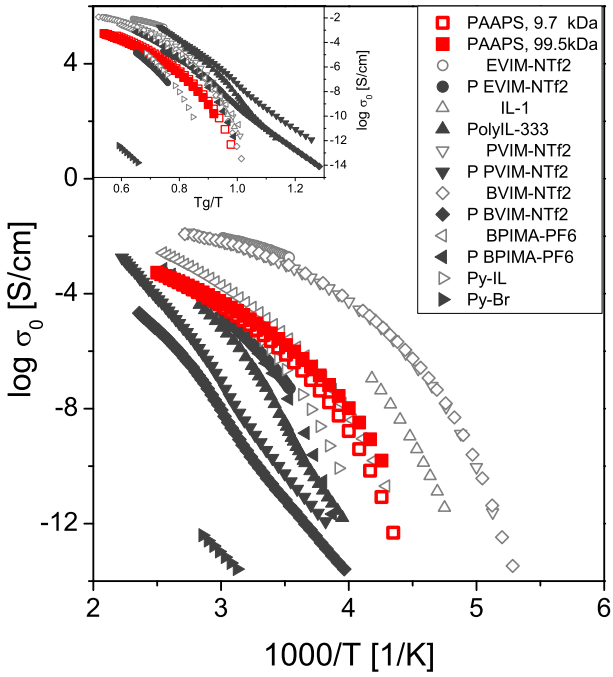

Figure 3.1: Comparative presentation of the DC-conductivity σ_0 vs. inverse temperature for the PILs with the lowest and highest molecular weights discussed in this study (red data points), as well as six other PILs and corresponding ILs analyzed over wide temperature and frequency range taken from the literature. The low molecular weight ILs are pictured as open symbols, the corresponding PILs as filled ones. The inset displays the same data rescaled to the calorimetric glass transition temperature T_g. The logarithm is to base 10; the error bars are smaller than the size of the symbols, unless explicitly specified otherwise.

Glassy dynamics and charge transport are studied for the polymeric ionic liquid (PIL) poly [tris-(2-(2-methoxyethoxy)-ethyl)-ammonium acryloxypropyl sulfonate] (PAAPS) with varying molecular weight (9700, 44200, 51600, and 99500 g/mol) by broadband dielectric spectroscopy (BDS) in a wide frequency (10^2–10^7 Hz) and temperature range (100–400 K) and by DSC- and AC-chip calorimetry. The dielectric spectra are characterized by a superposition of (i) relaxation processes, (ii) charge transport, and (iii) electrode polarization. The relaxation processes (i) are assigned to the dynamic glass transition and a secondary relaxation.[1, 2] Charge transport (ii) can be described by the random free-energy barrier model as worked out by Dyre et al.; the Barton-Namikawa-Nakajima (BNN) relationship is well fulfilled over more than 8 decades. Electrode polarization (iii) follows the characteristics as analyzed by Serghei et al., with deviations on the low frequency side.[2] The proportionality between the relaxation rate

of the dynamic glass transition and the charge carrier hopping rate reflects the nature of charge transport as glass transition assisted hopping. Hereby, the PIL under study exposes the highest DC-conductivity values observed for this class of materials below 100°C, so far; and for the first time a conductivity increase by rising degree of polymerization. The comparison of the polymeric ionic liquids under study with others implies conclusions on the design of novel highly conductive PILs.

[1] F. Frenzel, R. Guterman, A. M. Anton, J. Yuan, and F. Kremer, Macromolecules (2017) 50, 4022-4029
[2] A. M. Anton, F. Frenzel, and F. Kremer, Manuscript in preparation

3.3 Molecular Order in Cold Drawn, Strain-Recrystallized Poly-(Caprolactone)

W. Kossack, A. Seidlitz*,T. Thurn-Albrecht*, F. Kremer

*Institut für Physik, Martin-Luther-Universität Halle-Wittenberg, Halle

A novel experimental set-up is described which enables one to carry out Infrared Transition Moment Orientational Analysis (IR-TMOA) in dependence on temperature.[1] By that the three dimensional molecular order parameter tensors of IR-active transition dipole moments with respect to the sample coordinate system can be determined in its thermal evolution (35° C $< T <$ 59° C). As an example crystallinity and macroscopic order of Poly-ϵ-caprolcatone are monitored. Both remain largely unaltered up to $T \sim 50°$ C, above which they decline. These reductions are explained as the melting of flat on crystalline lamellae, that make up about 34% of the crystalline material.[2] The remaining crystallites are arranged into bulk-like, confined spherulitic structures and do not melt by more than (3±3)%. Therefore, flat on oriented lamellae are supposed to be kinetically favored by confinement during melt crystallization but thermo-dynamically less stable than two-dimensionally confined bulk-like spherulites.[4, 5]

[1] W. Kossack, P. Papadopoulos, P. Heinze, H. Finkelmann, und F. Kremer, Transition Moment Orientation Analysis on a Smectic C Liquid Crystalline Elastomer film, Macromolecules, 43 (18), 7532–7539, (2010).
[2] Kossack, W., Seidlitz, A., Thurn-Albrecht, T., Kremer, F., Macromolecules, 49, 3442–3451 (2016)
[3] Kossack, W., Seidlitz, A., Thurn-Albrecht, T., Kremer, F., Macromolecules, 50, 1056,1065 (2017)
[4] W. Kossack, M. Schulz, T. Thurn-Albrecht, J. Reinmuth, V. Skokow, und F. Kremer, Temperature-dependent IR-transition moment orientational analysis applied to thin supported films of poly-ϵ-caprolactone, Soft Matter, Vol. 13 (48), 9211–9219, (2017)
[5] G. Strobl, The physics of polymers: concepts for understanding their structures and behavior. Berlin: Springer (2010).

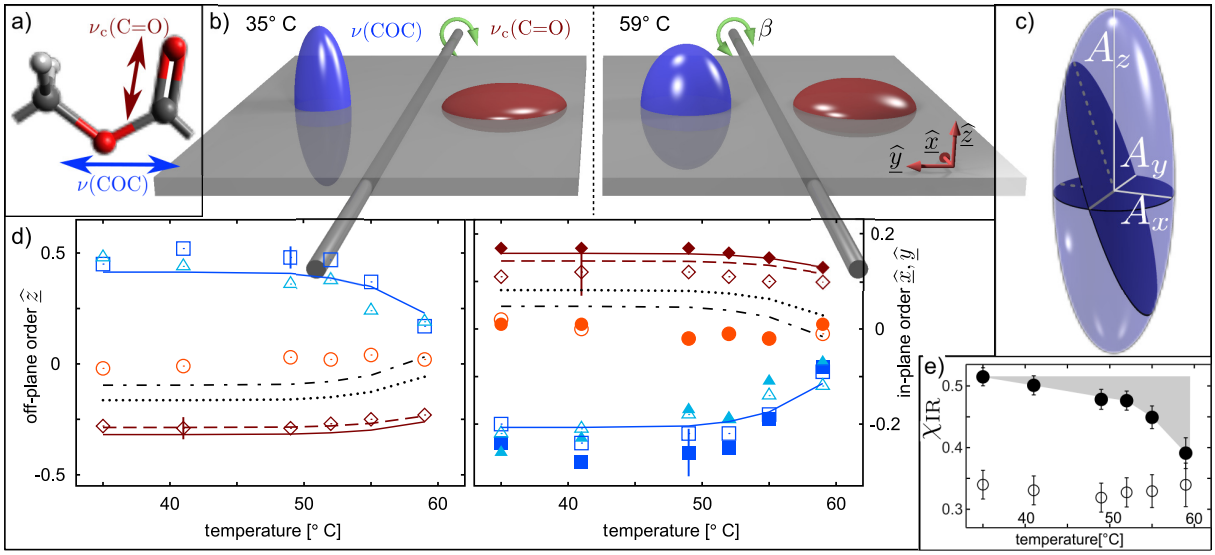

Figure 3.2: Thermal evolution of the molecular order parameter tensor for two representative IR-active Transition Dipole Moments: the extended back-bone-stretching and crystals' carbonyl-stretching (ν(COC), blue) and crystals' carbonyl-stretching (ν_c(C=O) red, a). The ellipsoids of absorption at $T = 35°$ C and 59° C, the sample plane (gray), its coordinate system ($\underline{\hat{x}}$, $\underline{\hat{y}}$, $\underline{\hat{z}}$), and the rotation axis are depicted in b). c) Order parameters are calculated from the principal axes (A_i) of the ellipsoids by $S_i = (3A_i - 1)/(2\sum_j A_j)$. The cross-sections refer to the planes of polarization measured for $\beta = 0°$ and 50°. Panel d) holds the order parameters along $\underline{\hat{z}}$ (left), and $\underline{\hat{x}}$ (right, open symbols), and $\underline{\hat{y}}$ (right, closed symbols) for back-bone segments (blue squares: ν'(COC) and cyan triangles: ν(COC)), crystalline (red diamonds: ν_c(C=O)),[3] and amorphous carbonyl groups (orange circles). Error bars are shown exemplary. The lines represent the results from the model superposition,[2] blue: $\underline{c}$, red: $\underline{b}$, dotted: $\underline{ab}$, and dash-dotted: $\underline{a}$. The red dashed line refers to the order parameter of a TM exhibiting an angle of 15° with $\underline{b}$. Mind the different scale of the $\underline{\hat{x}}$-$\underline{\hat{y}}$ and $\underline{\hat{z}}$ data. Panel e) depicts crystallinity (χ_{IR} filled circles), and the fraction of polymer strands within spherulitic structures (open symbols). The amount of molten material is indicated by the shaded area.

3.4 Inter- and intra-molecular interactions in an extraordinarily conductive Polymeric Ionic Liquid

A.M. Anton, F. Frenzel, F. Kremer

Polymeric Ionic Liquids (PILs) combine the advantages of neat ionic liquids, such as electrochemical and thermal stability or high ion conductivity, with the benefits of polymers like well-controllable processing and structure formation conditions. Because of these advantages, PILs are of principal importance for applications like super-capacitors or battery media. Recently, it has been reported from a novel PIL which exhibits the highest dc-conductivity at temperatures below 100° C, and contrary to the common dogma an intensified charge transport with rising degree of polymerization.[1] In order to shed light on the origin of the material's extraordinary performance, we examined temperature-dependent FTIR spectroscopy in combination with broadband dielectric spectroscopy.[2] On the one hand the pure cation exhibits a lower glass transition temperature than the polymeric system (170 vs. 220 K) and lower dc-conductivity (2×10^{-9}

vs. 2×10^{-7} S/cm at T_g + 50 K). On the other hand an extensive H-bond network is established, which is characterized through a distinct hysteresis during the cooling-heating cycles demonstrating the stabilization of the structure through intermolecular interactions. Thus, the interplay between polymer and cations leads to a higher dc-conductivity than that of every single part of the system (fig. 3.3).[2]

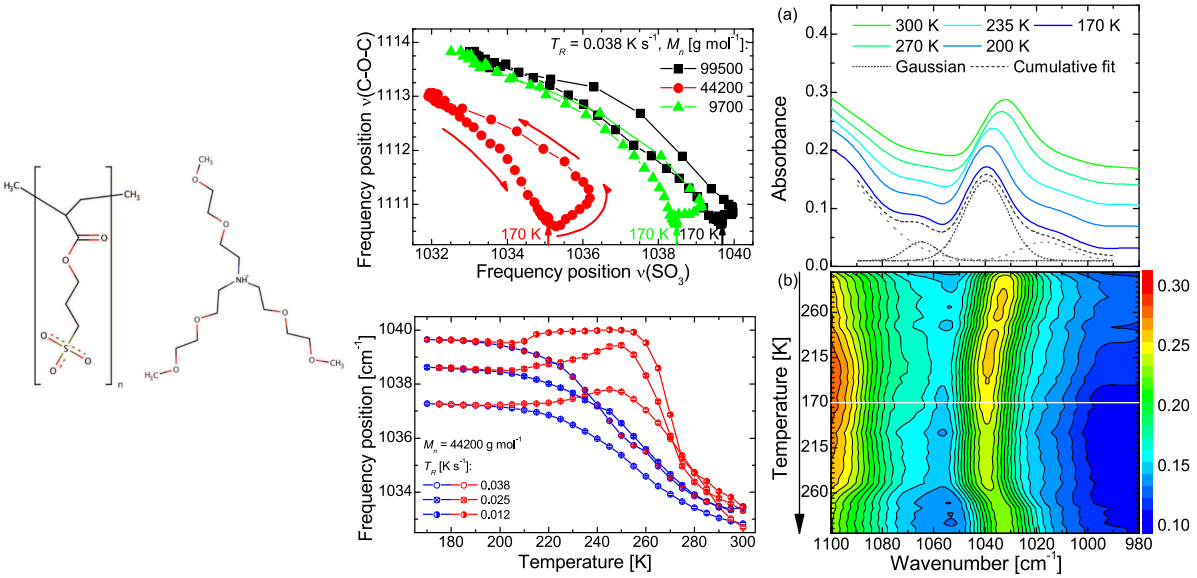

Figure 3.3: Left: Chemical structure of PAAPS. The isolated peak of the symmetric SO_3 stretching vibration at the outermost end of the PIL side chain. Bottom: With decreasing and subsequent increasing temperature the peak is shifted to higher and lower frequencies, respectively. A hysteresis in the frequency shift is evident during the temperature course. Bottom: Correlating the frequency shift of the symmetric SO_3 stretching vibration located at the outermost position in the polymer side chain with the shift of the antisymmetric stretching vibration of the C-O-C moiety in the counter ion (temperature as parameter, minimum 170 K) reveals the recovery of the C-O-C vibration (blue shift after initial red shift), whereas the SO_3 moiety is further blue shifted.

[1] F. Frenzel, R. Guterman, A. M. Anton, J. Yuan, and F. Kremer, Macromolecules (2017) 50, 4022-4029
[2] A. M. Anton, F. Frenzel, F. Kremer, Manuscript in preparation

3.5 Foundation of the outstanding toughness in biomimetic and natural spider silk

A.M. Anton, A. Heidebrecht*, N. Mahmood†, M. Beiner*, T.R. Scheibel†, F. Kremer

*Universität Bayreuth
†Martin-Luther-Universität Halle-Witteneberg

Spider dragline silk is distinguished through the highest toughness of all natural as well as artificial fiber materials. In order to unravel the toughness's molecular foundation

and to enable manufacturing biomimetic analogues, we investigated the morphological and functional structure of recombinant fibers with a similar toughness as the natural template; on the molecular scale by means of vibrational spectroscopy and on the meso-scale by X-ray scattering. In the case of natural spider silk its mechanical properties are based on a refined architecture of proteins with highly repetitive core motifs that aggregate into nanometer-sized crystals rich in alanine A_n in β-sheet secondary structure and surrounded by an amorphous glycine-rich matrix. During spinning the amorphous parts are elongated which orients both substructures and gives rise to an inherent non-equilibrium state. Thus, external stress is directly transferred to the nanocrystals, while the tendency to contract is counterbalanced by surrounding fiber structure.

In the case of the biomimetic silk we identified similar protein secondary structures as in natural silk, but less alignment as a consequence of subsequent wet spinning and straining. Furthermore, the proteins formed nanometer-sized crystallites. In addition, a spectral red shift of a crystal-specific IR absorption band demonstrated that macroscopically applied stress is directly transferred to the molecular scale, where it is finally dissipated. Concerning this feature, both the natural as well as the biomimetic fibers are almost indistinguishable, giving rise to the toughness of both fiber materials (fig. 3.4).[1]

[1] A. M. Anton, A. Heidebrecht, N. Mahmood, M. Beiner, T. R. Scheibel, and F. Kremer, Biomacromolecules (2017) 18, 3954-3962

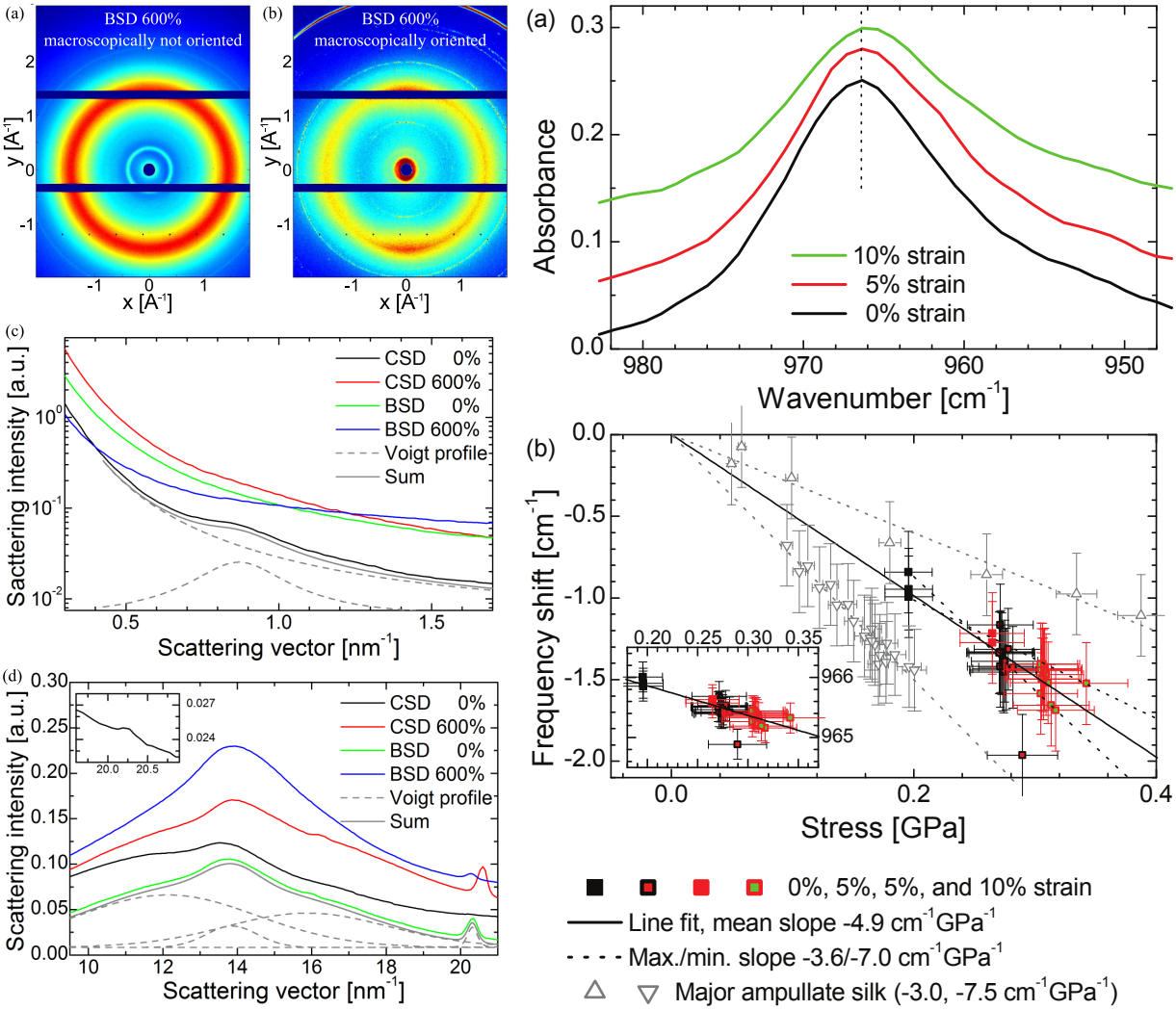

Figure 3.4: Left: X-ray scattering pattern of the recombinant fibers, (a) macroscopically not-oriented and (b) oriented (horizontally aligned). (c,d) Shoulders in the azimuthally integrated scattering patterns at (0.92 ± 0.05) and (11.86 ± 0.11) nm^{-1} arise from the long period and (200) reflections, respectively. The peaks at (13.92 ± 0.07) and (20.37 ± 0.15) nm^{-1} represent the (120) and (002) reflections.
Right: Microscopic response of the recombinant sample to macroscopic load. (a) The spectral position of the peak is shifted to lower wavenumbers as a consequence of the applied force (and hence stress). (b) Similar to natural spider the frequency shift is linear with the applied stress (inset) with a slope of -4.9 cm^{-1} GPa^{-1} being in full agreement with the literature. Because the A_n vibration is exclusively located within in the crystallites, it is demonstrated that the macroscopic load is transferred down the molecular scale, where it affects the crystalline parts of the peptide chains, even though the nanocrystals are embedded in an amorphous matrix.

3.6 Funding

SFB/TRR 102 "Polymers under multiple constraints: restricted and controlled molecular order and mobility", TP B05 "Structural levels of organisation in spider-silk - a combined mechanical and IR-spectroscopic study" (2011–2015), TP B08 "Broadband

Dielectric Spectroscopy to study the molecular dynamics in nanometer thin layers of block copolymers" (2011–2019)

New Polymer Materials on the Basis of Functionalized Ionic Liquids for Application in Membranes "Knowledge Transfer Project"
Prof. Dr. F. Kremer, Prof. Dr. Veronika Strehmel (Hochschule Niederrhein), KR 1138/24-1; STR 437/5-3; (2014–2017)

Establishment of spectroscopic techniques for operational in ovo-gender determination in domestic chicken (Gallus gallus f. dom.)
Prof. Dr. Frierich Kremer, Prof. Dr. Maria-Elisabeth Krautwald-Junghanns (Veterinärmedizinische Fakultät), GZ: 2813IP003 (2015–2017)

3.7 Organizational Duties

Friedrich Kremer

- Principal Investigator in the "Leipzig School of Natural Sciences - Building with Molecules and Nano-Objects" in the framework of a Graduate School funded by the "Ferderal Excellence Initiative". This supports several Ph.D. projects.

3.8 External Cooperations

Academic

- Technische Universität München
  Prof. Dr. C.M. Papadakis, J. Zhang
- Leibniz-Institut für Polymerforschung Dresden
  Dr. P. Uhlmann, R. Winkler
- Martin-Luther-Universität Halle-Wittenberg
  Prof. Dr. T. Thurn-Albrecht, A. Seidlitz
- Fraunhofer Institut für Mikrostrukturvon Werkstoffen und Mechanik IWMS, Halle/Saale
  PD Dr. M. Beiner, Dr. N. Mahmood
- Department of Chemical and Biomolecular Engineering, University of Tennessee, Knoxville
  Prof. Dr. J.R. Sangoro
- Department of Chemical and Biomolecular Engineering, University of Tennessee, Knoxville
  Dr. Martin Treß
- Hochschule Niederrhein, Institute of Organic Chemistry
  Prof. Dr. Strehmel
- Medizinische Fakultät Carl Gustav Carus der Technischen Universität Dresden
  Prof. Dr. Gerald Steiner
- Lehrstuhl für Biomaterialien, Universität Bayreuth
  Prof. Dr. Thomas Scheibel

Industry

- Novocontrol, Hundsangen, Germany
- MERCK KGaA, Darmstadt, Germany
- Lohmann Tierzucht GmbH
- EVONTA-Technology GmbH

3.9 Publications

Journals & Chapters

W.K. Kipnusu, M. Elsayed, R. Krause-Rehberg, F. Kremer: Glassy dynamics of polymethylphenylsiloxane in one-and two-dimensional nanometric confinement-a comparison. J. Chem. Phys. 146, 203302 (2017) DOI: 10.1063/1.4974767

W. Kossack, A. Seidlitz, T. Thurn-Albrecht, F. Kremer: Molecular Order in Cold Drawn, Strain-Recrystallized Poly(ϵ-Caprolactone). Macromolecules 50 (3), 1056 (2017) DOI: 10.1021/acs.macromol.6b02714

F. Frenzel, R. Guterman, M. Anton, J. Yuan, F. Kremer: Molecular Dynamics and Charge Transport in Highly Conductive Polymeric Ionic Liquids. Macromolecules 50 (10), 4022 (2017) DOI: 10.1021/acs.macromol.7b00554

M. Anton, A. Heidebrecht, N. Mahmood, M. Beiner, T. Scheibel, F. Kremer: Foundation of the Outstanding Toughness in Biomimetic and Natural Spider Silk. Biomacromolecules 18 (12), 3954 (2017) DOI: 10.1021/acs.biomac.7b00990

J. Ma, T. Stangner, F. Kremer: Frequency dependence of the electrophoretic mobility for single colloids as measured using optical tweezers. Phys. Rev. Fluids 2, 104306 (2017) DOI: 10.1103/PhysRevFluids.2.104306

W. Kossack, M. Schulz, T. Thurn-Albrecht, J. Reinmuth, V. Skokow, F. Kremer: Temperature-dependent IR-transition moment orientational analysis applied to thin supported films of poly-ϵ-caprolactone. Soft Matter 13, 9211 (2017) DOI: 10.1039/c7sm01988b

3.10 Talks

- F. Kremer: Glassy dynamics in one- and two-dimensional nanometric cofinement: a comparison. DPG-Spring Meeting, Dresden, März 2017 (invited talk)
- F. Kremer: Glassy dynamics in one- and two-dimensional nanometric cofinement: a comparison. Dynamics of Glass-forming Liquids, Valby, Dänemark, April 2017 (invited talk)
- F. Kremer: Molecular dynamics at nanometric length scales. Soft-Matter-Day at the University of Twente, Enschede, Holland, Juni 2017 (invited talk)

- F. Kremer: The extraordinary mechanical properties of spider silk and its molecular foundation. MULTIS Conference, Krakau, Polen, Juli 2017 (invited talk)

- F. Kremer: Molecular dynamics at nanometric length scales. CCP5 Annual General Meeting, University of Strathclyde, Glasgow, England, September 2017 (invited talk)

- F. Kremer: Glassy dynmics a reflected in its inter- and intra-molecular interactions, IDMRCS, Wisla, Polen, Juli 2017

- F. Frenzel: Molecular Dynamics and Charge Transport in Polymeric Ionic Liquids, DPG-Spring Meeting, Dresden, März 2017

- F. Frenzel: Charge transport and glassy dynamics in highly conductive Polymeric Ionic Liquids, SSI Meeting, Padua, Juli 2017

- F. Frenzel: Molecular Dynamics and Charge Transport in highly conductive Polymeric Ionic Liquids, IDMRCS, Wisla, Polen, August 2017

- A. M. Anton and F. Kremer: Soft and tough as well, morphology and fundamental structure of spider silk, DPG-Spring Meeting, Dresden, Deutschland, März 2017

- A. M. Anton and F. Kremer: Foundation of the outstanding toughness in natural and biomimetic spider silk, Soft matter day 2017, Leipzig, Deutschland, Juni 2017

- A. M. Anton and F. Kremer: The orientation of distinct subunits in an n-type copolymer as separately revealed by IR-TMOA, 81 Prague meeting on macromolecules, Prague, Czech Republic, September 2017

- A. M. Anton and F. Kremer: The functional role of nanocrystals in native and artificial spider silk, International discussion meeting on polymer crystallization 2017, Wittenberg, Deutschland, September 2017

- W. Kossack: Interface & confinement induced order and orientation in thin films of Poly-Caprolactone, APS March Meeting, März 2017, New Orleans. USA

- W. Kossack: Order and orientation in cold-drawn Poly-Capro-Lactone, Soft matter day 2017, Leipzig, Deutschland, June 2017

3.11 Posters

- W. Kossack, A. M. Anton, and F. Kremer: Broadband dielectric and IR spectroscopy to study molecular dynamics and order in nanometer domains of endfixed polymers; SFB/TRR Â 102 Minisymposium, Leipzig, Deutschland, Mai 2017

- A. M. Anton and F. Kremer: Spatial orientation and order of structure-defining subunits in thin films of a high electron mobility n-type copolymer, Soft matter day 2017, Leipzig, Deutschland, Juni 2017

- A. M. Anton and F. Kremer: Spatial orientation and order of molecular subunits in films of organic semiconductors. International discussion meeting on polymer crystallization 2017, Wittenberg, Deutschland, September 2017
- W. et. al: Temperature dependent IR-Transition Moment Orientational Analysis applied to thin supported films of Poly-ϵ-Caprolactone, International Discussion Meeting on Polymer Crystallization, September 2017, Wittenberg, Germany

3.12 Guests

- Prof. El-Habib Belarbi
  Université IBN KHALDOUN Tiaret, Algerien
  26.03.2017 bis 02.04.2017
- Dr. Mahdy M. Elmahdy
  University of Mansoura, Ägypten
  15.06.2017 bis 15.08.2017

4

Soft Matter Physics

4.1 Introduction

The Soft Matter Physics group focuses on the material properties of biological cells as key determinants of their character and functions, including tumour progression. This requires an integral approach that spans the length scales from molecules to tissues. It is the goal to develop a fundamental quantitative understanding of how cell jamming holds cells back through the yield stress generated by their micro environment. We will address the essential question in regards to under which tissue conditions of both the surrounding cellular tissue and the extra cellular matrix (ECM) a cancer cell cannot move. The fundamental reductionist approach based on collective material, rather than biochemical properties allows to investigate emergent tumour behaviour that can be universally applied despite its underlying molecular diversity and cellular heterogeneity. Our work incorporates molecular mechanisms into integral, coarse-grained physical variables. Moreover, we use a new class of artificial molecules, which simulate cytoskeletal functions in a bionic fashion, and thereby connect our results to the molecular cell interior.

Josef A. Käs

4.2 What Holds Cancer Cells Back?

J.A. Käs

Since decades the bulk of cancer research focusses on the genetic and molecular level. To complement this knowledge, I will focus on the collective behaviour of cancer cells in cell clusters and in the extracellular matrix (ECM). Conventional cancer research tackles issues like genetic changes, signalling pathways or intracellular mechanisms, I want to answer the question: When is a cancer cell jammed or when can it overcome the yield stress to actively „flow“ in a dense microenvironment (ME)? I have brought forward

the basic idea within the concept of Physics of Cancer that changes in a cancer cell's material properties determine its metastatic potential. As follows I propose the next breakthrough by determining a predictive phase diagram for unjamming transitions of cancer cells.

Cancer cell jamming is quantified by cell speed as a measure of the motile forces and by cellular shape to account for the interplay between cell contractility and adhesion. Our self-propelled Voronoi model (SPV) will explain whether a cell is jammed by its neighbours or the ECM, overcoming the limitations of existing theories which only apply to specific environments.

Building on my leadership in cell biomechanics and the exclusive access to two types of carcinomas (mamma, cervix), I will introduce highly innovative bionic modulators of intracellular mechanics and develop live cancer cell tracking in biopsies as a groundbreaking alternative to vital imaging. While these approaches are perfect to prove that unjamming transitions are key to tumour progression, I will investigate to what extent fluid, i.e. unjammed, tissue behaviour can be detected by magnetic resonance imaging elastography (MRE) as an individual predictive marker for metastasis. Moreover the results may guide surgeons when concerning the local spreading of cancer and thus greatly empower surgery in tumour therapies [1].

[1] J. A. Käs: ERC Advanced Grant in the context of Horizon 2020 (741350)

4.3 Jamming transitions in cancer

L. Oswald, S. Grosser, D. Smith*, J.A. Käs

*Fraunhofer IZI, Leipzig

The traditional picture of tissues, where they are treated as liquids defined by properties such as surface tension or viscosity has been redefined during the last few decades by the more fundamental question: Under which conditions do tissues display liquid-like or solid-like behaviour? As a result, basic concepts arising from the treatment of tissues as solid matter, such as cellular jamming and glassy tissues, have shifted into the current focus of biophysical research. Here, we review recent works examining the phase states of tissue with an emphasis on jamming transitions in cancer. When metastasis occurs, cells gain the ability to leave the primary tumour and infiltrate other parts of the body. Recent studies have shown that a linkage between an unjamming transition and tumour progression indeed exists, which could be of importance when designing surgery and treatment approaches for cancer patients [1].

[1] L. Oswald et al.: J. of Physics D: Appl. Physics **2017** 50:483001
[2] T. E. Angelini et al.: PNAS **2011** 108(12):4714
[3] K. D. Nnetu et al.: New J. Phys. **2015** 14:115012

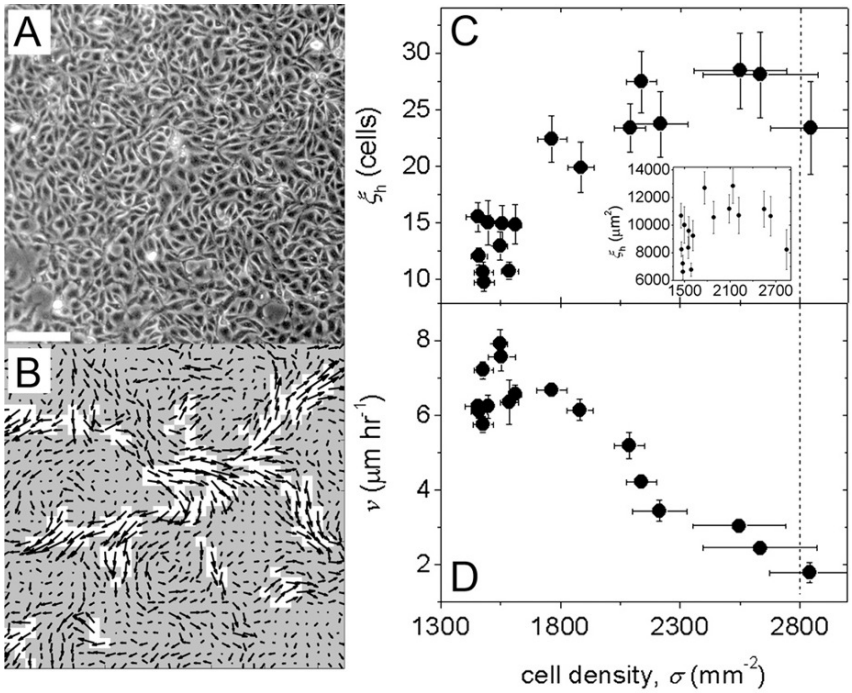

Figure 4.1: With increasing density, traits of collective motility develop. Velocity autocorrelation length increases and mean speed decreases. Reprinted from [2].

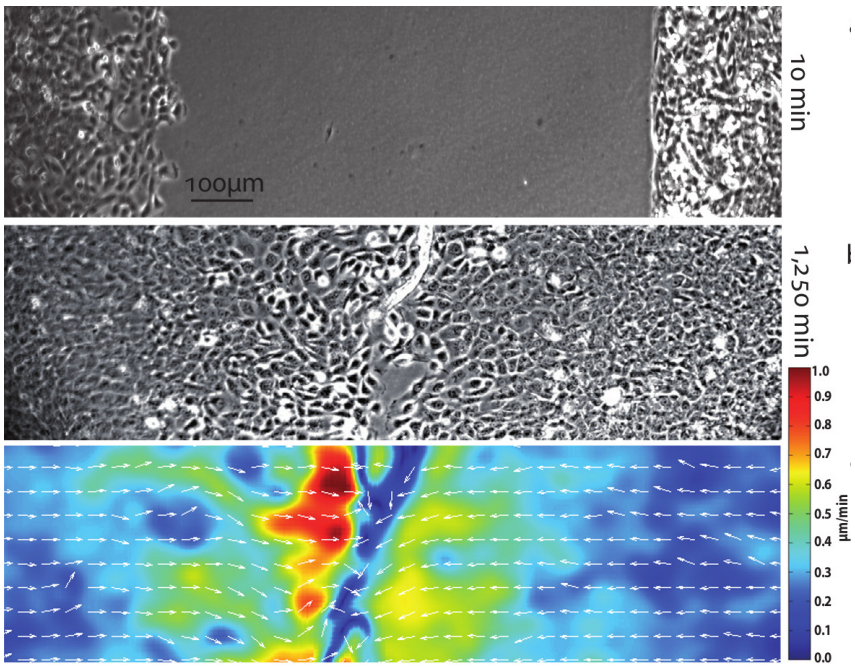

Figure 4.2: When two identical epithelial sheets meet in wound healing, cells from both layers do not intermix but form a jammed border. Reprinted from [3].

4.4 DNA Nanotubes as a Versatile Tool to Study Semiflexible Polymers

J. Schnauß*†, M. Glaser, J. Lorenz†, C. Schuldt, C. Möser†, M. Sajfutinow†, T. Händler, J.A. Käs, D. Smith†

*Peter Debye Institute of Soft Matter Physics, PWM
†Fraunhofer IZI, Leipzig

Mechanical properties of complex, polymer-based soft matter, such as cells or biopolymer networks, can be understood in neither the classical frame of flexible polymers nor of rigid rods. Underlying filaments remain outstretched due to their non-vanishing backbone stiffness, which is quantified via the persistence length (l_p), but they are also subject to strong thermal fluctuations. Their finite bending stiffness leads to unique, non-trivial collective mechanics of bulk networks, enabling the formation of stable scaffolds at low volume fractions while providing large mesh sizes. This underlying principle is prevalent in nature (e.g., in cells or tissues), minimizing the high molecular content and thereby facilitating diffusive or active transport. Due to their biological implications and potential technological applications in biocompatible hydrogels, semiflexible polymers have been subject to considerable study. However, comprehensible investigations remained challenging since they relied on natural polymers, such as actin filaments, which are not freely tunable. Despite these limitations and due to the lack of synthetic, mechanically tunable, and semiflexible polymers, actin filaments were established as the common model system. A major limitation is that the central quantity lp cannot be freely tuned to study its impact on macroscopic bulk structures. This limitation was resolved by employing structurally programmable DNA nanotubes, enabling controlled alteration of the filament stiffness. They are formed through tile-based designs, where a discrete set of partially complementary strands hybridize in a ring structure with a discrete circumference. These rings feature sticky ends, enabling the effective polymerization into filaments several microns in length, and display similar polymerization kinetics as natural biopolymers. Due to their programmable mechanics, these tubes are versatile, novel tools to study the impact of lp on the single-molecule as well as the bulk scale. In contrast to actin filaments, they remain stable over weeks, without notable degeneration, and their handling is comparably straightforward [1].

[1] J. Schnauß et al.: JoVE **2017** 56056
[2] C. Schuldt et al.: Phys. Rev. Lett. **2016** 117:197801

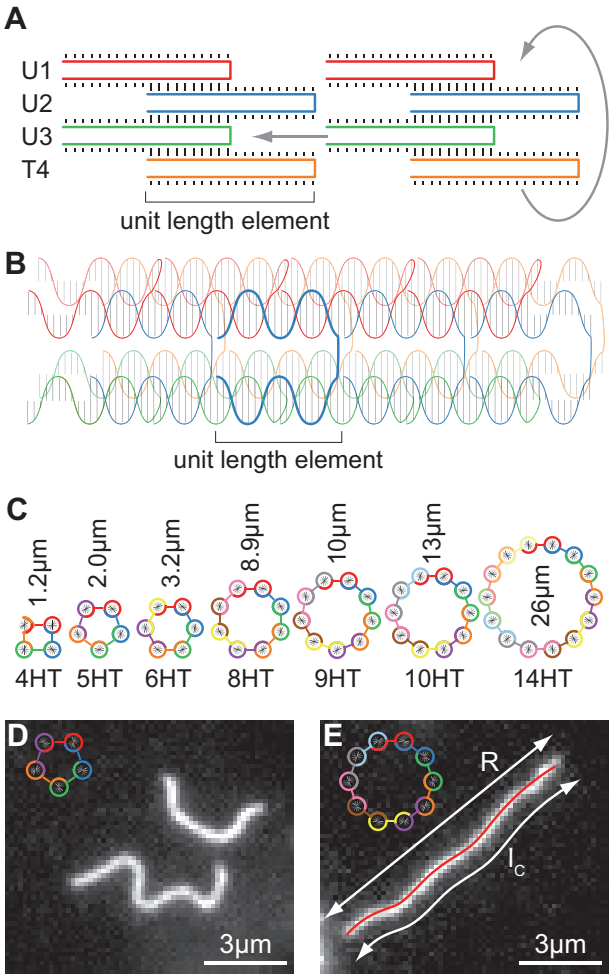

Figure 4.3: Tube assembly and architecture. DNA n-helix tube (nHT) allow to synthetically build semiflexible polymers featuring mechanical properties similar to natural cytoskeletal components such as actin or intermediate filaments. However, in contrast to their natural counterparts, the mechanical properties of the DNA tubes can be readily altered by changing their architectural design allowing to controllably study the impact of different persistence lengths (l_p) to the overall network. (A) Schematic of the assembly on the example of a 4HT formed of four distinct 42-mers. Adjacent single-stranded DNA strands hybridize through at a continuous alternating domains of 10-11 bases indicated by long black ticks. This half staggered motif features sticky ends on both sides along the axis, enabling axial growth indicated by the arrow. The boundary strands U1 and T4 also feature complementary domains and thus form a closed ring as indicated by the right arrow. (B) Quasi-3d-schematic of a 4HT tetramer with two double-helices covered in the shaded distant layer. Double helices form for complementary domains and are linked to both adjacent double helices of the tube once per unit length element. One U2 strand is drawn thicker for clarity. (C) Examples of seven different tube architectures are given with strand numbers ranging from 4HT to 14HT and l_p from 1.2 μm to 26 μm, respectively. (D & E) Epi-fluorescent images of Cy3-labeled, adsorbed 5 HT and 10HT illustrate the different stiffnesses via differently curved contours. The red overlay is the filament contour found via image analysis with end-to-end distance R and contour length l_c. Figure adapted from [2].

4.5 Single Actin Bundle Rheology

D. Strehle, P. Mollenkopf, M. Glaser, T. Golde, C. Schuldt, J.A. Käs, J. Schnauß*†

*Peter Debye Institute of Soft Matter Physics, PWM
†Fraunhofer IZI, Leipzig

Bundled actin structures play an essential role in the mechanical response of the actin cytoskeleton in eukaryotic cells. Although responsible for crucial cellular processes, they are rarely investigated in comparison to single filaments and isotropic networks. Presenting a highly anisotropic structure, the determination of the mechanical properties of individual bundles was previously achieved through passive approaches observing bending deformations induced by thermal fluctuations. We present a new method to determine the bending stiffness of individual bundles, by measuring the decay of an actively induced oscillation. This approach allows us to systematically test anisotropic, bundled structures. Our experiments revealed that thin, depletion force-induced bundles behave as semiflexible polymers and obey the theoretical predictions determined by the wormlike chain model. Thickening an individual bundle by merging it with other bundles enabled us to study effects that are solely based on the number of involved filaments. These thicker bundles showed a frequency-dependent bending stiffness, a behavior that is inconsistent with the predictions of the wormlike chain model. We attribute this effect to internal processes and give a possible explanation with regard to the wormlike bundle theory [1].

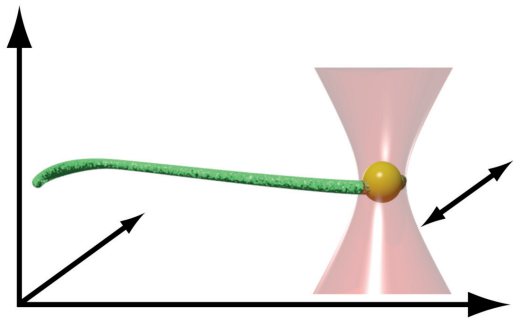

Figure 4.4: A 2-μm polystyrene bead coated with streptavidin is attached to an actin bundle enriched with biotinylated actin monomers. This bead is trapped by optical tweezers, and an oscillatory movement of the trap in the xy-plane induces oscillations in the bundle. The oscillation amplitudes subsequently decay when traveling through the bundle, a process which can be captured by fluorescence microscopy.

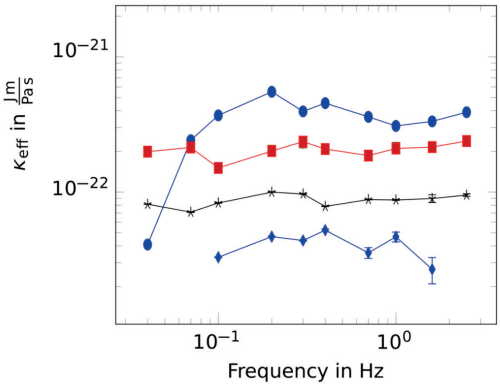

Figure 4.5: From the measured decay of the amplitudes, the hydrodynamic length was extracted. The acquired hydrodynamic length shows a scaling with frequency $l_\omega \propto \omega^{-1/4}$, as predicted by the theory for a wormlike chain translating to a constant bending rigidity.

[1] D. Strehle et al.: Molecules **2017** 22:1804

4.6 Actin and microtubule networks contribute differently to cell response for small and large strains

H. Kubitschke, J. Schnauß[*†], K.D. Nnetu, E. Warmt, R. Stange[‡], J.A. Käs

[*]Peter Debye Institute of Soft Matter Physics, PWM
[†]Fraunhofer IZI, Leipzig
[‡]RS Zelltechnik

Cytoskeletal filaments provide cells with mechanical stability and organization. The main key players are actin filaments and microtubules governing a cell's response to mechanical stimuli. We investigated the specific influences of these crucial components by deforming MCF-7 epithelial cells at small (5% deformation) and large strains (>5% deformation). To understand specific contributions of actin filaments and microtubules, we systematically studied cellular responses after treatment with cytoskeleton influencing drugs. Quantification with the microfluidic optical stretcher allowed capturing the relative deformation and relaxation of cells under different conditions.

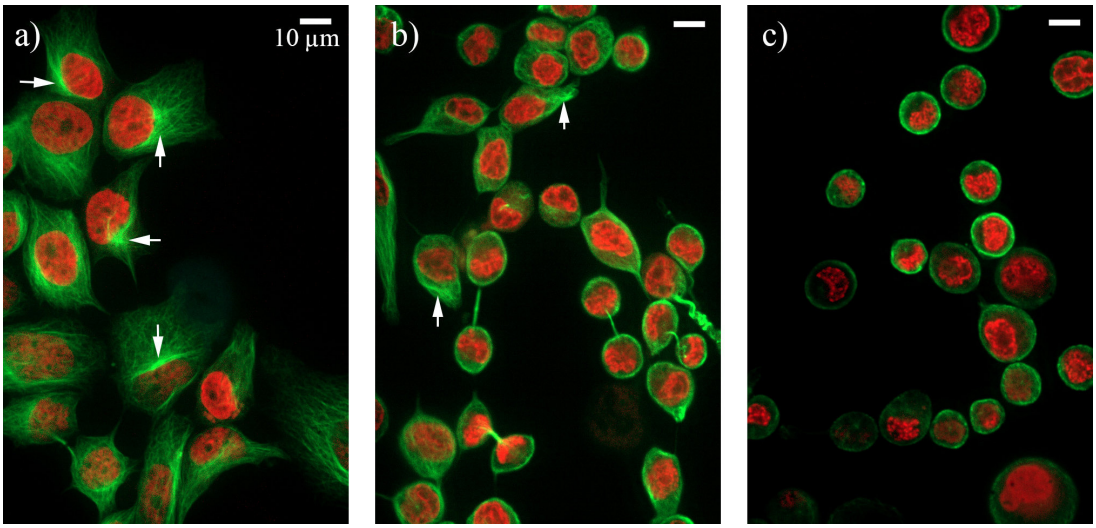

Figure 4.6: Time series of spinning disc microscope images of cells under influence of low concentration of trypsin-EDTA (0.025%). Microtubules stained in green (Tubulin Tracker Green) and nucleus stained in red (SiR-DNA). (a) Before adding trypsin, cells have well-structured microtubule networks with a microtubule organizing centre (MTOC, white arrows). Microtubule density decreases towards the cell membrane. (b) After 10 min of trypsination, the MTOC is barely recognizable and microtubules start to form a cortex-like structure. (c) After complete detachment from the substrate, the MTOC has dissolved and major parts of the microtubules have formed a microtubule cortex.

We separated distinctive deformational and relaxational contributions to cell mechanics for actin and microtubule networks for two orders of magnitude of drug dosages. Disrupting actinfilaments via latrunculin A, for instance, revealed a strain-independent softening. Stabilizing these filaments by treatment with jasplakinolide yielded cell softening for small strains but showed no significant change at large strains. In contrast, cells treated with nocodazole to disrupt microtubules displayed a softening at large

strains but remained unchanged at small strains. Stabilizing microtubules within the cells via paclitaxel revealed no significant changes for deformations at small strains, but concentration-dependent impact at large strains. This suggests that for suspended cells, the actin cortex is probed at small strains, while at larger strains; the whole cell is probed with a significant contribution from the microtubules [1].

[1] H. Kubitschke et al.: New J. Phys., **2017** 19, 093003

4.7 Optical stretching in continuous flows

E. Morawetz, R. Stange[*], T. Kießling, J. Schnauß[†‡], J.A. Käs,

[*]RS Zelltechnik
[†]Peter Debye Institute of Soft Matter Physics, PWM
[‡]Fraunhofer IZI, Leipzig

Rheology of living cells has developed an increasing need for high throughput measurements. Diseases such as cancer heavily remodel the cytoskeleton and impinge on cellular functions. Cells affected by such diseases show altered rheologic responses on many different levels rendering cell's mechanical fingerprints - a potential target for diagnostics. To counteract naturally occurring distributions of properties in samples of living cells and foster the validity of experiments, high numbers of single cell measurements are necessary. Here, we present the „in flow optical stretcher" (IFOS), a concept of non-invasive optical cytometry capable of high throughput rates, while working in a regime of long measurement times and low frequencies. The setup deforms whole cells in a continuous flow by optical forces, bypassing steps of cell positioning that are unavoidable in state-of-the-art optical stretcher devices. A prototype was built using polydimethylsiloxane soft lithography. In a proof of premise experiment, we show that in the IFOS it is possible to deform cells of mammalian origin which have been treated with cytochalasin. All recorded successful experiments took place in less than 2 s each, as opposed to 10-20 s in state-of-the-art optical stretcher devices. Although other microfluidic rheology devices achieve significantly higher throughput rates, they operate in different frequency regimes and probe different mechanical responses. The IFOS still captures viscoelastic properties and active responses of cells while aiming to maximize the throughput at creep times on the order of seconds. It can be assumed that an automatic IFOS reaches a throughput an order of magnitude higher than current devices that are based on optical stretching for cell rheology [1].

[1] E. Morawetz et al.: Converg. Sci. Phys. Oncol., **2017** 3, 024004

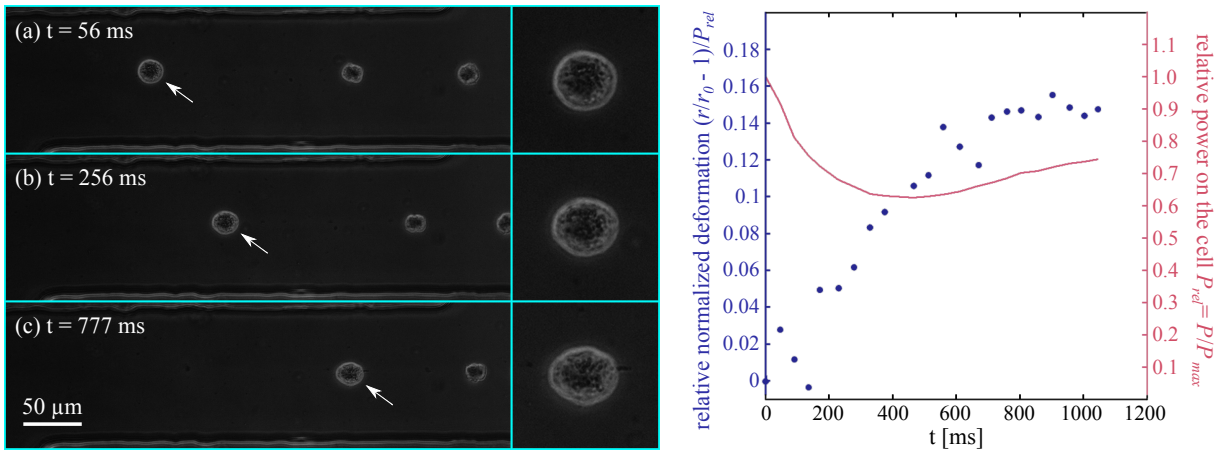

Figure 4.7: The in flow optical stretcher deforms cells while they are constant motion along an optical trap of two divergent Gaussian beams. Pictured is the deformation of a cell in the IFOS represented by three time points of the process as well as the deformation graph. The laser fibers are positioned left and right of the shown region and the beam axes go along the direction of movement of the pictured cell. The lasers are permanently turn on and emit radiation of 1200 mW at 1064 nm each. The cell - indicated by the white arrow - moves from the left to the right and is trapped (a), subsequently starts to deform (b) and eventually reaches the maximum deformation (c). Smaller cells may be stably trapped at the point where flow and radiation forces from the counter propagating laser beam cancel each other out. The moving cell is deformed continuously while flowing along the chamber although it is lined up behind other cells on the beam axis. The graph on the right shows the relative deformation of the moving cell in blue (analyzed with a self written edge detection algorithm). Data is normalized by the power experienced by the cell (red), which depends on the position in the chamber. Time is set to zero at the moment the cell is fully trapped by the dual beam trap and in focus.

4.8 Long-Term Tissue Culture of Adult Brain and Spleen Slices on Nanostructured Scaffolds

S. Kallendrusch*, F. Merz*, I. Bechmann*, S.G. Mayr†‡, M. Zink

*Institute of Anatomy, Leipzig University
†Leibniz Institute for Surface Modification (IOM), Leipzig
‡Division of Surface Physics, Felix Bloch Institute for Solid State Physics

Long-term tissue culture of adult mammalian organs is a highly promising approach to bridge the gap between single cell cultures and animal experiments, and bears the potential to reduce in vivo studies. Novel biomimetic materials open up new possibilities to maintain the complex tissue structure in vitro; however, survival times of adult tissues ex vivo are still limited to a few days with established state-of-the-art techniques. Here, it is demonstrated that TiO_2 nanotube scaffolds with specific tissue-tailored characteristics can serve as superior substrates for long-term adult brain and spleen tissue culture. High viability of the explants for at least two weeks is achieved and compared to tissues cultured on standard polytetrafluoroethylene (PTFE) membranes. Histological and immunohistochemical staining and live imaging are used

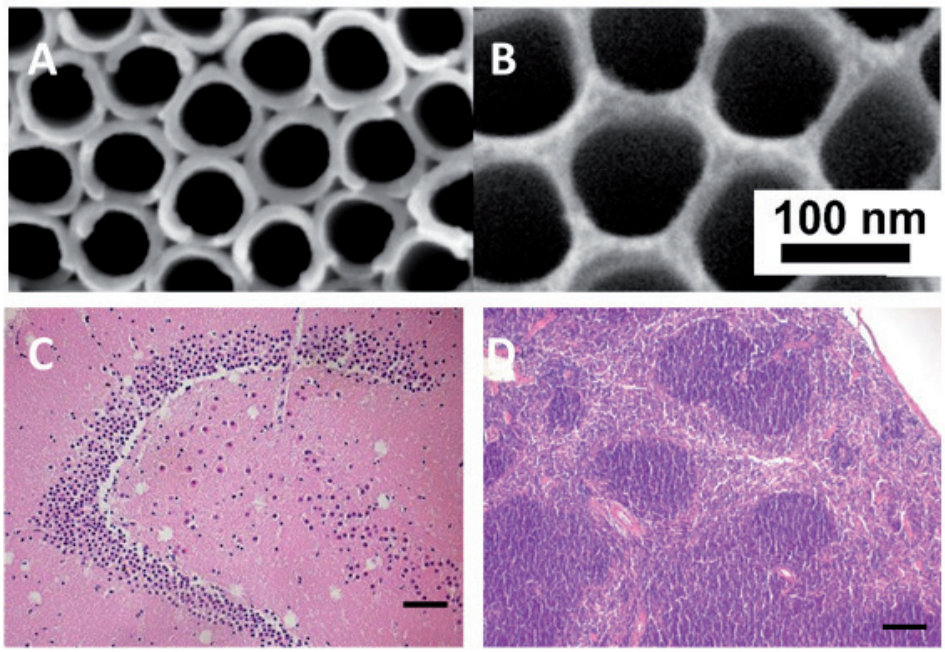

Figure 4.8: Freestanding (A) and nanoporous nanotubes (B) ideal for adult brain and spleen tissue culture. C: tissue from adult rat hippocampus cultured for 14 days on nanoporous nanotubes; D: spleen tissue cultured for 14 days on freestanding nanotubes (scale bar: 100 μm)

to investigate tissue condition after 5 and 14 d in vitro, while environmental scanning electron microscopy qualifies the interaction with the underlying scaffold. In contrast to tissues cultured on PTFE membranes, enhanced tissue morphology is detected in spleen slices, as well as minor cell death in neuronal tissue, both cultured on nanotube scaffolds. This novel biomimetic tissue model will prove to be useful to address fundamental biological and medical questions from tissue regeneration up to tumour progression and therapeutic approaches [1].

[1] S. Kallendrusch et al.: Adv. Healthcare Mater., **2017** 6(9):1601336

4.9 Micropatterning of reagent-free high energy cross-linked gelatin hydrogels for bioapplications

B. Heyart[*], A. Weidt, E. Wisotzki[*], M. Zink, S.G. Mayr[*†]

[*]Leibniz Institute for Surface Modification (IOM), Leipzig
[†]Division of Surface Physics, Felix Bloch Institute for Solid State Physics

Hydrogels are crosslinked polymeric gels of great interest in the field of tissue engineering, particularly as biocompatible cell or drug carriers. Reagent-free electron irradiated gelatin is simple to manufacture, inexpensive and biocompatible. Here, the potential to micropattern gelatin hydrogel surfaces during electron irradiation crosslinking was demonstrated as a promising microfabrication technique to produce thermally stable

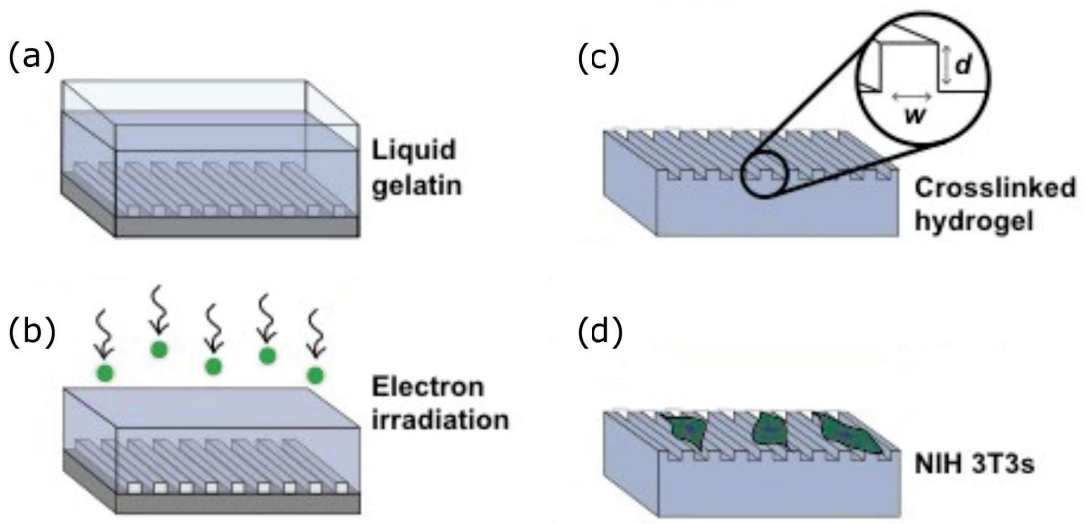

Figure 4.9: Schematic picture of the micro-patterning of reagent-free, high-energy electron irradiated gelatin hydrogels for bioapplications: (a) liquid gelatin is added onto the manufactured templates, (b) using high-energy electron irradiation, gelatin is crosslinked, (c) the sample topography of the moulded and irradiated gelatin samples is measured using an 3D confocal microscope after varying incubation times in simulated body fluid and (d) NIH/3T3 fibroblast cells are cultured on the crosslinked gelatin samples to evaluate contact guidance phenomena.

structures on highly relevant length scales for bioapplications. In the present work, grooves of 3.75 to 170 μm width and several hundred nanometers depth were transferred onto gelatin hydrogels during electron irradiation and characterized by 3D confocal microscopy after exposure to ambient and physiological conditions. The survival and influence of these microstructures on cellular growth was further characterized using NIH 3T3 fibroblasts. Topographical modifications produced surface structures on which the cultured fibroblasts attached and responded by adapting their morphologies. This developed technique allows for simple and effective structuring of gelatin and opens up new possibilities for irradiation crosslinked hydrogels in biomedical applications in which cell attachment and contact guidance are favored [1].

[1] B. Heyart et al.: J Biomed Mater Res Part B: Appl Biomater, **2017** published online before print

4.10 Funding

Leipziger Schule der Naturwissenschaften - Bauen mit Molekülen und Nano-Objekten (BuildMoNa)
Prof. Dr. E. Hey-Hawkins, Prof. Dr. M. Grundmann und Prof. Dr. J. A. Käs
GSC 185/1

Blebbing Driven or Actin Protrusive-Force Driven Cancer Cell Migration
Prof. Dr. J. A. Käs, Prof. Dr. C. T. Mierke
DFG, KA 1116/17-1

Mechanismen Aktin-vermittelter Krafterzeugung, Morphodynamik und Motilität einzelner Zellen
Prof. Dr. J. A. Käs, Prof. Dr. K. Rottner, Prof. Dr. M. Falcke
DFG, KA 1116/14-1

Dynamisch-mechanische Manipulation and Charakterisierung von Zellen mit Hilfe magnetischer Dehnung
Prof. Dr. M. Zink
DFG, Zi-1330/2-1

FORCE - Imaging the Force of Cancer, WP 6 - Mechanical Impact of Solid Tumours on Tissues
Prof. Dr. J. A. Käs
EU Horizon 2020, 668039

Plasmaunterstützte Funktionalisierung magnetischer Kern-Schale-Nanopartikel mit Biomolekülen für die medizinische Diagnostik - BIOCOAT
Prof. Dr. M. Zink
SAB, 100259235

Organotypische Langzeitkultivierung von adultem Augengewebe zur Erforschung von Krankheiten und Wirkstoffen in vitro - EYECULTURE - TP 1
Prof. Dr. M. Zink
BMBF, 031A574A

What Holds Cancer Cells Back? (HoldCancerBack)
Prof. Dr. J. A. Käs
ERC Advanced Grant - EU Horizon 2020, 741350

Korrelative Zell-Zell-Wechselwirkung in Geweben und Gewebemodellen fur neue Ansatze in Diagnostik und Therapie: Mechanische Aspekte (KOGEME), Geräteausstattung
Prof. Dr. J. A. Käs, Prof. Dr. C. T. Mierke, Prof. Dr. T. Pompe, Prof. Dr. M. Zink
SAB, 100299919

4.11 Organizational Duties

Prof. J. A. Käs

- Senator der Universität Leipzig
- Member of the Organizing Committee: 8th Annual Symposium - Physics of Cancer, Leipzig, October 2017
  involved organizers: Prof. H. Herrmann (German Cancer Research Center), Prof. Dr. Carsten Beta (Potsdam University), Dr. D. M. Smith (Fraunhofer Institute IZI)
- PWM Winterschool, Spindleruv Mlyn, Czech Republic, March 2017
- Journal review: Nature, Science, Cell, Physical Review Letters, Biophysical Journal, Biophysica and Proceedings of the National Academy of Science, Langmuir, Angewandte Chemie, Nature Physics, Journal of Biophotonics, Cytoskeleton, Optics Express, New Journal of Physics

- Grant review: National Science Foundation, Div. of Materials Research; National Science Foundation, Div. of Cellular Organization; National Science Foundation, Div. of Computational Biology; National Science Foundation, Div. of Physics, Special Programs; Deutsche Forschungsgemeinschaft, Alexander von Humboldt Foundation, Deutsche Studienstiftung, Centre National de Recherche
- Fellow, American Physical Society
- Full Member, Saxonian Academy of Sciences

4.12 External Cooperations

Academic

- Syracuse University, USA
  Prof. M. E. Manning
- Syracuse University, USA
  Prof. M. C. Marchetti
- University of Maryland, USA
  Prof. W. Losert
- Harvard University, Boston, USA
  Prof. J. J. Fredberg
- King's College London, Biomedical Engineering Department, GB
  Prof. R. Sinkus
- Politecnico Milano, Italy
  Dr. R. Osellame
- Deutsche Gesellschaft für Zellbiologie (DGZ)
  Prof. Dr. H. Herrmann
- Max-Delbrück-Zentrum für molekulare Medizin
  Dr. M. Falcke
- Charité Berlin, MR Elastographie
  Prof. Dr. I. Sack
- Technische Universität Braunschweig, Zoologisches Institut
  Prof. Dr. K. Rottner
- Universität Leipzig, Klinik u. Poliklinik für Frauenheilkunde
  Prof. Dr. M. Höckel
- Universität Leipzig, Institut für Pathologie
  Prof. Dr. L.-C. Horn
- Universität Leipzig, Institut für Experimentelle Physik I
  Prof. Dr. C. Mierke

Industry

- RS Zelltechnik GmbH, Leipzig
  R. Stange

4.13 Publications

Journals

D. Strehle, P. Mollenkopf, M. Glaser, T. Golde, C. Schuldt, J. A. Käs, J. Schnauß: *Single Actin Bundle Rheology*. Molecules, **22**, 1804 (2017)

J. Schnauß, M. Glaser, J. Lorenz, C. Schuldt, C. Möser, M. Sajfutinow, T. Händler, J. A. Käs, D. Smith: *DNA Nanotubes as a Versatile Tool to Study Semiflexible Polymers*. JoVE, 56056 (2017)

L. Oswald, S. Grosser, D. M. Smith, J. A. Käs: *Jamming transitions in cancer*. J. Phys. D: Appl. Phys., **50**, 483001 (2017)

H. Kubitschke, J. Schnauß, K. D. Nnetu, E. Warmt, R. Stange, J. A. Käs: *Actin and microtubule networks contribute differently to cell response for small and large strains*. New J. Phys., **19**, 093003 (2017)

E. Morawetz, R. Stange, T. Kießling, J. Schnauß, J. A. Käs: *Optical stretching in continuous flows*. Converg. Sci. Phys. Oncol., **3**, 024004 (2017)

F. Kage, M. Winterhoff, V. Dimchev, J. Mueller, T. Thalheim, A. Freise, S. Brühmann, J. Kolasser, J. Block, G. Dimchev, M. Geyer, H.-J. Schnittler, C. Brakebusch, T. Stradal, M.-F. Carlier, M. Sixt, J. A. Käs, K. Rottner: *FMNL formins boost lamellipodial force generation*. Nature Comm. **8**, 14832 (2017)

S. Kallendrusch, F. Merz, I. Bechmann, S. G. Mayr, M. Zink: *Long-Term Tissue Culture of Adult Brain and Spleen Slices on Nanostructured Scaffolds*. Adv. Healthcare Mater., **6**, 1601336 (2017)

B. Heyart, A. Weidt, E. Wisotzki, M. Zink, S. G. Mayr: *Micropatterning of reagent-free high energy crosslinked gelatin hydrogels for bioapplications*. J Biomed Mater Res Part B: Appl Biomater, published online before print (2017)

Books

J. Schnauß, J. A. Käs, D. Smith: *Contact-free Mechanical Manipulation of Biological Materials*. Chapter in: Springer Handbook of Nanotechnology, Bhushan B. (Ed.), Springer Handbooks, Springer, Berlin, Heidelberg (2017)

H. Kubitschke, E. W. Morawetz, J. A. Käs, J. Schnauß: *Physical Properties of Single Cells and Collective Behavior*. Chapter in: Quantification of Biophysical Parameters in Medical Imaging, Springer International Publishing, published online before print (2017)

Talks

J. A. Käs: *Tumor Cell Mechanics*. Status Report Meeting, EU-Project FORCE/HORIZON 2020, Paris, France, January 2017

J. A. Käs: *Rigid tumors and soft cells*. Gordon Research Conference: „Physical Sciences of Cancer“, Galveston, USA, February 2017 (invited talk)

S. Grosser, L. Oswald, J. Lippoldt, S. Pawlizak, A. Fritsch, J. A. Käs: *Jamming and liquidity in 3D cancer cell aggregates*. APS March Meeting, New Orleans, USA (2017)

E. Morawetz, Y. Ha, I. Fornaçon-Wood, J. A. Käs: *Changes in active and passive rheologic responses of epithelial cells during tumor progression*. PWM Winter School Spindleruv Mlyn, Czech Republic, March 2017

J. Lippoldt, S. Grosser, P. Heine, L. Oswald, J. A. Käs: *A new definition of jamming: Beyond T1 transitions and MSD*. PWM Winter School Spindleruv Mlyn, Czech Republic, March 2017

S. Grosser, L. Oswald, J. Lippoldt, P. Heine, J. A. Käs: *Cell Jamming across the EMT*. PWM Winter School Spindleruv Mlyn, Czech Republic, March 2017

E. Warmt, E. Morawetz, S. Grosser, J. A. Käs: *Myosin Induced Contractility in Suspended Cells*. PWM Winter School Spindleruv Mlyn, Czech Republic, March 2017

P. Mollenkopf, M. Glaser, J. Schnauß, T. Golde, T. Händler, J. A. Käs, D. Smith: *Extensibility measurements on DNA helix tubes*. PWM Winter School Spindleruv Mlyn, Czech Republic, March 2017

J. Schnauß, J. Lorenz, M. Glaser, M. Sajfutdinow, C. Schuldt, J. A. Käs, D. Smith: *Non-genetic programming of biology by DNA-based cross-linkers*. PWM Winter School Spindleruv Mlyn, Czech Republic, March 2017

T. Golde, M. Glaser, T. Händler, J. Schnauß, H. Herrmann, J. A. Käs: *Composite Networks of Actin and Intermediate Filaments*. PWM Winter School Spindleruv Mlyn, Czech Republic, March 2017

M. Glaser, P. Mollenkopf, C. Möser, C. Schuldt, J. Schnauß, T. Händler, J. A. Käs, D. Smith: *Altering Synthetic Semiflexible DNA Nanotube Networks by Tunable Cross-linking*. PWM Winter School Spindleruv Mlyn, Czech Republic, March 2017

T. Tschirner, M. Glaser, J. A. Käs, D. Smith, J. Schnauß: *Higher ordered assembly of chiral DNA nanotubes induced by depletion forces*. PWM Winter School Spindleruv Mlyn, Czech Republic, March 2017

J. Wittenbecher, T. Händler, M. Glaser, T. Golde, D. Smith, J. A. Käs, J. Schnauß: *Microrheology on mechanically tunable DNA nanotube networks*. PWM Winter School Spindleruv Mlyn, Czech Republic, March 2017

J. Schnauß: *Probing mechanical properties of biological, semiflexible polymers*. Seminar of Molecular Spectroscopy Group - Institute of Analytical Chemistry, Leipzig University, March 2017

J. Schnauß: *Driving Life's Engine: from Semiflexible Components to Cell Migration*. Vorstellungsvortrag Juniorprofessur - Experimentelle Medizinische Physik, Universität Düsseldorf, March 2017

S. Grosser, L. Oswald, J. Lippoldt, S. Pawlizak, A. Fritsch, J. A. Käs: *Jamming and Fluidity in 3D Cancer Cell Aggregates*. DPG Spring Meeting, Dresden, March 2017

M. Glaser, P. Mollenkopf, C. Möser, C. Schuldt, J. Schnauß, T. Händler, J. A. Käs, D. Smith: *Rheology on cross-linked DNA nanotube networks*. DPG Spring Meeting, Dresden, March 2017

A. Weidt, B. Heyart, E. Wisotzki, M. Zink, S. G. Mayr: *Micropatterning of reagent-free, high energy crosslinked gelatin hydrogels for bioapplications*. DPG Spring Meeting, Dresden, March 2017

P. Heine, J. Lippoldt, S. Grosser, L. Oswald, J. A. Käs: *How demixing and crowding behavior influence the invasive potential of composite tumor-like systems*. DPG Spring Meeting, Dresden, March 2017

J. Schnauß, J. Lorenz, M. Glaser, M. Sajfutdinow, C. Schuldt, J. A. Käs, D. Smith: *Emergent mechanics of DNA-crosslinked biopolymer hydrogels*. Workshop DNA Mitteldeutschland, Jena, May 2017

J. Schnauß, M. Glaser, T. Golde, J. Lorenz, P. Mollenkopf, T. Händler, C. Schuldt, D. Smith, J. A. Käs: *Mechanics and dynamics of semiflexible polymer structures*. Soft Matter Day, Leipzig, June 2017

A. Weidt, B. Heyart, E. Wisotzki, M. Zink, S. G. Mayr: *Micropatterning of reagent-free, high energy crosslinked gelatin hydrogels for bioapplications*. Soft Matter Day, Leipzig, June 2017

S. Grosser, J. Lippoldt, L. Oswald, J. A. Käs: *Mechanics and Structure of Multicellular Tumour Spheroids*. ERC Advanced Grant - kick off meeting, Freyburg/U., August 2017

P. Heine, J. Lippoldt, S. Grosser, L. Oswald, J. A. Käs: *How demixing and crowding behavior influence the invasive potential of composite tumor-like systems*. ERC Advanced Grant - kick off meeting, Freyburg/U., August 2017

E. Morawetz, Y. Ha, I. Fornaçon-Wood, E. Warmt, L.-C. Horn, S. Briest, M. Höckel, J. A. Käs: *Cadherins, Cancer & EMT*. ERC Advanced Grant - kick off meeting, Freyburg/U., August 2017

J. Lippoldt, S. Grosser, P. Heine, L. Oswald, J. A. Käs: *Dynamics of neighborhood exchanges and cellular jamming*. ERC Advanced Grant - kick off meeting, Freyburg/U., August 2017

F. Sauer, S. Grosser, C. T. Mierke, J. A. Käs: *Tunable collagen gels & their influence on cell jamming*. ERC Advanced Grant - kick off meeting, Freyburg/U., August 2017

H. Kubitschke, B. Wolf, E. Morawetz, U. Behn, J. A. Käs, M. Höckel: *Theory of Inverse Morphogenesis*. ERC Advanced Grant - kick off meeting, Freyburg/U., August 2017

E. Warmt, E. Morawetz, S. Grosser, J. A. Käs: *Myosin Induced Contractility in Suspended Cells*. ERC Advanced Grant - kick off meeting, Freyburg/U., August 2017

M. Glaser, P. Mollenkopf, C. Möser, C. Schuldt, J. Schnauß, T. Händler, J. A. Käs, D. Smith: *Altering Synthetic Semiflexible DNA Nanotube Networks by Tunable Cross-linking*. ERC Advanced Grant - kick off meeting, Freyburg/U., August 2017

J. Schnauß, M. Glaser, T. Golde, J. Lorenz, P. Mollenkopf, T. Händler, C. Schuldt, M. Sajfutdinow, D. Smith, J. A. Käs: *Mechanics and dynamics of the cytoskeleton*. ERC Advanced Grant - kick off meeting, Freyburg/U., August 2017

J. A. Käs: *Optical measurements of cell adhesion*. SPIE - Optics and Photonics Conference, San Diego, USA, August 2017 (invited talk)

J. A. Käs: *A new type of unjamming transitions in cancer*. International Symposium „Physics meets Medicine - the Heart of Active Matter", Göttingen, September 2017 (invited talk)

J. A. Käs: *Why do rigid tumours contain soft cancer cells?* MEIBioeng / MPEC2017 - Woolmer Lecture, Sandown Park Racecourse, Esher, Surrey, GB, September 2017 (invited talk)

S. Grosser, J. Lippoldt, L. Oswald, J. A. Käs: *Mechanics and Structure of Multicellular Tumour Spheroids*. Cell Jamming Meeting, Boston, USA, October 2017

J. Lippoldt, S. Grosser, P. Heine, L. Oswald, J. A. Käs: *Dynamics of neighborhood exchanges and cellular jamming*. Cell Jamming Meeting, Boston, USA, October 2017

T. Golde, C. Huster, M. Glaser, T. Händler, J. Schnauß, H. Herrmann, J. A. Käs: *Composite Networks of Actin and Intermediate Filaments*. Multiscale Mechanochemistry & Mechanobiology, Berlin, October 2017

J. A. Käs: *Why do rigid tumours contain soft cancer cells?* Physical Colloquium, University of Bremen, November 2017 (invited talk)

C. Ficorella, P. Heine: *Cell motility studies in constriction chips*. Joint Meeting at Politecnico di Milano, Italy, November 2017

P. Mollenkpopf, M. Glaser, J. Schnauß, T. Golde, T. Händler, J. A. Käs, D. Smith: *Single Molecule Manipulation and Extensibility Measurements on DNA Helix Tubes*. Workshop DNA Mitteldeutschland, Leipzig, November 2017

Posters

J. Lippoldt, P. Heine, S. Grosser, L. Oswald, J. A. Käs: *Connecting cell jamming with adhesion, contractility and cell stiffness*. DPG Spring Meeting, Dresden, March 2017

E. Warmt, E. Morawetz, S. Grosser, J. A. Käs: *Myosin Activity in Epithelial and Mesenchymal Cells*. DPG Spring Meeting, Dresden, March 2017

M. Glaser, P. Mollenkopf, C. Möser, C. Schuldt, J. Schnauß, T. Händler, J. A. Käs, D. Smith: *Altering Synthetic Semiflexible DNA Nanotube Networks by Tunable Cross-linking*. Soft Matter Day, Leipzig, June 2017

F. Sauer, L. Oswald, H. Tschätzsch, J. Braun, J. A. Käs, C. T. Mierke, I. Sack: *MR Elastography on polymer networks: a proof of concept for collagen gels*. Soft Matter Day, Leipzig, June 2017

H. Kubitschke, B. Wolf, E. Morawetz, U. Behn, J. A. Käs, M. Höckel: *Theory of Inverse Morphogenisis and Clinical Impact*. Soft Matter Day, Leipzig, June 2017

C. Ficorella, R. Martinéz Vazquéz, P. Heine, E. Lepera, J. Cao, R. Osellame, J. A. Käs: *Cell motion through a confined micro-environment: an attempt to understand cancer cell invasion*. Soft Matter Day, Leipzig, June 2017

T. Golde, M. Glaser, T. Händler, J. Schnauß, H. Herrmann, J. A. Käs: *Composite Networks of Actin and Intermediate Filaments*. CELLMECH2017, Windermere, GB, June 2017

F. Sauer, L. Oswald, H. Tschätzsch, J. Braun, J. A. Käs, C. T. Mierke, I. Sack: *MR Elastography on polymer networks: a proof of concept for collagen gels*. 1^{th} International MRE Workshop, Berlin, September 2017

E. Morawetz, Y. Ha, I. Fornaçon-Wood, E. Warmt, S. Grosser, J. A. Käs: *E-Cadherin as an upstream regulator of mechanical responses in the early EMT and cancer development*. 8^{th} Annual Symposium - Physics of Cancer, Leipzig, October 2017

M. Glaser, P. Mollenkopf, C. Möser, C. Schuldt, J. Schnauß, T. Händler, J. A. Käs, D. Smith: *Altering Synthetic Semiflexible DNA Nanotube Networks by Tunable Cross-linking*. 8^{th} Annual Symposium - Physics of Cancer, Leipzig, October 2017

C. Ficorella, R. Martinéz Vazquéz, P. Heine, E. Lepera, J. Cao, R. Osellame, J. A. Käs: *Cell motion through a confined micro-environment: an attempt to understand cancer cell invasion*. 8^{th} Annual Symposium - Physics of Cancer, Leipzig, October 2017

H. Kubitschke, B. Wolf, E. Morawetz, U. Behn, J. A. Käs, M. Höckel: *Theory of Inverse Morphogenisis and Clinical Impact*. 8^{th} Annual Symposium - Physics of Cancer, Leipzig, October 2017

J. Lippoldt, P. Heine, S. Grosser, L. Oswald, J. A. Käs: *Dynamics of cell jamming*. 8^{th} Annual Symposium - Physics of Cancer, Leipzig, October 2017

F. Sauer, L. Oswald, A. Ariza de Schellenberger, H. Tschätzsch, J. Braun, J. A. Käs, C. T. Mierke, I. Sack: *MR Elastography on polymer networks: a proof of concept for collagen gels*. 8^{th} Annual Symposium - Physics of Cancer, Leipzig, October 2017

E. Warmt, S. Grosser, E. Morawetz, J. A. Käs: *Cell Contractility might Determine Tissue Surface Tension*. 8^{th} Annual Symposium - Physics of Cancer, Leipzig, October 2017

Thomas Fuhs: *Direct measurement of surface charge distribution in phase separating supported lipid bilayers*. 8^{th} Annual Symposium - Physics of Cancer, Leipzig, October 2017

T. Golde, C. Huster, M. Glaser, T. Händler, J. Schnauß, H. Herrmann, J. A. Käs: *Glassy Dynamics in Composite Biopolymer Networks*. 8^{th} Annual Symposium - Physics of Cancer, Leipzig, October 2017

P. Mollenkopf, D. Strehle, M. Glaser, T. Golde, J. Schnauß, J. A. Käs, D. Smith: *Mechanical properties of anisotropic polymer structures investigated by optical tweezers*. 8^{th} Annual Symposium - Physics of Cancer, Leipzig, October 2017

4.14 Graduations

Doctorate

- Steve Pawlizak
  Cellular Cohesion and Segregation in Cancerous Tissues
  23.10.2017

Master

- Markus Sommerfeld
  Lamellopodial Protein Distribution and Force Generation
  January 2017
- Paul Mollenkopf
  Single Molecule Manipulation and Extensibility Measurements on DNA Helix Tubes
  May 2014
- Yonah Karkheck
  Versteckte Lipidreservoirs in Riesenplasmamembranvesikeln
  (Wissenschaftliche Arbeit nach Lehramtsprüfungsordnung I)
  November 2017

Bachelor

- Sebastian Henn
  Anti-hypertensives and the bending stiffness of cancer cell membranes: Thermal fluctuation analysis of Giant Plasma Membrane Vesicles
  June 2017
- Teresa Tschirner
  Higher ordered assembly of DNA nanotubes under varying nucleation conditions
  June 2017
- Isabella Fornaçon Wood
  Modelling tumour progression: Investigating cell rheology during the epithelial to mesenchymal transition.
  July 2017
- Diana Rodriguez Bonet
  Microrheology on Actin and Vimentin
  August 2017
- Yookyung Ha
  Epithelial Cadherin Dependent Cell Mechanics
  September 2017
- Carlotta Ficorella
  Cell migration through a confined microenvironment: an attempt to understand the motion of metastatic cells
  September 2017

- Pablo Gottheil
  Cell-cell Adhesion in the Optical Stretcher
  November 2017
- Cary Tutmarc
  Reptation of DNA Nanotubes in Semiflexible Biopolymer Networks
  November 2017

5

Biological Physics

5.1 Introduction

Besides genetic, morphological and biochemical alterations, the extracellular matrix stroma surrounding cancer cells represents a key characteristic feature of the malignant progression of cancer including cancer cell motility and the emergence of metastases. The current knowledge on the biophysical based experimental approaches in the field of cancer research is that mechanical aberrancies are major regulators of the malignant progression of cancer, in which the mechanical sensing of the stroma and the exertion of forces towards the stroma is crucial. However, the impact of the tumor stroma on cellular motility and hence on the metastatic cascade causing subsequently the malignant progression of cancer is still controversially discussed, as there exist two distinct and opposite effects of the local stroma.

On the one hand the stroma acts as tumor stroma and promotes all hallmarks of cancer enabling the cancer cells to overcome restrictive biological capabilities such as increased proliferation, enhanced survival and elevated migratory potential of cancer cells, altered metabolism and escape from programmed cell death through mechano-sensing and mechano-transduction processes caused by elevated stroma rigidity through the alignment of extracellular matrix fibers and on the other hand the stroma acts based on its structural constraints as a mechanical barrier for cancer cell motility in 3D extracellular matrix confinement, when the pore-size is much smaller than the cell's nuclear diameter.

In particular, the mechanical properties of the tumor stroma such as the tissue matrix stiffness and its entire architectural network are the major driving factors for providing the specific and optimal microenvironment for cancer cell penetration and invasion. Thus, biophysical methods determining the mechanical properties of the stroma such as the magnetic resonance elastography are critical for diagnosis and the prediction of early cancer stages, as tissue fibrosis and cancer are tightly associated, as there exists indeed an even elevated risk of cancer initiation upon cystic fibrosis or subsequently cirrhosis and even more important the malignant progression of cancer such as metastasis.

Prof. Dr. Claudia Tanja Mierke, Dipl. Phys. Tony Fischer

5.2 Focal adhesion kinase activity is required for actomyosin contractility-based invasion of cells into dense 3D matrices

T. Fischer, C.T. Mierke

Integrin-based adhesions are important for cell motility. They mediate interactions of cytoskeletal filaments with the local micro-environment. Activity of Focal Adhesion Kinase (FAK) is a vital component in the cell adhesion process. FAK is a cytoplasmic non-receptor tyrosine kinase, localized to cell-ECM contact sites, the focal adhesions. It is a crucial regulator of focal adhesion binding and thus for cell motility [1, 2].

Collagen Type I from rat tail and bovine skin (1:2 mass fraction) form a tunable ECM model with different mechanical and topological properties. Elastic properties of these collagen hydrogels were determined using Atomic Force Microscopy, see figure 5.5 for an illustration. A large bead ($\sim 45\,\mu m$) indents the scaffold, thus enabling fitting of the Hertz Model to the force-distance-curves and revealing the Young's Modulus. Results are shown in figure 5.1.

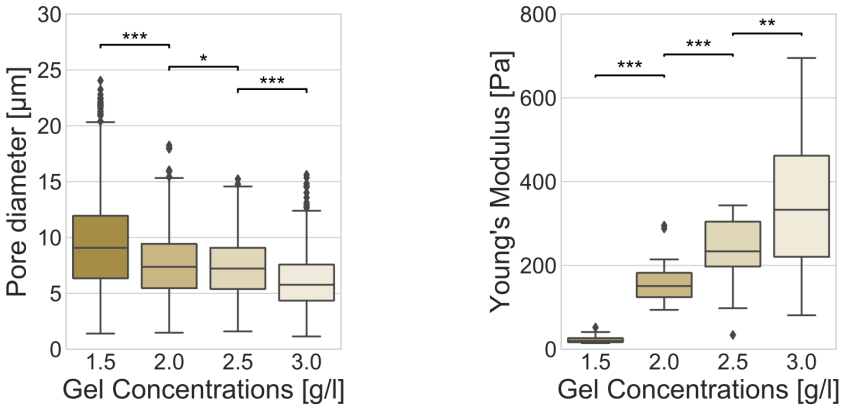

Figure 5.1: *Left:* pore-size decreases and *right:* gel stiffness drastically increases with increasing collagen monomer concentration

Cell migration, namely three-dimensional migration speed and persistance, are drastically hindered in $FAK^{R454/R454}$ cells. Z-Persistance is a measure for the directionality of migration in the z-dimension (height or depth) [3]. Both values were determined using life-cell phase-contrast image stacks and determining cell trajectories in 3D. Results are shown in figure 5.2.

These findings are supported by 3D invasion assays. These are fixed-timepoint assays, where cells are seeded on top of a $\sim 500\,\mu m$ high collagen gel and left migrating for 3 days. Afterwards, cells are fixated using Glutaraldehyde and cell nuclei are fluorescently stained using HOECHST33342. Three-dimensional fluorescence image stacks of the stained cell nuclei are recorded and analyzed using a custom built nuclei detection algorithm developed by group-member T. Fischer [4]. The most important of the many analysis values gathered are *invasivness* and *invasion depth*. The former measuring the fraction of cells invading into the gel, the latter determining the maximum depth the respective cells reached. We have shown that $FAK^{R454/R454}$ lacking FAK activity invade dense 3D matrices less efficiently, as shown in figure 5.3.

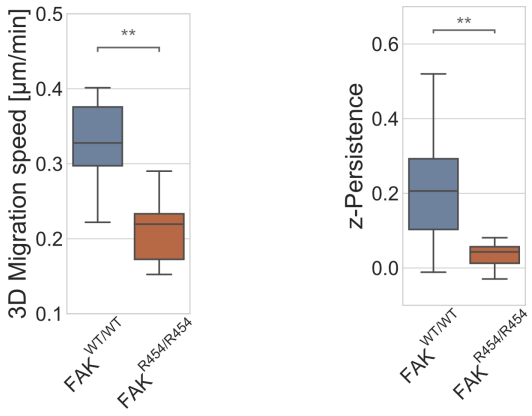

Figure 5.2: *Left:* three-dimensional migration speed and *right:* z-persistance are drastically reduced in $FAK^{R454/R454}$ compared to FAK widltype cells

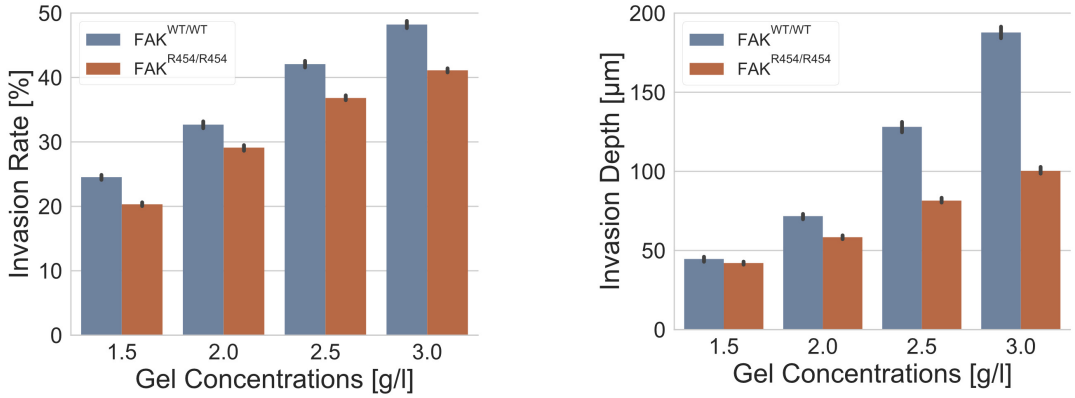

Figure 5.3: *Left:* invasion rate increases almost linearly with gel concentration and *right:* invasion depth increases more for FAK wildtype cell with increasing gel concentration than for kinase-dead cells

Invasion rate (percentage of cells migrated into the 3D scaffold) and depth determine the 3D migration and metastatic potential. While the number of invaded cells increases linearly with gel density and stiffness, invasion depth and thus ECM adhesion regulated migration seems to depend largely on FAK activity.

Due to the lack of substrate, cellular stiffness is overall reduced and impaired for adherent cells compared to non-adherent cells because matrix adhesion is crucial for overall cellular stiffness. We determined elasticity of adherent and non-adherent cells mainly using Atomic Force Microscopy, see figure 5.5 for an illustration. Results are shown in figure 5.4.

Cell morphology shows how a lack of matrix adhesion-sites leads decreased cell size. As mechano-coupling is decreased in kinase-dead cells, actin fiber-thickness is reduced accordingly, see figure 5.6.

Mechano-coupling is a crucial function of focal adhesions. We developed a novel approach to analyze 3D fiber displacements and thus measure a cells ability to deform its 3D micro-environment. This analysis is based on the well established Lucas-Kanade algorithm and incorporates a non-intrusive way to analyze 2D micro-environment deformations on a pixel-wise level. Depicted in figure 5.7 are absolute fiber displacements.

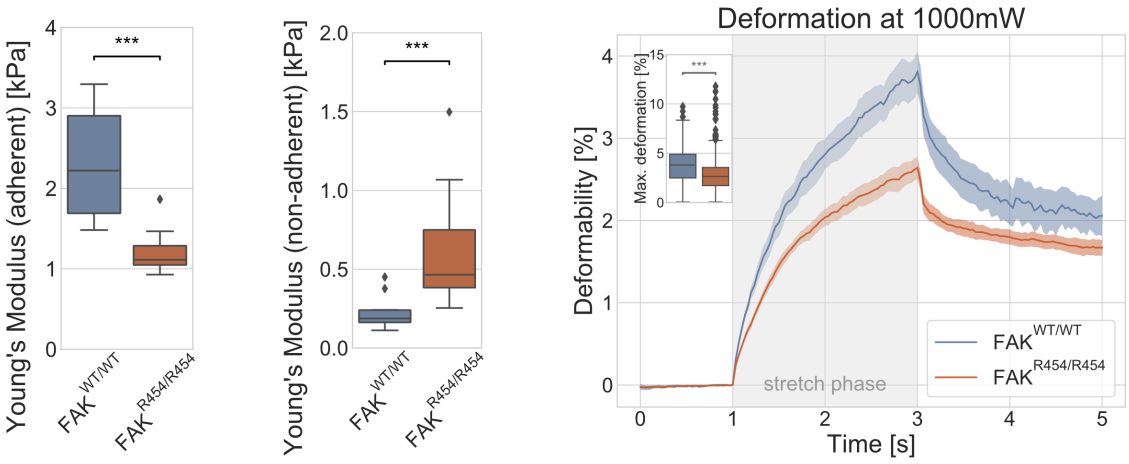

Figure 5.4: *Left and middle:* Young's Modulus for adherent and non adherent cells, *right:* proof of impaired cellular stiffness of non-adherent cells using Optical Stretcher. Note that cell deformability is reciprocal to cellular stiffness.

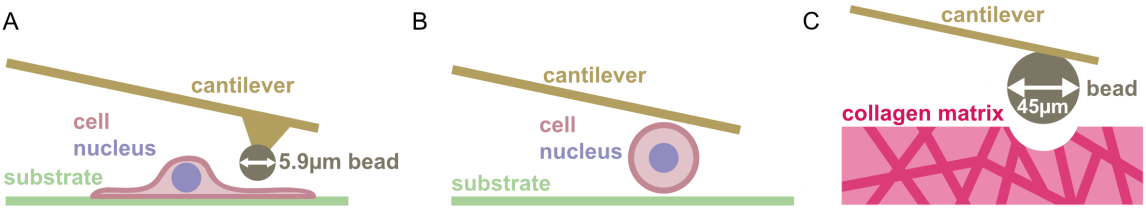

Figure 5.5: *A:* determination of adherent cell elasticity is done by probing the cytoskeleton with an *si m*6 µm bead and fitting the force-distance curve with the Hertz-Model, *B:* non-adherent cell elasticity determined using a modification to the Hertz-Model, *C:* gel elasticity determined using ~ 45 µm beads to measure large-scale scaffold elasticity

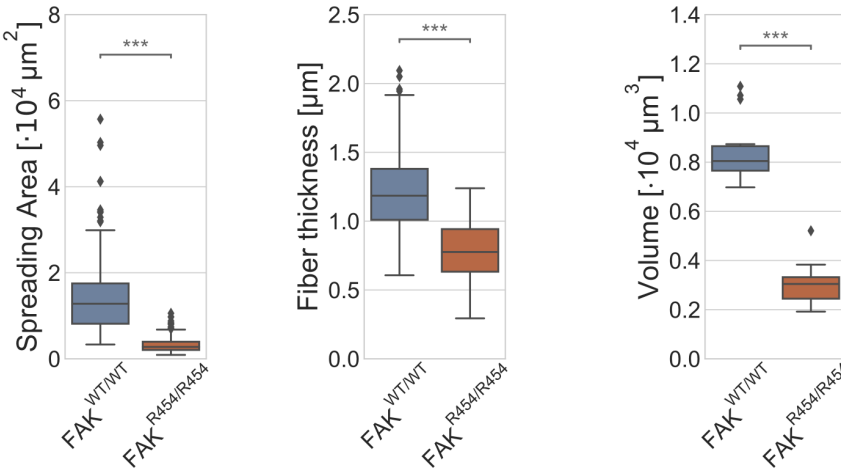

Figure 5.6: *Left:* spreading area of adherent cells on 2D substrate, *middle:* 3D cell volume of adherent cells in 3D collagen gel, *right:* actin fiber thickness of adherent cells in 3D collagen gel

Using a shell-approach where values in certain distances away from the cell boundary, we are able to analyze long-range force effects, see figure 5.7C for an illustration.

Fibroblasts expressing kinase-dead version of FAK are defective in integrin-dependent

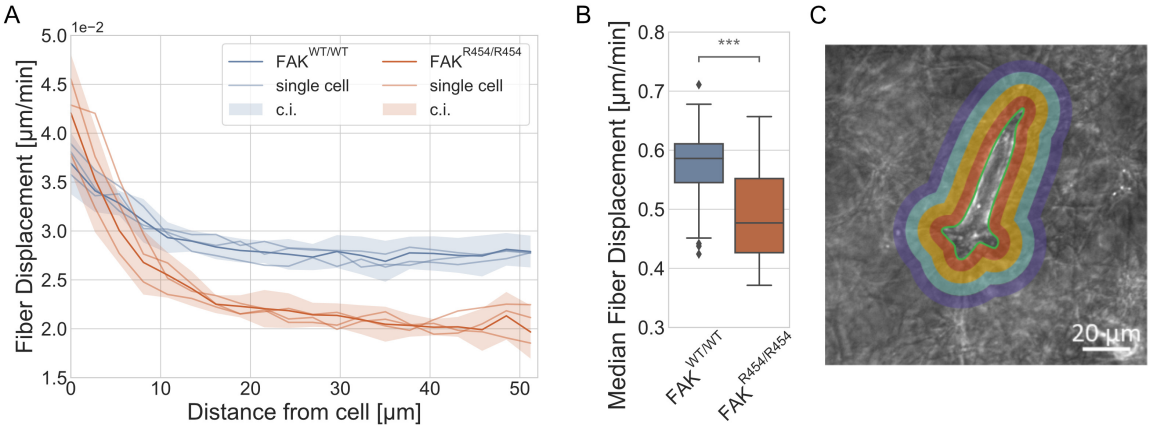

Figure 5.7: *A:* long range force-effects of different wildtype and kinase-dead cells, *B:* median fiber displacements, *C:* illustration of the shell-approach for long-range effect analysis

matrix remodeling and/or transmission of forces. This correlates with the invasion behavior in 3D ECMs.

Focal Adhesion Kinase activity plays a crucial role in cellular motility and facilitates 3D migration in collagen matrices. 3D pore size and scaffold stiffness seem to have a strong influence on cell migration. In future experiments, actin cytoskeleton and actual focal adhesions will be stained and observed during migration, leading to further insights in FAKs role on motility.

[1] F.J. Sulzmaier et al.: Nat. Rev. Cancer **14**, 598 (2014) doi:10.1038/nrc3792
[2] C.T. Mierke et al.: Phys Biol. **10**, 065005 (2013) doi:10.1088/1478-3975/10/6/065005
[3] S.T. Lim et al.: J. Biol. Chem. **285**, 21526 (2010) doi:10.1074/jbc.M110.129999
[4] T. Fischer et al.: Converg. Sci. Phys. Oncol. **3**, 044003 (2017) doi:10.1088/2057-1739/aa8bbb

5.3 Matrix and cellular mechanical properties are the driving factors for facilitating human cancer cell motility into 3D engineered matrices

T. Fischer, N. Wilharm, A. Hayn, C.T. Mierke

Cellular motility and invasion in connective tissue is a crucial process in tissue development, tissue regeneration and malignant progression of cancer and metastasis. Cell invasion requires cell-matrix adhesion via integrin receptors connected to the actomyosin cortex. Mechanical properties of tumor cells and their micro-environment are altered in many tumors. Tissue stiffness increase and cell stiffness decrease is associated with malignancy and metastasis.

We studied human breast cancer cell invasion into engineered 3D collagen I scaffolds and measured matrix and cell mechanical properties [1]. Both correlate with cellular invasiveness. We hypothesized that matrix and cellular mechanical properties regulate

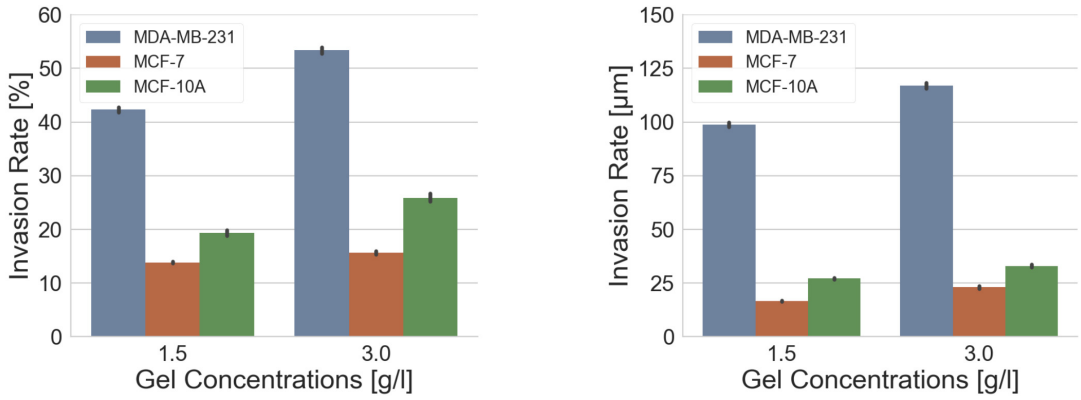

Figure 5.8: Invasion rate and invasion depth of used aggressive and non-aggressive cancer cell lines. As expected, aggressive cells invade more numerous and deeper than non-aggressive cells [1]

cancer cell motility in 3D collagen matrices. As seen in figure 5.8, results show exactly this behaviour.

To study 3D traction force of cells on their microenvironment, we developed a novel approach tzo determine 3D fiber displacement. In contrast to assays based on dislocation of beads [3], we use the well-established Lucas-Kanade algorithm for optical flow measurements. This ensures a significantly higher, pixel-wise resolution.

We analyzed the absolute fiber displacement by dislodging the cells using a Trypsin/CytochalasinD solution. This gives the overall fiber displacement of each cell [2]. As expected, aggressive cancer cells exhibit much higher absolute deformation on their surrounding ECM than non-aggressive control cell-lines. Figure 5.9 shows these results and the displacement vector-field of an exemplary MDA-MB-231 cell.

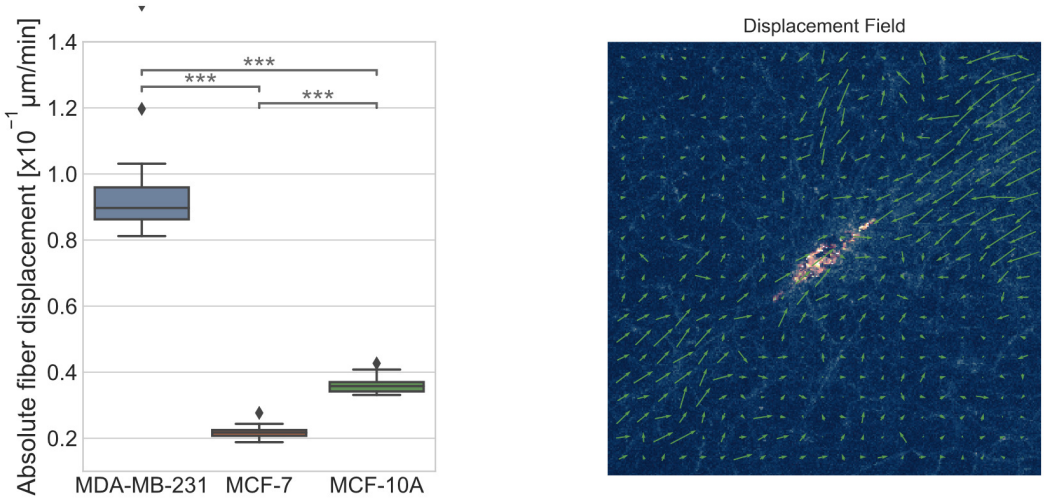

Figure 5.9: *Left:* Absolute fiber displacement of used aggressive and non-aggressive cancer cell lines, *right:* sample displacement vector-field of single image plane of 3D image stack and for a single time frame.

A more detailed analysis involves measurements over time with live cells and determination of long-range forces. Fiber displacement values in shells around each cell

and for each time frame are summed up, leading to overall displacements in dependence of distance from cell boundary. An illustration of the shell-analysis approach and time-distance development of a cell is shown in figure 5.10. Here, an exemplary cell initially pulled at its surrounding, relaxed, pulled again and finally relaxed in several steps. The graph depicts absolute displacements disregarding directionality.

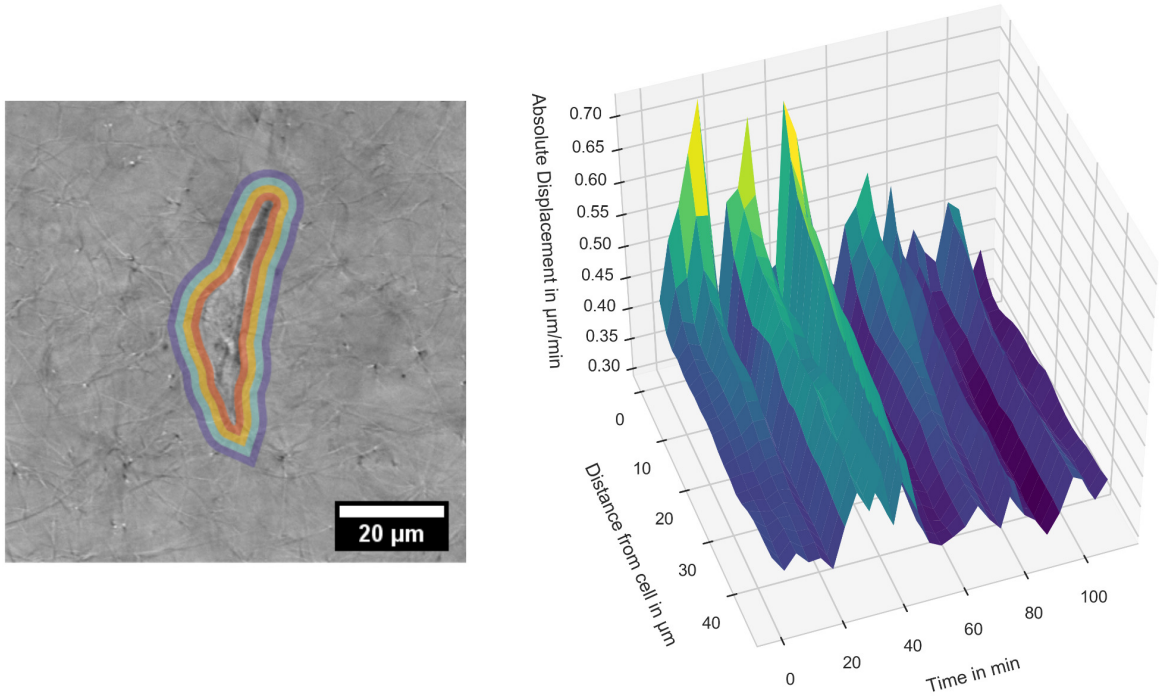

Figure 5.10: *Left:* Illustration of the shell-approach, *right:* displacement in dependence of distance from cell-boundary and time.

Besides cellular mechanical properties, an 18-fold higher matrix stiffness increased invasiveness of all three cell types suggesting that matrix stiffness indeed has an invasion-enhancing effect. Results are shown in figure 5.11.

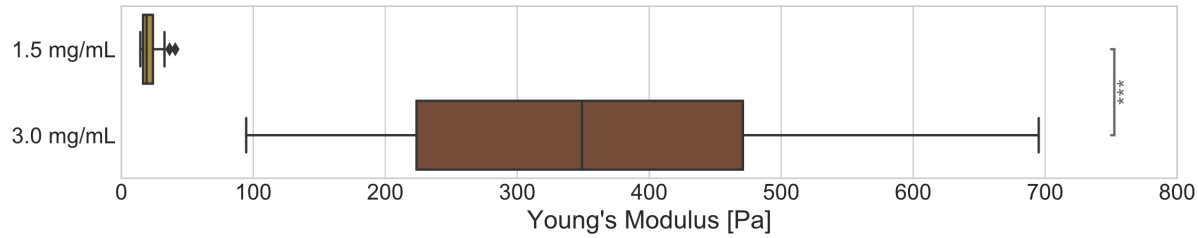

Figure 5.11: Gel elasticity of 1.5 g/l and 3.0 g/l collagen I gel. Due to the 18-fold increase, boxes are aligned vertically for better visibility.

Our findings demonstrate that mechanical properties of breast cancer cells and the 3D matrix environment facilitate 3D matrix invasion through increased actomyosin-dependent cellular stiffness and transmission of contractile force in dense 3D engineered collagen matrices [1].

[1] T. Fischer et al.: Converg. Sci. Phys. Oncol. **3**, 044003 (2017) doi:10.1088/2057-1739/aa8bbb

[2] C.T. Mierke et al.: Sci. Rep. **7**, 42780 (2017) doi:10.1038/srep42780
[3] J. Steinwachs et al.: Nat. Methods **13**, 171 (2015) doi:10.1038/nmeth.3685

5.4 Effects of rat tail and bovine dermal collagen I mixture on structural and elastic properties of 3D biomimetic ECM Models and their influence on cell migration

A. Hayn, T. Fischer, C.T. Mierke

Three-dimensional (3D) cell migration is studied mostly in biomimetic collagen I extracellular matrix (ECM) models. These *in vitro* collagen scaffolds are assumed to be mostly homogenous, unlike physiological *in vivo* ECM. How local variations of the extracellular matrix structure affect cell migration is mostly unknown. Thus, we investigated the effect of structure inhomogeneity on cell migration. We hypothesize that 3D pore size and elastic modulus of the surrounding matrix are the driving factors of 3D cell migration and invasion. Our findings implicate that these two parameters indeed seem to control both malignant and benign cancer cell invasion into these 3D collagen matrices.

By using mixes of rat tail and bovine dermal collagen I, we are able to mimic scaffold inhomogeneity. Collagen from rat tail self-assembles to elongated fibrils, whereas bovine collagen tends to build node-shaped scaffolds, illustrated in figure 5.12.

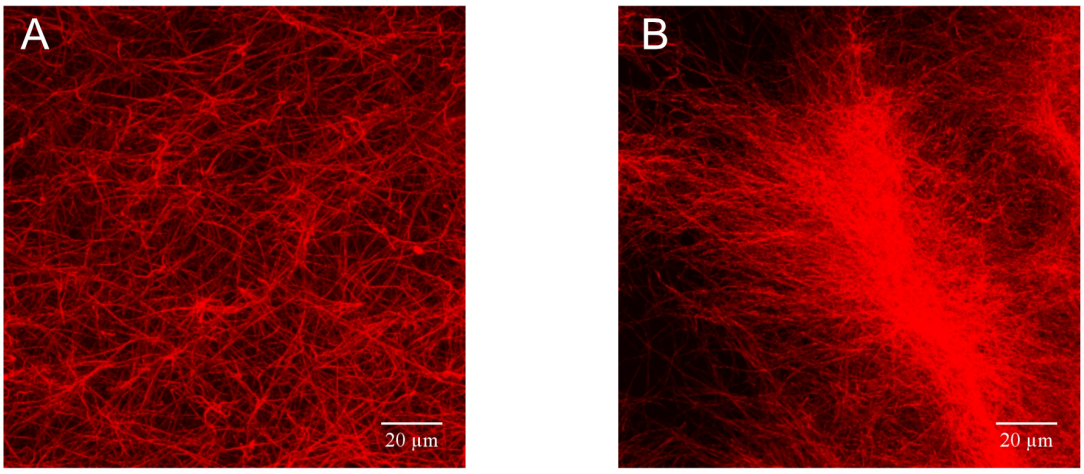

Figure 5.12: *A:* Collagen from rat tail (1.5 g/l), *B:* bovine dermal collagen (1.5 g/l)

Influence of collagen monomer concentration as well as single component matrices made from solely rat or bovine collagen on 3D pore-size and elastic modulus have been studied using confocal laser scanning microscopy (CLSM) and atomic force microscopy (AFM), respectively.

The occurrence of inhomogeneity, in form of node-like structures among all collagens observed, induced a matched approach to determine stiffness related characteristics, as shown in figure 5.13. Increased monomer concentration enhances collagen

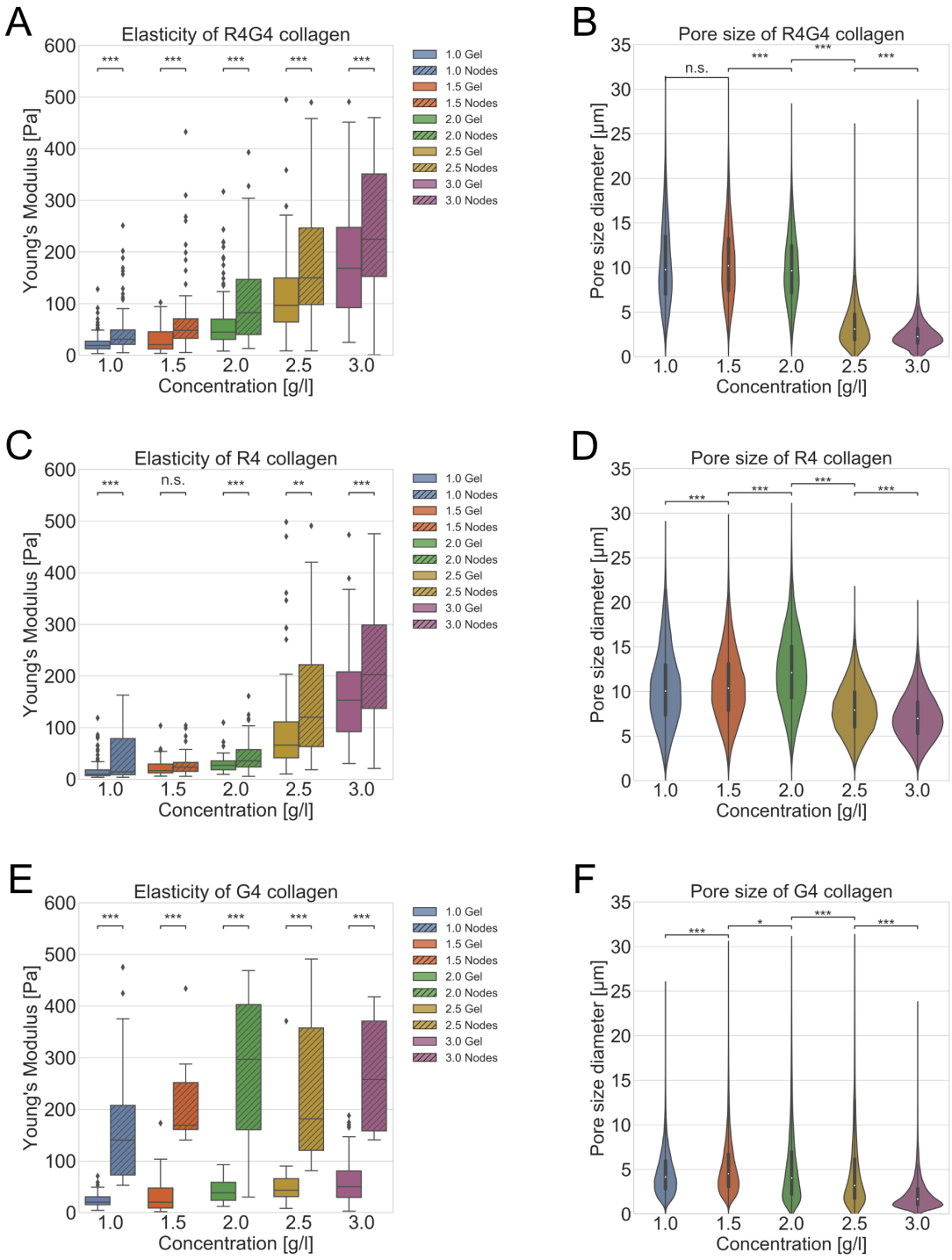

Figure 5.13: *A, C, E:* Stiffness measurements of different collagen compositions concerning the network stiffness and the stiffness of local inhomogenity, *B, D, F:* corresponding pore sizes of collagen networks

stiffness and reduces pore size what influence cancer cell invasion into these networks, illustrated in figure 5.13.

We found in consensus with [1] that collagen mixes with a concentration of 3 g/l and a median pore-size of around 2 µm and elastic modulus of around 200 Pa drastically promote migration and invasion of cancer cells. Softer networks with elastic modulus

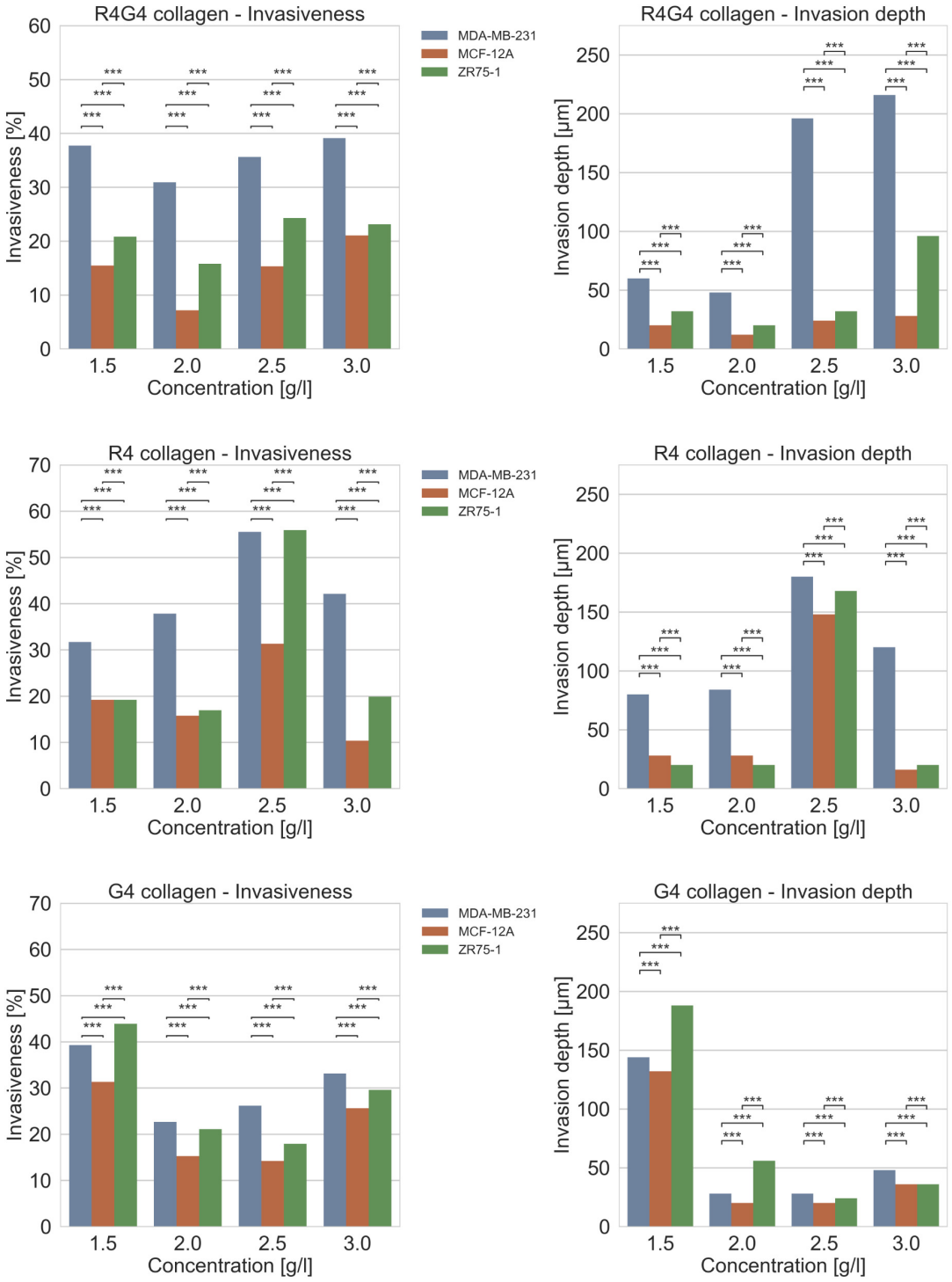

Figure 5.14: Cancer cell invasion into collagen networks with increased monomer concentration

of around 100 Pa with larger pores of around 7 µm promote migration and invasion of cancer cells into networks crafted solely from rat tail collagen, at a concentration of 2.5 g/l. The characteristics of these networks are similar to the findings of [2]. In case of bovine dermal collagen, the network structure is marked by large node-like structures. Due to this the promotion of cancer cell invasion is misaligned to a monomer

concentration of 1.5 g/l at which the parameters, like stiffness and pore size, are at comparable values.

Finally, our results show that 3D pore size and elastic modulus of the surrounding matrix are the driving factors of 3D cell migration and invasion. By mixing elongated fibril matrices from rat tail collagen and node-shaped scaffolds from bovine dermal collagen, we are able to adapt local inhomogeneity and matrix properties, without introducing other affecting parameters such as pH value, cross-linking proteins, etc., of in vivo ECM in biomimetic in vitro ECM models.

[1] T. Fischer et al.: Converg. Sci. Phys. Oncol. **3**, 044003 (2017) doi:10.1088/2057-1739/aa8bbb
[2] J. Sapudom et al.: Biomaterials **52**, 367 (2015) doi:10.1016/j.biomaterials.2015.02.022

5.5 Effect of Arp2/3 on 3D migration and cellular mechanical properties

S. Puder, C.T. Mierke

The migration of cells in 3D extracellular matrices (ECM) is regulated by the actin cytoskeleton. The actin related protein complex Arp2/3 facilitates nucleation and polymerization of new actin branches, which is supposed to impact cellular mechanical properties [1, 2]. The complex consist of 7 subunits whereas the two subfamilies Arp2 and Arp3 giving the complex its name [3–6]. Normally, the Arp2/3 complex is in an inactive state and is engaged by the so-called nucleation-promoting factor proteins (NPF) WASP and SCAR/WAVE [7, 8]. The activity of NPF's is regulated by the signaling-transduction pathways CDC42 and Rac [9]. In its active state, the complex initiate the formation of a new actin filament (daughter filament) that emerges from an existing mother filament in a y-branch configuration [8–10]. Interactions between Arp2/3 and mother and/ or daughter filament enable the disassembly of the branching and an inactivation of Arp2/3 [9], see figure 5.15.

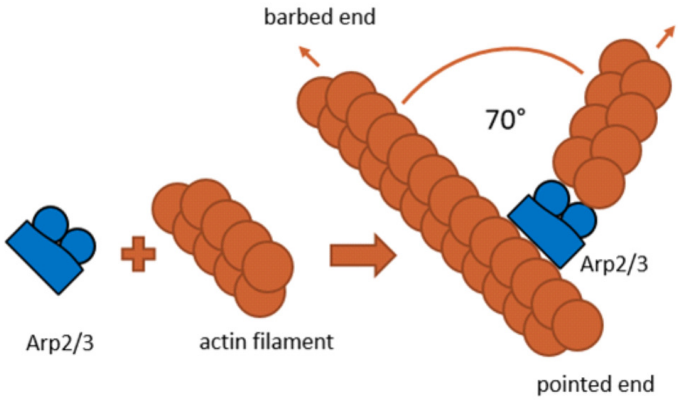

Figure 5.15: Schematic illustration of actin branching catalyzed by Arp2/3.

Actin filament nucleation and elongation catalyzed by the Arp2/3 complex has been implicated to be important for lamellipodia and filopodia initiation and formation. However, the importance of structures such as lamellipodia and filopodia for 3D motility and cellular mechanical properties are still not yet clear. We suggested that the Arp2/3 complex facilitates 3D motility into ECM by regulating cellular mechanical properties. Our study focuses on Arp3 conditional knock-down fibroblast cells induced by 2 µg/ml 4-OH-tamoxifen for at least 96 hours. Structural changes of the cytoskeleton were analyzed and acquired by a confocal laser scanning microscope (CLSM). Cells were fixated by paraformaldehyde and stained with phalloidin for actin and the nucleus was stained with Hoechst 33342 [11]. Arp3 knock-down cells show clear structural changes presented by an reduced branched actin network, showing straight and denser F-actin stress fibers.

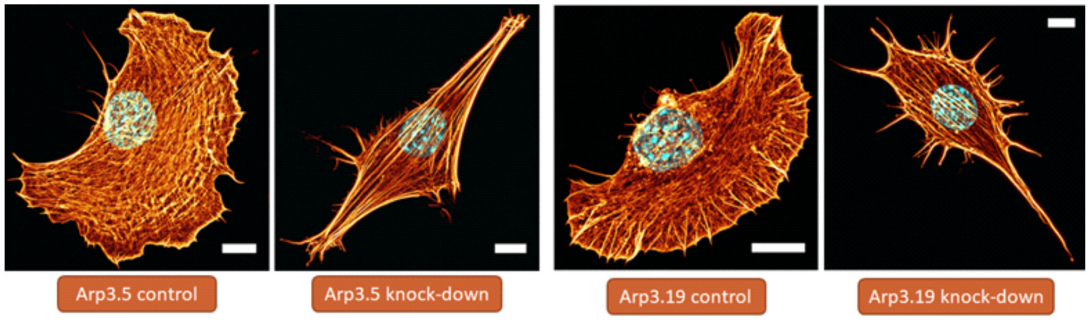

Figure 5.16: CLSM images (bar=10 µm) of control treated cells and Arp3 knock-down cells for two clones.

Cells were analyzed for their ability to migrate in dense 3D ECM. Therefore, we used well-established collagen networks consisting of 1/3 rat and 2/3 bovine collagen type I [11, 12]. The polymerized collagen mixture forms a structural network of collagen fibers and bundles. Cells were seeded on top of 1.5 g/l collagen networks and invaded for three days. Subsequently the percentage of invaded cells is analyzed [11]. The knock-down of Arp3 accompanies with a significant reduced invasiveness into 1.5 g/l dense collagen networks.

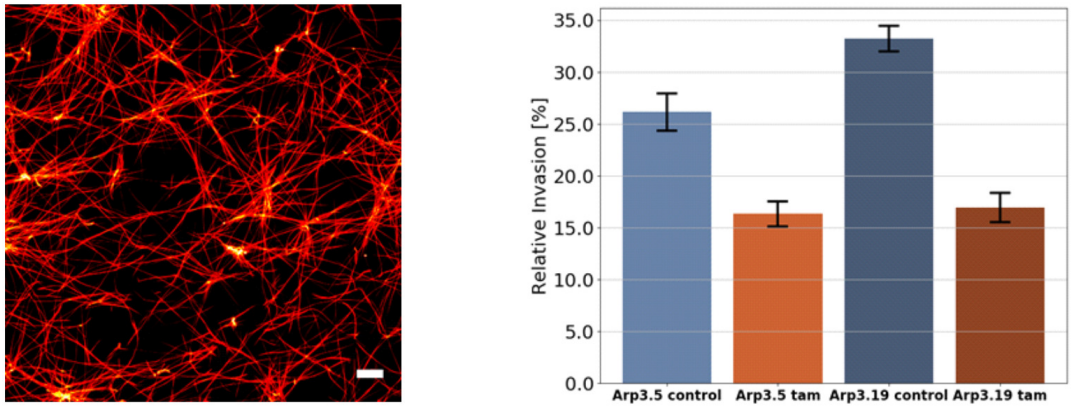

Figure 5.17: Representative image of 1.5 g/l collagen matrix (bar=10 µm) and relative cell invasion into 1.5 g/l dense collagen networks.

Mechanical properties of cells such as stiffness and contractile force generation have been demonstrated to regulate cell migration and invasion into 3D extracellular matrices [11, 13]. Cellular mechanical properties were quantified by an optical cell stretcher. A novel laser tool to observe viscoelastic behavior of suspended cells [14, 15]. A typical stress pattern of 800mW and 1200 mW was used. We determined the median creep deformation at the end of the stretch curve representing the maximal deformation. We found that Arp3 knock-down cells are less deformable (stiffer) compared to control treated cells.

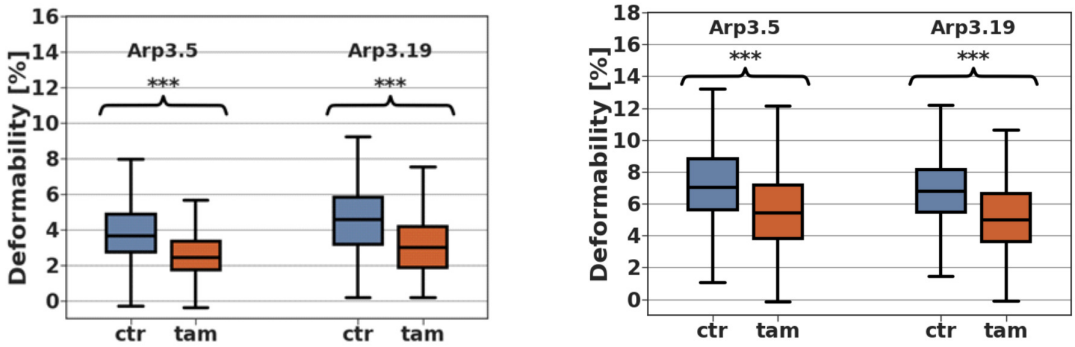

Figure 5.18: Cellular deformability of Arp3 knock-down cells for two different laser powers: 800 mW (left) and 1200 mW (right).

Further experiments consider the influence of the Arp2/3 complex on fibroblast cells. Cell permeable selective inhibitor CK869 was used to quantify results of ligand induced knock-down of Arp3. Cell migration and cellular mechanical properties under inhibition of Arp2/3 complex were analyzed as well as structural changes of the actin cytoskeleton. Cells were treated with 7.5 μM CK869 for 2 hours. Control cells treated with DMSO show a clear branched actin network, whereas inhibitor treated cells show straight actin filaments and a reduced branched actin network showing comparable results to our ligand induced Arp3 knock-down.

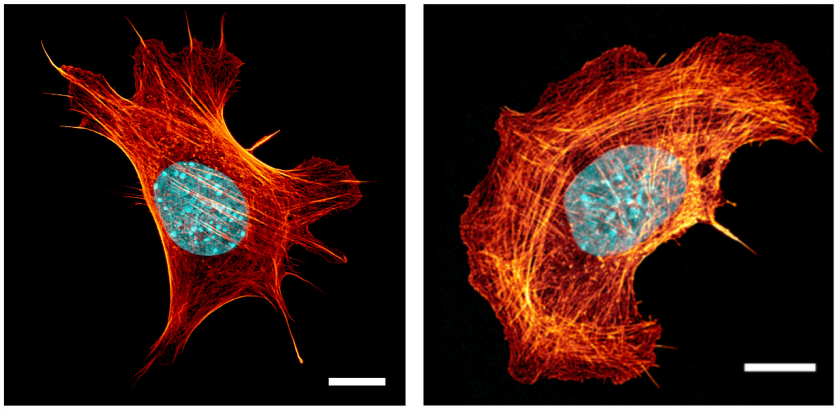

Figure 5.19: CLSM images (bar=10 μm) of control treated cells (left) and inhibitor treated cells (right) after 2 hours treatment with 7.5 μM CK869.

Cellular mechanical properties under inhibitor treatment show as well comparable results to the ligand induced knock-down of Arp3. We found that inhibitor treated

fibroblast cells are less deformable (stiffer) than control treated cells after 2 hours inhibitor treatment for both laser powers. Their migration ability into 3D collagen networks is as well reduced compared to control treated cells. Summarizing, both used methods showing comparable results for cellular mechanical properties and invasiveness.

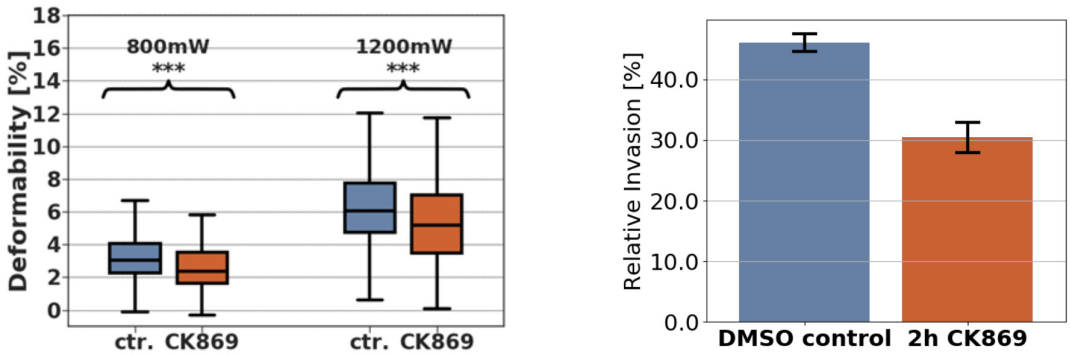

Figure 5.20: Cellular deformability of CK869 stimulated fibroblast cells for two different laser powers (left) and relative invasiveness into 1.5 g/l dense collagen networks (right).

In conclusion, Arp2/3 complex and its subunit Arp3 are essential for providing mechanical cellular stiffness regulating motility into 3D ECM. We demonstrated that Arp2/3 regulates cellular deformability, stiffness and transmission promoting Arp2/3-dependent cell invasion.

[1] J.G. Kiselar et al.: Proc. Natl. Acad. Sci. **104**, 1552 (2007) doi:10.1073/pnas.0605380104
[2] J. Pizzaro-Cerda et al.: Trends Cell Biol. **27**, 93 (2017) doi:10.1016/j.tcb.2016.08.001
[3] M. Carter et al.: *Guide to Research Techniques in Neuroscience*, 2nd Ed. (Elsevier, 2015)
[4] J.A. Cooper et al.: Cell **107**, 703 (2001) doi:10.1016/S0092-8674(01)00605-5
[5] K.J. Amann et al.: Proc. Natl. Acad. Sci. **97**, 15009 (2001) doi:10.1073/pnas.211556398
[6] L. Blanchoin et al.: Nature **404**, 1007 (2000) doi:10.1038/35010008
[7] L.M. Machesky et al.: Proc. Natl. Acad. Sci. **96**, 3739 (1999) doi:10.1073/pnas.96.7.3739
[8] B.A. Smith et al.: Proc. Natl. Acad. Sci. **110**, 1285 (2013) doi:10.1073/pnas.1211164110
[9] E.D. Goley et al.: Nat. Rev. Mol. Cell Bio. **7**, 713 (2006) doi:10.1038/nrm2026
[10] R.D. Mullins et al.: PNAS **95**, 6181 (1998) doi:10.1073/pnas.95.11.6181
[11] T. Kunschmann et al.: Biochim. Biophys. Acta **1864**, 580 (2016) doi:10.1016/j.bbamcr.2016.12.019
[12] T. Fischer et al.: Converg. Sci. Phys. Oncol. **3**, (2017) doi:10.1088/2057-1739/aa8bbb
[13] P. Friedl et al.: Cell Mol. Life Sci. **57**, 41 (2000) doi:10.1007/s000180050498
[14] J. Guck et al.: Phys. Rev. Lett. **84**, 5451 (2000) doi:10.1103/PhysRevLett.84.5451
[15] S. Pawlizak et al.: New J. Phys. **17**, (2015) doi:10.1088/1367-2630/17/8/083049

5.6 Deregulation (up and down) of myosin-II decreases the ability of cells to invade in artifical collagen matrices

T. Kunschmann, C.T. Mierke

Many publications have shown that myosin-II is crucial for the process of invasion [1] but it is still not clear if a upregulation of myosin enhances or reduces the ability to invade. We have shown that in myosin-II upregulated cell line (Rac1 -/-) a inhibition of myosin-II improves this ability. However, a further upregulation has no improved effect on the invasiveness. Moreover we showed that in a lower myosin-II expressed cell line (Rac1 fl/fl) the upregulation of myosin enhances the ability of cells to invade and the inhibition of myosin-II decreases it. Summarized we validated our hypothesis that there is a particular level of myosin-II which is optimal for the process of invasion.

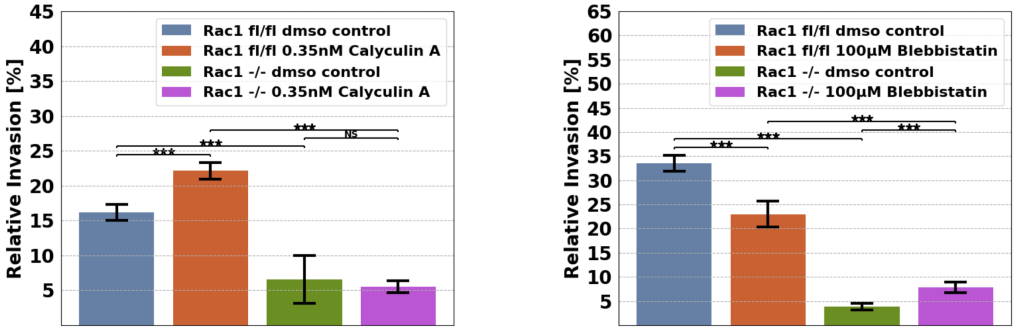

Figure 5.21: Invasiveness of myosin upregulated cell line (Rac1 -/-) and normal regulated cell line (Rac1 fl/fl) in presence of 100 µM Blebbistatin (myosin-II inhibition) and 0.35nM Calyculin A (myosin-II enhancer) respectively.

[1] J.B. Wyckoff et al.: Curr. Biol. **16**, 1515 (2006) doi:10.1016/j.cub.2006.05.065
[2] C. Beadle et al.: Mol. Biol. Cell **19**, 3179 (2008) doi:10.1091/mbc.e08-03-0319

5.7 The influence of Rac1 on motility into 3D extracellular matrices and mechanical properties

T. Kunschmann, C.T. Mierke

The migration and invasion of cell is a fundamental process regulating healthy functions such as the cell's regeneration and disease processes such as cancer as well as deregulation of wound healing events [1, 2] and Alzheimer disease [3]. Rac proteins such as Rac1 induce formation of lamellipodia and membrane ruffles [4, 5], but this is not unique to Rac, instead also other Rho proteins like the Rac-related Cdc42 and RhoG may induces lamellipodia structures [6]. The formation of lamellipodia has been shown to play a crucial role for motility in 2D. However, the importance of the structures such as lamellipodia for mechanical properties and 3D motility of cells is still yet not clear.

Hence, we suggested that Rac1 affects cellular mechanical properties and facilitates the invasion in 3D microenvironments.

The WAVE complex is found at high concentration at the leading edge of the lamellipodia [7, 8] and is a direct activation target of the Rho GTPase Rac1 [9, 10]. Moreover, Rac1 is and important upstream regulator of actin polymerization adn acto-myosin contractility that connects outside signals evoked by cell adhesion, chemokine and/or receptor tyrosine kinases to cytoskeletal acto-myosin dynamics [11–13]. Thus, Rac1 seems to control mechanosensory cell functions such as cell adhesion, cellular polarity and contractility. However, it is still controversial discussed how the suppression of lamellipodia formation affects cell motility and migration efficiency in 3D extracellular matrices [14, 15]. Moreover, even the effect of Rac1 expression on the cellular mechanical properties such as cellular deformability (or stiffness) is still not investigated yet.

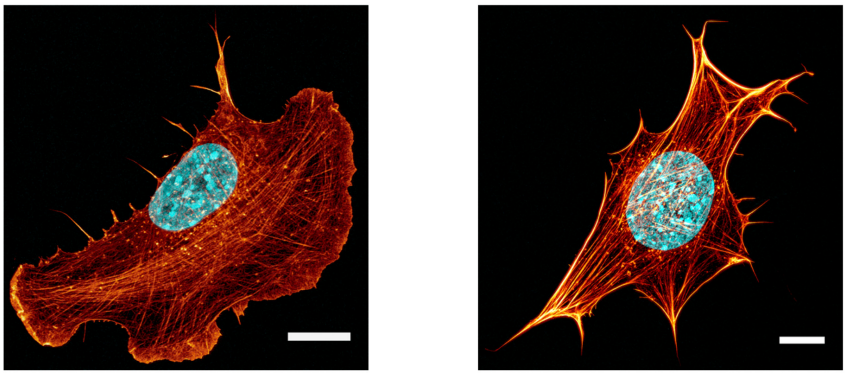

Figure 5.22: Confocal images of Rac1 fl/fl (left) and Rac1 -/- (right) stained with Hoechst 33342 (nucleus, cyan) and Phalloidin Alexa Fluor 546 (actin, red). Rac1 -/- cells lack of lamellipodia and show pronounced stress fibers compared to Rac1 fl/fl. (bar = 10 μm)

Measuring the cell motility in 3D, we used a invasion assay consisting of a artificial matrix made of two third type 1 rat collagen and one third type 1 bovine collagen. The cells were seeded on top of the collagen surfaces and invaded for 3 days into the matrix. The nucleus was stained with Hoechst 33342 and automatically recorded and detected with a custom made software. Rac1 -/- mouse fibroblasts of five different clones showed a drastically decreased. Additionally not only the ability to invaded into a collagen matrix was reduced, also the velocity was significant lowered.

Investigating the mechanical impact of Rac1, we used the optical stretcher and showed that Rac1 -/- causes a pronounced softening effect compared to Rac1 fl/fl (control) cells.

We showed that the mechanical alternation of Rac1 deficient cells can be reproduced in Rac1 fl/fl cells using the Rac1 inhibitor EHT1864. However, the inhibitor has a small working range in which the softening effects of Rac1 inhibition dominates the contrary side effect.

Rac1 inhibited cells showed also a lack of lamellipodia after cultivation in 35 μM EHT1864 for 2hours using confocal laser microscopy.

Additionally the ability to invade in a artificial collagen matrix was drastically reduced in Rac1 fl/fl cells using the EHT1864 inhibitor. This result is consistent with invasion assays of Rac1 deficient cells.

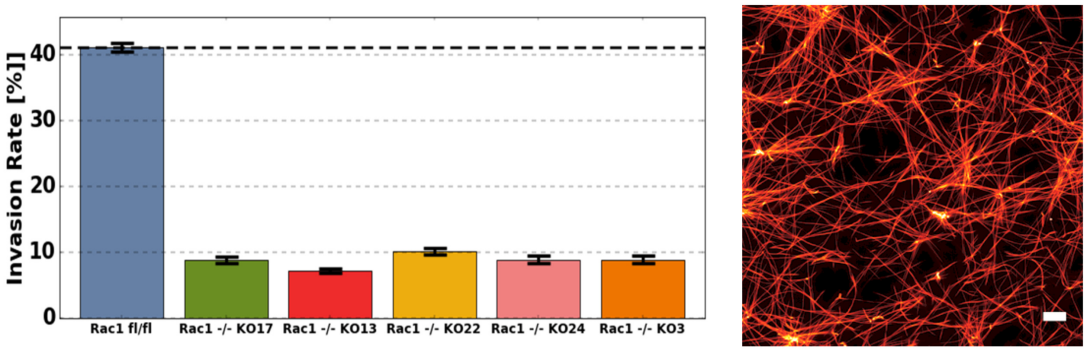

Figure 5.23: Invasion rates of Rac1 fl/fl and five different knock out in a 1.5 g/l RG-collagen matrix after 3 days (left) and Tamra stained collagen network (right)

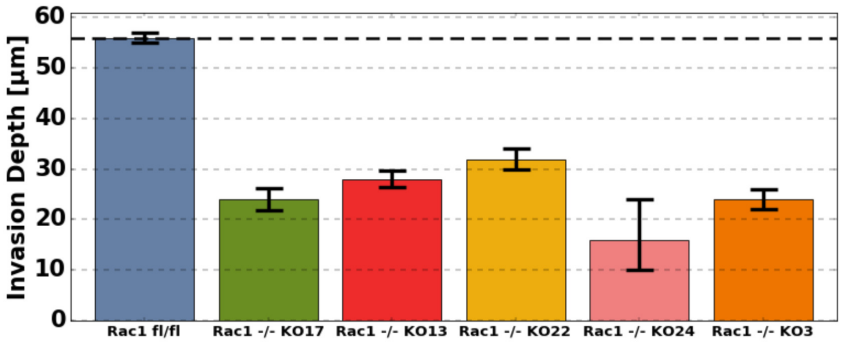

Figure 5.24: Invasion rates of Rac1 fl/fl and five different knock out in a 1.5 g/l RG-collagen matrix after 3 days (left), invasion schematic (right top) and Tamra stained collagen network (right bottom)

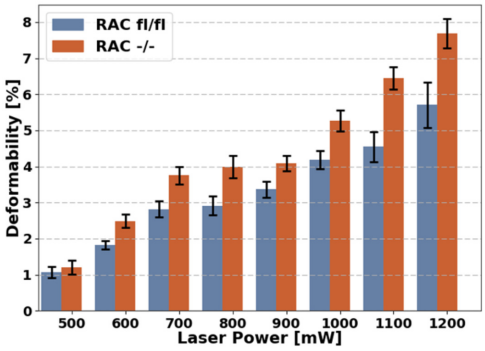

Figure 5.25: Maximal creep deformation after applying two seconds high laser power. Rac1 -/- cells showed a mechanical alternation compared to the Rac1 fl/fl cells over a wide range of forces.

[1] A.J. Ridley et al.: Science **302**, 1704 (2003) doi:10.1126/science.1092053
[2] P. Friedl et al.: Nature Immunology **9**, 960 (2008) doi:10.1038/ni.f.212
[3] L. Desire et al.: J. Biol. Chem. **280**, 37516 (2005) doi:10.1074/jbc.M507913200
[4] A.J. Ridley et al.: Cell **70**, 401 (1992) doi:10.1016/0092-8674(92)90164-8
[5] C.D. Nobes et al.: Cell **81**, 53 (1997) doi:10.1016/0092-8674(95)90370-4
[6] P. Aspenström et al.: Biochem J. **377**, 1552 (2004) doi:10.1042/BJ20031041
[7] P. Hahne et al.: FEBS Letters **492**, 1873 (2001) doi:10.1016/S0014-5793(01)02239-6

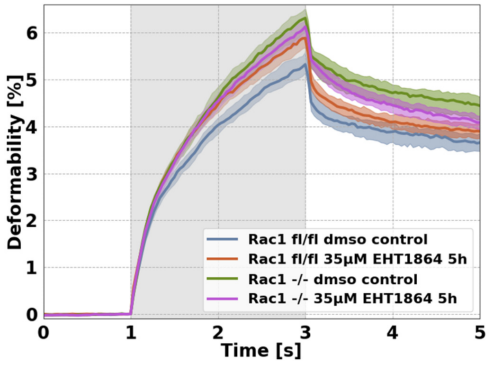

Figure 5.26: Creep curves (800 mW, gray area) of Rac1 fl/fl and Rac1 -/- cells using 35 µM EHT1864 for 5 hours. Rac1 deficient cells showed a small hardening effect which increases with drug concentration (data now shown). The underlying reason of this hardening effect is still unkown yet.

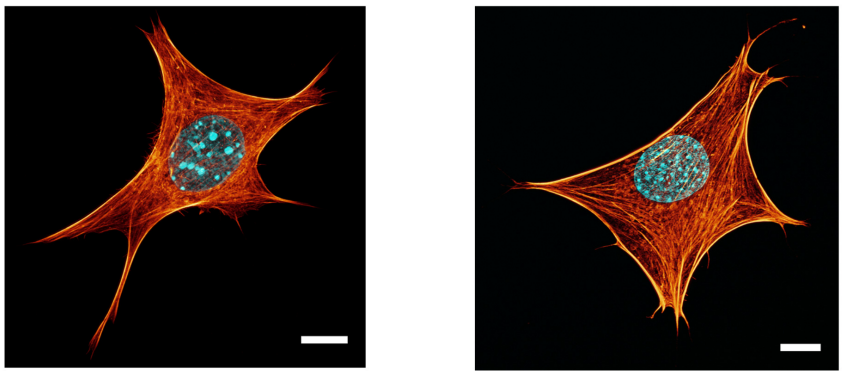

Figure 5.27: Rac1 fl/fl cells (left) treated with 35 µM EHT1864 for 2 hours and Rac1 -/- cell (right). Rac1 fl/fl cells lack of lamellipodia after the treatment.

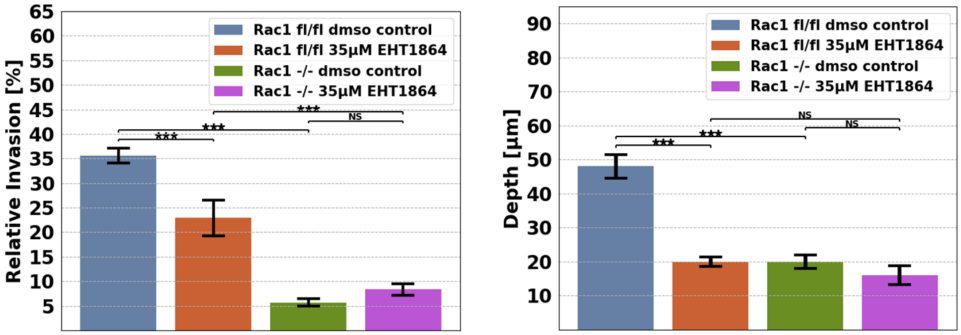

Figure 5.28: Invasion rate of Rac1 fl/fl and Rac1 -/- (left) and invasion depth (right) with 35 µM EHT1864 and dmso control in a 1.5 g/l RG-collagen matrix. EHT1864 had no significant effect on Rac1 deficient cells, however the invasion rate as well as the invasion depth of Rac1 fl/fl cells was significant decreased with EHT1864.

[8] M.Rehmsmeier et al.: RNA **10**, 1507 (2004) doi:10.1261/rna.5248604
[9] A.M. Ismail et al.: Nat. Struct. Mol. Biol. **16**, 561 (2009) doi:doi:10.1038/nsmb.1587
[10] A.M. Lebensohn et al.: Mol. Cell **36**, 512 (2009) doi:10.1016/j.molcel.2009.10.024
[11] A.J. Ridley et al.: Cell **145**, 1012 (2011) doi:10.1016/j.cell.2011.06.010

[12] A.A. Khali et al.: Integr. Biol. **2**, 568 (2010) doi:10.1039/C0IB00052C
[13] R.J. Buchsbaum et al.: J. Cell Sci. **120**, 1149 (2007) doi:10.1242/jcs.03428
[14] P. Suraneni et al.:J . Cell Biol. **217**, x (2018) doi:10.1083/jcb.201112113
[15] A. Wu et al.: Neural Netw. **36**, 1 (2012) doi:10.1016/j.neunet.2012.08.009

5.8 Impact of Rac1 on acto-myosin cortex contractility and mechanical changes due to myosin-II activity in suspended cells

T. Kunschmann, C.T. Mierke

It is known that myosin-II has a softening effect in actin networks in vitro [1]. Recently it was shown that myosin-II has also a influence on cellular stiffness in suspended mouse fibroblasts and cancer cells [2]. Moreover it was found that Rac1 regulates the contractility of smooth muscle cells from rats [3]. We were able to connect these statements and showed that Rac1 is responsible for myosin-II activity in the actin cortex of suspended non muscle cells. This deregulation causes a mechanical alternation which mainly depends on myosin-II. Additionally we showed that the stiffening effect of myosin inhibition occurs also in human non-cancer cell line MCF10A. We also showed that a upregulation of myosin-II causes a contrary effect (softening) which is consistent to the results of artificial actin networks crosslinked with myosin-II in vitro [1]. There is also some evidence that the cytoskeletal changes in Rac1 deficient cells (missing lamellipodia, pronounced stress fibers) are compensated by microtubule or intermediate filaments. The stiffening effect due to myosin inhibition can be seen for all cell lines and is shown in figure 5.30.

As seen in figure 5.29, one can observe that Rac1 -/- cells show a higher slope in relaxation phase, especially the passive relaxation is less present.

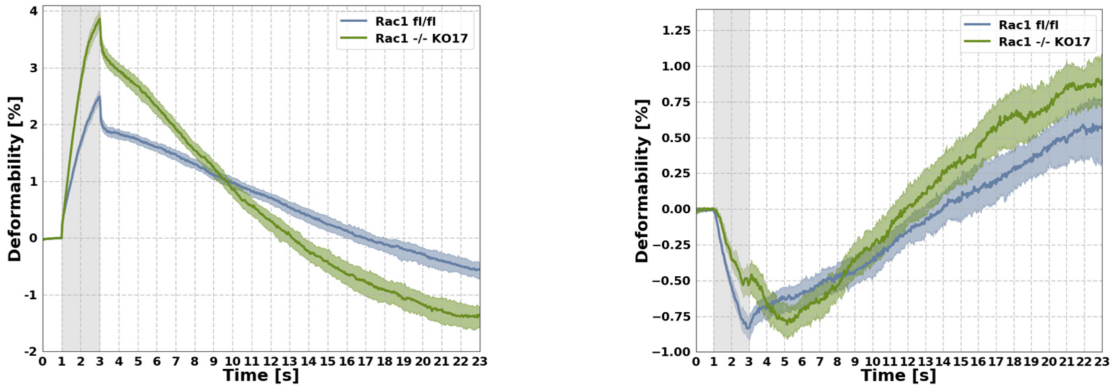

Figure 5.29: Creep curves (800 mW, gray area) of MCF10A after 2hours treatment in adherent state with Calyculin A and Blebbistatin and finally added drug in suspension. On the left side, the longaxis (cellular axis parallel to the beam axis) is shown and on the right side the shortaxis (cellular axis perpendicular to the beam axis) is shown.

In figure 5.30 it can be seen that myosin-II inhibition (Blebbistatin) as well as myosin-II enhancing (Calyculin A) leads to a stiffening and softening effect, respectively. Furthermore we showed that the alternation of mechanical properties due to myosin activity exists also for human non-cancer non-muscle cells. We showed also, that the actin-cortex contractility is mainly driven by myosin-II in non-muscle cells. The underlying reason the mechanical alternation caused by myosin-II is still not clear and is currently investigated. We showed that mechanical alternation due to lack of Rac1 is mainly caused due to myosin-II overregulation. Similar data were measured with Y27632 and ML7 (data not shown).

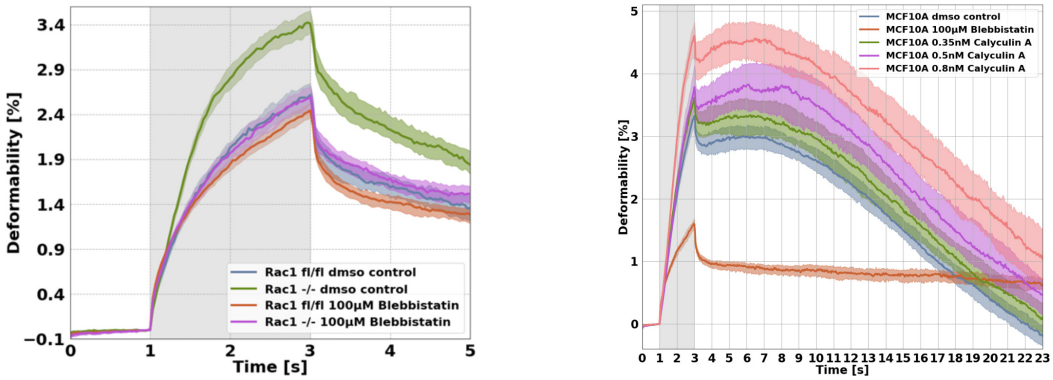

Figure 5.30: *Left:* Creep curves (800 mW, gray area) of Rac1 fl/fl and Rac1 -/- cells after treatment with 100 µM Blebbistatin in adherent state and added drug in suspension, *right:* Creep curves (800 mW, gray area) of MCF10A after 2hours treatment in adherent state with Calyculin A and Blebbistatin and finally added drug in suspension.

We showed that the effect of Latrunculin A is much larger on Rac1 fl/fl than on Rac1 -/- cells, see figure 5.31. Consequently, the actin is altered due to missing Rac1 but the overall effect of the cytoskeleton on the cellular mechanic seems to be compensated by other cytoskeletal components, e.g. microtubules or intermediare filaments. The involvement of other motor proteins were excluded by measuring both cell lines in Ca2+ / Mg2+ free PBS which blocks or at least reduces the activity of all calcium or magnesium driven motor proteins.

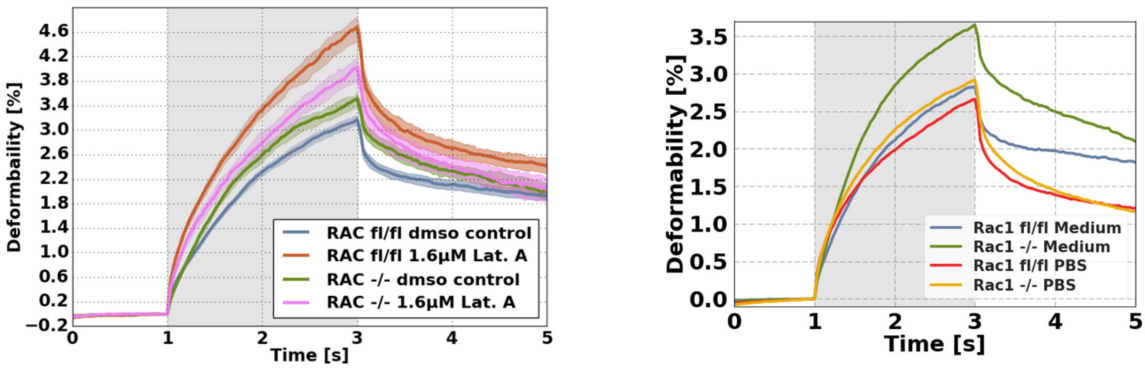

Figure 5.31: Creep curves (800 mW) of Rac1 fl/fl and Rac1 -/- cells after treatment with 1.6 µM Latrunculin A.

[1] D. Humphrey et al.: Nature **416**, 413 (2002) doi:10.1038/416413a
[2] C.J. Chan et al.: Biophys. J. **108**, 1856 (2015) doi:10.1016/j.bpj.2015.03.009
[3] K. Shibata et al.: J. Cell. Physiol. **230**, 1352 (2015) doi:10.1002/jcp.24878

5.9 Funding

Blebbing Driven or Actin Protrusive-Force Driven Cancer Cell Migration
C.T. Mierke, J.A. Käs
DFG-MI1211/18-1

Scientific Device: Confocal Scanning Microscope with Magnetic Tweezer Device and Life Cell Imaging
C.T. Mierke
DFG-INST 268/357-1

Optical Cell Stretcher und Dual Magnetic Tweezer Cell Cluster Device: Korrelative mechanische und molekulare Zell-Zell-Wechselwirkung in Geweben und Gewebemodellen für neue Ansätze in Diagnostik und Therapie
C.T. Mierke, J.A. Käs
ESF/SAB No. 100299919

5.10 Organizational Duties

C.T. Mierke

- Referee: Cancer Research, Journal of Cell Science, Advanced Biomaterials, Acta Biomaterials, British Journal of Cancer, Journal of Pharmacy and Pharmacology, Molecular Vision, International Journal of Nanomedicine, Plos One, Eur. J. Biophysics
- Special Issue Guest Editor for Physical Biology

5.11 External Cooperations

Academic

- University of Leipzig, Center for Biotechnology and Biomedicine (BBZ), Germany
  Prof. Dr. Andrea A. Robitzki
- Department of Paediatric Kidney, Liver and Metabolic Diseases, Hannover Medical School, Germany
  Dr. Wolfgang H. Ziegler
- GBF, National Research Center for Biotechnolog, Dept of Cell Biology, Germany
  Prof. Dr. Klemens Rottner
- Philipps-University Marburg, Department of Neurosurgery, Germany
  Prof. Dr. J.W. Bartsch

5.12 Publications

Journals

T. Kunschmann, S. Puder, T. Fischer, J. Perez, N. Wilharm, C.T. Mierke: *Integrin-linked kinase regulates cellular mechanics facilitating the motility in 3D extracellular matrices*, Biochim. Biophys. Acta BBA - Mol. Cell Res. **1864**, 580 (2017)
doi:10.1016/j.bbamcr.2016.12.019

C.T. Mierke, T. Fischer, S. Puder, T. Kunschmann, B. Soetje, W.H. Ziegler: *Focal adhesion kinase activity is required for actomyosin contractility-based invasion of cells into dense 3D matrices*, Sci. Rep. **7**, 42780 (2017)
doi:10.1038/srep42780

T. Fischer, N. Wilharm, A. Hayn, C.T. Mierke: *Matrix and cellular mechanical properties are the driving factors for facilitating human cancer cell motility into 3D engineered matrices*, Converg. Sci. Phys. Oncol. **3**, 044003 (2017)
doi:10.1088/2057-1739/aa8bbb

C.T. Mierke, F. Sauer, S. Grosser, S. Puder, T. Fischer, J.A. Käs: *The two faces of enhanced stroma: Stroma acts as a tumor promoter and a steric obstacle*, NMR Biomed., e3831 (2017)
doi:10.1002/nbm.3831

C.T. Mierke: *Physical role of nuclear and cytoskeletal confinements in cell migration mode selection and switching*, AIMS Biophys. **4**, 615 (2017)
doi:10.3934/biophy.2017.4.615

Posters

S. Puder, T. Kunschmann, T. Fischer, J.A. Käs, C.T. Mierke: *Down regulation of Arp2/3 complex affects cellular mechanics and motility into 3D extracellular matrices*, Soft Matter Day, Leipzig (23.06.2017)

T. Fischer, A. Hayn, S. Puder, T. Kunschmann, C.T. Mierke: *Focal adhesion kinase activity is required for actomyosin contractility-based invasion of cells into dense 3D matrices*, Soft Matter Day, Leipzig (23.06.2017)

S. Grosser, F. Sauer, J.A. Käs, C.T. Mierke: *Intricate features of cancer cell migration revealed by collagen live invasion assays*, Physics of Cancer, Leipzig (4.–6.10.2017)

II

Felix Bloch Institute for Solid State Physics

6

Magnetic Resonance of Complex Quantum Solids

6.1 Introduction

The electronic properties of quantum solids in which the electrons exhibit strong correlations with each other or with the lattice are particularly rich and will be of special importance in future functional materials. In addition, such solids are challenging for experiment, as well as theory, as the more than twenty five-year history of high-temperature superconductivity shows: we still do not understand the electronic structure of these systems. One particular aspect of strongly correlated electronic materials is their tendency towards nano-scale electronic phase separation. Even in perfect lattices, electronic nano-structures can form. The investigation of such materials requires the use of methods that can give detailed information. Here, magnetic resonance, on nuclei and electrons, is of particular interest as they not only have atomic scale resolution, but also yield bulk information in contrast to surface techniques. We explore the properties of these materials with tailored new techniques at the frontiers of magnetic resonance. For example, we are the leading laboratory when it comes to NMR at highest pressures and magnetic fields.

Jürgen Haase

6.2 Contrasting Phenomenology of NMR Shifts in Cuprate Superconductors

J. Haase, M. Jurkutat, J. Kohlrautz

Nuclear magnetic resonance (NMR) shifts, if stripped of their uncertainties, must hold key information about the electronic fluid in the cuprates. The early shift interpretation that favored a single-fluid scenario will be reviewed, as well as recent experiments that reported its failure. Thereafter, based on literature shift data for planar Cu, a contrasting shift phenomenology for cuprate superconductors is developed, which is very different from the early view while being in agreement with all published data. For example, it will be shown that the hyperfine scenario used up to now is

inadequate as a large isotropic shift component is discovered. Furthermore, the changes of the temperature dependences of the shifts above and below the superconducting transitions temperature proceed according to a few rules that were not discussed before. It appears that there can be substantial spin shift at the lowest temperature if the magnetic field is perpendicular to the CuO_2 plane, which points to a localization of spin in the $3d(x^2\text{-}y^2)$ orbital. A simple model is presented based on the most fundamental findings. The analysis must have new consequences for theory of the cuprates.

6.3 Different Efficiency of Zn^{2+} and ZnO Species for Methane Activation on Zn-Modified Zeolite

A.A. Gabrienko*, S.S. Arzumanov*, A.V. Toktarev*, I.G. Danilova*, I.P. Prosvirin*, D. Freude, V.V. Kriventsov*, V.I. Zaikovskii†, A.G. Stepanov†

*Boreskov Institute of Catalysis, Siberian Branch of the Russian Academy of Sciences, Novosibirsk, Russia
†Novosibirsk State University, Russia

Understanding methane activation pathways on Zn-modified high-silica zeolites (ZSM-5, BEA) is of particular importance because of the possibility of methane involvement in coaromatization with higher alkanes on this type of zeolites. Herein, two samples of Zn-modified zeolite BEA containing exclusively either small zinc oxide clusters or isolated Zn^{2+} cations have been synthesized and thoroughly characterized by a range of spectroscopic methods (^{1}H MAS NMR, DRIFTS, XPS, EXAFS, HRTEM) to show that only one of the Zn-species, either Zn^{2+} cations or ZnO small clusters, exists in the void of zeolite pores. The ability of zinc sites of different nature to promote the activation of methane C-H bond with the zeolite Brønsted acid sites (BAS) has been examined in the reactions of methane H/D hydrogen exchange with BAS and the alkylation of benzene with methane. It has been found that both ZnO and Zn^{2+} species promote the reaction of H/D exchange of methane with BAS. The rate of H/D exchange is higher by 2 and 3 orders of magnitude for the zeolite loaded with ZnO or Zn^{2+} species, respectively, compared to pure acid-form zeolite H-BEA. So, the promoting effect of Zn^{2+} cations is more profound than that of ZnO species for H/D exchange reaction (Figure 6.1). This implies that the synergistic effect of Zn-sites and BAS for C-H bond activation in methane is significantly higher for Zn^{2+} cations compared to small ZnO clusters. It has been revealed, however, that only Zn^{2+} cations promote the alkylation of benzene with methane, whereas ZnO species do not. The isolated Zn^{2+} cations provide the formation of zinc-methyl species, which are further transformed to zinc-methoxy species. The latter is the key intermediate for the performance of the alkylation reaction. Hence, while both zinc oxide clusters and Zn^{2+} cationic species are able to provide a synergistic effect for the activation of C-H bonds of methane displayed by the dramatic acceleration of H/D exchange reaction, only the Zn^{2+} cationic species perform methane activation toward the alkylation of benzene with methane. This implies that only the Zn^{2+} cations in Zn-modified zeolite can activate methane for the reaction of methane coaromatization with higher alkanes.

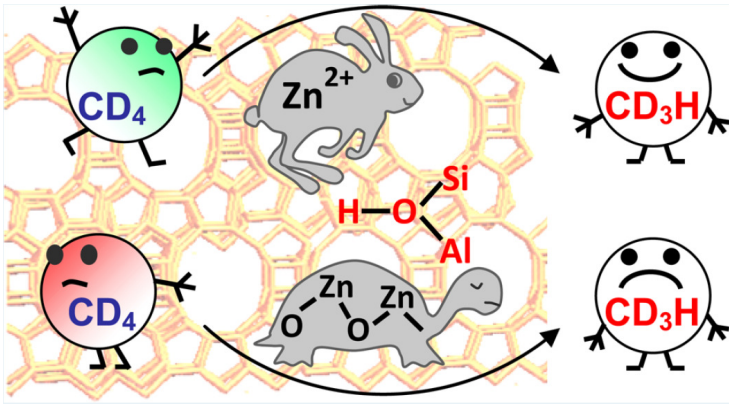

Figure 6.1: Methane activation in Zn-modified zeolites is preferably promoted by Zn^{2+} ions rather than ZnO species.

6.4 The importance of specific surface area in the geopolymerization of heated illitic clay

J. Dietel*, L.N. Warr*, M. Bertmer, A. Steudel†, G.H. Grathoff*, K. Emmerich†

*University of Greifswald, Institute of Geography and Geology, Greifswald, Germany
†Competence Center for Material Moisture and Institute for Functional Interfaces, Karlsruhe Institute of Technology, Eggenstein-Leopoldshafen, Germany

Geopolymers are inorganic binders formed by adding alkaline (hydroxide) solution to silicates such as blast furnace slag, fly ash or calcined clay to dissolve Si and Al that polymerizes and precipitates while hardening. The most common clay used as geopolymer raw material is kaolin. The aim of this study was to investigate the suitability of clays dominated by 2:1 dioctahedral layer silicates using the example of Friedland clay as a cheaper alternative to kaolin and determine the necessary preparation steps required to produce an effective geopolymer binder material. After a Rietveld-based quantification of the rawclay, the successive thermalmodifications of the mineral phases were analyzed using simultaneous thermal analysis coupled with mass spectrometer (STA-MS), temperature-resolved X-ray diffraction (TXRD), and ^{27}Al solid-state nuclear magnetic resonance spectroscopy (NMR)measurements. Friedland clay heated to 875 °C was found to produce a geopolymer with the highest compressive strength, but in contrast to the literature, the Si:Al ratio and the amount of 5-fold coordinated Al were not found to be the key parameters that determined the success of geopolymer synthesis. The specific surface area and the amount of Si and Al dissolved are here reported to be the key factors determining the suitability of clays dominated by 2:1 dioctahedral layer silicates as raw materials for geopolymer production.

6.5 An Untrodden Path: Versatile Fabrication of Self-Supporting Polymer-Stabilized Percolation Membranes (PSPMs) for Gas Separation

S. Friebe*, A. Mundstock*, D. Schneider, J. Caro*

*Leibniz University Hannover, Institute of Physical Chemistry and Electrochemistry, Hannover (Germany)

The preparation and scalability of zeolite or metal organic framework (MOF) membranes remains a major challenge, and thus prevents the application of these materials in large-scale gas separation. Additionally, several zeolite or MOF materials are quite difficult or nearly impossible to grow as defect-free layers, and require expensive macroporous ceramic or polymer supports. Here, we present new self-supporting zeolite and MOF composite membranes, called Polymer-Stabilized Percolation Membranes (PSPMs) (Figure 6.2), consisting of a pressed gas selective percolation network (in our case ZIF-8, NaX and MIL-140) and a gas-impermeable infiltrated epoxy resin for cohesion. We demonstrate the performance of these PSPMs by separating binary mixtures of H_2/CO_2 and H_2/CH_4. We report the brickwork-like architecture featuring selective percolation pathways and the polymer as a stabilizer, compare the mechanical stability of said membranes with competing materials, and give an outlook on how economic these membranes may become.

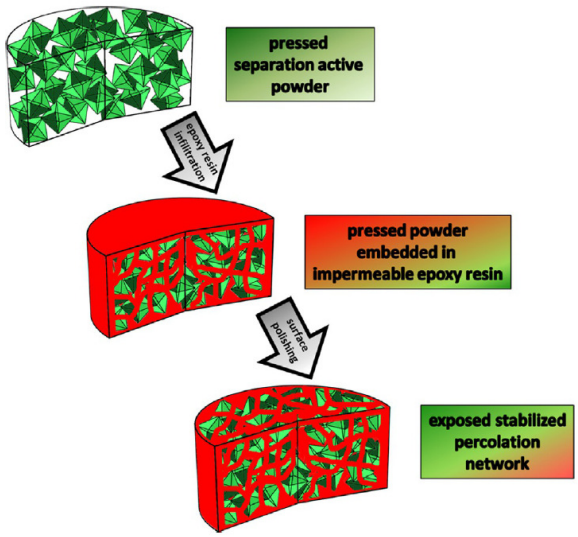

Figure 6.2: Schematic representation of the fabrication process of the PSPMs from the synthesized powders.

6.6 Structure-correlated diffusion anisotropy in nanoporous channel networks by Monte Carlo simulations and percolation theory

D. Kondrashova*, R. Valiullin, J. Kärger, A. Bunde*

*Institut für Theoretische Physik, Justus-Liebig-Universität Giessen, Giessen, Germany

Nanoporous silicon consisting of tubular pores imbedded in a silicon matrix has found many technological applications and provides a useful model system for studying phase transitions under confinement. Recently, a model for mass transfer in these materials has been elaborated, which assumes that adjacent channels can be connected by 'bridges' (with probability p_{bridge}) which allows diffusion perpendicular to the channels. Along the channels, diffusion can be slowed down by 'necks' which occur with probability p_{neck}. We use Monte-Carlo simulations to study diffusion along the channels and perpendicular to them, as a function of p_{bridge} and p_{neck}, and find remarkable correlations between the diffusivities in longitudinal and radial directions. For clarifying the diffusivity in radial direction, which is governed by the concentration of bridges, we applied percolation theory. We determine analytically how the critical concentration of bridges depends on the size of the system and show that it approaches zero in the thermodynamic limit. Our analysis suggests that the critical properties of the model, including the diffusivity in radial direction, are in the universality class of two-dimensional lattice percolation, which is confirmed by our numerical study.

6.7 Anomalous longitudinal relaxation of nuclear spins in CaF_2

C.M. Kropf*, J. Kohlrautz, J. Haase, B.V. Fine†

*Institute of Physics, University of Freiburg, Freiburg, Germany
†Skolkovo Institute of Science and Technology, Skolkovo Russia,
and Institute for Theoretical Physics, University of Heidelberg, Heidelberg, Germany

We consider the effect of non-secular resonances for interacting nuclear spins in solids which were predicted theoretically to exist in the presence of strong static and strong radiofrequency magnetic fields. These resonances imply corrections to the standard secular approximation for the nuclear spin-spin interaction in solids, which, in turn, should lead to an anomalous longitudinal relaxation in nuclear magnetic resonance experiments. We investigate the feasibility of the experimental observation of this anomalous longitudinal relaxation in calcium fluoride (CaF_2) and conclude that such an observation is realistic.

6.8 Influence of organic chemicals on aliphatic crystallites analyzed in whole soils

P. Ondruch*, A. Jäger, J. Kucerik*, M. Bertmer, G.E. Schaumann*

*University of Koblenz-Landau, Institute for Environmental Sciences, Workgroup of Environmental and Soil Chemistry, Landau, Germany

Crystalline aliphatic moieties in soil organic matter (SOM) have been under intensive investigation, but it is still unknown how they interact with organic chemicals in the unfractionated SOM. Our objective was to understand the changes in properties of soil aliphatic crystallites when being in contact with organic chemicals. For this, we treated an organic (sapric histosol) and a mineral soil (gleyic podzol) with phenol and naphthalene dissolved in different solvents. The crystallites were characterized in the unfractionated soil by their melting temperatures determined by differential scanning calorimetry (DSC) and by ^{13}C CPMAS NMR spectra from the trans (33.0 ppm) and gauche (30.0 ppm) signals. DSC identified two distinct types of crystalline domains differing in melting temperatures. Their reaction on solvent treatment and spiking allowed for the first time new insights into the nature of these domains in the unfractionated soil samples. Melting temperature and relative crystallinity were generally reduced by the presence of organic chemicals and solvent treatment, but in different way for each domain type. Thus, the domain types differ from each other in chemical nature. The domains melting at 68-75 °C (sapric histosol) responded similar to biopolymer residues and may originate from higher plants, while those melting at 82-93 °C (sapric histosol) and at 76-80 °C (gleyic podzol) responded similarly to lipids and are speculated to be of microbiological origin. These findings open new perspectives for the mechanistic analysis of sorption processes in soil. Aliphatic crystalline domains may have been underestimatedwith respect to their qualitative relevance for sorption processes in soil.

6.9 Hydrides of Alkaline Earth–Tetrel (AeTt) Zintl Phases: Covalent Tt–H Bonds from Silicon to Tin

H. Auer*, R. Guehne, M. Bertmer, S. Weber*, P. Wenderoth†, T.C. Hansen‡, J. Haase, H. Kohlmann*

*Department of Inorganic Chemistry, Leipzig University, Leipzig, Germany
†Department of Inorganic Solid-State Chemistry, Saarland University, Saarbrücken, Germany
‡Institut Laue-Langevin, Grenoble, France

Zintl phases form hydrides either by incorporating hydride anions (interstitial hydrides) or by covalent bonding of H to the polyanion (polyanionic hydrides), which yields a variety of different compositions and bonding situations. Hydrides (deuterides) of SrGe, BaSi, and BaSn were prepared by hydrogenation (deuteration) of the CrB-type Zintl phases AeTt and characterized by laboratory X-ray, synchrotron, and neutron diffraction, NMR spectroscopy (Figure 6.3), and quantum-chemical calculations. $SrGeD_{4/3-x}$ and $BaSnD_{4/3-x}$ show condensed boatlike six-membered rings of Tt

atoms, formed by joining three of the zigzag chains contained in the Zintl phase. These new polyanionic motifs are terminated by covalently bound H atoms with d(Ge-D) = 1.521(9) Å and d(Sn-D) = 1.858(8) Å. Additional hydride anions are located in Ae_4 tetrahedra; thus, the features of both interstitial hydrides and polyanionic hydrides are represented. $BaSiD_{2-x}$ retains the zigzag Si chain as in the parent Zintl phase, but in the hydride (deuteride), it is terminated by H (D) atoms, thus forming a linear (SiD) chain with d(Si-D) = 1.641(5) Å.

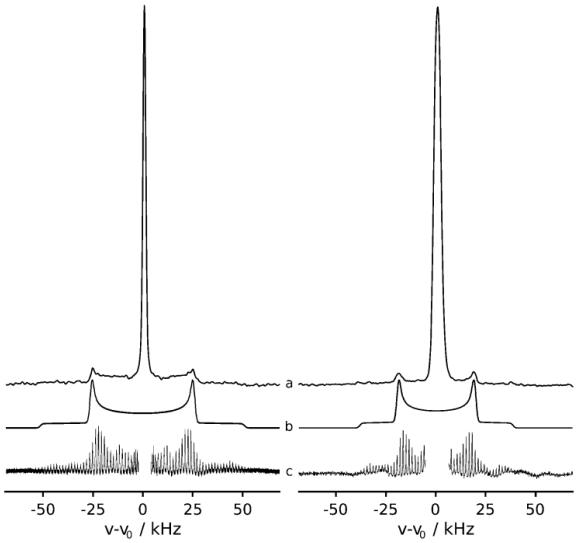

Figure 6.3: Static (a) and MAS (c) ^{2}H spectra of $BaSiD_{2-x}$ (left) and $SrGeD_{4/3-x}$ (right), together with simulation (b).

6.10 IR Microimaging of Direction-Dependent Uptake in MFI-Type Crystals

S. Hwang, B. Parditka*, C. Cserháti*, Z. Erdélyi*, R. Gläser† J. Haase, J. Kärger, W. Schmidt‡, C. Chmelik

*University of Debrecen, Department of Solid State Physics, Debrecen, Hungary
†Leipzig University, Institute of Chemical Technology
‡Max-Planck-Institut für Kohlenforschung, Mülheim an der Ruhr, Germany

Covering MFI-type zeolite crystals with Al_2O_3 by atomic layer deposition is shown to make the external zeolite crystal impermeable for guest molecules. By corresponding manipulations of the crystal certain faces can be opened for guest molecules. In this way, IR microimaging can be applied to record the evolution of transient intracrystalline concentration profiles along the crystals longitudinal extension. The introduced method of covering may provide the possibility of observing fluxes of reactant and product molecules within single zeolite crystals during catalytic reactions.

6.11 High-T_c Copper Oxide Superconductors and Related Novel Materials

M. Jurkutat, J. Kohlrautz, S. Reichardt, A. Erb*, G.V.M. Williams† J. Haase

*Walther Meissner Institute for Low Temperature Research, Garching, Germany
†The MacDiarmid Institute for Advanced Materials and Nanotechnology,
Victoria University of Wellington, Wellington, New Zealand

Since the discovery of high-temperature superconductivity in cuprates by Bednorz and Müller, NMR has contributed notably to our view and understanding of cuprate chemistry and physics, of which a brief account is given here. However, recent major insights from NMR that, at least in part, challenge certain views developed in the early years of cuprate research will be our focus: (i) The failure of a single-component spin susceptibility to adequately describe NMR shift data may indicate the presence of more than one electronic fluid. (ii) NMR quadrupole splittings provide a quantitative measure of local charges in the CuO_2 plane, and we find unexpectedly large differences between different cuprate families. These local charges, measured with NMR, appear to set the maximum T_c, and the superfluid density. A phase diagram using these local Cu and O charges rather than the total doping per CuO_2, gives a unified view of all cuprates and further insight can be expected if cuprate properties are discussed in this context. (iii) Based on magnetic field dependent and new pressure dependent NMR experiments, a review of NMR literature data, and the measurability of local charges with NMR, we argue that dynamic charge density variations are likely a universal phenomenon in cuprate superconductors.

6.12 Iron incorporation in biosilica of the marine diatom Stephanopyxis turris: dispersed or clustered?

J. Kaden*, S.I. Brückner*, S. Machill*, C. Krafft†, A. Pöppl, E. Brunner*

*School of Mathematics and Science, TU Dresden, Dresden, Germany
†Leibniz Institute of Photonic Technologies (IPHT) Jena, Jena, Germany

Iron incorporation into diatom biosilica was investigated for the species Stephanopyxis turris. It is known that several 'foreign' elements (e.g., germanium, titanium, aluminum, zinc, iron) can be incorporated into the siliceous cell walls of diatoms in addition to silicon dioxide (SiO_2). In order to examine the amount and form of iron incorporation, the iron content in the growth medium was varied during cultivation. Fe:Si ratios of isolated cell walls were measured by ICP-OES. SEM studies were performed to examine of a possible influence of excess iron during diatom growth upon cell wall formation. The chemical state of biosilica-attached iron was characterized by a combination of infrared, ^{29}Si MAS NMR, and EPR spectroscopy. For comparison, synthetic silicagels of variable iron content were studied. Our investigations show that iron incorporation in biosilica is limited. More than 95% of biosilica-attached iron is found in the form of

iron clusters/nanoparticles. In contrast, iron is preferentially dispersedly incorporated within the silica framework in synthetic silicagels leading to Si-O-Fe bond formation.

6.13 Monitoring the Diffusivity of Light Hydrocarbons in a Mixture by Magic Angle Spinning Pulsed Field Gradient NMR: Methane/Ethane/Ethene in ZIF-8

N. Dvoyashkina, D. Freude, S.S. Arzumanov*, A.G. Stepanov*

*Department of Physical Chemistry, Faculty of Natural Sciences, Novosibirsk State University, Novosibirsk, Russia

^{1}H magic angle spinning pulsed field gradient (MAS PFG) NMR was applied for the measurement of the diffusivities in a three-component mixture of the light hydrocarbons methane, ethane, and ethene, which were absorbed in the micropores of ZIF-8 metal-organic framework (MOF). It has been found that diffusivity in the mixture increases in the order ethane < ethene < methane with variance of self-diffusion coefficients D from 0.22×10^{-10} m^2 s^{-1} for ethane to 1.96×10^{-10} m^2 s^{-1} for methane at 313 K (Figure 6.4). This tendency in increasing of diffusivity from ethane to methane is similar to the tendency for individual hydrocarbons. It is concluded that the interaction of a hydrocarbon with the micropore wall of the ZIF-8 framework influences the mobility rather than the intermolecular hydrocarbon interaction. The latter plays no role for the molecules, when they overcome the energy barrier of the window connecting neighbor cages. The activation energies E_a for diffusivity of the hydrocarbons in mixture increases in the order methane (E_a = 2.4 kJ mol^{-1}) < ethene (E_a = 7.2 kJ mol^{-1}) < ethane (E_a = 11.5 kJ mol^{-1}). At the lowest studied temperature (273 K) D of methane is larger than D of ethane and ethene by 13.3 and 2.2 times, correspondingly, while the diffusivities of ethene and ethane differ by 5.8 times. This finding offers the possibility for separation of the three studied hydrocarbons on ZIF-8.

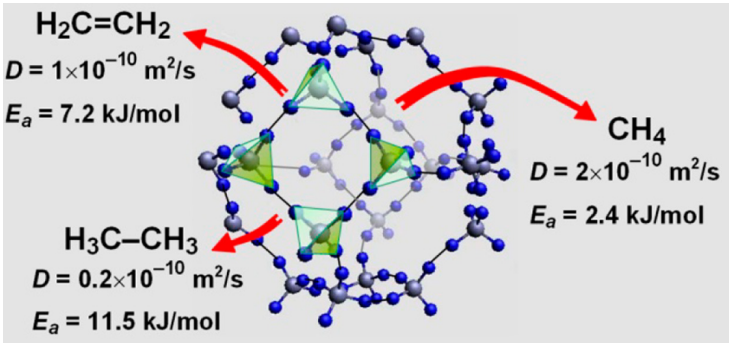

Figure 6.4: Sketch of ZIF-8 MOF with diffusivities for ethane, ethene, and methane.

6.14 Ice Nucleation in Periodic Arrays of Spherical Nanocages

S. Mascotto*, W. Janke, R. Valiullin

*Institute of Inorganic and Applied Chemistry, University of Hamburg, Hamburg, Germany

A silicious material containing massive array of spherical nanocages connected to each other by small micropores was used to study ice nucleation in confined water under conditions of well-defined pore geometry. By purposefully selecting small size of the interconnecting pores below 2 nm, ice nucleation and growth were limited to occur only within the nanocages. By exploitation of nuclear magnetic resonance, ice nucleation rates at different temperatures were accurately measured. These rates were obtained to be substantially higher than those typically observed for micrometer-sized water droplets in air. In addition, the occurrence of correlations between ice nucleation in one nanocage with the phase state in the adjacent cages were observed. These results have important implication for a deeper understanding of ice nucleation, especially in confined geometries.

6.15 Electron paramagnetic resonance and electric characterization of a perovskite metal formate framework

M. Simenas*, S. Balciunas*, M. Trzebiatowska†, M. Ptak†, M. Maczka†, G. Völkel, A. Pöppl, J. Banys*

*Faculty of Physics, Vilnius University, Vilnius, Lithuania
†Institute of Low Temperature and Structure Research, Polish Academy of Sciences, Wroclaw, Poland

We present a combined continuous-wave (CW) and pulse electron paramagnetic resonance (EPR), pulse electron-nuclear double resonance (ENDOR), pyrocurrent as well as broadband dielectric study of a $[CH_3NH_2NH_2][Zn(HCOO)_3]$ dense perovskite metal-organic framework (MOF). The pyroelectric current of a single crystal sample reveals two structural phase transitions at T_{c1} = 325 and T_{c2} = 173 K that are related to the ordering of $CH_3NH_2NH_2^+$ cations. The dielectric permittivity exhibits a small kink at T_{c1} implying improper ferroelectric phase transition, while much stronger anomaly is observed at T_{c2}. The dielectric spectra of the intermediate phase reveal a Cole-Cole relaxation process that is assigned to the hopping motion of the $CH_3NH_2NH_2^+$ cations. EPR and ENDOR experiments are performed on powder MOF samples doped with small amounts of paramagnetic Mn^{2+} and Cu^{2+} probe ions (Figure 6.5). CW EPR spectra reveal the successful incorporation of these ions at the Zn^{2+} lattice sites, while ENDOR measurements indicate several proton species that are in excellent agreement with the X-ray diffraction data. The CW EPR linewidth and intensity of the Mn^{2+} spectra demonstrate anomalies at the phase transition points. The direct measurements of the phase memory time Tm of the Mn^{2+} centers indicate a second motional process of $CH_3NH_2NH_2^+$ cations below T_{c2}. The measurements of the longitudinal relaxation time

T_1 of the low-temperature phase reveal a coupling between the electron spins and a hard optical phonon mode which undergoes a damping due to the coupling with the relaxational mode as T_{c2} is approached. The temperature dependent Mn^{2+} and Cu^{2+} spectra reflect the structural changes of the metal-oxygen octahedra. The fine structure splitting of Mn^{2+} ions is increasing as the temperature is decreased reflecting a distortion of the MnO_6 octahedra. The Cu^{2+} hyperfine interaction demonstrates a first-order character close to the tricritical limit of the phase transition at T_{c2}.

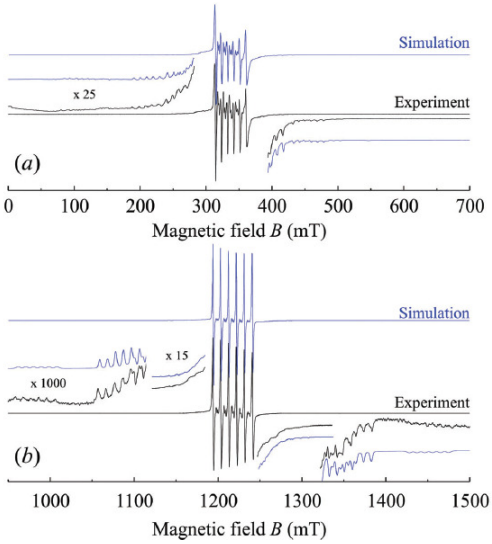

Figure 6.5: Experimental and simulated Mn^{2+} (a) X-band and (b) Q-band CW EPR spectra obtained at 140 K. The outer transitions are magnified for clarity.

6.16 Dynamical Shift of NMR Lines in Nanostructured Ga-In-Sn Melt

A.V. Uskova[*], D.Yu. Nefedova[*], E.V. Charnaya[*], D.Yu. Podorozhkin[*], A.O. Antonenko[*], J. Haase, D. Michel, M.K. Lee[†], L.J. Chang[†], Yu.A. Kumzerov[‡], A.V. Fokin[‡], A.S. Bugaev[§]

[*]St. Petersburg State University, St. Petersburg, Russia
[†]National Cheng Kung University, Tainan, Taiwan
[‡]Ioffe Institute, Russian Academy of Sciences, St. Petersburg, Russia
[§]Moscow Institute of Physics and Technology, Moscow, Russia

NMR spectrum and recovery of longitudinal nuclear magnetization after inverting pulses were measured for isotopes ^{69}Ga and ^{71}Ga in a liquid eutectic alloy Ga-In-Sn introduced in porous glasses having pores with the sizes of 25 and 7 nm. The measurements were conducted in the fields of 9.4, 11.7, and 17.6 T and compared with those for the bulk melt sample. Differences between the shape and position of the NMR lines in various fields and for different gallium isotopes were revealed in the melt introduced into the porous glass with the pores size of 7 nm. Data obtained for this sample were interpreted based on the theoretical model of dynamic quadrupolar shift, and correlation time of atomic motion was found within this model. Characteristics

of the atomic motion calculated based on the dynamic shift model and from the spin relaxation data were shown to agree with each other.

6.17 Funding

Energy efficient MOF-based Mixed Matrix Membranes for CO_2 Capture
Prof. Dr. Jürgen Haase
EU, 608490

Anwendungen der NMR-Spektroskopie zur Erforschung von Struktur-Beweglichkeits-Beziehungen an nanoporösen Wirt-Gast-Systemen im konzentrierten Einsatz mit dem Micro-Imaging
Prof. Dr. Jürgen Haase, Prof. Dr. Jörg Kärger
DFG, HA 1893/17-1

Metalle unter extremen Bedingungen
Prof. Dr. Jürgen Haase
DFG, HA 1893/12-1

Micro-Imaging transienter Konzentrationsprofile von Gastgemischen in Zeolithkristallen
Prof. Dr. Jürgen Haase, Prof. Dr. Jörg Kärger
DFG, HA 1893/15-1

Deuterium-Festkörper-NMR und ^1H MAS PFG NMR-Untersuchungen der Beweglichkeit des Wirtsgerüsts und der Gastmoleküle in nanoporösen Materialien
Prof. Dr. Jürgen Haase
DFG, HA 1893/16-1

EPR spectroscopy of paramagnetic centers and adsorption complexes in porous metal organic frameworks: Development and application of dielectric resonators and microresonators for investigations of small single crystals
Prof. Dr. Andreas Pöppl
DFG PO 426/11-2

Monitoring adsorption induced transformations of MOFs at a molecular level by in situ EPR spectroscopy
Prof. Dr. Andreas Pöppl
DFG PO 426/13-1

MOFs as carrier for nitric oxide delivery in biological systems - microscopic fundamentals of adsoprtion and controlled release studied by infrared and electron and nuclear spin resonance spectroscopy
PD Dr. Marko Bertmer, Prof. Dr. Andreas Pöppl, Prof. Dr. Martin Hartmann, Prof. Dr. Michael Fröba
DFG, BE 2434/4-2, PO 426/8-2

Charakterisierung der [2+2]-Photodimerisierung von photoaktiven Substanzen auf der Basis von Zimtsäure eingebaut in Polymeren oder in supramolekularen Strukturen mit

Festkörper-NMR-Spektroskopie
PD Dr. Marko Bertmer
DFG, BE 2434/2-3

Structure and Transport Characterization of Hierarchical Porous Solids
PD Dr. Rustem Valiullin
DFG

6.18 Organizational Duties

Professor Dr. Jürgen Haase

- Dean of the Faculty
- Vice Director of the Magnetic Resonance Center Leipzig
- Board Member of the Heisenberg Gesellschaft e. V.
- Full Member of the Saxonian Academy of Sciences in Leipzig
- Member of the German Physical Society
- Member of the American Physical Society
- Member of the 'ICAM Board of Goveners' of the Institute for Complex Adaptive Matter
- Referee: Physical Review, Science, IOP, German-Israeli Foundation for Scientific Research and Developement

Prof. Dr. Andreas Pöppl

- Referee: Journal of Magnetic Resonance, Journal of the American Chemical Society, Physical Chemistry Chemical Physics, Chemical Physics Letters
- Project Reviewer: German-Israeli Foundation for Scientific Research and Development

PD Dr. Marko Bertmer

- Referee: Angewandte Chemie, Chemistry of Materials, Journal of Physical Chemistry, Solid State Nuclear Magnetic Resonance, Microporous and Mesoporous Materials

PD Dr. Rustem Valiullin

- Member of the German Physical Society
- Scientific Advisory Board of the AMPERe Bologna Conference Magnetic Resonance in Porous Media
- Chairman of the IUPAC task group Diffusion in nanoporous solids
- Editorial Boards Diffusion Fundamentals, Dataset Papers in Physical Chemistry, Fluids
- Referee: Physical Review, RSC, ACS, Elsevier

Prof. Dr. Dieter Michel

- Full Member of the Saxonian Academy of Sciences in Leipzig
- Member of the German Physical Society
- Member of the Society of German Chemists
- German Coordinator of the German-Russian Centre 'Applied and Computational Physics (ACOPhys)' at the St. Petersburg State University

- Member at the International Advisory Committee of the International Meeting of Ferroelectricity
- Member at the International Advisory Committee of the European Meeting of Ferroelectricity
- Member at the International Advisory Committee of the Conference 'NMR of Condensed Matter St. Petersburg'
- Member of the German-Israeli Foundation for Scientific Research and Developement
- Referee: Physical Review, Journal of Physics: Condensed Matter, Langmuir, Journal of Magnetic Resonance, Phys. Stat. Sol., Materials Chemistry and Physics, German-Israeli Foundation for Scientific Research and Developement

Prof. Dr. Rolf Böttcher

- Referee: Physical Review, Journal of Physics: Condensed Matter, Langmuir, Journal of Magnetic Resonance

6.19 External Cooperations

Academic

- Technical University Munich, Physics Department, Crystal Lab, Garching, Germany
  Prof. Dr. Andreas Erb
- Washington University, St. Louis, MO, USA
  J. Schilling, M. Conradi
- Victoria University, Physics Department,Wellington, New Zealand
  Dr. Grant V. M.Williams
- University of Illinois at Urbana-Champaign, Department of Physics, USA
  Prof. Dr. C. P. Slichter
- University of New South Wales, School of Physics, Sydney, Australia
  Prof. Dr. O. Sushkov
- Washington University, Department of Chemistry, St. Louis, MO, USA
  Sophia E. Hayes
- Universität Koblenz-Landau, Abteilung Chemie, Landau, Germany
  Prof. Dr. Gabriele Schaumann
- Martin-Luther-Universität Halle-Wittenberg, Halle, Germany
  Dr. H. T. Langhammer
- Kazan State University, Tartastan, Russian Federation
  Prof. Dr. E. N. Kalabukhova
- Universität Erlangen-Nürnberg, Erlangen Catalysis Resource Center - ECRC, Erlangen, Germany
  Prof. Dr. Martin Hartmann
- Université du Maine, Laboratoire de Physique de l'Etat Condenseé, Le Mans, France
  Prof. Dr. A. Kassiba

- University of Vilnius, Faculty of Physics, Vilnius, Lithuania
  Prof. Dr. J. Banys
- University of Illinois at Chicago, USA
  Prof. Dr. D. K. Morr
- Skolkovo Institute of Science and Technology, Moscow, Russia and Institute for Theoretical Physics, University of Heidelberg, Heidelberg, Germany
  Prof. Dr. Boris V. Fine
- Boreskov Institute of Catalysis, Novosibirsk, Russia Novosibirsk State University, Novosibirsk, Russia
  Dr. Alexander G. Stepanov
- Institute of Physics, St. Petersburg State University, St. Petersburg, Russia
  Prof. Dr. Elena V. Charnaya
- Ruhr-University Bochum, Bochum, Germany
  R. A. Fischer
- University of Massachusetts, MA, USA
  Prof. P. Monson
- University of Giessen, Germany
  Prof. A. Bunde

Industry

- NMR-Service GmbH, Erfurt, Germany
  M. Braun
- Bruker BioSpin GmbH, Rheinstetten, Germany
  F. Engelke
- Quantachrome Ins., Boyton-Beach, FL, USA
  M. Thommes

6.20 Publications

Journals

J. Haase, M. Jurkutat, J. Kohlrautz
Contrasting Phenomenology of NMR Shifts in Cuprate Superconductors
arXiv, Cond. Matt. 2 (2017) 16.

M. Jurkutat, J. Kohlrautz, S. Reichardt, A. Erb, G. V. M. Williams, J. Haase
NMR of Cuprate Superconductors: Recent Developements.
In: High-T_C Copper Oxide Superconductors and Related Novel Materials
Ed. by. A. Bussmann-Holder, H. Keller, A. Bianconi
Springer International Publishing, pp. 77-97.

C. M. Kropf, J. Kohlrautz, J. Haase, B. V. Fine
Anomalous longitudinal relaxation of nuclear spins in CaF_2
Fortschr. Phys. 65 (2017) 6-8.

H. Auer, R. Guehne, M. Bertmer, S. Weber, P. Wenderoth, T. C. Hansen, J. Haase, H. Kohlmann
Hydrides of Alkaline Earth-Tetrel (AeTt) Zintl Phases: Covalent Tt-H Bonds from Silicon to Tin
Inorg. Chem. 56 (2017) 1061-1071.

A. E. Khudozhitkov, H. Jobic, D. I. Kolokolov, D. Freude, J. Haase, A. G. Stepanov
Probing the Guest-Mediated Structural Mobility in the UiO-66(Zr) Framework by ^{2}H NMR Spectroscopy
J. Phys. Chem. C 121 (2017) 11593-11600.

D. I. Kolokolov, A. G. Maryasov, J. Ollivier, D. Freude, J. Haase, A. G. Stepanov, H. Jobic
Uncovering the Rotation and Translational Mobility of Benzene Confined in UiO-66 (Zr) Metal-Organic Framework by the ^{2}H NMR-QENS Experimental Toolbox
J. Phys. Chem. C 121 (2017) 2844-2857.

D. Yu. Nefedov, A. O. Antonenko, D. Yu. Podorozhkin, A. V. Uskov, E. V. Charnaya, M. K. Lee, J. L. Chang, J. Haase, D. Michel, Yu. A. Kumzerov, A. V. Fokin, M. I. Samoilovich, A. S. Bugaev
Atomic mobility in a ternary liquid Ga-In-Sn alloy of the eutectic composition
Phys. Solid State 59 (2017) 362-367.

M. Šimėnas, A. Kultaeva, S. Balčiūnas, M. Trzebiatowska, D. Klose, G. Jeschke, M. Mączka, J. Banys, A. Pöppl
Single Crystal Electron Paramagnetic Resonance of Dimethylammonium and Ammonium Hybrid Formate Frameworks: Influence of External Electric Field
J. Phys. Chem. C. 121 (2017) 16533-16540.

M. Mendt, B. Barth, M. Hartmann, A. Pöppl
Low-Temperature Binding of NO Adsorbed on MIL-100(Al) - A Case Study for the Application of High Resolution Pulsed EPR Methods and DFT Calculations
J. Chem. Phys. 147 (2017) 224701.

M. Hartmann, T. Unruh, T. Schindler, A. Pöppl, Z. Zhou, V. Umamaheswari
Electron Paramagnetic Resonance Spectroscopic Study of Ascorbate Oxidase Immobilized on Mesoporous Silica Materials
Adv. Porous Mater. 5 (2017) 113-121.

M. Šimėnas, S. Balčiūnas, M. Trzebiatowska, M. Ptak, M. Mączka, G. Völkel, A. Pöppl, J. Banys
Electron paramagnetic resonance and electric characterization
of a $[CH_3NH_2NH_2][Zn(HCOO)_3]$ perovskite metal formate framework
J. Mater. Chem. C 5 (2017) 4526-4536.

J. Kaden, S. I. Brückner, S. Achill, C. Krafft, A. Pöppl, E. Brunner
Iron incorporation in basilica of the marine diatom Stephanopyxis turris: dispersed or clustered?
BioMetals 30 (2017) 71-82.

M. Bertmer
Paramagnetic solid-state NMR of materials
Solid State Nucl. Magn. Reson. 81 (2017) 1-7.

F. Bauer, S. Czihal, M. Bertmer, U. Decker, S. Naumov, S. Wassersleben, D. Enke
Water-based functionalization of mesoporous siliceous materials, Part 1: Morphology and stability of grafted 3-aminopropyltriethoxysilane
Microporous Mesoporous Mater. 250 (2017) 221-231.

P. Ondruch, A. Jäger, J. Kucerik, M. Bertmer, G. E. Schaumann
Influence of organic chemicals on aliphatic crystallites analyzed in whole soils
Geoderma 291 (2017) 40-46.

J. Dietel, L. N. Warr, M. Bertmer, A. Steudel, G. H. Grathoff, K. Emmerich
The importance of specific surface area in the geopolymerization of heated illitic clay
Appl. Clay Sci. 139 (2017) 99-107.

S. Friebe, A. Mundstock, D. Schneider, J. Caro
An Untrodden Path: Versatile Fabrication of Self-Supporting Polymer-Stabilized Percolation Membranes (PSPMs) for Gas Separation
Chem. Eur. J. 23 (2017) 6522-6526.

R. Řezníček, V. Chlan, H. Štěpánková, P. Novák, J. Żukrowski, A. Kozłowski, Z. Kąkol, Z. Tarnawski, J. M. Honig
Understanding the Mössbauer spectrum of magnetite below the Verwey transition: Ab initial calculations, simulation, and experiment Phys. Rev. B 96 (2017) 195124.

A. A. Gabrienko, S. S. Arzumanov, A. V. Toktarev, I. G. Danilova, I. P. Prosvirin, V. V. Kriventsov, V. I. Zaikovskii, D. Freude, A. G. Stepanov
Different Efficiency of Zn^{2+} and ZnO Species for Methane Activation on Zn-Modified Zeolite
ACS Catal. 7 (2017) 1818-1830.

R. Valiullin, J. Kärger
Chapter 12 Confined Fluids: NMR Perspectives on Confinements and on Fluid Dynamics, in Diffusion NMR of Confined Systems: Fluid Transport in Porous Solids and Heterogeneous Materials
R. Valiullin, Editor. 2017, The Royal Society of Chemistry. p. 390.

D. Schneider, D. Kondrashova, R. Valiullin
Phase transitions in disordered mesoporous solids
Sci. Rep. 7 (2017) 7216.

S. Mascotto, W. Janke, R. Valiullin
Ice Nucleation in Periodic Arrays of Spherical Nanocages
J. Phys. Chem. C 121 (2017) 23788-23792.

D. Kondrashova, R. Valiullin, J. Kärger, A. Bunde
Structure-correlated diffusion anisotropy in nanoporous channel networks by Monte Carlo simulations and percolation theory
Eur. Phys. J. B 90 (2017) 136.

D. Kondrashova, A. Lauerer, D. Mehlhorn, H. Jobic, A. Feldhoff, M. Thommes, D. Chakraborty, C. Gommes, J. Zecevic, P. de Jongh, A. Bunde, J. Kärger, R. Valiullin
Scale-dependent diffusion anisotropy in nanoporous silicon
Sci. Rep. 7 (2017) 40207.

N. Dvoyashkina, D. Freude, S. S. Arzumanov, A. G. Stepanov
Monitoring the Diffusivity of Light Hydrocarbons in a Mixture by Magic Angle Spinning Pulsed Field Gradient NMR: Methane/Ethane/Ethene in ZIF-8
J. Phys. Chem. C 121 (2017) 25372-25376.

A. V. Uskov, D. Yu. Nefedov, E. V. Charnaya, D. Yu. Podorozhkin, A. O. Antonenko, J. Haase, D. Michel, M. K. Lee, L. J. Chang, Yu. A. Kumzerov, A. V. Fokin, A. S. Bugaev
Dynamical shift of NMR lines in nanostructured Ga-In-Sn melt
Phys. Solid St. 59 (2017) 2481-2485.

S. Hwang, B. Parditka, C. Cserháti, Z. Erdélyi, R. Gläser, J. Haase, J. Kärger, W. Schmidt, C. Chmelik
IR Microimaging of Direction-Dependent Uptake in MFI-Type Crystals
Chem. Ing. Tech. 89 (2017) 1686-1693.

A. Kultaeva, T. Biktagirov, J. Bergmann, L. Hensel, H. Krautscheid, A. Pöppl
A combined continuous wave electron paramagnetic resonance and DFT calculations of copper-doped $^{3}_{\infty}[Cd_{0.98}Cu_{0.02}(prz\text{-}trz\text{-}ia)]$ metal-organic framework
Phys. Chem. Chem. Phys. 19 (2017) 31030-31038.

Books

R. Valiullin
Diffusion NMR of Confined Systems: Fluid Transport in Porous Solids and Heterogeneous Materials
The Royal Society of Chemistry
Cambridge, UK, 2017

Talks

J. Haase
Local charge density and its variation in cuprate superconductors from NMR
APS March Meeting 2017
New Orleans, USA, March 12, 2017

J. Haase
NMR and Cuprate Superconductors - A new phase diagram, proof of charge ordering, and a contrasting shift phenomenology
Solid State Seminar University of Sherbrooke
Sherbrooke, Kanada, July 20, 2017

J. Haase
NMR Changes the View of Cuprate Superconductivity
ISMAR Conference 2017
Quebec City, Kanada, July 23, 2017

J. Haase
New Ubiquitous Charge Order in Cuprate Superconductors Detected by NMR
Electron Correlation in Superconductors and Nanostructures
Odessa, Ukraine, August 16, 2017

J. Haase
Anvil Cell NMR of Solids
55th EHPRG Meeting
Poznan, Poland, September 3, 2017

J. Haase
Emergence of a new interpretation of NMR of cuprates superconductors
Perspectives on high-temperature superconductivity Workshop
Moskau, Russia, October 23, 2017

J. Haase
Emergence of a new interpretation of NMR of cuprates superconductor
Quantum Materials Seminar at School of Physics and Astronomy
Minnesota, USA, November 1, 2017

J. Haase
Emergence of a new interpretation of NMR of cuprates superconductors
Physics Colloquium at University of Illinois at Chicago
Chicago, USA, November 2, 2017

R. Gühne, G. V. W. Williams, J. Haase
Independent Confirmation of the Unique Electronic Susceptibility in Topological Insulator Bi_2Se_3 by ^{209}Bi Nuclear Magnetic Resonance
AMN8 International Conference
Queenstown, New Zealand, February 12-16, 2017

M. Jurkutat, S. Reichardt, J. Haase
Advances in Cuprate NMR - Local charges and charge order & NMR shift phenomenology
Superstripes 2017
Ischia, Italy, July 5, 2017

M. Jurkutat, S. Reichardt, A. Erb, J. Haase
Advances in Cuprate NMR - Local charge density and its variation in cuprate superconductors from NMR
APS March Meeting 2017
New Orleans, USA, March 15, 2017

A. Pöppl
Investigation of Structural Transformations and Defects in Flexible MOFs by Electron Paramagnetic Resonance Spectroscopy
International Microsymposium 'Switchability in Porous Metal-Organic Frameworks'
Dresden, Germany, March 13-14, 2017

A. Kultaeva, V. Bon, S. Kaskel, O. Ovchar, A. Belous, A. Pöppl
Continuous Wave Single Crystal Electron Paramagnetic Resonance of Cupric Ions in the Isostructural Elastic Layer-Structured Metal-Organic Framework ELM-11
DFG Priority Programm SPP 1601: Young researchers' workshop
Freudenstadt, Germany, 2017

Posters

Seungtaik Hwang
Transport diffusion of CO_2 in mixed matrix membranes
2017 Diffusion Fundamentals
Moskau, Russia, September 03-07, 2017

Seungtaik Hwang
CO_2 Adsorption and Diffusion Phenomna in Mixed Matrix Membranes
EuroMOF 2017
Delft, The Netherlands, October 29 - November 1, 2017

A. H. Khan, K. Peikert, F. Hoffman, M. Fröba, J. Haase, M. Bertmer
Nitric Oxide adsorption in amino modified $Cu_3(btc)_2$ type MOFs studied by solid-state NMR
39th FGMR Annual Discussion Meeting
Bayreuth, Germany, September 25-28, 2017

R. Gühne, M. Lindel, H. Auer, H. Kohlmann, J. Haase, M. Bertmer
Solid-state ^2H NMR of Zintl Phase Deuterides - Determination of Bonding Situations
39th FGMR Annual Discussion Meeting
Bayreuth, Germany, September 25-28, 2017

M. Mendt
EPR Insights into Switchable and Rigid Derivatives of the Metal-Organic Framework DUT-8(Ni) by NO Adsorption - Probing Defects
Switchability in Porous Metal-Organic Frameworks
Dresden, Germany, March 13-14, 2017

R. Gühne, G. V. W. Williams, J. Haase
^{209}Bi NMR Study of Topologial Insulator Bi_2Se_3

A. Pöppl
EPR spectroscopy of isomorphous Metal Organic Frameworks single crystals and powders with rtl-topology Xth EFEPR 2016 Conference
Torino, Italy, September 4-9, 2017

A. Pöppl
Continuous Wave Single Crystal Electron Paramagnetic Resonance of Cupric Ions in the Zn(II) Doped Porous Coordination Polymer $Cu_{2.965}Zn_{0.035}(btc)_2$ Xth EFEPR 2016 Conference
Torino, Italy, September 4-9, 2017

A. Pöppl
Continuous Wave Single Crystal Electron Paramagnetic Resonance of Cupric Ions in the Zn(II) Doped Porous Coordination Polymer $Cu_{2.965}Zn_{0.035}(btc)_2$
39th FGMR Annual Discussion Meeting
Bayreuth, Germany, September 25-28, 2017

A. Kultaeva, V. Bon, S. Kaskel, O. Ovchar, A. Belous, A. Pöppl
Continuous Wave Single Crystal Electron Paramagnetic Resonance of Cupric Ions in the Isostructural Elastic Layer-Structured Metal-Organic Framework ELM-11
DFG Priority Program SPP-1601: Young researchers' workshop, Freudenstadt, Germany, 2017

6.21 Graduations

Doctorate

- Jonas Kohlrautz
  Nuclear Magnetic Resonance - Advanced Concepts and Applications to Quantum Materials
  May 2017
- Stefan Friedländer
  Increasing Sensitivity for Electron Paramagnetic Resonance Spectroscopy of Cupric Ions in Metal-Organic Framework Single Crystals and Thin Films
  July 2017

Master

- Elisabeth Vonhof
  Investigation of water adsorption and ice formation on cloud forming aerosol kaolinite based on NMR
  September 2017

Bachelor

- Daniel Dernbach
  NMR Spin-Lattice Relaxation Time (T_1): Phenomenology in high-T_c Cuprates
  September 2017

6.22 Guests

- Sergei Bystrov
  Physikalisches Institut, Staatliche Universität St. Petersburg, St. Petersburg, Russian Federation
  11.12.2017–10.01.2018

- Seunghyun Khim
  Max-Planck-Institut für Chemische Physik fester Stoffe, Dresden, Germany
  19.10.2017
- Yoshimura Kazuyoshi
  Kyoto University, Department of Chemistry, Kyoto, Japan
  05.07.2017–08.07.2017
- Boris Fine
  Skolkovo Institute of Science and Technology Territory of Skolkovo Innovation Center, Moskau, Russian Federation
  16.05.2017–19.05.2017

7

Nuclear Solid State Physics

7.1 Introduction

Main goal of this group is to fabricate quantum devices on a solid-state basis and to develop new methods to fulfil this task using ion beam implantation. Ions with kinetic energies allow the three dimensional modification of all types of solid state materials in a very controlled way. We run different types of accelerators that deliver all types of ions of the periodic table with kinetic energies between a few eV and several MeV. This systems are able to modify or analyse all types of materials from the surface to depths of several micrometres. One of our challenges is to perform a deterministic single ion implantation in order to assemble single atoms or defects with nanometre lateral resolution within all three dimensions. This topic will be realised using focused ion beams with an image charge detector and installed at the Joint Lab in cooperation with the Leibniz Institute of Surface Engineering (IOM). Ion implantation is also used to build magnetic sensors with atom size lateral resolution to perform single molecule nuclear magnetic resonance (NMR). Beside the modification with ion beams, we run a different number of analytical tools like optically detected magnetic resonance (ODMR), Hanbury Brown and Twiss (HBT) setup, or spectroscopic measurements to investigate the outcome. The possibility of preparation, modification and quality control of quantum devices on the same place and with state of the art systems is unique and guarantees a fast optimisation. Beside the activities in quantum technology, we are specialised in defect engineering using ion beams, as well as nuclear analytics with high lateral resolution with proton induced X-ray emission (PIXE), Rutherford backscattering spectrometry (RBS), or channeling. These experiments can be performed routinely at a lateral resolution below 500 nm with the micro beam system LIPSION. In special cases the system is able to provide a 2 MeV proton beam with 40 nm in diameter and makes LIPSION one of the best MeV microbeam systems worldwide.

All these nice results are only possible due to our funding agencies, to whom we would like to express our deepest gratitude in particular the VolkswagenStiftung, the Deutsche Forschungsgemeinschaft (DFG), the European Social Fund (ESF), the European Union (EU), and the Senatsausschuss Wettbewerb (SAW) Project of the Leibniz Association.

Jan Meijer

7.2 Non-destructive measurement and detection of ion bunches

P. Räcke*†, D. Spemann†‡, J.W. Gerlach†‡, B. Rauschenbach†‡, J. Meijer*†

*Division of Nuclear Solid State Physics
†Leibniz Joint Lab "Single Ion Implantation", Leipzig
‡Leibniz Institute of Surface Engineering e.V., Leipzig

When a moving charge passes by a single electrode, the signal induced into that electrode is a peak in the time domain, as described by the Shockley-Ramo theorem. In image charge mass spectrometry, ions are commonly trapped and circulated, so that a periodic signal can be recorded and analysed. In terms of the signal-to-noise ratio (SNR), repeating a measurement N times improves the sensitivity by $1/\sqrt{N}$ for uncorrelated noise.

In the Leibniz Joint Lab "Single Ion Implantation", we work on methods for measuring and detecting small numbers of charges upon a single pass through an image charge detector (ICD). The detector consists of a linear array of electrodes, so that a periodic signal is formed, which can be analysed in the frequency domain (cp. Fig. 7.1**(a)**, **(b)**). The detection limit is determined by the SNR, considering the image charge signal

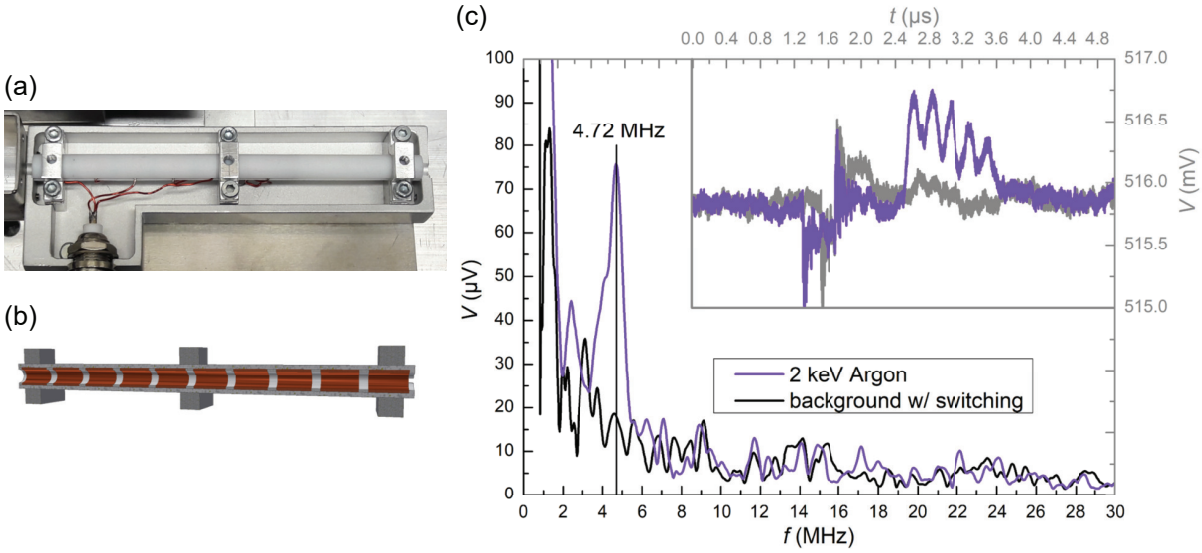

Figure 7.1: (a) Photograph of an image charge detector prototype. **(b)** Section of its 3D model, revealing the electrode geometry. **(c)** Time signal (*upper right, blue line, grey scale*) and its FFT spectrum (*bottom left, blue line, black scale*) of a 2 keV Ar bunch signal, shown together with the background spectrum (*black/grey line*) including switching interference, averaged over 100 acquisitions.

and the detector noise. The signal itself is proportional to the number of charges. Ion bunches and in future single highly charged ions are used for measurements to increase the SNR per measurement. In Fig. 7.1**(c)**, a typical measurement for a bunch of Ar ions is depicted. The time trace (inset, light scale) shows five clear peaks forming an approximate sinusoidal signal form between (2.4 – 3.8) µs. In its Fourier transform (black scale) this is translated into a peak at the frequency that results from the ion velocity

and the geometrical distance of the signal electrodes. Effectively, this detection set-up is a mass spectrometer, given that the accelerating potential of the ions is known.

There are important differences between measuring unknown properties in a mass-spectrometric experiment and detection of occurrence of a signal. The latter is relevant for the implantation of single ions with a pre-detection system. In this context, all unclear signals from the detector are rejected and not counted (false negative). However, if a noise component from the detector electronics resembles the expected signal and passes the detection threshold, a false positive event is registered. Since all parameters of the ions are known, very specific detection criteria can be applied, for example a threshold at a specific frequency in the Fourier spectrum. The point is, that even at low SNRs, a threshold can be found, where the probability of a false positive detection is sufficiently low, but the detection rate decreases to a still tolerable level.

7.3 Quantum and classical light emitters in silicon: Impurities and complex defects for nanophotonics

T. Herzig, C. Beaufils[*], W. Redjem[*], E. Rousseau[*], V. Jacques[*], A.Yu. Kuznetsov[†], C. Raynaud[‡], C. Voisin[‡], A. Benali[§], S. Pezzagna, J. Meijer, M. Abbarchi[§], G. Cassabois[*]

[*]Laboratoire Charles Coulomb, CNRS-UMR 5221, Université de Montpellier, France
[†]Department of Physics, University of Oslo, Norway
[‡]Laboratoire Pierre Aigrain, Ecole Normale Supérieure, Université Paris Diderot, CNRS-UMR 8551, Paris, France
[§]Institut Matériaux-Microélectronique-Nanosciences de Provence, IM2NP, CNRS-UMR 7334, Aix-Marseille Université, France

The steady demand of high performance electronics, be it in everyday life or ultramodern applications in science and engineering, requires continual improvement of processing power in computational calculations. Hitherto this was possible due to a decrease of the structure sizes on Si-based microchips with modern techniques. This downsizing process comes to its limit by the so called interconnect bottleneck problem. When the feature sizes of integrated circuits become too small, the signal delay is no longer dictated by the gate switching time but by the wiring delay [1]. Due to tighter packaging of metal conducting paths, parasitic capacitance increases and therefore signal propagation delay gets worse. Since this physical limitation is inevitable, new designs of circuits and computers are needed. One way to overcome this problem is the use of Si photonics.

Due to its indirect bandgap, radiative transitions in Si are highly improbable. By modifying the internal structure of the Si lattice with defects, one can suppress the indirect transitions and therefore generate light from Si itself. Together with physicists from the Aix-Marseille University and the University of Montpellier and funded by the DFG and ANR we investigate optimal conditions to create such defects with special focus on the so called G-centre. This defect has a sharp zero phonon line (ZPL) at around $\lambda \approx 1280\,\mathrm{nm}$, matching the optical telecommunications O-band wavelength with very low transmission losses. It consists of one interstitial- and one substitutional-C atom within the Si lattice and occurs in four different configurations, depending on

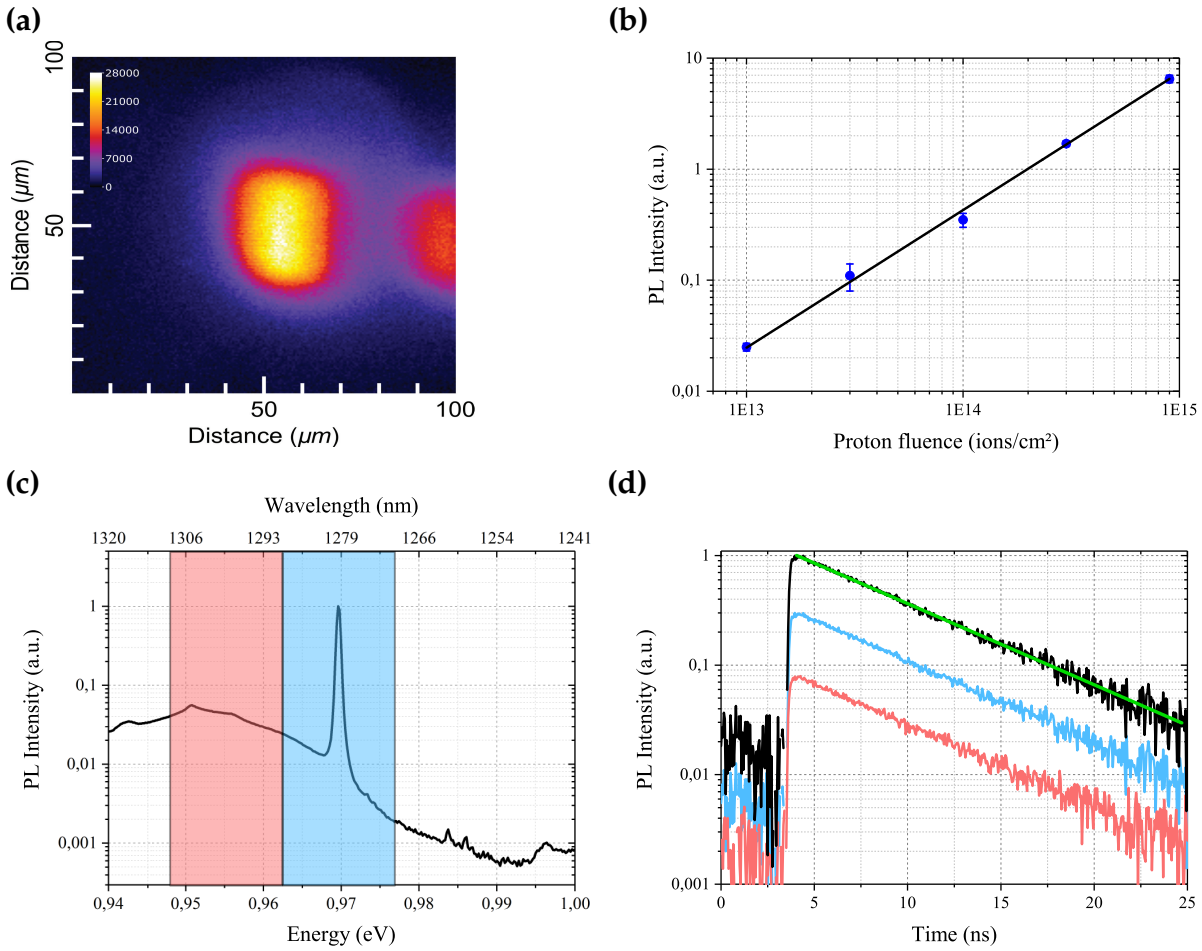

Figure 7.2: Measurements of a Si sample at $T = 10\,\mathrm{K}$ after irradiation with a proton fluence of $9\times10^{14}\,\mathrm{cm}^{-2}$: **(a)** PL raster scan to show the dimension of one irradiated spot. **(b)** H^+-fluence dependent PL intensity. **(c)** Typical PL spectrum of a G-centre, shaded areas indicate spectral width of two bandpass filters (phonon sideband (*red*), ZPL (*blue*)). **(d)** Spectrally selective, time-resolved PL signal intensity for phonon sideband (*red*), ZPL (*blue*), and full spectrum (*black*), the fit function (*green*) indicates an exponential decay with a time constant of $\tau = 5.9\,\mathrm{ns}$.

the orientation of the C atoms in the lattice [2]. It was first observed in the early 1960s after high energy electron irradiation of n-type Si [3] and later identified as a bistable C pair by electron paramagnetic resonance (EPR), optically detected magnetic resonance (ODMR), and infrared (IR) absorption measurements [4].

To generate these defects, we use a 100 kV accelerator with a source of negative ions by Cs sputtering (SNICS) for implantation of the different C isotopes with energies between (20 – 100) keV and ion fluences ranging from $\left(10^9 - 10^{16}\right)\,\mathrm{cm}^{-2}$. After an annealing step, executed with rapid thermal processing (1000 °C for 20 s) to incorporate the C atoms into the Si lattice, a high energy irradiation with light ions, implemented at the LIPSION Singletron accelerator with focussing setup and microbeam scanning system, leads to the C_i–C_s pair. Besides the investigation of the best conditions for implantation and irradiation, we also examine the influence of crystal orientation, Si-on-insulator (SOI) layers, and Si nanostructures on the generation and yield of G-centres.

Since start of the project we have been able to characterise the saturation power of an ensemble of G-centres. We investigated the recombination dynamics, leading to a new

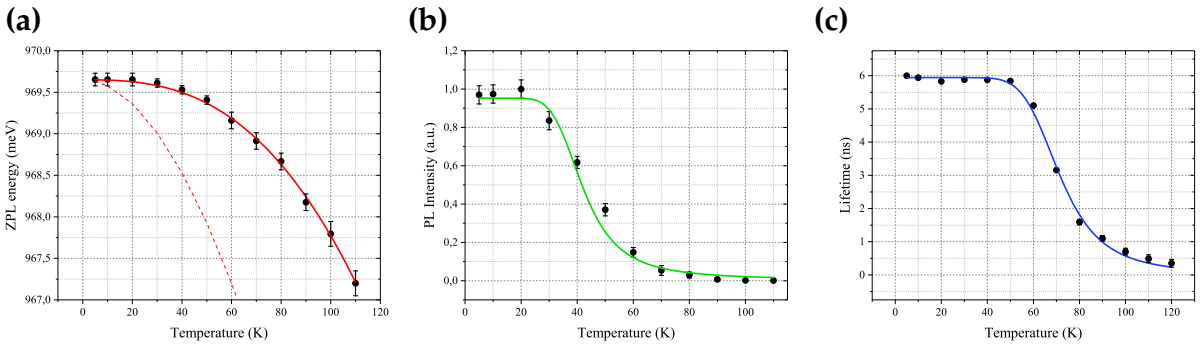

Figure 7.3: Temperature dependent measurements: **(a)** ZPL energy shift, **(b)** PL signal intensity losses, **(c)** Lifetime decrease.

value for the lifetime of the state of around $\tau \approx 6\,\text{ns}$ by means of photoluminescence (PL) at low temperature (Fig. 7.2). According to theoretical modelling of the vibronic spectrum we estimated the spatial extension of the electronic wave function in a G-centre to 1.6 Å. Moreover, the temperature dependence of the emission spectrum and recombination dynamics was recorded [5], leading to new insights of the characteristics of this fascinating defect (Fig. 7.3). With this knowledge, we want to entrench a method for straightforward production of lasers, light-emitting diodes (LED), and single photon sources directly within the Si itself, to herald the start of a new and revolutionary design for photonic based devices.

[1] L. Pavesi: J. Phys.: Condens. Matter **15**, R1169 (2003), doi:10.1088/0953-8984/15/26/201
[2] D. Timerkaeva et al.: J. Appl. Phys. **123**, 161421 (2018), doi:10.1063/1.5010269
[3] G.D. Watkins et al.: Phys. Rev. **121**, 1001 (1961), doi:10.1103/physrev.121.1001
[4] L.W. Song et al.: Phys. Rev. B **42**, 5765 (1990), doi:10.1103/physrevb.42.5765
[5] C. Beaufils et al.: Phys. Rev. B **97**, 035303 (2018), doi:10.1103/physrevb.97.035303

7.4 Development of nano apertures for ion beam collimation

C. Scheuner, P. Räcke, N. Raatz, St. Jankuhn, S. Pezzagna, C. Trautmann*, J. Meijer

*GSI Helmholtzzentrum für Schwerionenforschung GmbH, Darmstadt

For the creation of nitrogen–vacancy (NV) centres in diamond and other important applications ion beams with a very small diameter are needed. This is commonly done with micro probe devices. A less expensive alternative to this is nano collimation which can be applied to several applications [1, 2]. Especially for applications with very low ion currents and single ion implantation this method is useful. Another possible application is the focused ion beam (FIB) technique where liquid metal ion sources are used nowadays. There a liquid metal gets ionised due to an electron spray on a very sharp tip. The advantage of this source is that it emits ions on a very small area which can be demagnified down to a few nanometres. But the disadvantage is that it works

just for a few chemical elements which have their melting point in a useable region. This disadvantage can be overcome for low current applications with nano collimators which are mounted behind the ion source. Such that there is still a small point where the ions are emitted but it is possible to use different types of ion sources, so nearly every element can be ionised.

We used two different ways to create such nano apertures. One way is the ion-track-etching technique, the other is FIB-milling. For the first technique, Muscovite sheets were prepared at the GSI Darmstadt with high energetic Sm ions which traversed the sheets and left an ion-track of amorphous material. Subsequent etching with HF acid removed this material and created diamond shaped pores. The advantage of this method is that very high aspect ratios up to 100 can be archived. This leads to nano apertures with a thickness sufficient to stop ions in the low MeVrange [3]. But the disadvantage is that the pores are randomly distributed over the irradiated area of the sheets and further collimation is needed to select a single pore.

For FIB-milling thin membranes are irradiated with a well focused beam of Ga ions. This removes material due to sputtering and thus structures can be milled in the surface. One big advantage is that arbitrary shapes can be written with this in the material and used as a collimator. Furthermore, the only limitation on the collimator material is that one needs to obtain a certain sputter yield. But a limitation of this method is that the aspect ratios are not as good as for the track-etching-technique. Meaning that for pores in the range of a few ten nanometres the material needs to have a thickness in the order of a few hundred nanometre and thus the energy of the particles that should be collimated is limited to the lower keV range.

Another important parameter of collimators is the radiation hardness. In the literature was reported that nano pores reduce their diameter under ion and electron bombardment for certain circumstances [4–6]. This is an important feature for the desired use that was further investigated. Therefore, experiments with track-etched mica, diamond membranes, SiN membranes, and Pt foil were carried out (Fig. 7.4). With

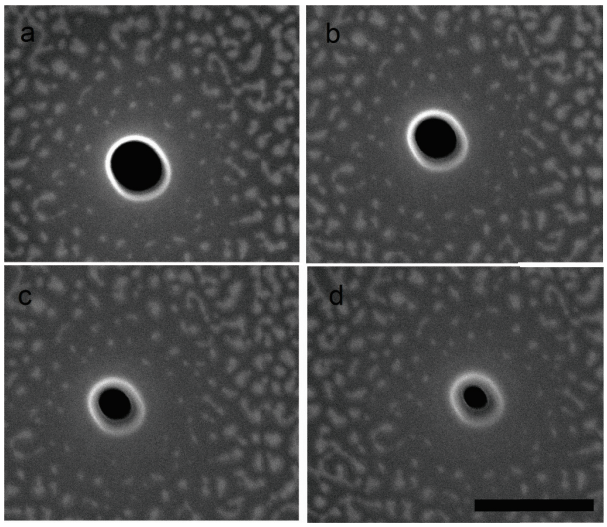

Figure 7.4: Scanning electron microscopy (SEM) micrograph of a pore created by FIB-milling in a SiN membrane with a diameter of 180 nm. The pore closes under electron irradiation. In **(a)** the irradiation was started, and it ended in figure **(d)** where the pore shrunk to 80 nm after an electron dose of 657 $nC/\mu m^2$.

these experiments we could confirm a temperature dependence of the closing rate for all materials. Furthermore, there was a dependence of the material and the used ion species. With this information we developed a model to describe the behaviour of the closing rate [7]. Using this model it is possible to keep track of the diameter variation during an implantation. Furthermore, it can be applied to create pores down to a few nanometres which is not possible with the before mentioned techniques.

[1] S. Pezzagna et al.: Phys. Status Solidi A **208**, 2017 (2011), doi:10.1002/pssa.201100455
[2] S. Pezzagna et al.: Small **6**, 2117 (2010), doi:10.1002/smll.201000902
[3] C. Scheuner et al.: Sci. Rep. **7**, 17081 (2017), doi:10.1038/s41598-017-17005-w
[4] H.B. George et al.: J. Appl. Phys. **108**, 014310 (2010), doi:10.1063/1.3452390
[5] J. Li et al.: Nature **412**, 166 (2001), doi:10.1038/35084037
[6] A.J. Storm et al.: Nat. Mat. **2**, 537 (2003), doi:10.1038/nmat941
[7] C. Scheuner: Master thesis, Universität Leipzig (2017)

7.5 Wide field imaging of magnetic fields using NV centres in diamonds

R. John, R. Staacke, S. Pezzagna, J. Meijer

The possibility to measure absolute magnetic fields simultaneously in all three dimensions from 4 K up to room temperature makes ensembles of nitrogen–vacancy (NV) centres in diamond a promising sensor for magnetometry. Fields down to 100 fT can be detected for sensor volumes of the order of 10^{-3} mm^3 [1]. By using a complementary metal-oxide-semiconductor (CMOS) camera we show, that it is possible to enhance the lateral resolution to the Abbe-limit of $\approx$ 400 nm with measurable fields down to $\approx$ 150 µT.

The NV centre is a defect in diamond consisting of a N atom replacing a C atom in the lattice with a neighbouring vacancy. The interesting feature of the NV centre is a difference in the possibilities for the fluorescence intensity depending on the magnetic spin quantum number m_s of the current state of the NV centre. For $m_s = 0$ the fluorescence is bright and for the states with $m_s = \pm 1$ the fluorescence is slightly darker. The energy difference between the $m_s = 0$ and $m_s = \pm 1$ ground states without any external magnetic field is 2.87 GHz [2]. The Zeeman splitting of the $m_s = \pm 1$ states is 28 GHz/T [3]. By sweeping a microwave around the resonances between the $m_s = 0$ and $m_s = \pm 1$ ground states, it is possible to measure the external magnetic field projection in the NV axis by fitting the shift of the fluorescence dips. Since the magnetic field projection is different for the four possible NV centre orientations, it is possible to reconstruct the magnetic field vector from the up to eight dips in the fluorescence.

With our current setup it is possible to measure absolute magnetic fields and their vector components simultaneously over large areas (e.g. Fig. 7.5). Fields down to $\approx$ 150 µT can be detected. In the future we can push this limit one to two orders of magnitudes down using pulsed techniques.

[1] T. Wolf et al.: Phys. Rev. X **5**, 041001 (2015), doi:10.1103/PhysRevX.5.041001

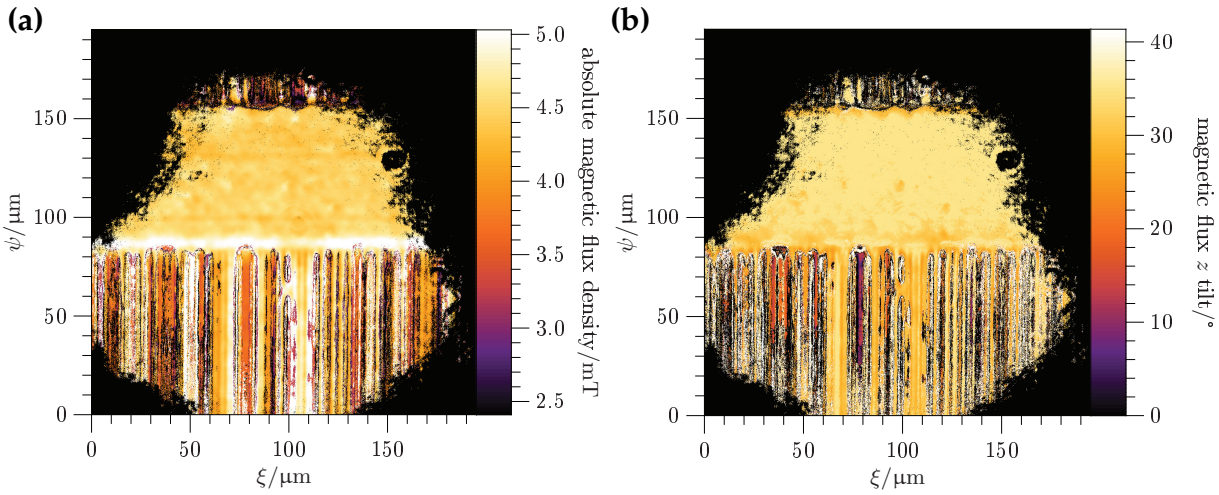

Figure 7.5: (a) Image of the absolute value of the magnetic field on the surface of a floppy disk. **(b)** Image of the tilt of the magnetic field with respect to the floppy disk surface normal.

[2] A. Gruber et al.: Science **276**, 2012 (1997), doi:10.1126/science.276.5321.2012
[3] R. Schirhagl et al.: Annu. Rev. Phys. Chem. **65**, 83 (2014), doi:10.1146/annurev-physchem-040513-103659

7.6 Investigation of the graphitization process of ion-beam irradiated diamond using ellipsometry, Raman spectroscopy and low temperature transport measurements

T. Lühmann, R. Wunderlich, R. Schmidt-Grund*, J. Barzola-Quiquia†, P. Esquinazi†, M. Grundmann*, J. Meijer

*Division of Semiconductor Physics
†Division of Superconductivity and Magnetism

Diamond and graphite are allotropes of carbon. Graphite is characterised by sp^2-hybridised bonds, it is electrically conductive, mechanically soft and optically highly absorbent. In contrast, diamond exhibits sp^3-hybridised bonds and it is the hardest natural material, chemically inert, has a wide band gap and is consequently optically transparent over a wide spectral range. Graphite is the stable phase of carbon and diamond is formed under extreme conditions. The complete or local transformation from one allotrope to the other is possible. On the one hand, if several sp^3 bonds are cracked by an input of energy, like laser beam or particle irradiation, diamond is transformed to disordered graphite-like diamond and, following temperature annealing process, transformed to graphite. On the other hand graphite undergoes a transformation to diamond at high pressure and high temperature. The two different bonding configurations of carbon are separated by a potential barrier, which is correlated to the

critical energy density $E_c = D_c \nu / X$ [1], where D_c is the critical fluence for the diamond-graphitisation, ν is the deposited energy per ion and X is the depth of the implanted ions. Different mixtures between sp^3- and sp^2-hybrid bonds are possible depending on the defect concentration. This leads to a large number of miscellaneous materials like thermally evaporated carbon [2], glassy carbon [3] and amorphous diamond [4], since mixing the two bond types and crystallinity result in different physical and chemical properties of these materials.

One possibility to induce local defects in diamond is ion beam irradiation. Controlling the energy loss of the ion beam via the ion mass or the kinetic energy and the ion fluence allows to form 3D structures inside the diamond by focusing the ion beam accordingly. The defect concentration and thus the degree of graphitisation can be controlled by the fluence of irradiation. At very high fluence a nearly complete transformation of non conductive diamond into a conductive graphite-like diamond phase [5] is possible [6–9]. This has been used to structure diamond samples, since the highly graphitised phase can be etched easily [6–10].

As a simple model, the graphitisation process can be described by the creation of sp^2-spheres inside a sp^3-matrix [1]. But so far, details of the real structure as well as the evolving macroscopic physical properties have not been studied thoroughly. In this work, we investigate buried thin film structures in diamond produced by focused He^+-ion beam irradiation. By modelling their optical response using the Bruggeman effective-medium-approximation-model (EMA) [11], in combination with Raman investigations, we were able to determine some structural properties by optical means. The determined structural parameters and the observed 3D variable-range hopping-mechanism (VRH) [1, 12–16] leads to an estimation of the localisation length parameter $\xi = 5$ Å and the density of states at the Fermi level (see Fig. 7.6).

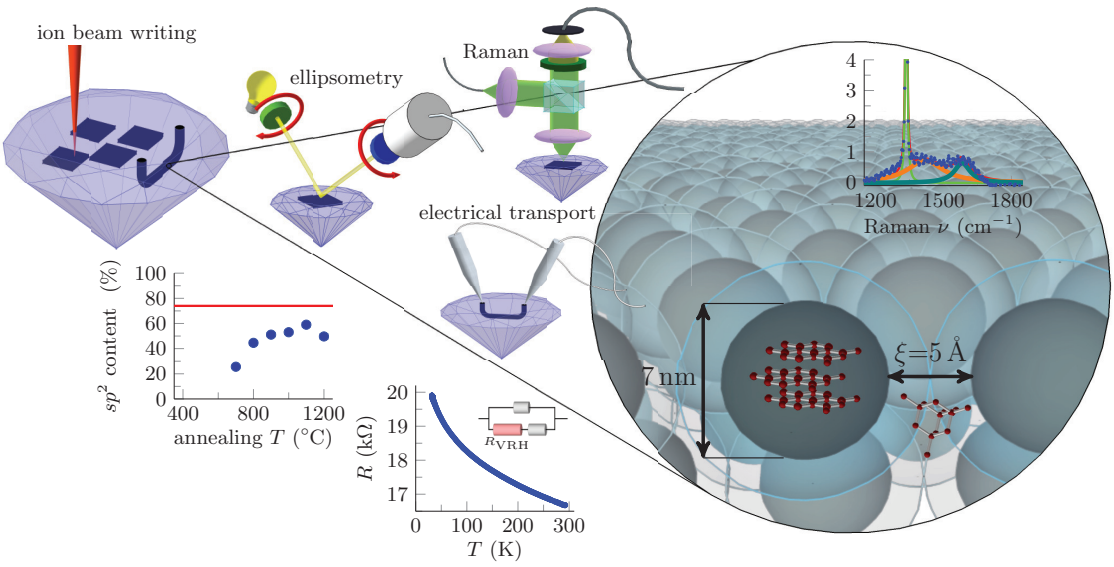

Figure 7.6: Illustration of the experiments and results. At first the graphite structures are made by high energy ion beam writing. Structural properties like the grain size and the localisation length parameter ξ were determined by combination of different methods: Raman, ellipsometry and temperature dependent electrical transport measurements.

[1] R. Kalish et al.: Rad. Eff. **52**, 153 (1980), doi:10.1080/00337578008210028
[2] X.D. Zhu et al.: J. Phys.: Condens. Matter **14**, 5083 (2002), doi:10.1088/0953-8984/14/20/304
[3] F.R. McFeely et al.: Phys. Rev. B **9**, 5268 (1974), doi:10.1103/physrevb.9.5268
[4] A.C. Ferrari et al.: Phil. Trans. R. Soc. A **362**, 2477 (2004), doi:10.1098/rsta.2004.1452
[5] V.S. Vavilov et al.: Rad. Eff. **22**, 141 (1974), doi:10.1080/00337577408232161
[6] A.A. Gippius et al.: Diamond Relat. Mater. **8**, 1631 (1999), doi:10.1016/s0925-9635(99)00047-3
[7] P. Olivero et al.: Europ. Phys. J. B **75**, 127 (2009), doi:10.1140/epjb/e2009-00427-5
[8] P. Olivero et al.: Diamond Relat. Mater. **18**, 870 (2009), doi:10.1016/j.diamond.2008.10.068
[9] R.S. Patti: Proc. IEEE **94**, 1214 (2006), doi:10.1109/jproc.2006.873612
[10] J.D. Hunn et al.: Appl. Phys. Lett. **65**, 3072 (1994), doi:10.1063/1.112959
[11] D.A.G. Bruggeman: Ann. Phys. **416**, 636 (1935), doi:10.1002/andp.19354160802
[12] S. Prawer et al.: Phys. Rev. B **51**, 15711 (1995), doi:10.1103/PhysRevB.51.15711
[13] J.J. Hauser et al.: Solid State Commun. **18**, 789 (1976), doi:10.1016/0038-1098(76)90205-2
[14] J.J. Hauser et al.: Appl. Phys. Lett. **30**, 129 (1977), doi:10.1063/1.89323
[15] J.F. Prins: Rad. Eff. Lett. **76**, 79 (1983), doi:10.1080/01422448308209641
[16] J.F. Prins: Phys. Rev. B **31**, 2472 (1985), doi:10.1103/physrevb.31.2472

7.7 Photoelectric investigations on nitrogen–vacancy centres

S. Becker, J. Meijer

For its application as a qubit in a solid-state, room-temperature quantum computer the quantum state of the nitrogen–vacancy (NV) centre in diamond has to be initialized, manipulated and read out. As a colour centre the NV can absorb electromagnetic radiation to get excited or ionized. This property is utilized in the three aforementioned processes. The state of the art here is an optical readout that is realized via the optically detected magnetic resonance (ODMR) method. But there are certain drawbacks of this compared to an electrical readout. These drawbacks relate to simple effectiveness questions like the collection efficiency as well as progressed considerations like the connection of the qubit to the electrically operating parts of a future quantum computer. The ODMR technique as well as a photoelectrical readout are based on the different probabilities of the spin sublevels for the direct decay between the triplets states or the decay via the metastable singlet state. The manipulation of the spin state is also realized in both approaches by irradiation of microwaves in an appropriate frequency range. First achievements for the photoelectrically detected approach have been published by Bourgeois et al. [1].

In our work we started with photoelectrical detection of the NV centres without any manipulation of the spin state by microwaves. By applying an electric field to the NV centres, that was realized with a DC voltage source, and lithographically produced contacts on the diamond surface and the excitation and ionization of the centres by

green laser light, we could measure a photocurrent. But since the substitutional N atom is a common defect in diamond that is susceptible to the applied laser light and whose occurrence is not separable from the production process of NV centres, the dependence of the magnitude of the photocurrent on the laser power ($I - P$) was investigated to differentiate between the signal of these two defect species. Because the ionization event for the NV centre is a two photon process, a quadratic $I - P$-dependence was expected in contrast to a linear dependence for the substitutional N atoms with a one photon ionization process. This quadratic dependence was indeed observed for very pure (electronic grade) diamond samples, but not for less pure (optical grade) samples (see Fig. 7.7), which can be explained by the high N concentration in the optical grade diamonds that simply dominated over the signal produced by the NV centres. The

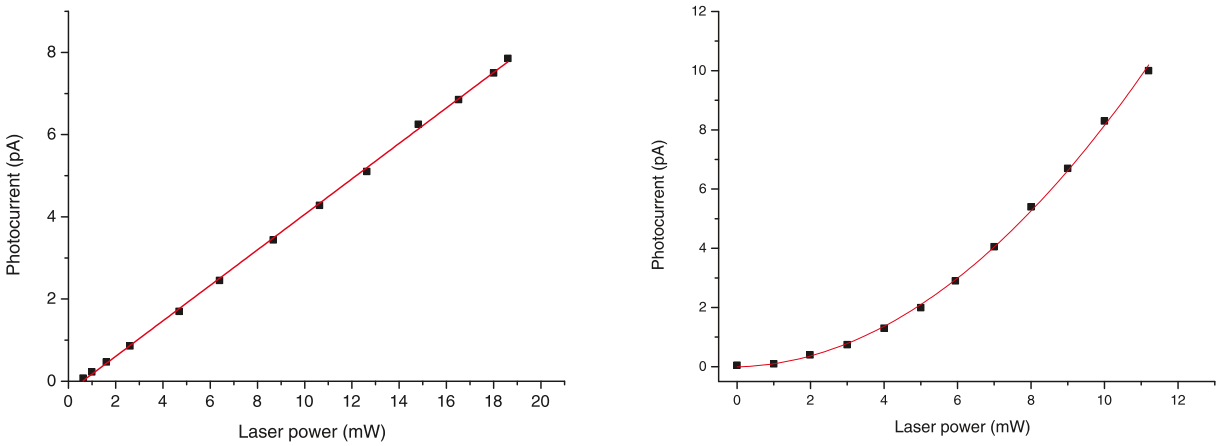

Figure 7.7: Dependence of the photocurrent on the laser power for an optical grade diamond (*left*) and an electronic grade diamond (*right*).

expansion of the setup by microwaves will then enable us to distinguish between the different spin states of the centre.

[1] E. Bourgeois et al.: Nat. Commun. **6**, 8577 (2015), doi:10.1038/ncomms9577

7.8 Polarising nitrogen–vacancy centre spins in the level-anti-crossing using ODMR technique

E. Wiedemann, R. John, S. Pezzagna, J. Meijer

The nitrogen–vacancy (NV) centre in diamond is an excellent candidate to realise quantum qubits. The quantum information is encoded in the spins of this electron system. The diamond material is a major advantage for the development of a quantum computer. It possesses a very large bandgap energy which makes diamond insulating. In addition, the basic diamond isotope ^{12}C is not spin-active. These two properties isolate the NV centre from interacting with the environment. Diamond's high transparency, resulting from the high band gap, makes it best suitable for detecting the centres fluorescence using laser experiments, which are comparatively simple and low-price.

The NV spin interacts with the microwave. Gruber et al. observed the so-called optically detected magnetic resonance (ODMR) in 1997 [1]. This experiment gave the first hints of the NV centres possible use as a relatively cheap and easy accessible qubit and quantum computation processor.

The transfer to the long-term storage of quantum information is still an immensely important topic when building a quantum computer with NV centres. Its comparatively long spin lifetime at room temperature is one of the NV centre's prevailing key features. It allows for a simpler information readout process without expensive cooling on a feasible time scale. These spin lifetimes occur due to the interactions of the electron spin with the atomic nuclei surrounding it. The relevant nuclei are the associated ^{14}N or ^{15}N atom and next neighbour ^{13}C atoms. Especially the ^{13}C atomic nuclei have very long spin-lattice relaxation times up to several hours, due to its weak lattice interaction. Hence, ^{13}C atoms are good candidates for logical operations and quantum memory [2].

To address these atomic nuclei and transfer quantum information between their nuclear spin and the NV's electron spin, we used the level anti-crossing (LAC) as a median. For the NV centre, LACs occur between the states $m_s = 0$ and $m_s = -1$ in both the excited state and the ground state. Applying ODMR techniques work as a quantum gate, polarising the spin to the minimal electron spin and the maximal nuclear spin eigenstate [3]. In terms of quantum information, this polarisation is an information transfer between electron and nuclei. For the excited state, the use of the LAC for polarisation has been shown [3, 4], but up to now the ground state LAC had not yet been utilised. The presented work establishes how to determine the ground state's nuclear spin polarisation of the NV centre working with the ODMR setup. In order to achieve the required magnetic fields, it was necessary to construct a module which fully controls the magnetic field applied to the NV centre within a diamond sample. To identify the LAC, we developed a method to find the alignment of the magnetic field's B_z direction and NV symmetry axis. Finally, we proved the polarisation of the NV centre in the LAC with ODMR measurements (Fig. 7.8).

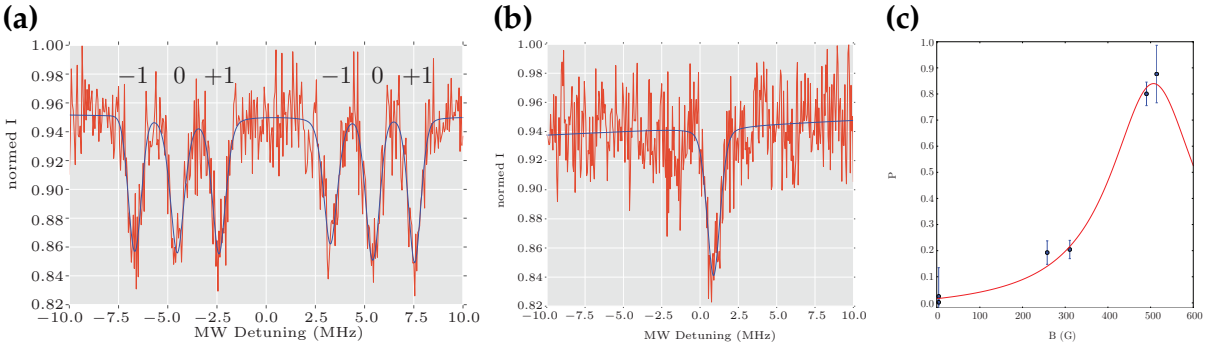

Figure 7.8: Nuclear spin polarisation of a single NV centre. **(a)** Hyperfine resolved spectra of ^{14}N at small field. The annotations appoint the nuclear spin transition. The central frequency is 2.870 GHz. The intensities of the resonance lines have approximately the same values, resulting in a polarisation degree of about 0 %. **(b)** Complete nuclear spin polarisation at 514 G. The field is perfectly aligned at a central frequency of 1.430 GHz. The polarisation degree is $P = 87.6$ %. **(c)** Degree of polarisation P depending on the magnetic field strength in an aligned field. The polarisation (*blue dots*) follows a Lorentzian distribution. The curve's form highly depends on the laser power.

[1] A. Gruber et al.: Science **276**, 2012 (1997), doi:10.1126/science.276.5321.2012
[2] F. Jelezko et al.: Phys. Rev. Lett. **93**, 130501 (2004), doi:10.1103/PhysRevLett.93.130501
[3] B. Smeltzer et al.: Phys. Rev. A **80**, 050302(R) (2009), doi:10.1103/PhysRevA.80.050302
[4] M. Steinert et al.: Phys. Rev. B **81**, 035205 (2010), doi:10.1103/PhysRevB.81.035205

7.9 Funding

Utilization of Ion Accelerators for Studying and Modelling of Radiation Induced Defects in Semiconductors and Insulators
Prof. Dr. J. Meijer
IAEA: CRP F11016

DIAmond Devices Enabled Metrology and Sensing (DIADEMS)
Prof. Dr. J. Meijer
EU: FP7-ICT-2013.9.7 611143

Joint Lab "Einzelionenimplantation": "Sensorik mit einzelnen Atomen"
Prof. Dr. Dr. h.c. B. Rauschenbach/Prof. Dr. J. Meijer
Leibniz-Gemeinschaft/EU

Diamond Materials for Quantum Application: Ultraprecise deterministic doping of diamond
Prof. Dr. J. Meijer
DFG: FOR1493

ECR-Ionenquelle
Prof. Dr. J. Meijer
DFG: HBFG

Kontrollierte Erzeugung von Defekt-Induziertem Magnetismus (DIM) in graphit- und diamantbasierten Filmen
Prof. Dr. J. Meijer/Prof. Dr. P. Esquinazi
DFG: ME 1564/11-1

Quanten und klassische Lichtquellen in Silizium: Verunreinigungen und komplexe Defekte für die Nanophotonik
Dr. S. Pezzagna, Prof. Dr. J. Meijer
DFG: ULYSSES

Leipzig School of Natural Sciences - Building with Molecules and Nano-objects (BuildMoNa)
Prof. Dr. M. Grundmann, Prof. Dr. J. Meijer
DFG: GS 185/2

Engineering Single Atoms for Quantum Technologies
Prof. Dr. J. Meijer
DAAD: 57319788

Integration of Molecular Components in Functional Macroscopic Systems: Coupling color centers into macroscopic quantum systems with an atomic nano-assembler
Prof. Dr. J. Meijer
VolkswagenStiftung

Functionalized Nanodiamonds for Biomedical Research and Therapy
Prof. Dr. J. Meijer
VolkswagenStiftung

EXMAD – Extreme Sensitive Magnetometry using Nitrogen–Vacancy Centers in Diamond
Prof. Dr. U.L. Andersen/Prof. Dr. J. Meijer
The Danish Council for Strategic Research

7.10 Organizational Duties

J. Meijer
- Member Study Commission (Physics): Faculty of Physics and Earth Sciences, Universität Leipzig
- Member PhD Board: Faculty of Physics and Earth Sciences, Universität Leipzig
- Principal Investigator: Graduate School BuildMoNa, Universität Leipzig
- Member User Selection Panel for the Ion Beam Center: Helmholtz-Zentrum Dresden–Rossendorf
- Member Advisory Board: ISTAC Croatian Nuclear Science
- Referee: Several journals

S. Pezzagna
- Referee: Several journals

P. Räcke
- Speaker Doctoral Candidates Committee: Graduate School BuildMoNa, Universität Leipzig
- Doctoral representative: Graduate Centre Mathematics/Computer Science and Natural Sciences, Research Academy Leipzig, Universität Leipzig
- Session Chair: Annual BuildMoNa Conference, Leipzig, 06.–07.03.2017

7.11 External Cooperations

Academic

- City University of New York, College of Staten Island, Department of Engineering Science and Physics, USA
  Assoc. Prof. Dr. A.M. Zaitsev
- Centre National de la Recherche Scientifique (CNRS), École normale supérieure (ENS), Laboratoire Aimé Cotton (LAC), Cachan, France
  Prof. Dr. J.-F. Roch

- Centre National de la Recherche Scientifique (CNRS), Laboratoire des Sciences des Procédés et des Matériaux (LSPM), Fabrication Processes of Advanced Materials (PEMA), Paris, France
  Prof. Dr. J. Achard
- Commissariat à l'énergie atomique et aux énergies alternatives (CEA), Institut Rayonnement Matière de Saclay (IRAMIS), Service de Physique de l'Etat Condensé (SPEC), Quantronique, Saclay, France
  Prof. Dr. D. Esteve
- ETH Zürich, Physikdepartement, Laboratorium für Festkörperphysik, Spin Physics and Imaging, Switzerland
  Prof. Dr. C. Degen
- Fraunhofer-Institut für Angewandte Festkörperphysik Freiburg, Mikro- und Nanosensoren
  Dr. C.E. Nebel
- Humboldt-Universität zu Berlin, Mathematisch-Naturwissenschaftliche Fakultät I, Institut für Physik, AG Nanooptik
  Prof. Dr. O. Benson
- Hungarian Academy of Sciences, Wigner Research Centre for Physics, Institute for Solid State Physics and Optics, Budapest, Hungaria
- Interuniversitair Micro-Electronica Centrum (imec) Leuven, Belgium
- Julius-Maximilians-Universität Würzburg, Fakultät für Chemie und Pharmazie, Institut für Organische Chemie
  Prof. Dr. A. Krüger
- Leibniz-Institut für Oberflächenmodifizierung e.V. Leipzig
  Prof. Dr. Dr. h.c. B. Rauschenbach, Prof. Dr. B. Abel
- Leibniz-Universität Hannover, Institut für Anorganische Chemie, AK Analytik
  Prof. Dr. C. Vogt
- Ludwig-Maximilians-Universität München, Fakultät für Physik, Experimentelle Quantenphysik
  Prof. Dr. H. Weinfurter
- Max-Planck-Institut für biophysikalische Chemie Göttingen, Karl-Friedrich-Bonhoeffer-Institut, Abt. NanoBiophotonik
  Prof. Dr. Dr. h.c. St.W. Hell
- Technische Universität München, Walter Schottky Institut, E25: Spins and Defects in Semiconductors
  Prof. Dr. M.S. Brandt
- Università di Torino, Dipartimento di Fisica Sperimentale, Gruppo di Fisica dello Stato Solido
  Prof. Dr. E. Vittone
- Universität Basel, Department of Physics, Quantum-Sensing Lab, Switzerland
  Prof. Dr. P. Maletinsky
- Universität Kassel

- Universität Konstanz, Mathematisch-Naturwissenschaftliche Sektion, Fachbereich Physik, Lehrstuhl für Ultrakurzzeitphysik und Photonik
  Prof. Dr. A. Leitenstorfer
- Universität Leipzig, Medizinische Fakultät, Institut für Medizinische Physik und Biophysik
  Prof. Dr. E. Donath, Dr. I. Estrela-Lopis, Priv.-Doz. Dr. U. Reibetanz
- Universität Mainz, Fachbereich Physik, Mathematik und Informatik, Institut für Physik, Arbeitsgruppe Quanten-, Atom- & Neutronenphysik (QUANTUM)
  Prof. Dr. F. Schmidt-Kaler, Priv.-Doz. Dr. K. Singer
- Universität Stuttgart, Fakultät Mathematik und Physik, 3. Physikalisches Institut
  Prof. Dr. J. Wrachtrup
- Universität Ulm, Fakultät für Naturwissenschaften, Institut für Quantenoptik
  Prof. Dr. F. Jelezko
- Universität Ulm, Fakultät für Naturwissenschaften, Institut für Theoretische Physik, Controlled Quantum Dynamics Group
  Prof. Dr. M.B. Plenio
- University of Warwick, Department of Physics, Condensed Matter Physics, Magnetic Resonance Cluster, Coventry, UK
  Prof. Dr. M. Newton
- Universität Wien
- Westfälische Wilhelms-Universität Münster, Physikalisches Institut
  Prof. Dr. R. Bratschitsch

Industry

- ARTTIC Paris, France
- attocube systems AG München
- Element Six Ltd. Shannon, Co. Clare, Ireland
- THALES Research & Technology Palaiseau, France

7.12 Publications

Journals

J. Barzola-Quiquia, T. Lühmann, R. Wunderlich, M. Stiller, M. Zoraghi, J. Meijer, P. Esquinazi, J. Böttner, I. Estrela-Lopis: *Fabrication and electrical transport properties of embedded graphite microwires in a diamond matrix*, J. Phys. D: Appl. Phys. **50**, 145301 (2017), doi:10.1088/1361-6463/aa6013

S. Ditalia Tchernij, T. Herzig, J. Forneris, J. Küpper, S. Pezzagna, P. Traina, E. Moreva, I.P. Degiovanni, G. Brida, N. Skukan, M. Genovese, M. Jakšić, J. Meijer, P. Olivero: *Single-Photon-Emitting Optical Centers in Diamond Fabricated upon* Sn *Implantation*, ACS Photonics **4**, 2580 (2017), doi:10.1021/acsphotonics.7b00904

R. John, J. Lehnert, M. Mensing, D. Spemann, S. Pezzagna, J. Meijer: *Bright optical centre in diamond with narrow, highly polarised and nearly phonon-free fluorescence at room temperature*, New J. Phys. **19**, 053008 (2017), doi:10.1088/1367-2630/aa6d3f

J. Lehnert, J. Meijer, C. Ronning, D. Spemann, E. Vittone: *Ion Beam Induced Charge analysis of diamond diodes*, Nucl. Instrum. Meth. Phys. Res. B **404**, 259 (2017), doi:10.1016/j.nimb.2017.01.021

D. Lichtenstein, J. Ebmeyer, T. Meyer, A.-C. Behr, C. Kästner, L. Böhmert, S. Juling, B. Niemann, C. Fahrenson, S. Selve, A.F. Thünemann, J. Meijer, I. Estrela-Lopis, A. Braeuning, A. Lampen: *It takes more than a coating to get nanoparticles through the intestinal barrier in vitro*, Eur. J. Pharm. Biopharm. **118**, 21 (2017), doi:10.1016/j.ejpb.2016.12.004

D. Lichtenstein, T. Meyer, L. Böhmert, S. Juling, C. Fahrenson, S. Selve, A. Thünemann, J. Meijer, I. Estrela-Lopis, A. Braeuning, A. Lampen: *Dosimetric quantification of coating-related uptake of silver nanoparticles*, Langmuir **33**, 13087 (2017), doi:10.1021/acs.langmuir.7b01851

T. Lühmann, R. Wunderlich, R. Schmidt-Grund, J. Barzola-Quiquia, P. Esquinazi, M. Grundmann, J. Meijer: *Investigation of the graphitization process of ion-beam irradiated diamond using ellipsometry, Raman spectroscopy and electrical transport measurements*, Carbon **121**, 512 (2017), doi:10.1016/j.carbon.2017.05.093

M. Pfender, N. Aslam, P. Simon, D. Antonov, G. Thiering, S. Burk, F.F. de Oliveira, A. Denisenko, H. Fedder, J. Meijer, J.A. Garrido, A. Gali, T. Teraji, J. Isoya, M.W. Doherty, A. Alkauskas, A. Gallo, A. Grüneis, P. Neumann, J. Wrachtrup: *Protecting a diamond quantum memory by charge state control*, Nano Lett. **17**, 5931 (2017), doi:10.1021/acs.nanolett.7b01796

C. Scheuner, St. Jankuhn, J. Vogt, S. Pezzagna, C. Trautmann, J. Meijer: *Nanometer collimation enhancement of ion beams using channeling effects in track-etched mica capillaries*, Sci. Rep. **7**, 17081 (2017), doi:10.1038/s41598-017-17005-w

S. Schmitt, T. Gefen, F.M. Stürner, T. Unden, G. Wolff, C. Müller, J. Scheuer, B. Naydenov, M. Markham, S. Pezzagna, J. Meijer, I. Schwarz, M. Plenio, A. Retzker, L.P. McGuinness, F. Jelezko: *Submillihertz magnetic spectroscopy performed with a nanoscale quantum sensor*, Science **356**, 832 (2017), doi:10.1126/science.aam5532

H. Sieg, C. Kästner, B. Krause, T. Meyer, A. Burel, L. Böhmert, D. Lichtenstein, H. Jungnickel, J. Tentschert, P. Laux, A. Braeuning, I. Estrela-Lopis, F. Gauffre, V. Fessard, J. Meijer, A. Luch, A.F. Thünemann, A. Lampen: *Impact of an Artificial Digestion Procedure on Aluminum-Containing Nanomaterials*, Langmuir **33**, 10726 (2017), doi:10.1021/acs.langmuir.7b02729

M. Stiller, J. Barzola-Quiquia, P.D. Esquinazi, S. Sangiao, J.M. De Teresa, J. Meijer, B. Abel: *Functionalized Akiyama tips for magnetic force microscopy measurements*, Meas. Sci. Technol. **28**, 125401 (2017), doi:10.1088/1361-6501/aa925e

J. Tentschert, P. Laux, H. Jungnickel, J. Brunner, B. Krause, I. Estrela-Lopis, C. Merker, J. Meijer, H. Ernst, L. Ma-Hock, J. Keller, R. Landsiedel, A. Luch: *Long-term low-dose*

exposure study of inhaled cerium dioxide – Organ burden quantification and pattern of particle distribution in organs, Toxicol. Lett. **280S**, S311 (2017), doi:10.1016/j.toxlet.2017.08.037

R. Wunderlich, J. Kohlrautz, B. Abel, J. Haase, J. Meijer: *Optically induced cross relaxation via nitrogen-related defects for bulk diamond* ^{13}C *hyperpolarization*, Phys. Rev. B **96**, 220407(R) (2017), doi:10.1103/physrevb.96.220407

Talks

Ph. Campagne-Ibarcq, S. Probst, P. Jamonneau, Y. Kubo, A. Bienfait, S. Pezzagna, P. Bertet *Toward strong coupling of a single NV center in diamond to a superconducting circuit*
APS March Meeting, New Orleans, LA, USA, 13.–17.03.2017

R. John
Optical properties of the L1 colour centre in diamond
Annual BuildMoNa Conference, Leipzig, 06.–07.03.2017

R. John, J. Lehnert, M. Mensing, D. Spemann, S. Pezzagna, J. Meijer
Bright optical centre in diamond with narrow, highly polarised and nearly phonon-free fluorescence at room temperature
68th Diamond Conference, Warwick, UK, 10.–13.07.2017

D. Lehmann
Ionisierende Strahlung – die "unsichtbare" Botschaft aus dem Inneren radioaktiver Atome. Eine Zeitreise über 5 Jahrzehnte von der Entdeckung der X-Strahlen bis zur Entdeckung der Kernspaltung
Seminar, Arnold-Sommerfeld-Gesellschaft e.V., Leipzig, 16.03.2017, invited

D. Lehmann
Ionisierende Strahlung – die "unsichtbare" Botschaft aus dem Inneren radioaktiver Atome. Der Start des geheimen Uranprojekts in Deutschland vor 78 Jahren, sein Verlauf und seine Ergebnisse aus heutiger Sicht. Der Beitrag der "Leipziger Physik"
Seminar, Arnold-Sommerfeld-Gesellschaft e.V., Leipzig, 22.06.2017, invited

D. Lehmann
Die Atombombe – vor 100 Jahren noch Science Fiction, vor 70 Jahren grausame Wirklichkeit
Seminar, Arnold-Sommerfeld-Gesellschaft e.V., Leipzig, 16.11.2017, invited

S. Pezzagna, D. Spemann, P. Räcke, N. Raatz, J.W. Gerlach, B. Rauschenbach, J. Meijer
Single Ion Implantation: An important tool for fabrication of quantum devices based on NV-centers
Quantum 2017, Torino, Italy, 07.–13.05.2017

N. Raatz, S. Pezzagna, J. Meijer
Single Ion Implantation with High Spatial Resolution
Workshop Ionenstrahlphysik, Göttingen, 13.–15.02.2017

N. Raatz, S. Pezzagna, S. Becker, St. Jankuhn, J. Meijer
Single Ion Implantation with High Lateral Resolution
Seminar, Centre for Quantum Computation & Communication Technology (CQC^{2}T), University of Melbourne, Australia, 22.06.2017, invited

P. Räcke, J. Meijer
Image Charge Detection for Ion Implantation
Workshop Ionenstrahlphysik, Göttingen, 13.–15.02.2017

P. Räcke, D. Spemann, J.W. Gerlach, S. Rauschenbach, B. Rauschenbach, J. Meijer
Image Charge Detection and Deterministic Ion Implantation
Seminar, Centre for Quantum Computation & Communication Technology (CQC^2T), University of Melbourne, Australia, 17.07.2017, invited

C. Scheuner, S. Pezzagna, P. Räcke, J. Meijer
Development of Nano Apertures for Ion Beam Collimation
Workshop Ionenstrahlphysik, Göttingen, 13.–15.02.2017

S. Schmitt, T. Gefen, F.M. Stürner, T. Unden, G. Wolff, C. Müller, J. Scheuer, B. Naydenov, M. Markham, S. Pezzagna, J. Meijer, I. Schwarz, M. Plenio, A. Retzker, L.P. McGuinness, F. Jelezko
Sub-millihertz magnetic spectroscopy with a nanoscale quantum sensor
DPG-Frühjahrstagung, Dresden, 19.–24.03.2017

R. Wunderlich, J. Kohlrautz, J. Haase, J. Meijer
Hyperpolarisation of ^{13}C via nitrogen vacancy centres
68th Diamond Conference, Warwick, UK, 10.–13.07.2017

R. Wunderlich, J. Kohlrautz, B. Abel, J. Haase, J. Meijer
Optically Induced Cross Relaxation via Nitrogen Vacancy Centers for Bulk Diamond C-13 Hyperpolarization
MRS Fall Meeting & Exhibit, Boston, MA, USA, 26.11.–01.12.2017

V. Zviagin, Y. Kumar, P. Huth, I. Lorite, A. Setzer, D. Spemann, J. Meijer, R. Denecke, P. Esquinazi, M. Grundmann, R. Schmidt-Grund
Optical Investigation of Structural Disorder in Normal Spinel Ferrites in Relation to Magnetic Properties
DPG-Frühjahrstagung, Dresden, 19.–24.03.2017

Posters

V. Zviagin, Y. Kumar, P. Huth, I. Lorite, A. Setzer, D. Spemann, K. Fleischer, J. Meijer, R. Denecke, P. Esquinazi, M. Grundmann, R. Schmidt-Grund
Spectroscopic Ellipsometry as a Method for Structural Investigation of Spinel Ferrite Thin Films
DPG-Frühjahrstagung, Dresden, 19.–24.03.2017

7.13 Graduations

Master

- J. Helbig
  Erzeugung von n-Typ in CVD-gewachsenem Diamanten mittels Ionenimplantation
  October 2017

- J. Küpper
  Änderung des Ladungszustandes von NV-Zentren durch p-i-p Dioden in Diamant
  November 2017
- M. Ritzschke
  Untersuchungen zu wasserstoffinduzierten Donator-Komplexen in Silizium
  September 2017
- C. Scheuner
  Entwicklung von Nanoaperturen zur Ionenstrahl-Kollimation
  July 2017
- E. Wiedemann
  Polarising Nitrogen Vacancy Centre Spins In The Level-Anti Crossing Using ODMR Technique
  March 2017

Bachelor

- C. Bräutigam
  Untersuchung zur Auswirkung einer niederfrequenten Sauerstoffplasmabehandlung auf oberflächennahe NV*-Zentren im Diamanten*
  January 2017
- F. Renner
  Einfluss von Defekten auf T_2^**-Zeiten von NV-Zentren im Diamanten*
  June 2017

7.14 Guests

- Dr. M. Abbarchi, A. Benali
  Aix-Marseille Université, IM2NP, Equipe Nanostructures Semiconductrices Epitaxiées, Marseille, France
  15.–17.03.2017
- F. Barbosa da Silva
  CEA, Quantronics Group, Saclay, France
  28./29.06.2017
- C. Beaufils, Prof. Dr. G. Cassabois, W. Redjem
  Université Montpellier, Laboratoire Charles Coulomb, Equipe Nanostructures quantiques, Propriétés optiques, Montpellier, France
  15.–17.03.2017
- S. Ditalia Tchernij
  University of Torino, Physics Department and "NIS" Inter-departmental Centre; Istituto Nazionale di Fisica Nucleare (INFN), Sez. Torino, Italy
  21.04.–21.06.2017
- Ph. Fuchs
  Universität des Saarlandes, Naturwissenschaftlich-Technische Fakultät, Fachrich-

tung Physik, AG Quantenoptik, Saarbrücken
02.–05.05., 18.–22.09.2017

- Prof. Dr. Ph.R. Hemmer
  Texas A&M University, Institute for Quantum Science and Engineering, Department of Electrical and Computer Engineering, College Station, TX, USA
  13.07., 13.–15.12.2017
- Mathias Holz
  nano analytik GmbH, Ilmenau
  01.03.2017
- Dr. V. Ivády
  Hungarian Academy of Science, Budapest, Hungary
  22./23.08.2017
- Prof. Dr. D.N. Jamieson
  Australian Research Council Centre of Excellence for Quantum Computation and Communication Technology; University of Melbourne, School of Physics, Parkville, VIC, Australia
  17.07.2017
- Marcus Kästner, Prof. Dr.-Ing. I.W. Rangelow
  TU Ilmenau, Fakultät für Elektrotechnik und Informationstechnik, FG Mikro- und nanoelektronische Systeme
  01.03.2017
- L. Nicolas
  ENS, Département de Physique, Laboratoire Pierre Aigrain, Groupe Optique Cohérente et Non Linéaire, Paris, France
  29./30.06.2017
- Xi Kong, Xiangyu Ye
  University of Science and Technology, Department of Modern Physics, Hefei, China
  11.–15.09.2017

8

Semiconductor Physics

Preface

We hope that our research report finds your interest and gives you an update about the recent discoveries in the Semiconductor research Group. Among others, you will find novel findings on exceptional points in optically anisotropic materials and microcavities, lasing in nanostructures and electrical properties of contacts to oxide semiconductors.

A highlight of 2017 was the TCO2017 conference that brought together national and international experts in the fields of transparent conductive oxides and oxide semiconductors. We are looking forward to TCO2019 (see back cover) becoming an equally large success.

A particularly interesting feature of anisotropic (biaxial) optical materials is the occurence of singular axes. For such axis only one polarization eigenmode exists. We had investigated this phenomenon in monoclinic gallia bulk crystals. Here, we extend this research to KTP, a popular crystal for non-linear optics, that additionally exhibits optical activity and a gyration pseudotensor (Chap. 8.12). A related phenomenon are

the polarization properties of anisotropic microcavities, i.e. cavities where the optic axis of the uniaxial cavity medium (e.g. GaN or ZnO) is inclined with respect to the mirror normal. Such medium turns out to be 'effectively' optically biaxial and the eigenmodes are generally elliptically polarized. Here, we present the first experimental evidence for this (Chap. 8.11.4).

Copper iodide has been proposed by us as a highly interesting and multi-functional p-type transparent semiconductor. It turns out that its thermoelectrical properties are unparalleled and we have measured the highest ZT value by far of any transparent p-type material (Chap. 8.7). We also have put forward a transport model for CuI thin films (Chap. 8.4); we propose that the high hole mobilities in the thin films are caused by the tunneling of holes through the grain boundaries.

A new topic in our group are carbon nano-dots and their optical properties, in particular in conjunction with embedding in optical cavities. This represents a very promising system with high efficiency at room temperature (Chap. 8.11.3)

We are largely indebted to our funding agencies in particular Deutsche Forschungsgemeinschaft (DFG). We are grateful for the continued funding of Sonderforschungsbereich SFB 762 "Functionality of Oxide Interfaces" that runs in its last period (2016–2019) and our project on nanowire heterostructures in the Forschergruppe FOR 1616 "Nanowire Optoelectronics" which will conclude soon (2015–2018). SAB is supporting our efforts on combinatorial pulsed laser deposition within the new project COSIMA (2017-2020). A project on flexible oxide electronics is funded in the DFG SPP FFLexCom (SPP 1796). The work of our students and researchers together with our academic and industrial partners near and far was fruitful and enjoyable and thus it is with pleasure that the semiconductor physics group presents their progress report.

Marius Grundmann

8.1 Rigorous modeling of Schottky contact characteristics

D. Splith, H. von Wenckstern, M. Grundmann

Schottky contacts (SCs) are both, the key element of electric unipolar devices like Schottky barrier diodes (SBDs) and metal-semiconductor field-effect transistors (MESFETs) as well as a gateway to electrical characterization of a semiconducting material by means of space charge region based measurements. While different models for the different current transport mechanisms and the influence of different inhomogeneities exist, certain non-idealities reported in literature are not fully understood. Here, we report on employing a rigorous model for the simulation of Schottky contact characteristics, taking into account thermionic emission (TE), thermionic field emission (TFE) and charging currents, lateral barrier height inhomogeneities[1] current spreading on local and global series resistance [2] as well as the doping profile of the semiconductor, in order to explain such non-idealities.

The characteristics were calculated by solving the Poisson equation for every height of the Gaussian barrier distribution and using the transfer-matrix method [3] to calculate the TE and TFE currents. Additional, the charging current of the space charge region capacitance is calculated using common sweep rates of measurement devices.

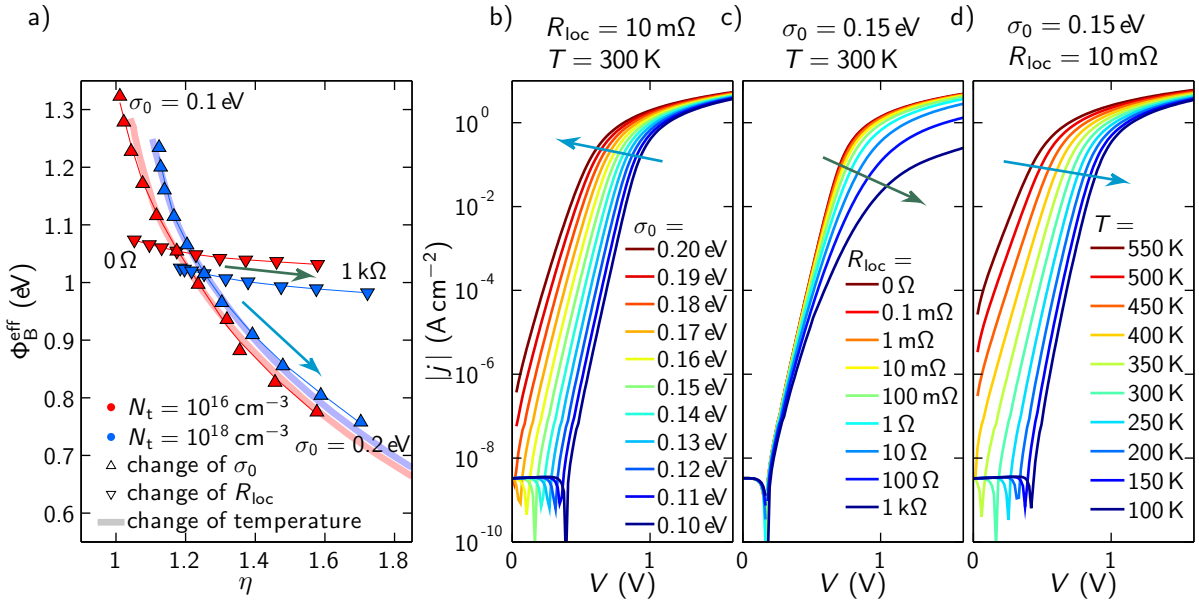

Figure 8.1: (a) Influence of σ_0, R_{loc} and T on $\Phi_B^{eff}(\eta)$ for both investigated doping concentrations. In (b-d), corresponding calculated characteristics for $N_t = 10^{18}\,cm^{-3}$ and (b) changing σ_0, (c) changing R_{loc} and (d) a change in temperature are plotted.

The different resistances are taken into account by using the bisection algorithm. Embedding the latter into a trust region reflective algorithm allows to fit both resistances of the calculated characteristic to the measured.

8.1.1 Evaluation of calculated characteristics

D. Splith, H. von Wenckstern, M. Grundmann

First, characteristics with given diode parameters were calculated. For this, a mean barrier height of 1.5 eV and two different doping concentrations N_t (10^{16} and $10^{18}\,cm^{-3}$) were used. The calculated curves were then fitted with the standard TE model in order to determine the effective barrier height Φ_B^{eff} and the ideality factor η. This was done in order to confirm that the model is self consistent as well as to understand the influence of different parameters on the relation between Φ_B^{eff} and η. In Fig. 8.1 (a), the behavior of $\Phi_B^{eff}(\eta)$ is shown when changing three different parameters: the standard deviation of the Gaussian barrier distribution σ_0, the local series resistance R_{loc} and the temperature T. Some of the corresponding calculated characteristics are shown in Fig. 8.1 (b-d). For both doping concentrations, the relation between Φ_B^{eff} and η for decreasing temperature and increasing standard deviation show the same behavior, namely an increase in ideality factor and a decrease in effective barrier height. However, an increase of the local series resistance also increases the ideality factor, but leaves the effective barrier height almost unchanged. From this plot, one can understand why the homogeneous barrier height determined by extrapolation of $\Phi_B^{eff}(\eta)$ to values of $\eta \approx 1.03$, which was established by empirical observations[4, 5], does not always agree with the mean barrier height of the Gaussian barrier distribution.

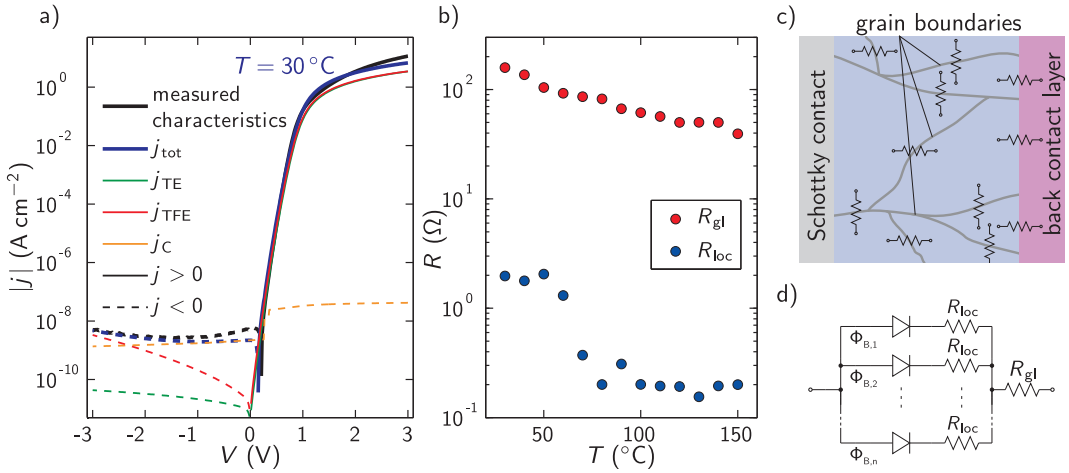

Figure 8.2: (a) Comparison between measured and calculated *j-V* characteristic at $T = 30\,°C$. The different contributions to the total current are plotted individually. In (b) the determined temperature dependencies of the local and the global series resistance are shown. (c) shows a schematic cross-section of the thin film, while in (d) the simplified equivalent circuit is depicted.

8.1.2 Analysis of Cu/β-Ga_2O_3 Schottky contact characteristics

D. Splith, S. Müller, H. von Wenckstern, M. Grundmann

The model was further used to calculate the characteristics of Cu Schottky contacts fabricated on heteroepitaxial β-Ga_2O_3 thin films with a ZnO back contact layer (BCL) [6] grown by pulsed laser deposition (PLD). In these characteristics the following deviations from the standard thermionic emission model are observed: a local minimum in the absolute value of the reverse current at about $-1.5\,V$, a reverse current that is about two orders of magnitude larger than expected from TE, the shifting of the zero-crossing of the characteristics in dependence on the sweep direction (negative to positive ($\Delta V > 0$) or positive to negative voltages ($\Delta V < 0$)) and a deviation in the series resistance region. Additionally, a discrepancy between homogeneous and mean barrier height was also observed. Using values determined from different measurements on these contacts, the temperature dependent IV characteristics for temperatures between $30\,°C$ and $150\,°C$ were calculated using the rigorous model [7].

In Fig. 8.2 (a), the calculated characteristic at $30\,°C$ is shown in comparison to the measured characteristic. Overall, a good agreement between measured and calculated characteristic is observed for this as well as all other temperatures investigated. Additionally to the total current, the different calculated contributions are plotted. From this plot, the high reverse current as well as the minimum in the absolute value in the reverse direction can be attributed to the combination of thermionic field emission and charging current. The shift of the zero crossing can be attributed to the charging current, which changes its sign in dependence on the measurement direction. The deviation in the series resistance region can be attributed to a high local series resistance. As mentioned before, the local and global series resistance can be fitted, such that the calculated curve fits the measured curve best. The resulting values determined in dependence on the temperature are shown in Fig. 8.2 (b). The global series resistance decreases exponentially, as expected for a semiconductor. From a fit, the activation energy of the corresponding defect can be determined to be around 180 meV. The local

series resistance shows a step like behavior around 50∘C. This behavior can be understood, if we assume that the individual grains of the PLD grown thin film are separated by grain boundary barriers. The resistance occurring at such barriers can to some extend be correlated to the local series resistances, connecting paths of different barrier height. A schematic of the thin film cross-section with grain boundary resistances and the simplified equivalent circuit of the model used are shown in Fig. 8.2 (c) and (d). If the thermal energy of the electrons becomes higher than the barrier height at the grain boundaries, a strong decrease in the resistance occurring at the grain boundary barriers and with that of the local series resistance is expected. This means that the grain boundary barrier height should be around 29 meV high. This assumptions can be confirmed by thermal admittance spectroscopy measurements. Here, on the one hand, a defect with an activation energy of 188 meV is observed, which is in good agreement with the value determined from the global series resistance. On the other hand, the determined grain boundary barrier height can be used to evaluate the freeze-out of the free carriers, resulting in an activation energy of the shallow donor of 37 meV. This values is in good agreement with the value determined by Irmscher *et al.* for the shallow donor from temperature dependent Hall-effect measurements [8].

[1] J. H. Werner and H. H. Güttler, J. Appl. Phys. 69, 1522 (1991)
[2] J. Osvald, J. Appl. Phys. 99, 033708 (2006)
[3] Y. Ando and T. Itoh, J. Appl. Phys. 61, 1497 (1987)
[4] R. T. Tung, Phys. Rev. B 45, 13509 (1992)
[5] R. F. Schmitsdorf and W. Mönch. EPJ B 7, 457 (1999)
[6] D. Splith *et al.*, Phys. Status Solidi A 211, 40 (2014)
[7] D. Splith *et al.*, Proc. SPIE 10533 (2018)
[8] K. Irmscher *et al.*, J. Appl. Phys. 110, 063720 (2011)

8.2 Electrical properties of vertical p-NiO/n-Ga_2O_3 and p-$ZnCo_2O_4$/n-Ga_2O_3 pn-heterodiodes

P. Schlupp, D. Splith, H. von Wenckstern, M. Grundmann

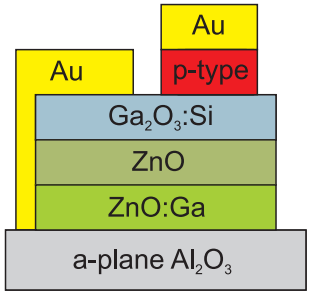

Figure 8.3: Sketch of the sample geometry of the pn-heterodiodes.

Wide band gap semiconductors like GaN oder SiC are used in high power rectifiers, transistors and UV photo detectors. Since it is not possible to fabricate cheap substrates

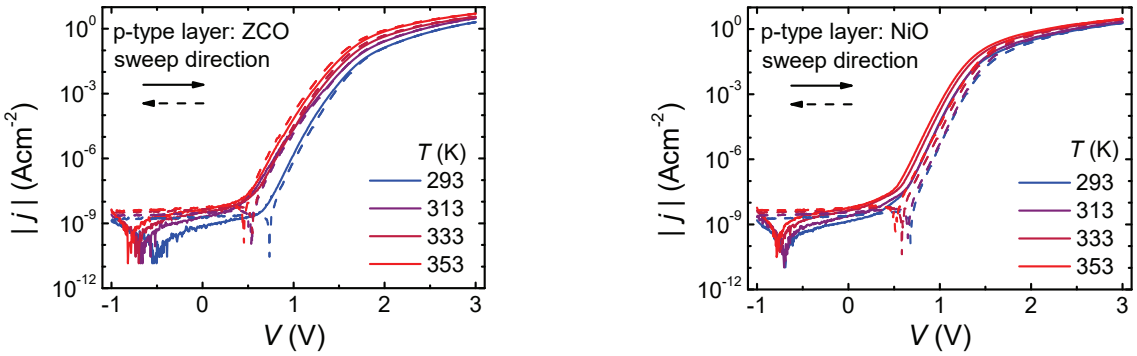

(a) (b)

Figure 8.4: Current density voltage characteristics obtained at different temperatures for the pn-heterodiode with p-type (a) ZCO and (b) NiO.

for these materials, alternatives are needed. Because of its large band gap of 4.9 eV and the possibility to fabricate high quality bulk material β-gallium oxide is an interesting candidate for high power electronics and also for solar-blind detectors [1–4]. For these applications, highly rectifying contacts are required. Further, these can be used for material characterization.

We report on vertical pn-heterojunction diodes comprising thin films of n-type $\beta-$gallium-oxide and p-type zinc cobalt oxide (ZCO) and nickel oxide fabricated by pulsed laser deposition. The back contact consists of highly conducting ZnO:Ga and a ZnO buffer deposited prior to the $\beta-$gallium-oxide layer on a-plane sapphire substrate. The sample structure is depicted in figure 8.3. The undoped ZnO layer avoids an electron barrier between the back contact and the gallium oxide [5]. Zinc oxide and gallium oxide layers were fabricated at about 650° C. The diodes realized with the two p-type materials were fabricated on pieces of one and the same gallium oxide sample.

The current density voltage characteristics for different measurement temperatures are depicted in figure 8.4. Both, ZCO as well as NiO forms highly rectifying diodes on $\beta-$gallium-oxide. The influence of the sweep direction during the measurement can be seen in the splitting of the zero-crossing of the current which can be explained by a parallel capacitance that is charged and discharged. Modeling the characteristics using the Shockley equation leads to ideality factors around 2 indicating that recombination at the heterointerface is the dominant current transport mechanism.

To both diodes thermal admittance spectroscopy was applied. The temperature dependence of the conductance is depicted in figure 8.5 (a) and (b) and shows two maxima corresponding to two defect levels for each diode. The activation energy as well as the corresponding capture cross section are summarized in table 8.1.

Both diodes show one defect level with activation energy of about 200 meV and a similar capture cross section. Since at room temperature the hole density in the p-type materials is higher than the electron density in the gallium oxide ($n(Ga_2O_3) \approx 10^{18}\,cm^{-3}$, $p(ZCO) > 10^{20}\,cm^{-3}$, $p(NiO) \approx 10^{18} - 10^{19}\,cm^{-3}$), meaning that the space charge region is mainly located within the gallium oxide, we attribute this defect to the gallium oxide. The shallow defect in the Ga_2O_3/ZCO diode is not observed in the Ga_2O_3/NiO diode. The reason for that may be that the decrease of the conductance in this diode is mainly due to the decrease of the conductance of the NiO. In the temperature range where the

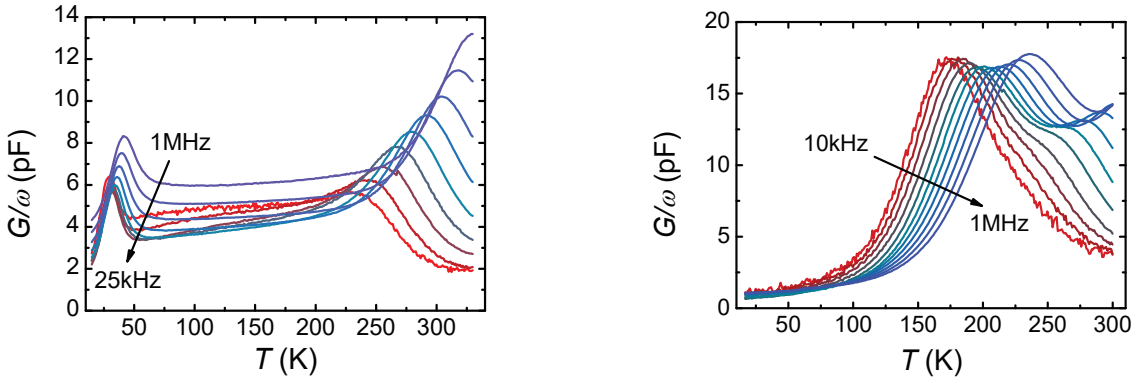

Figure 8.5: Temperature denpendence of the conductance obtained at different measurement frequencies. The peaks indicate defect levels.

defect level would be probed, the conductance shows no temperature and frequency dependence which could be due to the low-pass behavior because of the higher series resistance in the NiO at low temperature. This could be also a hint that the other deep defect in the Ga_2O_3/NiO diode may be located in the NiO. However, this behavior is not observed in In_2O_3/NiO diodes [7]. More investigations are needed at this point to fully understand the behavior.

p-type sem.	E_{act} (meV)	σ (cm^2)
ZCO	26±1	2×10^{-15}
ZCO	205±4	3×10^{-17}
NiO	194±8	2×10^{-17}
NiO	236±2	6×10^{-15}

Table 8.1: Thermal activation energy and apparent capture cross-sections of defect levels observed in ZCO/Ga_2O_3 and NiO/Ga_2O_3 heterostructures.

The work was supported by Leipzig School of Natural Science (BuildMoNa).

[1] M. Higashiwaki, K. Sasaki, H. Murakami, Y. Kumagai, A. Koukitu, A. Kuramata, T. Masui, S. Yamakoshi: Sem. Sc. Techn. **31**, 034001 (2016)
[2] S. I. Stepanov, V.I. Nikolaev, V. E. Bougrov, A. E. Romanov: Rev. Adv. Mater. Sci. **44**, 63 (2016)
[3] H. von Wenckstern: Adv. Electron. Mater. **3**, 1600350 (2017)
[4] Y. Kokobun, K. Miura, F. Endo, S. Nakagomi: Appl. Phys. Lett. **90**, 031912 (2007)
[5] D. Splith, S. Müller, F. Schmidt, H. von Wenckstern, J. J. van Rensburg, W. E. Meyer, M Grundmann: Phys. Status Solidi A **211**, 40 (2014)
[6] Y. Kokobun, S. Kubo, S. Nakagomi: Appl. Phys. Expr. **9**, 091101 (2016)
[7] H. von Wenckstern, D. Splith, S. Lanzinger, F. Schmidt, S. Müller, P. Schlupp, R. Karsthof, M. Grundmann: Adv. Electron. Mater. **1**, 1400026 (2015)

8.3 Vital Role of Oxygen for the Formation of Highly Rectifying Schottky Barrier Diodes on Amorphous Zinc-Tin-Oxide with Various Cation Compositions

S. Bitter, P. Schlupp, H. von Wenckstern, M. Grundmann

Amorphous oxide semiconductors are of great potential for the fabrication of large area, cost-efficient devices [1]. The most prominent example, amorphous gallium indium zinc oxide, is already used in modern mobile phones. However, due to the low availability and therefore high costs of indium and gallium, alternative materials are required. Among those amorphous zinc tin oxide (ZTO) is highly promising. It consists of naturally abundant and non-toxic elements only. The electrical and optical properties of this compound have been studied in great detail [2–5], e.g. their dependence on deposition pressure, deposition temperature and the zinc-to tin ratio [2–4]. In a previous report we used a continuous composition spread approach for pulsed laser deposition to efficiently study the electrical and optical properties of ZTO in dependence on the composition in the range from 0.08 to 0.82 Zn/(Zn+Sn) [4, 6]. Based on these results, we investigated the properties of Schottky diodes fabricated on thin films with compositions varying from 0.12 to 0.72 Zn/(Zn+Sn).In order to achieve smoother surfaces [4] we use four different, segmented targets to cover this composition range.

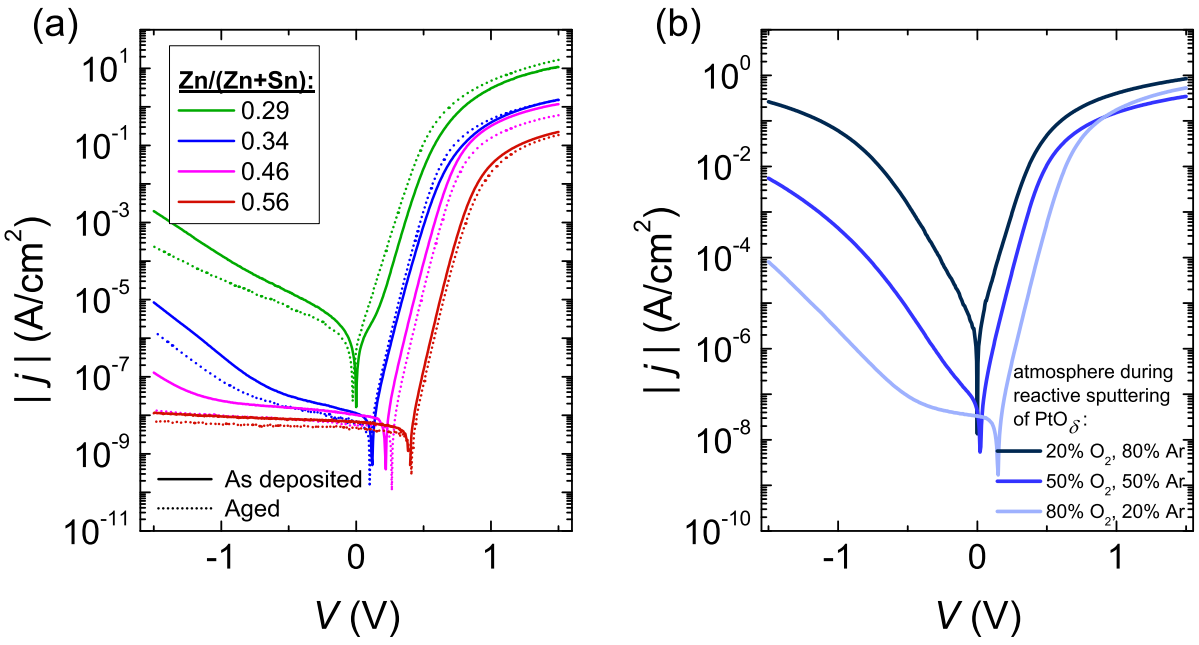

Figure 8.6: Current density-voltage characteristics (a) for selected zinc-to-tin ratios before and after aging for 100 days and (b) for different oxygen contents during the reactive sputtering of the platinum oxide.

The free carrier density of the thin films varied from 1×10^{16} to $3 \times 10^{19}\,\mathrm{cm}^{-3}$. The samples were cut into $5 \times 5\,\mathrm{mm}^2$ pieces and Schottky barrier diodes were fabricated thereon. The ohmic contact of the diodes was formed by sputtered gold, whereas the

Schottky barrier contact was formed by reactively sputtered platinum. Current density-voltage characteristics are depicted in Figure 8.6(a) for selected zinc-to-tin ratios . A decrease of the forward and reverse current density with decreasing carrier density (and increasing zinc content) was measured. This led to an increase of the rectification ratio. Additionally, a decrease of the ideality factor with increasing zinc content was observed. A maximum rectification ratio of 2.7×10^7 and a minimum ideality factor of 1.05 were observed for 0.63 and 0.72 Zn/(Zn+Sn), respectively. Upon re-measuring the samples after approximately 100 days, an increase of the rectification ratio to higher values (maximum 3.9×10^7) was observed, which is due to a reduction of the leakage current. For Zn/(Zn+Sn) > 0.4, the diode properties are very similar after the aging. A study with a thin film with fixed zinc-to-tin ratio was performed to investigate the aging with a better time revolution and to investigate the influence of the oxygen content during the reactive sputtering of the PtO_x contacts. An improvement of the diode characteristics with increasing oxygen content in the plasma was observed/measured as shown in Figure 8.6(b). The important role of oxygen in the formation of the Schottky barrier contact was demonstrated.

[1] H. Hosono *et al.*: J. Non-Cryst. Solids. **198-200**, 165 (1996)
[2] M. K. Jayaraj *et al.*: J. Vac. Sci. Technol. B **26**, 495 (2008)
[3] P. Görrn *et al.*: Advanced Materials **18**, 6, 738-741 (2006)
[4] S. Bitter *et al.*: ACS Comb. Sci. **18**, 4, 188-194 (2016)
[5] P. Schlupp *et al.*: Mater. Res. Soc. Symp. Proc. **1633**, 101 (2014)
[6] H. von Wenckstern *et al.* CrystEngComm. **15**, 10020 (2013)

8.4 Electrical Transport in Textured γ-CuI Thin Films

M. Kneiß, C. Yang, J. Barzola-Quiquia, G. Benndorf, H. von Wenckstern, P. Esquinazi, M. Lorenz, M. Grundmann

γ-CuI is a transparent p-type semiconductor with high hole mobility reaching up to $25\,\mathrm{cm}^2\,(\mathrm{Vs})^{-1}$ in textured thin films [1], it is the best known transparent p-type thermoelectric material [2], it has a wide band gap of 3 eV and large exciton binding energy rendering the material highly suited for transparent optoelectronic and thermoelectric device applications. Nevertheless, many material properties have not been investigated so far and among those are low-field transport properties of highly textured thin films. We have analyzed the electric transport properties of a large set of CuI thin films with thickness between 100 and 1500 nm grown on Corning1737 glass or fused silica substrates by thermal evaporation of CuI-powder, DC-reactive sputtering of Cu in iodine atmosphere and DC/RF sputtering of a CuI powder target, respectively [3]. However, the general behavior of the thin films in electrical transport measurements was not depending on the chosen deposition method. X-ray diffraction measurements showed that the films grow in the zincblende γ-phase with (111)-orientation and random in-plane orientation. Scanning electron microscopy (SEM) images (Fig. 8.7 (a)) show a rough granular structure. Hall-effect measurements at room temperature determined all thin films to be p-type conducting with hole concentrations in the range of $10^{18} - 10^{20}\,\mathrm{cm}^{-3}$ which is close to or above the Mott-limit of $3 \times 10^{18}\,\mathrm{cm}^{-3}$ [4]. The hole

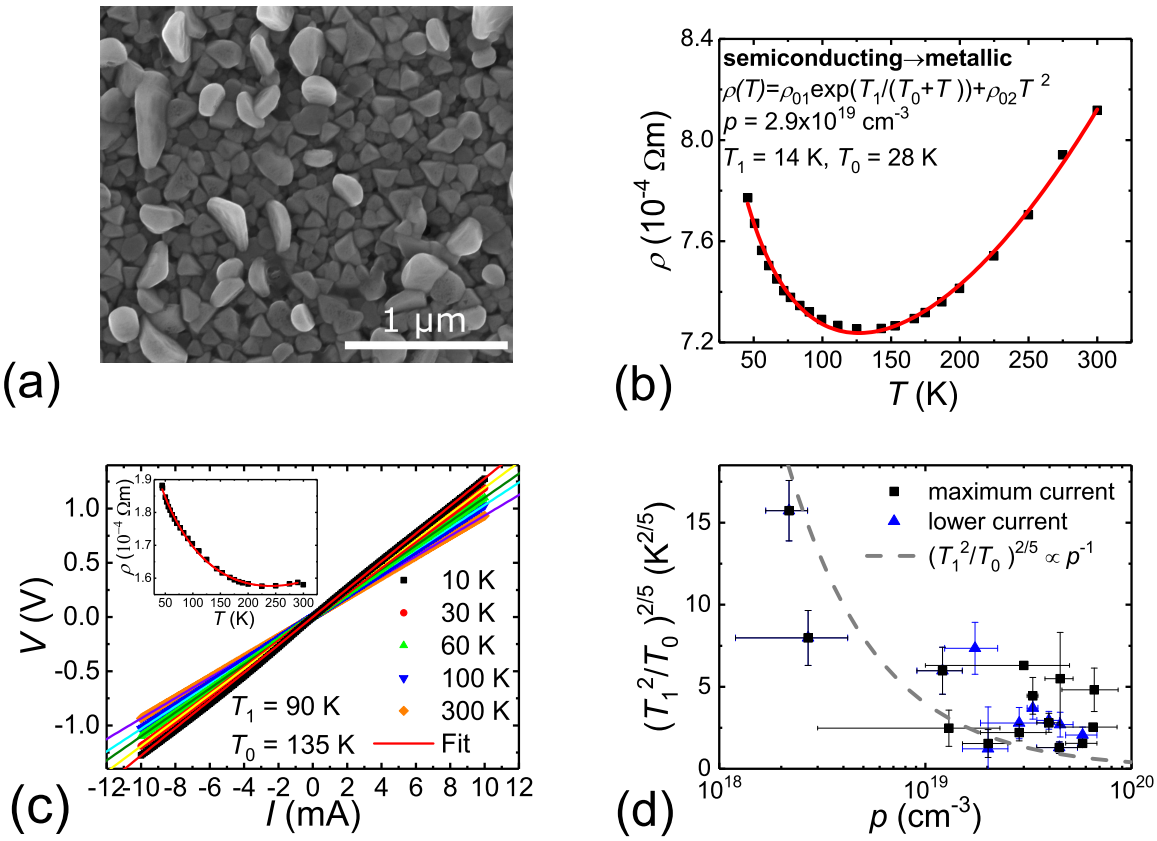

Figure 8.7: (a) Typical SEM image of a thermally evaporated CuI thin film. (b) Temperature-dependent resistivity of a CuI thin film. The resistivity shows a characteristic minimum. The solid line is a fit with the FITC model (exponential term in $\rho(T)$) in series with a metallic resistivity (quadratic term in $\rho(T)$). T_1 and T_0 are characteristic temperatures of the model. (c) Current-voltage (I-V)-characteristics of a CuI thin film for several selected temperatures. Solid lines are fits with the expected I-V dependence of the FITC model and an ohmic dependence for the metallic resistivity term in series. The characteristic temperatures are the same as in the resistivity model. The inset shows the temperature-dependent resistivity of the same thin film fitted with the same characteristic temperatures. (d) The term $\left(T_1^2/T_0\right)^{2/5} \propto V_0$ in dependence on the hole density p of the thin films. The dashed line is a $V_0 \propto 1/p$ dependence.

mobilities were surprisingly high with maximum values of about 12 $\mathrm{cm}^2\,(\mathrm{Vs})^{-1}$.
In temperature-dependent resistivity measurements ($T = 50-300$ K) most films showed a typical minimum in the resistivity at a certain temperature, with semiconducting behavior of the resistivity at lower and metallic behavior at higher temperatures. Since thermal activation of carriers is not expected, the semiconducting behavior could only be explained by the fluctuation-induced tunneling conductivity (FITC) model [3, 5]. The metallic part was modeled satisfyingly with a quadratic temperature dependence. Both contributions were combined in series to fit the complete resistivity curves, see also Fig.8.7 (b). The same model was also used by us in Ref. [6].
To further validate our model, temperature-dependent I-V-curves were measured and modeled. The FITC mechanism predicts non-ohmic I-V-characteristics, where the same characteristic temperatures T_1 and T_0 which were used in the modeling of the resistivity curves are included in the temperature and voltage dependency of the I-V-curves. Se-

lected measured curves are depicted in Fig. 8.7 (c), with the corresponding temperature-dependent resistivity in the inset. A clear S-shape is visible for low temperatures as predicted by the FITC model. The fits with the corresponding models are shown as solid lines and yielded similar characteristic parameters both for the resistance and *I*-*V*-curves.

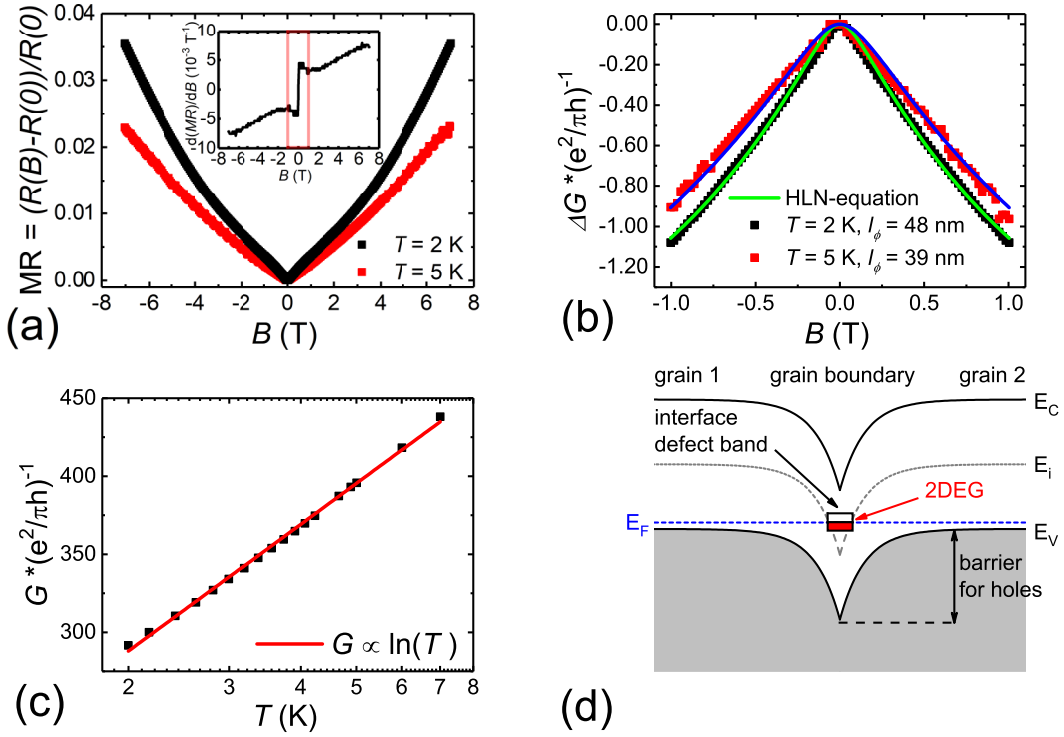

Figure 8.8: (a) MR of a reactively DC-sputtered γ-CuI thin film for two temperatures as indicated. A cusp typical for WAL processes is observable below ≈ 1 T. The anomaly is emphasized as red box in the inset where the derivative of MR with respect to the magnetic field is shown. (b) Normalized Magnetoconductance $\Delta G(B)$. Solid lines are fits according to a 2D WAL effect (Hikami-Larkin-Nagaoka (HLN-) equation). (c) Normalized zero-field conductance G in dependence on the logarithm of temperature. A linear behavior according to a 2D WAL effect in combination with 2D electron-electron interaction is emphasized as red solid line. (d) Band bending at the grain boundaries due to a defect band. E_F denotes the Fermi energy. E_C, E_V and E_i are the conduction band minimum, the valence band maximum and the Fermi energy for an intrinsic semiconductor, respectively.

Tunneling processes require energetic barriers, which we expect to be located at the grain boundaries. For such barriers, a carrier density dependent height is typically the case. We therefore determined the ratio $\left(T_1^2/T_0\right)^{2/5}$, which is proportional to the barrier height V_0 in the FITC model. This ratio is shown in Fig. 8.7 (d) in dependence on the hole density p and is decreasing with increasing hole density. It follows roughly a $V_0 \propto 1/p$ dependence (dashed line in Fig. 8.7 (d)) expected for barriers caused by defects at grain boundaries [7]. By analyzing the contribution of the FITC model to the total resistance, we found that this tunneling mechanism plays a vital role even at room temperature. Therefore, we propose that the high hole mobilities in the thin films are caused by the tunneling of carriers through the grain boundaries.

To gain further insight into the transport properties, magnetoresistance (MR) measurements were performed at low temperatures (T = 2 K and T = 5 K) and up to magnetic fields of 7 T on one reactively DC-sputtered thin film sample. The MR for this sample is shown in Fig. 8.8 (a) and shows a characteristic cusp for low magnetic fields typically associated with weak antilocalization (WAL) effects. A modeling of the low-field magnetoconductance $\Delta G(B)$ was possible using a two-dimensional (2D) WAL process [8], which is shown in Fig. 8.8 (b) as solid line. We determined phase coherence lengths of the carriers as large as ≈ 50 nm similar to other 2D systems [9]. The 2D nature of the effect was corroborated by a typical logarithmic temperature dependence [10] of the zero-field conductance G for temperatures below ≈ 8 K, see Fig. 8.8 (c). This is caused by the 2D WAL effect in combination with 2D electron-electron interaction. We propose a 2D electron gas (2DEG) in a defect band at the interfaces or grain boundaries as the cause of the 2D carrier system. The defects at the grain boundaries required for this can be due to dangling bonds or disorder at the interfaces and would also cause a band bending at the interfaces. This band bending in turn results in the tunneling barriers for the holes of the bulk material. The effect is schematically depicted in Fig. 8.8 (d).
In summary, the electrical transport properties of γ-CuI can be conclusively explained by barriers at the grain boundaries that are caused by a defect band which also contains a 2DEG. For the first time this leads to a thorough description of the transport properties of γ-CuI and also explains the high hole mobilities in heavily textured thin films which are due to interface tunneling currents.

[1] M. Zi *et al.*, phys. stat. sol. (a) **212**, 1466 (2015)
[2] C. Yang *et al.*, Nat. Commun. **8**, 16076 (2017)
[3] M. Kneiß *et al.*, Adv. Mater. Interfaces, 1701411 (2018)
[4] A. A. Klochikin *et al.*, J. Phys. C. Solid State Phys. **19**, 4237 (1987)
[5] P. Sheng, Phys. Rev. B **21**, 2180 (1980)
[6] C. Yang *et al.*, PNAS **113**, 12929 (2016)
[7] J. Y. W. Seto, J. Appl. Phys. **46**, 5247 (1975)
[8] S. Hikami *et al.*, Prog. Theor. Phys. **63**, 707 (1980)
[9] M. Jenderka *et al.*, Phys. Rev. B **88**, 045111 (2013)
[10] P. A. Lee, T. V. Ramakrishan, Rev. Mod. Phys. **57**, 287 (1985)

8.5 Investigations of Si-doped $(Al,Ga)_2O_3$ thin films

A. Werner, H. von Wenckstern, M. Grundmann

Transparent semiconductors, such as GaN and its alloys, are more and more used within technical applications like power devices, quantum well infrared photo detectors or deep UV-photo detectors, e.g. for flame sensors for missile plume detection, biological and chemical sensors for ozone detection or optical communications, such as intra- and inter-satellite secured communications [1–3]. Recently, the wide bandgap semiconductor Ga_2O_3 has attracted an increasing interest because of it's promising material properties. Ga_2O_3 occurs in five different crystallographic phases, denoted by $\alpha, \beta, \gamma, \delta$ and ϵ with the β-polymorph being the thermodynamically stable configuration [4]. Furthermore, it can be simply synthesized, has a large breakdown voltage and

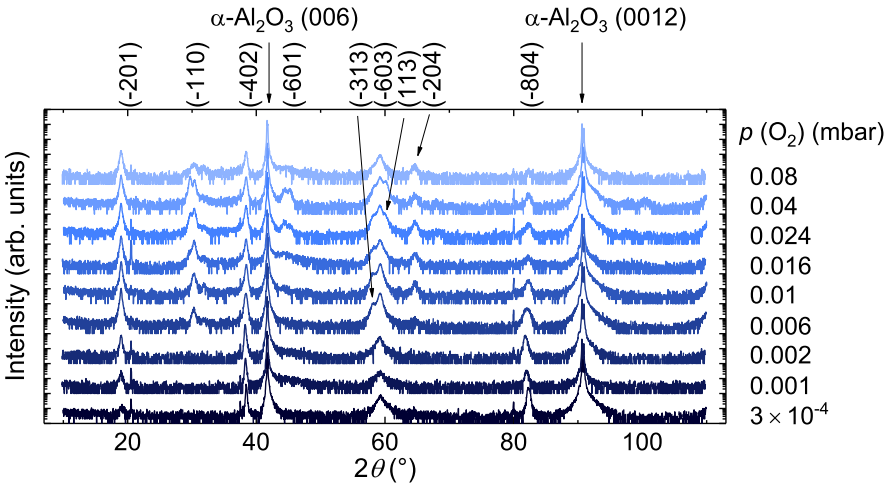

Figure 8.9: XRD 2θ-ω scan of $(Al,Ga)_2O_3$:Si thin films deposited at a growth temperature 670 °C and different oxygen partial pressures as labeled.

a high bandgap of about 4.7-5.0 eV[5]. Bandgap engineering is possible by alloying with In leading to a decrease in bandgap energy or by alloying with Al resulting in higher bandgap [6]. Here, we investigate Al alloyed thin films with bandgap energies above 5 eV.

The investigated $(Al,Ga)_2O_3$:Si thin films were grown by pulsed laser deposition (PLD) on (00.1)Al_2O_3. The target used consists of Ga_2O_3 + 5 wt.% Al_2O_3 and 5 wt.% SiO_2 to improve the electrical conductivity.

We investigated the influence of the growth temperature (T_g) and oxygen partial pressures ($p(O_2)$) on the alloy composition and structural, optical and electrical properties of the samples by energy-dispersive X-ray spectroscopy (EDX), X-ray diffraction (XRD), atomic force microscopy (AFM), transmission, and Hall effect measurements, respectively.

Figure 8.9 shows the XRD pattern of $(Al,Ga)_2O_3$ samples as a function of the oxygen partial pressures $p(O_2)$ during growth. For $p(O_2) \leq 2\times10^{-3}$ mbar the thin films grow in [-201] direction. For higher oxygen partial pressure polycrystalline samples are obtained as it was already reported for binary Ga_2O_3 [7]

EDX and transmission measurements revealed a correlation between bandgap energy E_g, cation concentration x, growth rate τ and the oxygen growth pressure. For low oxygen partial pressure the gallium content x_{Ga} and the growth rates τ are comparatively small (see fig.8.10(a)). Reason for this is a desorption process of volatile gallium suboxides (Ga_2O) during growth process. Vogt and Bierwagen already showed such a behavior for Ga_2O_3 and $(In,Ga)_2O_3$ thin films [8, 9]. Further, at a given T_g, the incorporation of Al is favored for lower $p(O_2)$ due to higher dissociation energy of the Al-O bond compared to the Ga-O bond. At a given $p(O_2)$, the incorporation of Al is favored for higher T_g due to desorption of gallium sub-oxides during growth. Further, the bandgap energy shows a linear dependence on the alloy composition. Figure 8.10(b) shows the root mean square surface roughness R_q estimated from AFM measurements. Here we observe an increase of R_q with increasing $p(O_2)$ up to a certain oxygen partial pressure ($p(O_2)$=0.01 mbar) and then it decreases again. For the highest chosen $p(O_2)$ value of 0.08 mbar, R_q increases slightly. To investigate the conductivity of the samples

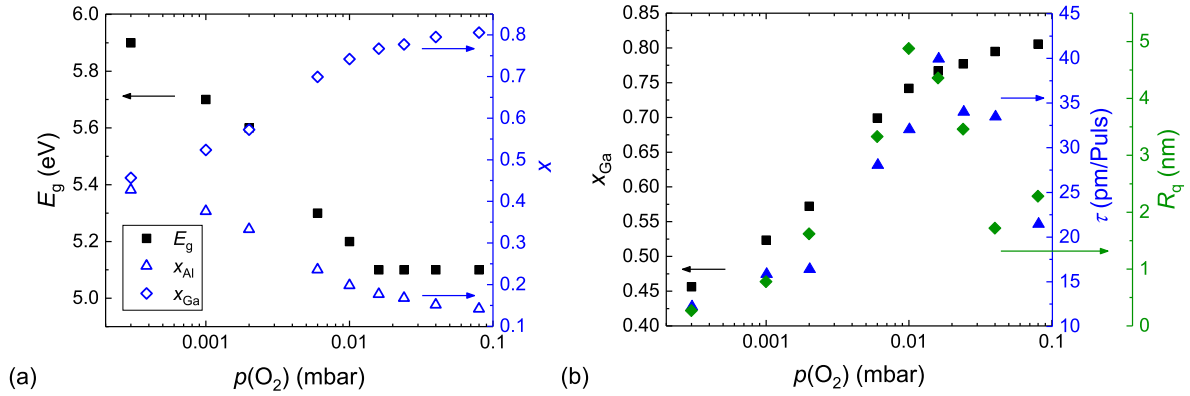

Figure 8.10: a) Bandgap energy E_g and cation content x, b) Ga concentration, growth rate τ and root mean square surface roughness versus logarithm oxygen partial pressure $p(O_2)$.

Hall effect and I-V measurements were executed. These measurements showed that the conductivity is too low to realize devices on the investigated thin films. Additional doping studies are required to provide means to tailor the electrical conductivity of $(Al,Ga)_2O_3$ thin films.

This work was supported by European Social Fund within the Young Investigator Group "Oxide Heterostructures" (SAB 100310460).

[1] M. Higashiwaki *et al.*, Appl. Phys. Lett. **100**, 013504 (2012).
[2] K.Sasaki *et al.*, Appl. Phys. Express **5**, 035502 (2012).
[3] T. Oshima *et al.*, J. J. Appl. Phys. **48**, 011605 (2009).
[4] R. Roy *et al.*, J. Am. Chem. Soc. **74**, 719 (1952).
[5] M. Orita *et al.*, Appl. Phys. Lett. 77 (2000).
[6] H. von Wenckstern, Adv. Electron. Mater **3**, 1600350 (2017).
[7] S. Müller *et al.*, Phys. Status Solidi A 211 (2014).
[8] P. Vogt and O. Bierwagen, Appl. Phys. Lett. **108**, 072101 (2016).
[9] P. Vogt and O. Bierwagen, APL Mater. **4**, 072101 (2016).

8.5.1 Low temperature ion irradiation of In_2O_3 and Ga_2O_3: implications on intrinsic defect formation and charge neutrality level

H. von Wenckstern, C. Bhoodoo,* L. Vines,* M. Grundmann

*Department of Physics/Centre for Materials Science and Nanotechnology, University of Oslo, PO Box 1048 Blindern, N-0316 Oslo, Norway

The transparent *n*-conducting group-III sesquioxides In_2O_3 and Ga_2O_3 behave dissimilar concerning realization of ohmic and rectifying metal contacts [1]. Whereas it is trivial to obtain ohmic contacts to indium oxide, it was until 2014 not possible to fabricate In_2O_3-based Schottky barrier diodes. Otherwise, it is challenging to realize ohmic contacts to Ga_2O_3. This typically requires multiple metal layers and adequate annealing steps, but Ga_2O_3 Schottky barrier diodes with excellent properties are commonly reported [1]. Within the electro-negativity based description of Schottky barrier height the

so-called branch-point energy also referred to as charge-neutrality level is the essential material parameter determining i) height of Schottky barrier at metal-semiconductor interfaces, ii) position and character of hydrogen level, iii) doping limits or the formation enthalpy of intrinsic defects [2]. The latter can be probed by monitoring of the Fermi level energy during the creation of intrinsic defects by, e.g., ion irradiation studies, for which thin films on electrically insulating substrate are well suited. We investigated changes of the electrical conductivity of In_2O_3 and Ga_2O_3:Si heteroepitaxial thin films as a function of the total irradiation dose for a given kinetic ion energy [3].

Thin films of In_2O_3 were grown by pulsed laser deposition (PLD) on (001)-oriented yttria-stabilized zirconia and (11.2)-oriented sapphire substrates with a thickness of about 450 nm. Ga_2O_3:Si thin films were grown by PLD on (100)MgO substrate with a thickness of about 225 nm. The free electron concentration of the as grown layers is about 1.5×10^{18} cm^{-3} for the nominally undoped In_2O_3 samples and about 5×10^{17} cm^{-3} for the Si-doped Ga_2O_3 layers, which are electrically insulating without doping. The irradiation experiments were carried out at the Centre for Materials Science and Nanotechnology of University of Oslo. For irradiation either 1.5 MeV C^+ or 3.2 MeV Si^+ ions were incident on the samples at a temperature of 35K. Monte Carlo simulations using the SRIM code revealed that the projected range of the implanted ions is 1, 3 μm or higher, implicating that the implanted species do not contribute to electrical conduction. Figure 8.11 shows that for In_2O_3 the resistivity decreases slightly for accumulated irradiation doses below about 5×10^{12} cm^{-2} (region I). The resistivity increases by about an order of magnitude as the accumulated dose increases from 5×10^{12} cm^{-2} to about 5×10^{14} cm^{-2} (region II). If the accumulated dose exceeds 5×10^{14} cm^{-2} (region III) the resistivity decreases to values clearly below that in the as-grown state. For Ga_2O_3:Si the resistivity is independent of the accumulated dose for region I. Within region II, the resistivity increases strongly by several orders of magnitude until the sample becomes electrically insulating for accumulated doses above 1×10^{14} cm^{-2}.

In general, for doses above 1×10^{14} cm^{-2} not only primary defects will form but the generation of defect complexes becomes more and more likely. Further, for irradiation doses above 1×10^{15} cm^{-2} the average distance between vacancies will be only 5 nm or lower and might lead to a hopping type of electrical transport instead of band transport. This leads to two possible scenarios explaining the unusual dependence of electrical conductivity of In_2O_3 on irradiation dose: i) decrease of conductivity due to tunnel-assisted hopping conduction, ii) formation of larger defect complexes which behave donor-like and lead to an increase of Fermi level energy in the In_2O_3 thin films. In Ga_2O_3 these vacancy complexes would behave acceptor-like and shift the Fermi level energy towards mid-gap. The second scenario is compatible with previously proposed microscopic view on charge neutrality level and its implications for the formation of intrinsic defects as well as properties of metal-semiconductor junctions and with the results of the current study.

[1] H. von Wenckstern, Adv. Electron. Mater. **3**, 1600350 (2017).
[2] C. G. Van de Walle and J. Neugebauer, Nature **423**, 626 (2003), W. Moench, J. Appl. Phys. **109**, 113724 (2011).
[3] L. Vines and C. Bhoodoo and H. von Wenckstern and M. Grundmann, Journal of Physics: Condensed Matter **30**, 025502 (2018).

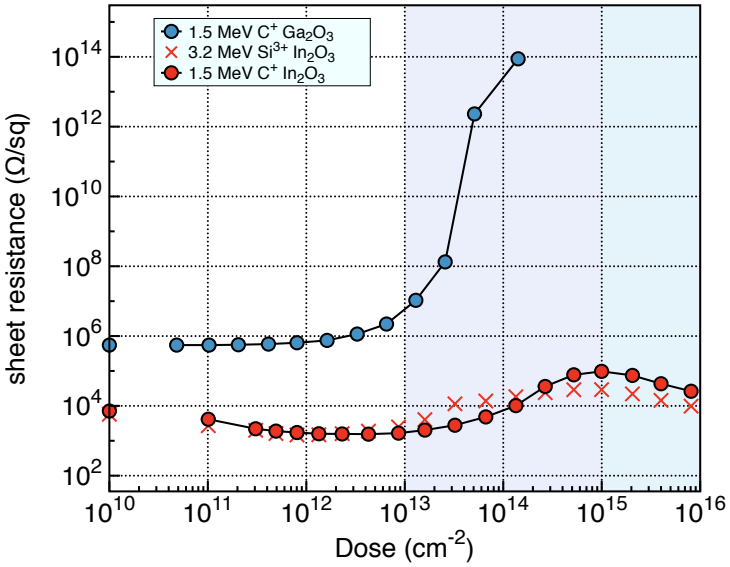

Figure 8.11: Dependence of sheet resistance on irradiation dose of 1.5 MeV C^+ and 3.2 MeV Si^{3+} ions in In_2O_3 and 1.5 MeV C^+ ions in Ga_2O_3 thin films. Regions I, II and III (as discussed in the text) have whitish, blueish and turquoise background color, respectively.

8.5.2 Single metal ohmic and rectifying contacts to ZnO nanowires

H. von Wenckstern, A. Jarjour,* J.W. Cox,* W.T. Ruane,* L.J. Brillson,* M. Grundmann

*The Ohio State University Department of Physics, 191 West Woodruff Ave., Columbus, Ohio 43210, USA

The fabrication of ohmic and Schottky barrier contacts to a semiconducting material requires metals with different work function, respectively. For instance, for an n-type semiconductor such as ZnO it is expected that metals with low work function are well suited for ohmic contacts and high work function metals are ideal for rectifying Schottky contacts. In a collaboration with the Ohio state University we could demonstrate that defect engineering allows formation of ohmic and Schottky barrier contacts by deposition of a single metal [1]. For the experiments ZnO nanowires, grown by pulsed laser deposition on (11.0)Al_2O_3 substrate, were collected by dragging lint-free clean room paper across the substrate and than transferred onto SiO_2 coated silicon wafers. Six platinum contacts were patterned along the wires by electron beam deposition in ultra-high vacuum and allow determination of the contact resistance. In order to tailor the contact behavior, a pre- and a post-deposition treatment step was used. In the pre-deposition step, the nanowires were milled using a focused Ga ion beam which removed the outermost layers of the wire that typically contain higher defect density than the bulk part of the wire. On such pre-treated wires current-voltage characteristics of Pt contacts show blocking behavior indicative for the formation of Schottky barrier diodes. If these contacts are subject to a post-deposition annealing at 450°C in nitrogen, current-voltage characteristics turn ohmic and the contact resistivity was determined to be $(2.59 \pm 0.08)\,m\Omega cm^2$. Depth-resolved cathodoluminescence measurements show that the initial change in contact behavior is accompanied by a change of defect densities in the vicinity of the metal/semiconductor interface. In figure 8.12

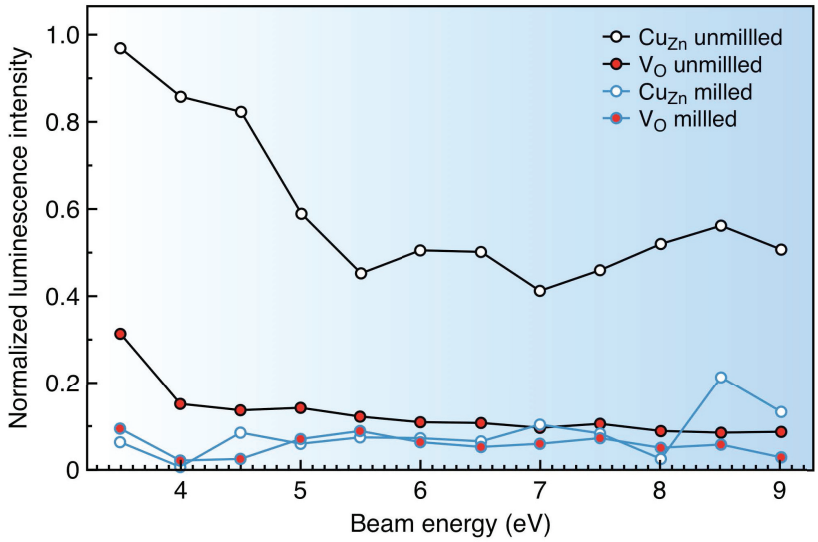

Figure 8.12: Variation of the integrated luminescence intensity of different defect related radiative transition channels normalized with respect to the intensity of the near band edge emission in dependence on the energy of the incident electrons. The excitation depth increases with increasing beam energy: whitish background indicates surface-near excitation, blueish background indicates excitation in the bulk of the wire.

the integrated intensity, normalized to the intensity of the near-band edge emission, of oxygen vacancy related luminescence and luminescence related to extrinsic defects (such as Cu_{Zn}) is compared for Pt contact layers on untreated and on Ga-milled wires. For untreated wires an increase of the defect density towards the metal/semiconductor interface (small beam energies) is obvious whereas a depth dependence of the defect density is not observed for Pt on pre-treated surfaces in accordance with the formation of rectifying contacts on the pre-treated wires.

[1] A. Jarjour, J. W. Cox, W. T. Ruane, H. Von Wenckstern, M. Grundmann, L. J. Brillson, Ann. Physik **530**, 1700335 (2018).

8.6 Strain in Pseudomorphic Monoclinic Heterostructures

M. Grundmann

Epitaxial heterostructures are the basis of basically all modern devices. Generally, they involve materials with different lattice constants, leading to pseudomorphic strain for layer thickness below the onset of plastic relaxation. First this has been investigated for cubic materials, such as silicon and III-V semiconductors, also representing the simplest case. Then, wurtzite-based heterostructures were investigated for GaN- and ZnO-based heterostructures; here polar, non-polar and semi-polar directions arise [1]. Recently, monoclinic heterostructures have become relevant through the availability of β-Ga_2O_3 substrates and epitaxy of $(In_xGa_{1-x})_2O_3$ and $(Al_xGa_{1-x})_2O_3$ alloy semiconductor thin films with applications in 2DEG-based heterostructure transistors, UV- and intersubband photodetectors and various other possible devices.

The usual monoclinic unit cell and its rotation by the angle θ around the b-axis is depicted in Fig. 8.13.

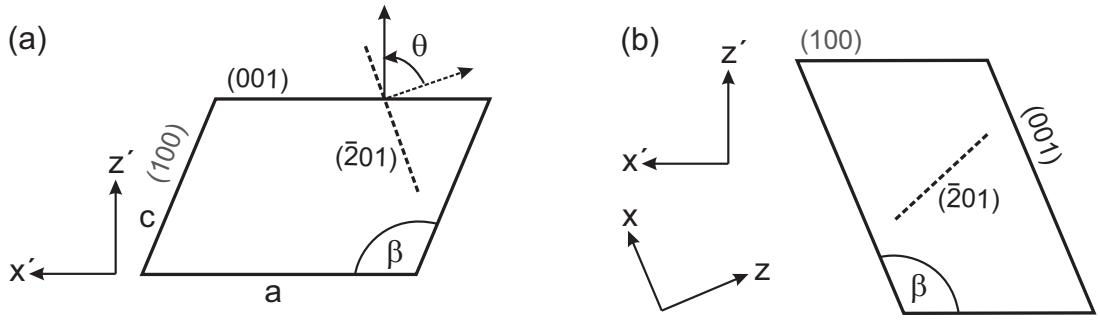

Figure 8.13: (a) Geometry of rotation by θ around y-axis. (b) Crystal and laboratory coordinate systems after rotation of the crystal by $\theta = \beta - \pi$ ($\theta < 0$) such that the normal of the (100) plane points in the z'-direction.

We have calculated analytically the epitaxial in-plane and out-of-plane strain components for pseudomorphic growth of monoclinic heterostructures for various substrate orientations, namely the (010) plane and all (*h*0*l*) planes, parametrized by the rotation angle θ against the (001) plane [2]. Also, numerical examples were given for the sesquioxide semiconductor systems $(In_{0.1}Ga_{0.9})_2O_3/Ga_2O_3$ (the alloy being under compressive strain) and $(Al_{0.1}Ga_{0.9})_2O_3/Ga_2O_3$ (tensile strain). In Fig. 8.14 we depict as an example the strain energy density of these epilayers for rotation of the epitaxial plane around the *b*-axis.

We note that by setting the monoclinic angle of the unit cell to $\pi/2$, our theory covers as well the simpler case of orthorhombic heterostructures.

[1] M. Grundmann, Jesús Zúñiga-Pérez, *Pseudomorphic ZnO-based heterostructures: from polar through all semipolar to nonpolar orientations*, phys. stat. sol. (b) **253**, 351–360 (2016).
[2] M. Grundmann, *Strain in Pseudomorphic Monoclinic Ga2O3-based Heterostructures*, phys. stat. sol. (b) **254**, 1700134 (2017).
[3] K. Momma, F. Izumi, *VESTA 3 for three-dimensional visualization of crystal, volumetric and morphology data*, J. Appl. Crystallogr. **44**, 1272–1276 (2011).

8.7 Flexible and Transparent Thermoelectric Copper Iodide Thin Film

C. Yang, D. Souchay, M. Kneiß, M. Lorenz, O. Oeckler, G. Benstetter, Y.Q. Fu, and M. Grundmann

Thermoelectric devices that are flexible and optically transparent hold unique promise for future electronics. However, development of invisible thermoelectric elements is hindered by the lack of p-type transparent thermoelectric materials. In this study, we present the superior room-temperature thermoelectric performance of p-type transparent copper iodide (CuI) thin films. Large Seebeck coefficients are observed and fitted

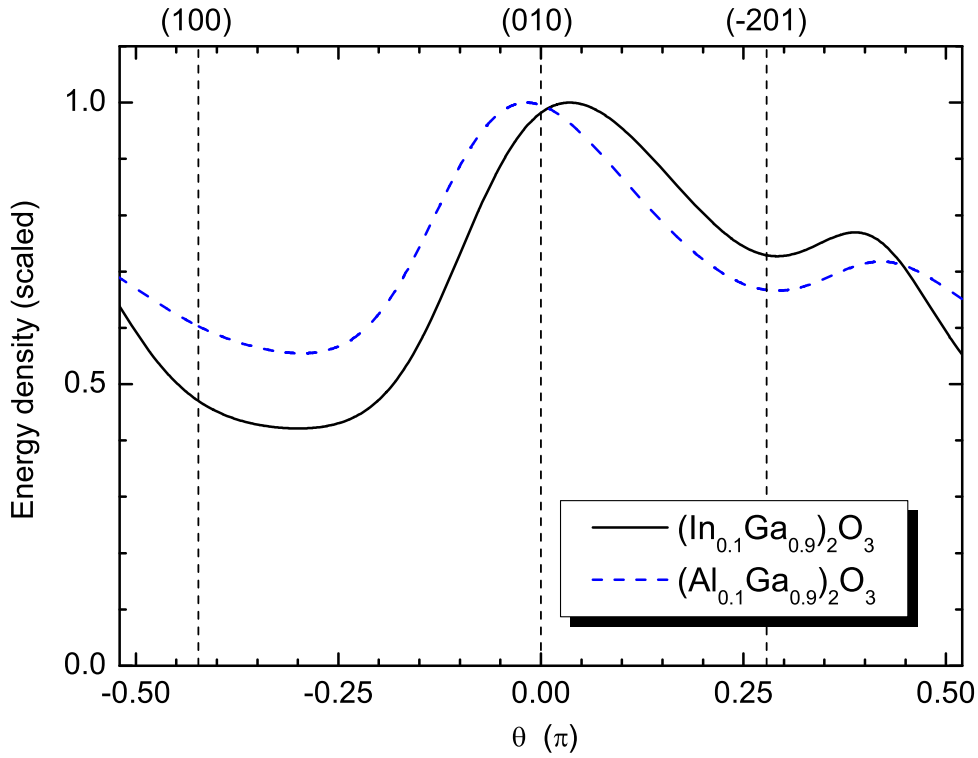

Figure 8.14: Energy density for $(In_{0.1}Ga_{0.9})_2O_3/Ga_2O_3$ (solid black line) and $(Al_{0.1}Ga_{0.9})_2O_3/Ga_2O_3$ (dashed blue line) scaled to their respective maxima as a function of angle θ in the (010) azimuth.

well with a single-band model. The low thermal conductivity near room temperature is attributed to the heavy element iodine as well as the strong phonon scattering within the obtained polycrystalline CuI thin films. At the same time, these films are transparent and exhibit a high transmission of 60–85 % in the visible spectral range. Accordingly, we have achieved a high thermoelectric figure of merit ZT 0.23 near room temperature for CuI films. In Fig. 8.15 we summarize the ZT of typical n- and p-type thermoelectric materials. The ZT value of our CuI thin film is 1000 times higher compared to any other p-type transparent material and almost twice compared to n-type materials.

A transparent and flexible CuI-based thermoelectric element has been demonstrated, as shown in Fig. 8.16 . Such device presents a high power density of 2.4 $mWcm^{-2}$ at $\delta T = 50$ K, which is comparable with those for Bi_2Te_3/Sb_2Te_3-based devices. In combination with available n-type transparent thermoelectric materials, such as Al-doped ZnO and Sn-doped In_2O_3, invisible thermoelectric modules can be readily constructed by coupling the transparent n- and p-type thermoelectric legs. Such invisible and flexible thermoelectric element can be used for designs of thermoelectric windows, body-heat-powered wearable devices, and on-chip cooling or power recovery for miniaturized chips. Our findings open a path for multifunctional technologies combing transparent electronics, flexible electronics and thermoelectricity [1].

[1] C. Yang et al., Nat. Commun. **8**, 16076 (2017), doi:10.1038/ncomms16076

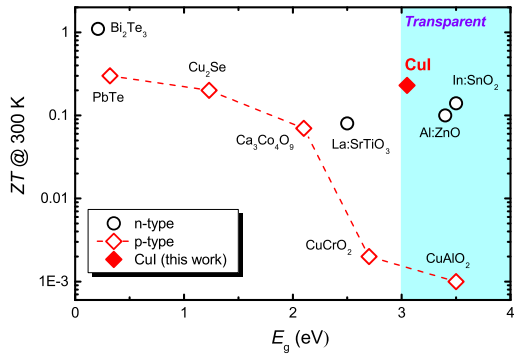

Figure 8.15: Comparing the thermoelectric ZT of typical n- and p-type thermoelectric materials and CuI thin films (this work) at room temperature. Dashed line is guide to the eyes.

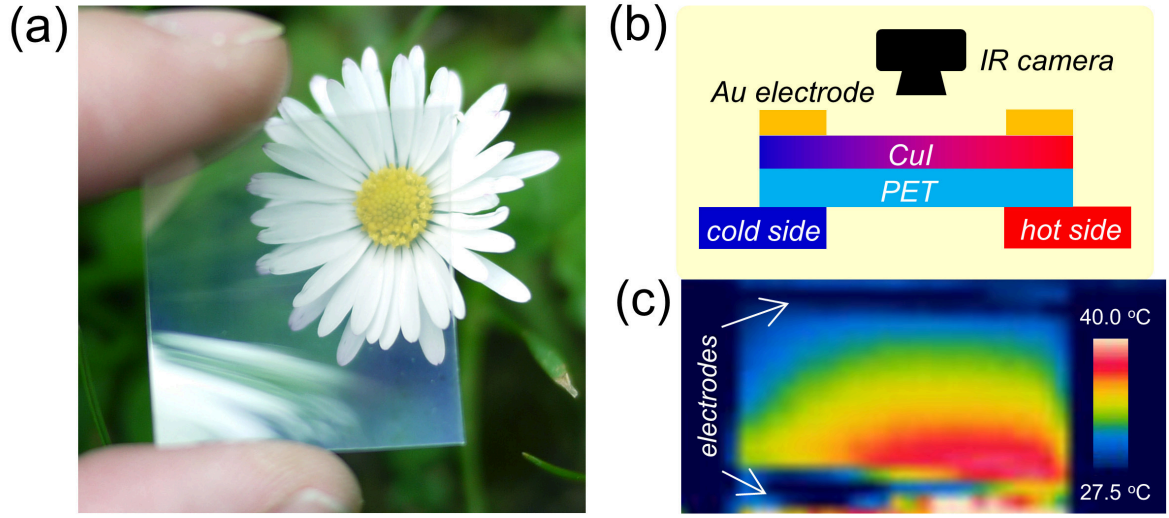

Figure 8.16: (a) The photo of a CuI thin film deposited on PET. (b) Schematic illustration for the power output measurement of the CuI/PET single-leg thermoelectric device. (c) The example IR image taken during one of the measurements.

8.8 Structural and optical properties of MgO/TiN superlattices

F. Jung, S. Ellis, V. Zviagin, C. Sturm, J. Lenzner, R. Schmidt-Grund, C. Patzig*, S. Selle*, T. Höche*, M. Lorenz and M. Grundmann

*Fraunhofer-Institut für Mikrostruktur von Werkstoffen und Systemen IMWS, Center for Applied Microstructure Diagnostics CAM, Halle D-06120, Germany

The growth and structural properties of MgO/TiN-based multilayers and superlattices with a lattice periodicity of a few nanometers were investigated. In these materials, the optical properties are described by an effective dielectric function tensor, consisting of two independent components: one for the electric field perpendicular to the layer interfaces and one for the electric field parallel to the interfaces, $\epsilon_\perp$ and $\epsilon_\parallel$, respectively. The real parts of these two contributions are expected to exhibit an opposite sign, which

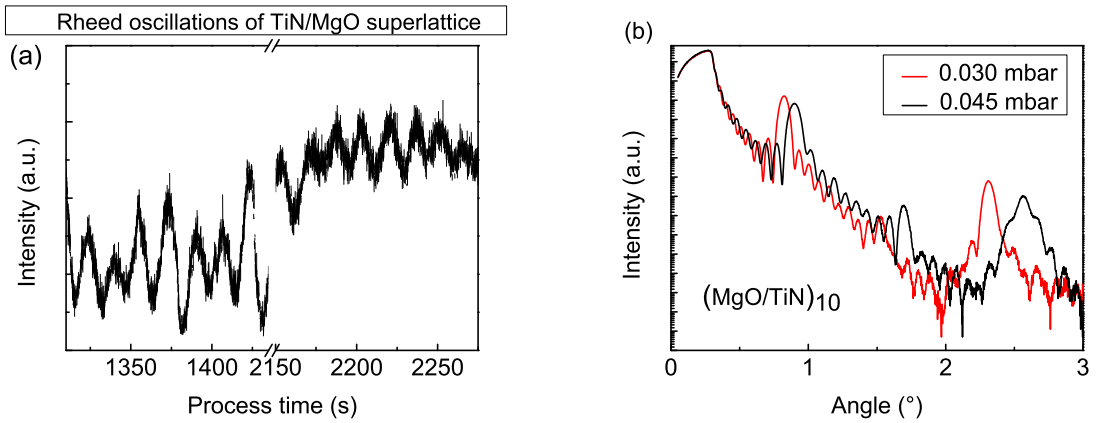

Figure 8.17: (a) *In-situ* RHEED oscillations of a superlattice grown at a pressure of $p = 0.045$ mbar. (b) XRR spectra for MgO/TiN-superlattices grown at different pressures. All superlattices consisted of 10 MgO/TiN double layers.

leads to a hyperbolic dispersion, whereas the imaginary part should be positive for both [1].

Planar periodic nanostructures employing titanium nitride as a plasmonic component have already been realised by Naik *et al.* [2], using (Al, Sc)N as a dielectric component. They are promising for realising hyperbolic dispersions in the visible spectral range. The use of MgO instead of (Al, Sc)N roots in it being a well-understood dielectric with the same crystal structure, namely rocksalt structure, as TiN and a small lattice mismatch.

Superlattices consisting of titanium nitride and magnesium oxide were deposited on TiN(100)-substrates using pulsed laser deposition (PLD) from sintered targets in an argon atmosphere. *In-situ* reflection high-energy electron diffraction (RHEED) has been employed to monitor the thickness of atomic mono-layers in the superlattice and to determine the growth mode. X-ray reflectometry (XRR) and x-ray diffraction (XRD) 2Θ-ω-scans allowed to evaluate the structural properties of the layers. In the XRR curves, single peaks arising from interferences are clearly visible for samples grown at high pressure. Equal spacing of the peak positions indicates homogeneous layer thicknesses (Fig. 8.17).

Analytical scanning transmission electron microscopy (STEM) analyses, employing a ring-shaped high-angle annular dark field (HAADF) detector, in combination with energy dispersive X-ray analysis (EDX) revealed smooth interfaces between the TiN and MgO layers, nearly homogeneous layer thicknesses and a minor diffusion of Mg into the TiN layers (Fig. 8.18). A subsequent layer-by-layer growth was also observed by the *in-situ* RHEED, as persistent RHEED oscillations were detected up to a total superlattice thickness of 100 nm (Fig. 8.17). Thus it was demonstrated that the subsequent growth of nitride and oxide materials is possible in a single deposition chamber [3].

Reproducibility of the optical properties of single TiN layers was inititally an obstacle. In the course of the investigation it became clear that the miscut and the growth pressure have a significant influence on the reproducibility. Ellipsometry measurements were performed *ex-situ* in the visible spectral range. By modelling the ellipsometry data, the dielectric function of the layers was obtained. It was observed that the reproducibility of optical properties was best for samples grown at a high miscut

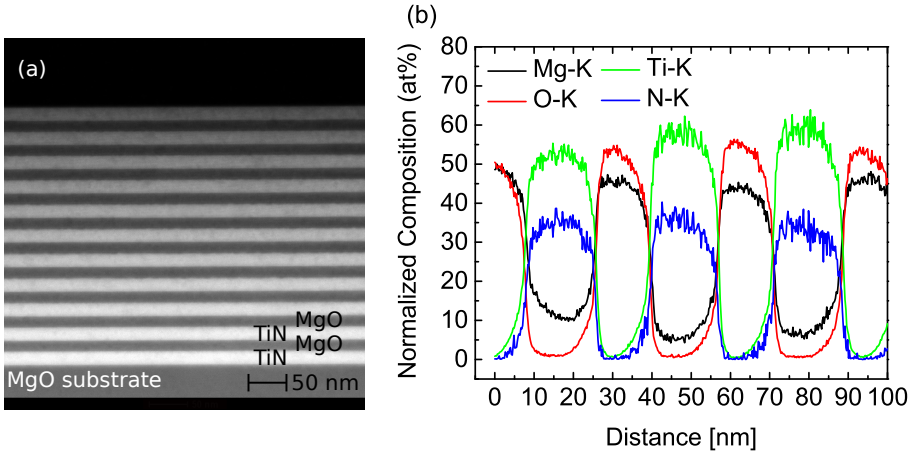

Figure 8.18: (a) STEM HAADF micrographs of a typical MgO/TiN-superlattice. (b) Normalized EDX linescan through the first few layers of the superlattice. The first five nanometers on the x-axis correspond to the MgO-substrate.

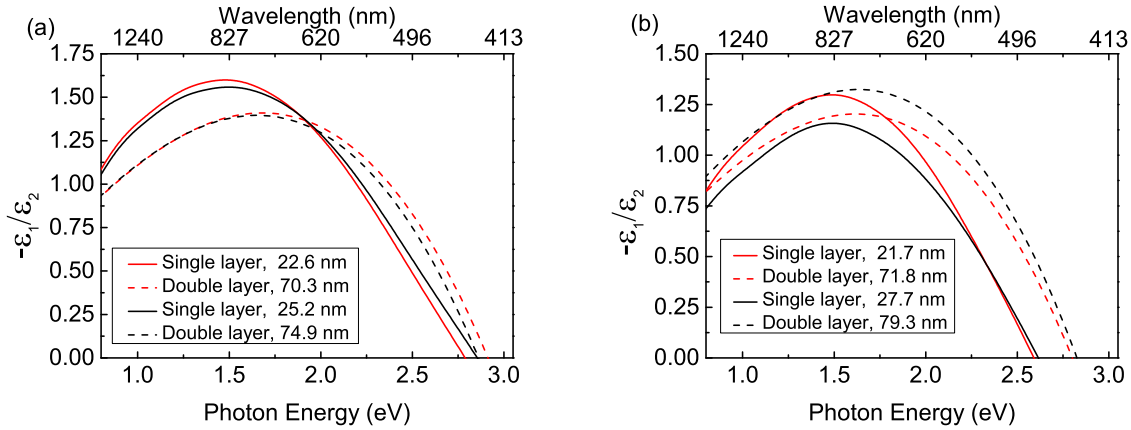

Figure 8.19: Figure of merit (*FOM*) of single TiN layers and TiN/MgO/TiN-double layers at a pressure of $p = 0.003$ mbar and a high (a) and low (b) substrate miscut, respectively.

angle of $0.1° < \gamma < 0.15°$ and a low pressure of $p = 0.003$ mbar. For some selected layers, an additional double layer of TiN/MgO was fabricated on top and evaluated using ellipsometry. The optical properties of the second TiN layers grown at the same pressure were similar, independent of the substrate miscut [4].

For the usage of TiN as a plasmonic component of a superlattice, an important quantity is the figure of merit (FOM), defined by $FOM = \frac{-\epsilon_1}{\epsilon_2}$. A maximal *FOM* of 1.87 was obtained for a single TiN-layer at a photon energy of $E = 1.52$ eV. It was further observed, that the the energy of the maximum of this ratio shifted towards the visible range for the second TiN-layer, compared to the first one, whereas its value decreased for most samples (Fig. 8.19).

[1] G.V. Naik *et al.*: Opt Mater Express **2**, 478 (2012),doi:10.1364/OME.2.000478.
[2] G.V. Naik *et al.*: PNAS **111**, 7546 (2014),doi:10.1073/pnas.1319446111.
[3] M. Lorenz *et al.*: J Mater Res **32**, 3936 (2017),doi:10.1073/pnas.1319446111.
[4] S. Ellis: *On the Properties and Reproducibility of PLD-grown MgO/TiN Thin Films*, Bachelor's thesis, Universität Leipzig, Leipzig, Germany (2017).

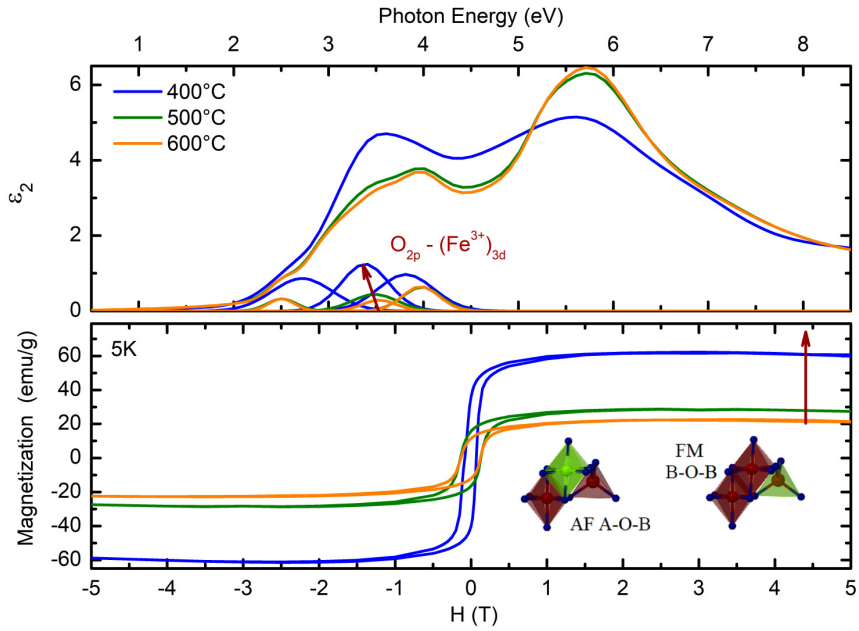

Figure 8.20: (Top) Imaginary part of the dielectric function (ϵ_2) determined from ellipsometry with the deposition temperatures indicated. (Bottom) Magnetization as a function of applied magnetic field of the ZFO thin films.

8.9 The Influence of Bulk and Surface Cationic Configuration on the Ferrimagnetic Behavior in Metastable $Zn_xFe_{3-x}O_4$ ($0 \leq x \leq 1.26$) Spinel Ferrite Systems.

V. Zviagin, P. Huth [*], M. Bonholzer [†], C. Sturm, J. Lenzner, A. Setzer, R. Denecke [*], P. Esquinazi, M. Grundmann, R. Schmidt-Grund

[*]Universtät Leipzig, Wilhelm-Ostwald-Institut für Physikalische und Theoretische Chemie, Leipzig, Germany.
[†]now with: Max-Planck-Institut für Extraterrestrische Physik, Garching, Germany.

Extensive variety of tunable properties make spinel transition-metal oxide AB_2O_4 system to a significant functional material for applications ranging from biomedical applications in cancer research [1], fabrication of novel Li-ion controlled electronic devices [2] to increasing energy conversion efficiency for renewable energy storage [3, 4]. These properties strongly depend on the choice of fabrication parameters, which result in various cationic site occupation. Ideally, antiferromagnetic and insulating $ZnFe_2O_4$ (ZFO) crystallizes in a normal spinel structure with the cation distribution formula being $(Zn^{2+})_A[Fe^{3+}]_BO_4^{2-}$. Round and square brackets indicate the tetrahedral (A) and octahedral (B) lattice sites, respectively. However, the ZFO structure, which is achieved by film deposition, is most likely to deviate from the ideal case and possess $(Zn^{2+}Fe^{3+})_A[Zn^{2+}Fe^{3+}Fe^{2+}]_BO_4^{2-}$ cationic distribution, depending on the deposition temperature and pressure. We have applied spectroscopic ellipsometry (SE) in order to probe bulk cationic configuration which is responsible for the observed ferrimagnetic response, measured by superconducting quantum interference device (SQUID) and

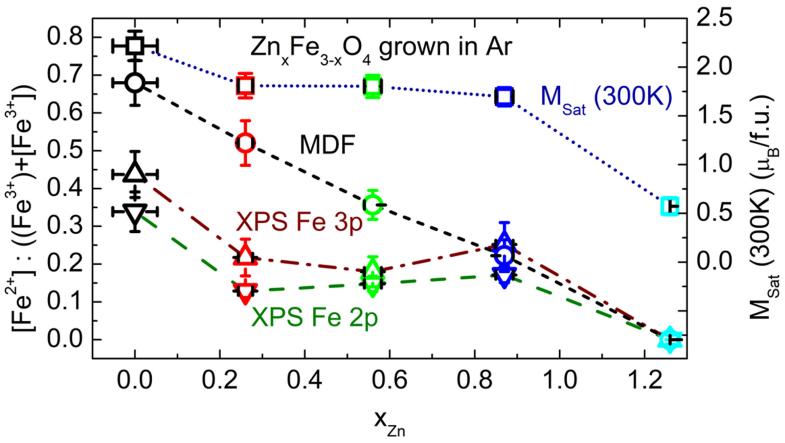

Figure 8.21: Cation ratio $[Fe^{2+}]/((Fe3+) + [Fe^{3+}])$ in the bulk (MDF) and surface (Fe3p and Fe2p) as well as room temperature magnetization saturation as a function of Zn concentration (x_{Zn}).

vibrating sample magnetometer (VSM). Transitions assigned to the model dielectric function (MDF) were electronic transitions between d orbitals of $[Fe^{2+}]_B$ at energies below 1 eV and between O_{2p} and cation 3d and 4s orbitals. Based on the strength of the transitions involving $[Fe^{2+}]_B$, $(Fe^{3+})_A$ and $[Fe^{3+}]_B$ cations, the relative cation concentration of individual cations was estimated. Furthermore, the analysis of the Fe2p and 3p core levels in the X-ray photoelectron spectroscopy spectra allowed for determination of surface sensitive cationic site occupation as well as estimation of relative concentration of individual cation.

ZFO thin films were deposited on $SrTiO_3$ substrates by pulsed laser deposition at temperatures varying from (400 – 600) ℃ and oxygen partial pressure of 0.016 mbar. The high oxygen pressure resulted in films without $[Fe^{2+}]$, confirmed by the absence of low-energy absorption in the MDF spectrum. The decrease in the crystal quality with the decrease in deposition temperature was confirmed by XRD. The tetrahedral occupation by $(Fe^{3+})_A$ was shown to increase with the decrease in deposition temperature, (Fig. 8.20), apparent by the increase in the strength of the oscillator located at ~ 3.5 eV. The increase in the magnetic response was attributed to the antiferromagnetic oxygen mediated super-exchange (SE) interaction between $(Fe^{3+})_A$ and $[Fe^{3+}]_B$ dominating over the ferromagnetic SE interaction between $[Fe^{3+}]_B$ and $[Fe^{3+}]_B$. A direct correlation between the amplitude of the transition involving (Fe^{3+}) and magnetization saturation and remanence measured at 5 K was drawn [5]. The presence of (Fe^{3+}) is likely to result from either inversion, where the Zn^{2+} moves to octahedral and Fe^{3+} moves to tetrahedral lattice site, or to Fe^{3+} occupying nominally unoccupied tetrahedral lattice sites.

The surface and bulk cation configuration was investigated as a function of Zn concentration in the $Zn_xFe_{3-x}O_4$ system with x_{Zn} varying from (0 – 1.26) . A deviation in the surface $[Fe^{2+}]/((Fe^{3+}) + [Fe^{3+}])$ cation ratio from the bulk was attributed the an excess of $[Fe^{3+}]_B$ cations in the surface layer (Fig. 8.21). The variation of cation configuration throughout the film depth is apparent for $x_{Zn} \leq 0.56$ and could serve as a possible explanation for the observed magnetic behavior. Although temperature dependent magnetization exhibits a jump at around the Verwey transition temperature, typical for magnetite, x = 0 , the room temperature magnetization saturation is lower than the

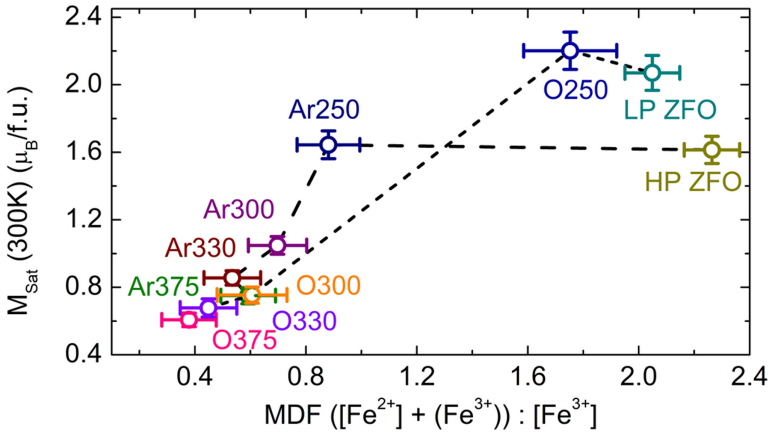

Figure 8.22: Room temperature magnetization satuation as a function of bulk (MDF) cation ratio ([Fe^{2+}] + (Fe^{3+}))/[Fe^{3+}]) for ZFO films annealed in oxygen (O) and argon (Ar) atmospheres at temperatures as indicated.

expected 4 μ_B/f.u., arising from the [Fe^{2+}] moments. A cusp at the Neel temperature as well as a low spin-freezing temperature is observed in the temperature dependent magnetization for x = 1.26, typical for ZFO system. However, Raman spectroscopy indicates the presence of octahedral Zn^{2+} and tetrahedral Fe^{3+} cations being present in the sample with highest x_{Zn}.

Low temperature (300 ℃) grown ZFO films were deposited at low and high oxygen partial pressures and subsequently annealed in oxygen and argon atmospheres, respectively, at temperatures varying from (250 – 375) ℃. The sample surface was found to become smooth and roughen after annealing in oxygen and argon environments, respectively. After annealing the films at a temperature lower than the deposition temperature, 250 ℃, the small change in room temperature magnetization saturation was attributed to defects such as oxygen vacancies and [Fe^{3+}] excess in the surface layer. At temperatures above 250 ℃, the bulk cationic structure tends to recrystallize towards the stable normal spinel phase structure. In this case a low ([Fe^{2+}] + (Fe^{3+}))/[Fe^{3+}] cation ratio is observed (Fig. 8.22). The octahedral crystal field parameter is closer to the literature value of 1.4 eV and the magnetization saturation is lower for films annealed in oxygen environment than for those annealed in argon at temperatures 300 ℃ and above, indicating a more stable spinel structure.

[1] V. Sawant *et al.*: J. Magn. Magn. Mater. **417**, 222 (2016), doi:10.1016/j.jmmm.2016.05.061.
[2] G. Wei *et al.*: Sci. Rep. **7**, 12554 (2017), doi:10.1038/s41598-017-12948-6.
[3] C. Suchomski *et al.*: Nanotechnol. **7**, 1350 (2016), doi:10.3762/bjnano.7.126.
[4] N. Guijarro *et al.*: Sustainable Energy Fuels **2**, 103 (2018), doi:10.1039/C7SE00448F.
[5] V. Zviagin *et al.*: Appl. Phys. Lett. **108**, 13 (2016), doi:10.1063/1.4944898.

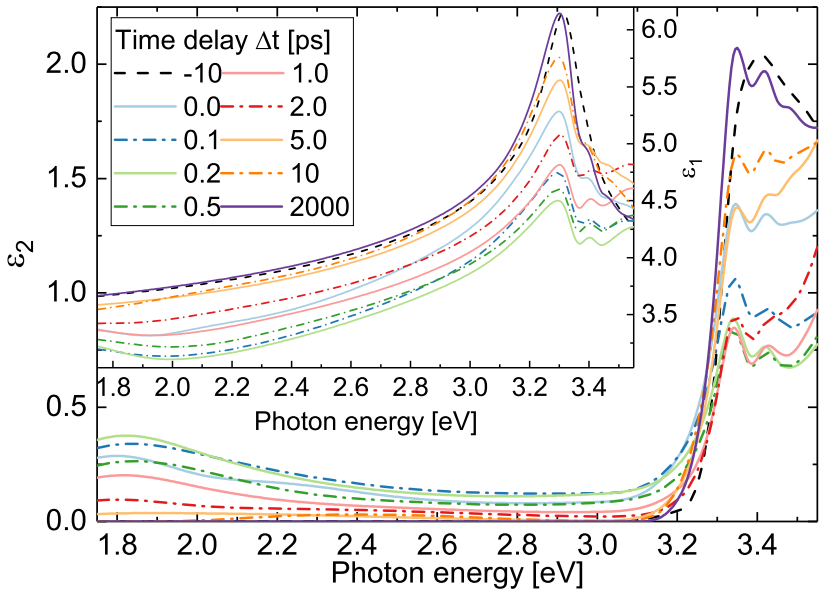

Figure 8.23: Real and imaginary part of the dielectric function of the *c*-plane oriented ZnO thin film calculated from pump-probe tSE measurements. The maximal created charge density amounts to 1×10^{20} cm^{-3}.

8.10 Femtosecond time-resolved spectroscopic ellipsometry

O. Herrfurth, S. Richter*, M. Rebarz*, S. Espinoza*, M. Kloz*, M. Grundmann, J. Andreasson†, R. Schmidt-Grund

*ELI Beamlines, Institute of Physics, Czech Academy of Science, Prague, Czech Republic
†Chalmers University of Technology, Condensed Matter Physics, Göteborg, Sweden

The recently established collaboration between ELI Beamlines (Czech Republic) and Universität Leipzig led to the development of a set-up for pump-probe femtosecond time-resolved spectroscopic ellipsometry (tSE). It enables ellipsometric measurements with very high time resolution (200 fs) in a broad observable spectral range (1.8 eV to 3.6 eV).

8.10.1 Time-resolved dielectric function and charge carrier dynamics of a ZnO thin film

To test the set-up capabilities, ZnO as promising candidate material for next-generation optoelectronic devices, was chosen. For this purpose, a 30 nm thin *c*-plane oriented ZnO film on an amorphous glass substrate was grown by pulsed laser deposition. In the tSE experiment, the film was pumped by ≈ 50 fs short pulses of 4.7 eV photons and reflectance-difference spectra of the probe whitelight were measured for different polarization states. The ellipsometric angles were computed utilizing Moore-Penrose pseudoinversion [1]. They where, in turn, modelled with B-Spline functions in a transfer

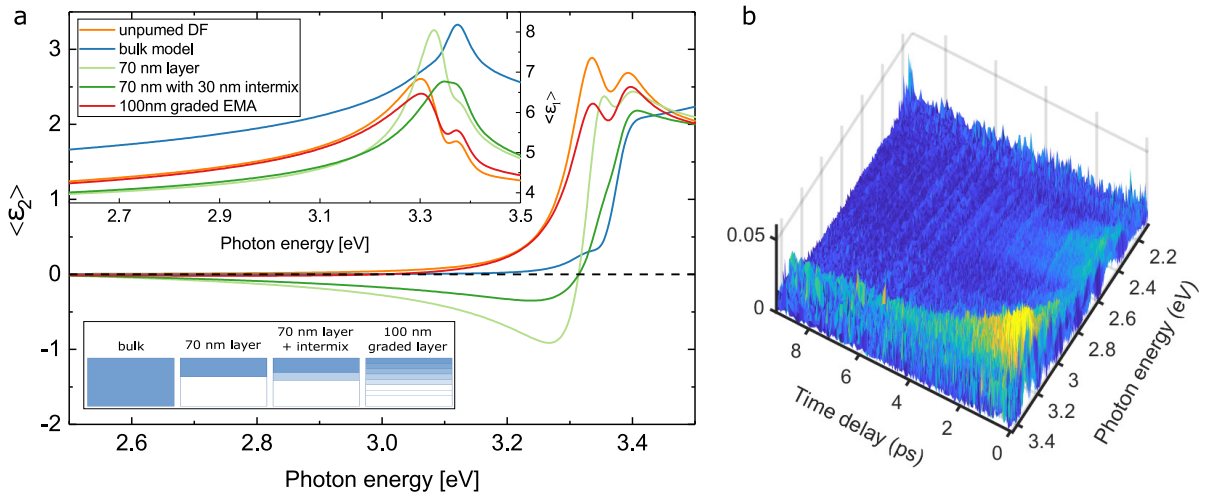

Figure 8.24: a Simulated pseudo-dielectric function of the pump laser-induced top layer within several model approaches differing from the unpumped bulk dielectric function below. The pumped and unpumped bulk dielectric function was chosen to be ZnO-like. The inset scheme depicts the different layer models given in the legend. **b** Depolarization profile of the *c*-plane oriented ZnO thin film measured with time-resolved spectroscopic ellipsometry.

matrix algorithm to obtain the dielectric function (DF) $\varepsilon = \varepsilon_1 + i\varepsilon_2$ for each time delay Δt. Selected DF spectra at various Δt are shown in figure 8.23.

The DF of the unpumped sample ($\Delta t < 0$) reveals the typical ZnO absorption spectrum with transparency regime up to 3.2 eV and broad exciton-related absorption peak at higher energies. Upon pumping the film a fine structure of the absorption is observable. This might be related to a lower local average potential acting on the charge carriers which now have high excess energy, an effect similar to motional narrowing observed in other spectroscopy techniques. Simultaneous to the pump pulse ($\Delta t \approx 0$), absorption in the formerly transparent regime (1.9 eV) sets in which represents absorption channels becoming available only due to the promotion of electrons from valence band or defect states to the conduction band. particular, intra-valence and intra-conduction band transitions to formerly occupied states as well as transitions to defect states might be involved. The mid-gap absorption disappears after about 3 ps when holes might have relaxed to the valence band maximum or fast electron capture by the defects appeared, both blocking the corresponding optical transitions.
Above band gap, the pump pulse induced electron-hole pair density immediately decreases absorption (bleaching) indicating that lower lying valence bands are involved. Otherwise, a certain onset time would be expected, but within the given time resolution absorption bleaching appears instantaneous. It is saturated after 300 fs, but surprisingly the excitonic peaks never disappear although the estimated maximal charge carrier density of 1×10^{20} cm^{-3} greatly exceeds the ZnO Mott density which can be expected to be around 5×10^{17} cm^{-3}. This could mean that electron-hole coupling is stronger than expected or that the actual charge carrier density near the respective band extrema never exceeds the Mott density. In both cases, this shines new light on the understanding of the charge carrier dynamics of non-resonantly pumped semiconductors. The absorption bleaching starts disappearing after 1 ps starting from higher energies indicating that optical transitions to the conduction band become available again as hot charge

carriers thermalize.
After 2 ns, absorption is restored and a remaining redshift of the absorption edge by 20 meV can be attributed to local heating of the sample by approximately 70 K which matches to theoretical estimations ending up with 95 K assuming that all energy of the pump laser pulse is transferred to the lattice. This data represents a charge carrier density-dependent DF, which can be compared to the results of the theoretical work of Marcel Wille [2]. as a consequence of stimulated emission of photons the wave vector of the stimulated light points to the sample backside and in a reflection experiment the wave vector of the detected light is opposite to it.
step should be worked out and on the experimental side optically anisotropic samples will be the next aim.

8.10.2 Strategies and problems of time-resolved spectroscopic ellipsometry data analysis

A general advantage of ellipsometry over unpolarized reflection and transmission measurements is that the depolarization of the probe light is measured. In particular, if physical processes altering the polarization state of the reflected light appear in the studied sample faster than the time resolution of the instrument, then several light polarization states are averaged over during the detector acquistion time effectively decreasing the degree of light polarization. This allows monitoring and effectively improving the time-resolution of the instrument. A depolarization profile of the previously introduced *c*-plane oriented ZnO thin film is shown in figure 8.24b. It is seen that the depolarization is largest in the spectral range around the exciton energy of ZnO for time delays smaller than a few ps.

Spectroscopic ellipsometry with femtosecond time resolution yields the ellipsometric parameters as a function of both energy and time in a two-dimensional data grid. The grid spacing is not equidistant as it is experimentally given by the temporal and spectral resolution of the set-up. In our first approach, the spectral resolution ΔE is implemented in the data analysis by convolution of the model data with a rectangle of the same width. In principle, both experimental uncertainties should be incorporated which can be realized by convolution of the model data grid with a two-dimensional profile (e.g. triangle, rectangle, 2D-Gaussian). This will be implemented in further steps of the data analysis.

A severe problem in data analysis is caused by the experimental scheme itself: the finite pump laser penetration depth leads to an exponential distribution of excited charge carriers in the probed sample depth. This distribution is further altered by time-dependent recombination and diffusion processes. To capture the therewith induced depth-dependence of the dielectric function (DF), the correct choice of the sample's layer model, most importantly for bulk-like samples, is therefore one of the most critical points. This problem is illustrated in figure 8.24a.

It shows the pseudo-DF of the pump laser-induced top layer simulated within several layer models: 1) bulk pumped layer, 2) thin pumped layer on top of bulk material, 3) thin pumped layer with intermix layer on top of bulk material and 4) thin exponentially graded layer on top of bulk material. It is seen, that the spectral form of $< \varepsilon_2 >$ differs significantly depending on the chosen layer model. In cases 2) and 3) negative $< \varepsilon_2 >$ is observed. Consequently, if such data is erroneously modelled as

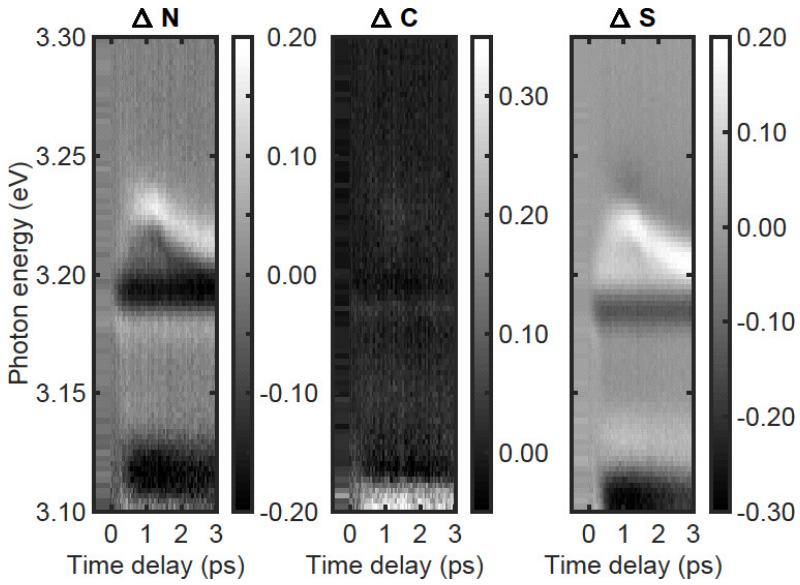

Figure 8.25: Pump-probe differences of ellipsometric parameters N, C and S of a ZnO-based microcavity measured with time-resolved spectroscopic ellipsometry.

bulk, then artificial optical gain ($\varepsilon_2 < 0$) seems to occur which is only a result of the wrong choice of the model.

These subtleties can be circumvented by choosing a thin film sample in order to neglect the correct form of the gradient. In particular, if the pump laser penetration depth is in the order of the sample thickness, then a homogeneously pumped volume can be assumed. Furthermore, diffusion in the lateral direction can be neglected since the probed sample area is only a quarter of the pumped area and the estimated diffusion length is much smaller compared to the diameter of the pumped area (400 µm).

8.10.3 Time-resolved mode dynamics of a ZnO-based microcavity

Semiconductor-based microcavities occur commonly in nowadays optoelectronic devices and are still a suitable structure to study fundamental light-matter interaction. We use a ZnO-based microcavity with wedge-shaped cavity layer an investigate its mode dynamics with tSE. The ZnO cavity layer is approximately 200 nm thick at the investigated position. In equilibrium, the cavity mode is situated at around 3.2 eV. Upon pumping, a large number of electron-hole pairs is created in the cavity layer which leads to a drastic decrease of its refractive index as can be seen in figure 8.23. As the mode condition inside the given resonator structure has to be still fulfilled, the lower refractive index is compensated by a blueshift of the mode energy (20 meV). The blueshift occurs during the first picosecond after pumping and vanishes on a time scale $\Delta t = 5$ ps. Nevertheless, the blueshifted cavity mode seems to coexist with the cavity mode at the initial spectral position which might be related to portions of the cavity volume containing a smaller number of electron-hole pairs as described in section 8.10.2.

[1] M. Bass: Handbook of Optics, (1995).
[2] M. Wille: PhD thesis, Universität Leipzig (2018), http://nbn-resolving.de/urn:nbn:de:bsz:15-qucosa2-172673 .

8.11 Microcavities

R. Schmidt-Grund, T. Michalsky, E. Krüger, S. Richter, L. Trefflich, M. Wille, S. Blaurock[*], F. Dissinger[†], J. Zúñiga-Pérez[‡], C. Deparis[‡], C. Sturm, H.G. Zirnstein[§], M. Kakei, V. Gottschalch[*], V. Zviagin, G. Benndorf, S.R. Waldvogel[†], H. Krautscheid[*], B. Rosenow[§], M. Grundmann

[*]Institut für Anorganische Chemie, Universität Leipzig, Leipzig, Germany
[†]Institute of Organic Chemistry, Johannes Gutenberg-University Mainz, Mainz, Germany
[‡]CRHEA-CNRS, Valbonne, France
[§]Universtät Leipzig, Institute for Theoretical Physics, Leipzig, Germany

Also in 2017, we continued our research on microcavities (MC) regarding applications as well as fundamental physical properties. MC physics is in focus of current research because it still provides new and fascinating fundamental physical effects like quantum-optical properties in the strong light-matter coupling regime or even topological non-trivial states [1] as well as a wide variety of (tunable) lasing properties in the weak coupling regime for applications in optoelectronic devices.

In ZnO-based microwire MC, we utilized the interplay between loss and gain for the demonstration of a wavelength tunable and mono-/multimode switchable laser (Sec. 8.11.1). In further developing microwire MC based on the newly emerging wide-gap p-type material CuI, we proved the lasing mode type to be of second order triangular whispering gallery mode (WGM) and found strong hints that the gain is related to exciton-exciton scattering (Sec. 8.11.2). For low-cost and wavelength tunable lasing structures, we developed planar MC with carbon nanodots as active material and demonstrated bright cavity mode emission (Sec. 8.11.3). In 2016 we found theoretically that in MC with low symmetry the optical mode structure becomes very complex, yielding so called exceptional points which are related to non-trivial topology physics. In 2017, we have experimentally validated the theoretical predictions by means of a ZnO-based MC with in-plane orientation of the ZnO optical axis (Sec. 8.11.4).

8.11.1 Tunable Lasing in ZnO microwires

As already reported last year, lasing properties in WGM type micro-/ nanowire MC are ruled by the balance of loss and gain as well as the effective length of the cavity. The total losses basically comprise photon escape to the surrounding and absorptive losses within the MC, while the latter is a function of the wire radius and the actual refractive index profile within the structure. We have shown, that in the case of strong optical excitation the dynamics of the excited charge carriers causes temporal dynamics of lasing modes [2] and that the ratio of excited to non-excited cavity volume determines the spectral range in which the lasing modes occur [3].

Utilizing these effects, we realized a wavelength tunable laser, which also can be switched between mono- and dual-mode operation [4]. The laser is based on a tapered ZnO microwire that is mechanically moved relative to the optical pumping area. The radius dependence of the whispering gallery mode properties is thus translated into wavelength tuning of the emission. Since the spectral separation of the WGMs is as large as the spectral width of the gain spectrum (both about 50 meV for the demonstrated wire

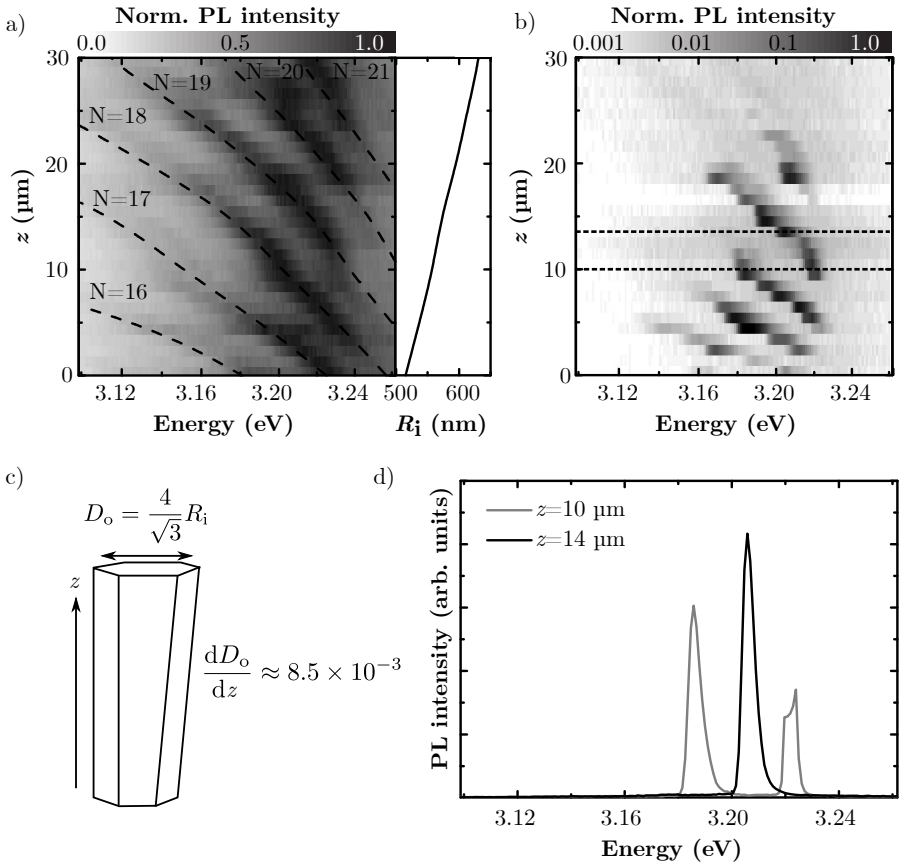

Figure 8.26: a) Spatial photoluminescence line scan along the wire z-axis for TE polarization at room temperature below the lasing threshold ($I \sim 0.3\,\mathrm{I_{th}}$) for $k_{||} = 0$. The right side of a) includes the determined inner wire radius R_i in dependence on the wire position. b) Same as a) but for an excitation energy density above threshold ($I \sim 2\,\mathrm{I_{th}}$). c) Sketch of a tapered microwire including length definitions and measured thickness gradient $\mathrm{d}D_0/\mathrm{d}z$. d) Two spectra from b) showing the spatial switch from mono- to dual mode lasing by changing the excitation spot position by $\Delta z = 4\,\mu\mathrm{m}$ (dashed lines in panel b).

with radius of around 0.5 µm), continuous mode tuning as well as switching between mono- and dual-mode operation is achieved (Fig. 8.26).

Comparing the WGM positions in the low-excitation case shown in Fig. 8.26a) and the mode energies which turned into the lasing regime under high-excitation shown in Fig. 8.26b), it becomes clear that although for each spatial position z at least two WGM modes are available, not each of them show lasing. This can be explained by the effective total loss or rather gain spectrum, which we thoroughly modeled based on a plane wave model, taking into account absorption and gain regions within the wire due to inhomogeneous pumping as well as optical losses of the microwire cavity (Fig. 8.27) [4].

8.11.2 Lasing in CuI microwires

We continued our research on CuI-based microcavities and investigated further properties of CuI microwires as potential candidates for new optoelectronic applications.

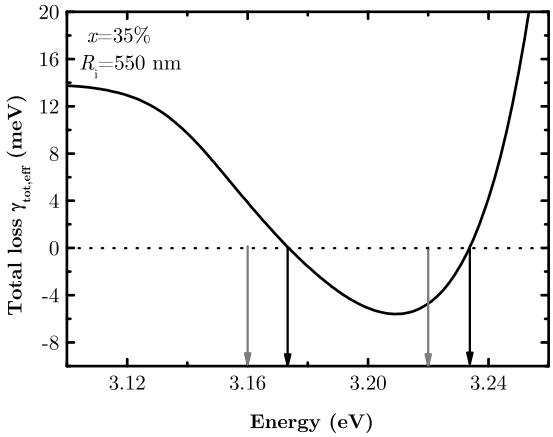

Figure 8.27: Modeled total loss γ_{tot} for a hexagonal ZnO cavity with $R_i = 550$ nm and a ratio of pumped to non-pumped cavity volume $x = 35$ % at room temperature and for TE polarization. In the spectral range (black arrows) where $\gamma_{tot} \leq 0$ holds gain is able to compensate cavity and absorption losses and lasing is supposed to appear. The experimentally observed lasing range is indicated by gray arrows. For the highly excited part of the cavity a carrier density of $\rho = 0.5 \times 10^{20}$ cm^{-3} has been taken into account.

The microwires were synthesized using a vapor-phase transport growth procedure. Last year we have allready demonstrated that the investigated microwires crystalize in zincblende CuI phase and exhibit a balanced stoichiometry of Cu:I 1:1. Further XRD-measurements proved, that the growth direction is the ⟨110⟩-direction. Furthermore the formation of twin planes along the ⟨111⟩-direction was observed similar to the dendritic growth of zincblende Germanium (Ge) [5].

The PL-measurements at low excitation density and 2 K substrate temperature exhibit a series of excitonic emission lines and their phonon replicas, which indicate the high optical quality of single microwires. The observed L-T-splitting energy of 6.1 meV fits well the known values for CuI [7]. The decay characteristics of the individual free and bound excitonic transitions were investigated with a time correlated single photon counting setup. The observed decay time in the spectral range of the free excitons is about (64 ± 30) ps. With increasing binding energy of the bound exciton the decay time increases and reaches values up to (680 ± 80) ps.

At higher optical excitation densities lasing emission of single CuI-microwires was demonstrated (see Fig. 8.28). The spectral mode positions were analyzed in order to deduce the dominant mode type of the microwire cavity. The experimental data match with the the calculated theoretical mode positions for second order triangular WGM. The refractive index for the theoretical calculations was extracted from ellipsometry data taken from CuI thin films. These findings indicate strongly that the triangular microwire acts as a whispering gallery type resonator. The dynamics of the microwire lasing was investigated for different temperatures and excitation densities. The observed decay constant was found to be independent of temperature and to fluctuate statistically in range of (3.5 – 8.5) ps. This small decay time reflects the ultra-fast recombination after the excitation pulse and is comparable to the values published by Ichida et. al. for the exciton-exciton scattering related P-Band in CuI films [6]. Nevertheless the formation of the EHP would also cause a sufficiently high gain in the same spectral range to overcome the optical losses in the microwire cavity and cause similar decay

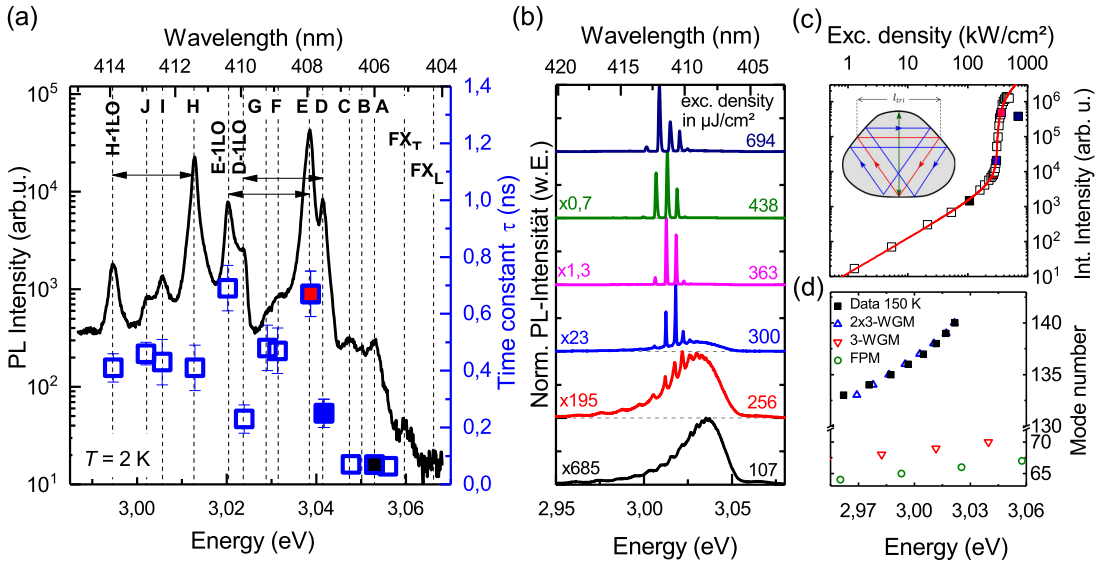

Figure 8.28: (a) Excitation density dependent μ-PL spectra (Ti:Sa, 200 fs, $\lambda_{ex} = 364$ nm) from a triangular microwire reveal a transition from broad spontaneuous emission to emission from narrow lasing modes. (b) Double logarithmic plot of the integrated μ-PL intensity of a lasing mode in dependence on the excitation density indicates a lasing threshold density $P_{th} = 300\ \mu J/cm^2$. The inset in (b) sketches different types of possible resonant modes in the triangular microwire cavity (green: Fabry-Perot modes (FPM), red and blue: first (3-WGM) and second (2x3-WGM) order triangular whispering gallery modes, respectivly). (c) A comparison of the experimental deduced mode positions at 150 K (black dots) and the calculated theoretical values for different types of resonant modes.

times for high excitaion densities. The laser action could be shown to be stable up to cryostat temperatures of about 150 K.

8.11.3 Carbon nanodots as active material in planar microcavities

Since their discovery in 2004 by Xu *et al.* [8] a lot of research on carbon nanodots (C-dots) has been done. Due to their facile synthesis from materials like coffee, tea, grass, candle soot [9] and more they are very eco-friendly and show good biocompatibility [10]. This leads to a wide range of applications like, photocatalysis, chemical sensing and cell imaging [11–13]. Because of their good photostability and strong, tuneable photoluminescence in the visible spectral range [14] they were used as active laser material [15]. Our goal is to incorporate carbon nanodots as active material into planar microcavities and explore their application for possible laser and white LEDs.
Carbon nanodots are discrete, quasispherical nanoparticles with sizes below 10 nm [9]. In order to minimize disorder effects and tune the thickness of the cavity layer, it was necessary to incorporate the C-dots in a transparent matrix. We chose commercial gelatin as cheap, eco-friendly and easy to process transparent material (Fig. 8.29 (a)). The C-dots were solved in Ethanol (10 mg C-dots in 10 ml Ethanol) and mixed with the heated (40°C) liquid gelatin (0.2 ml solved C-dots in 1 ml liquid gelatin). The solution was then spincoated (170 RPS, 2 min) onto a 8.5 layer pair distributed Bragg reflector (DBR, 95 % reflectivity) grown by pulsed laser deposition (PLD) [16]. Another 8.5 layer pair DBR was deposited on top, resulting in a microcavity with $\approx 2\lambda$ cavity layer

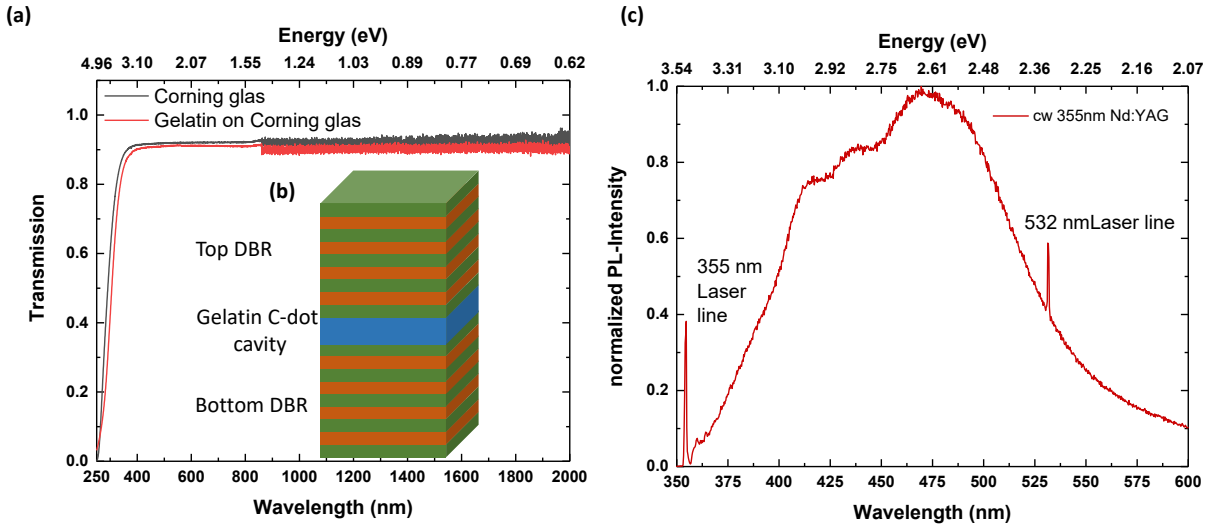

Figure 8.29: (a) Transmission measurement of gelatin on Corning glass. The Gelatin is transparent from 400 nm up to 2000 nm and therefore well suited as host matrix for the C-dots. (b) The microcavity consists of a PLD grown bottom DBR with 8.5 layer pairs yttria-stabilized zirconia (YSZ) and aluminium oxide(Al_2O_3), a 550 nm thick cavity layer of gelatin and C-dots and a top DBR with 8.5 layer pairs YSZ. (c) The cavity layer shows strong photoluminescence with maximum intensity around 470 nm.

thickness (Fig. 8.29 (b)). The ≈ 550 nm thick layer shows strong photoluminescence in the visible spectral range, with maximum intensity around 470 nm (Fig. 8.29 (c)).

The microcavity was investigated with angle-resolved photoluminescence spectroscopy (Fig. 8.30 (a)), revealing a cavity mode at 406 nm for $k_{\|} = 0\,\mu m^{-1}$. The stop-band of the DBR is also visible around 436 nm. The cavity mode as well as the stop band show dispersion in the measured k range of $\pm 6\,\mu m^{-1}$. For increasing excitation density we observed a linear increase of the integrated output intensity (at $k_{\|} = 0\,\mu m^{-1}$) (Fig. 8.30 (b)). The C-dot gelatin layer shows good photostability with possible peak excitation densities as high as $1\,GWcm^{-2}$.

Current research is focused on achieving better homogeneity of the cavity layer and an optimized microcavity design allowing for higher gain for possible laser applications.

8.11.4 Exceptional Points in the Dispersion of Optically Anisotropic Planar Microcavities

Planar optical microcavities are layered structures that confine the photon field in one dimension while allowing free propagation with wave vector $\vec{k}_{\|}$ in the cavity plane. Typically, a cavity layer is surrounded by distributed Bragg reflectors (DBR), i.e. multilayer mirrors revealing high-reflectivity bands. Here, we consider the 2D dispersion of radiative cavity-photon modes in structures comprising anisotropic media. The modes are described by complex energies $\tilde{E}_c = E_c - i\Gamma_c$; the real part E_c representing energetic position, the imaginary part Γ_c mode broadening in terms of half the width at half maximum. The latter arises due to dissipation by emission. Due to the quantization of the light field, several $m\frac{\lambda_c}{2}$ modes ($m \in \mathbb{N}$) can occur, all fulfilling phase matching

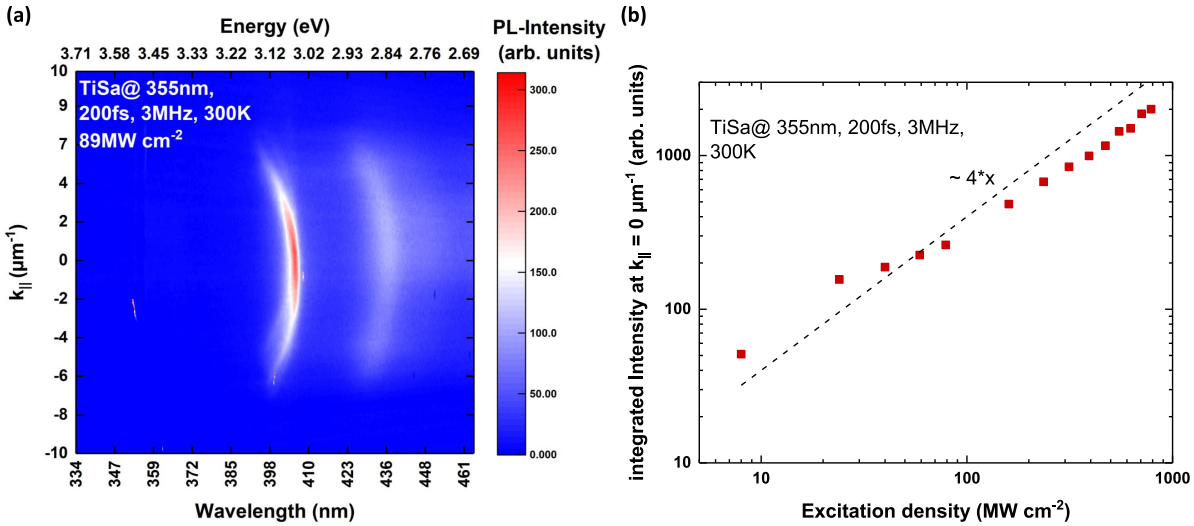

Figure 8.30: (a) Angle-resolved photoluminescence spectroscopy of the microcavity. The cavity mode (406 nm for $k_{||} = 0\,\mu m^{-1}$) and the stop-band of the DBR (436 nm for $k_{||} = 0\,\mu m^{-1}$) are visible. Both show dispersion in the measured k-space. (b) The input-output-characteristic of the microcavity shows a linear behaviour for peak excitation densities between 10 MWcm^{-2} and 1000 MWcm^{-2}.

by multiples of half-wavelengths fitting into the cavity. Depending on the in-plane wave-vector $\vec{k}_{||}$, each $m\frac{\lambda_c}{2}$ mode is polarization-split into two modes. In the case of microcavities consisting of optically anisotropic media, the two modes degenerate in the entire complex energy, i.e. in both, mode energy and broadening, for certain directions $\vec{k}_{||} \neq \vec{0}$ in momentum space. These are referred to as exceptional points [17].

Exceptional point degeneracies Exceptional points are simultaneous degeneracies of eigenvalues and eigenstates (eigenvectors), i.e. with reduced algebraic multiplicity. This requires non-Hermitian, complex-valued operators [18]. In the present case, at an exceptional point, the microcavity is described by a diverging transmission Jones matrix $\hat{J}_t$ such that its inverse matrix $\hat{J}_t^{-1}$ becomes [19]

$$\hat{J}_t^{-1} \propto \begin{pmatrix} a & \pm ia \\ \pm ia & -a \end{pmatrix}, \tag{8.1}$$

with $a \in \mathbb{C}$. For this symmetric (non-Hermitian) matrix this results in eigenstates describing either right- or left-circularly polarized light, $(1, i)^T$ or $(1, -i)^T$ in terms of Jones vectors. These states describe the light outside the microcavity, escaping from it. In contrast to other exceptional-point systems, the meaning of the eigenstates' chirality is hence directly given by the light polarization.

Exceptional points are topological charges and source of the Berry curvature [17]. This is also reflected by the complex-square-root topology in the vicinity of an exceptional point as depicted in Fig. 8.31. The exceptional point must be encircled twice in $\vec{k}_{||}$ space to return back to the same mode [20]. Moreover, an exceptional point establishes a center for a half-vortex in momentum space for the linear polarization of the modes, as illustrated in Fig. 8.32. However, as is also clear from Fig. 8.32, exceptional points in

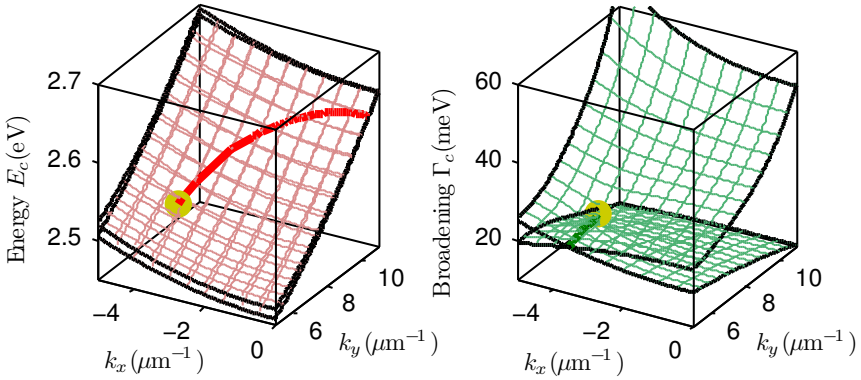

Figure 8.31: Example dispersion of photonic modes of an anisotropic microcavity near an exceptional point, representing a complex-square-root topology. Except for the exceptional point (yellow spheres), degeneracy of E_c (thick red line) is complementary to that of Γ_c (thick green line) in momentum space (wave vector $k_{x/y}$).

anisotropic microcavities occur pairwise with opposite circularity, resulting in a trivial net topology.

The phenomenon of exceptional points with circularly polarized propagation and vortices of the linear polarization is similar to singular optic axes in absorptive biaxial media [21, 22]. In fact, singular optic axes are also exceptional points in momentum space. This reflects the effective biaxiality of the anisotropic microcavity structure. For singular axes, the necessary dissipation is provided by absorption. In anisotropic microcavities, it is provided by the photonic loss due to emission, allowing the use of only transparent material for the entire structure. Furthermore, the exact orientation of singular axes in momentum space is fixed for biaxial absorptive crystals but for microcavities, it can be controlled by design [17].

ZnO-based microcavities We demonstrate ZnO-based microcavity structures grown on *m*-plane oriented ZnO substrates. The bottom DBR (16 pairs of ZnO/$Mg_{0.29}Zn_{0.71}O$) and the cavity layer were fabricated by means of molecular beam epitaxy [23]. All layers preserve *m*-plane orientation. The top DBR (6 pairs of polycristalline/amorphous Al_2O_3/YSZ[1]) were added by pulsed laser deposition. The width of the cavity layer was detuned with respect to the DBRs to result in an effective optical thickness of $9/8\lambda_c$. This results in directions of the exceptional points along emission angles of approx. 45° from normal incidence [17]. The photonic modes have been investigated by polarization-resolved transmission experiments, shining in unpolarized white light [19]. Figure 8.33 shows the resulting differences in mode energy and broadening in comparison to theoretical computations based on a transfer matrix model which was obtained by spectroscopic ellipsometry. Although the data still scatter a lot, the two pairs of exceptional points can be identified. Also the above-mentioned vortices of the linear polarization can be observed (not shown here).

[1] L. Lu *et al.*: Nat. Photonics **8**, 821 (2014), doi:10.1038/nphoton.2014.248.

[1] Y-stabilized ZrO_2

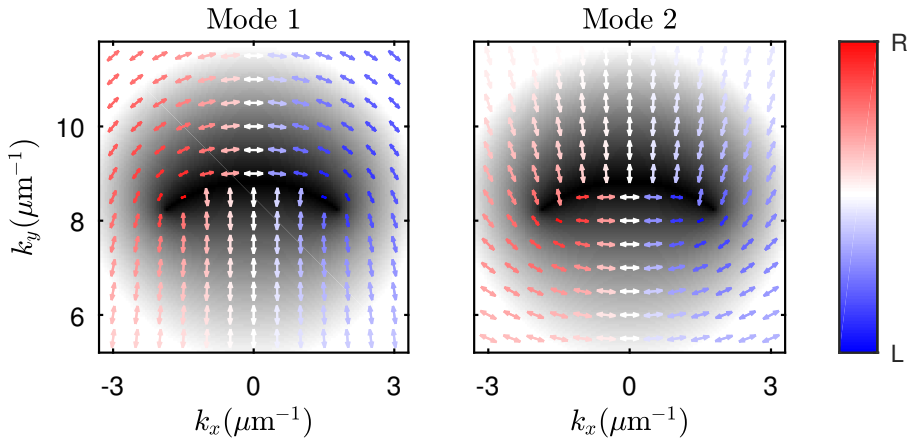

Figure 8.32: Representative mode polarization of the two cavity photon modes near a pair of exceptional points. Double arrows mark the orientation of the linear polarization, color the degree of circular polarization. Mode 2 has been chosen the one with higher energy, the material optic axis is oriented parallel to y. At the exceptional points (cf, Fig. 8.31), both modes become either left (L) or right (R) circularly polarized. For clarification, the energetic mode splitting is featured in both plots by gray scale (black depicting degeneracy).

[2] M. Wille *et al.*: Nanotechnology **27**, 225702 (2016), doi:10.1088/0957-4484/27/22/225702.
[3] M. Wille *et al.*: Appl. Phys. Lett. **109**, 061102 (2016), doi:10.1063/1.4960660.
[4] T. Michalsky: PhD thesis, Universität Leipzig (2017).
[5] D.R. Hamilton *et al.*: Journal of Applied Physics **31**, 1165 (1960), doi:10.1063/1.1735796.
[6] H. Ichida *et al.*: Physical Review B **72**, 045210 (2005), doi:10.1103/PhysRevB.72.045210.
[7] S. Suga *et al.*: Physical Review B **22**, 4931 (2005), doi:10.1103/PhysRevB.22.4931.
[8] X. Xu *et al.*: J Am Chem Soc **40**, 126 (2004), doi:10.1021/ja040082h.
[9] P. Roy *et al.*: Mater Today **8**, 18 (2015), doi:10.1016/j.mattod.2015.04.005.
[10] J.C.G.E. da Silva *et al.*: Trends Anal Chem **8**, 30 (2011), doi:10.1016/j.trac.2011.04.009.
[11] L. Cao *et al.*: J Am Chem Soc **13**, 133 (2011), doi:10.1021/ja200804h.
[12] Y. Dong *et al.*: Anal Chem **14**, 84 (2012), doi:10.1021/ac3012126.
[13] P. Roy *et al.*: Nanoscale **7**, 6 (2015), doi:10.1039/c4nr07005d.
[14] Y. Sun *et al.*: J Am Chem Soc **24**, 128 (2006), doi:10.1021/ja062677d.
[15] H. Liu *et al.*: ACS Appl Mater Interfaces **9**, 21 (2017), doi:10.1021/acsami.7b01067.
[16] H. Hilmer *et al.*: AIP Conf Proc **1199**, 151 (2010),

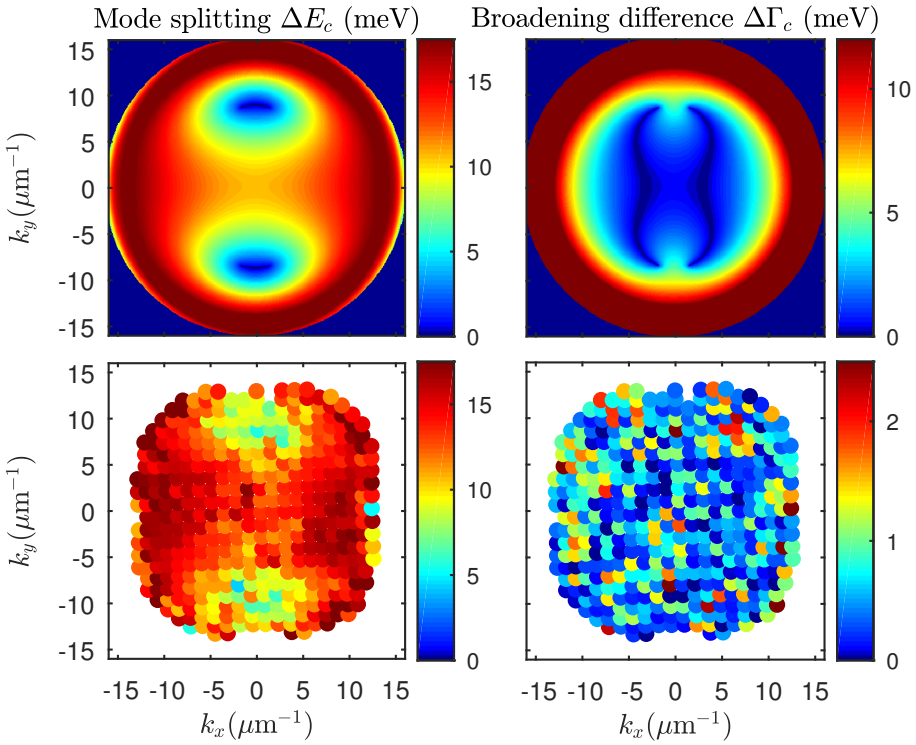

Figure 8.33: Difference in mode energy (left panels) and broadening (right panels) theoretically computed (upper panels) and experimentally obtained from transmission experiments (lower panels) depending on the in-plane wave-vector $k_{x/y}$ for an m-plane oriented ZnO-based microcavity. The material optic axis is oriented along y. The respective degeneracies (cf. Fig. 8.31) are recognized as minima.

doi:10.1063/1.3295340.
[17] S. Richter *et al.*: Phys. Rev. A **95**, 023836 (2017), doi:10.1103/PhysRevA.95.023836.
[18] M. V. Berry: Czech. J. Phys. **54**, 1039 (2004), doi:10.1023/B:CJOP.0000044002.05657.04.
[19] S. Richter: PhD thesis, Universität Leipzig (2018), http://nbn-resolving.de/urn:nbn:de:bsz:15-qucosa2-208912 .
[20] H. Cao, and J. Wiersig: Rev. Mod. Phys. **87**, 61 (2015), doi:10.1103/RevModPhys.87.61.
[21] M. Grundmann *et al.*: Phys. Status Solidi RRL **11**, 1600295 (2017), doi:10.1002/pssr.201600295.
[22] W. Voigt: Philos. Mag. 6$^{\text{th}}$ ser. **4**, 90 (1902), doi:10.1080/14786440209462820; W. Voigt: Götting. Nachr. **1**, 48 (1902), doi:10.1002/andp.19023141006.
[23] J. Zúñiga-Pérez *et al.*: Appl. Phys. Lett. **108**, 251904 (2016), doi:10.1063/1.4954796.

8.12 Dielectric tensor of KTP

C. Sturm, M. Grundmann

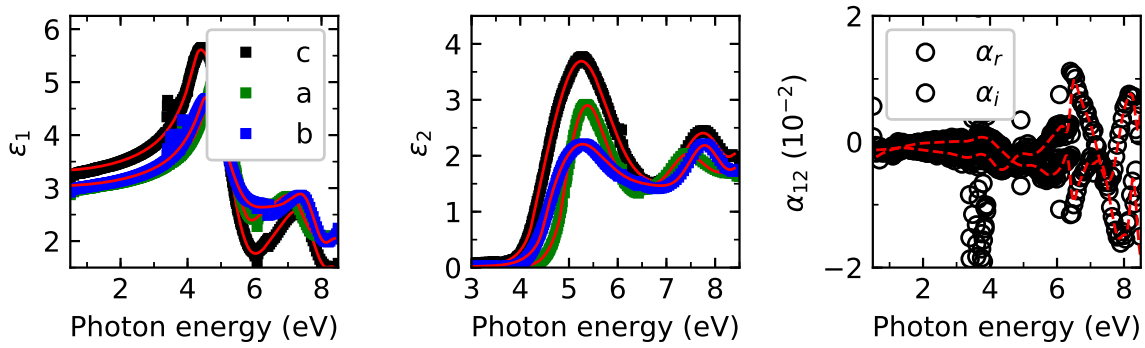

Figure 8.34: The determined dielectric function and gyration pseudotensor elements using the wavelength-by-wavelength analysis (symbols) and model dielectric functions (red solid lines). The red dashed lines for the gyration tensor element represent an interpolation of the experimental data by using a b-spline function.

Potassium titanyl phosphate ($KTiOPO_4$, KTP) is an optically biaxial material which is widely used in applications, e.g. for second harmonic generation (SHG) and frequency doubling in diode pumped lasers. Although the components of the dielectric tensor in the transparent spectral range are well known, there are only few reports for the absorption spectral range. Most of the reports were limited to the onset of the absorption which does not allow to deduce the dielectric function.

KTP belongs to the space group $Pna2_1$ and thus it is optically active. The impact of the optical activity on the electromagnetic wavepropagating within the material is typically described by means of the gyration pseudotensor α. For KTP this gyration pseudotensor is given by [1]

$$\alpha = \begin{pmatrix} 0 & \alpha_{12} & 0 \\ \alpha_{12} & 0 & 0 \\ 0 & 0 & 0 \end{pmatrix}. \tag{8.2}$$

In order to determine the dielectric tensor and the pseudo-gyration tensor we investigated a bulk single crystal by generalized spectroscopic ellipsometry in the spectral range from 0.5 eV up to 8.5 eV. The crystal exhibits two double side polished surfaces with the surface normal perpendicular to each other. In order to ensure a high sensitivity to the elements of the dielectric tensor and of the gyration pseudotensor, the crystal was rotated around the surface normal of the two polished surfaces from 0° to 180° by 15° and from 180° to 360° by 30° and the MÃ$\frac{1}{4}$ller matrix was measured. All orientations were analysed simultaneously by using a wavelength-by-wavelength analysis. The obtained dielectric function and gyration pseudotensor is shown in Fig. 8.34. In order to determine the band-gap energies, the DF deduced by the wavelength-by-wavelength analysis was parametrized by model dielectric functions. In doing so we determined a band-gap energy of (4.26 ± 0.10) eV for dipoles polarized along the *c*-axis, whereas for transitions polarized along the *a*- and *b*-axis the band-gap energies are blue shifted of about 0.6 eV and 0.2 eV, respectively.

[1] V.M. Agranovich, V.L. Ginzburg: *Crystal Optics with Spatial Dispersion, and Excitons*, 1st Ed. (Springer-Verlag, Berlin Heidelberg, 1984)

8.13 Funding

Polarisationswechselwirkung in Laser-MBE Wurtzit-Perowskit-Heterostrukturen
Prof. Dr. M. Lorenz
SFB 762/3, TP A2 within SFB 762 *Funktionalität Oxidischer Grenzflächen*

Optische Untersuchungen zu magneto-elektro-optischen Wechselwirkungen in ihrer Dynamik in oxidischen Heterostrukturen
Dr. Rüdiger Schmidt-Grund
SFB 762/3, TP B03 within SFB 762 *Funktionalität Oxidischer Grenzflächen*

Lateraler Transport in oxidischen Feldeffekt-Strukturen
Dr. H. von Wenckstern, Prof. Dr. M. Grundmann
SFB 762/3, TP B04 within SFB 762 *Funktionalität Oxidischer Grenzflächen*

Spinabhängiges Tunneln in oxidischen Heterostrukturen
Prof. Dr. M. Grundmann, Prof. Dr. I. Mertig (Martin-Luther-Universität Halle-Wittenberg)
SFB 762/3, TP B06 within SFB 762 *Funktionalität Oxidischer Grenzflächen*

Quantum Gases and Liquids in Semiconductor Rods conformally coated with Bragg Mirrors
Dr. R. Schmidt-Grund, Prof. Dr. M. Grundmann
DFG SCHM 2710/2-1, SCHM 2710/2-2, TP P1 within FOR 1616 *Dynamics and Interactions of Semiconductor Nanowires for Optoelectronics*

Whispering Gallery Moden: Einfluss der Resonatorform auf Lasing-Eigenschaften
Prof. Dr. M. Grundmann
DFG GR 1011/26-1

Amorphe Spinelle als p-Typ Halbleiter
Prof. Dr. M. Grundmann
DFG GR 1011/27-1

Kupferiodid: Epitaxie, Dioden und Ferromagnetismus
Prof. Dr. M. Grundmann
DFG GR 1011/28-1

Dioden auf der Basis von MBE und MoVPE oxid-Dünnfilmen
Prof. Dr. M. Grundmann
DFG GR 1011/30-2

Flexible analoge und digitale Grundschaltungen in amorphen Metalloxiden
Prof. Dr. M. Grundmann
DFG GR 1011/31-1, within SPP *High Frequency Flexible Bendable Electronics for Wireless Communication Systems (FFLexCom)*

Raman-Streuung in anisotropen Kristallen
Prof. Dr. M. Grundmann
GR 1011/33-1

Topologische Effekte in optisch-anisotropen Mikrokavitäten
Dr. R. Schmidt-Grund
DFG SCHM 2710/3-1

Graduiertenschule: Wolken, Aerosole und Strahlung am Beispiel des Mineralstaubes
Prof. Dr. M. Grundmann, Prof. Dr. A. Macke (Leibniz-Institut für Troposphärenforschung e. V.)
SAW-2012-IfT-4

SolarSens: Herstellung von wellenlängenselektiven DUV-Photoelektroden,
Dr. H. von Wenckstern
BMBF 01DR15008

High-resolution fingerprint sensing with piezoelectric nanowire matrices: PiezoMat
Prof. Dr. M. Grundmann
European Union, Seventh Framework Programme 611019

LOMID - Large cost-effective OLED microdisplays and their applications
Prof. Dr. M. Grundmann, Dr. H. von Wenckstern
European Union, Horizon 2020 644101

COSIMA - Combinatorisches Oxide-Screening für Materialien und Anwendungen
Prof. Dr. M. Grundmann
Europäischer Fonds für regionale Entwicklung (EFRE)
100282338 and 100315366

Nachwuchsforschergruppe - Oxid-Heterostrukturen: Anwendungen in Bauelementen
Prof. Dr. M. Grundmann
Europäische Sozialfonds (ESF)
100310460

8.14 Organizational Duties

M. Grundmann

- Director of the Felix Bloch Institute for Solid State Physics
- Stellvertretender Sprecher der Graduiertenschule "Leipzig School of Natural Sciences - Building with Molecules and Nano-objects" (BuildMoNa), http://www.buildmona.de/
- Stellvertretender Sprecher des Sonderforschungsbereiches "Funktionalität Oxidischer Grenzflächen" (SFB762), http://www.physik.uni-halle.de/sfb762/
- Stellvertretender Sprecher der Forschergruppe FOR 1616, http://www.for1616.uni-jena.de/
- Sprecher der Fächerübergreifenden Arbeitsgemeinschaft Halbleiterforschung Leipzig (FAHL), http://www.uni-leipzig.de/~fahl/
- Mitglied des wissenschaftlichen Beirats des Leibniz-Instituts für Oberflächenmodifizierung e. V., Leipzig (IOM)
- Member Editorial Board: Physica Status Solidi (a), (b), RRL
- Member International Advisory Board: Advanced Electronic Materials

- Project Reviewer: Deutsche Forschungsgemeinschaft (DFG), Alexander von Humboldt-Stiftung (AvH), Schweizerischer Nationalfonds zur Förderung der wissenschaftlichen Forschung (FNSNF), Fonds zur Förderung der Wissenschaften (FWF), EU, Österreichische Forschungsförderungsgesellschaft mbH (FFG), Agence Nationale de la Recherche (ANR, France)
- Referee: Applied PhysPhysics Letters, Electronics Letters, Journal of Applied Physics, Nature, Physica E, Physical Review B., Physical Review Letters, Physica Status Solidi, Advanced Materials, u.a.

M. Lorenz
- Editorial Board Member Journal of Physics D: Applied Physics (IOP, Bristol, U.K.)
- Project referee: Alexander von Humboldt Stiftung, Israeli Ministry of Science, Technology and Space
- Referee: ACS Applied Materials Interfaces, Acta Materialia, AIP Advances, Applied Physics Letters, CrystEngComm, IEEE Electron Device Letters, IEEE Magnetic Letters, Journal of Physics D: Applied Physics, Journal of Applied Physics, Journal of Materials Research, Journal of Colloid and Interface Science, Journal of Materials Chemistry C, Journal of Materials Science, Materials, Materials and Manufacturing Processes, Nano Letters (ASC), Physica Status Solidi A, Physica Status Solidi B, Surface and Coatings Technology, Thin Solid Films

H. von Wenckstern
- Project Reviewer: U.S. Department of Energy – Office of Science, National Research Fondation RSA
- Referee: Applied Physical Letters, Journal of Applied Physics, Thin Solid Films, Solid State Electronics, Physica Status Solidi, Journal of Electronic Materials, Turk. Journal of Physics, Journal of Material Sciences, u.a.

R. Schmidt-Grund
- Vice Chair of the German Association on Ellipsometry (Arbeitskreis Ellipsometrie – Paul Drude e.V.)
- Project Reviewer: Deutsche Forschungsgemeinschaft (DFG), US Department of Energy – Office of Science
- Referee: Thin Solid Films, Current Applied Physics, Physica Status Solidi C, Nature Communications, Applied Physics Letters, Optics Express, Journal of Electromagnetic Waves and Applications, Optical Materials, ACS Applied Materials & Interfaces

8.15 External Cooperations

Academic

- Leibniz-Institut für Oberflächenmodifizierung e. V., Leipzig, Germany
  Prof. Dr. A. Anders, Prof. Dr. B. Rauschenbach, Prof. Dr. S. Mayr, Dr. J. Gerlach, Dr. C. Bundesmann, Dr. A. Lotnyk
- Universität Leipzig, Fakultät für Chemie und Mineralogie, Germany
  Prof. Dr. H. Krautscheid, Prof. Dr. R. Denecke

- Universität Halle-Wittenberg, Germany
  Prof. Dr. I. Mertig, Prof. Dr. W. Widdra, Prof. Dr. S.G. Ebbinghaus, Prof. Dr. W. Hergert
- Max-Planck-Institut für Mikrostrukturphysik, Halle/Saale, Germany
  Dr. O. Breitenstein, Dr. A. Ernst, Dr. P. Werner
- Forschungszentrum Dresden-Rossendorf, Germany
  Prof. Dr. M. Helm, Dr. K. Potzger
- Technische Universität Berlin, Germany
  Prof. Dr. A. Hoffmann
- Universität Magdeburg, Germany
  Dr. J. Bläsing
- Universität Jena, Germany
  Prof. Dr. C. Ronning
- University of Pretoria, South Africa
  Prof. F. D. Auret
- University of Canterbury, Christchurch, New Zealand
  Prof. Dr. M. Allen
- Centre de Recherche sur l' Hétéro-Epitaxie et ses Applications (CNRS-CRHEA), Valbonne, France
  Dr. J. Zúñiga-Pérez, Dr. Guy Feuillet
- Western Michigan University, USA
  Prof. Dr. S. M. Durbin
- Katholieke Universiteit Leuven, Belgium
  Dr. V. Lazenka, Prof. Dr. K. Temst

Industry

- Freiberger Compound Materials GmbH, Freiberg, Germany
  Dr. G. Leibiger

8.16 Publications

Journals

S. Bitter, P. Schlupp, H. von Wenckstern, M. Grundmann: *The Vital Role of Oxygen for the Formation of Highly Rectifying Schottky Barrier Diodes on Amorphous Zinc-Tin-Oxide with Various Cation Composition*, ACS Appl. Mater. Interfaces **9**(31), 26574-26581 (2017)

K. Dorywalski, N. Lemée, B. Andriyevsky, R. Schmidt-Grund, M. Grundmann, M. Piasecki, M. Bousquet, T. Krzyzynski: *Optical properties of epitaxial $Na_{0.5}Bi_{0.5}TiO_3$ lead-free piezoelectric thin films: Ellipsometric and theoretical studies*, Appl. Surf. Sci. **421**, 367-372 (2017)

V. Gottschalch, S. Blaurock, G. Benndorf, J. Lenzner, M. Grundmann, H. Krautscheid: *Copper Iodide synthesized by iodization of Cu-films and deposited using MOCVD*, J. Cryst. Growth **471**, 21-28 (2017)

M. Grundmann: *Strain in Pseudomorphic Monoclinic Ga2O3-based Heterostructures*, phys. stat. sol. (b) **254**(9), 1700134:1-7 (2017)

M. Grundmann, C. Sturm, C. Kranert, S. Richter, R. Schmidt-Grund, C. Deparis, J. Zúñiga-Pérez: *Optically Anisotropic Media: New Approaches to the Dielectric Function, Singular Axes, Raman Scattering Intensities and Microcavity Modes*, phys. stat. sol. RRL **11**(1), 1600295:1-19 (2017)

M. Grundmann, S. Richter, T. Michalsky, C. Sturm, J. Zúñiga-Pérez, R. Schmidt-Grund: *Exceptional points in anisotropic photonic structures: From non-Hermitian physics to possible device applications*, Proc. SPIE **10105**, 101050K:1-8 (2017), Ferechteh H. Teherani, David C. Look, David J. Rogers, eds.

M. Grundmann, ed.: *Report Halbleiterphysik/Semiconductor Physics 2016*, Universität Leipzig (2017)

M. Grundmann, ed.: *Report of The Physics Institutes of Universität Leipzig 2016*, Universität Leipzig (2017)

V. Lazenka, M. Lorenz, H. Modarresi, J.K. Jochum, H.P. Gunnlaugsson, M. Grundmann, M.J. Van Bael, K. Temst, A. Vantomme: *Interface induced out-of-plane magnetic anisotropy in magnetoelectric $BiFeO_3$-$BaTiO_3$ superlattices*, Appl. Phys. Lett. **110**(9), 092902:1-5 (2017)

M. Lorenz: *Pulsed Laser Deposition*, chapter 5 in Encyclopedia of Applied Physics (Wiley VCH, Weinheim) (2017)

M. Lorenz, H. Wei, F. Jung, S. Hohenberger, H. Hochmuth, M. Grundmann: *Two-dimensional Frank - van der Merwe growth of functional oxide and nitride thin film superlattices by pulsed laser deposition*, J. Mat. Res. **32**(21), 3936-3946 (2017)

M. Lorenz, J. Barzola-Quiquia, C. Yang, C. Patzig, T. Höche, P. Esquinazi, M. Grundmann, H. Wei: *Charge transfer-induced magnetic exchange bias and electron localization in (111)- and (001)-oriented $LaNiO_3$/$LaMnO_3$ superlattices*, Appl. Phys. Lett. **110**(10), 102403:1-5 (2017)

M. Lorenz, D. Hirsch, C. Patzig, T. Höche, S. Hohenberger, H. Hochmuth, V. Lazenka, K. Temst, M. Grundmann: *Correlation of interface impurities and chemical gradients with magnetoelectric coupling strength in multiferroic $BiFeO_3$-$BaTiO_3$ superlattices*, ACS Appl. Mater. Interfaces **9**(22), 18956-18965 (2017)

T. Lühmann, R. Wunderlich, R. Schmidt-Grund, J. Barzola-Quiquia, P. Esquinazi, M. Grundmann, J. Meijer: *Investigation of the graphitization process of ion-beam irradiated diamond using ellipsometry, Raman spectroscopy and electrical transport measurements*, Carbon **121**, 512-517 (2017)

A. de Pablos Martín, M. Lorenz, M. Grundmann, Th. Höche: *Laser Welding of Fused Silica Glass with Sapphire Using a Non- Stoichiometric, Fresnoitic $Ba_2TiSi_2O_8$·3 SiO_2 Thin Film as an Absorber*, Optics & Laser Technol. **92**, 85-94 (2017)

S. Müller, H. von Wenckstern, F. Schmidt, D. Splith, H. Frenzel, M. Grundmann: *Method of choice for fabrication of high-quality β-gallium oxide-based Schottky diodes*, Semic. Sci. Technol. **32**, 065013:1-8 (2017)

Y. Kumar, I. Lorite, M. Lorenz, P. Esquinazi, M. Grundmann: *Effect of annealing on the magnetic properties of zinc ferrite thin films*, Mater. Lett. **195**, 89-91 (2017)

Y. Kumar, I. Lorite, M. Lorenz, P.D. Esquinazi, M. Grundmann: *Effect of annealing on the magnetic properties of zinc ferrite thin films*, arxiv: 1702.06033 (2017)

S. Richter, T. Michalsky, C. Sturm, B. Rosenow, M. Grundmann, R. Schmidt-Grund: *Erratum: Exceptional points in anisotropic planar microcavities*, Phys. Rev. A **96**, 059902E:1-2 (2017)

S. Richter, T. Michalsky, C. Sturm, B. Rosenow, M. Grundmann, R. Schmidt-Grund: *Exceptional points in anisotropic planar microcavities*, Phys. Rev. A **95**, 023836:1-9 (2017)

P. Schlupp, H. von Wenckstern, M. Grundmann: *Schottky barrier diodes based on room temperature fabricated amorphous zinc tin oxide thin film*, phys. stat. sol. (a) **214**(10), 1700210:1-8 (2017)

A. Shkurmanov, C. Sturm, H. Franke, J. Lenzner, M. Grundmann: *Low temperature PLD-growth of ultrathin ZnO nanowires by using $Zn_xAl_{1-x}O$ and $Zn_xGa_{1-x}O$ seed layers*, Nanoscale Res. Lett. **12**, 134:1-7 (2017)

C. Sturm, M. Wille, J. Lenzner, S. Khujanov, M. Grundmann: *Non-linear optical deformation potentials in uniaxially strained ZnO microwires*, Appl. Phys. Lett. **110**(6), 062103:1-4 (2017)

C. Sturm, R. Schmidt-Grund, V. Zviagin, M. Grundmann: *Temperature dependence of the dielectric tensor of monoclinic dielectric Ga2O3 single crystals in the spectral range 0.5-8.5 eV*, Appl. Phys. Lett. **111**(8), 082102:1-4 (2017)

L. Vines, C. Bhoodoo, H. von Wenckstern, M. Grundmann: *Electrical conductivity of In_2O_3 and Ga_2O_3 after low temperature ion irradiation; implications for instrinsic defect formation and charge neutrality level*, J. Phys. D: Appl. Phys. **30**(2), 025502:1-6 (2017)

H. Wei, C. Yang, J.L. Barzola-Quiquia, M. Welke, R. Denecke, C. Patzig, T. Höche, P. Esquinazi, M. Grundmann, M. Lorenz: *Ferromagnetic phase transition and single-gap type electrical conductivity of epitaxial $LaMnO_3/LaAlO_3$ superlattices*, J. Phys. D: Appl. Phys. **50**(43), 43LT02:1-6 (2017)

M. Welke, K. Brachwitz, M. Lorenz, M. Grundmann, K.-M. Schindler, A. Chasse, R. Denecke: *Structure and cation distribution in $(Mn_{0.5}Zn_{0.5})Fe_2O_4$ thin films on $SrTiO_3(001)$*, J. Appl. Phys. **121**(22), 225305:1-7 (2017)

M. Wille, E. Krüger, S. Blaurock, V. Zviagin, R. Deichsel, G. Benndorf, L. Trefflich, V. Gottschalch, H. Krautscheid, R. Schmidt-Grund, M. Grundmann: *Lasing in cuprous iodide microwires*, Appl. Phys. Lett. **111**(3), 031105:1-5 (2017)

C. Yang, D. Souchay, M. Kneiß, M. Bogner, H.M. Wei, M. Lorenz, O. Oeckler, G. Benstetter, Y.Q. Fu, M. Grundmann: *Transparent Flexible Thermoelectric Material Based on Non-toxic, Earth-Abundant p-Type Copper Iodide Thin Film*, Nature Commun. **8**, 16076:1-7 (2017)

M. Zapf, R. Röder, K. Winkler, L. Kaden, J. Greil, M. Wille, M. Grundmann, R. Schmidt-Grund, A. Lugstein, C. Ronning: *Dynamical Tuning of Nanowire Lasing Spectra*, Nano Lett. **17**(11), 6637-6643 (2017)

H.-E. Zschau, M. Schütze, M.C. Galetz, B.M. Gleeson, S. Neve, M. Lorenz, M. Grundmann: *Surface Chemistry Evolution of F-doped Ni-base Superalloy upon Heat Treatment*, Materials and Corrosion**68**(2), 220-227 (2017)

Talks

M. Grundmann: *Exceptional points in anisotropic photonic structures: From non-Hermitian physics to possible device applications*, SPIE Photonics West,San Francisco, CA, USA, January 2017 (invited)

M. Grundmann: *Interfacing Bragg Mirrors with Tilted Uniaxial Media: Exceptional Points and Chiral States*, 16th International Conference on the Formation of Semiconductor Interfaces (ICFSI-16), Hannover, Germany, July 2017 (invited)

O. Herrfurth, S. Richter, M. Rebarz, M. Kloz, S. Espinoza, J. Andreasson, M. Grundmann, R. Schmidt-Grund: *Towards fs-time-resolved spectroscopic ellipsometry*, DPG Spring Meeting, Dresden, Germany, March 2017

O. Herrfurth, S. Richter, M. Rebarz, M. Kloz, S. Espinoza, J. Andreasson, M. Grundmann, R. Schmidt-Grund: *Femtosecond time-resolved spectroscopic ellipsometry at ELI Beamlines*, 2nd ELIps Workshop, Dolní Brezany, Czech Republic, October 2017 (invited)

M. Lorenz, D. Hirsch, C. Patzig, T. Höche, V. Lazenka, K. Temst, M. Grundmann: *Multiferroic $BiFeO_3$-$BaTiO_3$ superlattices: Chemical interface features by TOF-SIMS and STEM-EDX*, EU-COST project: Towards Oxide Based Electronics, TO-BE Fall meeting, Riga, Lettland, September 2017

M. Kneiß, P. Storm, G. Benndorf, H. von Wenckstern, M. Grundmann: *A new pulsed laser deposition technique to control the composition of ternary thin films in growth direction demonstrated on the transparent $Mg_xZn_{1-x}O$ alloy*, TCO2017, Leipzig, Germany, September 2017

M. Rebarz, S.J. Espinoza, S. Richter, O. Herrfurth, R. Schmidt-Grund, J. Andreasson, S. Zollner: *Femtosecond Spectroscopic Ellipsometry on Optoelectronic Materials and Photonic Structures*, AVS 64th Internaional Symposium and Exhibition, Tampa, Florida, USA, November 2017

S. Richter, O. Herrfurth, S. Espinoza, M. Rebarz, M. Kloz, J. Andreasson, M. Grundmann, R. Schmidt-Grund: *Analysis of Time Resolved Ellipsometry Data and ZnO Results*, 2nd ELIps Workshop, Dolní Brezany, Czech Republic, October 2017 (invited)

R. Schmidt-Grund: *Topical materials: Ferrite Spinels, Cuprous Iodide, buried Graphite in Diamond*, 2nd ELIps Workshop, Dolní Brezany, Czech Republic, October 2017 (invited)

C. Sturm, V. Zviagin, C. Kranert, J. Furthmüller, F. Bechstedt, R. Schmidt-Grund, M. Grundmann: *Temperature dependence of the full dielectric tensor of monoclinic Ga_2O_3*, 2nd International Workshop on Ga_2O_3 and Related Materials, Parma, Italy, September 2017 (invited)

C. Sturm: *Optics and Tensor Properties of Anisotropic Materials Determined by Spectroscopic Ellipsometry*, Humboldt Forum, Bejing, China, September 2017 (invited)

C. Sturm: *Optics and tensor properties of β-Ga_2O_3*, GraFox, Berlin, November 2017 (invited)

L. Wägele, T. Jawinski, C. Bahret, H. von Wenckstern, E. López, A. Martí, M. Grundmann, R. Scheer: *Preparation and Analysis of In_2S_3:V Intermediate Band Thin-Film Absorbers for Solar Cells*, DPG Spring Meeting, Dresden, Germany, March 2017

M. Wille, E. Krüger, S. Blaurockb, V. Zviagin, R. Deichsel, G. Benndorf, L. Trefflich, V. Gottschalch, H. Krautscheid, R. Schmidt-Grund, M. Grundmann: *Lasing in Cuprous Iodide Microwires*, International Workshop on Transparent Conductive Oxides - TCO 2017, Leipzig, Germany, September 2017

C. Yang, D. Souchay, M. Kneiß, M. Bogner, H. M. Wei, M. Lorenz, O. Oeckler, G. Benstetter, Y. Q. Fu, M. Grundmann: *Towards Flexible and Transparent Thermoelectric Devices with Copper Iodide*, TCO2017 meeting, Leipzig, Germany, September 2017

C. Yang, M. Kneiß, M. Lorenz, M. Grundmann: *Advances in the Development of High Performance p-Type Transparent Conducting Materials: A Study of Copper Iodide Thin Film*, Compound Semiconductor Week 2017, Berlin, Germany, May 2017

C. Yang: *Towards Transparent and Flexible Thermoelectric Devices using Copper Iodide*, Scientific Networking Workshop "Thermoelectricity", Krippen, Germany, March 2017

C. Yang, M. Kneiß, M. Lorenz, M. Grundmann: *Room-temperature domain-epitaxy of p-type transparent conductor copper iodide for transparent CuI/ZnO heterojunctions*, E-MRS Spring Meeting, Lille, France, May 2016.

V. Zviagin, Y. Kumar, P. Huth, I. Lorite, A. Setzer, D. Spemann, J. Meijer, R. Denecke, P. Esquinazi, M. Grundmann, R. Schmidt-Grund: *Optical Investigation of Structural Disorder in Normal Spinel Ferrites in Relation to Magnetic Properties*, DPG Spring Meeting, Dresden, Germany, March 2017

Posters

M. Himmerlich, S. Shokhovets, J. Pezoldt, L. Kirste, V. M. Polyakov, J.H. Leach, R. Schmidt-Grund, V. Zviagin, M. Grundmann, S. Krischok: *Impact of Surface Polish on the Structural and Optical Properties of bulk GaN crystals prepared by HVPE*, ICNS12, Strasbourg, France, July 2017

S. Hohenberger, M. Lorenz, V. Lazenka, M. Grundmann: *Effect of Bi-content and Gd-doping on the multiferroic properties of $BaTiO_3$-$BiFeO_3$ superlattices*, DPG Spring Meeting, Dresden, Germany, March 2017.

M. Kneiß, G. Benndorf, T. Schultz, H. von Wenckstern, M. Grundmann: *MgZnO/ZnO quantum wells with distinct quantum-confined Stark effect grown on a highly conductive ZnO:Al back contact layer*, Annual Conference of the Graduade School BuildMoNa, Leipzig, Germany, March 2017

M. Kneiß, G. Benndorf, T. Schultz, H. von Wenckstern, M. Grundmann: *MgZnO/ZnO quantum wells with distinct quantum-confined Stark effect grown on a highly conductive ZnO:Al back contact layer*, DPG Spring Meeting, Dresden, Germany, March 2017

C. Kranert, C. Sturm, R. Schmidt-Grund, M. Grundmann: *Determination of the Raman Tensor of monoclinic Ga_2O_3*, 2nd International Workshop on Ga2O3 and Related Materials, Parma, Italy, September 2017

T. Jawinski, L.A. Wägele, E. López, H. von Wenckstern, A. Martí, M. Grundmann, R. Scheer: *Preparation and Analysis of In_2S_3:V Intermediate Band Solar Cells*, DPG Spring Meeting, Dresden, Germany, March 2017

F. Jung, V. Zviagin, M. Bonholzer, S. Selle, C. Sturm, J. Lenzner, R. Schmidt-Grund, M. Lorenz, M. Grundmann: *Structural and optical properties of TiN/MgO superlattices*, DPG Spring Meeting, Dresden, Germany, March 2017

T. Michalsky, M. Wille, E. Krüger, S. Lange, M. Grundmann, R. Schmidt-Grund: *Spatial and temporal evolution of coherent polariton modes in ZnO microwire cavities*, DPG Spring Meeting, Dresden, Germany, March 2017

T. Michalsky, E. Krüger, M. Wille, M. Grundmann, R. Schmidt-Grund: *Spatial and temporal evolution of coherent polariton modes in ZnO microwire cavities*, Conference on Physics of Light-Matter Coupling in Nanostructures, Würzburg, Germany, July 2017

S. Richter, T. Michalsky, C. Sturm, B. Rosenow, M. Grundmann, R. Schmidt-Grund: *Exceptional points in optically anisotropic microcavities*, DPG Spring Meeting, Dresden, Germany, March 2017

S. Richter, J. Zúñiga-Pérez, C. Deparis, L. Trefflich, T. Michalsky, C. Sturm, B. Rosenow, M. Grundmann, R. Schmidt-Grund: *Anisotropic microcavities and the occurrence of circularly polarized exceptional points*, Conference on Physics of Light-Matter Coupling in Nanostructures, Würzburg, Germany, July 2017

S. Richter, J. Zúñiga-Pérez, C. Deparis, L. Trefflich, T. Michalsky, C. Sturm, B. Rosenow, M. Grundmann, R. Schmidt-Grund: *Exceptional points in the dispersion of cavity photon and polariton modes*, International Conference on Optics of Excitons in Confined Systems - OECS 2017, Bath, Uhnited Kingdom, September 2017

L. Trefflich, G. Benndorf, R. Schmidt-Grund, H. Krautscheid, M. Grundmann: *Optical properties of (CuI)-based inorganic-organic hybrid materials as active semiconductor in planar microcavities*, DPG Spring Meeting, Dresden, Germany, March 2017

L.A. Wägele, T. Jawinski, C. Bahret, E. López, H. von Wenckstern, A. Martí, M. Grundmann, R. Scheer: *Preparation and analysis of In_2S_3:V solar cells*, MRS Spring Meeting, Phoenix, Arizona, USA, April 2017

H. Wei, M. Grundmann, M. Lorenz: *Possible Superconductivity in (001)- and (111)-Oriented $LaNiO_3$-Based Superlattices: Metal-Insulator Transition and Polarity-Controlled Conductivity*, ISEC 2017, 16th International Superconductive Electronics Conference, Sorrento (NA), Italy, June 2017

M. Wille, T. Michalsky, C. Sturm, E. Krüger, M. Grundmann, R. Schmidt-Grund: *Absorptive lasing mode suppression in highly excited ZnO nano- and microcavities*, DPG Spring Meeting, Dresden, Germany, March 2017

M. Wille, C. Sturm, O. Herrfurth, S. Richter, T. Michalsky, R. Röder, C. Ronning, R. Schmidt-Grund, M. Grundmann: *Ultrafast Dynamics of the Optical Properties of ZnO-based Nanocavities*, Conference on Physics of Light-Matter Coupling in Nanostructures, Würzburg, Germany, July 2017

M. Wille, E. Krüger, S. Blaurock, V. Zviagin, R. Deichsel, G. Benndorf, L. Trefflich, V. Gottschalch, H. Krautscheid, R. Schmidt-Grund, M. Grundmann: *Lasing in Cuprous Iodide Microwires*, Conference on Physics of Light-Matter Coupling in Nanostructures, Würzburg, Germany, July 2017

M. Wille, V. Zviagin, S. Blaurock, R. Deichsel, G. Benndorf, L. Trefflich, H. Krautscheid, M. Grundmann, R. Schmidt-Grund: *Demonstration of Lasing in Cuprous Iodide Microwires*, International Conference on Optics of Excitons in Confined Systems - OECS 2017, Bath, Uhnited Kingdom, September 2017

V. Zviagin, Y. Kumar, P. Huth, I. Lorite, A. Setzer, D. Spemann, K. Fleischer, J. Meijer, R. Denecke, P. Esquinazi, M. Grundmann, R. Schmidt-Grund: *Spectroscopic Ellipsometry as a Method for Structural Investigation of Spinel Ferrite Thin Films*, DPG Spring Meeting, Dresden, Germany, March 2017

8.17 Graduations

Doctorate

- Marcus Jenderka
  Pulsed Laser Deposition of Iridate and $YBiO_3$ Thin Films
  February 2017
- Haoming Wei
  Conductivity behavior of $LaNiO_3$- and $LaMnO_3$- based thin film superlattices
  April 2017
- Daniel Splith
  Schottky-Kontakte auf β-Galliumoxid- und Indiumoxid-Dünnfilmen: Optimierung der Probenstruktur und Modellierung der Diodenkennlinien
  October 2017
- Martin Thunert
  Exciton-Polaritons in ZnO-based Microresonators: Disorder Influence and Coherence Properties
  October 2017

Master

- Anna Werner
  Strukturelle und elektrische Untersuchung an $(Ga,Al)_2O_3$ - Dünnfilmen
  June 2017
- Stefan Lange
  Aufbau und Charakterisierung eines Photokorrelationsmessplatzes
  July 2017

Bachelor

- Philipp Storm
  Erprobung einer neuen PLD-Technik zur Realisierung vertikaler Kompositionsgradienten in $Mg_{(x)}Zn_{(1-x)}O$ Dünnfilmen für das Wachstum von gradierten Quantengrabensystemen
  November 2017

8.18 Guests

- Vera Prozheeva
  Aalto University, Espoo, Finland
  April 2017 – June 2017
- Dr.-Ing. Krzysztof Grzegorz Dorywalski
  Politechnika Koszalinska, Koszalin, Poland
  October 2017 – June 2018

9

Superconductivity and Magnetism

9.1 Introduction

The main interests of the group at the division are phenomena related to superconductivity and magnetism in solids. In the last few years the research activities in superconductivity have been mainly concentrated in searching for its existence in graphite, especially at graphite interfaces between Bernal-like crystalline regions. This research issue started in our division in Leipzig in the year 2000 and became supporting experimental evidence quite recently, indicating the existence of superconductivity at temperatures above 100 K. Future work will be concentrated in the localization of the superconducting phases and the increase of the superconducting yield.

Our division was the first to show that atomic lattice defects can produce magnetic order in graphite without the need of magnetic ions. This phenomenon is known nowadays as Defect-Induced Magnetism and it is found in a broad spectrum of different materials. We are involved in a collaborative research project with the aim of triggering this phenomenon in nominally non-magnetic oxides, via vacancies and/or hydrogen doping. Further research topic is the study of the electrical and magnetic properties of oxide multilayers of thickness starting from a few unit cells. Main research issues are related to the magnetic coupling at the interfaces of oxide layers, i.e. exchange bias phenomena, with different magnetic properties as well as the possibility to develop a two-dimensional electron gas at the interfaces.

In 2017 the group organized the "Topological Matter and Flat Bands (TMFB) Conference" which took place in Leipzig 17.-20. August 2017. This meeting was an official satellite conference of the 28th International Conference on Low Temperature Physics, LT28, held in Gothenburg/Sweden.

Pablo Esquinazi

9.2 Electrical Transport Properties of Polycrystalline and Amorphous TiO_2 Single Nanotubes

M. Stiller[*], J. Barzola-Quiquia[*], P. Esquinazi[*], S. Seulgi[†], I. Hwang[†], P. Schmuki[†], J. Böttner[‡], I. Estrela-Lopis[‡]

[*]Division of Superconductivity and Magnetism, Institute for Experimental Physics II, University of Leipzig, 04103 Leipzig, Germany
[†]Chair for Surface Science and Corrosion Department Material Science and Engineering, University of Erlangen, D-91058 Erlangen, Germany
[‡]Institute of Medical Physics and Biophysics, University of Leipzig, 04107 Leipzig, Germany

The electrical transport properties of anodically grown TiO_2 nanotubes was investigated. Amorphous nanotubes were anodically grown on titanium foil and transformed through annealing into the anatase phase. Amorphous and polycrystalline single nanotubes were isolated and contacted for measurements of the electrical resistance. Nonlinear current-voltage characteristics were explained using the fluctuation induced tunneling conduction model. A clear enhancement of the conductance was induced in an insulating anatase nanotube through low-energy Ar/H ion irradiation. Confocal Raman spectroscopy shows that the annealed samples were in anatase phase and a blueshift due to phonon confinement was observed.

9.3 Functionalized Akiyama tips for magnetic force microscopy measurements

M. Stiller[*], J. Barzola-Quiquia[*], P. Esquinazi[*], S. Sangiao[†], J.M. DeTeresa[†], J. Meijer[‡], B. Abel[§]

[*]Division of Superconductivity and Magnetism, Institute for Experimental Physics II, University of Leipzig, 04103 Leipzig, Germany
[†]Laboratorio de Microscopías Avanzadas (LMA), Instituto de Nanociencia de Aragón (INA), Universidad de Zaragoza, E-50018 Zaragoza, Spain
[‡]Division of Nuclear Solid State Physics, Felix-Bloch Institute for Solid-state Physics, University of Leipzig, 04103 Leipzig, Germany
[§]Leibniz Institute of Surface Modification, 04318 Leipzig, Germany

In this work we have used focused electron beam induced deposition of cobalt to functionalize atomic force microscopy Akiyama tips for application in magnetic force microscopy. The grown tips have a content of $\approx$ 90 % Co after exposure to ambient air. The magnetic tips were characterized using energy dispersive X-ray spectroscopy and scanning electron microscopy. In order to investigate the magnetic properties, current loops were prepared by electron beam lithography. Measurements at room temperature as well as 4.2 K were carried out and the coercive field of $\approx$ 6.8 mT of the Co tip was estimated by applying several external fields in the opposite direction of the tip magnetization. Magnetic Akiyama tips open new possibilities for wide-range temperature magnetic force microscopy measurements.

9.4 Funding

Defect-induced Magnetism in Oxides
Prof. Dr. Pablo Esquinazi
DFG SFB 762/3, B1

Magnetic and electric properties of ultrathin oxide films
Prof. Dr. Pablo Esquinazi and Prof. Dr. Michael Ziese
DFG SFB 762/3, B5

Study of the reentrant metallic behavior of the interfaces in graphite at very high fields
Prof. Dr. Pablo Esquinazi
DAAD-PPP USA 2016/2017

Controlled creation of defect-induced magnetism (DIM) in graphite- and diamond-based films
Prof. Dr. Pablo Esquinazi
DFG-ES86/29-1

International conference of topological matter and flat bands (TMFB)
Prof. Dr. Pablo Esquinazi
DFG-ES86/30-1

9.5 Organizational Duties

P. Esquinazi

- Project Reviewer: Deutsche Forschungsgemeinschaft (DFG), National Science Foundation (USA), German-Israeli Foundation (GIF), Israel Science Foundation, Department of Energy (Washington), DAAD
- Referee: Phys. Rev. Lett, Phys. Rev. B., Appl. Phys. Lett., Chem. Phys. Lett., Nature Physics, Nature Materials, Physica C, Phys. Lett. A, phys. stat. sol., J. Low Temp. Phys., Carbon, J. Chem. Phys., Eur. J. Phys. B, J. Magn. Magn. Mater.

M. Ziese

- Head of the Basic Physics Laboratory
- Dean of Studies
- Referee: Phys. Rev. Lett., Phys. Rev. B., Adv. Mater., Appl. Phys. A, Current Nanoscience, Eur. Phys. J. B, IEEE Trans. Magn., J. Phys.: Condens. Matter, J. Phys. D: Appl. Phys., J. Alloys Comp., J. Appl. Phys., J. Am. Ceram. Soc., J. Magn. Magn. Mater., J. Mater. Research, J. Mater. Science, Materials Science and Engineering B, Nanotechnology, phys. stat. sol., Thin Solid Films

W. Böhlmann

- Referee: J. Physical Chemistry, J. of American Chemical Society, Microporous and Mesoporous Materials

9.6 External Cooperations

Academic

- State University of Campinas, Campinas, Brazil
  Prof. Dr. Yakov Kopelevich
- Universität zu Köln, Cologne, Germany
  Dr. Ionela Vrejoiu
- Max-Planck Institute of Microstructure Physics, Halle, Germany
  Dr. Arthur Ernst
- Martin-Luther Universität Halle-Wittenberg, Halle, Germany
  Prof. Ingrid Mertig
- Martin-Luther Universität Halle-Wittenberg, Halle, Germany
  Prof. Wolfram Hergert
- Martin-Luther Universität Halle-Wittenberg, Halle, Germany
  Dr. Angelika Chassé
- Martin-Luther Universität Halle-Wittenberg, Halle, Germany
  Dr. Manfred Dubiel
- Stanford Synchrotron Radiation Laboratory, USA
  Dr. Hendrik Ohldag
- Laboratorio de Física de Sistemas Pequeños y Nanotecnologíia, Consejo Superior de Investigaciones Científicas, Madrid, Spain
  Prof. N. García (Madrid)
- Forschungszentrum Dresden-Rossendorf e.V., Institut für Ionenstrahlphysik und Materialforschung, Germany
  Dr. W. Anwand
- Forschungszentrum Dresden-Rossendorf e.V., Institut für Ionenstrahlphysik und Materialforschung, Germany
  Dr. G. Brauer
- Tucuman University, Argentina
  Prof. S. P. de Heluani
- University of La Plata, Argentina
  Dr. C. E. Rodriguez Torres
- Universidad Autónoma de Madrid, Spain
  Prof. Dr. Miguel Angel Ramos
- Bar Ilan University, Israel
  Dr. G. D. Nessim

9.7 Publications

Journals

X. Li, I. Lindfors-Vrejoiu, M. Ziese, A. Gloter and P. A. von Aken:
Impact of interfacial coupling of oxygen actahedra on ferromagnetic order in $La_{0.7}Sr_{0.3}MnO_3/SrTiO_3$ heterostructures
Sci. Rep. **7**, 40068 (2017)

C. E. Precker, P. D. Esquinazi, A. Champi, J. Barzola-Quiquia, M. Zoraghi, S. Muinos-Landín, A. Setzer, W. Böhlmann, D. Spemann, J. Meijer, T. Muenster, O. Baehre, G. Kloess and H. Beth:
On the Quest of Superconductivity at Room Temperature
2Physics, 015013 (2017)

M. Zoraghi, J. Barzola-Quiquia, M. Stiller, A. Setzer and P. Esquinazi:
Influence of rhombohedral stacking order in the electrical resistance of bulk and mesoscopic graphite
Phys. Review B **95**, 045308 (2017)

J. Barzola-Quiquia, T. Lühmann, R. Wunderlich, M. Stiller, M. Zoraghi, J. Meijer, P. Esquinazi, J. Böttner and I. Estrella-Lopis:
Fabrication and electrical transport properties of embedded graphite microwires in a diamond matrix
Appl. Phys. **50**, 145301 (2017)

H. Wei, J. Barzola-Quiquia, C. Yang, C. Patzig, T. Höche, P. Esquinazi, M. Grundmann and M. Lorenz:
Charge transfer-induced magnetic exchange bias and electron localization in (111)- and (001)-oriented $LaNiO_3/LaMnO_3$ superlattices
App. Phys. Lett. **110**, 102403 (2017)

M. Stiller, J. Barzola-Quiquia, P. Esquinazi, S. So, I. Hwang, P. Schmuki, J. Böttner and I. Estrela-Lopis:
Electrical transport properties of polycrystalline and amorphous TiO_2 single nanotubes
Nano-Structures & Nano-Objects **10**, 51 (2017)

L. Botsch, I. Lorite, Y. Kumar and P. Esquinazi:
Indirect experimental evidence of a persistent spin helix in H^+ implanted Li-doped ZnO by photogalvanic spectroscopy
Phys. Review B **95**, 201405(R) (2017)

T. Lühmann, R. Wunderlich, R. Schmidt-Grund, J. Barzola-Quiquia, P. Esquinazi, M. Grundmann and J. Meijer:
Investigation of the graphitization process of ion-beam irradiated diamond using ellipsometry, Raman spectroscopy and electrical transport measurements
Carbon **121**, 512 (2017)

J. L. Cholula-Díaz, J. Barzola-Quiquia, M. Videa, C. Yin and P. Esquinazi:
The frequency-dependent AC photoresistance behavior of ZnO thin films grown on

different sapphire substrates
Phys. Chem. Chem. Phys. **19**, 23919 (2017)

H. Wei, C. Yang, J. Barzola-Quiquia, M. Welke, R. Denecke, C. Patzig, T. Höche, P. Esquinazi, M. Grundmann and M. Lorenz:
Ferromagnetic phase transition and single-gap type electrical conductivity of epitaxial $LaMnO_3/LaAlO_3$ superlattices
Appl. Phys. **50**, 43LT02 (2017)

M. Stiller, J. Barzola-Quiquia, P. Esquinazi, S. Sangiao, J. M de Teresa, J. Meijer and B. Abel:
Functionalized Akiyama tips for magnetic force microscopy measurements
Meas. Sci. Technol. **28**, 125401 (2017)

I. Lindfors-Vrejoiu and M. Ziese:
Topological Hall effect in antiferromagnetically coupled $SrRuO_3/La_{0.7}Sr_{0.3}MnO_3$ epitaxial heterostructures
Phys. Status Solidi B **254**, 1600556 (2017)

in press

P. D. Esquinazi, C. E. Precker, M. Stiller, T. R. S. Cordeiro, J. Barzola-Quiquia, A. Setzer and W. Böhlmann:
Evidence for room temperature superconductivity at graphite interfaces
Quantum Stud.: Math. Found. **5**, 41 (2018)

C. Hanisch, F. Hofmann and M. Ziese:
Linear momentum, angular momentum and energy in the linear collision between two balls
Eur. J. Phys. **39**, 015003 (2018)

C. Hanisch, F. Hofmann and M. Ziese:
Impuls-, Drehimpuls- und Energieerhaltung beim eindimensionalen Stoß zweier Kugeln: Impressionen aus dem Praktikumsalltag
PhyDid **1/17**, 13 (2018)

9.8 Guests

- David Boamah
  Kwame Nkrumah University of Science and Technology, Knust/Ghana
  06/2017 - 08/2017
- Abisheik John Samuel Victor Jothi
  Karunya University, Karunya Institute of Technology and Sciences, Karunya Nagar, Coimbatore/Indien
  06/2017 - 08/2017
- Prof. Dr. Ana Melva Champi Farfán
  Universidade Federal do ABC, Santo André, São Paulo/Brazil
  09/2017 - 08/2018

- Prof. Dr. Markus Bernd Raschke
  Department of Physics, 390 UCB, University of Colorado, Boulder, CO 80309-0390, USA
  10/2017

III

Institute for Theoretical Physics

10

Computational Quantum Field Theory

10.1 Introduction

The Computational Physics Group performs basic research into classical and quantum statistical physics with special emphasis on phase transitions and critical phenomena. In the centre of interest are the physics of spin glasses, diluted magnets and other materials with quenched, random disorder, soft condensed matter physics with a focus on fluctuating paths and interfaces, biologically motivated problems such as polymer collapse/folding, adsorption and aggregation as well as related properties of proteins, and the intriguing physics of low-dimensional quantum spin systems.

The methodology is a combination of numerical and analytical techniques. The numerical tools are mainly Monte Carlo (MC) and Molecular Dynamics (MD) computer simulations, chain-growth algorithms, and exact enumeration techniques. The computational approach to theoretical physics is expected to gain more and more importance with the future advances of massively parallel computer technologies, and is likely to become the third cornerstone of physics besides experiment and analytical theory as sketched in Fig. 10.1. Already now it often helps to bridge the gap between experiments and the often necessarily approximate calculations in analytic approaches. To achieve the desired high efficiency of the numerical studies we develop new algorithms and, to guarantee the flexibility required by basic research, all computer codes are implemented by ourselves. The technical tools are Fortran, C, C++, and Python programs running under Unix or Linux operating systems and computer algebra using Maple or Mathematica. The software is developed and tested at the Institute on a cluster of PCs and workstations, where also most of the numerical analyses are performed. Currently we are also exploring the possibilities of the rapidly developing graphics card computing, that is computer simulations on general purpose graphics processing units (GPGPUs) with a very large number of cores. High-performance simulations requiring vast amounts of computer time are carried out at the Institute on quite powerful compute servers, at the parallel computers of the Saxon computing centre in Dresden, and, upon successful grant application, at the national supercomputing centres in Jülich, Stuttgart and München on parallel high-capability computers. This hierarchy of various platforms gives good training and qualification opportunities for the students, which offers promising job perspectives in many different fields for their future careers.

Our research activities are closely integrated into the Graduate School "BuildMoNa": Leipzig School of Natural Sciences – *Building with Molecules and Nano-*

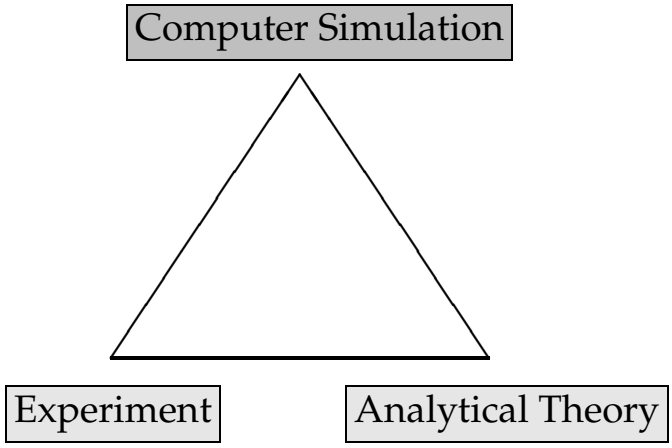

Figure 10.1: Sketch of the "triangular" relationship between experiment, analytical theory and computer simulation.

objects, the International Max Planck Research School (IMPRS) *Mathematics in the Sciences*, and the International Doctoral College *Statistical Physics of Complex Systems* with Université de Lorraine in Nancy, France, supported by the Deutsch-Französische Hochschule (DFH-UFA). In the second funding period 2011–2013, Coventry University in England has been integrated as an associated partner, and in the third funding period 2014–2016, also the National Academy of Sciences of Ukraine in Lviv has joined as another associated partner institution, offering our PhD students now several interesting options for secondments. For instance, in 2014, one PhD student started a "co-tutelle de thèse" jointly supervised with a colleague from Coventry University. Currently the DFH-UFA Doctoral College under the acronym "$\mathbb{L}^4$" is in its fourth funding period 2017–2020. The three Graduate Schools are all "Classes" of the Research Academy Leipzig (RALeipzig), providing the organizational frame for hosting visiting students and senior scientists, offering language courses, organizing childcare and for many other practical matters.

At a more post-graduate level our research projects are embedded into the Sonderforschungsbereich/Transregio SFB/TRR 102 *Polymers under Multiple Constraints: Restricted and Controlled Molecular Order and Mobility* together with Halle University. Our group also actively contributes to two of the top level research areas ("Profillinien") and the Centre for Theoretical Sciences (NTZ) of the University. Beside "BuildMoNa" the latter structures are particularly instrumental for our cooperations with research groups in experimental physics and biochemistry on the one hand and with mathematics and computer science on the other.

On an international scale, our research projects are carried out in a wide net of collaborations which are currently mainly funded by the Alexander von Humboldt Foundation through an Institute Partnership with the National Academy of Sciences in Lviv, Ukraine, on *Polymers in Porous Environments and on Disordered Substrates* and the EU IRSES Network DIONICOS: *Dynamics of and in Complex Systems*, a consortium of 6 European and 12 non-European partners, including sites in Austria, England, France and Germany as well as in Armenia, Russia, Ukraine, India, the United States and Venezuela, which commenced work in 2014. Further close contacts and

collaborations are established with research groups in Armenia, Austria, China, France, Great Britain, India, Israel, Italy, Japan, Poland, Russia, Spain, Sweden, Taiwan, Turkey, Ukraine, and the United States. These contacts are refreshed and furthered through topical Workshops, Advanced Training Modules and Tutorials, and our International Workshop series *CompPhys: New Developments in Computational Physics*, taking annually place at the end of November just before the first advent weekend.

Wolfhard Janke

10.2 Monte Carlo simulations of poly(3-hexylthiophene) (P3HT): Comparison of three coarse-grained models

J. Gross, M. Ivanov, N. Oberthür, W. Janke

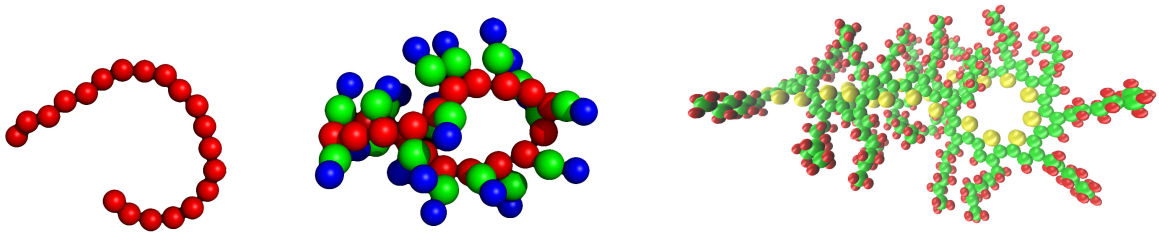

(a) (b) (c)

Figure 10.2: Hairpin conformations of poly(3-hexylthiophene) for a degree of polymerization $DP_n = 20$ in three different models. (a) One-particle coarse-grained model (one bead per monomer), (b) three-particle coarse-grained model, and (c) fully atomistic model.

Regioregular poly(3-hexylthiophene) (P3HT) is a very interesting conjugated polymer due to its electronic and optical properties [1]. One of its applications is the use as semiconducting layer in organic photovoltaics [2]. Studies of P3HT on the microscopic level are of great importance for a fundamental understanding of the tuneability of electronic properties and their dependence on external constraints, e.g., the adsorption on electrode surfaces. Hence a number of experimental studies addressed for example the influence of structure formation by polymer self-assembly on ideal surfaces on the electronic properties of oligo- and polythiophenes [3]. Due to the complexity of these macromolecules many of the experimental findings have not been supported with simulations so far, which in contrast is well-established for studies of small organic molecules. Our previous study [4] reported on an collaborative effort within the DFG SFB/TRR 102 project to combine the experimental observation of polymer chain conformations adsorbed on a metal surface with Monte Carlo simulations of a coarse-grained P3HT model developed by Huang *et al.* [5]. Based on our previous work on a three beads per monomer coarse-grained model, we expanded our studies in two directions. We focused our interest on the polymer itself and, firstly, investigated an even coarser model with one bead per monomer [6] using Monte Carlo simulations.

Secondly, we simulated a fully atomistic representation of P3HT using molecular dynamics. The different levels of resolution are illustrated in Fig. 10.2. We pursue these two routes to gauge the level of detail that is necessary to reproduce experimental findings more accurately. Another interest is the development of our own simplified model by systematically performing the coarse-graining procedure ourselves. For this we looked at the iterative Boltzmann inversion method [7]. A comparative analysis of all three models regarding structural observables, but also the computational effort is discussed in Ref. [8]. Recently we extended our simulations with the three-particle coarse-grained P3HT model also to the fully adsorbed (two-dimensional) case [9].

[1] X. Bai, S. Holdcroft: Macromolecules **26**, 4457 (1993); Z. Bao et al.: Appl. Phys. Lett. **69**, 4108 (1996); M.R. Andersson et al.: J. Mater. Chem. **9**, 1933 (1999); B.W. Boudouris et al.: Macromolecules **44**, 6653 (2011)
[2] J.M. Frost et al.: Nano Letters **6**, 1674 (2006); M. Campoy-Quiles et al.: Nat. Mater. **7**, 158 (2008); A.M. Ballantyne et al.: Adv. Funct. Mater. **18**, 2373 (2008)
[3] Z.Y. Yang et al.: ACS Nano **2**, 743 (2008); Y.F. Liu et al.: Nanoscale **5**, 7936 (2013)
[4] S. Förster et al.: J. Chem. Phys. **141**, 164701 (2014)
[5] D.M. Huang et al.: J. Chem. Theory Comput. **6**, 526 (2010)
[6] C.K. Lee et al.: Energy Environ. Sci. **4**, 4124 (2011)
[7] D. Reith et al.: J. Comput. Phys. **24**, 1624 (2003); Macromolecules **36**, 5406 (2003)
[8] J. Gross et al.: J. Phys.: Conf. Ser. **750**, 012009 (2016); Eur. Phys. J. – Special Topics **226**, 667 (2017)
[9] N. Oberthür et al.: *Two-dimensional Monte Carlo simulations of coarse-grained poly(3-hexylthiophene) (P3HT) adsorbed on striped substrates*, Leipzig preprint (2018), submitted to J. Chem. Phys. (under revision)

10.3 Polymer knots as a topological order parameter

M. Marenz, W. Janke

For the investigation of the generic behaviour of polymers and proteins with computer simulations, it is common to use minimalistic, coarse-grained models since this is the only possibility to investigate large time scales, length scales or parameter ranges. In this study we used a bead-stick model for a semiflexible polymer defined by the Hamiltonian

$$H = E_{\mathrm{LJ}} + \kappa E_{\mathrm{Bend}} = 4 \sum_{i=1}^{N-2} \sum_{j=i+2}^{N} \left(\frac{1}{r_{ij}^{12}} - \frac{1}{r_{ij}^{6}} \right) + \kappa \sum_{i} (1 - \cos \theta_i) \ , \tag{10.1}$$

where r_{ij} is the distance between non-adjacent monomers, and θ_i is the angle of two adjacent bonds. The parameter κ allows to vary the bending stiffness of the polymer from flexible over semiflexible to stiff [1, 2].

To simulate the system in the complete (T, κ)-plane we used two advanced Monte Carlo algorithms. A parallel multicanonical algorithm [3] combined with a one-dimensional replica exchange in the κ direction and a two-dimensional replica-exchange method, which simulates the system in parallel in the T and κ direction. Employing

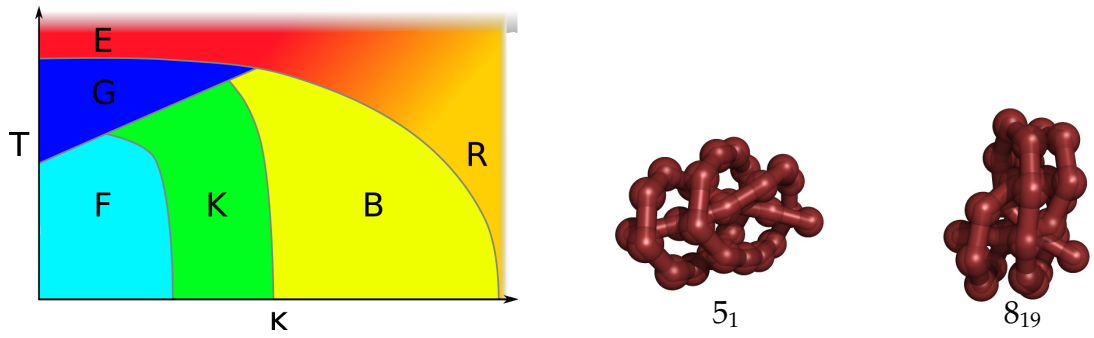

Figure 10.3: Sketch of the phase diagram for a semiflexible bead-stick model exhibiting several phases: E – elongated, R – rod-like, G – globular, F – frozen, K – knotted, B – bent. Next to the phase diagram two typical knots of types 5_1 and 8_{19} for a 28mer are shown.

both algorithms, we calculated surface plots of various observables (energy, end-to-end distance, radius of gyration, eigenvalues of gyration tensor) to construct the full pseudo-phase diagram for several polymer lengths ($N = 14, 28, 42$) [4, 5].

Despite the simplicity of the model, the phase diagram sketched in Fig. 10.3 is remarkably rich. Compared to former work simulating similar coarse-grained models [6], we observed a novel type of phases labeled by "K", which are characterized by thermodynamically stable knots [7], which may be considered as topological order parameters. The transitions into these knot phases exhibit some intriguing characteristics. Although we observed clear signals of a first-order transition between the knotted and unknotted phases, the transition apparently shows no latent heat [4, 5]. Instead the two sub-energies, the Lennard-Jones energy and the bending energy, are transformed into each other while the polymer knots itself, see Fig. 10.4.

[1] J. Zierenberg et al.: Polymers **8**, 333 (2016)
[2] W. Janke et al.: Lobachevskii J. Math. **38**, 978 (2017)
[3] J. Zierenberg et al.: Comput. Phys. Commun. **184**, 1155 (2013)
[4] M. Marenz, W. Janke: Phys. Rev. Lett. **116**, 128301 (2016)
[5] M. Marenz, W. Janke: In *Computer Simulation Studies in Condensed-Matter Physics XXIX*, eds. D.P. Landau, H.-B. Schüttler, S. Lewis, M. Bachmann, J. Phys.: Conf. Ser. **750**, 012006 (2016)
[6] D.T. Seaton et al.: Phys. Rev. Lett. **110**, 028103 (2013)
[7] L.H. Kauffman: *Knots and Physics*, 2nd ed. (World Scientific, Singapore, 1991)

10.4 Polymer adsorption to a nano-sphere

H. Arkın*, W. Janke

*Department of Physics Engineering, Faculty of Engineering, Ankara University, Tandogan, 06100 Ankara, Turkey

The interaction of macromolecules with differently shaped substrates is particularly important for interdisciplinary research and nano-technological applications including, e.g., the fabrication of biosensors and peptide adhesion to metals or semiconductors.

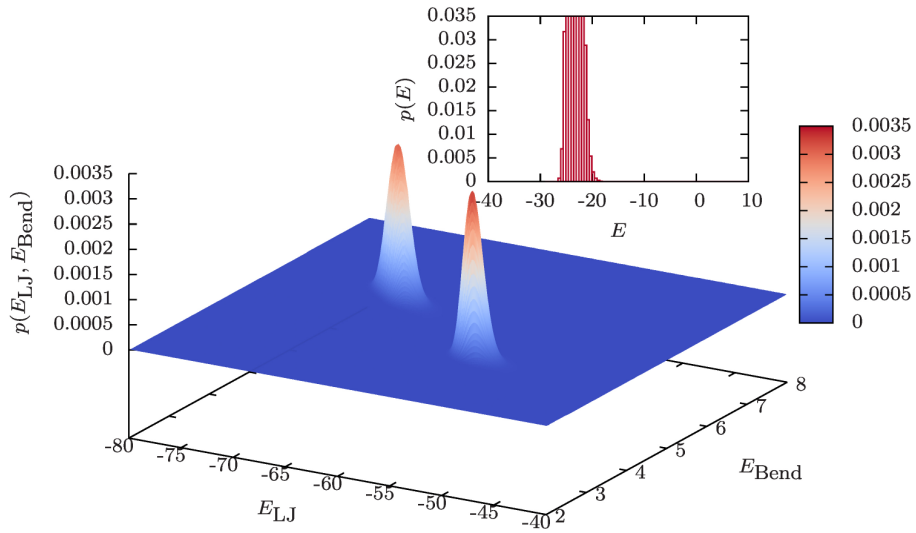

Figure 10.4: Two-dimensional energy histogram $p(E_{\mathrm{LJ}}, E_{\mathrm{Bend}})$ of a 28mer at the transition into the knot phase signaling clear phase coexistence. The inset shows the one-dimensional energy histogram $p(E)$ of the total energy $E = E_{\mathrm{LJ}} + \kappa E_{\mathrm{Bend}}$, which corresponds to a projection along the diagonal of the two-dimensional histogram. In this projection, the two peaks fall on top of each other, so only a single peak is visible in $p(E)$.

The knowledge of structure formation for a variety of interfaces has therefore been a challenging subject of numerous experimental and computational studies.

Recently we have investigated the purely steric confinement effect of a spherical cage enclosing a simple flexible polymer chain to determine its influence on the location of the collapse and freezing transitions [1]. Another hybrid system under consideration was a polymer chain inside an attractive spherical cage for which we have constructed the finite-temperature phase diagram depending on the attraction strength of the sphere inner wall and the temperature [2, 3] and investigated the ground-state properties [4]. We have also compared the results with an attractive flat surface [5, 6]. These systems exhibit a rich phase behaviour ranging from highly ordered, compact to extended, random coil structures.

Here, we consider the opposite situation: A nano-sphere whose attractive outer spherical surface is the target for the adsorbing polymer. This problem could have practical implications for a broad variety of applications ranging from protein-ligand binding, designing smart sensors to molecular pattern recognition and for the discovery of new drugs that bind to specific receptors. Therefore it is interesting to study the adsorption of macromolecules on different types of substrates and identify the conformational changes that a polymer can experience at the interface.

In this project we investigate a simple coarse-grained polymer model interacting with a spherical surface of varying radius (and consequently curvature) by means of extensive generalized-ensemble Monte Carlo computer simulations [7]. The employed multicanonical method enables us to describe the different phases of the finite chain over a wide range of sphere radius and temperature. In a comparative study, we determined how the structural phase diagram changes with the sphere radius and

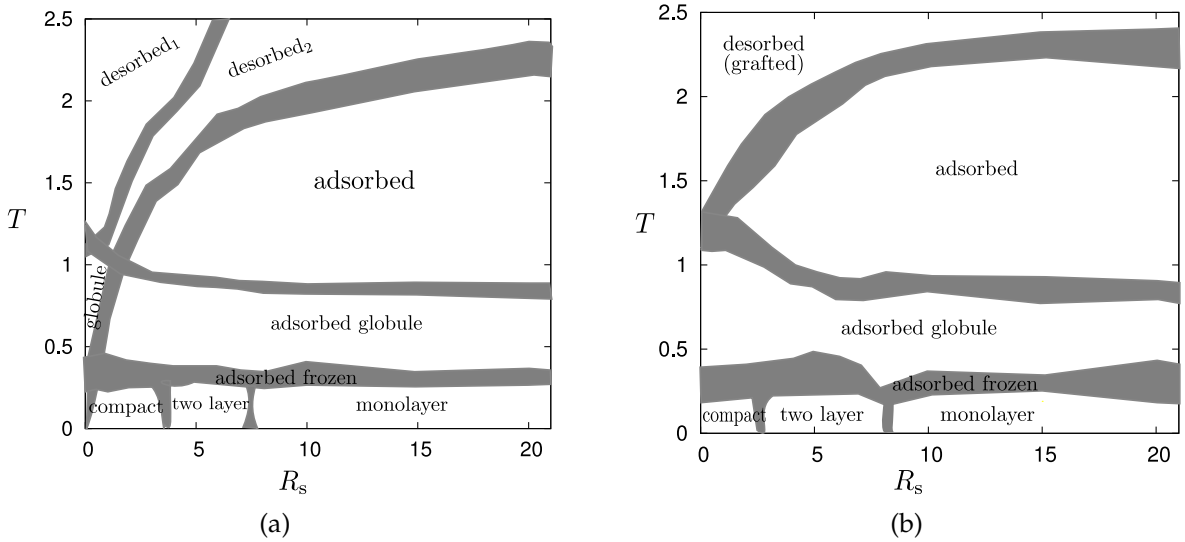

Figure 10.5: The phase diagram of a homopolymer interacting with an attractive spherical surface of radius R_s for (a) a non-grafted and (b) an end-grafted 20mer.

temperature, both for non-grafted and end-grafted polymer chains. The band widths of the boundaries separating the individual conformational phases in Fig. 10.5 indicate the variation of the peak locations of temperature derivatives of different structural observables which we have analyzed simultaneously [7]. Typical conformation for the case of a non-grafted polymer are shown in Fig. 10.6.

[1] M. Marenz et al.: Condens. Matter Phys. **15**, 43008 (2012)
[2] H. Arkın, W. Janke: Phys. Rev. E **85**, 051802 (2012)
[3] H. Arkın, W. Janke: J. Chem. Phys. **138**, 054904 (2013)
[4] H. Arkın, W. Janke: J. Phys. Chem. B **116**, 10379 (2012)
[5] M. Möddel et al.: J. Phys. Chem. B **113**, 3314 (2009); Phys. Chem. Chem. Phys. **12**, 11548 (2010); Macromolecules **44**, 9013 (2011)
[6] H. Arkın, W. Janke: Eur. Phys. J. – Special Topics **216**, 181 (2013)
[7] H. Arkın, W. Janke: Phys. Rev. E **96**, 062504 (2017)

10.5 Adsorption of semiflexible polymers

K.S. Austin, J. Zierenberg*, W. Janke

*Max Planck Institute for Dynamics and Self-Organization, Am Fassberg 17, 37077 Göttingen, Germany

The conformational properties of a semiflexible polymer in the vicinity of an attractive surface is of relevance for a wide range of applications from material design to catalysis to DNA sequencing through nanopores. If the polymer adsorbs, which is not always desired in applications, there may occur different structural conformations. Often, the discussion of semiflexible polymer adsorption considers polymers under good

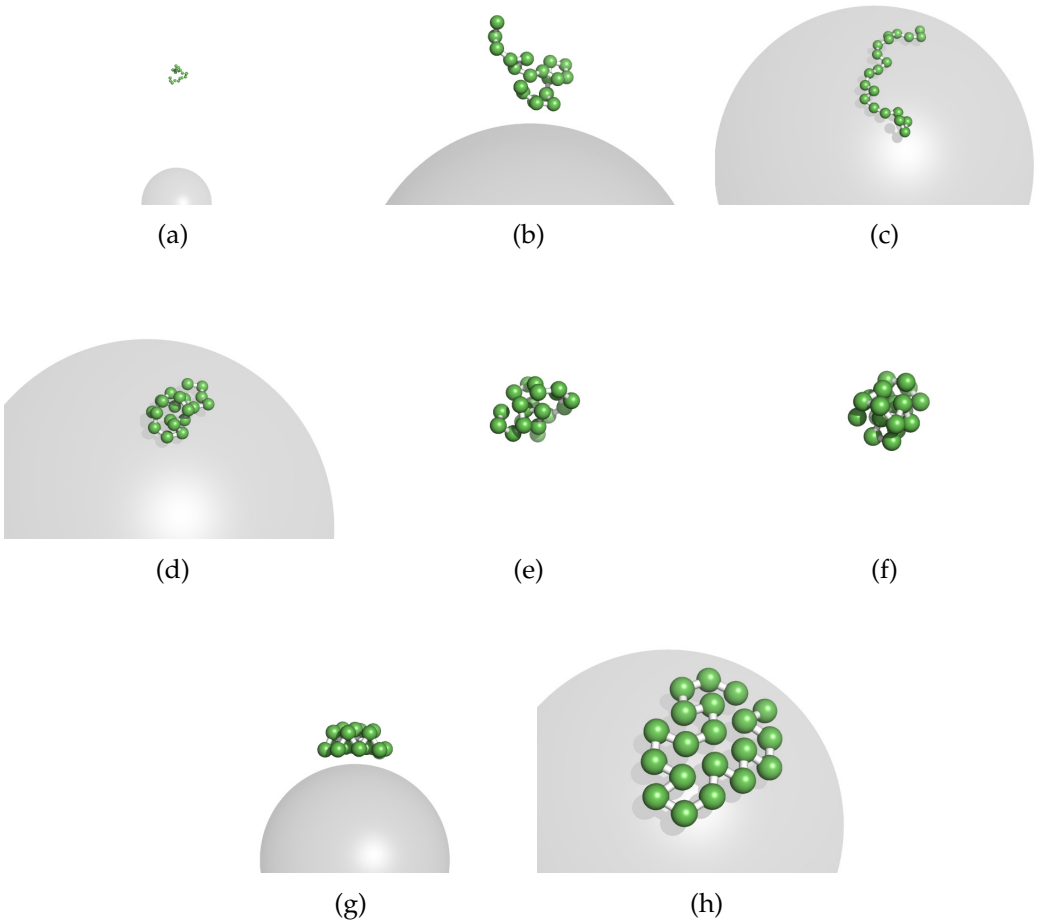

Figure 10.6: Typical conformations for the regions (a) desorbed$_1$, (b) desorbed$_2$, (c) adsorbed, (d) adsorbed globule, (e) globule, (f) compact, (g) two layer, and (h) monolayer in the phase diagram of a non-grafted polymer.

solvent conditions with purely *repulsive* monomer-monomer interactions [1, 2]. Finite-size scaling analyses of computer simulation data show that the adsorption transition temperature increases linearly with persistence length for stiff polymers as predicted [2]. This may be expected to be maintained under poor solvent conditions. However, additional short-range *attractive* monomer-monomer interactions will lead to a rich conformational phase space as a result of the competition of polymer stretching and collapse close to an attractive surface.

In general, there has been an extensive theoretical and numerical effort towards the study of flexible polymers near attractive surfaces. Under poor solvent conditions, the final adsorbed states range from partially adsorbed to fully flat conformations, demonstrated for an entire class of flexible polymers [3, 4]. Similar observations were made for the adsorption of specific lattice proteins [5]. If the surface shows complex attractive motifs, one observes in addition pattern recognition effects [5, 6].

Semiflexible, *self-attractive* polymers undergoing a collapse transition exhibit a rich variety of structural phases already in the case of an isolated chain [7, 8]. These include collapsed, toroidal, hairpin, and knotted conformations, partially depending on the

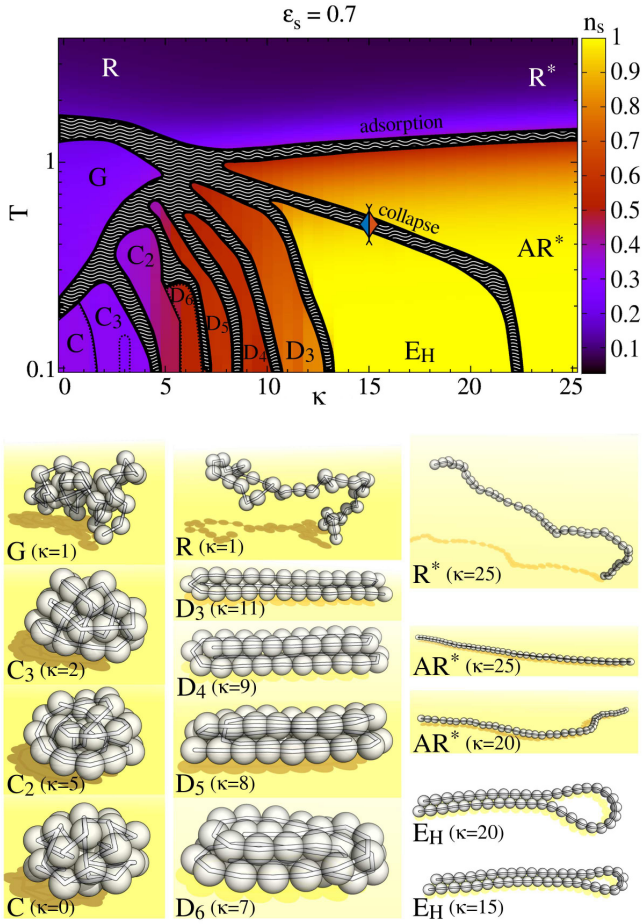

Figure 10.7: Structural phase diagram for a semiflexible polymer of length $N = 40$ grafted to a weakly attractive surface ($\epsilon_s = 0.7$). The background color encodes the average fraction of surface contacts $n_s = N_s/N$. Dotted lines indicate that signals are found only in a small subset of observables. Representative conformations from the respective conformational regimes are shown below. They comprise globule-like (G), compact (C), and random coil-like (R) conformations, as well as folded bundles (D_m), desorbed and adsorbed weakly bent rods (R* and AR*, respectively), and hairpins (E_H). The (blue-red) rhombus at $\kappa \approx 15$ marks the crossover from a second-order-like to a first-order-like collapse transition.

geometric and energetic constraints of the model. This plays a crucial role for practical purposes, since semiflexibility is a common property of biopolymers such as DNA. The question arises how semiflexibility influences the structural and thermal adsorption properties of dilute self-attractive polymers. A detailed study of the interplay of (effective) polymer stiffness and surface adsorption for the full range of self-attracting polymer models was so far lacking and in Ref. [9] we intended to fill this gap.

This study comprises sophisticated Monte Carlo computer simulations of a linear homopolymer consisting of $N = 40$ monomers connected by anharmonic springs fluctuating around an "equilibrium" bond length r_0. We consider the cases of a completely free polymer and a polymer grafted to a non-interacting as well as an attractive substrate (i.e., the first monomer remains at a fixed location on the surface). Our polymer description is intended to model a full class of (grafted) semiflexible polymers in a range of solvent conditions. The resulting coarse-grained model incorporates four en-

ergy terms: bond-vibrational energy, non-neighboring 12-6 Lennard-Jones interactions, bending energy parametrized by the bending stifness κ, and 9-3 Lennard-Jones surface interaction parametrized by the interaction strength ε_s. As a typical example of our results, Fig. 10.7 shows the κ-T phase diagram for a weakly attractive surface with $\varepsilon_s = 0.7$.

[1] T. Sintes et al.: Macromolecules **34**, 1352 (2001)
[2] H.-P. Hsu, K. Binder: Macromolecules **46**, 2496 (2013)
[3] J. Luettmer-Strathmann et al.: J. Chem. Phys. **128**, 064903 (2008)
[4] M. Möddel et al.: Phys. Chem. Chem. Phys. **12**, 11548 (2010)
[5] A.D. Swetnam, M.P. Allen: Phys. Chem. Chem. Phys. **11**, 2046 (2009); Phys. Rev. E **85**, 062901 (2012)
[6] M. Möddel et al.: Phys. Rev. Lett. **112**, 148303 (2014)
[7] D.T. Seaton et al.: Phys. Rev. Lett. **110**, 028103 (2013)
[8] M. Marenz, W. Janke: Phys. Rev. Lett. **116**, 128301 (2016)
[9] K.S. Austin et al.: Macromolecules **50**, 4054 (2017)

10.6 Binding transition of two grafted polymers

K. Tholen, J. Zierenberg*, W. Janke

*Max Planck Institute for Dynamics and Self-Organization, Am Fassberg 17, 37077 Göttingen, Germany

In this project we studied the binding of two flexible polymers grafted closeby to a steric surface. More specifically, we fixed one of their end points to a steric surface covering the $x - y$ plane at $z = 0$. No monomer was allowed to cross this geometric constraint, i.e., monomer coordinates with $z_i < 0$ were forbidden. No further interactions with the (inert) surface are assumed. The end points are grafted with distance $d = r_0$ (the equilibrium bond length of a FENE spring connecting the monomers) and are immobilized. If the polymers are not grafted, we enclose them in a cubic box of side length L with steric walls. For an illustration see Fig. 10.8.

As "binding" we refer to the process where two polymers attach to each other, in our case flexible polymers. If specific inter-polymer interactions are considered this may quickly lead to effects also characterized as zipping. Even more interesting is the equivalence between two-polymer binding of directed polymers and adsorption [1]. This should qualitatively remain valid also for flexible polymers, especially if one imagines the crossover scenario of a flexible polymer adsorbed to a nanowire, equivalent to the stiff limit of a polymer chain [2, 3], or a flexible polymer adsorbing to a flexible surface [4]. In fact, it was shown that grafting alters the first-order-like adsorption transition to a second-order-like transition [5].

From our Monte Carlo simulation data we conclude [6] that when grafting two polymers to a steric surface at a close distance an analogous scenario holds true, i.e., we observe a second-order-like binding transition, which is in contrast to the first-order-like finite-size binding transition for free polymers in a steric box. This is relevant for an experimental study of polymer binding, where in vitro polymers would be

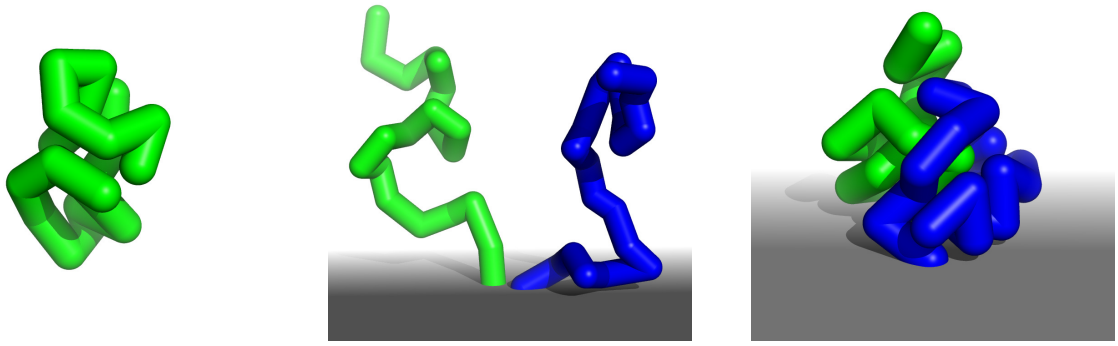

(a) (b) (c)

Figure 10.8: Snapshots of (a) a single polymer of length $N = 20$ in the globular phase below the collapse transition ($T = 0.7$) and two polymers of length $N = 20$ grafted to a steric surface (b) above (T = 4) and (c) below ($T = 0.7$) the binding transition.

commonly grafted. In this case, one will neither observe a latent heat nor hysteresis effects associated with first-order-like transitions, which would be expected to occur in vivo. Still, grafted polymers may be studied with respect to aggregate properties and their dynamics which are expected to sufficiently coincide for observables which are not directly influenced by the geometric constraint. One exception is the average end-to-end distance and subsequently (no longer isotropic) geometric properties. Interesting effects may be anticipated for interacting surfaces, where the binding of polymers would compete with the surface attraction. Connecting to experimental setups, the surfaces may be considered both flat or curved, e.g., when grafting polymers to nanoparticles.

[1] J. Kierfeld, R. Lipowsky: Europhys. Lett. **62**, 285 (2003)
[2] T. Vogel et al.: J. Chem. Phys. **142**, 104901 (2015)
[3] J. Gross et al.: Phys. Chem. Chem. Phys. **17**, 30702 (2015)
[4] S. Karalus et al.: Phys. Rev. E **84**, 031803 (2011)
[5] M. Möddel et al.: Macromolecules **44**, 9013 (2011)
[6] J. Zierenberg et al.: Eur. Phys. J. – Special Topics **226**, 683 (2017)

10.7 Polymer versus particle condensation

J. Zierenberg*, P. Schierz, W. Janke

*Max Planck Institute for Dynamics and Self-Organization, Am Fassberg 17, 37077 Göttingen, Germany

A common approach to study nucleation rates is the estimation of free-energy barriers. This usually requires knowledge about the shape of the forming droplet, a task that becomes notoriously difficult in macromolecular setups starting with a proper definition of the cluster boundary or a proper ensemble choice. Here, we demonstrate that a shape-free determination of temperature-driven cluster formation is directly accessible in the canonical ensemble for particle as well as polymer systems. Combined with rigorous results on canonical equilibrium droplet formation, this allows for a well-defined

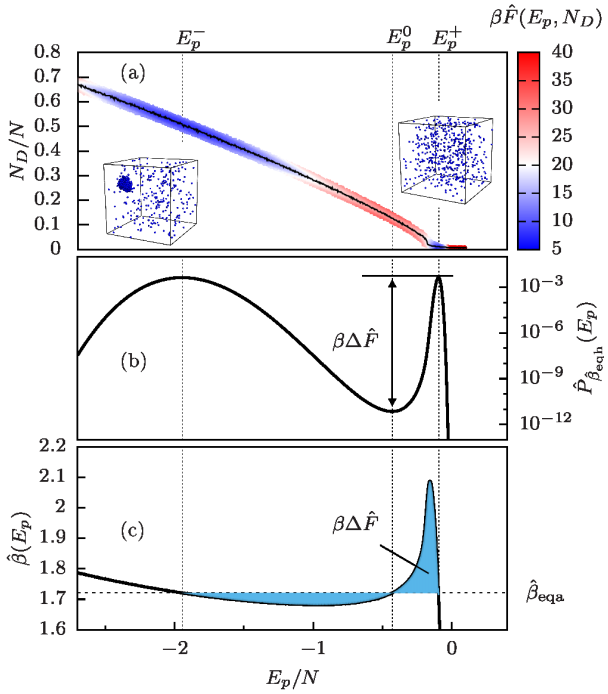

Figure 10.9: (a) Illustration of the free-energy landscape $\beta\hat{F}(E_p, N_D)$ (color map) as a function of potential energy E_p and droplet size N_D for $N = 512$ Lennard-Jones particles. The minimal free-energy path (black solid line) connects a droplet ($E_p \approx E_p^-$) and a gaseous ($E_p \approx E_p^+$) phase, visualized by the snapshots at $E_p^\pm$. The projection onto the reaction-coordinate E_p yields the canonical potential-energy probability distribution $\hat{P}_\beta(E_p)$, where the free-energy barrier $\beta\Delta\hat{F}$ is encoded in the ratio between maximum and minimum at $\hat{\beta}_{\rm eqh}$. (c) Equivalently, $\beta\Delta\hat{F}$ is the (equal) area size enclosed between the microcanonical inverse temperature $\hat{\beta}(E_p)$ and the accordingly defined transition temperature $\hat{\beta}_{\rm eqa}$, where $\hat{\beta}_{\rm eqa} = \hat{\beta}_{\rm eqh} = 1.72099(3)$.

finite-size scaling analysis of the effective interfacial free energy at fixed density as illustrated in Fig. 10.9. We first verified the theoretical predictions for the formation of a liquid droplet in a supersaturated particle gas by (parallelized) generalized-ensemble Monte Carlo simulations [1–3] of a Lennard-Jones system [4–6]. Going one step further, we then generalized this approach to the aggregation process in a dilute polymer solution [6], cf. Fig. 10.10. Our results suggest an analogy between particle condensation and polymer aggregation, when the macromolecules are interpreted as extended particles.

Because the standard approach in Monte Carlo simulations is to work in the conformational ensemble governed by potential energy only, we show that excluding the kinetic energy from the partition function leads to finite-size differences in the free energy compared to the full ensemble [7, 8] but retains intensive parameters in the thermodynamic limit [6]. Our study of nucleation rates at fixed density corresponds to a heating-cooling framework where simulation and experiment may meet at the nanometer scale.

[1] B.A. Berg, T. Neuhaus: Phys. Lett. B **267**, 249 (1991); Phys. Rev. Lett. **68**, 9 (1992)
[2] W. Janke: Int. J. Mod. Phys. C **03**, 1137 (1992); Physica A **254**, 164 (1998)
[3] J. Zierenberg et al.: Comput. Phys. Commun. **184**, 1155 (2013)

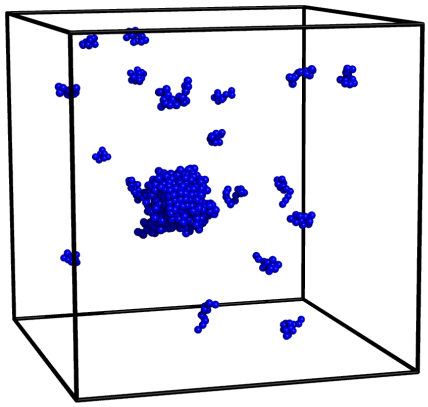

Figure 10.10: Illustration of an aggregate of polymers in a dilute solution ($N = 64$ bead-spring polymers with 13 monomers each; monomer density $\rho = 10^{-2}$). The snapshot stems from the droplet phase ($E_p \approx E_p^-$).

[4] J. Zierenberg, W. Janke: Phys. Rev. E **92**, 012134 (2015)
[5] J. Zierenberg, W. Janke: in *Computer Simulation Studies in Condensed-Matter Physics XXIX*, eds. D.P. Landau, H.-B. Schüttler, S. Lewis, M. Bachmann, J. Phys.: Conf. Ser. **750**, 012017 (2016)
[6] J. Zierenberg et al.: Nat. Commun. **8**, 14546 (2017)
[7] P. Schierz et al.: Phys. Rev. E **94**, 021301(R) (2016)
[8] W. Janke et al.: in *Computer Simulation Studies in Condensed-Matter Physics XXX*, eds. D.P. Landau, M. Bachmann, S.P. Lewis, H.-B. Schüttler, J. Phys.: Conf. Ser. **921**, 012018 (2017)

10.8 Computer simulations of semiflexible polymers in disordered environments

J. Bock, W. Janke

Single-molecule experiments have established the wormlike chain (WLC) as a standard model for semiflexible polymers [1]. Exploiting the analogy of the WLC with a one-dimensional Heisenberg ferromagnet, it can be shown that the equilibrium tangent-tangent correlation function decays exponentially. The decay rate defines the thermal persistence length l_p. When the same polymer is embedded in a quenched, disordered environment in three dimensions, this property may change quantitatively or even qualitatively. We addressed this problem by performing extensive numerical simulations of semiflexible polymers in a simple lattice disorder and in a gaseous disorder constructed by microcanonical Lennard-Jones gas simulation which represents the disordered environment. Further plans are to simulate the polymers in algebraically correlated

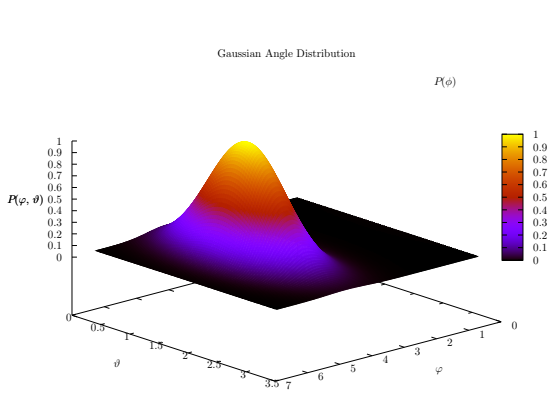

(a) Weighting histogram

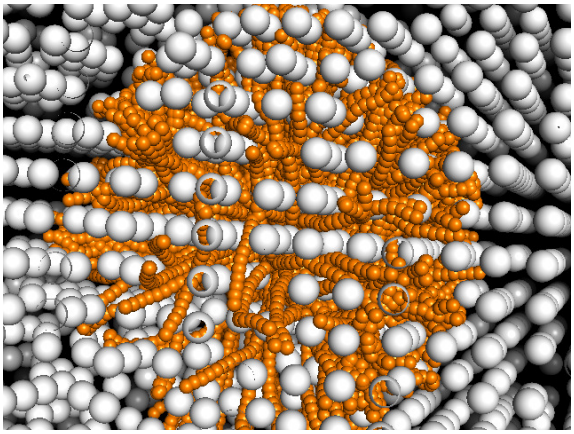

(b) Semiflexible polymer in 3D disorder

Figure 10.11: (a) Histogram used for the guiding field in 3D and (b) an examplary configuration of a polymer with $N = 30$ and $\xi = 1$.

disorder. Only the space between the spheres is accessible to the polymer. The extreme strength and density of the environmental constraints are a great challenge to conventional Monte Carlo simulation schemes, which we found hard to overcome even with a sophisticated multicanonical histogram reweighting procedure [2]. We have therefore adopted a breadth-first chain-growth algorithm [3] that resolves this difficulty by circumventing energy barriers instead of trying to cross them [2, 4], see examples in Fig. 10.11. Therefore the already existing procedures were expanded to the third dimension to investigate the behaviour of the tangent-tangent correlation length, the mean square end-to-end distance and the end-to-end probability distribution function, see Fig. 10.12. A difference in behaviour is clear and the task now is to check wether the differences scale similarly as in two dimensions, where the disorder renormalization is stated to be [5]:

$$\frac{1}{l_p^*} = \frac{1}{l_p} + \frac{1}{l_p^D},$$

with l_p^* the renormalized persistence length, l_p the persistence length given as simulation parameter and l_p^D the measured disorder persistence length.

[1] O. Otto et al.: Nat. Commun. **4**, 1780 (2013)
[2] S. Schöbl et al.: Phys. Rev. E **84**, 051805 (2011)
[3] T. Garel, H. Orland: J. Phys. A: Math. Gen. **23**, L621 (1999)
[4] S. Schöbl et al.: J. Phys. A: Math. Theor. **45**, 475002 (2012)
[5] S. Schöbl et al.: Phys. Rev. Lett. **113**, 238302 (2014)

10.9 Periodically driven DNA: A comparative study of Langevin and Brownian dynamics

R. Kumar, S. Kumar*, W. Janke

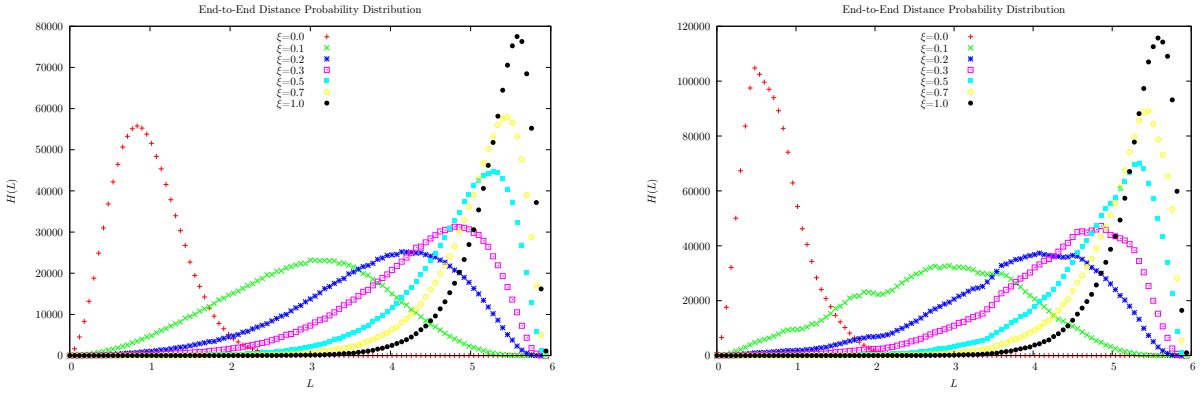

(a) Free polymers (b) Polymers in disorder

Figure 10.12: End-to-end distance distributions for (a) free polymers and (b) polymers in gaseous disorder, both in 3D.

*Department of Physics, Banaras Hindu University, Varanasi 221 005, India

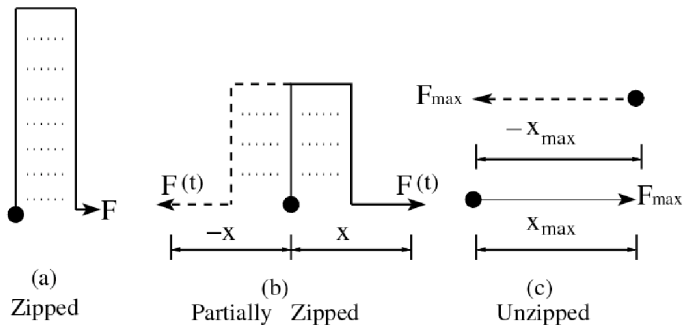

Figure 10.13: Schematic representations of DNA: (a) zipped, (b) partially zipped, and (c) unzipped state. One end is kept fixed (indicated by solid circles), while the other end may move.

DNA replication is one of the most important biological processes in living organisms. Under the influence of special enzymes, two strands of the DNA double helix can separate themselves like a zip. The first step in the process of DNA replication is to unzip the double-helix structure of the DNA molecule. Therefore, it is very important to study the unzipping of DNA. There has been some experimental studies at a constant force or loading rate used in SMFS experiments to unzip the DNA *in vitro*. In these experiments one end of the DNA was fixed and a constant force was applied on its other end. However, such processes are driven by different types of molecular motors *in vivo* [1].

A constant force or loading rate used in SMFS experiments provides a limited picture of these processes *in vitro*. Hence, the picture provided by constant force unzipping is not complete. This has been highlighted in recent studies, where it was suggested that by varying the frequency and amplitude of the applied force new aspects of a force-driven transition can be introduced [2–5], which otherwise would not be possible in the case of a steady force. The considered situation is sketched in Fig. 10.13.

This model was further simplified in [6, 7] by reducing the degrees of freedom

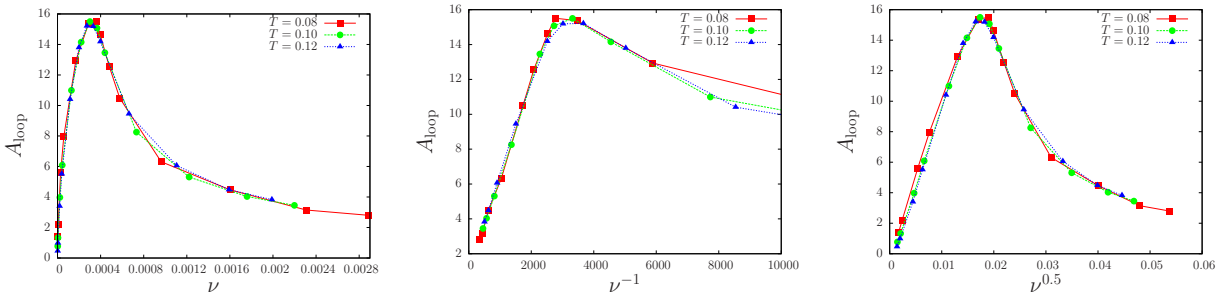

(a) (b) (c)

Figure 10.14: Effect of temperature on the area of the hysteresis loop for the model with parameters $L = 32$, $F = 1.0$, and $\gamma = 0.4$ for (a) $A_{\rm loop}$ vs. ν, (b) area vs. ν^{-1} in the higher frequency regime, and (c) area vs. $\nu^{0.5}$ in the lower frequency regime. Here the x-axis is rescaled in order to show the data collapse for all temperatures.

and studying the overdamped limit using Brownian dynamics. This simplified model was investigated only at zero temperature. Therefore, it became crucial to further investigate how the temperature effects the dynamics of such system using the detailed model described in [3]. Emphasis was placed on the effect of different temperatures on the scaling properties. Moreover, we compared results of the Langevin dynamics for the detailed model and Brownian dynamics for the simplified model. We observed that the temperature and over-damped limit does not effect the scaling exponentsi, cf. Fig. 10.14. Hence, the model proposed by us is good enough to study the scaling properties and provides a possibility of analytic studies within certain limits. Moreover, currently we are trying to understand the effect of the over-damped limit in the detailed model proposed in [3].

[1] B. Alberts et al.: *Molecular Biology of the Cell* (Garland Publishing, New York, 1994)
[2] S. Kumar, M. S. Li: Phys. Rep. **486**, 1 (2010)
[3] S. Kumar, G. Mishra: Phys. Rev. Lett. **110**, 258102 (2013)
[4] G. Mishra et al.: Phys. Rev. E **87**, 022718 (2013)
[5] R.K. Mishra et al.: J. Chem. Phys. **138**, 244905 (2013)
[6] S. Kumar et al.: Phys. Rev. E **93**, 010402(R) (2016)
[7] R. Kumar et al.: *Comparative study of Brownian and Langevin dynamics for periodically driven DNA* , Leipzig/Varanasi preprint (2017), to be published

10.10 Effect of temperature on the scaling laws governing the kinetics of collapse of a homopolymer

S. Majumder, J. Zierenberg*, W. Janke

*Max Planck Institute for Dynamics and Self-Organization, Am Fassberg 17, 37077 Göttingen, Germany

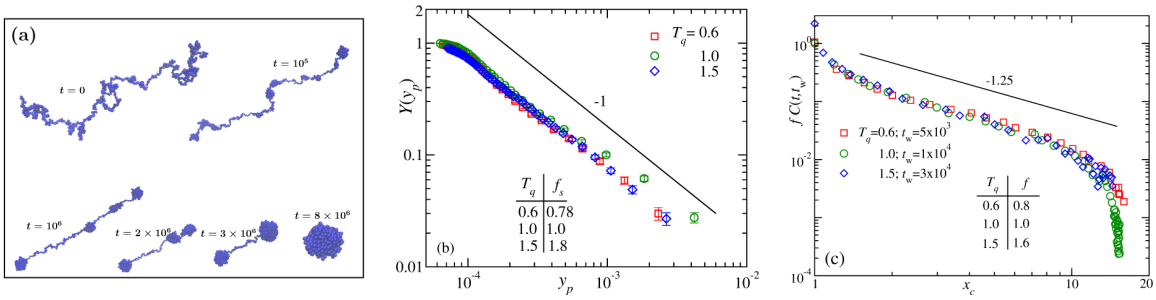

Figure 10.15: (a) Snapshots [1] showing the sequence of events occurring during the collapse of a polymer upon being quenched from an expanded state (at high temperature) into the globular phase (at low temperatures). (b) Universal finite-size scaling function $Y(y_p)$ with a non-universal metric factor (f_p) in the scaling variable y_p describing the scaling in the cluster growth during the collapse [2]. (c) Temperature-independent scaling plot for the aging and related dynamical scaling, probed by the behavior of a suitable density-density autocorrelation function $C(t, t_w)$ against $x_c = C_s(t)/C_s(t_w)$, the ratio of cluster sizes $C_s(t)$ at the observation time (t) and the waiting time (t_w) [2].

The collapse transition of a polymer upon transfer from a good solvent (high temperature) to a poor solvent (low temperature) bears significant connection to the folding process of a proteins and other biomolecules. Thus understanding the kinetics of a homopolymer in that respect may provide useful primary information on the underlying mechanism of more realistic problems [1, 2]. On the other hand, if one considers the usual "pear-necklace" like picture of the collpase [1] as shown in Fig. 14.1(a), it also resembles coarsening phenomena popular in spin and particle systems [6]. Over the last two years we have been exploiting this connection to understand the kinetics of collapse of a homopolymer [7, 8].

In this work, from the state of the art Monte Carlo simulations of an off-lattice polymer model, we understand the effect of the quench temperature (T_q) on the various scaling laws related to the collapse viz., scaling of the cluster growth and the dynamical scaling related to the aging. Our results in conjunction with the nonequilibrium finite-size scaling analysis [9] show that the cluster growth is rather universal in nature and can be described by a universal finite-size scaling function with a non-universal metric factor that depends on the amplitudes of the growth [2], see Fig. 14.1(b). This observation has recently been confirmed in a related lattice model for the polymer [3]. For a direct comparison of the lattice and off-lattice formulations, see Ref. [4]. Furthermore, the scaling related to the aging (which is probed by a suitable two-time density-density autocorrelation function) is also found to be independent of the quench temperature T_q, shown in Fig. 14.1(c).

[1] S. Majumder, W. Janke: J. Phys.: Conf. Ser. **750**, 012020 (2016)
[2] S. Majumder et al.: Soft Matter **13**, 1276 (2017)
[3] H. Christiansen et al.: J. Chem. Phys. **147**, 094902 (2017)
[4] S. Majumder et al.: J. Phys.: Conf. Ser. **955**, 012008 (2018)
[5] A. Halperin, P. Goldbart: Phys. Rev. E **61**, 565 (2000)
[6] A.J. Bray: Adv. Phys. **51**, 481 (2002)
[7] S. Majumder, W. Janke: Europhys. Lett. **110**, 58001 (2015)
[8] S. Majumder, W. Janke: Phys. Rev. E **93**, 032506 (2016)

[9] S. Majumder, S.K. Das: Phys. Rev. E **81**, 050102(R) (2010); Phys. Rev. E **84**, 021110 (2011)

10.11 Coarsening and aging of lattice polymers: Influence of bond fluctuations

H. Christiansen, S. Majumder, W. Janke

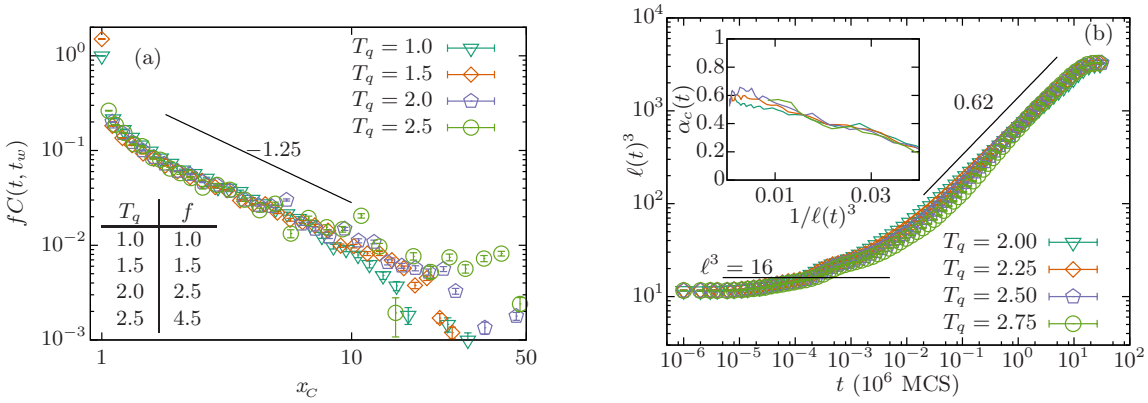

Figure 10.16: (a) The two-time correlation function $C(t, t_w)$ against the ratio of length-scales $x_C = \ell(t)/\ell(t_w)$ for the model with fixed bonds and different quench-temperatures T_q. In (b) the growth of the length-scales for the model with flexible bonds is shown for different T_q. Here the growth is independent of T_q and follows a power law with exponent $\alpha = 0.62(5)$.

The nonequilibrium properties of homopolymer collapse were investigated using Monte Carlo simulations of the interacting self-avoiding walk on a simple cubic lattice (with lattice-spacing 1) using fixed bond lengths 1 and flexible bond lengths; 1, $\sqrt{2}$, and $\sqrt{3}$ [1]. The phenomenological picture of pearl necklace polymer collapse [2] was observed, in which a polymer, when transferred from a good solvent ($T_h > T_\theta$) to a bad solvent ($T_q < T_\theta$), undergoes a collapse transition from an expanded coil by forming clusters at locally higher densities which then subsequently coalesce with each other until only a single globular cluster is left. The aging exponent $\lambda \approx 1.25$ was found to be independent of the bond conditions and the same as in the off-lattice exponent [4] (see Fig. 10.16(a) for the model with fixed bonds at different quench temperatures T_q). For the model with flexible bonds, the power-law growth exponent of the clusters of monomers was likewise observed to be independent of temperature $\alpha = 0.62(5)$ (see Fig. 10.16(b)), while the same exponent was found to be dependent on the temperature in the fixed bond model. In the off-lattice model on the other hand, $\alpha = 1$ was found [3]. The discrepency in the exponent α is attributed to the constraints introduced by the lattice structure.

[1] H. Christiansen et al.: J. Chem. Phys. **147**, 094902 (2017)
[2] A. Halperin, P. M. Goldbart: Phys. Rev. E **61**, 565 (2000)
[3] S. Majumder, W. Janke: Phys. Rev. E **93**, 032506 (2016)
[4] S. Majumder, W. Janke: Europhys. Lett. **110**, 58001 (2015)

10.12 Scaling laws during collapse of a homopolymer: Lattice versus off-lattice

S. Majumder, H. Christiansen, W. Janke

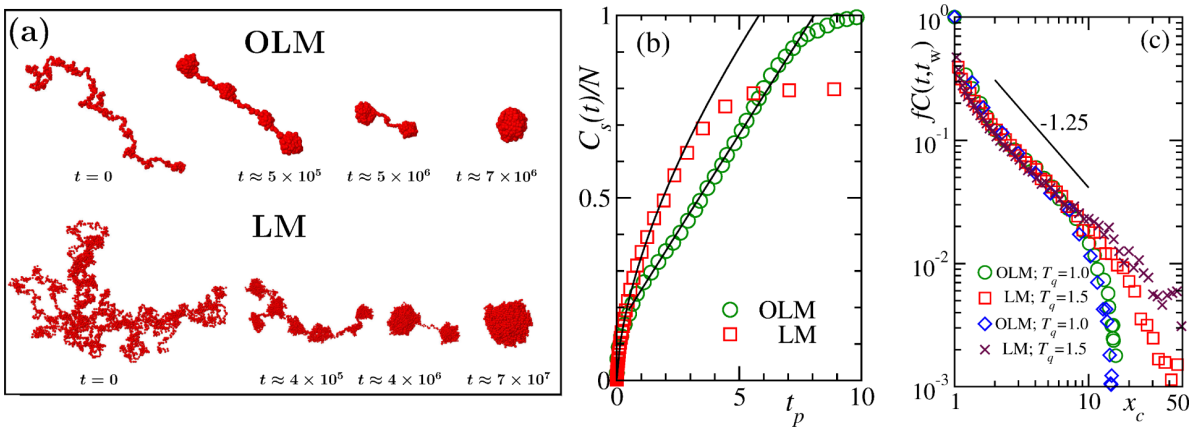

Figure 10.17: (a) Time evolution snapshots of the collapse of a homopolymer, after being quenched from an extended coil phase to a temperature, $T_q = 1$ for OLM, and $T_q = 2.5$ for LM, in the globular phase.(b) Plots of the average cluster size $C_s(t)/N$ as function of time for the two models. To make both the data visible on the same plot, we divide the time axis by a factor m to obtain $t_p = t/m$, where $m = 1 \times 10^6$ and 3.5×10^6, respectively, for OLM and LM. The solid lines there are fits to the form $C_s(t) = C_0 + At^{\alpha_c}$ with $\alpha_c = 0.98$ for OLM and $\alpha_c = 0.62$ for LM. (c) Plot showing that universal aging scaling at different T_q for the two models can be described by a single master-curve behavior. The solid line here also corresponds to $C(t, t_w) = A_C x_c^{-\lambda_C}$ with $\lambda_C = 1.25$. Note that $C(t, t_w)$ is multiplied by a factor f to make them collapse onto the same curve. For OLM $t_w = 10^4$ whereas for LM $t_w = 10^3$.

The pathways of collapse of a homopolymer, upon a transfer from a good to a poor solvent, bears resemblance to coarsening processes. Simulation results in this context can be explained by the phenomenonlogical "pearl-necklace" picture of Halperin and Goldbart (HG) [1]. Recently we have shown via Monte Carlo simulations of both a lattice model (LM) and an off-lattice model (OLM) polymer that this nonequilibrium evolution dynamics is also a scaling phenomenon [2]. In this work we compared the results obtained from the LM and OLM, in particular the scaling of the cluster growth [3] and the aging scaling [4] probed by the two-time density-density autocorrelation function.

For the OLM, we opt for the bead-spring model of a flexible homopolymer in $d = 3$ dimensions where bonds between successive monomers are maintained via the standard finitely extensible non-linear elastic (FENE) potential

$$E_{\mathrm{FENE}}(r_{ii+1}) = -\frac{KR^2}{2} \ln\left[1 - \left(\frac{r_{ii+1} - r_0}{R}\right)^2\right], \tag{10.2}$$

with $K = 40$, $r_0 = 0.7$ and $R = 0.3$. The nonbonded interaction energy is modeled by $E_{\mathrm{nb}}(r_{ij}) = E_{\mathrm{LJ}}(\min(r_{ij}, r_c)) - E_{\mathrm{LJ}}(r_c)$, where

$$E_{\mathrm{LJ}}(r) = 4\epsilon\left[\left(\frac{\sigma}{r}\right)^{12} - \left(\frac{\sigma}{r}\right)^{6}\right] \tag{10.3}$$

is the standard Lennard-Jones (LJ) potential with $\sigma = r_0/2^{1/6}$ as the diameter of the monomers, ϵ (= 1) as the interaction strength and $r_c = 2.5\sigma$ as the cut-off radius.

For LM, we consider [5] a variant of the interactive self-avoiding walk on a simple-cubic lattice, where each lattice site can be occupied by a single monomer. The energy is given by

$$E_{\mathrm{LM}} = -\frac{1}{2}\sum_{i\neq j, j\pm 1} w(r_{ij}), \quad \text{where} \quad w(r_{ij}) = \begin{cases} J & r_{ij} = 1 \\ 0 & \text{else} \end{cases}. \tag{10.4}$$

In Eq. (10.4), r_{ij} is the Euclidean distance between two nonbonded monomers i and j, $w(r_{ij})$ is an interaction parameter that considers only nearest neighbors, and J(= 1) is the interaction strength. We allow a fluctuation in the bond length by considering diagonal bonds, i.e., the possible bond lengths are 1, $\sqrt{2}$, and $\sqrt{3}$.

Phenomenonlogically both LM and OLM show intermediate structures consistent with the "pear-necklace" picture of HG [Fig. 10.17(a)]. However, the cluster-growth scaling in LM and OLM are different. While the OLM yields a linear growth ($\alpha_c \approx 1$), in the LM the growth is slower ($\alpha_c \approx 0.62$) [Fig. 10.17(b)], which could be attributed to the topological constraints one experiences in a lattice model. On the other hand, surprisingly, both the models show evidence of simple aging scaling having the same autocorrelation exponent $\lambda_C \approx 1.25$ [Fig. 10.17(c)], thus implying that the aging scaling is rather universal. This allowed us to demonstrate that scaling of the autocorrelation functions for the two models can be described by a single master curve.

[1] A. Halperin, P. M. Goldbart: Phys. Rev. E **61**, 565 (2000)
[2] S. Majumder et al.: J. Phys.: Conf. Ser. **955**, 012008 (2018)
[3] S. Majumder, W. Janke: Europhys. Lett. **110**, 58001 (2015)
[4] S. Majumder, W. Janke: Phys. Rev. E **93**, 032506 (2016)
[5] H. Christiansen et al.: J. Chem. Phys. **147**, 094902 (2017)

10.13 Universal finite-size scaling for kinetics of phase separation in mixtures with varying number of components

S. Majumder, S.K. Das*, W. Janke

*Theoretical Sciences Unit, Jawaharlal Nehru Centre for Advanced Scientific Research, Jakkur P.O., Bangalore, India

In this work [1] we have presented results for the kinetics of phase separation in multicomponent solid mixtures, from Monte Carlo simulations of the q-state conserved Potts model, in space dimension $d = 2$, for $2 \leq q \leq 10$. Evolution snapshots for $q = 4$ are shown in Fig. 10.18 (left). In agreement with previous reports [2], we also find that, even though for a fixed q various morphology-characterizing functions obey the expected scaling relations, there exists no common scaling function for different q. The primary interest in our work was to quantify the domain-growth kinetics, cf. Fig. 10.18 (middle).

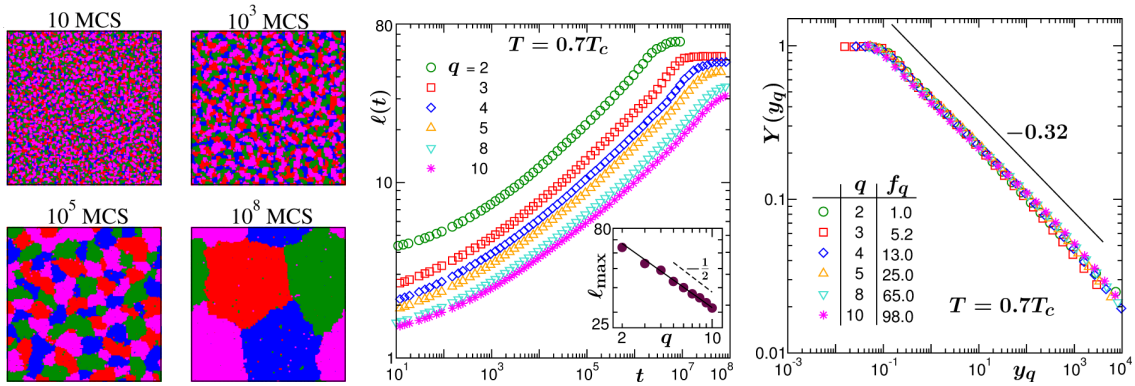

Figure 10.18: (left) Evolution snapshots from different times for 4-state Potts model, obtained from the MC simulations following a quench from the high-temperature homogeneous phase to $T = 0.7\,T_c$, that lies inside the miscibility gap. The used system size is $L = 128$. Different colors correspond to different states. (middle) Double-log plots of the average domain length, $\ell(t)$, versus time. Data for few different q-component mixtures are presented, all from $T = 0.7\,T_c$, using $L = 128$. Inset: Plot showing the dependence of the saturated domain length, $\ell_{\rm max}$, on q. The solid line is a fit to the form $\ell_{\rm max} = Kq^{\eta}$, that yields $\eta = -0.45$. The dashed line shows the expected power-law decay with an exponent $-1/2$, corresponding to the behavior $\ell_{\rm max} \sim q^{-1/d}$. (right) Demonstration of the fact that the finite-size scaling curves in domain growth for different q can be collapsed onto a single master curve, such that there exists a universal finite-size scaling function $Y(y_q)$, when plotted against the modified scaling variable y_q. The values of the metric factor f_q, used to obtain the optimum collapse of data, are tabulated inside the figure. The results correspond to $L = 128$ and $T = 0.7\,T_c$. The solid line represents the behavior $Y(y_q) \sim y_q^{-\alpha}$, with $\alpha = 0.32$.

This we achieve via the application of appropriate finite-size scaling analysis [3, 4]. Like in critical phenomena [5], this technique allows one to obtain a precise estimation of the growth exponent α, without using very large systems. We observe that finite-size effects are weak, as in the Ising model [3, 4]. By considering an initial domain length [3] in the scaling ansatz, we show that one obtains the Lifshitz-Slyozov growth, for all q, from rather early time, like in the Ising case. This was previously confirmed [2] to be true in the asymptotic limit, via the application of a renormalization group method of analysis to the Monte Carlo results.

Furthermore, we show that the growth for different q could be described by a universal finite-size scaling function, with a nonuniversal, q-dependent, metric factor [6], arising from the amplitude of growth (that varies with q), see Fig. 10.18 (right). In a similar way, for a range of quench depth, viz. $T \in [0.5T_c, 0.8T_c]$, we show that the growth follows Lifshitz-Slyozov law, irrespective of the temperature, for all q. This also can be described by a similar common finite-size scaling function. We have also shown the equivalence between the evolution of a equi-proportion q-component mixture and an off-critical binary mixture with composition of the minority species $m_c = 1/q$.

[1] S. Majumder et al.: Leipzig/Bangalore preprint (2018), submitted to Phys. Rev. E
[2] S.K. Das, S. Puri: Phys. Rev. E **65**, 026141 (2002)
[3] S. Majumder, S.K. Das: Phys. Rev. E **81**, 050102(R) (2010)
[4] S.K. Das et al.: Europhys. Lett. **97**, 66006 (2012).
[5] M.E. Fisher: *The theory of critical point singularities*, in *Critical Phenomena*, Proc.

51st Enrico Fermi Summer School, Varenna, Italy, edited by M.S. Green (Academic Press, London, 1971), p. 1
[6] S. Majumder et al.: Soft Matter **13**, 1276 (2017)

10.14 Adsorption and diffusion of H_2/CH_4 gas mixture in ZIF-90

T. Chokbunpiam*, S. Fritzsche, J. Caro†, C. Chmelik‡, W. Janke, S. Hannongbua§

*Department of Chemistry, Faculty of Science, Ramkhamhaeng University, Bangkok 10240, Thailand
†Institute of Physical Chemistry and Electrochemistry, Leibniz University Hannover, Germany
‡Peter-Debye-Institut für Physik der weichen Materie, Universität Leipzig, Germany
§Computational Chemistry Unit Cell (CCUC), Department of Chemistry, Faculty of Science, Chulalongkorn University, Bangkok 10330, Thailand

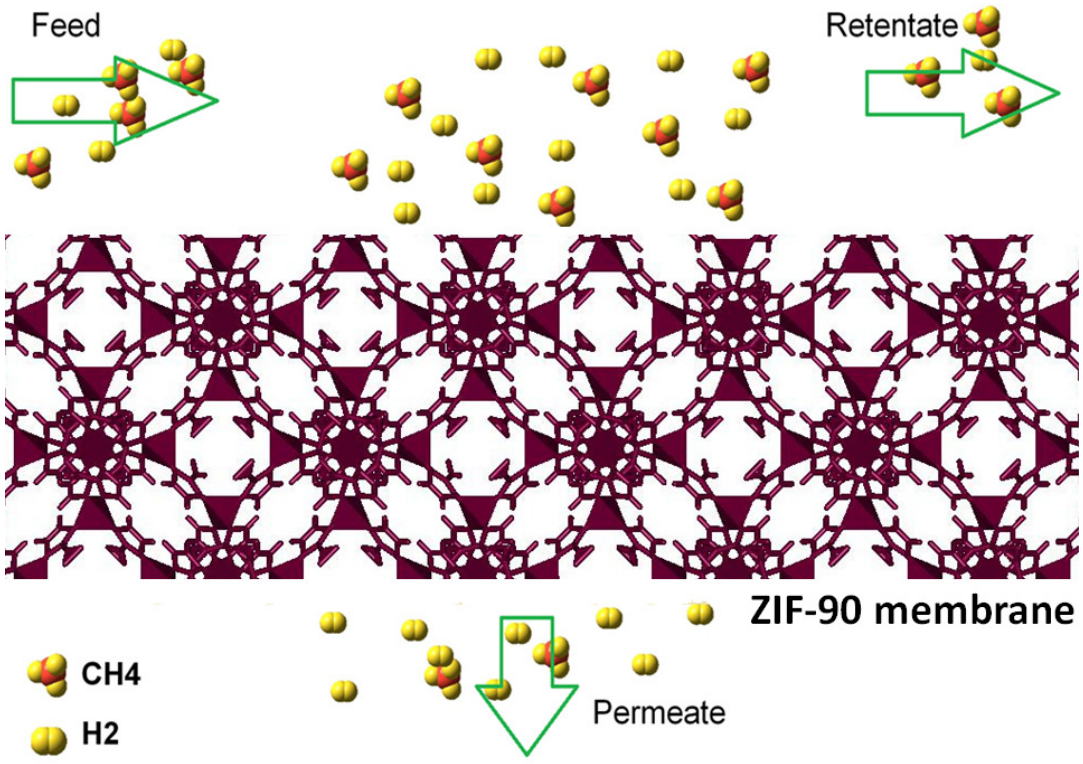

Figure 10.19: Illustration of the considered experimental setup based on a ZIF-90 membrane.

Adsorption and diffusion of the gas mixture H_2/CH_4 in the metal-organic framework (MOF) of structure type zeolitic imidazolate framework-90 (ZIF-90) [1, 2] are revisited in this project [3]. The considered setup is sketched in Fig. 10.19. While the adsorption can successfully be examined in Gibbs ensemble Monte Carlo (GEMC) simulations using the common approximation of a rigid lattice, the dynamics of methane in ZIF-90 is remarkably influenced by the lattice flexibility [4]. Molecular dynamics (MD)

simulations not only show a strong influence of the lattice flexibility on the diffusion of methane but even find a slight structural phase transition of the lattice. This structural change appeared at higher temperatures and was not caused by the content of guest molecules like in most former discoveries of gate opening. For prediction of mixed gas ZIF-90 membrane selectivity, the adsorption and diffusion results show that the high CH_4 adsorption selectivity is overcompensated by the high H_2 mobility. The comparison of our results for the H_2/CH_4 membrane selectivity with experimental findings from mixed gas permeation through supported ZIF-90 membranes shows better agreement than other simulations that use a rigid lattice for MD [3]. Also, the increase of the membrane selectivity by increased temperature could be found.

[1] W. Morris et al.: J. Am. Chem. Soc. **130**, 12626 (2008)
[2] A. Huang et al.: J. Am. Chem. Soc. **132**, 15562 (2010)
[3] T. Chokbunpiam et al.: J. Phys. Chem. C **121**, 10455 (2017)
[4] V.T. Phuong et al.: Microporous Mesoporous Mater. **235**, 69 (2016)

10.15 Self-avoiding walks on critical percolation clusters in 2 – 7 dimensions

N. Fricke, W. Janke

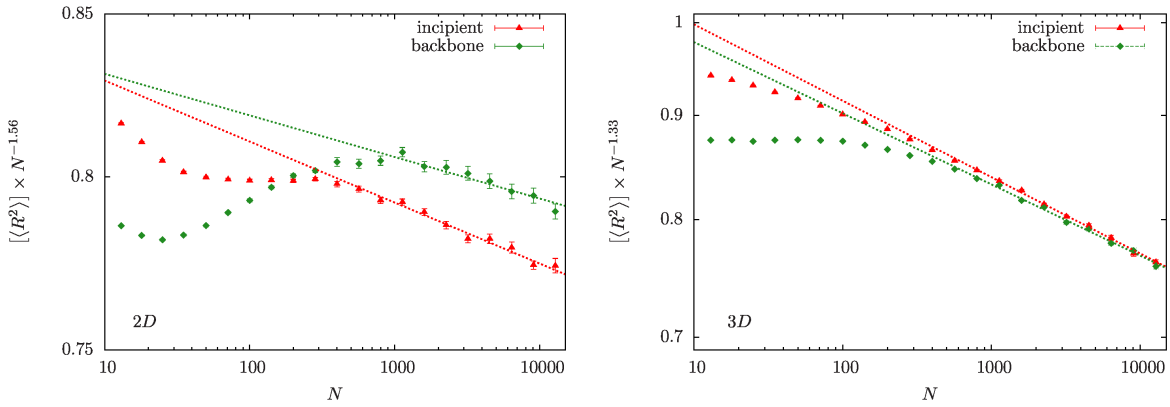

Figure 10.20: Scaled disorder averages of the mean squared end-to-end distance as a function of the number of SAW steps on critical clusters and cluster backbones in (a) 2D and (b) 3D on a double-logarithmic scale. The values have been divided by $\approx N^{2\nu_{pc}}$ for better visibility. Straight lines show least-squares power-law fits to the data in the range $N = 800 - 12\,800$ for 2D and 3D incipient clusters and $N = 1131 - 12\,800$ for 3D backbones.

Self-avoiding walks (SAWs) on critical percolation clusters are a simple model for polymers in highly disordered environments such as porous rocks or a biological cell [1, 2]. The system is also appealing from a theoretical perspective as it combines two of the most ubiquitous models from statistical physics. It has therefore been studied

intensely in the past both analytically and numerically. However, despite its conceptual simplicity, the problem proved extremely challenging. Few reliable predictions exist for the SAWs' scaling exponents, and our qualitative understanding of the model is also still limited. In particular, it is unclear how the disorder and the medium's fractal structure, characterized by its various fractal dimensions, impacts the SAWs' asymptotic scaling behavior. This understanding is crucial when we want to generalize from the results and make predictions for real-world systems.

The main difficulty for numerical investigation of the problem can be overcome by making use of the self-similar geometry of critical percolation clusters to factorize the problem, in an approach that we called scale-free enumeration (SFE) [3, 4]. In two preceding studies, we had used this method to investigate SAWs on critical percolation clusters in 2D [5] and 3D [6]. Recently we have expanded this perspective and looked at systems in up to 7D [7], above the supposed upper critical dimension of $D_{\mathrm{uc}} = 6$.

We mainly focused on the scaling of the increase of the mean squared end-to-end distance with the number of steps,

$$[\langle R^2 \rangle] \sim N^{2\nu} \tag{10.5}$$

where ν is a universal scaling exponent. The reduced time complexity of our recently introduced SFE method allows us to exactly enumerate SAWs of over $N = 10^4$ steps, easily amounting to 10^{2000} conformations. Previously, only up to $N = 45$ steps on 2D clusters and 40 steps on 3D clusters could be handled by the standard "brute-force" enumeration method.

In 2D and 3D we studied walk lengths increasing in multiplicative steps of $\sqrt{2}$ from $N = 13$ up to $N = 12\,800$ ($= 100 \times 2^7$). For each length we took independent samples of at least 5×10^4 randomly generated percolating clusters and backbones. The results for the mean squared end-to-end distance as a function of N and least-squares fits of Eq. (10.5) to the data are shown in Fig. 10.20 on a double-logarithmic scale. The y-axes have been rescaled by $\approx N^{-2\nu_{pc}}$, so that the slopes are close to zero and more details are visible. Note that while the conformational averages are evaluated exactly, we still have statistical fluctuations of the disorder averages reflected by the error bars.

Repeating this procedure in 4D – 7D, we finally arrive at Fig. 10.21, where we have also included a comparison with analytical predictions from various sources.

[1] D. Ben-Avraham, S. Havlin: *Diffusion and Reactions in Fractals and Disordered Systems* (Cambridge University Press, Cambridge, 2000)
[2] B.K. Chakrabarti (ed.): *Statistics of Linear Polymers in Disordered Media* (Elsevier, Amsterdam, 2005)
[3] N. Fricke, W. Janke: Eur. Phys. J. – Special Topics **216**, 175 (2013)
[4] N. Fricke, W. Janke: *How to enumerate* 10^{1000} *self-avoiding walk conformations on a critical percolation cluster*, Leipzig preprint (2017), to be published
[5] N. Fricke, W. Janke: Europhys. Lett. **99**, 56005 (2012)
[6] N. Fricke, W. Janke: Phys. Rev. Lett. **113**, 255701 (2014); Phys. Rev. Lett. **115**, 149902 (2015)
[7] N. Fricke, W. Janke: J. Phys. A: Math. Theor. **50**, 264002 (2017)
[8] C. von Ferber et al.: Phys. Rev. E **70**, 035104 (2004)
[9] H.K. Janssen, O. Stenull: Phys. Rev. E **75**, 020801 (2007); Phys. Rev. E **85**, 051126 (2012)

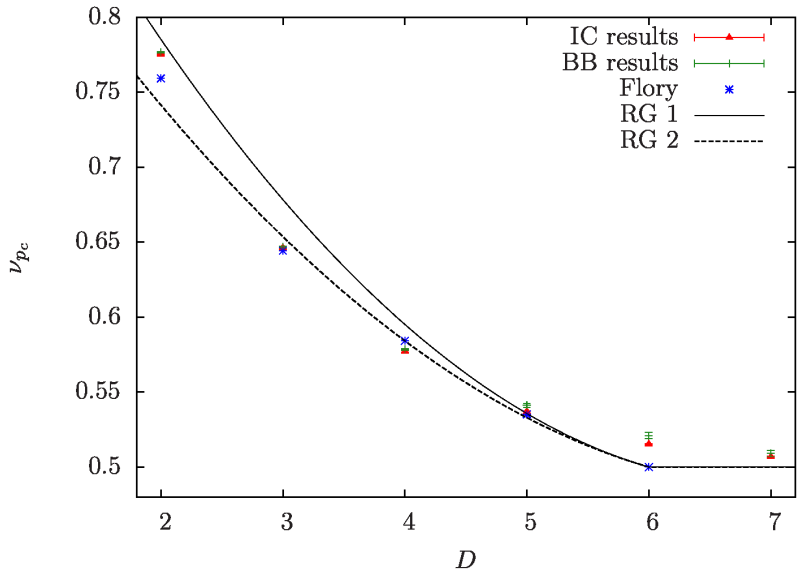

Figure 10.21: Results for ν_{p_c} on incipient clusters (IC, red) and backbones (BB, green) as a function of dimension compared to various analytical predictions. The blue asterisks correspond to Flory estimates [7]. The lines represent the field-theory estimates from [8] (RG1, solid) and [9] (RG2, dashed).

10.16 Percolation on square lattices with long-range correlated defects

J. Zierenberg*, N. Fricke, M. Marenz, F.P. Spitzner, V. Blavatska†, W. Janke

*Max Planck Institute for Dynamics and Self-Organization, Am Fassberg 17, 37077 Göttingen, Germany

†Institute for Condensed Matter Physics of the National Academy of Sciences of Ukraine, 79011 Lviv, Ukraine

Structural obstacles (impurities) play an important role for a wide range of physical processes as most substrates and surfaces in nature are rough and inhomogeneous [1]. For example, the properties of magnetic crystals are often altered by the presence of extended defects in the form of linear dislocations or regions of different phases. Another important class of such disordered media are porous materials, which often exhibit large spatial inhomogeneities of a fractal nature. Such fractal disorder affects a medium's conductivity, and diffusive transport can become anomalous [2, 3]. This aspect is relevant, for instance, for the recovery of oil through porous rocks [4], for the dynamics of fluids in disordered media [5], or for our understanding of transport processes in biological cells [6].

In nature, inhomogeneities are often not distributed completely at random but tend to be correlated over large distances. To understand the impact of this, it is useful to consider the limiting case where correlations asymptotically decay by a power law rather than exponentially with distance:

$$C(r) \sim |r|^{-a} \tag{10.6}$$

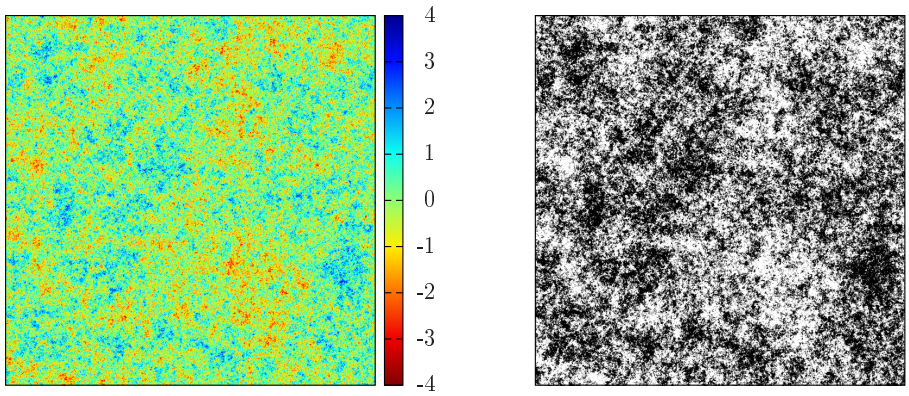

(a) (b)

Figure 10.22: Correlated continuous variables on a $2^{11} \times 2^{11}$ lattice for (a) correlation strength $a = 0.5$ and (b) corresponding discrete lattice at the percolation threshold with defects shown in black.

where a is the correlation parameter. If a is smaller than the spatial dimension D, the correlations are considered long-range or "infinite." An illustration of such power-law correlations for continuous and discrete site variables on a square lattice is shown in Fig. 10.22.

In this project we studied long-range power-law correlated disorder on square and cubic lattices [7, 8]. In particular, we obtained high-precision results for the percolation thresholds and the fractal dimension of the largest clusters as a function of correlation parameter a. The correlations are generated using a discrete version of the Fourier filtering method [9]. We consider two different metrics to set the length scales over which the correlations decay, showing that the percolation thresholds are highly sensitive to such system details. By contrast, we verify that the fractal dimension d_f is a universal quantity and unaffected by the choice of metric. We also show that for weak correlations, its value coincides with that for the uncorrelated system. In two dimensions we observe a clear increase of the fractal dimension with increasing correlation strength, approaching $d_f \to 2$. The onset of this change, however, does not seem to be determined by the extended Harris criterion.

[1] D. Avnir et al.: Nature (London) **308**, 261 (1984)
[2] J.-P. Bouchaud, A. Georges: Phys. Rep. **195**, 127 (1990)
[3] I. Goychuk et al.: Phys. Rev. E **96**, 052134 (2017)
[4] M. Sahimi: *Flow and Transport in Porous Media and Fractured Rock* (VCH, Weinheim, 1995)
[5] M. Spanner et al.: Phys. Rev. Lett. **116**, 060601 (2016)
[6] F. Höfling, T. Franosch: Rep. Prog. Phys. **76**, 046602 (2013)
[7] N. Fricke et al.: Condens. Matter Phys. **20**, 13004 (2017)
[8] J. Zierenberg et al.: Phys. Rev. E **96**, 062125 (2017)
[9] H.A. Makse et al.: Phys. Rev. E **53**, 5445 (1996)

10.17 Dynamical greedy algorithm for the Edwards-Anderson model

S. Schnabel, W. Janke

One of the most intuitive and natural approaches to optimization problems is realized by so-called greedy algorithms. These methods create trajectories in the space of possible solution by always choosing the next step such that the energy is maximally reduced (or a fitness function maximally increased). Naturally, this will usually not find the global optimum, just as starting at a random spot and always walking uphill will usually not lead a wanderer to the summit of Mt. Everest. Therefore, in practice many attempts with randomly created starting points are made and if the problem is not too difficult the global optimum may be found this way.

On the other hand, there is practically no chance of success if the energy landscape is as complicated and possesses as many local minima as in the case of the Edwards-Anderson spin-glass model [1], whose Hamiltonian is given by

$$\mathcal{H} = \sum_{\langle ij \rangle} J_{ij} S_i S_j,$$

where the spins can take two values $S_i \in \{-1, 1\}$ and adjacent spins interact via normally distributed random couplings J_{ij}. If such a model on a three-dimensional cubic lattice of 1000 spins is considered, about 10^{30} attempts would be necessary in order to find the ground state this way.

However, the greedy algorithm can still be a very helpful tool, since it is a comparatively simple and reliable method to reach states of low energy. We devised a method to efficiently update the greedy algorithm, i.e., to reuse the data created during a minimization from a configuration $\mathbf{S}$ to the configuration $\mathbf{S}_{\min}$ to obtain the result $\mathbf{S}'_{\min}$ of the minimization from a configuration $\mathbf{S}'$ which differs from $\mathbf{S}$ only in the values of one or very few spins [2]. If furthermore, both, the terminal configuration, delivered by the greedy algorithm, and its energy are understood as attributes of the starting configuration, it is possible to use the energy of the minimized configurations $\mathbf{S}_{\min,t}$ to steer a path in the space of starting configurations $\mathbf{S}_t$.

A simple application is to apply the greedy algorithm again: It is tested which alteration (e.g., which single spin flip) of the starting configuration will reduce the energy of the *minimized* configuration by the largest amount and this locally optimal step is performed. Repeating this simple procedure as long as viable as a "second order greedy algorithm" will lead to much lower energies albeit not the ground state.

Alternatively, the energy of the minimized configuration can be used as argument for the occupation probability for a generalized ensemble [3]:

$$P(\mathbf{S}) = P(\mathbf{S}_{\min}),$$

which can then be sampled using Monte Carlo techniques. All states in the same "valley" in the energy landscape, i.e., all configuration which minimize to the same local energy minimum, now occur with the same probability and the barriers of high energy which greatly hamper standard Monte Carlo simulations simply vanish. In consequence, the configuration space is sampled much more easily and the performance of ground-state search is greatly improved.

[1] S.F. Edwards, P.W. Anderson: J. Phys. F **5**, 965 (1975)
[2] S. Schnabel, W. Janke: Comput. Phys. Commun. **220**, 74 (2017)
[3] D.J. Wales: J. Phys. Chem. A **101**, 5111 (1997)

10.18 Distribution of local minima for the Edwards-Anderson model

S. Schnabel, W. Janke

In statistical physics the term "complex behavior" is usually used to characterize systems that posses a rough free-energy landscape with many metastable states. This can be the result of competing interactions on different scales like in the case of protein folding or it may arise from quenched disorder as for spin glasses. A conceptually simple model for such a system is the Edwards-Anderson model [1], whose Hamiltonian is given by

$$\mathcal{H} = \sum_{\langle ij \rangle} J_{ij} S_i S_j,$$

where the spins sit on the sites of a cubic lattice, can take two values $S_i \in \{-1, 1\}$, and adjacent spins interact via normally distributed random couplings J_{ij}. Since these interactions can be either ferromagnetic (positive) or antiferromagnetic (negative), there is no trivial order established at low temperatures. Instead, many very different pure states might coexist, each one of them corresponding to a minimum in free energy.

Albeit not identical, minima of the energy, i.e. spin configurations that are stable against single spin flips are closely related to these pure states. It is thought that minima in energy form the end-points of hierarchical tree-like structures with branches corresponding to different pure states. Understanding their properties might, therefore, improve our understanding of the behavior of the system. However, they have proven to be a very demanding subject of inquiry.

We have developed an advanced Monte Carlo method that in its basic form allows to sample the local energy minima with uniform distribution, i.e., each minimum configuration is occupied with equal probability. This is achieved by establishing within the simulation the combination of a spin configuration together with a random minimization thereof. I.e., the repeated flipping of spins with positive energy until a local minimum is reached. If one now alters the spin configuration and the parameters of the minimization in a suitable way it is possible to ensure that all local minima are equally likely found this way. This corresponds to 'simple sampling' in the space of local minima. It is also possible to perform 'importance sampling' by including suitable weight functions. We can for instance sample a canonical distribution of local minima in energy by including the Boltzmann weight.

A basic application of this method is the measurement of the distribution of the energy minima. Since existing algorithms are unable to perform such a task, there is no numerical data for comparison. However, we can use our results to test analytical approximations [2] that are based on the expansion of meanfield solutions. We found that there are considerable deviations (Fig. 10.23) [3]. In fact, the distributions much more closely – although not entirely – resemble Gaussian distributions.

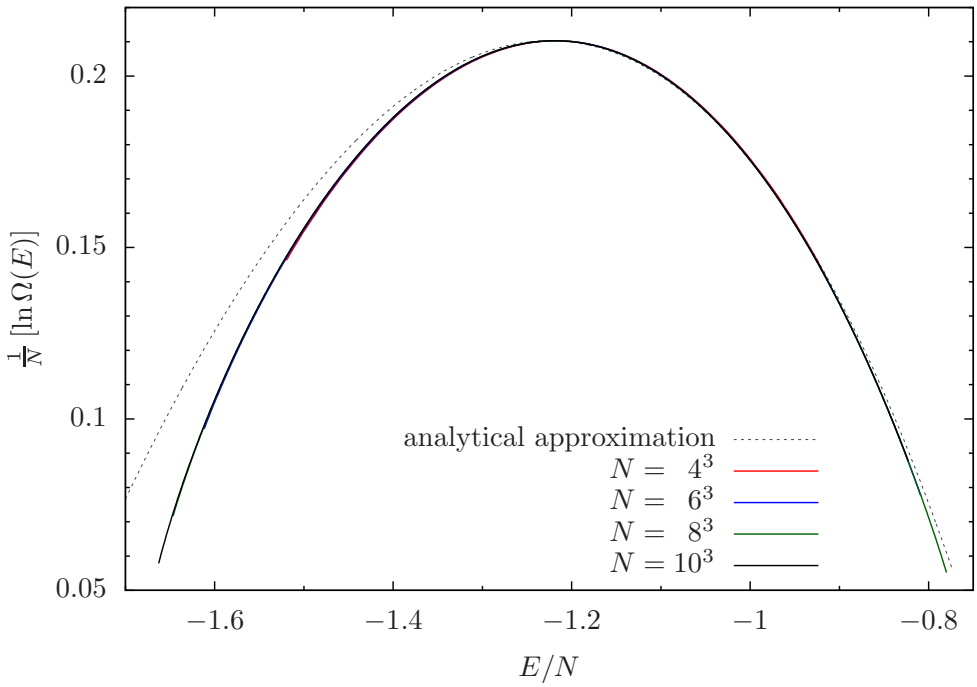

Figure 10.23: The distribution of local minima for different system sizes and the analytical approximation.

[1] S.F. Edwards, P.W. Anderson: J. Phys. F **5**, 965 (1975)
[2] A.J. Bray, M.A. Moore: J. Phys. C **14**, 1313 (1981)
[3] S. Schnabel, W. Janke: Phys. Rev. B **97**, 174204 (2018)

10.19 Spin glasses with variable frustration

R. Kumar, M. Weigel*, W. Janke

*Applied Mathematics Research Centre, Coventry University, England, UK

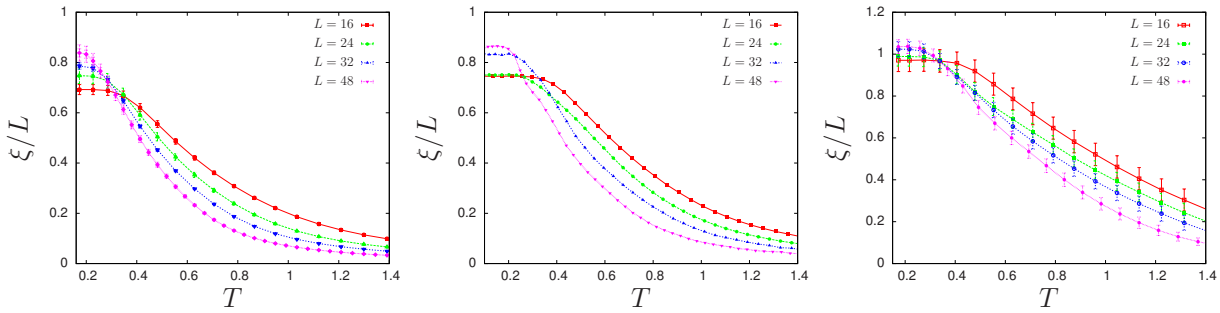

Figure 10.24: Correlation length as a function of temperature for (a) stochastically frustrated system, (b) a system with 46% frustration, and (c) a system with 20% frustration.

Together with randomness, frustration is believed to be a crucial prerequisite for the occurrence of glassy behaviour in spin systems. The degree of frustration is normally the result of a chosen distribution of exchange couplings in combination with the structure of the lattice under consideration. Here, however, we discuss a process for tuning the frustration content of the Edwards-Anderson model on arbitrary lattices. With the help of extensive parallel-tempering Monte Carlo simulations we study such systems on the square lattice and compare the outcomes to the predictions of a recent study employing the Migdal-Kadanoff real-space renormalization procedure [1]. We use a cluster algorithm proposed in [2] in order to reduce the equilibration time. The phase transition studies are done by looking at the divergence of the correlation length, see Fig. 10.24. The results are benchmarked by comparing to the stochastic case described in [3]. We also study the freezing temperature of such a system and observe a different behaviour compared to the stochastically frustrated case. Studies on larger system sizes are very crucial to confirm these differences.

We find that the divergence of the correlation length occurs at non-zero finite temperature for the 2D Ising spin glass. This gives hints of a phase transition, but such transitions have to be studied carefully in order to fully understand the phases [4].

[1] E. Ilker, A.N. Berker: Phys. Rev. E **89**, 042139 (2014)
[2] J. Houdayer: Eur. Phys. J. B **22**, 479 (2001)
[3] H.G. Katzgraber, L.W. Lee: Phys. Rev. B **71**, 134404 (2005)
[4] A. Hartmann: Phys. Rev. B **67**, 214404 (2003)

10.20 Random field q-state Potts model: Ground states and low-energy excitations

R. Kumar[*], M. Kumar[†‡], M. Weigel[§], V. Banerjee[‡], S. Puri[†], W. Janke

[*]Doctoral College for the Statistical Physics of Complex Systems, Leipzig-Lorraine-Lviv-Coventry ($\mathbb{L}^4$)
[†]School of Physical Sciences, Jawaharlal Nehru University, New Delhi – 110067, India
[‡]Department of Physics, Indian Institute of Technology, Hauz Khas, New Delhi – 110016, India
[§]Applied Mathematics Research Centre, Coventry University, England, UK

While the ground-state (GS) problem for the random-field Ising model is polynomial and can be solved by using a number of well-known algorithms for maximum flow [1–4], the analogue random-field q-state Potts model with $q \geq 3$ corresponds to a multi-terminal flow problem that is known to be NP hard. Hence an efficient exact algorithm is extremely unlikely to exist [5]. Still, it is possible to employ an embedding of binary degrees of freedom into the Potts spins to use graph-cut methods (GCMs) to solve the corresponding ground-state problem approximately with polynomial methods. It is shown in this project [6] that this works relatively well. We compare results produced by this heuristic algorithm to energy minima found by an appropriately tuned parallel tempering method that is configured to find ground states for the considered system sizes with high probability. The method based on graph cuts finds the same states in

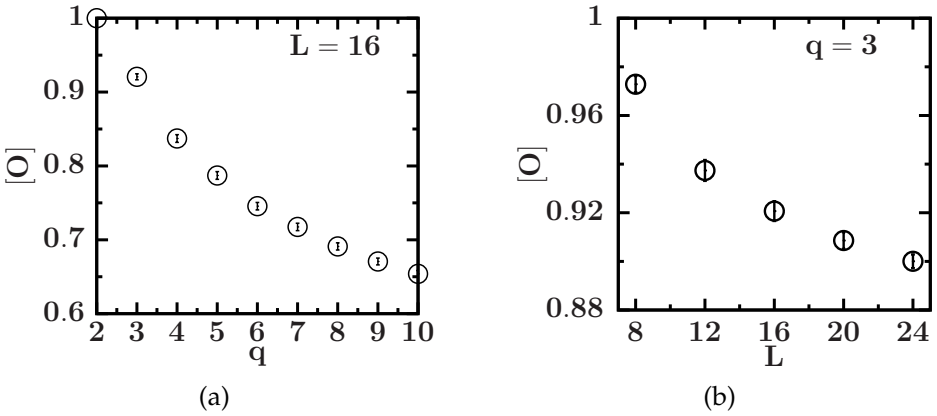

Figure 10.25: Overlap between the lowest states found by graph-cut methods (GCM) and the putative ground state (a) as a function of the number of Potts states q and (b) as a function of system size L.

a fraction of the time. The new method is used for a first exploratory study of the random-field Potts model in $d = 2, 3$.

We observe that the probability of finding a ground state decreases exponentially with q for GCM, but for parallel tempering this decay is linear [Fig. 10.25(a)]. Hence, GCM is more suitable for lower q studies. We also find that the lower energies found by GCM are very close to the ground state and the excess energy is very small. The probability of finding the ground state falls exponentially with the system size, whereas for GCM it falls linearly [Fig. 10.25(b)]. Therefore, GCM is better suited for studying larger system sizes. This is one very good feature of GCM as for the smaller system sizes we have larger finite-size effects. The overlap between the states found by GCM and the ground state is observed to be very large. Hence, we conclude that GCM produces the approximate GS which can be treated as an exact GS for sufficiently small q ($q = 3, 4$) for studying the critical behaviour and ground-state morphologies.

[1] G.P. Shrivastav et al.: Europhys. Lett. **96**, 36003 (2011)
[2] G.P. Shrivastav et al.: Phys. Rev. E **90**, 032140 (2014)
[3] G.P. Shrivastav et al.: Eur. Phys. J. E **37**, 98 (2014)
[4] V. Banerjee et al.: Ind. J. Phys. **88**, 1005 (2014)
[5] J.C. Angles d'Auriac et al.: J. Physique Lett. **46**, L173 (1985)
[6] M. Kumar et al.: Phys. Rev. E **97**, 053307 (2018)

10.21 Gonihedric plaquette models of Fuki-Nuke type: Boundary conditions and non-local constraints

M. Müller, D.A. Johnston*, W. Janke

*Department of Mathematics and the Maxwell Institute for Mathematical Sciences, Heriot-Watt University, Edinburgh, Scotland, UK

An anisotropic limit of the $3d$ plaquette Ising model, in which the plaquette couplings in one direction were set to zero, was solved for free boundary conditions by Suzuki [1],

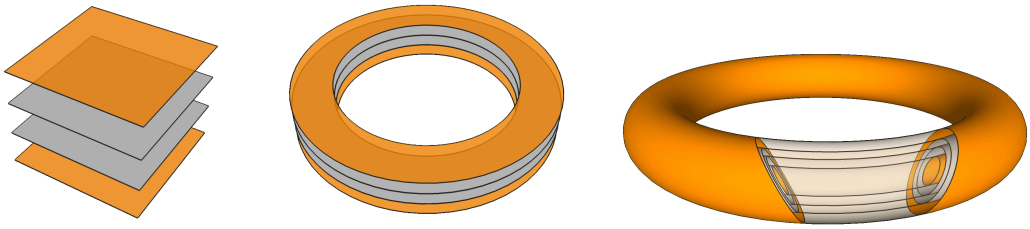

Figure 10.26: Fuki-Nuke models with free boundary conditions in one direction permit different topology of the lattice. We sketch the layers of independent layers of spins: (a) free boundary conditions in *all* directions, (b) periodic boundary conditions are set in one, and only one direction, and (c) periodic boundary conditions are set in both other directions.

who later dubbed it the fuki-nuke, or "no-ceiling", model. Defining new spin variables as the product of nearest-neighbour spins transforms the Hamiltonian into that of a stack of (standard) $2d$ Ising models and reveals the planar nature of the magnetic order, which is also present in the fully isotropic $3d$ plaquette model [2]. More recently, the solution of the fuki-nuke model was discussed for periodic boundary conditions applied to the spin lattice, which require a slightly different approach to defining the product spin transformation, by Castelnovo et al. [3].

We find that the essential features of the differences between free and periodic boundary conditions when using a product spin transformation are already present in the $1d$ Ising model [4], which thus provides an illuminating test case for its use in solving plaquette spin models and an alternative method for solving the $1d$ Ising model with periodic boundary conditions.

We clarify the exact relation between partition functions expressed in terms of the original and product spin variables for the $1d$ Ising model, $2d$ plaquette and $3d$ fuki-nuke models with free and periodic boundary conditions. Representing graphically the combinatorial factors that contribute to the partition function, we are able to solve the $2d$ plaquette model with free, periodic and helical boundary conditions and various combination of these in x- and y-directions, see Fig. 10.26. The various exactly solved examples illustrate how correlations can be induced in finite systems as a consequence of the choice of boundary conditions.

For the three-dimensional fuki-nuke model the exact finite-size partition function may be written as a product of $2d$ Ising partition functions in the case of free boundary conditions using the product variable transformation. A similar decoupling is not manifest with periodic boundary conditions, where all n-point $2d$ Ising spin-spin correlations also contribute to the expression for the $3d$ fuki-nuke partition function. As illustrated in Fig. 10.27, this can be most easily understood in a pictorial way by employing the high-temperature expansion/dimer approach. It is perhaps worth remarking that the discussion of the fuki-nuke model in [3] conflates the discussion of free and periodic boundary conditions, although the overall picture of a $2d$ Ising-like transition in the thermodynamic limit of the $3d$ fuki-nuke model remains, of course, correct in both cases.

A further consequence of the planar flip symmetry is found in a Hamiltonian related to the quantum dual of the plaquette model. This fits into the general framework developed in [5, 6] in which novel fracton topological phases are constructed by gauging

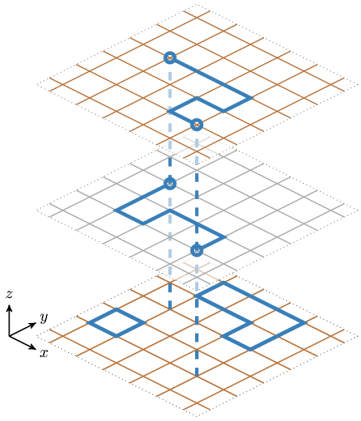

Figure 10.27: A dimer configuration of the Fuki-Nuke model with $L_z = 3$ that can contribute to the partition function, although the mid and top layer have dangling ends (symbolised by open circles). These are connected through the constraints (dashed vertical lines) and contribute to the two-point function in each of the two upper layers. Notice that additional, standard $2d$ Ising loops may appear, as those shown in the bottom layer, which are the standard contributions to the partition function of each layer.

symmetries acting on subsystems of dimension $2 \leq d_s < d$. Since the spin-flip symmetry in the $3d$ plaquette model acts on $2d$ planes it has precisely this property. The procedure for constructing the fracton Hamiltonian follows closely that of the Kitaev toric code, giving commuting electric and magnetic operators. We outline the role played by the spin-flip symmetry in enabling the appearance of fracton topological defects in a Hamiltonian related to the dual of the quantum version of the model [7].

[1] M. Suzuki: Phys. Rev. Lett. **28**, 507 (1972)
[2] M. Mueller et al.: Nucl. Phys. B **894**, 1 (2015); D.A. Johnston et al.: Mod. Phys. Lett. **B29**, 1550109 (2015)
[3] C. Castelnovo et al.: Phys. Rev. B **81**, 184303 (2010)
[4] M. Mueller et al.: Nucl. Phys. B **914**, 388 (2017)
[5] S. Vijay et al.: Phys. Rev. B **94**, 235157 (2016)
[6] D.J. Williamson: Phys. Rev. B **94**, 155128 (2016)
[7] D.A. Johnston et al.: Eur. Phys. J. – Special Topics **226**, 749 (2017)

10.22 The two-dimensional Blume-Capel model: Scaling and universality

J. Zierenberg[*], N.G. Fytas[†], M. Weigel[†], W. Janke, A. Malakis[‡]

[*]Max Planck Institute for Dynamics and Self-Organization, Am Fassberg 17, 37077 Göttingen, Germany
[†]Applied Mathematics Research Centre, Coventry University, England, UK
[‡]Department of Physics, University of Athens, Greece

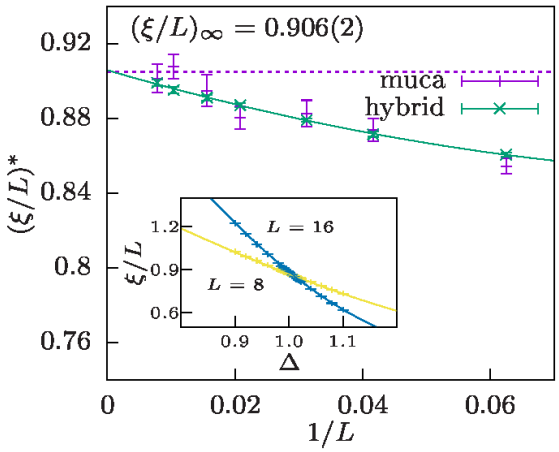

Figure 10.28: Finite-size scaling at $T = 1.398$ of the correlation length crossings $(\xi/L)^*$. The dashed horizontal shows the asymptotic value for the square-lattice Ising model with periodic boundaries. Compared are data from the multicanonical ("muca") and hybrid methods. The line shows a quadratic fit in $1/L$ to the data from the hybrid method. The inset demonstrates the crossing point of $L = 8$ and $L = 16$ obtained from both the muca (lines) and hybrid (data points) method.

The Blume-Capel model [1, 2] is a perfect test model for studies of phase transitions. We consider this spin-one Ising model in a crystal field on a square lattice in two dimension (2D), described by the Hamiltonian

$$\mathcal{H} = -J \sum_{\langle ij \rangle} \sigma_i \sigma_j + \Delta \sum_i \sigma_i^2 = E_J + \Delta E_\Delta \,. \tag{10.7}$$

We investigate the behaviour in the vicinity of the first-order and second-order regimes of the ferromagnet-paramagnet phase boundary, respectively [3]. To achieve high-precision results, we utilize a combination of (i) a parallel version of the multicanonical algorithm and (ii) a hybrid updating scheme combining Metropolis and generalized Wolff cluster moves. These techniques are combined to study for the first time the correlation length ξ of the model, using its scaling with system size L in the regime of second-order transitions to illustrate universality through the observed identity of the limiting value of ξ/L with the exactly known result for the Ising universality class, see Fig. 10.28.

In contrast to most previous work, we focused on crossing the phase boundary at constant temperature by varying the crystal field Δ [4]. Employing a multicanonical scheme in Δ allowed us to get results as continuous functions of Δ and to overcome the free-energy barrier in the first-order regime of the transitions. A finite-size scaling analysis based on a specific-heat-like quantity and the magnetic susceptibility provided us with precise estimates for the transition points in both regimes of the phase diagram that compare very well to the most accurate estimates of the current literature. In the first-order regime, we found a somewhat surprising $1/L$ correction in the scaling of the conventionally defined magnetic susceptibility χ. As it turns out, this is due to the explicit symmetry breaking by using the absolute value of the magnetisation (i.e., $|M|$ instead of M) in the definition of χ. For a modified symmetry breaking prescription that leaves the disordered peak invariant, this correction disappears. It would be interesting

to see whether similar corrections are found in other systems with first-order transitions, such as the Potts model.

[1] M. Blume: Phys. Rev. **141**, 517 (1966)
[2] H.W. Capel: Physica (Utr.) **32**, 966 (1966)
[3] J. Zierenberg et al.: Eur. Phys. J. – Special Topics **226**, 789 (2017)
[4] J. Zierenberg et al.: Phys. Rev. E **91**, 032126 (2015)

10.23 Finite-size scaling properties of the real microcanonical ensemble

P. Schierz, J. Zierenberg*, W. Janke

*Max Planck Institute for Dynamics and Self-Organization, Am Fassberg 17, 37077 Göttingen, Germany

The definition of the microcanonical ensemble can be found in any standard text book on statistical physics. Usually this ensemble is quickly dismissed in favor of the canonical ensemble since it is quite unrealistic for most physical systems in a laboratory. In the literature on phase transitions, however, this ensemble gained some interest also due to the development of the generalized ensemble methods MUCA [1, 2] and Wang-Landau [3]. Here, however, one refers to the microcanonical ensemble at constant *potential* energy while the "real" microcanonical ensemble was originally defined at constant *total* energy.

We previously investigated the behaviour of molecular dynamics and Monte Carlo simulations within this ensemble and made the interesting observation that a Monte Carlo simulation in this ensemble sampled the first-order aggregation transition in a very efficient way [4]. Such a behaviour behaviour was previously described by Martin-Mayor [5] for the temperature-driven first-order phase transition in the Potts lattice model. We further investigated this simulation technique in the real microcanonical ensemble for a continuous Lennard-Jones system and found the same sampling advantage [7]. We reached the same amount of particles with these simulations as with the sophisticated MUCA simulation technique.

In Ref. [6] we were able to develop a framework based on the generalization of the equal-area rule which allowed us to explain the obtained simulation behaviour of the real microcanonical ensemble. For comparison we introduced the transition barrier of an ensemble as

$$B = \ln\left[P^{\mathrm{eqh}}\left(E_p^{\pm}\right)/P^{\mathrm{eqh}}\left(E_p^{0}\right)\right], \tag{10.8}$$

where $P^{\mathrm{eqh}}\left(E_p^{\pm}/E_p^{0}\right)$ denotes the equal-height histogram emerging due to phase coexistence, $E_p^{\pm}$ the positions of the two maxima and E_p^{0} the position of the minimum in between, cf. Fig. 10.29(a). This quantity hence allows one to evaluate how "hard" the first-order transition between two phases is within an ensemble. This framework leads to the conclusion that the barrier in the canonical ensemble is always larger than in the microcanonical ensemble, $B_{\mathrm{NVT}} > B_{\mathrm{NVE}}$. In the microcanonical ensemble the transition

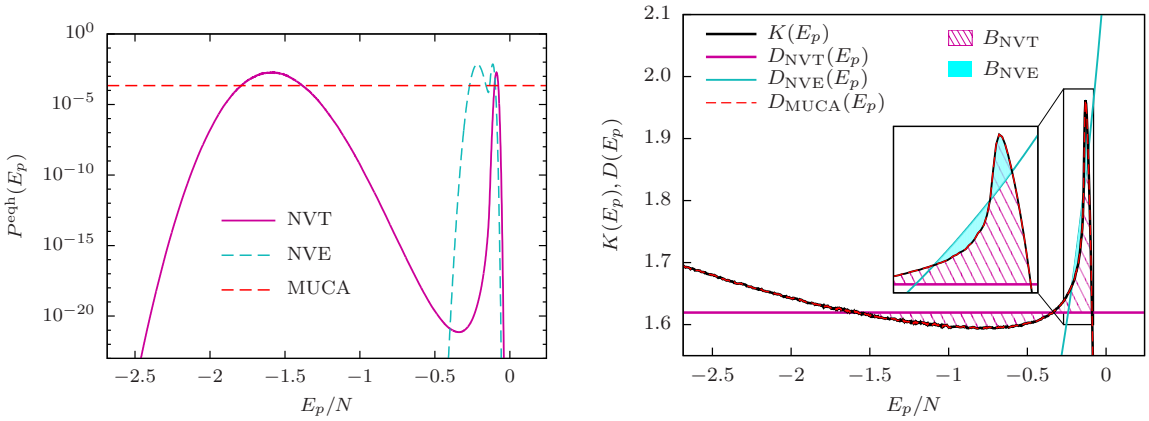

Figure 10.29: (a) The potential-energy histogram at equal height for three different ensembles for the $N = 2048$ Lennard-Jones system [6]. (b) The system dependent quantity $K(E_p)$ and the ensemble dependent $D(E_p)$ for the considered ensembles as defined in [6].

barrier can even vanish as it was observed in [4, 8] for polymer aggregation and by reproducing the data from Ref. [5]. For the example of the Lennard-Jones system with $N = 2048$ particles we discovered that the sampling with the microcanonical ensemble is of the order of $\exp\left(B_{\rm NVT} - B_{\rm NVE}\right) \approx 10^{16}$ more efficient than simulations in the canonical ensemble due to the difference of the barriers. The underlying mechanism is discussed in Ref. [6] and sketched in Fig. 10.29(b).

[1] B.A. Berg, T. Neuhaus: Phys. Lett. B **267**, 249 (1991); Phys. Rev. Lett. **68**, 9 (1992)
[2] W. Janke: Int. J. Mod. Phys. C **03**, 1137 (1992); Physica A **254**, 164 (1998)
[3] F. Wang, D.P. Landau: Phys. Rev. Lett. **86**, 2050 (2001); Phys. Rev. E **64**, 056101 (2001)
[4] P. Schierz et al.: J. Chem. Phys. **143**, 134114 (2015)
[5] V. Martin-Mayor: Phys. Rev. Lett. **98**, 137207 (2007)
[6] P. Schierz et al.: Phys. Rev. E **94**, 021301(R) (2016)
[7] J. Zierenberg et al.: Nat. Commun. **8**, 14546 (2017)
[8] W. Janke et al.: in *Computer Simulation Studies in Condensed-Matter Physics XXX*, eds. D.P. Landau, M. Bachmann, S.P. Lewis, H.-B. Schüttler, J. Phys.: Conf. Ser. **921**, 012018 (2017)

10.24 Stochastic Approximation Monte Carlo versus modified Wang-Landau algorithms: Convergence tests for the Ising model

S. Schneider, M. Müller, W. Janke

The Wang-Landau algorithm [1] has proven to be a very efficient tool for determining the density of states (DOS) of statistical systems near phase transitions where traditional local importance sampling algorithms like the Metropolis algorithm are likely to run into critical slowing down or become trapped in local free-energy minima [2]. It has,

however, been pointed out that the error of the estimator for the DOS obtained by the Wang-Landau algorithm cannot be made arbitrarily small just by using longer simulations [3], the (systematic) error saturates at some (small) value. To overcome this, it has been suggested to change the behaviour of the refinement parameter in the $1/t$ modification ($1/t$-WL) of the Wang-Landau algorithm in order to circumvent the error saturation [4].

Another approach is the Stochastic Approximation Monte Carlo (SAMC) algorithm [5], which works similar to the modified Wang-Landau algorithm regarding the choice of refinement scheme. While the $1/t$ algorithm has been tested for the Ising model, the calculation of multidimensional integrals, and in applications to lattice polymer models, the SAMC algorithm has only been tested for an artificial, non-physical model with a very small number of states [5] and for a special off-lattice polymer model [6]. The standard test case, the Ising model, however, was still missing and we closed this gap [7].

The $1/t$-method inherits the problem of needing to know the range of admissible energies for the considered model from the Wang-Landau algorithm. In SAMC, this needs not to be known beforehand, since histogram checking is not necessary in principle. The SAMC algorithm, on the other hand, sometimes failed to converge in our examined run times. This is caused by the simulation failing to explore the low-energy states. Therefore no flat histogram can be produced, see Fig. 10.30. Since both variants of the Wang-Landau algorithm regularly check the histogram for adequate flatness, it is ensured that all energies are visited at least once. While the SAMC algorithm should converge to the desired distribution if all conditions are met, it is necessary to check if the histogram measured during the simulation was really flat at the end. This dampens the advantage of a predictable run time, since it is possible that a complete run of the algorithm turns out to be unusable due to an inappropriate choice of t_0. Monitoring the flatness of the histogram during the run is no help, because this would introduce a stochastic quantity into the algorithm, making the run time unpredictable and require the same *a-priori* knowledge of the admissible energy range as the Wang-Landau algorithm and its modifications. The rule of thumb for the choice of t_0 given by Liang et al. [5] is violated even by the 128×128 Ising model, showing that finding an appropriate t_0 can be a quite cumbersome task. The $1/t$-WL algorithm suffers from a similar restriction in this regard: While we could not find anything comparable in the Ising model, other studies suggest that the overall convergence behaviour can also be sensitive to the details of the $1/t$-refining scheme for more complicated models [4, 8]. Regarding the common features of the SAMC and $1/t$-WL algorithms, it seems reasonable to assume that the proof of convergence for SAMC also extends to the $1/t$-WL algorithm as well, since their long-time behaviour is the same. Therefore the choice of algorithm to apply to a certain problem is a practical one. With the various refinements allowing it to adapt to *a-priori* unknown energy ranges and to determine the right time for the onset of the $1/t$-refinement, the $1/t$-WL algorithm might be able to overcome its drawback for complicated systems with unknown ground states. SAMC still has the advantage of allowing to generate weights not only according to the density of states, but also according to other distributions [5], which can improve estimators and might prove useful for complex systems like spin glasses or polymers, because sampling with distributions other than the inverse density of states can speed up round trip times significantly [9].

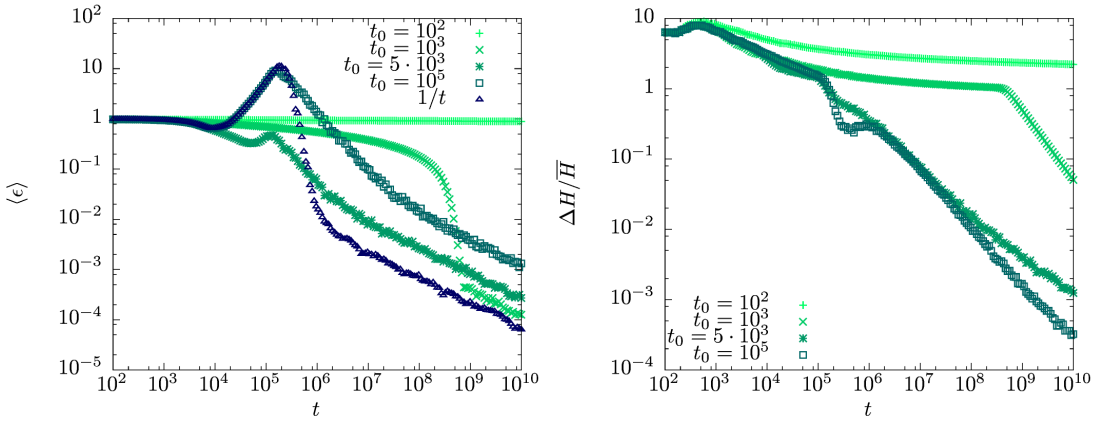

(a) (b)

Figure 10.30: (a) The behaviour of the average deviation from the exact solution $\langle \epsilon(t) \rangle_E$ over MC time t for SAMC for different t_0 and $1/t$-WL simulations of the 16×16 Ising model. Obviously, tweaking the free parameter t_0 is essential for practical convergence. (b) The flatness of the histogram over MC time t for different choices of t_0. All data was obtained by averaging over 40 independent runs of the algorithm to reduce statistical noise.

[1] F. Wang, D.P. Landau: Phys. Rev. Lett. **86**, 2050 (2001); Phys. Rev. E **64**, 056101 (2001)
[2] W. Janke, W. Paul: Soft Matter **12**, 642 (2016)
[3] Q. Yan, J.J. de Pablo: Phys. Rev. Lett. **90**, 035701 (2003)
[4] R.E. Belardinelli, V.D. Pereyra: J. Chem. Phys. **127**, 184105 (2007); Phys. Rev. E **75**, 046701 (2007); C. Zhou, J. Su: Phys. Rev. E **78**, 046705 (2008)
[5] F. Liang: J. Stat. Phys. **122**, 511 (2006); J. Amer. Statist. Assoc. **102**, 305 (2007)
[6] B. Werlich et al.: Comput. Phys. Commun. **186**, 65 (2015)
[7] S. Schneider et al.: Comput. Phys. Commun. **216**, 1 (2017)
[8] A. D. Swetnam, M. P. Allen: J. Comput. Chem. **32**, 816 (2011); T. Wüst, D.P. Landau: Phys. Rev. Lett. **102**, 178101 (2009)
[9] B. Hesselbo, R.B. Stinchcombe: Phys. Rev. Lett. **74**, 2151 (1995); S. Trebst et al.: Phys. Rev. E **70**, 046701 (2004)

10.25 Population annealing: A massively parallel simulation scheme

M. Weigel[*], L.Yu. Barash[†‡], M. Borovský[§], L.N. Shchur[†‡¶], W. Janke

[*]Applied Mathematics Research Centre, Coventry University, England, UK
[†]Landau Institute for Theoretical Physics, 142432 Chernogolovka, Russia
[‡]Science Center in Chernogolovka, 142432 Chernogolovka, Russia
[§]P.J. Šafárik University, Park Angelinum 9, 040 01 Košice, Slovak Republic
[¶]National Research University Higher School of Economics, 101000 Moscow, Russia

The canonical technique for Monte Carlo simulations in statistical physics is importance sampling via a suitably constructed Markov chain [1]. While such approaches are quite

successful, they are not particularly well suited for parallelization as the chain dynamics is sequential, and if replicated chains are used to increase statistics each of them relaxes into equilibrium with an intrinsic time constant that cannot be reduced by parallel work. Population annealing is a sequential Monte Carlo method that simulates an ensemble of system replica under a cooling protocol. This method was first suggested in 2001 by Iba [2] and later on discussed in more detail by Hukushima and Iba [3] as a method to tackle potentially difficult sampling problems, but with no particular view to a parallel implementation. More recently, Machta [4] used a variant that avoids the recording of weight functions through population control in every step. This is the variant we adapted in our own implementation.

The population element makes this method naturally well suited for massively parallel simulations, and bias can be systematically reduced by increasing the population size. To demonstrate this, we developed an implementation of population annealing on graphics processing units (GPUs) [5] and benchmarked its behaviour for different systems undergoing continuous and first-order phase transitions [6, 7].

[1] D.P. Landau, K. Binder: *A Guide to Monte Carlo Simulations in Statistical Physics*, 4th ed. (Cambridge University Press, Cambridge, 2015)
[2] Y. Iba: Trans. Jpn. Soc. Artif. Intell. **16**, 279 (2001)
[3] K. Hukushima, Y. Iba: AIP Conf. Proc. **690**, 200 (2003)
[4] J. Machta: Phys. Rev. E **82**, 026704 (2010)
[5] L.Yu. Barash et al.: Comput. Phys. Commun. **220**, 341 (2017)
[6] L.Yu. Barash et al.: Eur. Phys. J. – Special Topics **226**, 595 (2017)
[7] M. Weigel et al.: in *Computer Simulation Studies in Condensed-Matter Physics XXX*, eds. D.P. Landau, M. Bachmann, S.P. Lewis, H.-B. Schüttler, Phys.: Conf. Ser. **921**, 012017 (2017)

10.26 Framework for programming Monte Carlo simulations (βMC)

M. Marenz, J. Zierenberg*, W. Janke

*Max Planck Institute for Dynamics and Self-Organization, Am Fassberg 17, 37077 Göttingen, Germany

Monte Carlo (MC) computer simulations are a very powerful tool for investigating and understanding the thermodynamic behaviour of a wide variety of physical systems. These systems range from such simple ones like the Ising spin model to complex ones like the adsorption properties of proteins on surfaces. In contrast to Molecular Dynamics (MD) simulations, the other important class of algorithm to simulate microscopic systems, MC simulations are not suitable to investigate dynamical properties. On the other hand, the ability of modern MC methods to explore effectively the phase space of physical systems, especially those with a phase transition, makes them a very powerful and indispensable tool.

Another difference to MD simulations is the lack of a widely used program package for generic MC simulations. One reason for this lack is the versatility of modern MC

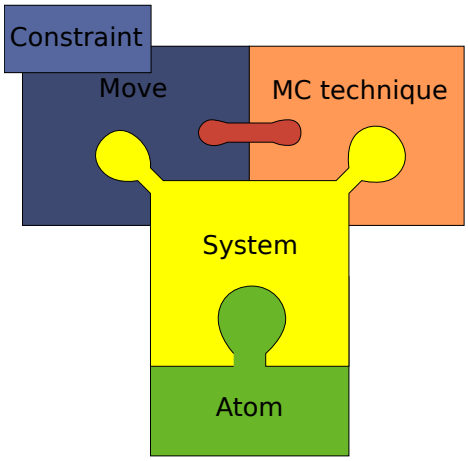

Figure 10.31: The 5 basic building blocks.

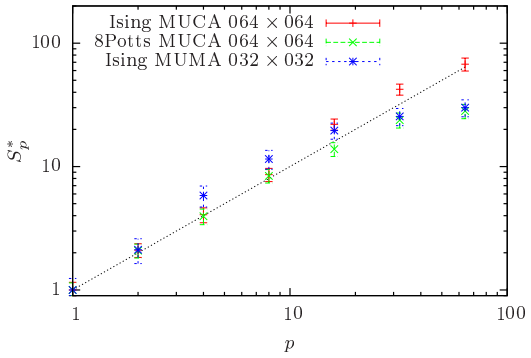

Figure 10.32: Scaling properties of the parallel multicanonical algorithm as a function of the number of processors p.

algorithms – there are various different algorithm and many different possibilities to adjust a MC simulation to a specific problem. This was the starting point for the development of our framework for advanced MC algorithms. The aim of the framework is to enable the programmer to implement specific simulations in an easy and efficient way, without the need to implement all the tricky details for every new problem. The framework is implemented in the C++ programming language and is designed such that it separates basics parts of a MC algorithm in separate building blocks. These building blocks can be used by the programmer to implement a specific simulation.

There are 5 basic building blocks as illustrated in Fig. 10.31: The first one is the "system", which defines the Hamiltonian and the structure of the physical system. This means that the "system" building block encapsulates the energy calculation and the structure of the considered physical problem. For off-lattice system this block contains a smaller subpart, the "atom" block, which encodes the geometry of the system (e.g., boundary conditions). As systems we have implemented so far different kinds of coarse-grained homopolymers, the Lennard-Jones gas, the TIP4P water model, lattice polymers and the Potts model in different dimensions. On top of the "system" are the last two other building blocks, the "move" and the "MC technique". A "move" defines a single update proposal, propagating the system from the current state to the next one. Additionally a "constraint" can be added to every "move" in order to simulate efficiently systems with geometrical confinements. The "MC technique" implements the Monte Carlo algorithm itself. At the moment we have implemented various algorithms such as Metropolis MC, parallel tempering, multicanonical MC, multimagnetic MC and the Wang-Landau MC algorithm. One of the most advanced MC algorithms we have implemented is a parallel version of the multicanonical algorithm [1, 2], see Fig. 10.32.

The boundaries between these blocks are well defined, so that one can easily exchange one of them. For example one can use two different algorithm to simulate a specific system without implementing a completely new program. The framework is already in practical use for different studies, for example the investigation of the influence of bending stiffness on a coarse-grained homopolymer, the influence of a spherical confinement to pseudo-phase transitions of homopolymers, and the study of polymer aggregation of several polymers for a large set of parameters (temperature, bending

stiffness). Thus, the framework is very useful and has led already to several publications [3–9].

[1] J. Zierenberg et al.: Comput. Phys. Commun. **184**, 1155 (2013)
[2] J. Gross et al.: Comput. Phys. Commun. **224**, 387 (2018)
[3] J. Zierenberg et al.: J. Chem. Phys. **141**, 114908 (2014)
[4] J. Zierenberg, W. Janke: Europhys. Lett. **109**, 28002 (2015)
[5] J. Zierenberg et al: Phys. Rev. E **91**, 032126 (2015)
[6] M. Marenz, W. Janke: Phys. Rev. Lett. **116**, 128301 (2016)
[7] J. Zierenberg et al: Polymers **8**, 333 (2016)
[8] J. Zierenberg et al.: Nat. Commun. **8**, 14546 (2017)
[9] N.G. Fytas et al.: Phys. Rev. E **97**, 040102(R) (2018)

10.27 Funding

Sonderforschungsbereich/Transregio SFB/TRR 102 *Polymers under Multiple Constraints: Restricted and Controlled Molecular Order and Mobility*
W. Janke (Principal Investigator, project B04)
Deutsche Forschungsgemeinschaft (DFG)

Free-Energy Landscapes of Semiflexible Theta-Polymer Aggregation with and without External Force
W. Janke
Deutsche Forschungsgemeinschaft (DFG), Grant No. JA 483/31-1

Stable Knotted Phases in Semiflexible Polymers
W. Janke
Deutsche Forschungsgemeinschaft (DFG), Grant No. JA 483/33-1

Institute Partnership with the Institute for Condensed Matter Physics of the National Academy of Sciences of Ukraine, Lviv, Ukraine, *Polymers in Porous Environments and on Disordered Substrates*
W. Janke (with V. Blavatska, Lviv)
Alexander von Humboldt Foundation (AvH)

Marie Curie IRSES Network *DIONICOS: Dynamics of and in Complex Systems*
W. Janke (Principal Investigator, Head of Leipzig node)
European Union (EU), Contract No. PIRSES-GA-2013-612707

Doctoral College *Statistical Physics of Complex Systems* ($\mathbb{L}^4$)
W. Janke (with B. Berche, Nancy)
Deutsch-Französisches Doktorandenkollegium (DFDK) with "Co-tutelle de Thèse", jointly with Université de Lorraine, Nancy, France, and Coventry University, UK, and National Academy of Sciences of Ukraine, Lviv, Ukraine, as associated partners
Deutsch-Französische Hochschule (DFH-UFA), Grant No. CDFA-02-07

Graduate School *"BuildMoNa": Leipzig School of Natural Sciences – Building with Molecules and Nano-objects*
W. Janke (Principal Investigator)

International Max Planck Research School (IMPRS) *Mathematics in the Sciences*
W. Janke (Scientific Member)
Max Planck Society and Klaus Tschira Foundation

Free-Energy Landscapes of Semiflexible Polymer Aggregation
W. Janke, J. Zierenberg
NIC Jülich (computer time grant for "JURECA"), Grant No. HLZ24

10.28 Organizational Duties

Wolfhard Janke

- *Adjunct Professor* of The University of Georgia, Athens, Georgia, USA
- *International Visiting Professor* of Coventry University, England, UK
- Director, Institute for Theoretical Physics (ITP), Universität Leipzig
- Director, Naturwissenschaftlich-Theoretisches Zentrum (NTZ), Universität Leipzig
- Member of Department Council ("Fakultätsrat"), Faculty for Physics and Earth Sciences, Universität Leipzig
- Member of the Steering Committee ("Direktorium") of the Graduate Centre *Mathematics/Computer Science and Natural Sciences*, Research Academy Leipzig
- Principal Investigator of the Graduate School "BuildMoNa"
- Scientific Member of the International Max Planck Research School (IMPRS) *Mathematics in the Sciences*
- Principal Investigator of the DFG Sonderforschungsbereich/Transregio SFB/TRR 102 *Polymers under Multiple Constraints: Restricted and Controlled Molecular Order and Mobility*
- Principal Investigator of "Profillinie" *Complex Matter*, Universität Leipzig
- Principal Investigator of "Profillinie" *Mathematical and Computational Sciences*, Universität Leipzig
- Spokesperson of the German-French Graduate College *Statistical Physics of Complex Systems* with Nancy (France), and associated partners in Coventry (England, UK) and Lviv (Ukraine), of the Deutsch-Französische Hochschule (DFH-UFA)
- Spokesperson of the German-Ukrainian Institute Partnership Leipzig-Lviv of the Alexander von Humboldt Foundation (AvH)
- External Member of the Jagiellonian University Graduate School *International Ph.D. Studies in Physics of Complex Systems*, Krakow, Poland
- Permanent Member of the International Advisory Board for the Annual *Conference of the Middle European Cooperation in Statistical Physics (MECO)*
- Organizer (with W. Paul, Universität Halle) of the *1st Discussion Meeting HalLei17*, ITP, Universität Leipzig, 19. July 2017
- Organizer of the Workshop *CompPhys17* – 18th International NTZ Workshop on *New Developments in Computational Physics*, ITP, Universität Leipzig, 30. November – 02. December 2017
- Organizer of the Workshop *CompPhys18* – 19th International NTZ Workshop on *New Developments in Computational Physics*, ITP, Universität Leipzig, 29. November – 01. December 2018

- Editor "Computational Physics", Central European Journal of Physics, Krakow, Poland
- Member of Editorial Board, Condens. Matter Phys., Lviv, Ukraine
- External Reviewer for Deutsche Forschungsgemeinschaft (DFG), Humboldt-Stiftung (AvH), Studienstiftung des deutschen Volkes, Fond zur Förderung der wissenschaftlichen Forschung (FWF), Österreich, The Royal Society, UK, The Engineering and Physical Sciences Research Council (EPSRC), UK, Israel Science Foundation, Israel, National Science Foundation (NSF), USA, Natural Sciences and Engineering Research Council of Canada (NSERC), Canada, The Jeffress Memorial Trust, Bank of America, Virginia, USA, Universität Mainz, Germany, The University of Warwick, England, UK, Coventry University, England, UK, CECAM, Lyon, France
- Referee for Physical Review Letters, Physical Review B, Physical Review E, Journal of Chemical Physics, Europhysics Letters, Physics Letters A, Physics Letters B, The European Physical Journal B, Physica A, Proceedings of the Royal Physical Society, Journal of Physics A, Computer Physics Communications, JSTAT, Condens. Matter Phys., PLOS ONE, New Journal of Physics, International Journal of Modern Physics C

10.29 External Cooperations

Academic

- Institute of Physics, Jagiellonian University, Kraków, Poland
  Prof. Dr. Piotr Białas, Dr. Leszek Bogacz, Prof. Dr. Zdzisław Burda
- CEA/Saclay, Service de Physique Théorique, France
  Dr. Alain Billoire
- Institut für Physik, Universität Mainz, Germany
  Prof. Dr. Kurt Binder, Andreas Nußbaumer, Prof. Dr. Friderike Schmid
- Institut für Theoretische Physik, Universität Heidelberg, Germany
  Dr. Elmar Bittner
- Laboratoire de Physique des Matériaux (UMR CNRS No 7556), Université de Lorraine, Nancy, France
  Prof. Dr. Bertrand Berche, Dr. Christophe Chatelain, Dr. Olivier Collet, Prof. Dr. Malte Henkel, Prof. Dr. Dragi Karevski
- Groupe de Physique des Matériaux (UMR CNRS No 6634), Université de Rouen, France
  Dr. Pierre-Emmanuel Berche
- SUPA, School of Physics and Astronomy, University of Edinburgh, Scotland, UK
  Dr. Richard A. Blythe, Prof. Dr. Martin R. Evans, Dr. Bartłomiej Wacław
- P.J. Šafárik University, Košice, Slovak Republic
  Dr. Michal Borovský
- Istituto Nazionale di Fisica Nucleare, Sezione di Milano-Bicocca, Milano, Italy
  Prof. Dr. Pablo Butera

- Applied Mathematics Research Centre, Coventry University, England, UK
  PD Dr. Christian von Ferber, Dr. Nikolaos G. Fytas, Prof. Dr. Ralph Kenna, Dr. Thierry Platini, Dr. Martin Weigel
- Jülich Supercomputing Centre (JSC), Forschungszentrum Jülich, Germany
  Prof. Dr. Peter Grassberger
- IAC-1, Universität Stuttgart, Germany
  Prof. Dr. Rudolf Hilfer, Prof. Dr. Christian Holm
- Max Planck Institute for Polymer Research, Mainz, Germany
  Dr. Hsiao-Ping Hsu, Prof. Dr. Kurt Kremer
- Complex Systems Division, Department of Theoretical Physics, Lunds Universitet, Lund, Sweden
  Prof. Dr. Anders Irbäck
- Department of Mathematics and the Maxwell Institute for Mathematical Sciences, Heriot-Watt University, Edinburgh, Scotland, UK
  Prof. Dr. Desmond A. Johnston
- Inst. für Theoretische Physik, FU Berlin, Germany
  Prof. Dr. Hagen Kleinert
- Department of Physics, University of Athens, Zografou, Greece
  Prof. Dr. Anastasios Malakis
- Atominstitut, TU Wien, Austria
  Prof. Dr. Harald Markum
- Jacobs Universität Bremen, Germany
  Prof. Dr. Hildegard Meyer-Ortmanns, Darka Labavić
- Institute of Physics, Polish Academy of Sciences, Warsaw, Poland
  Dr. Panagiotis E. Theodorakis
- Applied Mathematics, Universitat Pompeu Fabra, Barcelona, Spain
  Prof. Dr. Ramon Villanova
- CERN (PH-SFT), Geneva, Switzerland
  Dr. Sandro Wenzel
- Department of Engineering of Physics, Ankara University, Ankara, Turkey
  Prof. Dr. Handan Arkın-Olgar, Mustafa Bilsel, Buket Taşdizen
- Dept. of Physics, Hacettepe University, Ankara, Turkey
  Prof. Dr. Tarik Çelik, Gökhan Gökoğlu
- Dept. of Physics Engineering, Hacettepe University, Ankara, Turkey
  Prof. Dr. Fatih Yaşar
- Institute for Condensed Matter Physics, National Academy of Sciences, Lviv, Ukraine
  Dr. Viktoria Blavatska, Prof. Dr. Yurij Holovatch
- Yerevan Physics Institute, Yerevan, Armenia
  Prof. Dr. David B. Saakian
- Alikhanyan National Science Laboratory, Yerevan, Armenia
  Prof. Dr. Nerses Ananikyan, Dr. Nikolay Izmailyan

- Landau Institute for Theoretical Physics, Chernogolovka, Russia
  Dr. Lev Yu. Barash, Prof. Dr. Lev N. Shchur
- Center for Simulational Physics, The University of Georgia, Athens, USA
  Prof. Dr. Michael Bachmann, Prof. Dr. David P. Landau
- Dept. of Physics, Florida State University, Tallahassee, USA
  Prof. Dr. Bernd A. Berg
- Dept. of Chemistry and Biochemistry, University of Oklahoma, Norman, USA
  Prof. Dr. Ulrich H.E. Hansmann
- Los Alamos National Laboratory, Los Alamos, USA
  Dr. Christoph Junghans
- Dept. of Physics and Astronomy, Texas A&M, College Station, USA
  Prof. Dr. Helmut G. Katzgraber
- Dept. of Physics, Virginia Tech, Blacksburg, USA
  Prof. Dr. Michel Pleimling, Prof. Dr. Royce K.P. Zia
- Physics Department, Carnegie Mellon University, Pittsburgh, USA
  Prof. Dr. Robert H. Swendsen
- University of North Georgia, Dahlonega, USA
  Dr. Thomas Vogel
- Banaras Hindu University, Varanasi, India
  Prof. Dr. Sanjay Kumar
- Jawaharlal Nehru Centre for Advanced Scientific Research (JNCASR), Jakkur, India
  Prof. Dr. Subir K. Das
- School of Physical Sciences, Jawaharlal Nehru University, New Delhi, India
  Manoj Kumar, Prof. Dr. Sanjay Puri
- Department of Physics, Indian Institute of Technology, Hauz Khas, New Delhi, India
  Prof. Dr. Varsha Banerjee
- Computational Chemistry Unit Cell (CCUC), Department of Chemistry, Chulalongkorn University, Bangkok, Thailand
  Prof. Dr. Supot Hannongbua, Dr. Oraphan Saengsawang
- Ramkhamhaeng University, Department of Chemistry, Faculty of Science, Bangkok, Thailand
  Dr. Tatiya Chokbunpiam
- Laboratory of Statistical and Computational Physics, Institute of Physics, Academia Sinica, Nankang, Taipei, Taiwan
  Prof. Dr. Chin-Kun Hu
- Zhejiang Institute of Modern Physics, Zhejiang University, Hangzhou, P.R. China
  Prof. Dr. He-Ping Ying, Prof. Dr. Bo Zheng
- The University of Tokyo, Tokyo, Japan
  Prof. Dr. Nobuyasu Ito
- Nagoya University, Nagoya, Japan
  Dr. Tetsuro Nagai, Prof. Dr. Yuko Okamoto

10.30 Publications

Journals

H. Arkın, W. Janke: *Polymer Adsorption on Curved Surfaces*, Phys. Rev. E **96**, 062504-1–14 (2017)

K.S. Austin, J. Zierenberg, W. Janke: *Interplay of Adsorption and Semiflexibility: Structural Behavior of Grafted Polymers under Poor Solvent Conditions*, Macromolecules **50**, 4054–4063 (2017)

L.Yu. Barash, M. Weigel, M. Borovský, W. Janke, L.N. Shchur: *GPU Accelerated Population Annealing Algorithm*, Comput. Phys. Commun. **220**, 341–350 (2017)

L. Yu. Barash, M. Weigel, L.N. Shchur, W. Janke: *Exploring First-Order Phase Transitions with Population Annealing*, Eur. Phys. J. – Special Topics **226**, 595–604 (2017)

T. Chokbunpiam, S. Fritzsche, J. Caro, C. Chmelik, W. Janke, S. Hannongbua: *Importance of ZIF-90 Lattice Flexibility on Diffusion, Permeation, and Lattice Structure for an adsorbed H_2/CH_4 Gas Mixture: A Re-Examination by Gibbs Ensemble Monte Carlo and Molecular Dynamics Simulations*, J. Phys. Chem. C **121**, 10455–10462 (2017)

H. Christiansen, S. Majumder, W. Janke: *Coarsening and Aging of Lattice Polymers: Influence of Bond Fluctuations*, J. Chem. Phys. **147**, 094902-1–12 (2017)

N. Fricke, W. Janke: *Exact Enumeration of Self-Avoiding Walks on Critical Percolation Clusters in 2–7 Dimensions*, J. Phys. A **50**, 264002-1–17 (2017)

N. Fricke, J. Zierenberg, M. Marenz, F. P. Spitzner, V. Blavatska, W. Janke: *Scaling Laws for Random Walks in Long-Range Correlated Disordered Media*, Condens. Matter Phys. **20**, 13004-1–11 (2017)

J. Gross, M. Ivanov, W. Janke: *Single-Chain Behavior of Poly(3-hexyl-thiophene)*, Eur. Phys. J. – Special Topics **226**, 667–681 (2017)

W. Janke, M. Marenz, J. Zierenberg: *Generalized Ensemble Computer Simulations for Structure Formation of Semiflexible Polymers*, Lobachevskii J. Math. **38**, 978–985 (2017)

W. Janke, P. Schierz, J. Zierenberg: *Transition Barrier at a First-Order Phase Transition in the Canonical and Microcanonical Ensemble*, in *Computer Simulation Studies in Condensed-Matter Physics XXX*, eds. D.P. Landau, M. Bachmann, S.P. Lewis, H.-B. Schüttler, J. Phys.: Conf. Ser. **921**, 012018-1–5 (2017)

D.A. Johnston, M. Mueller, W. Janke: *Plaquette Ising Models, Degeneracy and Scaling*, Eur. Phys. J. – Special Topics **226**, 749–764 (2017)

S. Majumder, J. Zierenberg, W. Janke: *Kinetics of Polymer Collapse: Effect of Temperature on Cluster Growth and Aging*, Soft Matter **13**, 1276–1290 (2017)

S. Mascotto, W. Janke, R. Valiullin: *Ice Nucleation in Periodic Arrays of Spherical Nanocages*, J. Phys. Chem. C **121**, 23788–23792 (2017)

M. Mueller, D.A. Johnston, W. Janke: *Exact Solutions to Plaquette Ising Models with Free and Periodic Boundaries*, Nucl. Phys. B **914**, 388–404 (2017)

S. Schnabel, W. Janke: *Dynamic Greedy Algorithms for the Edwards-Anderson Model*, Comput. Phys. Commun. **220**, 74–80 (2017)

S. Schneider, M. Mueller, W. Janke: *Convergence of Stochastic Approximation Monte Carlo and Modified Wang-Landau Algorithms: Tests for the Ising Model*, Comput. Phys. Commun. **216**, 1–7 (2017)

M. Weigel, L.Yu. Barash, M. Borovský, W. Janke, L.N. Shchur: *Population Annealing: Massively Parallel Simulations in Statistical Physics*, in *Computer Simulation Studies in Condensed-Matter Physics XXX*, eds. D.P. Landau, M. Bachmann, S.P. Lewis, H.-B. Schüttler, J. Phys.: Conf. Ser. **921**, 012017-1–10 (2017)

J. Zierenberg, N. Fricke, M. Marenz, F.P. Spitzner, V. Blavatska, W. Janke: *Percolation Thresholds and Fractal Dimensions for Square and Cubic Lattices with Long-Range Correlated Defects*, Phys. Rev. E **96**, 062125-1–11 (2017)

J. Zierenberg, N.G. Fytas, M. Weigel, W. Janke, A. Malakis: *Scaling and Universality in the Phase Diagram of the 2D Blume-Capel Model*, Eur. Phys. J. – Special Topics **226**, 789–804 (2017)

J. Zierenberg, P. Schierz, W. Janke: *Canonical Free-Energy Barrier of Particle and Polymer Cluster Formation*, Nat. Commun. **8**, 14546-1–7 (2017)

J. Zierenberg, K. Tholen, W. Janke: *Effect of Grafting on the Binding Transition of Two Flexible Polymers*, Eur. Phys. J. – Special Topics **226**, 683–692 (2017)

in press

K.S. Austin, M. Marenz, W. Janke: *Efficiencies of Joint Non-Local Update Moves in Monte Carlo Simulations of Coarse-Grained Polymers*, Comput. Phys. Commun. **224**, 222–229 (2018)

N.G. Fytas, J. Zierenberg, P.E. Theodorakis, M. Weigel, W. Janke, A. Malakis: *Universality from Disorder in the Random-Bond Blume-Capel Model*, Phys. Rev. E **97**, 040102(R)-1–6 (2018)

J. Gross, J. Zierenberg, M. Weigel, W. Janke: *Massively Parallel Multicanonical Simulations*, Comput. Phys. Commun. **224**, 387–395 (2018)

W. Janke: *Generalized Ensemble Computer Simulations of Macromolecules*, invited Ising Lecture Notes 2016, in *Order, Disorder and Criticality: Advanced Problems of Phase Transition Theory*, Vol. 5, ed. Y. Holovatch (World Scientific, Singapore, 2018), pp. 173–225

W. Janke, J. Zierenberg: *From Particle Condensation to Polymer Aggregation*, Invited Plenary Talk, International Conference *Computer Simulations in Physics and beyond (CSP2017)*, 09–12 October 2017, Moscow, Russia, J. Phys.: Conf. Ser. **955**, 012003-1–10 (2018)

M. Kumar, R. Kumar, M. Weigel, V. Banerjee, W. Janke, S. Puri: *Approximate Ground States of the Random-Field Potts Model from Graph Cuts*, Phys. Rev. E **97**, 053307-1–10 (2018)

S. Majumder, H. Christiansen, W. Janke: *Scaling Laws During Collapse of a Homopolymer: Lattice Versus Off-Lattice*, J. Phys.: Conf. Ser. **955**, 012008-1–6 (2018)

S. Schnabel, W. Janke: *Distribution of Metastable States of Ising Spin Glasses*, Phys. Rev. B **97**, 174204-1–10 (2018)

S. Schnabel, W. Janke: *Distribution of Metastable States of Spin Glasses*, to appear in *Computer Simulation Studies in Condensed-Matter Physics XXXI*, eds. D.P. Landau, M. Bachmann, S.P. Lewis, H.-B. Schüttler, J. Phys.: Conf. Ser. (2018), in print

Talks

H. Christiansen, S. Majumder, W. Janke: *The Influence of Bond Fluctuations on the Coarsening and Aging of Lattice Polymers*, Joint Steering Committee Meeting of the IRSES Projects DIONICOS and STREVCOMS, Lviv, Ukraine, 14. June 2017

H. Christiansen, S. Majumder, W. Janke: *Efficient Method of Simulating with Long-Range Interactions: The Case of Coarsening in the Ising Model*, 18th International NTZ-Workshop on *New Developments in Computational Physics – CompPhys17*, Universität Leipzig, Germany, 30. November – 02. December 2017

J. Gross, M. Ivanov, W. Janke: *Poly(3-hexylthiophene) Interacting with Gold and "other" Striped Substrates*, 1st Discussion Meeting HalLei17, Universität Leipzig, Germany, 19. July 2017

W. Janke: *Canonical Free-Energy Barrier of Particle and Polymer Cluster Formation*, Conference of the Middle European Cooperation in Statistical Physics – MECO42, Lyon, France, 08.–10. February 2017

W. Janke: *The Real Microcanonical Ensemble: Free-Energy Barriers for Particle and Polymer Aggregation*, 30th Annual CSP Workshop on *Recent Developments in Computer Simulation Studies in Condensed Matter Physics*, The University of Georgia, Athens, USA, 20.–24. February 2017

W. Janke: *Knots as Stable Topological Order Parameter for Semiflexible Polymers*, invited talk ("Hauptvortrag"), Focus Session *Topological Problems in the Physics of Polymers, Biopolymers and Fibers* within DPG Frühjahrstagung 2017, TU Dresden, Germany, 23.–24. March 2017

W. Janke: *Knots as Stable Topological Order Parameter for a Semiflexible Polymer*, Workshop on *Polymer Physics and Chemistry*, State Key Laboratory of Polymer Physics and Chemistry, Changchun Institute of Applied Chemistry, Chinese Academy of Sciences, Changchun, China, 27.–30. March 2017

W. Janke: *Exact Enumeration of Self-Avoiding Walks on Critical Percolation Clusters in Two to Seven Dimensions*, ICMP Workshop, Lviv, Ukraine, 14.–16. June 2017

W. Janke: *Exact Enumeration of Self-Avoiding Walks on Critical Percolation Clusters in Two to Seven Dimensions*, International Workshop and Young Scientist School on *Critical Phenomena and Phase Transitions CPPT17*, A.I. Alikhanyan National Science Laboratory, Yerevan, Armenia, 20.–24. September 2017

W. Janke: *From Particle Condensation in the Ising Lattice Gas to Polymer Aggregation: Computer Simulation Studies*, invited talk, Workshop on *Stochastic Spin Systems: models, theory, simulation and real world applications*, ZIF Bielefeld, Germany, 28.–30. September 2017

W. Janke: *From Particle Condensation to Polymer Aggregation*, invited plenary talk, International Conference on *Computer Simulation in Physics and beyond*, National Research University Higher School of Economics, Moscow, Russia, 09.–12. October 2017

M. Kumar, R. Kumar, V. Banerjee, S. Puri, M. Weigel, W. Janke: *Approximate Ground States of the Random-Field Potts Model from Graph Cuts and Parallel Tempering*, DPG Frühjahrstagung 2017, TU Dresden, Germany, 19.–24. March 2017

S. Majumder, H. Christiansen, W. Janke: *Universal Scaling for Coarsening and Aging During Collapse of a Polymer*, 1st Discussion Meeting HalLei17, Universität Leipzig, Germany, 19. July 2017

S. Majumder, W. Janke: *Scaling laws in Kinetics of Collapse of a Polymer*, International Conference on *Computer Simulation in Physics and beyond*, Moscow, Russia, 09.–12. October 2017

S. Schnabel, W. Janke: *Coarse-Graining the State Space of a Spin Glass*, 18th International NTZ-Workshop on *New Developments in Computational Physics – CompPhys17*, Universität Leipzig, Germany, 30. November – 02. December 2017

M. Weigel, L.Yu. Barash, L.N. Shchur, W. Janke: *Understanding Population Monte Carlo Simulations*, DPG Frühjahrstagung 2017, TU Dresden, Germany, 19.–24. March 2017

Posters

H. Christiansen, S. Majumder, W. Janke: *The Influence of Bond Fluctuations on the Coarsening and Aging of Lattice Polymers*, Soft Matter Day, Universität Leipzig, Germany, 23. June 2017

J. Gross, W. Janke: *Monte Carlo Studies of Polymer Aggregation*, International Discussion Meeting on *Polymer Crystallization 2017 – From Classical Systems to Functional Materials and Biopolymers*, Wittenberg, Germany, 17.–20. September 2017

J. Gross, M. Ivanov, D.N. Oberthür, W. Janke: *Monte Carlo Studies of P3HT Aggregation*, 18th International NTZ-Workshop on *New Developments in Computational Physics – CompPhys17*, Universität Leipzig, Germany, 30. November – 02. December 2017

S. Kazmin, W. Janke: *Site-Diluted Ising Model in Two Dimensions – Towards Long-Range Correlated Defects* 18th International NTZ-Workshop on *New Developments in Computational Physics – CompPhys17*, Universität Leipzig, Germany, 30. November – 02. December 2017

S. Majumder, W. Janke: *Universal Scaling of Cluster growth and Aging During Collapse of a Polymer*, DPG Frühjahrstagung 2017, TU Dresden, Germany, 19.–24. March 2017

F. Müller, S. Schnabel, W. Janke: *Non-Flat Histogram Methods for Spin Glasses*, 18th International NTZ-Workshop on *New Developments in Computational Physics – Comp Phys17*, Universität Leipzig, Germany, 30. November – 02. December 2017

F.P. Spitzner, J. Zierenberg, W. Janke: *Two Perspectives on the Condensation-Evaporation Transition*, 18th International NTZ-Workshop on *New Developments in Computational Physics – CompPhys17*, Universität Leipzig, Germany, 30. November – 02. December 2017

10.31 Graduations

Doctorate

- Philipp Schierz
  Liquid-Gas-Like Phase Transitions in Various Ensembles: A Computational Study of Liquid-Gas-Like Phase Transitions with Various Simulation Techniques and a Focus on Polymer Aggregation
  11. January 2017

Master

- Franz Paul Spitzner
  Two Perspectives on the Condensation-Evaporation Transition of the Lennard-Jones Gas in 2D
  06. July 2017
- Fabio Müller
  Non-Flat Histogram Methods for Spin Glasses
  12. September 2017

Bachelor

- Christopher Allen
  Microcanonical Simulations of Phase Transitions in the Potts Model
  04. October 2017

10.32 Guests

- Prof. Dr. George Savvidy
  Demokritos Nat. Res. Center, Athens, Greece

NTZ/DFH-UFA Colloquium (03. November 2016)
The Gonihedric Ising Model
01. November 2016 – 31. January 2017

- Prof. Dr. Subir K. Das
Jawaharlal Nehru Centre for Advanced Scientific Research, Bangalore, India
18.–21. May 2017

- Prof. Dr. Ulrich H.E. Hansmann
University of Oklahoma, Norman, USA
Sabbatical, NTZ/DFH-UFA Seminar (12. September 2017)
Direct Coupling Analysis
01. June – 31. December 2017

- Dr. Lev Yu. Barash
Landau Institute, Chernogolovka, Russia
NTZ/DFH-UFA and EU IRSES Network DIONICOS Colloquium (08. June 2017)
Applying Population Annealing to First- and Second-Order Phase Transitions
02.–12. June 2017

- Prof. Dr. Lev Shchur
Landau Institute, Chernogolovka, Russia
04.–10. June 2017

- Prof. Dr. Handan Arkın-Olgar
Ankara University, Turkey
Alexander-von-Humboldt Fellowship for Experienced Researchers
15. June – 15. September 2017

- Marina Fadeeva
Landau Institute, Chernogolovka, and Higher School of Economics, Moscow, Russia
NTZ/DFH-UFA and EU IRSES Network DIONICOS Colloquium (20. July 2017)
Control of Accuracy in the Wang-Landau Algorithm
27. June – 28. July 2017

- Dr. Johannes Zierenberg
Max Planck Institute for Dynamics and Self-Organization, Göttingen, Germany
NTZ/DFH-UFA Seminar (07. July 2017)
Homeostatic Plasticity in Neural Networks Induces a Diverse Range of Dynamic States
06.–08. July 2017

- Prof. Dr. Jutta Luettmer-Strathmann
University of Akron, Ohio, USA
1st Discussion Meeting HalLei17 (19. July 2017)
Sexithiophene Phase Diagram from Simulations of a Gay-Berne Type Model
19. July 2017

- Prof. Dr. Mark P. Taylor
Dept. of Physics, Hiram College, USA
1st Discussion Meeting HalLei17 (19. July 2017)
Polymer Collapse and Folding in a Crowded Environment
19. July 2017

- Kseniia Shapovalova
  Far Eastern Federal University, Vladivostok, Russia
  DAAD Michail-Lomonosov-Programm
  NTZ/DFH-UFA Seminar (09. November 2017)
  High-Performance Algorithms for the Research of Frustrated Systems of Spin Ice and Spin Glass
  01. October 2017 – 31. March 2018

- Dr. Khristine Haydukivska
  ICMP, National Academy of Sciences of Ukraine, Lviv, Ukraine
  22. November – 09. December 2017

- Dr. Viktoria Blavatska
  ICMP, National Academy of Sciences of Ukraine, Lviv, Ukraine
  01. – 31. December 2017

- Dr. Elmar Bittner
  Universität Heidelberg, Germany
  On the Interface Tension of the Ising Model
  29. November – 02. December 2017

- Dr. Nathan Clisby
  Swinburne University of Technology, Hawthorn, Victoria, Australia
  Efficient Implementation of Connectivity Changing Moves for Dense Polymers
  29. November – 02. December 2017

- Dr. Eren Metin Elçi
  Monash University, Clayton, Victoria, Australia
  On Critical Speeding-up in an Irreversible Worm Dynamics for High-Dimensional Ising Models
  29. November – 02. December 2017

- Dr. Nikolaos Fytas
  Coventry University, England, UK
  On the Effect of Disorder on First-Order Phase Transitions: The Case of the 2D Random-Bond Blume-Capel Model
  29. November – 02. December 2017

- Dr. Antonio Gordillo
  Universidad de Extremadura, Badajoz, Spain
  Crumpling Transition and Low-Temperatures Properties of Crystalline Membranes with Perforation Patterns
  29. November – 02. December 2017

- Prof. Dr. Ulrich H.E. Hansmann
  University of Oklahoma, Norman, OK, USA
  Enhanced Sampling Simulations of Folding and Aggregation
  29. November – 02. December 2017

- Prof. Dr. Alexander Hartmann
  Universität Oldenburg, Germany
  High-Precision Simulation of Height Distribution for Directed Polymers in Random

Media
29. November – 02. December 2017

- Priv.-Doz. Dr. Martin Hasenbusch
Humboldt Universität zu Berlin, Germany
Interface Tension and the Cluster Exchange Algorithm
29. November – 02. December 2017

- Dr. Hsiao-Ping Hsu
MPI Polymer Research, Mainz, Germany
Non-Linear Viscoelasticity of Highly Strained Polymer Melts: Primitive Path Analysis
29. November – 02. December 2017

- Dr. Fred Hucht
Universität Duisburg-Essen, Germany
Analytic Finite-Size Scaling Functions in the Anisotropic Ising Rectangle
29. November – 02. December 2017

- Prof. Dr. Ferenc Igloi
Wigner Research Centre, Budapest, Hungary
Contact Process in Inhomogeneous Environment
29. November – 02. December 2017

- Prof. Dr. Viktor Ivanov
Moscow State University, Russia
29. November – 02. December 2017

- Prof. Dr. Desmond A. Johnston
Heriot-Watt University, Edinburgh, Scotland, UK
Spin Chain SUSY
29. November – 02. December 2017

- Prof. Dr. David P. Landau
The University of Georgia, Athens, GA, USA
Complexity and Optimization: Physical Science Meets Biological Science via Computer Simulations
29. November – 02. December 2017

- Daria Maltseva
Moscow State University, Russia
29. November – 02. December 2017

- Prof. Dr. Arnulf Möbius
IFW Dresden, Germany
Simulated Annealing, Effective but Inefficient? A Case Study for the 3D136 Instance of the HP Model of Protein Folding
29. November – 02. December 2017

- Prof. Dr. Juan J. Ruiz-Lorenzo
Universidad de Extremadura, Badajoz, Spain
Numerical Construction of the Aizenman-Wehr Metastate
29. November – 02. December 2017

- Prof. Dr. Lev N. Shchur
  Landau Institute and Science Center, Chernogolovka, Moscow Region, Russia
  Control of Accuracy in the Wang-Landau Algorithm
  29. November – 02. December 2017
- Dr. Francesco Parisen Toldin
  Universität Würzburg, Germany
  Finite-Size Effects in Canonical and Grand-Canonical Quantum Monte Carlo Simulations for Fermions
  29. November – 02. December 2017
- Dr. Erol Vatansever
  Dokuz Eylul University, Izmir, Turkey
  Dynamically Order-Disorder Transition in Triangular Lattice Driven by a Time Dependent Magnetic Field
  29. November – 02. December 2017
- Dr. Zeynep Demir Vatansever
  Dokuz Eylul University, Izmir, Turkey
  Monte Carlo Study of Hysteresis Features of a Cylindrical Nanowire under Quenched Disorder
  29. November – 02. December 2017
- Dr. Dimitris Voliotis
  University of Sao Paulo, Brazil
  Critical Behavior of the Quantum Potts Chain with Aperiodic Perturbation
  29. November – 02. December 2017
- Dr. Johannes Zierenberg
  Max Planck Institute for Dynamics and Self-Organization, Göttingen, Germany
  Diversity of Dynamic States in Neural Networks induced by Homeostatic Plasticity
  29. November – 02. December 2017

11

Quantum Field Theory and Gravity

11.1 Introduction

The focus of investigation in the group of Quantum Field Theory and Gravity consists of three main strands: (1) Quantum field theory in curved spacetimes (Prof. Dr. R. Verch, Dr. T. P. Hack), (2) mathematical structure of gauge field theories and their quantization (Prof. Dr. G. Rudolph (retired), Dr. M. Schmidt) and (3) quantum fields under the influence of external conditions (PD Dr. M. Bordag).

In quantum field theory in curved spacetimes, several research fields are pursued, such as mathematical and conceptual foundations of local covariant quantum field theory and of the early epoch of cosmology, characterization of locally thermal states and their application to the Unruh effect, and in cosmology; and furthermore some aspects of quantum field theory on spacetimes that contain closed timelike curves. A sideline of this research is quantum field theory on non-commutative geometries. One of the aims is to gain a better understanding of essential ingredients for a potential theory of quantum gravity. In the research on gauge theories, one focus is on the topological structure of gauge orbit spaces. A complementary line of research is devoted to a better understanding of gauge field theories on lattices. In quantum field theory under the influence of external conditions, a central research field is the influence of boundaries, as in the Casimir effect, and singular potentials and their role in quantization. Some of the effects studied in this line of research have concrete applications in experiments.

Prof. Dr. Rainer Verch

11.2 Causal pathologies in quantum field theory

R. Verch, J. Tolksdorf*

*Max Planck Institute for Mathematics in the Sciences

Analogue models for states in the presence of closed timelike curves which are popular in quantum information theory are studied within quantum field theory together with J. Tolksdorf (Max Planck Institute for Mathematics in the Sciences).

[1] J. Tolksdorf and R. Verch: Commun. Math. Phys. **357** (2018) no.1, 319, doi:10.1007/s00220-017-2943-5

11.3 Thermal and non-equilibrium steady states in quantum field theory

R. Verch, D. Buchholz[*], C. J. Fewster[†], M. Gransee[‡], T.-P. Hack, N. Pinamonti[§]

[*]Universität Göttingen
[†]University of York
[‡]Max Planck Institute for Mathematics in the Sciences
[§]University of Genoa

A new description of local thermal equilibrium is being investigated together with M. Gransee and N. Pinamonti (University of Genova).

Fundamental aspects of the Unruh effect are studied together with D. Buchholz (Universität Göttingen) and C. J. Fewster (University of York).

Non-equilibrium steady states of the interacting scalar field in four spacetime dimensions are constructed and investigated.

[1] M. Gransee, N. Pinamonti and R. Verch: J. Geom. Phys. **117** (2017) 15, doi:doi:10.1016/j.geomphys.2017.02.014
[2] D. Buchholz and R. Verch: Gen. Rel. Grav. **48** (2016) no.3, 32, doi:doi:10.1007/s10714-016-2029-2

11.4 Quantum field theory and cosmology

R. Verch, R. Brunetti[*], K. Fredenhagen[†], M. B. Fröb[‡], T.-P. Hack, M. Hänsel, A. Higuchi[‡], I. Khavkine[§], N. Pinamonti[¶], K. Rejzner[‡]

[*]University of Trento
[†]Universität Hamburg
[‡]University of York
[§]University of Prague
[¶]University of Genoa

Fundamental aspects of stability in cosmology (pertaining to solutions to the semiclassical Friedmann equations) are under investigation together with M. Hänsel.

An all-order perturbative description of the quantum theory of inflationary perturbations is developed together with R. Brunetti (University of Trento), K. Fredenhagen (Universität Hamburg), N. Pinamonti (University of Genova) and K. Rejzner (University of York) [1].

The localisation, infrared properties and completeness of observables in the theory of inflationary perturbations are investigated together with M. Fröb (University of York), A. Higuchi (University of York) [2] and I. Khavkine (University of Prague) [2, 3].

[1] R. Brunetti, K. Fredenhagen, T.-P. Hack, N. Pinamonti and K. Rejzner: JHEP **1608** (2016) 032, doi:10.1007/JHEP08(2016)032

[2] M. B. Fröb, T.-P. Hack and A. Higuchi, JCAP **1707** (2017) 043, doi:10.1088/1475-7516/2017/07/043
[3] M. B. Fröb, T.-P. Hack and I. Khavkine, arXiv:1801.02632 [gr-qc].

11.5 Stability of black holes and dynamical Hawking-radiation

R. Verch, T.-P. Hack, F. Kurpicz, N. Pinamonti*

*University of Genoa

The dynamical stability of black holes is investigated by considering the backreaction of quantum fields on non-stationary black hole backgrounds. A related project is the analysis of Hawking-radiation of quantum fields on non-stationary black hole backgrounds which model evaporating black holes.

11.6 Structure of the gauge orbit space and study of gauge theoretical models

G. Rudolph, Sz. Charzynski*, E. Fuchs, H. Grundling†, J. Huebschmann‡, P. Jarvis§, J. Kijowski*, M. Schmidt

*U Warsaw
†U Sydney
‡U Lille
§U Hobart

The investigation of gauge theories in the Hamiltonian approach on finite lattices with emphasis on the role of nongeneric strata was continued.

As a further step towards a generalization of stratified Kähler quantization to larger lattices, the defining relations for lattice gauge models with gauge group SU(2) have been derived . E. Fuchs worked on the formulation of stratified Kähler quantization in terms of coherent states.

In collaboration with H. Grundling, the investigation of the structure of the algebra of observables and its representations for specific models of quantum lattice gauge theory in terms of gauge invariant quantities was continued.

In collaboration with Johannes Huebschmann, symplectic reduction for field theories was studied [2].

Investigation of the deformation quantization of classical lattice gauge theory in collaboration with Markus Pflaum (U Boulder) was continued.

[1] H. Grundling, G. Rudolph, Commun. Math. Phys. **318** (2013) 717–766 ; Commun. Math. Phys. **349** (2016) pp 1163–1202
[2] T. Diez, J. Huebschmann, Yang-Mills moduli spaces over an orientable closed surface via Fréchet reduction. arXiv: 1704.01982

11.7 Dispersion forces and dissipation

M. Bordag

With increasing precision of Casimir and van der Waals force measurements, the question of the influence of dissipation becomes increasingly interesting. Sources of dissipation are primarily ohmic losses in the interacting bodies. The intriguing question is how such losses will influence the groundstate of a quantum system, which by definition is the lowest state (in energy) and cannot loose energy any further. In order to gain understanding in this question we consider a typical setup from first principles by coupling the internal degrees of freedom of the interacting bodies to heat bathes. We derive a representation of the free energy as an integral over real frequencies, which can be viewed as an generalization of the 'remarkable formula' introduced by Ford et. al. 1985. For instance, we obtain a nonperturbative representation for the atom-atom and atom-wall interactions. We investigate several limiting cases. From the limit $T \to 0$ we show that the third law of thermodynamics cannot be violated within the given approach, where the dissipation parameter cannot depend on temperature 'by construction'. We conclude, that the given approach is insufficient to resolve the thermodynamic puzzle connected with the Drude model when inserted into the Lifshitz formula. Further we consider the transition to Matsubara representation and discuss modifications of the contribution from the zeroth Matsubara frequency.

11.8 Funding

Symplektische Reduktion im Unendlichdimensionalen mit Anwendung auf das Cauchy-Problem der Yang-Mills Gleichung
T. Diez
IMPRS fellowship, MPI-MIS

Stability in cosmology
M. Hänsel
Universität Leipzig

Stability of black holes
F. Kurpicz
IMPRS fellowship, MPI-MIS

11.9 Organizational Duties

Prof. Dr. Rainer Verch

- Ansprechpartner, Forschungsprofilbereich "Mathematical and Computational Sciences", Universität Leipzig
- Berufungsbeauftragter des Rektorats
- Book Series Editor, Fundamental Theories of Physics (Springer)
- IMPRS Board Member
- Referee for DFG, AvH Stiftung

- Referee: Ann. H. Poincaré, Commun. Math. Phys., Found. Phys., Class. Quantum Grav., J. Geom. Phys.
- Organization of Workshop: LQP 40, Foundations and Constructive Aspects of Quantum Field Theory, Universität Leipzig und MPI-MIS Leipzig, 23.-24.6.2017, sponsored by Research Academy Leipzig

Prof. Dr. G. Rudolph
- Referee: Class. Quant. Grav., J. Math. Phys., J. Geom. Phys., J. Phys. A, Rep. Math. Phys., Commun. Math. Phys.
- Referee for the German Research Council (DFG) and the Alexander von Humboldt Foundation

Priv.-Doz. Dr. Michael Bordag
- Organization of the workshop
  Dispersion forces and dissipation
  Leipzig, 1.11.2017
- Referee: J. Phys. A, Phys. Rev. D, J. Math. Phys.

Dr. T.-P. Hack
- Referee for AvH Stiftung
- Referee: Ann. H. Poincaré, Class. Quantum Grav., Phys. Lett. B, Gen. Rel. Grav., Math. Rev. (AMS)

Dr. Matthias Schmidt
- Referee: J. Phys. A and Int. J. Mod. Phys. A

11.10 External Cooperations

Academic

- Mathematisches Institut, Universität Göttingen
  Prof. Dr. D. Bahns
- Dipartimento di Matematica, Universitá di Trento, Italy
  Prof. Dr. Romeo Brunetti
- Institut f. Theoretische Physik, Universität Göttingen
  Prof. Dr. D. Buchholz
- Department of Mathematics, University of York, England
  Prof. Dr. C. J. Fewster
- II. Institut f. Theoretische Physik, Universität Hamburg
  Prof. Dr. K. Fredenhagen
- Department of Mathematics, University of York, England
  Dr. M. B. Fröb
- Department of Mathematics, University of York, England
  Dr. A. Higuchi

- Department of Mathematics, University of Prague, Czech Republic
  Dr. I. Khavkine
- Department of Mathematics, University of York, England
  Dr. K. Rejzner
- Dipartimento di Matematica, Universitá di Genova, Italy
  Prof. Dr. N. Pinamonti
- Department of Mathematics, University of York, England
  Dr. K. Rejzner
- Max Planck Institute for Mathematics in the Sciences, Leipzig
  Dr. J. Tolkstorf
- University of Paderborn, Institute for Mathematics
  Prof. Dr. C. Fleischhack
- Polish Academy of Sciences, Center for Theoretical Physics, Warsaw
  Prof. Dr. J. Kijowski, Dr. Sz. Charzynski
- University of Boulder
  Prof. Dr. Markus Pflaum
- University of Tasmania, Hobart
  Prof. Dr. P. Jarvis
- Université des Sciences et Technologies de Lille
  Prof. Dr. J. Huebschmann
- University of New South Wales, Sydney
  Prof. H. Grundling
- National University, Dnepropetrovsk
  Prof. V. Skalozub
- Central Astronomical Observatory at Pulkovo of the Russian Academy of Science,
  Prof. V.M.Mostepanenko
- Baylor University, Texas
  Prof. K. Kirsten
- VIK Dubna
  Dr. V. Nesterenko, Dr. I. Pirozhenko

11.11 Publications

Journals

M. Bordag: Casimir and Casimir-Polder forces with dissipation from first principles. *Phys. Rev. A*, 96:062504, Dec 2017.

M. Bordag, I. Fialkovsky, and D. Vassilevich: *Casimir Interaction of Strained Graphene*. *Phys. Lett. A*, 381:2439, 2017.

M. Bordag and I.G. Pirozhenko: *Casimir Effect for Dirac Lattices*. *Phys. Rev. D*, 95:056017, 2017. ArXiv: 1701.0261.

M. B. Fröb, T.-P. Hack and A. Higuchi: *Compactly supported linearised observables in single-field inflation*, JCAP **1707** (2017) 043, doi:10.1088/1475-7516/2017/07/043

N. Drago, T. P. Hack and N. Pinamonti: *The generalised principle of perturbative agreement and the thermal mass*, Annales Henri Poincare **18** (2017) no.3, 807, doi:10.1007/s00023-016-0521-6

F. Fürstenberg, G. Rudolph, M. Schmidt: Defining relations for the orbit type strata of SU(2)-lattice gauge models. J. Geom. Phys. **119** (2017) 66–81.

M. Gransee, N. Pinamonti and R. Verch: *KMS-like Properties of Local Equilibrium States in Quantum Field Theory*, J. Geom. Phys. **117** (2017) 15, doi:10.1016/j.geomphys.2017.02.014

Books

G. Rudolph, M. Schmidt: *Differential Geometry and Mathematical Physics. Part II. Fibre Bundles, Topology and Gauge Fields*, Springer Series in Theoretical and Mathematical Physics, 2017, p840

In press

M Bordag, G L Klimchitskaya, and V M Mostepanenko: *Nonperturbative theory of atom-surface interaction: corrections at short separations. Journal of Physics: Condensed Matter*, 30(5):055003, 2018.

M. Bordag: *Vacuum and thermal energies for two oscillators interacting through a field.* arXiv: 1707.06214, to appear in Theor.Mat.Phys.

J. Tolksdorf and R. Verch: *Quantum physics, fields and closed timelike curves: The D-CTC condition in quantum field theory*, Commun. Math. Phys. **357** (2018) no.1, 319, doi:10.1007/s00220-017-2943-5

Preprints

M. B. Fröb, T.-P. Hack and I. Khavkine: *Approaches to linear local gauge-invariant observables in inflationary cosmologies*, arXiv:1801.02632 [gr-qc]

Talks

T. Diez: *Smoothness of the holonomy map.* Higher Differential Geometry Seminar, MPI Bonn 2017-08-02

T. Diez: *Normal form of momentum maps in infinite dimensions.* Workshop Geometry and PDEs 2017-06-13

T. Diez *On the universality of the incompressible Euler equation.* Shanghai Jiao Tong University 2017-11-03

T. Diez: *Central extensions using holonomy preserving diffeomorphisms in infinite dimensions.* Shanghai Jiao Tong University 2017-11-16

Dr. T.-P. Hack: *Non-equilibrium steady states for the Klein-Gordon Field in 1+3 dimensions*, invited talk, Universität Göttingen (3 July 2017)

Dr. T.-P. Hack: *Non-equilibrium steady states for the Klein-Gordon Field in 1+3 dimensions*, Seminar on QFT, Gravity and Theoretical Particle Physics, Universität Leipzig (6 November 2017)

Prof. R. Verch: *The D-CTC condition in quantum field theory*, invited talk, DPG-Tagung Bremen, März 2017

Prof. R. Verch: *Closed timelike curves and the D-CTC condition in quantum field theory*, invited talk, Conference Quantum Field Theory: Concepts, Constructions and Curved Spacetimes, University of York, 04.4.2017 to 07.4.2017

Prof. R. Verch: *Wick-Moyal rotation for quantum fields non (degenerate) Moyal Space/Time*, invited talk, Workshop Reflection Positivity, Mathematisches Forschungsinstitut Oberwolfach, 2.-6.12.2017

11.12 Graduations

Bachelor

- Mohamed Belhassen
  Backflow in Quantum Mechanical Potential Scattering
  Date 25.09.2017

11.13 Guests

- Prof. Dr. Christopher J. Fewster
  U York
  December 2 - December 9, 2017
- Prof. Dr. Nicola Pinamonti
  U Genova
  November 1, 2017 - February 28, 2018, Funding: DAAD

12

Statistical Physics

12.1 Introduction

The focus of research in the STP group is on low-dimensional and mesoscopic interacting systems. These systems are fascinating because on the one hand they allow to study fundamental questions of quantum statistical mechanics, and on the other hand they have a great potential for technological applications. The interplay of a reduced dimensionality with enchanced interaction effects, non-equilibrium physics, and possibly disorder allows the observation of many interesting phenomena, which pose a stimulating challenge for theoretical analysis. The mathematical language used for the description of these systems is quantum field theory, including techniques like functional integrals, renormalization group, instanton calculus, the Keldysh technique for non-equilibrium situations, and the replica method for disordered systems. These analytical tools are suplemented by the use of computer algebra (Mathematica) and numerical calculations (Matlab, Perl, C++). We try to combine the analysis of theoretically interesting problems with relevance to experiments on nanostructures.
Fractional quantum hall (QH) systems display perhaps the richest and most beautiful physics of all condensed matter systems. They are a prime example for the idea that the whole is more than the sum of its parts, as low lying excitations of a fractional QH fluid carry only a faction of the electron charge and are thus qualitatively different from the system constituents. Recently, interest in fractional QH physics has been reinvigorated by the prospect that quasiparticles (QPs) of the fractional QH state at filling fraction 5/2 may be non-abelian anyons, i.e. their braiding may not only give rise to a multiplication of the wave function with a complex phase, but in addition corresponds to a unitary transformation of the highly degenerate ground state. Due to the topological nature of braiding, these unitary transformations are robust against local perturbations and guarantee a high degree of stability of the quantum weave of braids, lending it to the construction of topological quantum bits. Future research in this field will concentrate on both the analysis of qualitative properties of topologically ordered systems and the description of experimentally relevant consequences in nanostructured systems.
Similarly to the edge states of QH systems, in single channel nanowires interactions strongly modify the dynamics of electrons. In the presence of strong spin-orbit coupling and in proximity to a superconductor, nanowires can support a topologically ordered state suitable for the formation of topological quantum bits. In multimode nanowires, a quantum phase transition between superconductor and diffusive metal can occur,

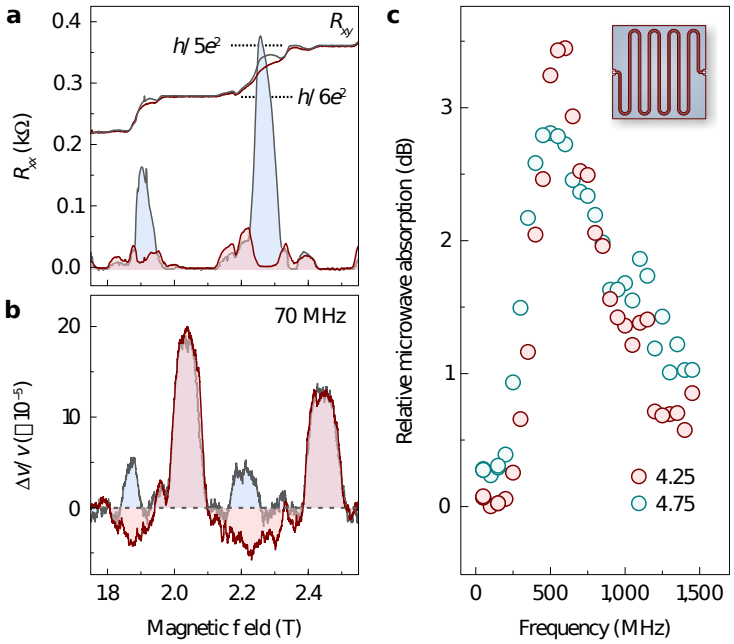

Figure 12.1: On the origin of the negative velocity shift (a) Longitudinal and Hall resistance between filling factor 5 and 7 in the crystallographic directions [110] (blue) and [110] (red). (b) SAW velocity change measured along the same directions at a SAW frequency of 70 MHz. (c) Frequency dependence of the microwave adsorption at filling factor 4.25 (red circles) and 4.75 (green circles). The measurement was done using a coplanar stripline configuration as shown in the inset. A clear resonance is observed at a frequency of 500-600 MHz.

which is tuned by an external magnetic field and is experimentally realized in niobium and molybdenum-germanium systems. Comparatively small changes in the external magnetic field can give rise to a large change in conductivity. Quantum mechanical fluctuations of the superconducting phase can restore part of the density of states, which is reduced due to scattering of electrons off the superconducting order parameter.

B. Rosenow

12.2 Negative permittivity in bubble and stripe phases

B. Friess*, Y. Peng†, B. Rosenow, F. vonOppen†, V. Umansky‡, K. vonKlitzing*, J.H. Smet*

*Max-Planck Insitute for Solid State Research, Stuttgart
†Dahlem Center for Theoretical Physics, Free University of Berlin
‡Weizmann Institute of Science

The physics of itinerant electrons in condensed matter is by and large governed by repulsive Coulomb forces. However, cases exist where attractive interactions emerge and prevail in determining the ground state of the system despite the concomitant and pervasive Coulomb repulsion. The most notable example is no doubt electron pairing, which leads to superconductivity and is mediated by electron-phonon coupling or more intricate mechanisms such as antiferromagnetic spin order in high-temperature superconductors. The interplay of attractive and repulsive interaction components may also instigate spontaneous symmetry lowering and clustering of charges in geometric

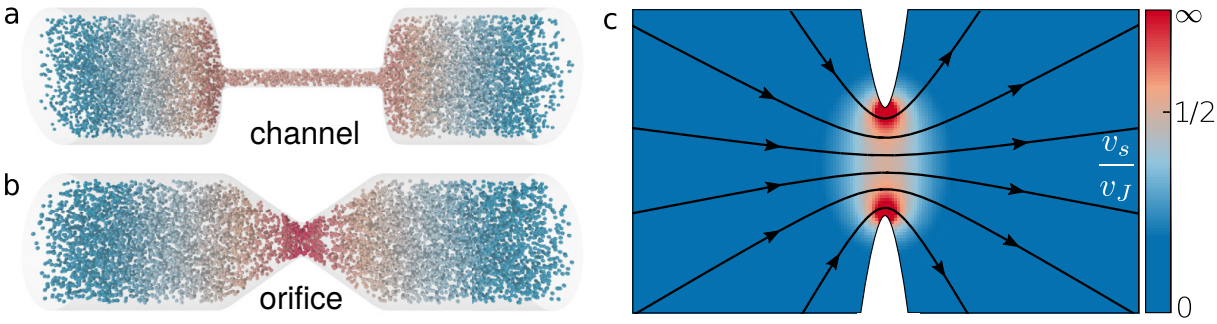

Figure 12.2: a A current of superfluid atoms driven through a long channel with a homogeneous (radius independent) flow profile. **b** Flow through a narrow orifice formed from the surface of revolution of a hyperbola around the flow axis. **c** Velocity field v_s for the potential flow though an orifice in units of the average flow speed v_J . The flow direction is indicated by black lines, with the magnitude diverging as a power law at the orifice boundary.

patterns such as bubbles and stripes. No net attractive interaction is required for such clustering, but an important prerequisite is that the opposing interaction components act on different length scales. In high-temperature superconductors, fluctuating stripe or nematic ordering is intertwined with superconductivity itself. Both types of attractive interaction triggered physics, pairing and charge ordering, are also at play in high-quality two-dimensional electron systems exposed to a quantizing perpendicular magnetic field. The charge ordering has been concluded indirectly from transport behaviour. Here we report the observation of negative permittivity present solely when bubble and stripe phases form. In conjunction with a theoretical model, the negative permittivity can be traced back to the exchange-correlation energy which sufficiently countervails Coulomb repulsion at small distances to enable and mediate charge clustering [1]. The implemented technique based on surface acoustic waves offers true directionality and confirms the stripe phase to be a strongly anisotropic medium.

[1] B. Friess, Y. Peng, B. Rosenow, F. von Oppen, V. Umansky, K. von Klitzing, and J.H. Smet, *Negative permittivity in bubble and stripe phases*, Nature Physics **13**, 1124 (2017).

12.3 Dissipation in mesoscale superfluids

A. Del Maestro*, B. Rosenow

*Department of Physics, University of Vermont, Burlington, VT 05405, USA

We investigate the maximum speed at which a driven superfluid can flow through a narrow constriction with a size on the order of the healing length. Considering dissipation via the thermal nucleation of quantized vortices, we calculate the critical velocity for superfluid 4He and ultracold atomtronic circuits, identify fundamental length and velocity scales, and are thus able to present results obtained in widely different temperature and density ranges in a universal framework. For ultra-narrow channels we predict a drastic reduction in the critical velocity as the energy barrier for flow reducing thermally activated phase slip fluctuations is suppressed.

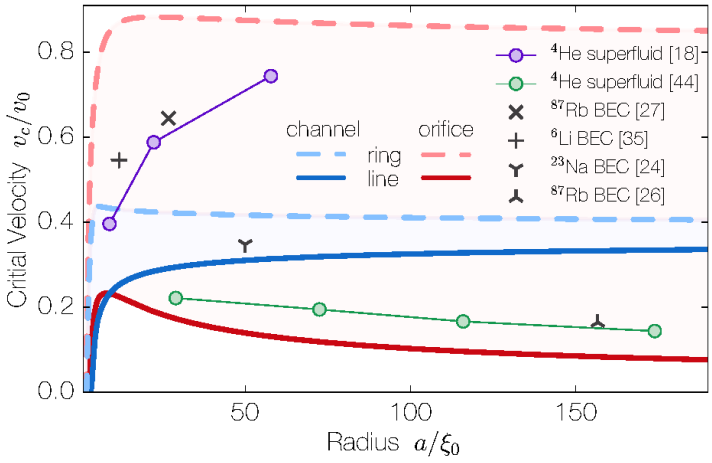

Figure 12.3: Upper and lower bounds on the critical velocity are indicated by lines from the channel ($L = 10^3\xi_0$, blue) and orifice ($L = 10\xi_0$, red) flow profiles for both ring (dashed) and line vortices (solid) at $T = 0.7T_c$, $\hbar\Gamma?? = 0.1k_BT_c$, and $\nu = 0.6717$. Symbols show experimental massflow results for superfluid helium and Bose-Einstein condensates.

The flow of dissipationless atomic supercurrents in neutral superfluids is one of the most dramatic manifestations of macroscopic quantum coherence, with applications to matter wave interferometry. Recently, there has been increased interest in dimensionally confined superfluids, due to progress in manufacturing nanoscale channels and fountain effect devices for studying the flow of superfluid helium and the availability of trapped non-equilibrium atomic Bose-Einstein condensates. Common to these experiments in vastly different density and interaction regimes is an observed increase in dissipation for highly confined systems.

In this project, we consider confined mesoscale superflow through quasi-one-dimensional (1d) constrictions with a characteristic size a approaching the temperature (T) dependent correlation (healing) length $\xi(T)$, and find a strong increase in dissipation when $a/\xi(T)$ approaches one [1]. Going beyond previous studies, we (i) quantitatively predict the temperature, size, and drive dependence of the critical velocity without adjustable parameters, (ii) use a paradigmatic orifice geometry to model the enhancement of vortex creation in spatially inhomogeneous flow near a sharp boundary, which significantly lowers critical velocities, (iii) point out the universality between high density 4He and low density atomic condensates, by characterizing constrictions via the dimensionless length a/ξ and measuring velocities in units of $v_0 = \kappa/(4\pi\xi_0)$, and (iv) describe the crossover to the purely 1d limit, a Luttinger liquid in the thermal regime. Predictions are expected to be logarithmically accurate in the critical regime while corrections of order unity may arise when extrapolating to lower T.

[1] Adrian Del Maestro, Bernd Rosenow, *Dissipation in mesoscale superfluids*, Phys. Rev. B **95**, 140507(R) (2017).

12.4 Disorder, synchronization and phase locking in non-equilibrium Bose-Einstein condensates

P.R. Eastham*, B. Rosenow

*Trinity College Dublin, Ireland

It is twenty years since Bose-Einstein condensation (BEC) was achieved, in its ideal setting of a weakly-interacting ultracold gas. In other settings, namely superconductivity (which we understand in terms of a Bose-Einstein condensate of Cooper pairs), Bose-Einstein condensates have been available in laboratories for over a century. Yet their behaviour is still startling. Because the many particles of the condensate occupy the same quantum state, collective properties become described by a macroscopic wavefunction, with an interpretation parallel to that of the single-particle wavefunction of Schrödinger's equation. Thus, many of the phenomena of single-particle quantum mechanics appear as behaviours of the condensate.

The aim of this project is to review some theories of how these phenomena generalize to non-equilibrium Bose-Einstein condensates [1]. We have in mind, primarily, the Bose-Einstein condensate of polaritons. Here there is a continuous gain and loss of particles in the condensate, due to pumping and decay. However, the concepts are also relevant to other topical non-equilibrium condensates, including those of magnons and photons, and are linked to aspects of laser physics. Our aim is not a comprehensive review. Rather we hope to indicate a unifying framework for understanding non-equilibrium condensates in inhomogeneous settings, from Josephson-like double-well systems, to complex disorder potentials. We think that these problems can be understood in terms of the synchronization and phase-locking of coupled oscillators, as well as the related phenomenology of mode selection in lasers.

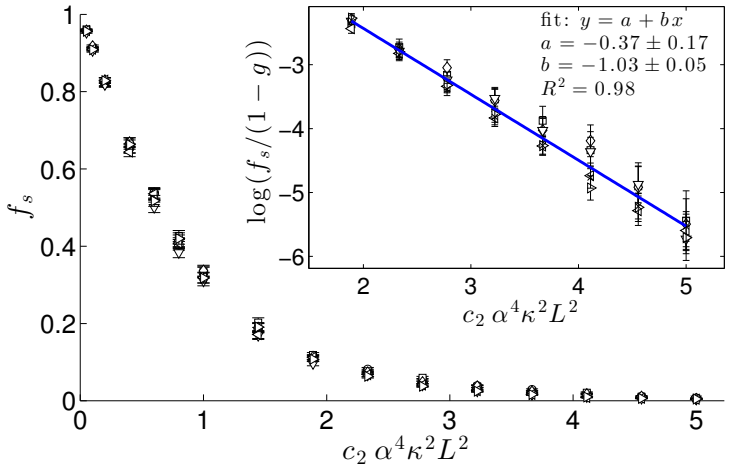

Figure 12.4: Test of the scaling form for the stiffness of a non-equilibrium condensate, $f_s \propto e^{-c_2\,\alpha^4\kappa^2L^2}$. A clear data collapse is observed when plotting the numerically obtained superfluid stiffness as a function of $c_2\alpha^4\kappa^2L^2 \sim L^2/{\mathcal{L}_s}^2$. Inset: exponentially small tail of f_s compared to the scaling form , using the perturbative values c_2 and g. Data points for $L \times L$ lattices with $L = 64$ and 96; $\alpha = 0.9, 1$ and 1.2, and for up to 1320 disorder realizations.

[1] Paul R. Eastham and Bernd Rosenow, *Disorder, synchronization and phase locking in non-equilibrium Bose-Einstein condensates*, contributed chapter for book "Universal themes of Bose-Einstein condensation", edited by David Snoke, Peter Littlewood and Nick Proukakis, Cambridge University Press, (2017).

12.5 Transient Features in Charge Fractionalization, Local Equilibration and Non-equilibrium Bosonization

A. Schneider, M. Milletari*, B. Rosenow

*Centre for Advanced 2D Materials and Department of Physics, National University of Singapore

Interactions play a major role in the physics of one-dimensional systems. Due to the reduced dimensionality, excitations in one dimension can only occur collectively, and the system is therefore strongly correlated. As a consequence, the quasiparticle concept of Fermi liquid theory does not apply and these systems are better understood in the framework of Luttinger liquid theory, where for instance the quantum critical behaviour of the system is captured by non-trivial power law exponents. A convenient way to study Luttinger liquids is through the method of bosonization, where a system of interacting fermions is related to an equivalent system of non-interacting bosons. This remarkable identity allows one to evaluate fermionic correlation functions exactly for the important case of forward scattering interactions, where the peculiar phenomena of spin charge separation is observed. From a mathematical point of view, the exact solution of the model is due to its integrability, i.e. the existence of an infinite number of conserved quantities that in turn precludes the systems from global equilibration. This "equilibrium bosonization" framework has been very useful in the past years to study systems such as carbon nanotubes, polymers, quantum wires or quantum Hall edge states.

In quantum Hall edge states and in other one-dimensional interacting systems, charge fractionalization can occur due to the fact that an injected charge pulse decomposes into eigenmodes propagating at different velocities. If the original charge pulse has some spatial width due to injection with a given source-drain voltage, a finite time is needed until the separation between the fractionalized pulses is larger than their width.

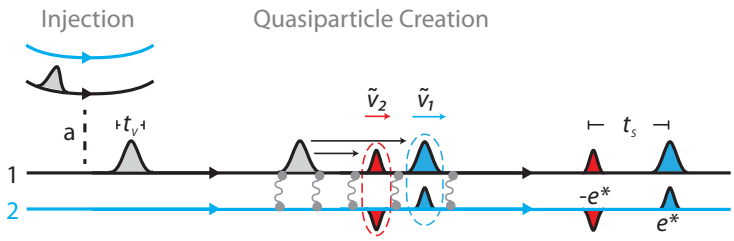

Figure 12.5: A charge pulse of time duration t_v is injected into edge mode 1. Due to the interaction quench, the injected pulse decomposes into a charge and a neutral pulse, propagating with different velocities $\tilde{v}_i$. After the quench, two oppositely and fractionally charged pulses e^* are separated in time by t_s in edge mode 2.

In the formalism of non-equilibrium bosonization, the above physics is reflected in the separation of initially overlapping square pulses in the effective scattering phase. When expressing the single particle Green's function as a functional determinant of counting operators containing the scattering phase, the time evolution of charge fractionalization is mathematically described by functional determinants with overlapping pulses. We develop a framework for the evaluation of such determinants, describe the system's equilibration dynamics, and compare our theoretical results with recent experimental findings [1].

[1] Alexander Schneider, Mirco Milletari, and Bernd Rosenow, *Transient Features in Charge Fractionalization, Local Equilibration and Non-equilibrium Bosonization*, SciPost Phys. 2, 007 (2017).

12.6 Time-reversal-symmetric topological magnetoelectric effect in three-dimensional topological insulators

H.-G. Zirnstein, B. Rosenow

Topological insulators [1, 2], are electronic materials that are insulating in the bulk, but feature conducting surface states which are protected against smooth perturbations, as long as these perturbations preserve certain symmetries. For instance, a time-reversal symmetric topological insulator will have conducting surface states even when the crystal structure is deformed or disorder is introduced, as these types of perturbations preserve time-reversal symmetry. Concrete examples that exist as 3D bulk materials are Bi_2Se_3 and Bi_2Te_3.

In Ref. [3], we have studied the symmetries of the electromagnetic response of the surface states of such time-reversal (TR) symmetric topological insulators more closely. One of their hallmark responses is the topological magnetoelectric effect, where a magnetic field induces an electric charge and vice-versa. So far, a variant of this effect has attracted much attention where time-reversal is, however, broken explicitly. Thus, we face the puzzling situation where these surface states are protected by TR-symmetry, yet their hallmark effect requires explicit TR-breaking. We have resolved this conundrum and presented a topological magnetoelectric effect that is explicitly time-reversal-symmetric.

In particular, we have shown that threading a thin magnetic flux tube of one flux quantum through the material and applying a uniform electric field will induce a half-integer charge $\Delta Q = e/2 \cdot sgn(E_z)$ on the surface of the topological insulator if the system has mesoscopic size. This is illustrated in the figure. A key point of this effect is that the sign of this induced charge does not depend on the direction of magnetic field, only on the direction of the electric field. This is the defining characteristic of a time-reversal symmetric charge response.

The effect can be understood in terms of the surface states of the topological insulator. Threading the flux tube through the material will lead to two electronic states, which are located at the two places where the flux tube meets the surface. Without electric field, these states will hybridize and a superposition of these states with has equal weight in

either place will be occupied. In the presence of a small electric field, one state will be occupied, while the other one will be emptied. This corresponds to a transfer of charge $e/2$. The validity of this argument depends on how well these two particular states can be separated from the other electronic states on the surface. By a combination of analytic and numerical arguments, we have shown that there are two energy scales: The energy splitting of the two states, which vanishes with decreasing flux tube size, and the energy of the other states, which is determined by the system size, but independent of the (relative) flux tube size. By choosing the electric potential in between these two energy scales, it is possible to single out the response of these two states. In the limit of a vanishing flux tube size, this leads to the half-integer charge as described. For a finite flux tube size, which is experimentally more relevant, we have shown numerically that the effect still yields an appreciable charge response. This means that the effect could be observed experimentally, though realizing the proposed setup is likely challenging.

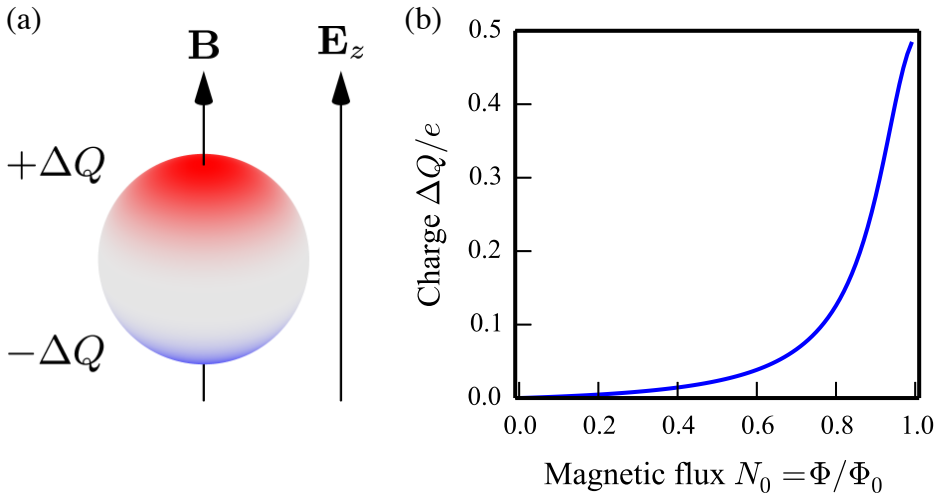

Figure 12.6: Spherical topological insulator threaded by a thin magnetic flux tube with flux Φ and subject to an electric field E_z in vertical direction. Insertion of one flux quantum induces a charge $\Delta Q = e/2$. (a) Geometry. (b) Analytical result for the charge difference in the top hemisphere, $\Delta Q(E_z, \Phi)$, in the thin flux tube limit for an external electric field E_z, giving rise to a potential difference $e2RE_z$ between top and bottom, with $e2RE_z = 0.2v_F/R$. Here, R denotes the radius of the sphere and v_F is the Fermi velocity on the surface.

[1] M. Z. Hasan and C. L. Kane, *Colloquium: Topological insulators*, Rev. Mod. Phys. **82**, 3045 (2010).

[2] X.-L. Qi and S.-C. Zhang, *Topological insulators and superconductors*, Rev. Mod. Phys. **83**, 1057 (2011).

[3] H.-G. Zirnstein and B. Rosenow, *Time-reversal-symmetric topological magneto-electric effect in three-dimensional topological insulators*, Phys. Rev. B **96**, 201112 (2017).

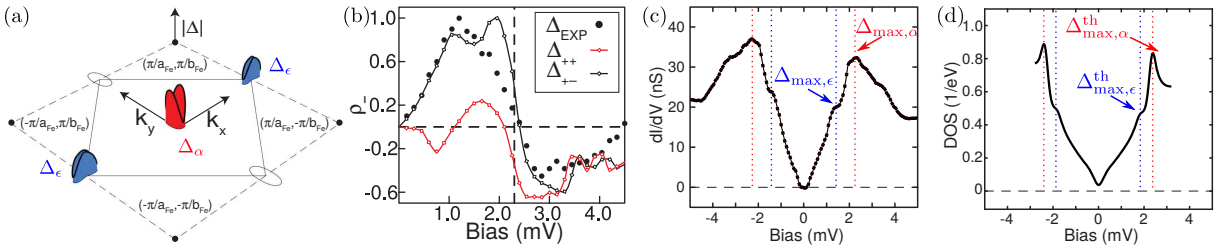

Figure 12.7: (a) Result of the deduction of the Fermi surface and the superconducting order parameter (magnitude) for FeSe on the α and ε Fermi surface sheet together with the information about the sign change (red/blue)[3]. (b) Calculated antisymmetrized QPI signal as introduced in Ref. [2] (integrated over momenta corresponding to intrapocket scattering) using a sign changing order parameter Δ_{+-} and an order parameter without sign change Δ_{++} as input and compared to the experimental data (dots) revealing a sign change of the order parameter. (c) Typical experimental spectrum of the homogeneous superconductor and corresponding calculated spectrum exhibiting two features from the gap maxima on the two Fermi surfaces (d)[3]

12.7 Discovery of Orbital-Selective Cooper Pairing in FeSe

P.O. Sprau*, A. Kostin*, A. Kreisel, A.E. Böhmer†, V. Taufour†, P.C. Canfield†, S. Mukherjee‡, P.J. Hirschfeld§, B.M. Andersen¶, J.C. SéamusDavis*

*Laboratory of Atomic and Solid State Physics, Department of Physics, Cornell University, Ithaca, NY 14853, USA
†Ames Laboratory, U.S. Department of Energy, Ames, IA 50011, USA
‡Department of Physics, Binghamton University, State University of New York, Binghamton, NY, USA
§Department of Physics, University of Florida, Gainesville, FL 32611, USA
¶Niels Bohr Institute, University of Copenhagen, Juliane Maries Vej 30, DK 2100 Copenhagen, Denmark

The superconductor FeSe is of intense interest thanks to its unusual non-magnetic nematic state. Its Cooper pairing mechanism has not been determined partly because an accurate knowledge of the momentum-space structure of superconducting energy gaps on the different electron-bands is missing. We use Bogoliubov quasiparticle interference imaging to determine the Fermi surface geometry of the bands surrounding the Γ and X points of FeSe, and to measure the corresponding superconducting energy gaps. We show that both gaps are extremely anisotropic but nodeless, and have opposite sign with respect to each other which is deduced from a phase sensitive measurement based on the antisymmetric QPI signal $\rho_-(\omega)$[2]. This complex gap configuration reveals orbital-selective Cooper pairing of electrons from the d_{yz} rbitals of iron atoms. A theoretical approach for a modified spin-fluctuation theory[1] which includes reduced coherence of quasiparticles due to correlations finds agreement to the measured gap magnitude and the sign change as well as to simulated spectra, see Fig.12.7.

[1] P. O. Sprau, A. Kostin, A. Kreisel, A. E. Böhmer, V. Taufour, P. C. Canfield, S. Mukherjee, P. J. Hirschfeld, B. M. Andersen, and J. C. S. Davis, *Discovery of orbital-selective Cooper pairing in FeSe*, Science **357**, 75 (2017).

[2] D. Altenfeld, P. J. Hirschfeld, I. I. Mazin, and I. Eremin, *Detecting sign-changing superconducting gap in LiFeAs using quasiparticle interference*, Phys. Rev. B **97**, 054519 (2018).
[3] A. Kreisel, B. M. Andersen, P. O. Sprau, A. Kostin, J. C. S. Davis, and P. J. Hirschfeld, *Orbital selective pairing and gap structures of iron-based superconductors*, Phys. Rev. B **95**, 174504 (2017).

12.8 Orbital selective pairing and gap structures of iron-based superconductors

A. Kreisel, B.M. Andersen*, P.O. Sprau†, A. Kostin†, J.C. SéamusDavis† P.J. Hirschfeld‡

*Niels Bohr Institute, University of Copenhagen, Juliane Maries Vej 30, DK 2100 Copenhagen, Denmark
†Laboratory of Atomic and Solid State Physics, Department of Physics, Cornell University, Ithaca, NY 14853, USA
‡Department of Physics, University of Florida, Gainesville, FL 32611, USA

We discuss the influence on spin-fluctuation pairing theory of orbital selective strong correlation effects in Fe-based superconductors, particularly Fe chalcogenide systems. We propose that a key ingredient for an improved itinerant pairing theory is orbital selectivity, i.e., incorporating the reduced coherence of quasiparticles occupying specific orbital states. This modifies the usual spin-fluctuation via suppression of pair scattering processes involving those less coherent states and results in orbital selective Cooper pairing of electrons in the remaining states. We show that this paradigm yields remarkably good agreement with the experimentally observed anisotropic gap structures in both bulk and monolayer FeSe, as well as LiFeAs (see Fig. 12.8), indicating that orbital selective Cooper pairing plays a key role in the more strongly correlated iron-based superconductors.

In both copper-based and iron-based high temperature superconductors, fundamental issues include the degree of electron correlation and its consequences for enhancing superconductivity. In both archetypes, there are multiple active orbitals (two O p orbitals and one Cu d orbital in the former, and five Fe d orbitals in the latter). This implies the possibility of orbital-selective physics, where states dominated by electrons of one orbital type may be weakly correlated and others much more strongly correlated, leading to substantial differences in quasiparticle spectral weights, interactions, magnetism and orbital ordering[7]. Cooper pairing itself could then become orbital-selective, with the electrons of a specific orbital character binding to form the Cooper pairs of the superconductor. The superconducting energy gaps of such a material would therefore generically be highly anisotropic, i.e., large only for those Fermi surface regions where a specific orbital character dominates. Such phenomena, although long the focus of theoretical research on higher temperature superconductivity in correlated multi-orbital superconductors, have remained largely unexplored because orbital-selective Cooper pairing has not been experimentally accessible.

Spin fluctuations are proposed as the dominant mechanism driving Cooper pairing in a wide variety of unconventional superconductors: heavy-fermion systems, cuprates,

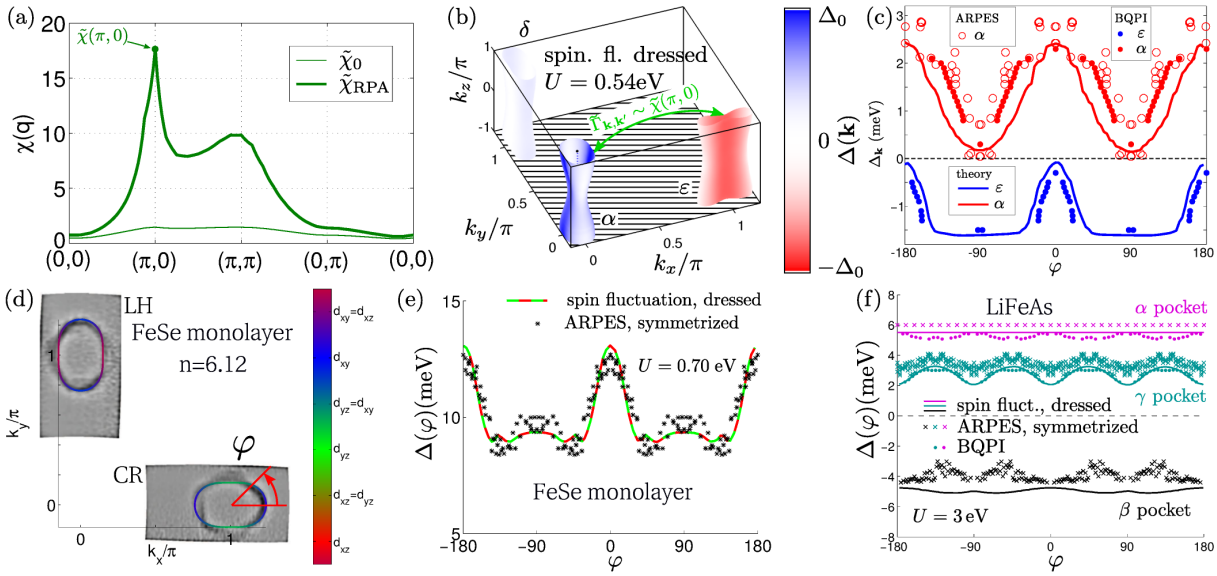

Figure 12.8: (a) Calculated interacting susceptibility in the scenario of an orbital-selective Fermi liquid for FeSE. It exhibits a large static susceptibility at $(\pi, 0)$ which drives (b) the sign change of the order parameter on the bands forming the α and ε Fermi surfaces. This, in turn agrees with the experimental observations (c)[1, 3, 3]. The same tight binding model without orbital order and doped to yield an electron density of $n = 6.12$ electrons per elementary cell describes the experimentally observed Fermi surface almost perfectly (d)[1, 4] and the orbital-selective pairing scenario can reproduce the gap structure with two (local) maxima (e)[4]. (f) Similar conclusions about the scenario of reduced coherence can be drawn when calculating the superconducting order parameter for LiFeAs and compare it to experimentally available data[5, 6].

two-dimensional organic charge transfer salts, and iron-based superconductors (FeSC). One of the employed calculational schemes is referred to as random phase approximation (RPA) has achieved considerable qualitative progress for unconventional systems.

While material-specific calculations of the critical temperature T_c within spin-fluctuation theory appear distant, considerable success has been achieved understanding qualitative aspects of pairing, particularly in Fe-pnictide systems.

The consequences of correlations for the band structure of FeSC are more profound than simple Fermi surface shifts, however. If one examines compounds where the d-bands are closer to half-filling (5 electrons/Fe), the effect of electron-electron interactions are enhanced in a way distinctly different from one-band systems: different d orbital effective masses are enhanced by different factors. This "orbital selectivity" predicted by theory[7] has been confirmed by ARPES experiments. In Fermi liquid theory, excitations in a system of interacting fermions are described by quasiparticles that have the same quantum numbers but deviate from the free particles in properties such as the quasiparticle mass, which renormalizes the Fermi velocity. Generally, interactions in electronic systems also lead to reduced quasiparticle weights, corresponding to reduced values of the residue at the pole of the Green's function describing those dressed electrons.

In this work, we implement a simple scheme to incorporate aspects of renormalization of the electronic band structure, including reduced quasiparticle coherence that is orbital selective into spin-fluctuation pairing theory, and apply it to several FeSC. This orbital selective approach to pairing provides an excellent description for the super-

conducting gap deduced from quasiparticle interference measurements on the nematic Fermi surface pockets of bulk FeSe, as shown already in Ref. [3]. Here we discuss the generality of this approach, and show how it explains the exotic gap structures of FeSe, FeSe monolayers and in the LiFeAs system as well. These findings encourage us to believe that the proposed paradigm is the correct way to understand the physics in these materials, but we cannot rule out completely that other effects affecting the gap such as spin-orbit coupling or orbital fluctuations may contribute. While the microscopic origin of the phenomenology remains an open challenge, we believe that it provides a major step towards a quantitative, material-specific theory of superconductivity in strongly correlated FeSC and reveal an immediate challenge to determine if our approach can be combined with microscopic calculations of quasiparticle weights to yield a material-specific theory with predictive power for strongly correlated FeSC.

[1] A. Kreisel, B. M. Andersen, P. O. Sprau, A. Kostin, J. C. S. Davis, and P. J. Hirschfeld, *Orbital selective pairing and gap structures of iron-based superconductors*, Phys. Rev. B **95**, 174504 (2017).

[2] P. O. Sprau, A. Kostin, A. Kreisel, A. E. Böhmer, V. Taufour, P. C. Canfield, S. Mukherjee, P. J. Hirschfeld, B. M. Andersen, and J. C. S. Davis, *Discovery of orbital-selective Cooper pairing in FeSe*, Science **357**, 75 (2017).

[3] H. C. Xu, X. H. Niu, D. F. Xu, J. Jiang, Q. Yao, Q. Y. Chen, Q. Song, M. Abdel-Hafiez, D. A. Chareev, A. N. Vasiliev, Q. S. Wang, H. L. Wo, J. Zhao, R. Peng, and D. L. Feng, *Highly Anisotropic and Twofold Symmetric Superconducting Gap in Nematically Ordered* $FeSe_{0.93}S_{0.07}$, Phys. Rev. Lett. **117**, 157003 (2016).

[4] Y. Zhang, J. J. Lee, R. G. Moore, W. Li, M. Yi, M. Hashimoto, D. H. Lu, T. P. Devereaux, D.-H. Lee, and Z.-X. Shen, *Superconducting Gap Anisotropy in Monolayer FeSe Thin Film*, Phys. Rev. Lett. **117**, 117001 (2016).

[5] M. P. Allan, A. W. Rost, A. P. Mackenzie, Y. Xie, J. C. Davis, K. Kihou, C. H. Lee, A. Iyo, H. Eisaki, and T.-M. Chuang, *Anisotropic Energy Gaps of Iron-Based Superconductivity from Intraband Quasiparticle Interference in LiFeAs*, Science **336**, 563 (2012).

[6] S. V. Borisenko, V. B. Zabolotnyy, A. A. Kordyuk, D. V. Evtushinsky, T. K. Kim, I. V. Morozov, R. Follath, and B. Büchner, *One-Sign Order Parameter in Iron Based Superconductor*, Symmetry **4**, 251 (2012).

[7] A. van Roekeghem, P. Richard, H. Ding, and S. Biermann, *Spectral properties of transition metal pnictides and chalcogenides: Angle-resolved photoemission spectroscopy and dynamical mean-field theory*, C. R. Phys. **17**, 140 (2016).

12.9 Robustness of a quasiparticle interference test for sign-changing gaps in multiband superconductors

J.H.J. Martiny*, A. Kreisel, B.M. Andersen*, P.J. Hirschfeld†

*Niels Bohr Institute, University of Copenhagen, Juliane Maries Vej 30, DK 2100 Copenhagen, Denmark

†Department of Physics, University of Florida, Gainesville, FL 32611, USA

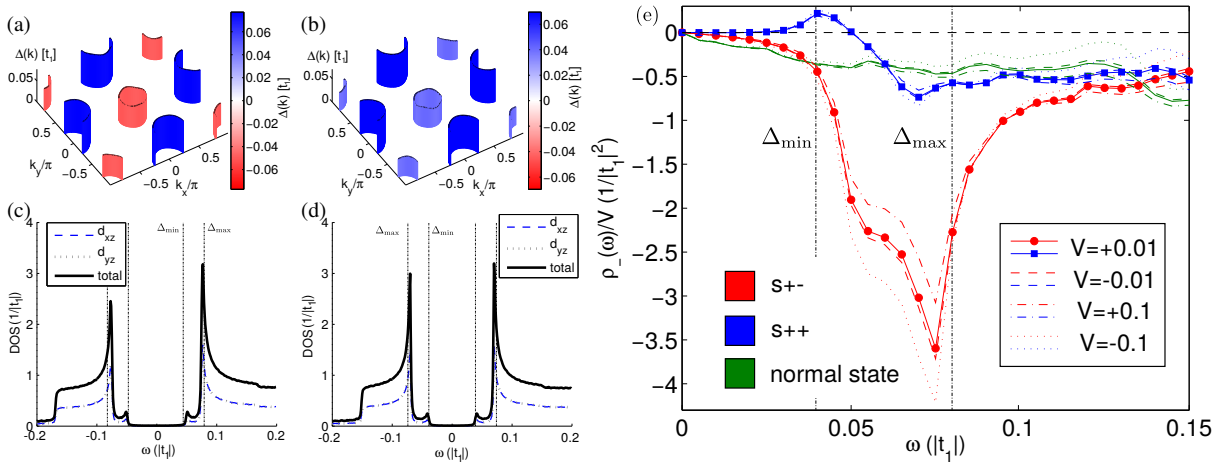

Figure 12.9: (a) Fermi surface and superconducting gap for the two band model as used in the present study. The superconducting order parameter exhibits a sign change between the electronlike and holelike Fermi surface sheets where the gap has sligtly different magnitude. (b) Similar order parameter, but without sign change such that the density of states from the model with sign change (c) and without sign change (d) cannot be distinguished. (e) Result of a realistic calculation of the antisymmetric QPI signal $\rho_-(\omega)$ in the normal state (green) and for the two superconducting order parameters. $\rho_-(\omega)$ clearly exhibits a sign change for the s_{++} order paramter which is absent for the s_{+-} case. This result is fully robust under changes of the impurit potential (different curves).

The most fundamental question that can be posed about a newly discovered superconductor is why conduction electrons pair. In particular, it is important to know whether the pairing mechanism is unconventional, i.e. based on an effective attraction that arises from the Coulomb interaction rather than from the exchange of phonons as in a traditional BCS system. While this question is difficult to answer directly, a good hint is often provided by whether the gap changes sign over the Fermi surface of the candidate material, since such a state is generically produced by repulsive interactions. Even this indirect type of proof has been particularly vexing to establish in the iron-based superconductors (FeSC)[1], however, since many of them have rather isotropic gaps, and the sign-change may occur between different Fermi surface sheets, leading to a quasiparticle spectrum without zero-energy states, very similar to that which would occur were the system to have the same gaps without a sign change.

Recently, a test ("HAEM" method) for a sign-changing gap function in a candidate multiband unconventional superconductor involving quasiparticle interference data was proposed[2]. The test was based on the antisymmetric, Fourier-transformed conductance integrated over a range of momenta $\mathbf{q}$ corresponding to interband processes, which was argued to display a particular resonant form, provided the gaps changed sign between the Fermi surface sheets connected by $\mathbf{q}$. The calculation was performed for a single impurity, however, raising the question of how robust this measure is as a test of sign-changing pairing in a realistic system with many impurities. Here we reproduce the results of the previous work within a model with two distinct Fermi surface sheets (see Fig. 12.9), and show explicitly that the previous result, while exact for a single nonmagnetic scatterer and also in the limit of a dense set of random impurities, can be difficult to implement for a few dilute impurities. We show that the

HAEM result is indeed obscured for a dilute impurity system, but also that a clear signal can generally be recovered by properly windowing an isolated impurity that occurs in such a context, a technique already successfully employed on the Fe-based superconductor FeSe.[3] We further investigate and discuss the effect of stronger and magnetic impurity potentials. Finally, we discuss how to apply the HAEM method to non-*s*-wave pair states in multiband systems. An interesting distinction arises in the case of *d*-wave states in systems without hole pockets, proposed e.g. for monolayer FeSe on $SrTiO_3$ and various FeSe intercalates (for a discussion see Ref. [1]. Since the gap sizes on the two electron pockets are identical by symmetry, the simplest nodeless *d*-wave case yields a sharp, antisymmetrized momentum-integrated conductance peak whose width is due only to on-pocket anisotropy and thermal broadening. Such a signal should be easy to distinguish from that arising from both $s_{\pm}$ and s_{++} gap symmetries. In summary, this work demonstrates three possible ways to recover the robust determination of inter-pocket gap sign changes, and we conclude that the HAEM procedure is a realistic method to be used for this purpose.

[1] P. J. Hirschfeld, *Using gap symmetry and structure to reveal the pairing mechanism in Fe-based superconductors*, C. R. Phys. **17**, 197 (2016).
[2] P. J. Hirschfeld, D. Altenfeld, I. Eremin, and I. I. Mazin, *Robust determination of the superconducting gap sign structure via quasiparticle interference*, Phys. Rev. B **92**, 184513 (2015).
[3] P. O. Sprau, A. Kostin, A. Kreisel, A. E. Böhmer, V. Taufour, P. C. Canfield, S. Mukherjee, P. J. Hirschfeld, B. M. Andersen, and J. C. S. Davis, *Discovery of orbital-selective Cooper pairing in FeSe*, Science **357**, 75 (2017).

12.10 Imaging the Real Space Structure of the Spin Fluctuations in an Iron-based superconductor

S. Chi[*], R. Aluru[†], S. Grothe[*], A. Kreisel, U.R. Singh[‡], B.M. Andersen[§], W.N. Hardy[*], R. Liang[*], D.A. Bonn[*], S.A. Burke[*], P. Wahl[†]

[*]Department of Physics and Astronomy, University of British Columbia, Vancouver BC, Canada V6T 1Z1
[†]SUPA, School of Physics and Astronomy, University of St. Andrews, North Haugh, St. Andrews, Fife, KY16 9SS, United Kingdom
[‡]Max-Planck-Institut für Festkörperforschung, Stuttgart, Germany
[§]Niels Bohr Institute, University of Copenhagen, Copenhagen, Denmark

Spin fluctuations are a leading candidate for the pairing mechanism in high temperature superconductors, supported by the common appearance of a distinct resonance in the spin susceptibility across the cuprates, iron-based superconductors and many heavy fermion materials. The information we have about the spin resonance comes almost exclusively from neutron scattering. Here we demonstrate that by using low-temperature scanning tunneling microscopy and spectroscopy we can characterize the spin resonance in real space. Theoretical calculations for the inelastic tunneling contributions show show that the spectra should exhibit a characteristic dip-hump feature

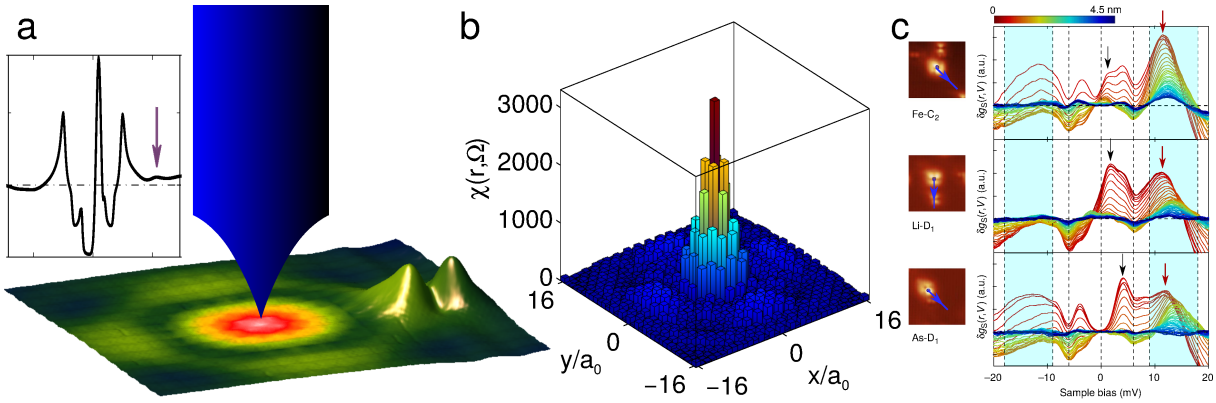

Figure 12.10: (a) Schematic of the experimental method to detect the real space structure: The STM tip probes the real space structure of the spin excitations (colored on the surface) by using the large density of states of an impurity (height profile) which gives rise to the dip-hump feature (purple arrow) in the spectrum. (b) Real space structure of spin excitations in the superconducting state as calculated from an itinerant approach together with a sign-changing superconducting order parameter that produces a neutron resonance in the spin susceptibility. (c) Examples of impurities and differential spectra as the STM tip is moved away (color scale for curves). While the impurity peak is quickly suppressed (black arrow), the dip-hump feature (purple arrow) is visible at much larger distances which enables to measure the size of the spin fluctuation modes in real space.

if a strongly peaked bosonic mode is assumed. We argue that the feature seen in tunneling spectra in high temperature superconductors arises from excitations of the spin fluctuations. Spatial mapping of this feature near defects allows us to probe non-local properties of the spin susceptibility and to image its real space structure, see Fig. 12.10.

12.11 Universality of scanning tunneling microscopy in cuprate superconductors

P. Choubey*, A. Kreisel, B.M. Andersen†, P.J. Hirschfeld‡

*Department of Physics, Indian Institute of Science, Bengaluru 560012, India
†Niels Bohr Institute, University of Copenhagen, Copenhagen, Denmark
‡Department of Physics, University of Florida, Gainesville, FL 32611, USA

We consider the problem of local tunneling into cuprate superconductors, combining model based calculations for the superconducting order parameter with wavefunction information obtained from first principles electronic structure. For some time it has been proposed that scanning tunneling microscopy (STM) spectra do not reflect the properties of the superconducting layer in the CuO_2 plane directly beneath the STM tip[1], but rather a weighted sum of spatially proximate states determined by the details of the tunneling process through the layers above the CuO_2 plane which differ from material to material, see Fig. 12.11(a,b). These "filter" ideas have been countered with the argument that similar conductance patterns have been seen around impurities and charge ordered states in systems with atomically quite different barrier layers. Here we use a recently developed Wannier function based method[2, 3] to calculate topograph-

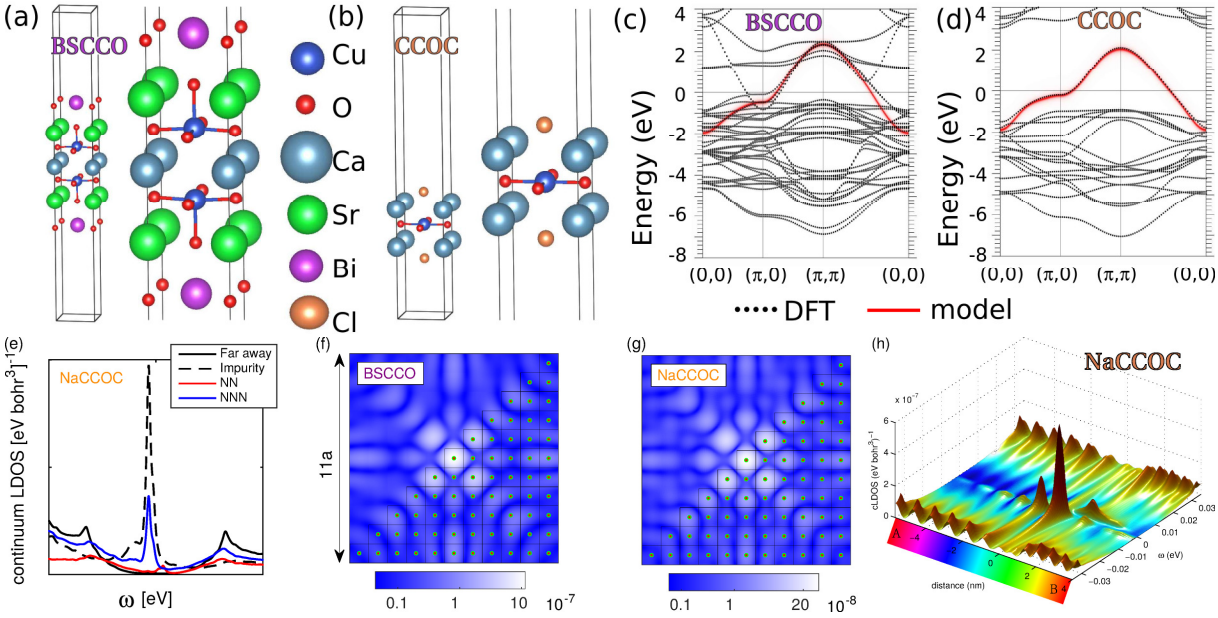

Figure 12.11: Crystal structures of of the $Bi_2Sr_2CaCu_2O_8$ and $Ca_{2-x}Na_xCuO_2Cl_2$system exhibiting different layers above the CuO_2 plane (a,b). The electronic structure of the relevant degrees of freedom is almost identical (c,d); similar for the Wannier functions (not shown). (e) Typical expected spectrum close to a strong impurity in $Ca_{2-x}Na_xCuO_2Cl_2$. (f,g) Real space pattern as expected close to a strong impurity in $Bi_2Sr_2CaCu_2O_8$ and $Ca_{2-x}Na_xCuO_2Cl_2$and (h) spectral behavior as a function of position.

ies, spectra, conductance maps and normalized conductance maps close to impurities. We find that it is the local planar Cu $d_{x^2-y^2}$ Wannier function, qualitatively similar for many systems, that controls the form of the tunneling spectrum Fig. 12.11(e,h) and the spatial patterns near perturbations Fig. 12.11(f,g). We explain how, despite the fact that STM observables depend on the materials-specific details of the tunneling process and setup parameters, there is an overall universality in the qualitative features of conductance spectra. In particular, we discuss why STM results on $Bi_2Sr_2CaCu_2O_8$ (BSCCO) and $Ca_{2-x}Na_xCuO_2Cl_2$(NaCCOC) are essentially identical.

[1] I. Martin, A. V. Balatsky, and J. Zaanen, *Impurity States and Interlayer Tunneling in High Temperature Superconductors*, Phys. Rev. Lett. **88**, 097003 (2002).
[2] P. Choubey, T. Berlijn, A. Kreisel, C. Cao, and P. J. Hirschfeld, *Visualization of atomic-scale phenomena in superconductors: Application to FeSe*, Phys. Rev. B **90**, 134520 (2014).
[3] A. Kreisel, P. Choubey, T. Berlijn, W. Ku, B. M. Andersen, and P. J. Hirschfeld, *Interpretation of Scanning Tunneling Quasiparticle Interference and Impurity States in Cuprates*, Phys. Rev. Lett. **114**, 217002 (2015).

12.12 Funding

Engineering the coherency of fractional and non-abelian electronic interferometers
B. Rosenow
DFG grant RO 2247/8-1

Spin-dependent tunneling in oxide heterostructures
B. Rosenow
SFB 762: Functionality of Oxide Interfaces

Particle Partition Entanglement After a Quantum Quench
B. Rosenow
DFG, Grant RO 2247/10-1, 2017/18

MPI for Mathematics in the Sciences
G. Frigeri
International Max Planck Research Schools

12.13 Organizational Duties

B. Rosenow

- Member of the Qualitätssicherungskommission of the Faculty of Physics and Earth Sciences
- Referee for Science, Phys. Rev. Lett., Phys. Rev. B, Europhys. Lett. Adv. Con. Matter, JSTAT, Physica A, NSF, Studienstiftung des Deutschen Volkes
- Vertrauensdozent (Studienstiftung des Deutschen Volkes)

A. Kreisel

- Referee for Phys. Rev. Lett., Phys. Rev. B, Europhys. Lett., Nature Physics, Nature Communications, Physica Status Solidi B, Annals of Physics, Commucations Physics, DOE

12.14 External Cooperations

Academic

- University of Vermont, USA
  Adrien Del Maestro
- Universität Heidelberg, Germany
  Dr. Michael M. Scherer
- Max-Planck-Institut für Festkörperforschung, Stuttgart, Germany
  G. Khaliullin
- RWTH Aachen, Germany
  Prof. Dr. Carsten Honerkamp
- Universiteit Leiden, Netherlands
  Dr. Timo Hyart
- School of Physics and CRANN, Trinity College, Ireland
  Prof. Paul Eastham
- Weizmann Institute for Science, Israel
  Prof. Yuval Gefen, Prof. Ady Stern, Prof. Yuval Oreg

- Harvard University, USA
  Prof. Bert Halperin
- McGill University, Canada
  Pierre/Francois Duc, Michel Savard, Matei Petrescu, Guillaume Gervais
- University of California, Los Angeles, USA
  So Takei
- Universität zu Köln, Germany
  Prof. Dr. Alexander Altland
- Princeton University, USA
  Curt von Keyserlingk
- University of Oxford, United Kingdom
  Steve Simon
- Niels Bohr Institute, Denmark
  Brian M. Andersen, Kim Lefmann
- University of Florida, USA
  Peter J. Hirschfeld
- Cornell University, USA
  J.C. Séamus Davis
- Unversity of St. Andrews, Scotland
  Peter Wahl
- Oak Ridge National Labatory, USA
  Tom Berlijn
- STFC Rutherford Appleton Laboratory, Oxfordshire, UK
  Pabitra K. Biswas

12.15 Publications

Journals

B. Friess, Y. Peng, B. Rosenow, F. von Oppen, V. Umansky, K. von Klitzing, and J.H. Smet, *Negative permittivity in bubble and stripe phases*, Nature Physics **13**, 1124 (2017)

Paul R. Eastham and Bernd Rosenow, *Disorder, synchronization and phase locking in non-equilibrium Bose-Einstein condensates*, contributed chapter for book "Universal themes of Bose-Einstein condensation", edited by David Snoke, Peter Littlewood and Nick Proukakis, Cambridge University Press, (2017).

Adrian Del Maestro, Bernd Rosenow, *Dissipation in mesoscale superfluids*, Phys. Rev. B **95**, 140507(R) (2017).

Alexander Schneider, Mirco Milletari, and Bernd Rosenow, *Transient Features in Charge Fractionalization, Local Equilibration and Non-equilibrium Bosonization*, SciPost Phys. 2, 007 (2017).

Steffen Richter, Tom Michalsky, Chris Sturm, Bernd Rosenow, Marius Grundmann, Rüdiger Schmidt-Grund, *Exceptional points in anisotropic planar microcavities*, Phys. Rev. A **95**, 023836 (2017)

H.-G. Zirnstein and B. Rosenow, *Time-reversal-symmetric topological magnetoelectric effect in three-dimensional topological insulators*, Phys. Rev. B **96**, 201112 (2017).

P. O. Sprau, A. Kostin, A. Kreisel, A. E. Böhmer, V. Taufour, P. C. Canfield, S. Mukherjee, P. J. Hirschfeld, B. M. Andersen, and J. C. S. Davis, *Discovery of orbital-selective Cooper pairing in FeSe*, Science **357**, 75 (2017).

A. Kreisel, B. M. Andersen, P. O. Sprau, A. Kostin, J. C. S. Davis, and P. J. Hirschfeld, *Orbital selective pairing and gap structures of iron-based superconductors*, Phys. Rev. B **95**, 174504 (2017).

J. H. J. Martiny, A. Kreisel, P. J. Hirschfeld, and B. M. Andersen, *Robustness of a quasiparticle interference test for sign-changing gaps in multiband superconductors*, Phys. Rev. B **95**, 184507 (2017).

S. Chi, R. Aluru, S. Grothe, A. Kreisel, U. R. Singh, B. M. Andersen, W. N. Hardy, R. Liang, D. A. Bonn, S. A. Burke, and P. Wahl, *Imaging the real space structure of the spin fluctuations in an iron-based superconductor*, Nature Communications **8**, 15996 (2017).

P. Choubey, A. Kreisel, T. Berlijn, B. M. Andersen, and P. J. Hirschfeld, *Universality of scanning tunneling microscopy in cuprate superconductors*, Phys. Rev. B **96**, 174523 (2017).

in press

Giovanni A. Frigeri, Daniel D. Scherer, Bernd Rosenow, Subperiods and apparent pairing in integer quantum Hall interferometers

S. L. Holm, A. Kreisel, T. K. Schäffer, A. Bakke, M. Bertelsen, U. B. Hansen, M. Retuerto, J. Larsen, D. Prabhakaran, P. P. Deen, Z. Yamani, J. O. Birk, U. Stuhr, Ch. Niedermayer, A. L. Fennell, B. M. Andersen, K. Lefmann, Magnetic ground state and magnon-phonon interaction in multiferroic h-$YMnO_3$

Anna E. Böhmer, Andreas Kreisel, Nematicity, magnetism and superconductivity in FeSe

Talks

Bernd Rosenow, Topological superconductivity in quantum Hallsuperconductor hybrid systems, Topological Matter & Flat Bands Conference, Leipzig, August 2017

Bernd Rosenow, Enhanced Bulk-Edge Coulomb Coupling in Fractional Fabry-Perot Interferometers, Conference Frontiers in Quantum Hall Physics, Niels Bohr Institute Copenhagen, July 2017.

Bernd Rosenow, Theory of quantum Hall interferometers: subperiods and apparent electron pairing, Symposium Celebrating Physics with a good excuse, Paul-Scherrer Institute, July 2017.

Andreas Kreisel, Orbital-Selective Pairing and Gap Structures of Iron-Based Superconductors, Institut für Theoretische Physik, Universität Frankfurt, February 2017

Andreas Kreisel, Towards a quantitative description of tunneling conductance of superconductors, APS March Meeting 2017, New Orleans, LA, March 2017

Andreas Kreisel, New Developments in the Theory of STM on Unconventional Superconductorsm, DPG-Frühjahrstagung 2017 Dresden, March 2017

Andreas Kreisel, Orbital-Selective Pairing in FeSe, School of Physics and Astronomy, University of St. Andrews, Scotland, April 2017

Andreas Kreisel, Orbital-Selective Pairing in iron-based superconductors, RWTH Aachen, July 2017

Timo Hyart, Overview of my research interests in topological matter, IFPAN, Warsaw, November 2017.

Timo Hyart, Interplay of spontaneous symmetry breaking and topology in condensed matter systems, IFW Dresden, December 2017.

Timo Hyart, Interplay of spontaneous symmetry breaking and topology in condensed matter systems, Uppsala University, December 2017.

Heinrich-Gregor Zirnstein and Bernd Rosenow, A time-reversal symmetric topological magnetoelectric effect in 3D topological insulators, Annual BuildMoNa Conference 2017, March 2017

Heinrich-Gregor Zirnstein and Bernd Rosenow, A time-reversal symmetric topological magnetoelectric effect in 3D topological insulators, DPG-Frühjahrstagung Dresden, March 2017

Giovanni A. Frigeri, Daniel D. Scherer, Bernd Rosenow, "Apparent pairing and subperiods in integer quantum Hall interferometers", DPG-Frühjahrstagung Dresden, March 2017

Posters

Heinrich-Gregor Zirnstein and Bernd Rosenow, "A time-reversal symmetric topological magnetoelectric effect in 3D topological insulators", CRC183 Bad Honnef School on Disorder Effects in Topological Systems, Bad Honnef, June 2017

Heinrich-Gregor Zirnstein and Bernd Rosenow "A time-reversal symmetric topological magnetoelectric effect in 3D topological insulators", Topological Matter & Flat Bands Conference, Leipzig, August 2017

Andreas Kreisel, "Orbital-Selective Pairing in iron-based superconductors", Workshop on Fundamentals on Quantum Transport, ICTP Trieste, August 2017

Giovanni A. Frigeri, Daniel D. Scherer, Bernd Rosenow "Apparent pairing and subperiods in integer quantum Hall interferometers", Workshop on Fundamentals on Quantum Transport, August 2017

12.16 Graduations

Master

- Zeid Zandi
  Geometrical entanglement and matrix product states of many body quantum systems

Bachelor

- Elias Enache
  Majorana-Fermionen als Randzustände topologischer Supraleiter

- Sina Teichert
  Quanten-Spin-Hall-Effekt in invertierten Quanten-Doppeltrögen

- Thomas Suchanek
  Gebundene Zustände an Störstellen in unkonventionellen Supraleitern
  03.11.2017

12.17 Guests

- Julia S. Meyer
  CEA Grenoble, France
  11.04.2017
- Casey Nosiglia
  Technion Department of Physics, Israel
  20.03.-07.04.2017
- Edvin Idrisov
  University of Luxembourg, Israel
  04.-06.05.2017
- Yuval Gefen
  Weizmann Institute of Science, Israel
  05.-08.06.2017
- Timo Hyart
  Aalto University, Finland
  20.-28.08.2017
- Adrian Del Maestro
  University of Vermont, USA
  03.-09.09.2017

13

Theory of Condensed Matter

13.1 Introduction

Major research topics of our group include nonequilibrium phenomena and pattern formation in systems of various nature, e.g. in soft condensed matter and in biological systems. Modern analytic methods of statistical physics and computer simulations complement and stimulate each other. Cooperations with mathematicians, theoretical and experimental physicists, biologists and medical researchers in Germany, Europe and around the world are well established.

The group's activities can be subsumed under the name of "Soft Mesoscopics", the study of emerging properties in soft and biological matter. Studied phenomena range from structure formation by wind-blown sand resulting in ripples and dunes, through non-equilibrium dynamics of hot nanoparticles, proteins and polymers, the viscoelastic and inelastic mechanics of the cytoskeleton, to the tension propagation in single DNA molecules under strong externalfields. (Related experimental work is currently in progress at EXP1: MON, MOP, PWM.) A common theme is the presence of strong fluctuations and stochastic dynamics on the microscale. The emergence of the mesoscopic structure and transport is to be understood. The applied methods comprise a broad statistical mechanics toolbox including stochastic (integro-)differential equations, liquid-state theories, effective hydrodynamic equations, various systematic coarse-graining techniques, and massively parallel numerical simulations on GPUs.

Klaus Kroy

13.2 Stirling cycle for microscopic active environments

S. Steffenoni, V. Holubec, G. Falasco*, K. Kroy

*Physics and Materials Science Research Unit, University of Luxembourg

The strong interest of physicists and engineers for thermodynamics cycles has origin in the early 19th century. Only recently, due to the improved ability of realizing nano-structures, such an interest has been addressing to smaller and smaller systems, e.g. colloidal particles in contact with a bath of smaller particles. Indeed, if confined by a time-periodic external potential, the colloids can exhibit cyclic dynamics. At this

scale, the thermodynamics of the system, strongly influenced by the thermal fluctuations of the surrounding medium, naturally meets the Brownian Motion. Such a theory endows thermodynamics with new tools and approaches, leading to a new branch of physics, the so-called stochastic thermodynamics. Many experiments and theoretical studies have treated small systems cycles, focusing, for example, on the fluctuations of heat, work and efficiency of a colloidal particle embedded in an equilibrium bath. Limited and only very recent, is the extension to nonequilibrium baths, e.g. made by active particles. Strong is the interest in this direction focused on understanding if the truly non-equilibrium nature of active particles is able to improve the cycle. Namely, if the harvesting of the bath fluctuations, known to be non-Gaussian too, is able to enhance the efficiency and override the upper limit imposed by classical equilibrium thermodynamics.

A recent experiment has been focused on the so-called active thermodynamic cycles and has observed an increase of the efficiency, compared to the same cycle in contact with an equilibrium bath instead. In order to theoretically explain such findings, we use a Langevin equation, describing a colloidal particle, coupled to an active particles fluid and confined by a time periodic harmonic potential able to induce the colloid to carry out a Stirling cycle [2]. We define (average) work, heat and efficiency from the underlying dynamics. Activity strongly influences the thermodynamics quantities and is able to increase the work extracted from the colloid, as well as the heat dissipated. Efficiency can be enhanced if the increase of the heat is small compared to the work one. The achievement of that is helped by the introduction of an active effective temperature.

[1] S. Steffenoni, G. Falasco, and K. Kroy: Phys. Rev. E **95**, 052142 (2017)
[2] S. Steffenoni, V. Holubec, G. Falasco, and K. Kroy: *Active heat engine: Dynamics and average thermodynamics* (in preparation)

13.3 Polarization of Janus spheres

S. Auschra, A. Bregulla*, F. Cichos*, K. Kroy

*Molecular Nano-Photonics, Institute for Experimental Physics I

Plenty of scientists from a broad range of research fields are attracted by the manifold phenomenology of active matter. Motivated by flocks of fish, birds or bees, collective motion and swarming is one of the most studied phenomena displayed by active matter. A key interaction for the flocking and schooling of animals is alignment. It has been incorporated in simple versatile models like the Viscek model [1].

Here, we consider a two-faced artifically manufactured microswimmer (Janus particle) passively thermophoretically driven by an external temperature gradient stemming from a nearby heat source. Our experimental as well as theoretical and numerical studies verify that Janus swimmers exhibit an alignment with respect to the external gradient. Since this effect originates from the asymmetric temperature gradients across the particle surface as well as its distinct surface properties on both half caps, we suggest that this effect also exists for other types of phoretically driven microswimmers.

[1] T. Vicsek *et al.*: Phys. Rev. Lett. **57**, 6 (1995)

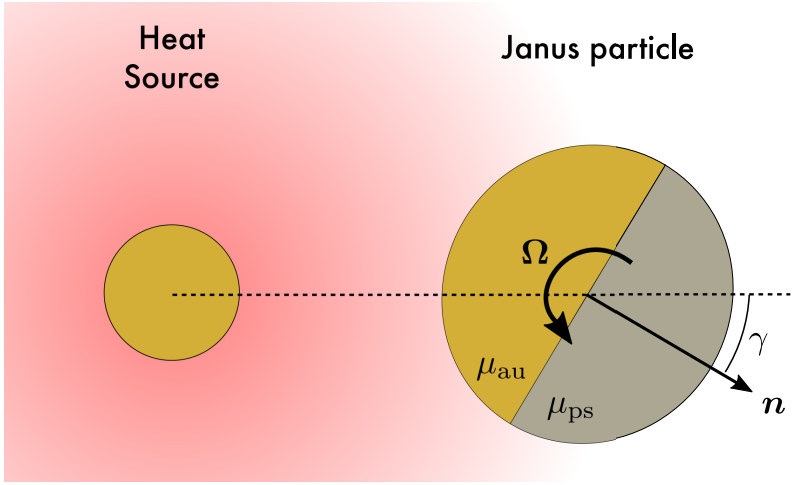

Figure 13.1: Polarization of passively swimming Janus particles. Driven by an external temperature gradient, which stems from a close-by heated nano-bead, one observes an alignment of the particle's symmetry axis $\boldsymbol{n}$ with respect to the external temperature gradient (dotted line). That is, whenever there is a discrepancy between the symmetry axis of the particle and the direction of the external temeprature gradient, which is measured by the angle γ, we both theoretically predict and experimentally observe on average a non-zero angular velocity $\boldsymbol{\Omega}$ realigning the particle with the external gradient. The magnitude of $\boldsymbol{\Omega}$ is found to be proportional to the difference of the phoretic mobilities μ_{au} and μ_{ps} on the gold and polystyrene half caps, respectively.

13.4 Properties of active Brownian particles under imhomogeneous activity

S. Auschra, P. Cervenak, V. Holubec, N. Söker*, F. Cichos*, K. Kroy

*Molecular Nano-Photonics, Institute for Experimental Physics I

Driven by laser heating, two-faced Janus particles are presumably the simplest realization of synthetic (self-)thermophoretic microswimmers. Their properties have been well-studied, most of the times assuming that the supply of "fuel" is homogeneous in space and not varying over time. However, in general, there exist artificial microswimmers as well as living cells whose propulsion strength fluctuates in space and time due to inhomogeneous fuel supply.

We have experimentally studied the spatial and orientational distribution of a single thermophoretically driven Brownian swimmer exploring well-defined regions of inhomogeneous activity by switching on/off the laser heating. According to our observations, Brownian swimmers are less likely to find within regions of higher activity and tend to polarize when experiencing activity gradients. Brownian dynamics simulations and a recently presented numerical solver for Fokker-Planck equations [1] were used to reproduce the experiemntal observation and to investigate the sensitivity of the swimmer's spatial and the orientational distributions to the strength of the activity gradient and the corresponding size of activity regions. By a simple run-and-tumble process (in one dimension) [2, 3], we can qualitatively explain all the features observed by the experiments as well as the numerical and simulation methods.

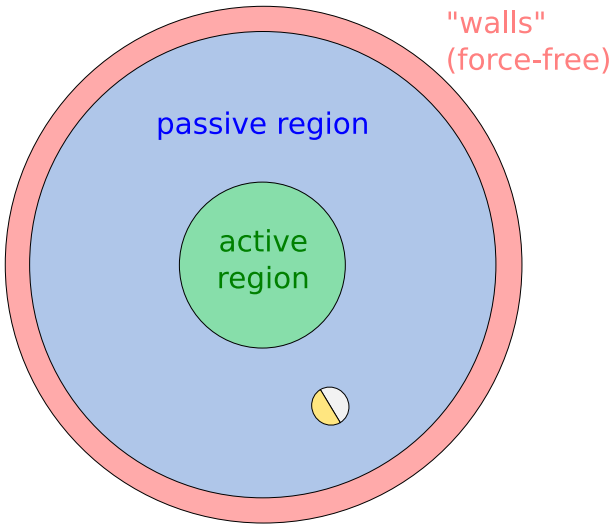

Figure 13.2: Sketch of a Janus swimmer confined in a two-dimensional circular geometry. It is supplied by "fuel" (laser light) whenever it wanders inside a predefined active region (green area). The Janus particle runs out of fuel if it enters the passive region (blue area) an thus becomes an ordinary Brownian particle. For the Janus sphere to stay inside the predefined geometry, the photon-nudging technique of the Molecular Nano-Photonics group by Frank Cichos was applied in the experiments, which allows for a force-free confinement of the microswimmer.

[1] V. Holubec, K. Kroy and S. Steffenoni: arxiv.org/pdf/1804.01285v1 (2018)
[2] T. Demaerel and C. Maes: arXiv:1801.01894v1 (2018)
[3] K. Malakar *et al.*: arXiv:1711.08474v2 (2017)

13.5 Non-Markov bond kinetics and its application in dynamic force spectroscopy

J. T. Bullerjahn, S. Sturm, K. Kroy

Single-molecule force spectroscopy data are conventionally analysed using a schematic model, wherein a molecular bond is modeled as a virtual particle diffusing in a one-dimensional free-energy landscape [1]. However, this simplistic, albeit efficient, approach is unable to account for the "anomalous" bond-breaking kinetics increasingly observed in high-speed force spectroscopy experiments and simulations, such as non-exponential distributions of bond lifetimes under constant load [2]. Here, we show that such characteristic traits arise naturally in a rigorous extension of the one-dimensional theory that accounts for the transient dynamics of a generic set of coupled degrees of freedom. These "hidden modes" affect the reaction dynamics in various ways, depending on their relaxation spectrum. In two complementary asymptotic limits, we are able to find exact analytical expressions for pertinent experimental observables, such as the mean rupture force and the rupture force distribution. Intriguingly, our asymptotic results become unconditionally exact at high loading rates, thus providing us with a microscopically consistent theory of rapid force spectroscopy that avoids the usual Markov assumption.

[1] J. T. Bullerjahn, S. Sturm & K. Kroy, Nat. Commun. **5**, 4463 (2014).
[2] J. Brujić, R. I. Hermans Z., K. A. Walther & J. M. Fernández, Nat. Phys. **2**, 282 (2006).

13.6 Aeolian sand sorting and megaripple formation

M. Lämmel, A. Meiwald, Y. Hezi, H. Tsoar, I. Katra, K. Kroy

Sand is blown across beaches and deserts by turbulent winds. The seemingly chaotic process creates monumental dunes [1, 3] and delicate ripple patterns [2], but hardly anything in between. By the very same process, grains are constantly sorted, as smaller ones advance faster, heavier ones trail behind. In this work [6], we argue that sand sorting and structure formation under prevalent erosive wind conditions can conspire to create distinct bedforms in the "forbidden wavelength gap" between aeolian ripples and dunes [4]. These so-called megaripples are shown to co-evolve with an unusual, predominantly bimodal grain-size distribution [5]. Combining theory and field measurements, we generate a mechanistic understanding of their shape and migration speed, as well as their cyclic aging, renewal, and sedimentary memory, in terms of the intermittent wind statistics. Our results demonstrate that megaripples exhibit close similarities to dunes and can indeed be mechanistically characterized as a special type of ("reptation") dune.

[1] K. Kroy, G. Sauermann, H. J. Herrmann: Phys. Rev. Lett. **88**, 054301 (2002)
[2] O. Durán, P. Claudin, B. Andreotti, Bruno: Proc. Natl. Acad. Sci. U.S.A. **111**, 15665 (2014)
[3] B. Andreotti, P. Claudin, S. Douady: Eur. Phys. J. B **28**, 341 (2002)
[4] J. M. Ellwood, P. D. Evans, I. G. Wilson: J. Sediment. Res. **45**, 554 (1975)
[5] H. Yizhaq, I. Katra and O. Isenberg, H. Tsoar: Aeolian Research **6**, 1 (2012)
[6] M. Lämmel, A. Meiwald, Y. Hezi, H. Tsoar, I. Katra, K. Kroy: Accepted for publication in Nat. Phys.

13.7 Analytical mesoscale modeling of aeolian sand transport

M. Lämmel, K. Kroy

The mesoscale structure of aeolian sand transport plays a crucial role for the understanding and control of a variety of natural phenomena in planetary and Earth science. In Ref. [1], we analyze it beyond the mean-field level, combing insights we gained from a previously proposed two-species transport model [2] with a recently developed parametrization scheme of the collision process between hopping grains and the sand bed [3]. The predicted height-resolved sand flux and other important characteristics of the aeolian transport layer agree remarkably well with a comprehensive compilation of field and wind tunnel data, suggesting that the model robustly captures the essential mesoscale physics.

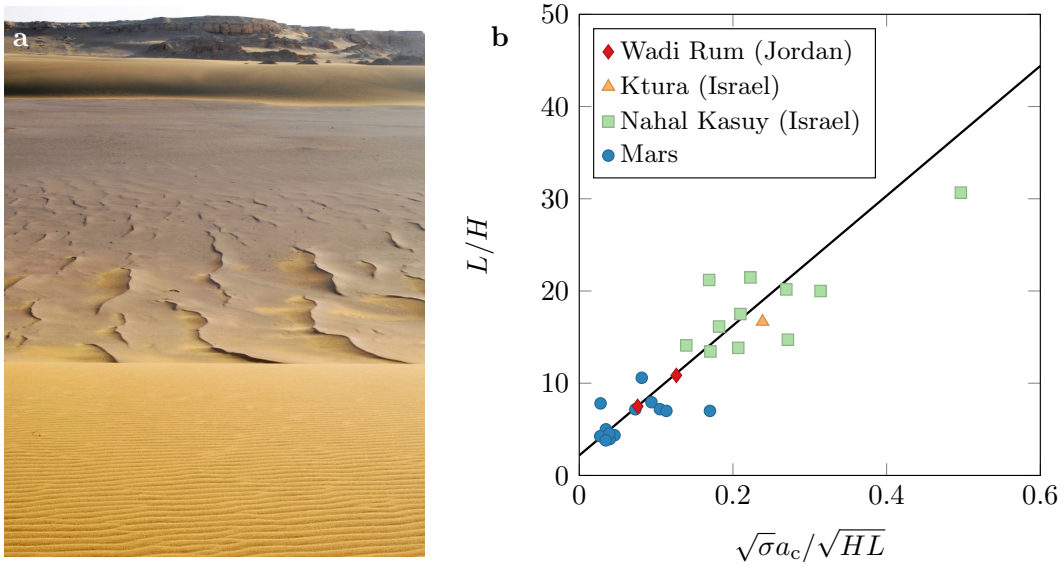

Figure 13.3: a), Ripples, megaripples, and large sand dunes colocated in the same area. Monodisperse wind-blown sand creates centimeter-scale ripples (front) and decameter-scale dunes (back). Polydisperse wind-blown sand gets sorted, the heavier grains forming decimeter-scale megaripples (middle) in the otherwise forbidden wavelength gap. Closer to ripples in size, they share their morphology and migration dynamics with dunes. (Photo taken at al-Fayyum, Egypt. Image credit: Hezi Yizhaq.) **b)**, Our "reptation dune" model predicts an affine relation (solid line) between the inverse aspect ratio L/H of the megaripple and the combination $\sqrt{\sigma}a_c/\sqrt{HL}$, where σ is the sand–air density ratio, a_c the size of the coarse grains armoring the megaripple crest, and H and L its height and base length, respectively.

On the basis of our model, we were able to reconcile a long-standing debate on the wind-dependence of the saturation length, which is the characteristic response length of the transport process to wind perturbations. It is theoretically expected to set the minimum length of the sand dunes. Our "bare" theory predicts it to be almost constant and to follow the characteristic length of the grain trajectories for all wind strengths but those very close to the transport threshold, where it features a singularity.A second version, "dressed" with intermittent wind fluctuations, smears out this singularity and brings the effective saturation length close to the wind-dependent minimum dune length as measured in the field.

[1] M. Lämmel, K. Kroy: Phys. Rev. E **96**, 052906 (2017)
[2] M. Lämmel, D. Rings, K. Kroy: New J. Phys. **14**, 093037 (2012)
[3] M. Lämmel, K. Dzikowski, K. Kroy, L. Oger, A. Valance: Phys. Rev. E **95**, 022902 (2017)

13.8 Grain-scale modeling and splash parametrization for aeolian sand transport

M. Lämmel, K. Dzikowski, L. Oger, A. Valance, K. Kroy

The collision of a spherical grain with a granular bed is commonly parametrized by the splash function, which provides the velocity of the rebounding grain and the velocity distribution and number of ejected grains [1]. In Ref. [3], we derived a rebound parametrization for the collision of a spherical grain with a granular bed, starting from elementary geometric considerations and physical principles, like momentum conservation and energy dissipation in inelastic pair collisions. Combined with a recently proposed energy-splitting model [2] that predicts how the impact energy is distributed among the bed grains, this yields a coarse-grained but complete characterization of the splash as a function of the impact velocity and the impactor–bed grain-size ratio. The predicted mean values of the rebound angle, total and vertical restitution, ejection speed, and number of ejected grains are in excellent agreement with experimental literature data and with our own discrete-element computer simulations. We extract a set of analytical asymptotic relations for shallow impact geometries, which can readily be used in coarse-grained analytical modeling or computer simulations of geophysical particle-laden flows.

[1] J. E. Ungar, P. K. Haff: Sedimentology **34**, 289 (1987)
[2] T. D. Ho, P. Dupont, A. Ould El Moctar, A. Valance: Phys. Rev. E **85**, 052301 (2012)
[3] M. Lämmel, K. Dzikowski, K. Kroy, L. Oger, A. Valance: Phys. Rev. E **95**, 022902 (2017)
[4] D. Beladjine, M. Ammi, L. Oger, A. Valance: Phys. Rev. E **75**, 061305 (2007)

13.9 Funding

DFG "Non-isothermal Brownian Motion"
K. Kroy
DFG, KR 3381/4-1

DFG SPP 1726 "Thermophoretic Propulsion and Interaction of Hot Brownian Swimmers"
K. Kroy in collaboration with F. Cichos
DFG, KR 3381/5-1

Humboldt Foundation "Optimal control of information-driven hot micro-swimmers"
Victor Holubec (Humboldt postdoc position)

Czech Science Foundation "Stochastic thermodynamics of molecular systems: from classical to quantum"
Victor Holubec
17-06716S

International Max Planck Research Schools
Stefano Steffenoni

13.10 Organizational Duties

K. Kroy

- Member of the graduation grants committee of the University
- Study counselor for physics
- Scientific Member of the International Max Planck Research School "Mathematics in the Sciences"
- Referee for Nature Commun., Proc. Natl. Acad. Sci. (USA), Phys. Rev. Lett., Phys. Rev. E, J. Chem. Phys., Biophysical Journal, Soft Matter, Physica A, J. Phys. Cond. Mat., and various funding organizations (e.g. DFG)

13.11 External Cooperations

Academic

- Heidelberger Institut für Theoretische Studien
  Prof. Dr. Frauke Gräter
- Indian Institute of Science Education and Research, Mohalo
  Prof. Dr. D. Chakraborty
- Ben-Gurion University of the Negev, Israel
  H. Yizhaq, I. Katra, H. Tsoar
- Université de Rennes, France
  A. Valance

13.12 Publications

Journals

S. Steffenoni, G. Falasco, and K. Kroy, "Microscopic derivation of the hydrodynamics of active-Brownian-particle suspensions", Phys. Rev. E **95**, 052142, 2017

M. Lämmel, K. Kroy, "Analytical mesoscale modeling of aeolian sand transport Marc", Phys. Rev. E **96** (5), 052906, 2017

M. Lämmel, K. Dzikowski, K. Kroy, L. Oger, A. Valance: "Grain-scale modeling and splash parametrization for aeolian sand transport", Phys. Rev. E **95** (2), 022902, 2017

J.A. Wagner, P.P. Sandeep, I. Greving, M. Lämmel, K. Gkagkas, T. Seydel, M. Müller, B. Markert, F. Gräter: "Stress-induced long-range ordering in spider silk", Sci. Rep. **7**, 15273, 2017

K. Kroy: "Cell mechanics: The benefits of getting high", Nat. Phys. **13**, 728-729, 2017

S. Landmann, N. Preuss, U. Behn: "Self-tolerance and autoimmunity in a minimal model of the idiotypic network", J. Theor. Biol. **426**, 17-39, 2017.

Talks

J. T. Bullerjahn: *Analytical catch-slip bond model for arbitrary forces and loading rates*, DPG Annual Meeting, Dresden, March 20, 2017

J. T. Bullerjahn: *Non-Markovian bond kinetics and its application in dynamic force spectroscopy*, Conference on Multiscale mechanochemistry & mechanobiology, Berlin, October 18, 2017

K. Kroy: *Forcible bond breaking and polymer dynamics*, Institut National de la Santé et de la Recherche Médicale, Marseille, January 17

K. Kroy: *Aeolian sand transport and megaripples*, GIF-Delegates, Ben-Gurion-University, Beer Sheva, February 21

K. Kroy *Exact symmetries in the velocity fluctuations of a hot Brownian swimmer*, 8th Nordic Workshop on Statistical Physics: Biological, Complex and Non-Equilibrium Systems, Nordita, Stockholm, March 9

K. Kroy *Exact symmetries of a hot Brownian swimmer*, Physik Kolloquium, Uni Konstanz, July 15

K. Kroy *Quantifying the distance from equilibrium*, CENS Workshop, Venice International University, San Servolo, September 18

13.13 Graduations

Doctorate

- Jakob Tómas Bullerjahn
  A unified theory for single-molecule force spectroscopy experiments and simulations
  July 10, 2017
- Gianmaria Falasco
  Four out-of-equilibrium stories
  May 29, 2017
- Rüdiger Kürsten
  Critical Phenomena in Non-Markovian and Nonlinear Diffusion Processes
  March 29, 2017

Bachelor

- Omer Rochman
  Stability of Symmetric Barchan Dunes
  November 13, 2017
- Joscha Mecke
  Investigation of the non-isothermal oscillator
  September 22, 2017

- Roland Wiese
  Iron Balance of Hemochromatosis Patients under Phlebotomy: A Simple Mathematical Model
  December 19, 2017

13.14 Guests

- Markus Gruber
  University of Konstanz
  October 11, 2017
- Matteo Smerlak
  Perimeter Institute for Theoretical Physics
  July 5, 2017
- Aidan Schuhmann
  University of Puget Sound
  May 26, 2017 – August 4, 2017
- Kerstin Blank
  MPI of Colloids and Interfaces
  April 19, 2017
- Matti Gralka
  University of California, Berkeley
  January 1, 2017

14

Theory of Elementary Particles

14.1 Introduction

Our group is interested in the properties of matter at very high energies (small scales) or under other extreme conditions, covering a broad variety of research topics ranging from the study of elementary particles and their properties to the study of quantized matter fields in the presence of strong gravitational fields. The underlying theme of our research and teaching activity is the theory of such quantized fields in its various manifestations, and applications, including:

1. Quantum fields on discrete spacetimes (lattices) and their numerical and theoretical study
2. Quantum fields on curved spacetimes and in the presence of background (gauge) fields
3. Applications of ideas from integrable systems to the study of quantum gauge theories
4. Dualities and relation with classical General Relativity

Quantum field theories on lattices are discretized counterparts of continuum models describing elementary particles in quantum field theoretic models such as the standard model of particle physics. They were introduced in order to investigate certain non-perturbative features of these models in a controlled approximation. A substantial fraction of the current work being done in this area are numerical simulations and the development of new theoretical methods leading to improved numerical schemes. Our group is participating in this endeavor.

Quantum gauge theories such as the standard model can also be treated as continuum field theories, and can thereby be studied using for instance by perturbative methods. The task of finding improved ways of handling perturbative calculations is an important aspect of quantum field theory and is actively pursued in our group from a variety of different viewpoints, including operator product expansion techniques, methods from integrability, renormalization group methods, holographic ideas, and more.

We also pursue the quest to generalize quantum field theory to curved spacetime (QFTCS), which is inspired by the ideas and principles of General Relativity. On account

of its classical treatment of the metric, QFTCS cannot be a fundamental theory of nature. However, QFTCS is expected to provide an accurate description of quantum phenomena in a regime where the effects of curved spacetime may be significant, but effects of quantum gravity itself may be neglected. In particular, it is expected that QFTCS should be applicable to the description of quantum phenomena occurring in the early universe and near (and inside of) black holes, provided that one does not attempt to describe phenomena occurring so near to singularities that curvatures reach Planckian scales and the quantum nature of the spacetime metric would have to be taken into account. Quantum field theory in curved spacetimes has provided important physical insights into the quantum nature of black holes, indicating that they should, if left alone, gradually evaporate due to the emission of quanta whose energies are distributed thermally at the famous Hawking temperature.

In parallel to direct approaches to quantum field theory via perturbative, or numerical, techniques, there are now also more indirect approaches via so-called "holographic dualities", or methods from "operator algebras". Holographic dualities typically establish a connection with a quantum field theory living on some sort of boundary of a space and a classical, gravitational, theory living in the higher dimensional space itself. This type of duality is believed to probe rather different regimes of quantum field theory (strong coupling, "large N"), and is hence complementary to other methods. At the technical level, it motivates studies into higher dimensional gravity theories, which turn out to have a rather rich mathematical structure. The study of such structures is another research topic in our group. Operator algebraic methods become useful e.g. when trying to apply concepts from quantum information theory in the context of quantum field theories, such as entanglement, relative entropies etc.

More information may be found on the group's webpages, www.uni-leipzig.de/~tet

Prof. S. Hollands

14.2 Gravitational radiation and memory effect

S. Hollands

The physical reality of gravitational waves emitted in the course of black hole- or neutron star mergers is now experimentally confirmed. Not least for this reason, the investigation of the theoretical foundations of this phenomenon is now an active research area, which still brings to light new and unforeseen structures/phenomena. One aspect of gravitational radiation which has relevance also in quantum field theory (via an analogous mechanism in quantum field theories containing massless particles such as the photon) is the so-called "memory effect". It states that a permanent displacement freely falling test-masses can remain after a burst of gravitational radiation from a distant source has passed through. The memory effect is connected in a profound way to the notion of "BMS symmetry", which is a fundamental concept in the description of asymptotically flat spacetimes.

[1] D. Garfinkle, S. Hollands, A. Ishibashi, A. Tolish and R. M. Wald, Class. Quant. Grav. **34**, no. 14, 145015 (2017) doi:10.1088/1361-6382/aa777b [arXiv:1702.00095 [gr-qc]].

[2] S. Hollands, A. Ishibashi and R. M. Wald, Class. Quant. Grav. **34**, no. 15, 155005 (2017) doi:10.1088/1361-6382/aa777a [arXiv:1612.03290 [gr-qc]].

14.3 Operator product expansions in quantum field theory

S. Hollands, J.W. Holland, M.B. Fröb

All quantum field theories with well-behaved ultra violet behavior are believed to have an operator product expansion (OPE) [1]. This means that the product of any two local fields located at nearby points x and y in spacetime can be expanded in the form

$$O_A(x)O_B(y) \sim \sum_C C^C_{AB}(x-y)\, O_C(y), \tag{14.1}$$

where A, B, C are labels for the various local fields in the given theory (incorporating also their tensor character/spin), and where C^C_{AB} are certain numerical coefficient functions—or rather distributions—that depend on the theory under consideration, the coupling constants, etc. The sign "$\sim$" indicates that this can be understood as an asymptotic expansion: If the sum on the right side is carried out to a sufficiently large but finite order, then the remainder goes to zero fast as $x \to y$ in the sense of operator insertions into a quantum state, or into a correlation function. The operator product expansion is on the one hand an important tool for calculations in asymptotically free quantum field theories (such as Quantum Chromo Dynamics, QCD). At a conceptual level, the OPE may be viewed as a kind of algebraic skeleton of quantum field theory, and its understanding may shed some light on fundamental open questions in this theory. Our work has been directed in the following directions:

1. Algebraic aspects of the expansion ("associativity", "crossing symmetry")
2. Recursive procedures for calculating the OPE coefficients in perturbation theory, functional equations for the OPE coefficients.
3. Ways to construct the OPE beyond perturbation theory.
4. Understanding the role of gauge invariance with in the OPE in non-abelian gauge theories.

[1] K. G. Wilson and W. Zimmermann, "Operator product expansions and composite field operators in the general framework of quantum field theory," Commun. Math. Phys. **24**, 87 (1972).
[2] S. Hollands, "Action principle for OPE," Nucl. Phys. B **926**, 614 (2018) [arXiv:1710.05601 [hep-th]].
[3] M. B. Fröb and J. Holland, "All-order existence of and recursion relations for the operator product expansion in Yang-Mills theory," arXiv:1603.08012 [math-ph].
[4] M. B. Fröb, J. Holland and S. Hollands, "All-order bounds for correlation functions of gauge-invariant operators in Yang-Mills theory," J. Math. Phys. **57**, no. 12, 122301 (2016) [arXiv:1511.09425 [math-ph]].

[5] J. Holland and S. Hollands, "Associativity of the operator product expansion," J. Math. Phys. **56**, no. 12, 122303 (2015) [arXiv:1507.07730 [math-ph]].
[6] S. Hollands and C. Kopper, "The operator product expansion converges in massless φ^4_4 theory," Commun. Math. Phys. **313** (2012) 257 [arXiv:1411.1785 [hep-th]].
[7] J. Holland and S. Hollands, "Recursive construction of operator product expansion coefficients," Commun. Math. Phys. **336**, no. 3, 1555 (2015) [arXiv:1401.3144 [math-ph]].
[8] J. Holland and S. Hollands, "A small cosmological constant due to non-perturbative quantum effects," Class. Quant. Grav. **31** (2014) 125006 [arXiv:1305.5191 [gr-qc]].

14.4 Entanglement entropy of quantum fields

K. Sanders*, S. Hollands

*Dublin City University

A typical state of a quantum field theory (QFT) exhibits entanglement between spacelike separated regions. In Minkowski space this is due to the Reeh-Schlieder theorem, which has partial extensions to curved spacetimes [2]. In order to quantify the amount of entanglement of a state between two given regions, one may adopt the notion of entanglement entropy as used in quantum mechanics (QM). Computing entanglement entropies is difficult, even for free fields [3], but the results show some interesting features. E.g., when space is divided into two regions by a boundary surface S, the entanglement entropy of the vacuum is divergent and the coefficient of the leading divergent order is proportional to the area of S ("area law").

Unfortunately, the existing computations have a number of drawbacks: they often only work for ground states (using path integrals), and they introduce regulators and subtle computational tricks whose physical meaning is unclear (e.g. the replica method). In this project we endeavour to provide an alternative approach to entanglement entropy, with a better physical motivation, and compare with the existing results. We focus on the following questions [5, 6]:

- The definition of entanglement entropy in terms of density matrices, familiar from QM, requires modification, due to the existence of inequivalent Hilbert space representations in QFT. For this reason we resort to the relative entropy of Araki [1], leading to a well-defined entanglement entropy in a very general setting, taking values in $[0, \infty]$.

- For two quasi-free states in QM, we obtained an explicit formula for their relative entropy, relying heavily on literature from quantum information theory [4]. This general result allows us to find upper and lower bounds for entanglement entropies.

- For quasi-free states of a free scalar QFT, we expect to find their relative entropy as a generalisation of the formula from QM, and the upper and lower bounds should generalise as well.

- In simple explicit cases, such as the Minkowski vacuum and spacelike separated regions with sufficiently simple geometry, it may be possible to evaluate or approximate the bounds on the entanglement entropy. This allows for a comparison of computational methods and results with the existing literature (e.g. the area law).

[1] H. Araki, Publ. Res. Inst. Math. Sci. **11** (1975/76), 809–833
[2] K. Sanders, Commun. Math. Phys. **288** (2009), no.1, 271–285
[3] S.N. Solodukhin, Living Rev. Relativity **14** (2011), no.8
[4] C. Weedbrook, S. Pirandola, R. García-Patrón, N.J. Cerf, T.C. Ralph, J.H. Shapiro and S. Lloyd, Rev. Mod. Phys. **84** (2012), no.2, 621–669
[5] S. Hollands and K. Sanders, "Entanglement measures and their properties in quantum field theory," arXiv:1702.04924 [quant-ph].
[6] S. Hollands, O. Islam and K. Sanders, "Relative entanglement entropy for widely separated regions in curved spacetime," arXiv:1711.02039 [math-ph].

14.5 Yangians and symmetric correlators

R. Kirschner, J. Fuksa, A.P. Isaev, D. Karakhanyan

We have studied Yang-Baxter relations with the symmetry of the the orthosymplectic Lie super-algebras, in particular the RLL relations involving the fundamental R-matrix. The work is based on the classical results [1–3] and continues recent work [4, 5].

The concept of Yangian symmetric correlators has been proposed as a tool for the calculation of amplitudes in gauge field theories, where the Yangian of the type $s\ell_4$ applies [6, 7]. We have studied now in detail such symmetric correlators in the simpler case of type $s\ell_2$. Symmetric correlators can be used to define integral operators obeying Yang-Baxter relations. The latter can be used to solve completely the spectral problem of those operators. An application to the kernels of the evolution equation of generalized parton distributions has been pointed out.

[1] A.B. Zamolodchikov and Al.B. Zamolodchikov, "Factorized S Matrices in Two-Dimensions as the Exact Solutions of Certain Relativistic Quantum Field Models," Annals Phys. **120** (1979) 253.
[2] B. Berg, M. Karowski, P. Weisz and V. Kurak, "Factorized U(n) Symmetric s Matrices in Two-Dimensions," Nucl. Phys. B **134** (1978) 125.
[3] N.Yu. Reshetikhin, Integrable models of quantum one-dimensional models with $O(n)$ and $Sp(2k)$ symmetry, Theor. Math. Fiz. **63** (1985) 347-366.
[4] D. Chicherin, S. Derkachov and A. P. Isaev, "The spinorial R-matrix," J. Phys. A **46** (2013) 485201. arXiv:1303.4929 [math-ph].
[5] A. P. Isaev, D. Karakhanyan, R. Kirschner, "Orthogonal and symplectic Yangians and Yang-Baxter R operators," Nucl. Phys. **B904** (2016) 124147, arXiv:1511.06152
[6] D. Chicherin and R. Kirschner, *Yangian symmetric correlators,* Nucl. Phys. B **877** (2013) 484 doi:10.1016/j.nuclphysb.2013.10.006 [arXiv:1306.0711 [math-ph]].
[7] D. Chicherin, S. Derkachov and R. Kirschner, *Yang-Baxter operators and scattering amplitudes in N=4 super-Yang-Mills,* Nucl. Phys. B **881** (2014) 467 doi:10.1016/j.nuclphysb.2014.02.016 [arXiv:1309.5748 [hep-th]].

14.6 High-spin parton splitting in generalised Yang-Mills theory

R. Kirschner, G. Savvidy

The generalised Yang-Mills theory [1] involves gauge bosons of higher spin, based on a consistent extension of the Poincare group [2]. As in ordinary gauge field theory the tree-level amplitudes can be calculated from the action as well as by the BCFW rules [3] related to $s\ell_4$ Yangian symmetry.

Following the hypothesis [4] that the high-spin gluons contribute to the structure of hadrons in analogy to the ordinary gluons, we calculate the corresponding Lipatov-Altarelli-Parisi parton splitting kernels. Relying on results of [5] derived by Yangian symmetry we obtain a convenient universal form of the splitting kernels in dependence on the helicities of the involved partons.

[1] G. Savvidy, *Non-abelian tensor gauge fields.* Int. J. Mod. Phys. A **21** (2006) 4931 and 4959.
[2] I. Antoniadis, L. Brink and G. Savvidy, *Extensions of the Poincare group,* J. Math. Phys. **52** (2011) 072303 doi:10.1063/1.3607971 [arXiv:1103.2456 [hep-th]].
[3] R. Britto, F. Cachazo, B. Feng and E. Witten, *Direct proof of tree-level recursion relation in Yang-Mills theory,* Phys. Rev. Lett. **94** (2005) 181602 [arXiv:hep-th/0501052].
[4] G. Savvidy, *Asymptotic freedom of non-Abelian tensor gauge fields,* Phys. Lett. B **732** (2014) 150.
[5] J. Fuksa and R. Kirschner, *Correlators with $s\ell_2$ Yangian symmetry,* Nucl. Phys. B **914** (2017) 1 doi:10.1016/j.nuclphysb.2016.10.019 [arXiv:1608.04912 [hep-th]].

14.7 Hadron physics using background from lattice QCD

H. Perlt, A. Schiller

It is well known that the sea quark and gluon content of hadrons (Fig. 14.1) can be traced back to flavor singlet hadron matrix elements, following the operator product expansion. The calculation of these matrix elements is one of the greatest technical challenges left in lattice QCD. This is due to the fact that the lattice calculation of so-called "disconnected diagrams" is extremely noisy and gives a poor signal. An improved determination of these disconnected contributions is one of the main aims of this project.

For that we have proposed an alternative to the conventional three-point function technique for the study of hadron matrix elements in lattice QCD. By adapting the so called Feynman-Hellmann theorem (FH) to the lattice setting, we were able to isolate matrix elements in terms of energy shifts in the presence of appropriate weak external background fields. Our spin results contribute to a solution of the so called spin crisis of the proton and allow for a direct comparison of our lattice form factor results to experimental measurements at JLab. The HPC system JUQUEEN has been used to generate part of the necessary lattice configurations at different lattice couplings, quark masses, sizes and background fields. Among the results let us to mention here:

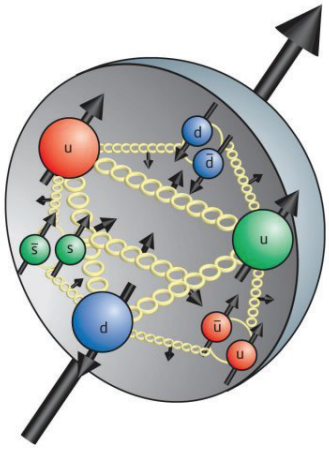

Figure 14.1: Schematic view of the proton with spin arrows of the quarks and gluon (from https://www.quantumdiaries.org/wp-content/uploads/2012/03/SPT78-proton.jpg).

- Calculation of spin distributions in the hadrons including the sea quark content [2, 10] (see Fig. 14.2).

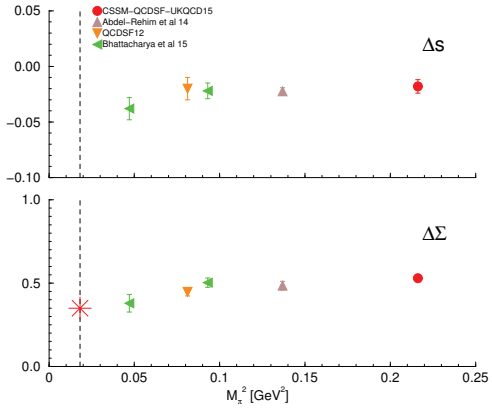

Figure 14.2: Strange quark and total quark spin for various lattice pion masses (in red our collaboration).

- Elastic form factors at large momentum transfer unreachable by standard lattice techniques [3–5] (see Fig. 14.3).
- Determination of the flavor-singlet axial-vector and scalar renormalisation constants [9].

[1] A. J. Chambers *et al.* [QCDSF and UKQCD Collaborations], Phys. Rev. D **90** (2014) 014510 [arXiv:1405.3019 [hep-lat]].
[2] A. J. Chambers *et al.*, Phys. Rev. D **92** (2015) no.11, 114517 [arXiv:1508.06856 [hep-lat]].
[3] A. J. Chambers *et al.*, PoS LATTICE **2015** (2016) 125 [arXiv:1511. [hep-lat]].
[4] A. Chambers *et al.*, PoS LATTICE **2016**, 168 (2017).

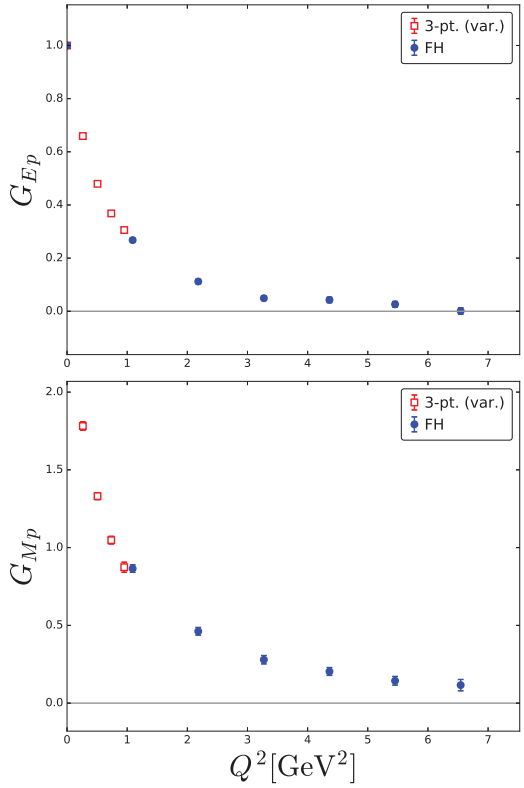

Figure 14.3: Electric and magnetic form factor vs. momentum transfer Q^2 compared to a standard variational three-point method [6].

[5] A. J. Chambers *et al.* [QCDSF and UKQCD and CSSM Collaborations], Phys. Rev. D **96**, no. 11, 114509 (2017) [arXiv:1702.01513 [hep-lat]].
[6] J. Dragos *et al.*, Phys. Rev. D **94** (2016) no.7, 074505 doi:10.1103/PhysRevD.94.074505 [arXiv:1606.03195 [hep-lat]].
[7] A. J. Chambers *et al.* [QCDSF Collaboration], Phys. Lett. B **740** (2015) 30 [arXiv:1410.3078 [hep-lat]].

14.8 Nucleon structure functions from lattice forward Compton amplitude

H. Perlt, A. Schiller

Traditionally, parton distribution functions (PDFs) are obtained from global fits to the experimental data. However, there are gaps in the experimental coverage, and hence it is highly desired to have robust results from numerical simulations in lattice QCD. So far lattice calculations have been limited to a few low Mellin moments of selected PDFs. Though providing useful information, both as benchmarks of lattice QCD calculations and as constraints in global fits, this is insufficient to reconstruct the total momentum dependence of the structure functions without significant model dependence.

Our approach is based on the computation of the structure functions from the forward Compton scattering amplitude [1]. Here, one has to compute the current-current correlator

$$T_{\mu\nu}(p,q) = \int \mathrm{d}^4x\, \mathrm{e}^{iqx} \langle p,s|TJ_\mu(x)J_\nu(0)|p,s\rangle \tag{14.2}$$

at large q^2, which involves the time ordered product of electromagnetic currents J_μ sandwiched between states of momentum p and spin s. We started with the calculation of the structure function F_1. Its relation to the Compton scattering amplitude is given by ($\omega = 2pq/q^2$)

$$T_{33}(p,q) = \mathcal{F}_1(\omega,q^2) = 4\omega \int_0^1 dx\, \frac{\omega x}{1-(\omega x)^2}\, F_1(x,q^2) \tag{14.3}$$

The Compton amplitudes can be computed most efficiently, including disconnected contributions, by a simple extension of existing implementations of the Feynman-Hellmann technique to lattice QCD [2]. We consider local vector and axial vector currents only. The corresponding renormalisation constants Z_V, Z_A are known [8]. No further renormalisation is needed. To compute the Compton amplitude T_{33} from the Feynman-Hellmann relation, we introduce the perturbation to the Lagrangian

$$\mathcal{L}(x) \to \mathcal{L}(x) + \lambda \mathcal{J}_3(x)\,, \quad \mathcal{J}_3(x) = Z_V \cos(\vec{q}\cdot\vec{x})\, e_q\, \bar{q}(x)\gamma_3 q(x)\,, \tag{14.4}$$

where q is the quark field, $q = u,d,s$ in our case, to which the photon is attached, and e_q is its electric charge. Note that λ has dimension mass. Taking the second derivative of the nucleon two-point function $\langle N(\vec{p},t)\bar{N}(\vec{p},0)\rangle_\lambda \simeq C_\lambda\, \mathrm{e}^{-E_\lambda(p,q)\,t}$ with respect to λ on both sides, we obtain

$$-2E_\lambda(p,q)\, \frac{\partial^2}{\partial\lambda^2} E_\lambda(p,q)\,\Big|_{\lambda=0} = T_{33}(p,q)\,. \tag{14.5}$$

Only one insertion is needed to compute $E_\lambda(p,q)$ for all momenta p at any value of q and parameter λ. Varying q^2 will allow us to test the twist expansion and, in particular, isolate twist-four contributions. A conventional calculation of the four-point function $\langle p,s|J_\mu(x)J_\nu(0)|p,s\rangle$, in contrast, would involve all-to-all quark propagators twice consecutively, which is not practical.

After a successfull test calculation with mock data[1] (which were taken from experiments) we made a first run with data from lattice simulation. It turns out that the second derivative of the nucleon energy can be computed rather accurately. In a proof-of-principle study we have computed (14.5) from $O(900)$ configurations generated at the SU(3) symmetric point [4] on a $32^3\times 64$ lattice with lattice spacing $a \approx 0.074$ fm generated at rather heavy quark masses, $m_\pi = m_K = 465$ MeV. First results are presented in Figs. 14.4 and 14.5, where the contribution from

$$\mathcal{F}_1(0,q^2) = -2\, E_\lambda(0,q)\, \partial^2 E_\lambda(0,q)/\partial\lambda^2\,\big|_{\lambda=0} \tag{14.6}$$

has been subtracted. We used momenta $\vec{p} = (2,-1,0), (-1,1,0), (1,0,0), (0,1,0), (2,0,0), (-1,2,0), (1,1,0), (0,2,0), (2,1,0), (1,2,0)$, from left to right, and $\vec{q} = (3,5,0)$, in lattice units. For our lattice this translates into $q^2 \approx 9.3\ \mathrm{GeV}^2$. Z_V has been taken from [8]. The

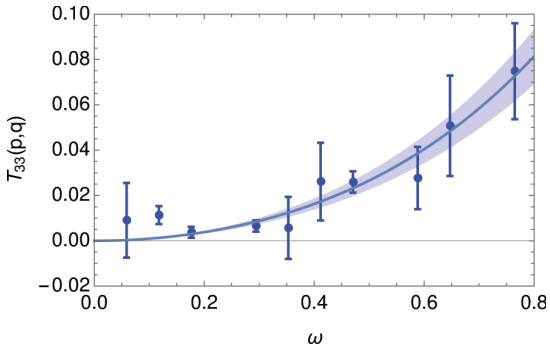

Figure 14.4: The proton Compton amplitude $T_{33}(p,q)$ for the lattice described in the text. The solid line shows a sixth order polynomial fit (giving $\chi^2/\text{dof} = 0.9$), and the shaded area shows the error.

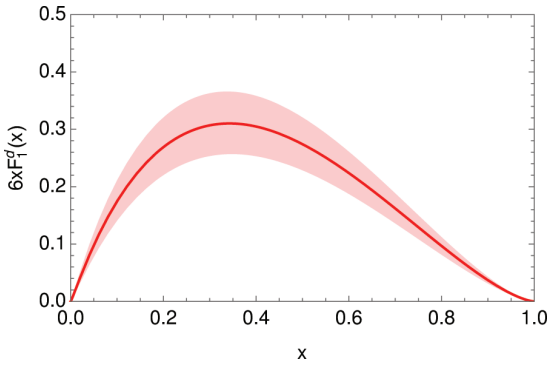

Figure 14.5: The structure function $F_1^{u-d}(x)$ as obtained from the Compton amplitude shown in Fig. 14.4. The shaded area shows the error.

precision for lattice momenta $\vec{p}^2 = 1$ and 2 is already quite impressive. We emphasise that the lattice computation has been done away from the physical point. However, one recognises already a fairly good agreement in the shape compared to the result of the mock data in [1]. We should be able to improve on the precision of the data at higher momenta by employing 'momentum smearing' techniques, which has not been attempted here.

[1] A. J. Chambers, R. Horsley, Y. Nakamura, H. Perlt, P. E. L. Rakow, G. Schierholz, A. Schiller, K. Somfleth, R. D. Young, J. M. Zanotti, Phys. Rev. Lett. **118** (2017) no.24, 242001, [arXiv:1703.01153 [hep-lat]].

[2] R. Horsley, R. Millo, Y. Nakamura, H. Perlt, D. Pleiter, P.E.L. Rakow, G. Schierholz, A. Schiller, F. Winter, J.M. Zanotti, Phys. Lett. B **714** (2012) 312 [arXiv:1205.6410 [hep-lat]].

[3] M. Constantinou, R. Horsley, H. Panagopoulos, H. Perlt, P. E. L. Rakow, G. Schierholz, A. Schiller and J. M. Zanotti, Phys. Rev. D **91** (2015) 1, 014502 [arXiv:1408.6047 [hep-lat]].

[4] W. Bietenholz *et al.* [QCDSF Collaboration], Phys. Rev. D **84** (2011) 054509 [arXiv:1102.5300 [hep-lat]].

14.9 Global anomalies on Lorentzian spacetimes

A. Schenkel*, J. Zahn

*Nottingham U

Global anomalies are very interesting aspects of Quantum Field Theories (QFT). From a practical point of view, the condition of the absence of anomalies is an important constraint for model building. This is in particular the case for QFTs in higher dimensions such as those inspired by superstring theory. On the other hand, global anomalies are a non-perturbative effect, and are thus of interest in their own right, being

one of the few aspects of this regime which is accessible with our current theoretical tools.

Global anomalies are usually discussed in a formal path integral setting on compact Riemannian spaces [1] and are computed with the help of the mod 2 index theorem or more generally family index theory. There exists also a formulation in the Hamiltonian framework [2]. Nevertheless, the actual computation of the anomaly relies on the results obtained on compact Riemannian spaces.

We think that this state of affairs is unsatisfactory: Physical spacetimes are neither Riemannian nor compact. Furthermore, in the above formulations it is not clear whether the anomaly is a feature of the (ground) state, or a property of the algebra of observables.

The aim of our project [3] was thus two-fold: To find an algebraic characterization of global anomalies, in order to make the state-independence explicit. And to carry out the actual computation in a proper Lorentzian setting. Our criterion for the presence of global anomalies is a non-trivial phase of the S matrix for scattering of free fermions off a gauge transformed background potential. As a by-product, we thus provide a definition for the phase of the S matrix in such a situation. For the computation of the anomaly, we follow ideas developed in [4, 5]. This also leads to a clarification of the relation of *perturbative agreement* [6, 7] and the *Wess-Zumino consistency condition* [8].

[1] E. Witten, "An SU(2) Anomaly," Phys. Lett. **117B**, 324 (1982).
[2] P. C. Nelson and L. Alvarez-Gaume, "Hamiltonian Interpretation of Anomalies," Commun. Math. Phys. **99**, 103 (1985).
[3] A. Schenkel and J. Zahn, "Global anomalies on Lorentzian space-times," Annales Henri Poincare **18**, no. 8, 2693 (2017).
[4] E. Witten, "Global Aspects of Current Algebra," Nucl. Phys. B **223** (1983) 422.
[5] S. Elitzur and V. P. Nair, "Nonperturbative Anomalies in Higher Dimensions," Nucl. Phys. B **243**, 205 (1984).
[6] S. Hollands and R. M. Wald, "Conservation of the stress tensor in interacting quantum field theory in curved spacetimes," Rev. Math. Phys. **17**, 227 (2005) [gr-qc/0404074].
[7] J. Zahn, "Locally covariant charged fields and background independence," Rev. Math. Phys. **27**, no. 07, 1550017 (2015).
[8] J. Wess and B. Zumino, "Consequences of anomalous Ward identities," Phys. Lett. **37B**, 95 (1971).

14.10 Generalized Wentzell boundary conditions and quantum field theory

J. Zahn

Quantum Field Theory in the presence of boundaries has technologically relevant applications, the Casimir effect, but is also important for recent developments in high energy physics, in particular holography (the AdS/CFT correspondence). The goal of the project is to study exotic boundary conditions involving second order derivatives,

known in the mathematical literature as *generalized Wentzell boundary conditions*. These occur for example for a spinning string with a mass attached to the boundary [1], but also in the context of the AdS/CFT correspondence [2].

In our project [3], we investigate different aspects of these boundary condition. As a first step, we establish well-posedness of the wave equation at the classical level, including a proof of causal propagation. We then quantize the system and in particular discuss holographic aspects.

[1] J. Zahn, "The excitation spectrum of rotating strings with masses at the ends," JHEP **1312**, 047 (2013).
[2] K. Skenderis, "Lecture notes on holographic renormalization," Class. Quant. Grav. **19**, 5849 (2002).
[3] J. Zahn, "Generalized Wentzell boundary conditions and quantum field theory," Annales Henri Poincare **19**, no. 1, 163 (2018).

14.11 Semi-classical energies of rotating strings

J. Zahn

For several reasons, the Nambu-Goto string is an interesting model: It exhibits diffeomorphism invariance, making it a toy model for (quantum) gravity. It also provided motivation for the Polyakov string, which led to string theory as a candidate for a fundamental theory. Furthermore, it constitutes a phenomenological model for QCD (Quantum Chromo-Dynamics) vortex lines connecting quarks, i.e., for the description of hadrons.

It is well-known that in the covariant quantization of the open Nambu-Goto string, the *intercept* a is a free parameter, only constrained by the fact that the theory is consistent only for $a \leq 1$ and $D \leq 25$ or $a = 1$ and $D = 26$. Furthermore, the ground state energies $E_{\ell_{1,2}}$ for a given angular momentum $\ell_{1,2} > 0$, say in the $1-2$ plane, lie on the *Regge trajectory*

$$E^2_{\ell_{1,2}} = 2\pi\gamma(\ell_{1,2} - a),$$

with γ the string tension. In other approaches to quantization, the critical dimension $D = 26$ with intercept $a = 1$ are singled out. One way to compute a for $D < 26$ is to use the effective action of Polchinski and Strominger [1]. With this, the result $a = 1$ is obtained for any dimension D [2].

Another approach to string theory in non-critical dimensions is via perturbation theory around classical solutions [3], using concepts from quantum field theory on curved space-times. It is a priori not clear that the two approaches yield the same result. The second approach has the advantage that also the case of masses at the endpoints can be treated, a model which is particularly interesting in the context of QCD phenomenology [4]. With our method [5], we find $a = 1$ for any D, consistent with the results found in [2].

[1] J. Polchinski and A. Strominger, "Effective string theory," Phys. Rev. Lett. **67**, 1681 (1991).

[2] S. Hellerman and I. Swanson, "String Theory of the Regge Intercept," Phys. Rev. Lett. **114**, no. 11, 111601 (2015).
[3] D. Bahns, K. Rejzner and J. Zahn, "The effective theory of strings," Commun. Math. Phys. **327**, 779 (2014).
[4] J. Sonnenschein and D. Weissman, "Rotating strings confronting PDG mesons," JHEP **1408**, 013 (2014).
[5] J. Zahn, "The semi-classical energy of open Nambu-Goto strings," accepted for publication in Phys. Rev. D, arXiv:1605.07928 [hep-th].

14.12 Funding

Flavor singlet physics with background fields from lattice QCD
A. Schiller
SCHI 422/10-1

14.13 Organizational Duties

Prof. S. Hollands
- Group leader
- Group speaker
- Erasmus coordinator
- Kolloquium organizer

Dr. A. Schiller
- Referee Phys. Rev. D
- Referee Europhysics Journal C

Dr. J. Zahn
- Referee J. Math. Phys., Ann. Henri Poincaré

14.14 External Cooperations

Academic

- DESY Hamburg
  Prof. G. Schierholz (QCDSF collaboration)
- Edinburgh U., UK
  Dr. R. Horsley (QCDSF collaboration)
- Liverpool U., UK
  Dr. P.E.L. Rakow (QCDSF collaboration)
- Adelaide U., Australia
  Dr. J. Zanotti (QCDSF collaboration)
- Cyprus U. Nikosia
  Prof. H. Panagopoulos and collaborators

- Jena U.
  Dr. A. Sternbeck
- Dubna, Russia
  Dr. E.-M. Ilgenfritz
- U Chicago, USA
  Prof. R. M. Wald
- Kinki U., Japan
  Prof. A. Ishibashi
- U Michigan, USA
  Prof. D. Garfinkle
- Dublin City U, Ireland
  Dr. J. Sanders
- York U., UK
  Dr. M. Fröb
- Dubna, Russia
  Prof. A. Isaev (Heisenberg-Landau grant)
- St. Petersburg, Steklov Inst., Russia
  Dr. S.E Derkachov
- Yerevan Phys. Inst., Armenia
  Dr. D. Karakhanyan
- Nottingham U, UK
  Dr. A. Schenkel

14.15 Publications

Journals

V. G. Bornyakov *et al.* [QCDSF-UKQCD Collaboration], "Flavour breaking effects in the pseudoscalar meson decay constants," Phys. Lett. B **767**, 366 (2017).

A. Chambers *et al.*, "Hadron Structure from the Feynman-Hellmann Theorem," PoS LATTICE **2016**, 168 (2017).

A. J. Chambers *et al.*, "Nucleon Structure Functions from Operator Product Expansion on the Lattice," Phys. Rev. Lett. **118**, no. 24, 242001 (2017).

A. J. Chambers *et al.* [QCDSF and UKQCD and CSSM Collaborations], "Electromagnetic form factors at large momenta from lattice QCD," Phys. Rev. D **96**, no. 11, 114509 (2017).

D. Garfinkle, S. Hollands, A. Ishibashi, A. Tolish and R. M. Wald, "The Memory Effect for Particle Scattering in Even Spacetime Dimensions," Class. Quant. Grav. **34**, no. 14, 145015 (2017).

S. Hollands, A. Ishibashi and R. M. Wald, "BMS Supertranslations and Memory in Four and Higher Dimensions," Class. Quant. Grav. **34**, no. 15, 155005 (2017).

J. Fuksa, A. P. Isaev, D. Karakhanyan and R. Kirschner, "Yangians and Yang-Baxter R-operators for ortho-symplectic superalgebras," Nucl. Phys. B **917**, 44 (2017).

J. Fuksa and R. Kirschner, "Correlators with $s\ell_2$ Yangian symmetry," Nucl. Phys. B **914**, 1 (2017).

A. P. Isaev, D. Karakhanyan and R. Kirschner, "Metaplectic R-matrices," Phys. Part. Nucl. Lett. **14**, no. 2, 360 (2017).

D. R. Karakhanyan and R. Kirschner, "Second-order evaluations of orthogonal and symplectic Yangians," Theor. Math. Phys. **192**, no. 2, 1154 (2017).

R. Kirschner and G. Savvidy, "Yangian and SUSY symmetry of high spin parton splitting amplitudes in generalised Yang-Mills theory," Mod. Phys. Lett. A **32**, no. 23, 1750121 (2017).

A. Schenkel and J. Zahn, "Global anomalies on Lorentzian space-times," Annales Henri Poincare **18**, no. 8, 2693 (2017).

M. Wrochna and J. Zahn, "Classical phase space and Hadamard states in the BRST formalism for gauge field theories on curved spacetime," Rev. Math. Phys. **29**, 1750014 (2017).

M. T. Tehrani, "Self-consistency of Conformally Coupled ABJM Theory at the Quantum Level," JHEP **1711**, 153 (2017).

in press

M. B. Fröb and M. Taslimi Tehrani, "Green's functions and Hadamard parametrices for vector and tensor fields in general linear covariant gauges," Phys. Rev. D **97**, no. 2, 025022 (2018) [arXiv:1708.00444 [gr-qc]].

S. Hollands, "Action principle for OPE," Nucl. Phys. B **926**, 614 (2018) [arXiv:1710.05601 [hep-th]].

S. Hollands and G. Lechner, "$SO(d,1)$ -Invariant Yang-Baxter Operators and the dS/CFT Correspondence," Commun. Math. Phys. **357**, no. 1, 159 (2018) [arXiv:1603.05987 [gr-qc]].

J. Zahn, "Generalized Wentzell boundary conditions and quantum field theory," Annales Henri Poincare **19**, no. 1, 163 (2018) [arXiv:1512.05512 [math-ph]].

S. Pottel, "BPHZ renormalization in configuration space for the $\mathcal{A}^4$-model," Nucl. Phys. B **927**, 274 (2018) [arXiv:1709.10194 [hep-th]].

J. Zahn, "The semi-classical energy of open Nambu-Goto strings," accepted for publication in Phys. Rev. D, arXiv:1605.07928 [hep-th].

Talks

S. Hollands, "Gravitational Memory, Information, and Black Holes" plenary talk at DPG spring meeting, Bremen (March 2017).

S. Hollands, "Entanglement Measures in Quantum Field Theory" talk at conference "Quantum Field Theory: Concepts, Constructions & Curved Spacetimes", York (April 2017).

S. Hollands, "Recent progress in Operator Product Expansion" talk at "Wolfhard Zimmermann Memoriam Symposium", MPI Munich (May 2017).

S. Hollands, "Quantum Field Theory in de Sitter spacetime" talk at summer school "Quantum Field Theories on Curved Spacetime", Lyon (June 2017).

S. Hollands, "Entanglement Measures in Quantum Field Theory" talk at Perimeter Institute, Canada (August 2017).

S. Hollands, "Entanglement Measures in Quantum Field Theory" talk at conference "Advances in Mathematics and Theoretical Physics", Rome (September 2017).

S. Hollands, "Dynamical and Thermodynamical (In-)stabilities" talk at workshop "General Relativity & AdS/CFT", Fields Institute, Toronto, Canada (October 2017).

S. Hollands, "Flows of conformal field theories" talk at workshop "Quantum Physics meets Mathematics", Hamburg University (December 2017).

M. T. Tehrani, "Background-independence in gauge theories" talk at workshop "Foundational and structural aspects of gauge theories", Mainz Institute for Theoretical Physics (May 2017).

J. Zahn, "Local gauge covariance and global anomalies" seminar at Faculty of Physics, University of Warsaw, Poland (March 2017).

J. Zahn, "The Nambu-Goto string as an effective field theory and its semi-classical limit" seminar at Faculty of Physics, University of Warsaw, Poland (March 2017).

J. Zahn, "The Nambu-Goto string as an effective field theory and its semi-classical limit" invited talk (Hauptvortrag) at DPG spring meeting, Bremen (March 2017).

14.16 Graduations

Master

- Onirban Islam
  Entanglement Entropy of Dirac Field in Curved Spacetime
  July 2017

Bachelor

- Carlos Serrano (Erasmus)
  Time observables in Quantum Mechanics
  September 2017

14.17 Guests

- Prof. George Savvidy
  Demokritos National Research Center, Athens, Greece
  November 2016–February 2017.
- En-Hung Chao
  Ecole Polytechnique, France
  March–July 2017.
- Dr. Markus Fröb
  U York
  April 24, 2017.
- Prof. Andreas Wipf
  U Jena
  May 29, 2017.
- Dr. David Hilditch
  U Jena
  June 26, 2017.
- Dr. David Karakhanyan
  Yerevan Phys. Inst.
  October – November 2017.
- Dr. Daniela Cadamuro
  TU München
  November 19–21, 2017.
- Prof. Glenn Barnich
  U Brussels
  December 3–5, 2017.
- Dr. Pawel Duch
  U Cracow
  December 17–19, 2017.

15

Theory of Elementary Particles: Correlate to The Report 2016

15.1 Introduction

Our group is interested in the properties of matter at very high energies (small scales) or under other extreme conditions, covering a broad variety of research topics ranging from the study of elementary particles and their properties to the study of quantized matter fields in the presence of strong gravitational fields. The underlying theme of our research and teaching activity is the theory of such quantized fields in its various manifestations, and applications, including:

1. Quantum fields on discrete spacetimes (lattices) and their numerical and theoretical study

2. Quantum fields on curved spacetimes and in the presence of background (gauge) fields

3. Applications of ideas from integrable systems to the study of quantum gauge theories

4. Dualities and relation with classical General Relativity

Quantum field theories on lattices are discretized counterparts of continuum models describing elementary particles in quantum field theoretic models such as the standard model of particle physics. They were introduced in order to investigate certain non-perturbative features of these models in a controlled approximation. A substantial fraction of the current work being done in this area are numerical simulations and the development of new theoretical methods leading to improved numerical schemes. Our group is participating in this endeavor.

Quantum gauge theories such as the standard model can also be treated as continuum field theories, and can thereby be studied using for instance by perturbative methods. The task of finding improved ways of handling perturbative calculations is an important aspect of quantum field theory and is actively pursued in our group from a variety of different viewpoints, including operator product expansion techniques,

methods from integrability, renormalization group methods, holographic ideas, and more.

We also pursue the quest to generalize quantum field theory to curved spacetime (QFTCS), which is inspired by the ideas and principles of General Relativity. On account of its classical treatment of the metric, QFTCS cannot be a fundamental theory of nature. However, QFTCS is expected to provide an accurate description of quantum phenomena in a regime where the effects of curved spacetime may be significant, but effects of quantum gravity itself may be neglected. In particular, it is expected that QFTCS should be applicable to the description of quantum phenomena occurring in the early universe and near (and inside of) black holes, provided that one does not attempt to describe phenomena occurring so near to singularities that curvatures reach Planckian scales and the quantum nature of the spacetime metric would have to be taken into account. Quantum field theory in curved spacetimes has provided important physical insights into the quantum nature of black holes, indicating that they should, if left alone, gradually evaporate due to the emission of quanta whose energies are distributed thermally at the famous Hawking temperature.

In parallel to direct approaches to quantum field theory via perturbative, or numerical, techniques, there are now also more indirect approaches via so-called "holographic dualities". Such dualities typically establish a connection with a quantum field theory living on some sort of boundary of a space and a classical, gravitational, theory living in the higher dimensional space itself. This type of duality is believed to probe rather different regimes of quantum field theory (strong coupling, "large N"), and is hence complementary to other methods. At the technical level, it motivates studies into higher dimensional gravity theories, which turn out to have a rather rich mathematical structure. The study of such structures is another research topic in our group.

More information may be found on the group's webpages, www.uni-leipzig.de/~tet

Prof. S. Hollands

15.2 Stability of higher dimensional black holes

S. Hollands

Black holes are a key feature of Einstein's theory of General Relativity, as well as cousins of this theory in higher dimensions or with a more elaborate field content inspired by holographic ideas. A central question is the stability of such objects under perturbations. For the Schwarzschild and Kerr-spacetimes in four spacetime dimension, this question appears more or less settled, but remains wide open e.g. in higher dimensions, or as soon as more elaborate field content is considered. In a work with Wald [1], we have established a novel method that makes use of ideas from black hole thermodynamic. We have applied these ideas to a variety of interesting situations, most recently for a thorough investigation of so-called "super-radiant" instabilities of fast rotating black holes in AdS-type spacetimes [2]. Such investigations are of interest in their own right as well as for holographic descriptions of field theories within the gauge-gravity duality.

[1] S. Hollands and R. M. Wald, "Stability of Black Holes and Black Branes," Commun. Math. Phys. **321** (2013) 629 [arXiv:1201.0463 [gr-qc]].

[2] S. R. Green, S. Hollands, A. Ishibashi and R. M. Wald, "Superradiant instabilities of asymptotically anti-de Sitter black holes," Class. Quant. Grav. **33**, no. 12, 125022 (2016) doi:10.1088/0264-9381/33/12/125022 [arXiv:1512.02644 [gr-qc]].

15.3 Operator product expansions in quantum field theory

S. Hollands, J.W. Holland, M.B. Fröb, Y. Honma

All quantum field theories with well-behaved ultra violet behavior are believed to have an operator product expansion (OPE) [1]. This means that the product of any two local fields located at nearby points x and y in spacetime can be expanded in the form

$$O_A(x)O_B(y) \sim \sum_C C_{AB}^C(x-y)\, O_C(y), \tag{15.1}$$

where A, B, C are labels for the various local fields in the given theory (incorporating also their tensor character/spin), and where C_{AB}^C are certain numerical coefficient functions—or rather distributions—that depend on the theory under consideration, the coupling constants, etc. The sign "$\sim$" indicates that this can be understood as an asymptotic expansion: If the sum on the right side is carried out to a sufficiently large but finite order, then the remainder goes to zero fast as $x \to y$ in the sense of operator insertions into a quantum state, or into a correlation function. The operator product expansion is on the one hand an important tool for calculations in asymptotically free quantum field theories (such as Quantum Chromo Dynamics, QCD). At a conceptual level, the OPE may be viewed as a kind of algebraic skeleton of quantum field theory, and its understanding may shed some light on fundamental open questions in this theory. Our work has been directed in the following directions:

1. Algebraic aspects of the expansion ("associativity", "crossing symmetry")
2. Recursive procedures for calculating the OPE coefficients in perturbation theory, functional equations for the OPE coefficients.
3. Ways to construct the OPE beyond perturbation theory.
4. Understanding the role of gauge invariance with in the OPE in non-abelian gauge theories.

This is a longer term research project funded by an ERC grant.

[1] K. G. Wilson and W. Zimmermann, "Operator product expansions and composite field operators in the general framework of quantum field theory," Commun. Math. Phys. **24**, 87 (1972).
[2] M. B. Fröb and J. Holland, "All-order existence of and recursion relations for the operator product expansion in Yang-Mills theory," arXiv:1603.08012 [math-ph].

[3] J. Holland and S. Hollands, "Associativity of the operator product expansion," J. Math. Phys. **56**, no. 12, 122303 (2015). doi:10.1063/1.4937811
[4] S. Hollands and C. Kopper, "The operator product expansion converges in massless φ^4_4 theory," Commun. Math. Phys. **313** (2012) 257 [arXiv:1411.1785 [hep-th]].
[5] J. Holland and S. Hollands, "Recursive construction of operator product expansion coefficients," arXiv:1401.3144 [math-ph].
[6] J. Holland and S. Hollands, "A small cosmological constant due to non-perturbative quantum effects," Class. Quant. Grav. **31** (2014) 125006 [arXiv:1305.5191 [gr-qc]].

15.4 Entanglement entropy of quantum fields

K. Sanders, S. Hollands

A typical state of a quantum field theory (QFT) may exhibit a lot of entanglement between spacelike separated regions. In Minkowski space this is due to the Reeh-Schlieder theorem, which has partial extensions to curved spacetimes [2]. In order to quantify the amount of entanglement of a state between two given regions, one may adopt the notion of entanglement entropy as used in quantum mechanics (QM). Computing entanglement entropies is difficult, even for free fields [3], but the results show some interesting features. E.g., when space is divided into two regions by a boundary surface S, the entanglement entropy of the vacuum is divergent and the coefficient of the leading divergent order is proportional to the area of S ("area law").

Unfortunately, the existing computations have a number of drawbacks: they often only work for ground states (using path integrals), and they introduce regulators and subtle computational tricks whose physical meaning is unclear (e.g. the replica method). In this project we endeavour to provide an alternative approach to entanglement entropy, with a better physical motivation, and compare with the existing results. We focus on the following questions:

- The definition of entanglement entropy in terms of density matrices, familiar from QM, requires modification, due to the existence of inequivalent Hilbert space representations in QFT. For this reason we resort to the relative entropy of Araki [1], leading to a well-defined entanglement entropy in a very general setting, taking values in $[0, \infty]$.

- For two quasi-free states in QM, we obtained an explicit formula for their relative entropy, relying heavily on literature from quantum information theory [4]. This general result allows us to find upper and lower bounds for entanglement entropies.

- For quasi-free states of a free scalar QFT, we expect to find their relative entropy as a generalisation of the formula from QM, and the upper and lower bounds should generalise as well.

- In simple explicit cases, such as the Minkowski vacuum and spacelike separated regions with sufficiently simple geometry, it may be possible to evaluate or approximate the bounds on the entanglement entropy. This allows for a comparison

of computational methods and results with the existing literature (e.g. the area law).

[1] H. Araki, Publ. Res. Inst. Math. Sci. **11** (1975/76), 809–833
[2] K. Sanders, Commun. Math. Phys. **288** (2009), no.1, 271–285
[3] S.N. Solodukhin, Living Rev. Relativity **14** (2011), no.8
[4] C. Weedbrook, S. Pirandola, R. García-Patrón, N.J. Cerf, T.C. Ralph, J.H. Shapiro and S. Lloyd, Rev. Mod. Phys. **84** (2012), no.2, 621–669

15.5 Modular nuclearity in curved spacetimes

K. Sanders, G. Lechner

Nuclearity conditions were introduced in quantum field theory by [1], and modular nuclearity, which makes use of Tomita-Takesaki theory, has recently played an important role in certain integrable interacting algebraic QFTs in two dimensional Minkowski space [2]. Although conditions of this sort are physically desirable, mathematically useful, and expected to hold quite generally, they have only been verified in very few cases, even for free fields.

The general formulation of a nuclearity condition requires a reference Hilbert space (obtained from a reference state), a (bounded) region of spacetime, and an operator representing the energy. For free scalar fields, the condition has been verified e.g.

- For the Hamilton operator in the ground state on an ultrastatic spacetime, using localisation in arbitrary bounded regions [3].

- For the modular operator of a wedge region in the Minkowski vacuum, using localisation in any smaller wedge region [2].

In this project we have exploited modular operators to formulate a modular nuclearity condition for generally covariant quantum field theories, formulated in terms of C^*-algebras. At this level of generality we have established that this condition is preserved under pull-backs and under mixing of states, and that it behaves well under space-time deformations. For free scalar fields (with arbitrary potential energy functions, including all masses and scalar curvature couplings) we were able to verify this condition for all quasi-free Hadamard states, both at the one-particle and at the second quantised levels, making use of results of Verch [4].

[1] D. Buchholz and E. Wichmann, Commun. Math. Phys. **106** (1986), no.2, 321–344
[2] D. Buchholz and G. Lechner, Ann. Henri Poincaré **5** (2004), no.6, 1065–1080
[3] R. Verch, Lett. Math. Phys. **29** (1993), no.4, 297–310
[4] R. Verch, Commun. Math. Phys. **160** (1994), no.3, 507–536

15.6 Categories and space-time

K. Sanders

The classical concept of space-time is generally believed to be an approximation, which should arise as an emergent concept in theories of quantum gravity. In order to understand what requirements this imposes on quantum gravity theories, it is necessary to have a good understanding of the classical structure of space-time.

The most advanced in which space-time is treated classically are quantum field theories (QFTs) in curved space-times. Such theories can be discussed in the language of locally covariant QFT (LCQFT), which provides a general, precise and flexible framework [1]. A key aspect of this language is its use of category theory to implement locality and general covariance in a unified way.

In this project we review an interpretation of the categorical language used in LCQFT [3], linking it to modal logic and to an implicit notion of space-time. We consider the importance of the categorical language for the studies of Fewster and Verch on doing the "same physics in all space-times" [2], and we consider its repercussions for the notion of space-time in general and for theories of quantum gravity.

[1] R. Brunetti, K. Fredenhagen and R. Verch, Commun. Math. Phys. **237**, 31–68 (2003)
[2] C. Fewster and R. Verch, Ann. Henri Poincaré **13** (2012), 1613–1674
[3] K. Sanders, PhD Thesis, University of York (2009), arXiv:0809.4828v1 [math-ph]

15.7 Local vs. global temperature

K. Sanders

A state of a quantum field theory can be said to be in thermodynamic equilibrium when it satisfies the KMS-condition [1]. This condition is motivated by strong analogies to quantum statistical mechanics, but it has some drawbacks. In general curved space-times, the analogies used are questionable (see e.g. [3] for the case of accelerated observers). Furthermore, the KMS condition is a global condition, and its relation to a locally measured temperature is unclear.

For a massless free scalar field, a mathematical model of a local thermometer was proposed in [2]. The local temperature is defined in terms of the expectation value of a generally covariant Wick square, assuming that this expectation value is non-negative. This definition is local, generally covariant and reduces to global temperature for KMS states in Minkowski space. However, its usefulness in general curved space-times is unclear, because the local temperature may be ill-defined even for many KMS states in stationary space-times. One known cause for this lies in the acceleration of the stationary observers.

In this project we compare the global and local definitions of temperature. We will show that the local temperature can also be ill-defined for ground states in ultra-static space-times, when the space-time violates the weak energy condition. However, in ultra-static space-times with non-negative scalar curvature, compact Cauchy surface, and minor other conditions, we will show that the local temperature is well-defined

for all stationary states in any flat region. Furthermore, when both local and global temperature are well-defined, we show that both notions give qualitatively similar behaviour.

[1] O. Bratteli and D.W. Robinson, "Operator Algebras and Quantum Statistical Mechanics 2," Springer, Berlin (1997)
[2] D. Buchholz and J. Schlemmer, Class. Quantum Grav. **24**, F25–F31 (2007)
[3] J. Earman, Stud. Hist. Philos. Sci. B Stud. Hist. Philos. Mod. Phys. **42** (2011), no.2, 81–97
[4] R. Schoen and S.-T. Yau, Phys. Rev. Lett. **42**, 547–548 (1979)
[5] R. Schoen, J. Differential Geom. **20** (1984), no.2, 479–495
[6] K. Sanders, "Local Versus Global Temperature Under a Positive Curvature Condition," [arXiv:1605.00895 [math-ph]].

15.8 Orthogonal and symplectic Yangians

R. Kirschner, A.P. Isaev, D. Karakhanyan

We have studied Yang-Baxter relations with symmetry based on orthogonal and symplectic Lie algebras, in particular the RLL relations involving the fundamental R-matrix. The generators of the related Yangian algebra are obtained from the expansion of the L-operator in inverse powers of the spectral parameter. In the case when this expansion is truncated the involved algebra generators have to obey additional conditions which can be fulfilled in distinguished representations only. The spinor representation in the orthogonal case and the metaplectic representation in the symplectic case allow L-operators with only one non-trivial term in the expansion. The generator matrix obeys a quadratic relation. Second order L-operators can be constructed for Jordan-Schwinger type representations. The generator matrix obeys a cubic relation. The Yangian algebra concept provides a deeper understanding of the classical results [1–3]. Our work continues recent work [4].

[1] A.B. Zamolodchikov and Al.B. Zamolodchikov, "Factorized S Matrices in Two-Dimensions as the Exact Solutions of Certain Relativistic Quantum Field Models," Annals Phys. **120** (1979) 253.
[2] B. Berg, M. Karowski, P. Weisz and V. Kurak, "Factorized U(n) Symmetric s Matrices in Two-Dimensions," Nucl. Phys. B **134** (1978) 125.
[3] N.Yu. Reshetikhin, Integrable models of quantum one-dimensional models with $O(n)$ and $Sp(2k)$ symmetry, Theor. Math. Fiz. **63** (1985) 347-366.
[4] D. Chicherin, S. Derkachov and A. P. Isaev, "The spinorial R-matrix," J. Phys. A **46** (2013) 485201. arXiv:1303.4929 [math-ph].

15.9 Applications of numerical stochastic perturbation theory to lattice QCD

H. Perlt, A. Schiller

In collaboration with authors from different locations we have continued our research program using numerical stochastic perturbation theory (NSPT).

It is well known that lattice perturbation theory (LPT) is much more involved compared to its continuum QCD counterpart. The complexity of diagrammatic approaches increases rapidly beyond the one-loop approximation. By now only a limited number of results up to two-loop accuracy have been obtained.

Applying the standard Langevin dynamics [1, 2] to the problem of weak coupling expansions for lattice QCD, a powerful numerical approach for higher loop calculations – called numerical stochastic perturbation theory (NSPT) – has been proposed in [3].

With colleagues from the QCDSF collaboration we have calculated Wilson loops of various sizes up to 20 loops in SU(3) pure lattice gauge theory at different lattice sizes for Wilson gauge action using the technique of numerical stochastic perturbation theory [4]. This allowed us to investigate the perturbative series for various Wilson loops at high loop orders. In we have calculated [5] the SU(3) beta function from Wilson loops to 20th order numerical stochastic perturbation theory. An attempt has been made to include massless fermions, whose contribution is known analytically to 4th order. The question whether the theory admits an infrared stable fixed point is addressed.

The subtraction of hypercubic lattice corrections, calculated at one-loop order in lattice perturbation theory, is common practice, e.g., for determinations of renormalization constants in lattice hadron physics (see the next project). One may overcome the limitation to one-loop and calculate hypercubic corrections for any operator and action beyond the one-loop order using Numerical Stochastic Perturbation Theory (NSPT). Together with colleagues from Regensburg and Dubna we started [6] a first check whether NSPT can by used to subtract hypercubic lattice corrections and provide (in a parametrization valid for arbitrary lattice couplings) the lattice corrections up to three-loop order for the SU(3) gluon and ghost propagators in Landau gauge. In [7] we explored the practicability of such an approach to operators including fermions and considered, as a first test, the case of Wilson fermion bilinear operators in a quenched theory. Our results allow us to compare boosted and unboosted perturbative corrections up to three-loop order.

[1] G. Parisi and Y. s. Wu, Sci. Sin. **24** (1981) 483.
[2] G. G. Batrouni, G. R. Katz, A. S. Kronfeld, G. P. Lepage, B. Svetitsky and K. G. Wilson, Phys. Rev. D **32** (1985) 2736.
[3] F. Di Renzo, E. Onofri, G. Marchesini and P. Marenzoni, Nucl. Phys. B **426** (1994) 675 [arXiv:hep-lat/9405019].
[4] R. Horsley, G. Hotzel, E.-M. Ilgenfritz, R. Millo, Y. Nakamura, H. Perlt, P. E. L. Rakow, G. Schierholz and A. Schiller, Phys. Rev. D **86** (2012) 054502 [arXiv:1205.1659 [hep-lat]].
[5] R. Horsley, H. Perlt, P. E. L. Rakow, G. Schierholz and A. Schiller, Phys. Lett. B **728** (2014) 1 [arXiv:1309.4311 [hep-lat]].
[6] J. Simeth, A. Sternbeck, E. -M. Ilgenfritz, H. Perlt and A. Schiller, PoS LATTICE **2013** (2014) 459 [arXiv:1311.1934 [hep-lat]].
[7] J. Simeth, A. Sternbeck, M. Göckeler, H. Perlt and A. Schiller, arXiv:1501.06322 [hep-lat].

15.10 Aspects in the determination of renormalization constants on the lattice

H. Perlt, A. Schiller

Renormalization factors in lattice Quantum Chromodynamics (QCD) relate observables computed on finite lattices to their continuum counterparts in specific renormalization schemes. Therefore, their determination should be as precise as possible in order to allow for a reliable comparison with experimental results. One approach is based on lattice perturbation theory [1]. However, it suffers from its intrinsic complexity, slow convergence and the impossibility to handle mixing with lower-dimensional operators. Therefore, nonperturbative methods have been developed and applied. Among them the so-called regularization-invariant momentum (RI-MOM) scheme [2] is widely used because of its simple implementation.

Like (almost) all quantities evaluated in lattice QCD also renormalization factors suffer from discretization effects. One can attempt to cope with these lattice artifacts by extrapolating the nonperturbative scale dependence to the continuum (see Ref. [3]) or one can try to suppress them by a subtraction procedure based on perturbation theory. Here we were dealing with the latter approach.

In a recent paper of the QCDSF/UKQCD collaboration [4] a comprehensive discussion and comparison of perturbative and nonperturbative renormalization have been given. Particular emphasis was placed on the perturbative subtraction of the unavoidable lattice artifacts. For the simplest operators and lattice actions this can be done with reasonable effort in one-loop order completely by computing the corresponding diagrams for finite lattice spacing numerically. An alternative approach can be based on the subtraction of one-loop terms of order a^2 with a being the lattice spacing. The computation of those terms has been developed by the Cyprus group [6] and applied to various operators for different actions.

In collaboration with colleagues from QCDSF and Cyprus university we have used in works [7] and [8] some of those results for the analysis of lattice Monte Carlo data of the QCDSF collaboration to determine as precisely as possible the renormalization constants in the so-called renormalization group invariant (RGI) scheme Z^{RGI}.

A novel method for nonperturbative renormalization of lattice nonsinglet as well as singlet operators has been introduced by our lattice collaboration [9], which is based on the Feynman-Hellmann relation (for more details see [10]). The Feynman-Hellmann technique offers a promising alternative for calculations of quark line disconnected contributions to hadronic matrix elements. The method involves computing two-point correlators in the presence of generalized background fields arising from introducing additional operators into the action. As a first application, and test of the method, we computed the renormalization factors of the axial vector current and the scalar densityfor both nonsinglet and singlet operators for three quark flavors of SLiNC fermions. For nonsinglet operators, where a meaningful comparison is possible, perfect agreement with recent calculations using standard three-point function techniques has been found.

[1] S. Capitani, Phys. Rept. **382** (2003) 113 [arXiv:hep-lat/0211036]

[2] G. Martinelli, C. Pittori, C. T. Sachrajda, M. Testa and A. Vladikas, Nucl. Phys. B **445** (1995) 81 [arXiv:hep-lat/9411010]
[3] R. Arthur and P. A. Boyle (RBC and UKQCD Collaborations), Phys. Rev. D **83** (2011) 114511 [arXiv:1006.0422 [hep-lat]].
[4] M. Göckeler, R. Horsley, Y. Nakamura, H. Perlt, D. Pleiter, P. E. L. Rakow, A. Schäfer, G. Schierholz, A. Schiller, H. Stüben and J. M. Zanotti, (QCDSF/UKQCD Collaboration) Phys. Rev. D **82** (2010) 114511 [Erratum-ibid. D **86** (2012) 099903] [arXiv:1003.5756 [hep-lat]].
[5] M. Göckeler, R. Horsley, E.-M. Ilgenfritz, H. Perlt, P. E. L. Rakow, G. Schierholz and A. Schiller, Phys. Rev. D **54** (1996) 5705 [arXiv:hep-lat/9602029].
[6] M. Constantinou, V. Lubicz, H. Panagopoulos and F. Stylianou, JHEP **0910** (2009) 064 [arXiv:0907.0381 [hep-lat]].
[7] M. Constantinou, M. Costa, M. Göckeler, R. Horsley, H. Panagopoulos, H. Perlt, P. E. L. Rakow, G. Schierholz and A. Schiller, Phys. Rev. D **87** (2013) 9, 096019 [arXiv:1303.6776 [hep-lat]].
[8] M. Constantinou, R. Horsley, H. Panagopoulos, H. Perlt, P. E. L. Rakow, G. Schierholz, A. Schiller and J. M. Zanotti, Phys. Rev. D **91** (2015) 1, 014502 [arXiv:1408.6047 [hep-lat]].
[9] A. J. Chambers *et al.* [QCDSF Collaboration], Phys. Lett. B **740** (2015) 30 [arXiv:1410.3078 [hep-lat]].
[10] A. J. Chambers *et al.* [CSSM and QCDSF/UKQCD Collaborations], Phys. Rev. D **90** (2014) 1, 014510 [arXiv:1405.3019 [hep-lat]].

15.11 Global anomalies on Lorentzian spacetimes

A. Schenkel* J. Zahn

*Nottingham U

Global anomalies are very interesting aspects of Quantum Field Theories (QFT). From a practical point of view, the condition of the absence of anomalies is an important constraint for model building. This is in particular the case for QFTs in higher dimensions such as those inspired by superstring theory. On the other hand, global anomalies are a non-perturbative effect, and are thus of interest in their own right, being one of the few aspects of this regime which is accessible with our current theoretical tools.

Global anomalies are usually discussed in a formal path integral setting on compact Riemannian spaces [1] and are computed with the help of the mod 2 index theorem or more generally family index theory. There exists also a formulation in the Hamiltonian framework [2]. Nevertheless, the actual computation of the anomaly relies on the results obtained on compact Riemannian spaces.

We think that this state of affairs is unsatisfactory: Physical spacetimes are neither Riemannian nor compact. Furthermore, in the above formulations it is not clear whether the anomaly is a feature of the (ground) state, or a property of the algebra of observables.

The aim of our project [3] was thus two-fold: To find an algebraic characterization of global anomalies, in order to make the state-independence explicit. And to carry out

the actual computation in a proper Lorentzian setting. Our criterion for the presence of global anomalies is a non-trivial phase of the S matrix for scattering of free fermions off a gauge transformed background potential. As a by-product, we thus provide a definition for the phase of the S matrix in such a situation. For the computation of the anomaly, we follow ideas developed in [4, 5]. This also leads to a clarification of the relation of *perturbative agreement* [6, 7] and the *Wess-Zumino consistency condition* [8].

[1] E. Witten, "An SU(2) Anomaly," Phys. Lett. **117B**, 324 (1982).
[2] P. C. Nelson and L. Alvarez-Gaume, "Hamiltonian Interpretation of Anomalies," Commun. Math. Phys. **99**, 103 (1985).
[3] A. Schenkel and J. Zahn, "Global anomalies on Lorentzian space-times," [arXiv:1609.06562 [hep-th]].
[4] E. Witten, "Global Aspects of Current Algebra," Nucl. Phys. B **223** (1983) 422.
[5] S. Elitzur and V. P. Nair, "Nonperturbative Anomalies in Higher Dimensions," Nucl. Phys. B **243**, 205 (1984).
[6] S. Hollands and R. M. Wald, "Conservation of the stress tensor in interacting quantum field theory in curved spacetimes," Rev. Math. Phys. **17**, 227 (2005) [gr-qc/0404074].
[7] J. Zahn, "Locally covariant charged fields and background independence," Rev. Math. Phys. **27**, no. 07, 1550017 (2015).
[8] J. Wess and B. Zumino, "Consequences of anomalous Ward identities," Phys. Lett. **37B**, 95 (1971).

15.12 Generalized Wentzell boundary conditions and quantum field theory

J. Zahn

Quantum Field Theory in the presence of boundaries has technologically relevant applications, the Casimir effect, but is also important for recent developments in high energy physics, in particular holography (the AdS/CFT correspondence). The goal of the project is to study exotic boundary conditions involving second order derivatives, known in the mathematical literature as *generalized Wentzell boundary conditions*. These occur for example for a spinning string with a mass attached to the boundary [1], but also in the context of the AdS/CFT correspondence [2].

In our project [3], we investigate different aspects of these boundary condition. As a first step, we establish well-posedness of the wave equation at the classical level, including a proof of causal propagation. We then quantize the system and in particular discuss holographic aspects.

[1] J. Zahn, "The excitation spectrum of rotating strings with masses at the ends," JHEP **1312**, 047 (2013).
[2] K. Skenderis, "Lecture notes on holographic renormalization," Class. Quant. Grav. **19**, 5849 (2002).
[3] J. Zahn, "Generalized Wentzell boundary conditions and quantum field theory," [arXiv:1512.05512 [math-ph]].

15.13 Funding

ERC Starting Grant
Prof. S. Hollands
QC & C 259562

DFG Grant
Dr. A Schiller
Projektnummer 276092138

15.14 Organizational Duties

Prof. S. Hollands

- Group leader
- Group speaker
- Erasmus coordinator
- Kolloquium organizer

Dr. A. Schiller

- Referee Phys. Rev. D
- Referee Europhysics Journal C

Dr. J. Zahn

- Referee J. Math. Phys., Ann. Henri Poincaré

15.15 External Cooperations

Academic

- DESY Hamburg
  Prof. G. Schierholz (QCDSF collaboration)
- Edinburgh U., UK
  Dr. R. Horsley (QCDSF collaboration)
- Liverpool U., UK
  Dr. P.E.L. Rakow (QCDSF collaboration)
- Adelaide U., Australia
  Dr. J. Zanotti (QCDSF collaboration)
- Cyprus U. Nikosia
  Prof. H. Panagopoulos and collaborators
- Jena U.
  Dr. A. Sternbeck
- Dubna, Russia
  Dr. E.-M. Ilgenfritz

- U Chicago, USA
  Prof. R. M. Wald
- Kinki U., Japan
  Prof. A. Ishibashi
- U Michigan, USA
  Prof. D. Garfinkle
- Perimeter Institute, Canada
  Dr. S. Greene
- York U., UK
  Dr. M. Fröb
- Grenoble U., France
  Dr. M. Wrochna
- Dubna, Russia
  Prof. A. Isaev (Heisenberg-Landau grant)
- St. Petersburg, Steklov Inst., Russia
  Dr. S.E Derkachov
- Yerevan Phys. Inst., Armenia
  Dr. D. Karakhanyan
- Nottingham U, UK
  Dr. A. Schenkel

15.16 Publications

Journals

S. R. Green, S. Hollands, A. Ishibashi and R. M. Wald, "Superradiant instabilities of asymptotically anti-de Sitter black holes," Class. Quant. Grav. **33**, no. 12, 125022 (2016).

M. B. Fröb, J. Holland and S. Hollands, "All-order bounds for correlation functions of gauge-invariant operators in Yang-Mills theory," J. Math. Phys. **57**, no. 12, 122301 (2016).

J. Holland, S. Hollands and C. Kopper, "The operator product expansion converges in massless φ^4_4- theory," Commun. Math. Phys. **342**, no. 2, 385 (2016).

M. B. Fröb, A. Higuchi and W. C. C. Lima, "Mode-sum construction of the covariant graviton two-point function in the Poincaré patch of de Sitter space," Phys. Rev. D **93**, no. 12, 124006 (2016).

M. B. Fröb and E. Verdaguer, "Quantum corrections to the gravitational potentials of a point source due to conformal fields in de Sitter," JCAP **1603**, no. 03, 015 (2016).

D. Karakhanyan and R. Kirschner, "Yang-Baxter relations with orthogonal or symplectic symmetry," J. Phys. Conf. Ser. **670**, no. 1, 012029 (2016).

A. P. Isaev, D. Karakhanyan and R. Kirschner, "Orthogonal and symplectic Yangians and Yang-Baxter R-operators," Nucl. Phys. B **904**, 124 (2016).

R. Horsley *et al.* [QCDSF-UKQCD Collaboration], "Towards a determination of the ratio of the kaon to pion decay constants," PoS LATTICE **2016**, 284 (2016).

R. Horsley, S. Kazmin, Y. Nakamura, H. Perlt, P. E. L. Rakow, G. Schierholz, A. Schiller and J. M. Zanotti, "Partially conserved axial vector current and applications," PoS LATTICE **2016**, 149 (2016).

R. Horsley *et al.* [QCDSF-UKQC Collaboration], "Determining the scale in Lattice QCD," PoS LATTICE **2015**, 264 (2016).

A. J. Chambers *et al.*, "Applications of the Feynman-Hellmann Theorem in Hadron Structure," PoS LATTICE **2015**, 125 (2016).

R. Horsley, Y. Nakamura, H. Perlt, P. E. L. Rakow, G. Schierholz, A. Schiller and J. M. Zanotti, "Improving the lattice axial vector current," PoS LATTICE **2015**, 138 (2016).

R. Horsley *et al.*, "QED effects in the pseudoscalar meson sector," JHEP **1604**, 093 (2016).

R. Horsley *et al.*, "Isospin splittings of meson and baryon masses from three-flavor lattice QCD + QED," J. Phys. G **43**, no. 10, 10LT02 (2016).

Y. Honma and M. Manabe, "Open Mirror Symmetry for Higher Dimensional Calabi-Yau Hypersurfaces," JHEP **1603**, 160 (2016).

S. Pottel and K. Sibold, "Conjugate variables in quantum field theory and a refinement of Pauli's theorem," Phys. Rev. D **94**, no. 6, 065008 (2016).

A. Much, S. Pottel and K. Sibold, "Preconjugate variables in quantum field theory and their applications," Phys. Rev. D **94**, no. 6, 065007 (2016).

Talks

S. Hollands, "Operator Product Expansion" talk at conference "Local Quantum Physics and Beyond", Hamburg (September 2016).

J. Zahn, "Generalized Wentzell boundary conditions and holography" talk at workshop "Recent Mathematical Developments in Quantum Field Theory", Mathematisches Forschungsinstitut Oberwolfach (July 2016).

M. Fröb, "The operator product expansion for Yang-Mills theories" talk at workshop "Recent Mathematical Developments in Quantum Field Theory", Mathematisches Forschungsinstitut Oberwolfach (July 2016).

K. Sanders, "Modular ℓ^p-conditions for QFT in curved spacetimes" talk at workshop "Recent Mathematical Developments in Quantum Field Theory", Mathematisches Forschungsinstitut Oberwolfach (July 2016).

J. Zahn, "Generalized Wentzell boundary conditions and holography" talk at workshop "LQP38 - Foundations and Constructive Aspects of QFT", TU Munich (May 2016).

G. Collini, "Fedosov quantization and Quantum Field Theories" talk at workshop "LQP37 - Foundations and Constructive Aspects of QFT", Göttingen (January 2016).

15.17 Graduations

Doctorate

- Giovanni Collini
  Fedosov Quantization and Perturbative Quantum Field Theory
  December 2016

Master

- Maximilian Schambach
  Quantization of the Proca field in curved spacetimes - A study of mass dependence and the zero mass limit
  May 2016
- Tobias Jerabek (external)
  Interacting Quantum Fields in the Rindler Spacetime
  July 2016

Bachelor

- Sebastian Drawert
  Die nichtabelsche Eichgruppe SU(3) und ihre Anwendung in der Quantenchromodynamik
  January 2016
- Melanie Weber
  Event Classification with Convolutional Neural Networks for Diboson Channels in the ATLAS Experiment at the Large Hadron Collider
  September 2016

15.18 Guests

- Prof. Roberto Longo
  U Rome
  January 25-26, 2016.
- Dr. Daniela Cadamuro
  U Göttingen
  February 22, 2016.
- Dr. Carla Cederbaum
  U Tübingen
  May 2-3, 2016.

- Dr. Wojciech Dybalski
  TU München
  May 9-10, 2016.
- Prof. Harald Grosse
  U Wien
  May 29-31, 2016.
- Gabriele Nosari
  U Pavia
  June 6-7, 2016.
- Prof. Lars Andersson
  Albert-Einstein-Institut Golm
  October 10, 2016.
- Prof. George Savvidy
  Demokritos National Research Center, Athens, Greece
  November 2016-February 2017.
- Prof. Hans-Werner Diehl
  U Duisburg-Essen
  November 13-14, 2016.
- Prof. Martin Reuter
  U Mainz
  November 28-29, 2016.
- Prof. Bert Schroer
  FU Berlin & CBPF Rio de Janeiro
  December 5, 2016.

Author Index

C

D

E

F

G

H

I

J

K

L

M

N

O

P

R

S

T

U

V

W

Y

Z

UNIVERSITÄT LEIPZIG

TCO2019

Transparent Conductive Oxides – Fundamentals and Applications

23-27 September 2019

Transparent materials are used for ohmic applications such as transparent contacts in displays and solar cells or electro-magnetic shielding. Also semiconducting transparent oxides for diodes and transistors have gained tremendous interest due to applications in transparent and flexible active electronics.

Special topics of TCO2019 include:

- **theory of oxide electronic materials**
- **epitaxial oxide heterostructures**
- **metal-like n-type TCOs**
- **novel transparent semiconductors**
- **2D oxides**
- **point defects in oxides**
- **integrated devices and applications**

supported by

BuildMoNa

Malvern Panalytical
a spectris company

DFG Deutsche Forschungsgemeinschaft

Fächerübergreifende Arbeitsgemeinschaft Halbleiterforschung Leipzig

Historical focus:

120 years of Drude theory of the electron gas

$$n^2(\varkappa^2 - 1) = 2\sum \frac{\sigma\vartheta}{1+(\vartheta/\tau)^2} - 1$$

$$2n^2\varkappa = 2\tau\sum \frac{\sigma}{1+(\vartheta/\tau)^2}$$

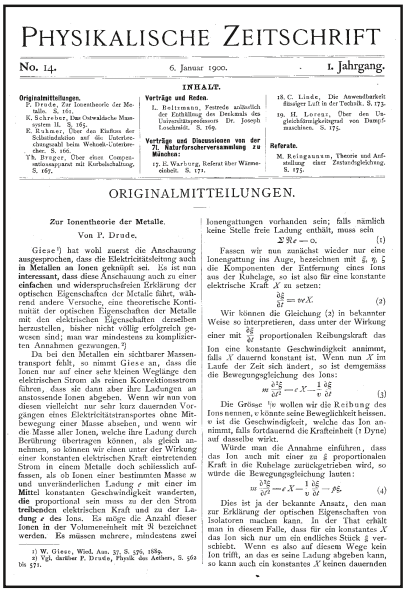

PHYSIKALISCHE ZEITSCHRIFT

No. 14. 6. Januar 1900. 1. Jahrgang.

INHALT.

Originalmitteilungen.
P. Drude, Zur Ionentheorie der Metalle. S. 161.
K. Schreber, Das Ostwaldsche Manometer II. S. 165.
E. Rukmer, Über den Einfluss der Schlussdrahtlänge auf die Unterbrechungszahl beim Wehnelt-Unterbrecher. S. 166.
Th. Bruger, Über einen Compensationsapparat mit Kreisbewicklung. S. 167.

Vorträge und Reden.
L. Boltzmann, Festrede anlässlich der Enthüllung des Denkmals des Universitätsprofessors Dr. Joseph Loschmidt. S. 169.

Vorträge und Discussionen von der 71. Naturforscherversammlung zu München:
17. E. Warburg, Referat über Wärmeschutz. S. 171.
18. C. Linde, Die Anwendbarkeit flüssiger Luft in der Technik. S. 173.
19. H. Lorenz, Über den Ungleichförmigkeitsgrad von Dampfmaschinen. S. 175.

Referate.
M. Reinganum, Theorie und Aufstellung einer Zustandsgleichung. S. 175.

ORIGINALMITTEILUNGEN.

Zur Ionentheorie der Metalle.

Von P. Drude.

Giese[1]) hat wohl zuerst die Anschauung ausgesprochen, dass die Elektricitätsleitung auch in Metallen an Ionen geknüpft sei. Es ist nun interessant, dass diese Anschauung auch zu einer einfachen und widerspruchsfreien Erklärung der optischen Eigenschaften der Metalle führt, während andere Versuche, eine theoretische Kontinuität der optischen Eigenschaften der Metalle mit den elektrischen Eigenschaften derselben herzustellen, bisher nicht völlig erfolgreich gewesen sind; man war mindestens zu komplicierten Annahmen gezwungen.[2])

Da bei den Metallen ein sichtbarer Massentransport fehlt, so nimmt Giese an, dass die Ionen nur auf einer sehr kleinen Wegstrecke den elektrischen Strom als reinen Konvektionsstrom führen, dass sie dann aber ihre Ladungen an anstossende Ionen abgeben. Wenn wir nun von diesen vielleicht nur sehr kurz dauernden Vorgängen eines Elektricitätstransportes ohne Mitbewegung einer Masse absehen, und wenn wir die Masse aller Ionen, welche ihre Ladung durch Berührung übertragen können, als gleich annehmen, so können wir einen unter der Wirkung einer konstanten elektrischen Kraft eintretenden Strom in einem Metalle doch schliesslich auffassen, als ob Ionen einer bestimmten Masse m und unveränderlichen Ladung ε mit einer im Mittel konstanten Geschwindigkeit wanderten, die proportional sein muss zu der den Strom treibenden elektrischen Kraft und zu der Ladung ε des Ions. Es möge die Anzahl dieser Ionen in der Volumeneinheit mit $\mathfrak{N}$ bezeichnet werden. Es müssen mehrere, mindestens zwei Ionengattungen vorhanden sein; falls nämlich keine Stelle freie Ladung enthält, muss sein

$$\Sigma\,\mathfrak{N}\varepsilon = 0. \quad (1)$$

Fassen wir nun zunächst wieder nur eine Ionengattung ins Auge, bezeichnen mit ξ, η, ζ die Komponenten der Entfernung eines Ions aus der Ruhelage, so ist also für eine konstante elektrische Kraft X zu setzen:

$$\frac{d\xi}{dt} = vX. \quad (2)$$

Wir können die Gleichung (2) in bekannter Weise so interpretieren, dass unter der Wirkung einer mit $\frac{d\xi}{dt}$ proportionalen Reibungskraft das Ion eine konstante Geschwindigkeit annimmt, falls X dauernd konstant ist. Wenn nun X im Laufe der Zeit sich ändert, so ist demgemäss die Bewegungsgleichung des Ions:

$$m\frac{d^2\xi}{dt^2} = \varepsilon X - \frac{1}{v}\frac{d\xi}{dt}. \quad (3)$$

Die Grösse $\frac{1}{v}$ wollen wir die Reibung des Ions nennen, v könnte seine Beweglichkeit heissen. v ist die Geschwindigkeit, welche das Ion annimmt, falls fortdauernd die Krafteinheit (1 Dyne) auf dasselbe wirkt.

Würde man die Annahme einführen, dass das Ion auch mit einer zu $\frac{d\xi}{dt}$ proportionalen Kraft in die Ruhelage zurückgetrieben wird, so würde die Bewegungsgleichung lauten:

$$m\frac{d^2\xi}{dt^2} = \varepsilon X - \frac{1}{v}\frac{d\xi}{dt} - p\xi. \quad (4)$$

Dies ist ja der bekannte Ansatz, den man zur Erklärung der optischen Eigenschaften von Isolatoren machen kann. In der That erhält man in diesem Falle, dass für ein konstantes X das Ion sich nur um ein endliches Stück ξ verschiebt. Wenn es also auf diesem Wege kein Ion trifft, an das es seine Ladung abgeben kann, so kann auch ein konstantes X keinen dauernden

1) W. Giese, Wied. Ann. 37, S. 570, 1889.
2) Vgl. darüber P. Drude, Physik des Aethers, S. 562 bis 571.

Please register and submit your oral or poster contribution via www.buildmona.de/TCO2019

Venue: Lecture Hall for Theoretical Physics, Linnéstraße 5, Leipzig